CR-102725

RADIAL AND AXIAL TRANSMISSIBILITY CHARACTERISTICS OF TYPICAL ROCKET VEHICLE STRUCTURE

SD 69-766

TECHNICAL SUMMARY REPORT

CONTRACT NAS8-21426

Prepared for

National Aeronautics and Space Administration, Marshall Space Flight Center

* * * * * * * * *

Prepared by
STUART Y. LEE
Research and Engineering

Space Division
North American Rockwell

Technical Summary Report

SD 69-766

RADIAL AND AXIAL TRANSMISSIBILITY CHARACTERISTICS OF TYPICAL ROCKET VEHICLE STRUCTURE

(Contract NAS8-21426)

December 1969

Prepared by

S. Y. Lee, Program Manager

Approved by
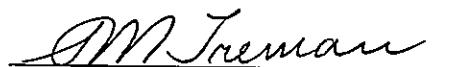
S.M. Treman

S. M. Treman, Director
Structural Systems and Mechanisms

Space Division
North American Rockwell
Downey, California
for
National Aeronautics and Space Administration
George C. Marshall Space Flight Center
Huntsville, Alabama

FOREWORD

This report is a description of the work performed under NASA Contract NAS8-21426, Radial and Axial Transmissibility Characteristics for Typical Rocket Vehicle Structure, by the Space Division (SD) of North American Rockwell Corporation (NR) for the George C. Marshall Space Flight Center, Huntsville, Alabama, during the period of 7 October 1968 to 30 November 1969.

The work was conducted at NR SD by Stuart Y. Lee with support in test operations from the Structural Dynamics Laboratory of NR's Los Angeles and Atomics International Divisions.

Appreciation is extended to Messrs. J. Farrow, R. Jewell, C. Lifer, R. Schock, R. McComas, and Dr. J. Admire of NASA, Messrs. S. Treman and J. West of NR SD for their encouragement and support; and to Dr. R. Guyan, Mr. J. Gee, Mrs. T. Willis, and Mr. H. Hsung for their assistance in computer applications.

PRECEDING PAGE BLANK NOT FILMED.

ABSTRACT

Dynamic transmissibility is a major concern in
preliminary design of advanced systems and finalized
design and analyses of typical aerospace vehicles. A
cylindrical shell mounted with discrete masses simu-
lating a primary structure of a typical rocket vehicle
mounted with equipment or components is analytically
and experimentally investigated under vibratory and
shock excitations. The results indicate significant
mass loading effects upon the vibration responses.
These effects include some shift of frequencies,
many eliminations of resonances, substantial amounts
of amplitude attenuation in the responses, some change
of mode shapes, and an amplification of the response
at resonance dwellings. Little was found affecting the
shock peak responses. The effective forcing areas of
mass loading may be defined by the vibratory patterns,
which are changing in accordance with the resonance
attenuation and disappearance characteristics. The
transmissibility characteristics indicated some dif-
ferences for beams, plates, honeycomb panels, rings,
and shells.

CONTENTS

✓ APPENDIXES

ILLUSTRATIONS

Figure

Page

TABLES

INTRODUCTION

Dynamically induced interactions of primary structures with equipment and components often affect the program safety and mission objectives of a typical rocket vehicle and its advanced systems such as space station, space shuttle vehicles, Apollo, and Saturn; consequently, it becomes a major concern in environmental predictions, preliminary designs, detailed analyses, and finalized design and test evaluations of equipment, components, primary structures, and the combined vehicle systems.

No conclusive solution is known at present on dynamic transmissibility characteristics of these interacted structures. As a result, almost all current designs and analyses of aerospace vehicles, even simple structures, rely upon guessed transmissibilities or arbitrarily assumed dampings which, in either case, may lead to solutions of substantial error, sometimes as much as several thousand percent. There may be some information available in predicting the frequencies and modal response of an unloaded shell, but no practical method exists for computing the transmissibility characteristics without some arbitrary assumptions. This analytical problem becomes more complicated for mass-loaded shell structures and requires the investigation of response attenuation characteristics, change of mode shapes, disappearance of resonances, shift of frequencies, coupling of resonances and the amplifications, as well as the shock spectrum responses and the affected area around the equipment mounted on the primary structure of a typical aerospace vehicle.

Most aerospace equipment or components are affected by the dynamic behavior of the primary structures, which are generally shell structures. During the earlier studies of vibratory transmissibilities in the related research program, NAS8-20019, emphasis was placed on investigations of the mass-loading effects on local structures, i.e., beams, plates, honeycomb panels, and rings, with some preliminary work done on shell structures. In the present study, the combined theoretical and experimental investigation of the mass-loading effect on shell vibrations was continued. Essentially, the primary structure of a typical aerospace vehicle is represented by a cylindrical shell while the components and equipment by discrete masses. Vibratory and shock excitations are employed to generate the forcing functions. Noncontact shakers and instrumentation were specifically used to eliminate the undesirable effects of their masses and frequency coupling to the specimen. For shock tests, a shock form synthesis device in conjunction with an electromechanical shaker is applied longitudinally to determine the axial and radial transmissibility characteristics. Earlier

- 1 -

exploratory studies (References 1 through 10) and the preceding research programs (References 11 through 15) provided the background for the present investigation and formed the bases for the methods of approach.

The shock and vibration loads induced by engine oscillations, aerodynamic pressure fluctuations, acoustics, equipment noise, rough handling, transportation, static firing, ignition, liftoff, powered flight, thrust termination, stage separation, docking, and landing constitute some of the most crucial forcing functions to which rocket and aerospace vehicles are subjected. Also, responses to these sources of excitation often impose the maximum stresses encountered by the spacecraft, payload, or vehicle components. As a result, mission success often hinges on the reliability of the prediction of the radial responses and axial loads propagated along the structure and the confidence in estimates of shock and vibration transmissions along the launch vehicle for design. This criticality is widely appreciated by dynamicists and has been the inspiration for a considerable research and literary effort, particularly in recent years in connection with aerospace vehicle advanced development programs.

Because of technical and financial considerations, the evolution of aerospace programs has been accompanied by great emphasis on the success of individual components and on the assembly of components and local structures. These components and local structures are subjected to crucial environments of shock, vibration, and acoustics during ground operations and in flight; nevertheless, insufficient design progress has been realized from related experience and practical applications in the areas of shock, vibration, environmental prediction, dynamic analysis, testing, and evaluation.

Dynamic problems increase and, simultaneously, become more critical when local structures serve as supports for other components or pieces of equipment. In such cases, the dynamicist is confronted with two problems. One is the estimation of the effect of the equipment on the response of the supporting structure in order to predict realistically the vibratory environment experienced by the mounted component. The other is the calculation of the vibration response of the combined interacting system for the design of local and primary structures.

In environmental dynamics, Mahaffey and Smith (Reference 32) published their study of the local vibration data of airplane flights in 1960. Eldred, Roberts, and White (Reference 33) presented a similar investigation on aircraft and missiles in late 1961. In 1962, Franken (Reference 16) reported the results of his study on the vibration environment of Titan missiles. The data obtained from these studies have been widely used

- 2 -

throughout the aerospace industry to predict dynamic environments for missiles and space vehicles. The primary concern during these studies, however, was the statistical regression of the airplane or missile flight vibration data at a given vehicle zone, and the lack of mass-loading effects specifically due to the mounted equipment. Because there is no unique method available for predicting mass-loading effects on vibration environment, another objective of this study was to investigate these effects on environmental dynamics. During 1963 and 1968, Schock, Barrett, Jewel, Winter, and Lifer (References 18 through 23) of NASA/MSFC, aware of the mass-loading phenomenon, introduced an empirical prediction technique that allowed some amplitude reduction of the vibration environment due to the increase of weights. The technique is a result of their statistical study of Saturn firing test data. They also initiated and recommended theoretical and experimental research studies to investigate the dynamic response phenomenon.

In performing dynamic analyses, scientists and engineers have relied on experimental data or assumptions of the quality factor, complex modulus of elasticity, or damping factor in order to compute the vibration response of a structure. With respect to mass-loaded structures, however, two problems arise immediately: (1) the applicability of the experimental data or assumptions for unloaded structures to mass-loaded structures, and (2) information to support the new assumptions for mass-loaded structures. In consideration of these two problems, one of the major objectives of this study is to explore the relationship between the transmissibility character-istics of the mass-loaded structures and those of the unloaded structures undergoing forced vibration and free vibration.

The first documentation of mass-loading effects on vibration environ-ment appears to be MIL-E-5272, but the mass-loading provision presented appears to have been determined rather arbitrarily. These mass-loading effects criteria were endorsed and specified in the new specification standards, MIL-STD-810, by an evaluation committee (Reference 17) of Government and industry shock and vibration specialists selected by the USAF in late 1962. No information could be found, however, regarding the author, date of initiation, or the technical basis used in establishing the arbitrary mass-loading criteria.

At the laboratory of the former Missiles Development Division of NR in 1956, mass-loading effects on vibrating structures were brought to the author's attention. These phenomena later were found repeatedly at work with Douglas Aircraft Company in connection with 12 missile and space systems. The analytical investigation of the vibration characteristics of mass-loaded structures emphasizing the frequency shifts and modal isolation studies in research papers (References 1 and 6) was initiated in 1959 for the

University of Southern California. In 1962, a preliminary experimental and theoretical investigation of the mass-loading and coupling problem was launched at the Space Division of North American Rockwell Corporation (References 3 and 4). A consistent trend of the mass-loading effect on transmissibility characteristics then became apparent. These basic concepts were followed with further development through the related programs (References 11 through 15).

The preceding study programs on Axial Transmissibilities Characteristics of Typical Rocket Vehicle Structures have analytically and experimentally shown the amplification of shock response for an aerospace vehicle having vibratory characteristics susceptible to the frequency range characterized by the shock durations and the waveforms characterized by the shock shapes. Because these shock response phenomena are closely related to modal characteristics and have some similarity to the mass-loading effects on structural vibration, a correlation of the shock response and vibration response may be beneficial in finding the solution for defining the forcing area and the response attenuation corresponding to the increasing mass load.

This program emphasizes equally in theoretical and experimental studies the attainment of a practical solution to shock and vibration problems, specifically in connection with environmental prediction and response analysis of aerospace vehicles. The analytical and experimental approaches of this study are established by following the basic philosophy of the previous research programs: to concentrate acquiring specifically pertinent information to supplement and extend the previous study, and to emphasize the development of a practical solution satisfying the theoretical requirements and application needs. Because of the continuation nature, this program follows and incorporates some of the theoretical and experimental effort of five previous study projects.

N70-31062

FREQUENCY AND MODAL ANALYSES BY
SERIES-EXPANSION TECHNIQUE

Dynamic analysis of shell structures may be accomplished by a mathematical treatment of the describing partial differential equations of motion, which, in very simple cases only, lend themselves to a closed-form exact solution. Some of these theories of cylindrical shells are compared in Table 1 by listing various sets of differential equations of shell structures developed by different authors, such as Donnell, Flugge, Vlasov, Kennard, Timoshenko, and Naghdi. There are some physical simplification such as gridwork and finite-element approaches, suggesting a replacement of the shell structure by a set of simplified structural elements on which matrix iteration technique can be applied. These structural simplification approaches would result in approximate solutions and may require large computer operations for matrix iteration

During the earlier programs (References 13 and 15), a method was developed using a series-expansion technique in conjunction with Lagrange's approach, and it resulted in a favorable solution in computing the natural frequencies as compared to experimental data and to some previous work by Arnold, Warburton, and Weingarten (References 29, 30, and 31). The process of computation is efficient and can be conveniently modified to compute the interacted mode shapes, in addition to the modal frequencies, by the application of more harmonic waves to describe a single mode.

The present study emphasizes the series-expansion technique and considers the finite-element approach as an alternative method. Both approaches are briefly discussed in this report. Timoshenko-Love notations are mainly used. A mass-loaded shell and the coordinate system are shown in Figure 1.

NOTATIONS

A_{mn}, B_{mn}, C_{mn} = Fourier coefficients of displacements u, v, and w

$$D_A = \frac{E\pi^2 h m}{1.82}$$

$$D_B = \frac{E\pi^2 h^3 m}{21.84}$$

Table 1. Comparison of the Theories of Cylindrical Shells

Characteristic Eq. $\lambda^8 - (4n^2 + A)\lambda^6 + (6n^4 + \frac{1-\nu^2}{K} + B)\lambda^4 - (4n^6 + C)\lambda^2 + n^4(n^2-1)^2 + D = 0$

A	B	C	D	Authors
0	0	0	0	Donnell
-2ν	$-6n^2$	$-2(4-\nu)n^4 + 2(2-\nu)n^2$	0	Flugge and Byrne
-2ν	$-(4+\nu)n^2 + 1$	$-(8-\nu)n^4 + 2n^2$	0	Vlasov
0	$-\frac{4-\nu}{2(1-\nu)}n^2 + \frac{2+\nu}{2(1-\nu)}$	$-\frac{8-8\nu-3\nu^2}{4(1-\nu)}n^2 + \frac{(2+\nu)(2-3\nu)}{4(1-\nu)}$	0	Kennard
0	$-2(2+\nu)n^2$	$-2(3+\nu)n^4 + \frac{1}{2}(5+3\nu)n^2$	0	Naghdi and Berry
0	$-(6+\nu-\nu^2)n^2 + 2(1-\nu^2)$	$-(7+\nu)n^4 + (3+\nu)n^2$	0	Timoshenko
0	$-2(4-\nu^2)n^2 + 4(1-\nu^2)$	$-4(2n^2+1)n^2$	0	Novozhilov
-2	$-6n^2 + 1$	$2(-3n^2+1)n^2$	0	Morley
-2ν	$-6n^2 + 4 - 3\nu^2$	$-2(4-\nu)n^4 + 2(2-\nu)n^2$	0	Biezeno and Grammel
0	$-(6+\nu-\nu^2)n^2$	$-(7+\nu)n^4$	$-p^4$	Bijlaard

Following are additional terms for more accuracy

A	B	C	D	Authors
$-\frac{3-\nu}{1-\nu}\gamma p^2$	$-\gamma p\left[\frac{3(3-\nu)}{1-\nu}n^2 + \frac{1}{K}\right]$ $+\frac{2}{1-\nu}\gamma^2 p^4$	$-\gamma p^2\left[\frac{3(3-\nu)}{1-\nu}n^4 + 2\frac{n^2}{K} - 2(3+\nu)n^2 + \frac{3+2\nu}{K}\right]$ $+\gamma^2 p^2\left[\frac{3-\nu}{1-\nu}\frac{1}{K} + \frac{4}{1-\nu}n^2\right]$	$-\gamma p^2\left(\frac{3-\nu}{1-\nu}n^6 + \frac{n^4}{K} + \frac{n^2}{K} - \frac{3-\nu}{1-\nu}n^2\right) + \gamma^2 p^4\left[\frac{3-\nu}{1-\nu}\frac{n^2}{K} + \frac{2}{1-\nu}n^4\right]$ $+\frac{2}{(1-\nu)}\frac{1}{K} - \frac{4n^2}{1-\nu} + \frac{2}{1-\nu}\right] - \frac{2}{(1-\nu)}\frac{1}{K}\gamma^3 p^6$	Vlasov
$-\frac{3-\nu}{1-\nu}\gamma p^2$	$-\gamma p^2\left[\frac{3(3-\nu)}{1-\nu}n^2 + \frac{1}{K}\right]$ $+\frac{2}{1-\nu}\gamma^2 p^4$	$-\gamma p^2\left[\frac{3(3-\nu)}{1-\nu}n^4 + 2\frac{n^2}{K} - \frac{(4-\nu)(3-\nu)}{2(1-\nu)^2}n^2 + \frac{3+2\nu}{K}\right.$ $\left. + \frac{(2+\nu)(3-\nu)}{2(1-\nu)^2}\right] + \gamma^2 p^4\left[\frac{3-\nu}{(1-\nu)K} + \frac{4n^2}{1-\nu}\right]$	$-\gamma p^2\left[\frac{3-\nu}{1-\nu}n^6 + \frac{n^4}{K} + \frac{n^2}{K} + \frac{(4+\nu)(3-\nu)}{2(1-\nu)^2}n^4 + \frac{(3-\nu)(2-\nu)}{2(1-\nu)^2}n^2\right]$ $+ \gamma^2 p^4\left[\frac{3-\nu}{1-\nu}\frac{n^2}{K} + \frac{2}{1-\nu}n^4 + \frac{2}{(1-\nu)}\frac{1}{K} + \frac{2+\nu}{(1-\nu)^2} - \frac{4-\nu}{(1-\nu)^2}n^2\right]$ $-\frac{2}{(1-\nu)K}\gamma^3 p^6$	Kennard
$-\frac{3-\nu}{1-\nu}\gamma p^2$	$-\gamma p^2\left[\frac{3(3-\nu)}{1-\nu}n^2 + \frac{1}{K}\right]$ $+\frac{2}{1-\nu}\gamma^2 p^4$	$-\gamma^2 p^2\left[\frac{3(3-\nu)}{1-\nu}n^4 + 2\frac{n^2}{K} + \frac{3+2\nu}{K}\right]$ $+\gamma^2 p^4\left(\frac{3-\nu}{1-\nu}\frac{1}{K} + \frac{4}{1-\nu}n^2\right)$	$-\gamma p^2\left(\frac{3-\nu}{1-\nu}n^6 + \frac{n^4}{K} + \frac{n^2}{K}\right) + \gamma^2 p^4\left[\frac{3-\nu}{1-\nu}\frac{n^2}{K} + \frac{2}{1-\nu}n^4 + \frac{2}{(1-\nu)K}\right]$ $-\frac{2}{(1-\nu)K}\gamma^3 p^6$	Naghdi and Berry

R = radius of cylindrical shell

n = number of circumferential waves

$K = h^2/(12R^2)$

h = shell thickness

λ = root of characteristic equation

ν = Poisson's ratio

$\gamma = \frac{1-\nu^2}{E}\rho R^2$

ρ = mass density

p = exponential index in expression for displacements u, v, w.

Space Division
North American Rockwell

E	= Young's modulus
I_x, I_θ	= centroidal mass moments of inertia of m_a
L	= length of shell
M	= largest value for integer m
M_S	= mass of shell
N	= largest value for integer n
T	= kinetic energy
V	= strain energy
x_o	= length of the mass m_a
a	= mean radius of shell
e	= eccentric distance between mid-surface of shell to mass m_a
h	= skin thickness of shell
h_o	= thickness of the mass m_a
m	= number of half-waves along longitudinal axis
n	= number of circumferential waves along radial direction
m_a	= attached mass
t	= time
u, v, w	= displacements of a point on the mid-surface of the shell in the direction of x, θ, and z.
x, θ, z	= longitudinal, circumferential and radial coordinates
α_m	$= \dfrac{m\pi}{L}$
α_i	$= \dfrac{i\pi}{L}$

λ $\qquad = \dfrac{1}{\omega^2}$

θ_0 $\qquad$ = width of mass m_a

ν $\qquad$ = Poisson's ratio

ρ $\qquad$ = mass density

ω $\qquad$ = frequency of vibration in cps or Hz

Subscripts

i, j $\qquad$ = positive integers

s $\qquad$ = refer to shell

$\cdot$ $\qquad$ = differentiation with respect to time

i $\qquad = \sqrt{-1}$

To describe the mode shape of the mass-loaded shell incorporating the change due to mass-loading effects, sufficient numbers of sine and cosine waves must be used in the expression of shell motion. Fourier-series representation is, therefore, adequate for this purpose. The displacement functions of the mass-loaded shell in free vibration can then be expressed in the following forms.
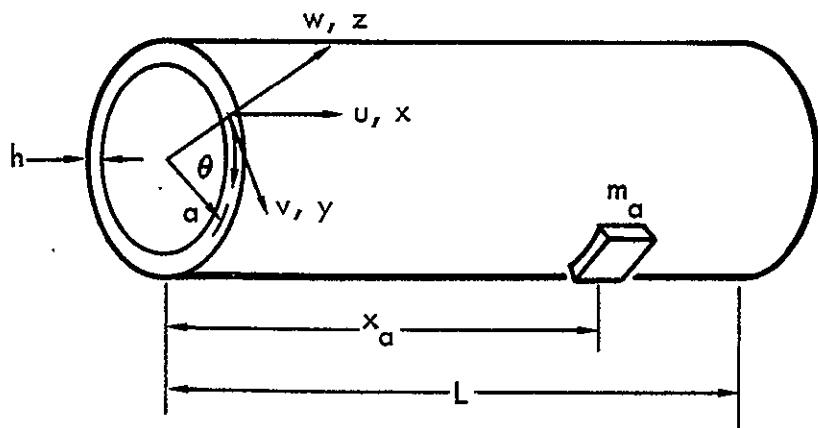
Figure 1. Mass-Loaded Shell

- 8 -

SYMMETRICAL CASE

$$u(\theta, x, t) = \sum_{m=1}^{M} \sum_{n=0}^{N} A_{mn} \cos \alpha_m x \cos n\theta e^{-i\omega t}$$

$$v(\theta, x, t) = \sum_{m=1}^{M} \sum_{n=0}^{N} B_{mn} \sin \alpha_m x \sin n\theta e^{-i\omega t}$$

$$w(\theta, x, t) = \sum_{m=1}^{M} \sum_{n=0}^{N} C_{mn} \sin \alpha_m x \cos n\theta e^{-i\omega t} \tag{1}$$

ANTISYMMETRICAL CASE

$$u(\theta, x, t) = \sum_{m=1}^{M} \sum_{n=0}^{N} A_{mn} \cos \alpha_m x \sin n\theta e^{-i\omega t}$$

$$v(\theta, x, t) = \sum_{m=1}^{M} \sum_{n=0}^{N} B_{mn} \sin \alpha_m x \cos n\theta e^{-i\omega t}$$

$$w(\theta, x, t) = \sum_{m=1}^{M} \sum_{n=1}^{N} C_{mn} \sin \alpha_m x \sin n\theta e^{-i\omega t} \tag{2}$$

The shell structure is treated as a continuous system whose motions can be described by a set of partial differential equations in Lagrange's form as follows:

$$\frac{d}{dt}\left(\frac{\partial T}{\partial \dot{A}_{mn}}\right) - \frac{\partial T}{\partial A_{mn}} + \frac{\partial V}{\partial A_{mn}} = 0$$

$$\frac{d}{dt}\left(\frac{\partial T}{\partial \dot{B}_{mn}}\right) - \frac{\partial T}{\partial B_{mn}} + \frac{\partial V}{\partial B_{mn}} = 0$$

$$\frac{d}{dt}\left(\frac{\partial T}{\partial \dot{C}_{mn}}\right) - \frac{\partial T}{\partial C_{mn}} + \frac{\partial V}{\partial C_{mn}} = 0 \tag{3}$$

where, T and V represent the kinetic and strain energies, as follows:

$$T = \frac{ha\rho}{2g} \int_0^{2\pi} \int_0^L \left[\left(\frac{\partial u}{\partial t}\right)^2 + \left(\frac{\partial v}{\partial t}\right)^2 + \left(\frac{\partial w}{\partial t}\right)^2 \right] dx\, d\theta$$

$$+ \frac{h_o \rho}{2g} \int_0^{\theta_o} \int_0^{x_o} \left\{ \left(\frac{\partial w}{\partial t}\right)^2 + \left(\frac{\partial u}{\partial t} - e\, \frac{\partial^2 w}{\partial x \partial t}\right)^2 \right.$$

$$\left. + \left[\frac{\partial v}{\partial t} - e \left(\frac{\partial v}{a \partial t} + \frac{\partial^2 w}{\partial \theta \partial t} \right) \right]^2 \right\} \quad d x_o\, d\, \theta_o$$

$$\Big|_{x_a\ \theta_a}$$

$$+ I_\theta \left(\frac{\partial w}{\partial x \partial t}\right)_{x_a\ \theta_a} + \frac{I_x}{a} \left(\frac{\partial v}{\partial t} + \frac{\partial^2 w}{\partial \theta \partial t}\right)_{x_a\ \theta_a} \tag{4}$$

$$V = \frac{E\, h}{2(1-\nu^2)} \int_0^{2\pi} \int_0^L \left\{ \left[\frac{\partial u}{\partial x} + \frac{1}{a} \left(\frac{\partial v}{\partial \theta} - w \right) \right]^2 - 2(1-\nu) \right.$$

$$\left. \left[\frac{1}{a} \left(\frac{\partial u}{\partial x} \frac{\partial v}{\partial \theta} - w \frac{\partial u}{\partial x} \right) - \frac{1}{4} \left(\frac{1}{a} \frac{\partial u}{\partial \theta} + \frac{\partial v}{\partial x} \right)^2 \right] \right\} a\, dx\, d\theta$$

$$+ \frac{E\, h^3}{24(1-\nu^2)} \int_0^{2\pi} \int_0^L \left[\left(\frac{\partial^2 w}{\partial x^2} + \frac{\partial v}{a^2 \partial \theta} + \frac{\partial^2 w}{a^2 \partial \theta^2} \right)^2 \right.$$

$$\left. - \frac{2(1-\nu)}{a^2} \left(\frac{\partial^2 w}{\partial x^2} \frac{\partial v}{\partial \theta} + \frac{\partial^4 w}{\partial x^2 \partial \theta^2} \right) - \frac{2(1-\nu)}{a^4} \left(\frac{\partial v}{\partial x} + \frac{\partial^2 w}{\partial x \partial \theta} \right)^2 \right] a\, dx\, d\theta \tag{5}$$

- 10 -

A set of linear algebraic equations can be obtained from the equations of motion by substitution of the kinetic energy expression of the mass-loaded shell, the strain energy of the shell, and the displacement functions. The resulting frequency equations for a symmetrical case are given in Equations 6a, 6b, and 6c.

$$-0.3\ D_A\ C_{mn} + 0.65\ D_A\ B_{mn} - D\left(\alpha_m\ a + 0.35\frac{n^2}{\alpha_m\ a^2}\right)A_{mn}$$

$$+\ \omega^2\left[0.5\ M_S\ A_{mn} + m_a\ \cos\ \alpha_m\ x_a\ \cos\ \frac{n\pi}{2}\ \sum_{i=1}^{M}\ \sum_{j=0}^{N}\right.$$

$$\left.(-e\ \alpha_i\ C_{ij} + A_{ij})\ \cos\ \alpha_i x_a\ \cos\ \frac{j\pi}{2}\right] = 0 \tag{6a}$$

$$0.65\ D_B\ n\ A_{mn} - \left[D_A\left(\frac{n}{\alpha_m\ a} + 0.35\ \alpha_m\right) + D_B\left(\frac{n^2}{\alpha_m\ a^3} + 1.4\ \frac{\alpha_m}{a}\right)\right]B_{mn}$$

$$+\left[D_A\ \frac{n}{\alpha_m\ a} + D_B\left(1.7\ \alpha_m\ \frac{n}{a} + \frac{n^3}{\alpha_m\ a^3}\right)\right]C_{mn} + \omega^2\left\{0.5\ M_S B_{mm}\right.$$

$$+\ M_a\left(1 - \frac{e}{a}\right)\sin\ \alpha_m x_a\ \sin\ \frac{n\pi}{2}\ \sum_{i=1}^{M}\ \sum_{j=0}^{N}\left[\frac{ej}{a}\ C_{ij}\right.$$

$$+\left(1 - \frac{e}{a}\right)B_{ij}\right]\sin\ \alpha_i x_a\ \sin\ \frac{j\pi}{2} + \frac{1}{a^2}\ I_x\ \sin\ \alpha_m x_a\ \sin\ \frac{n\pi}{2}$$

$$\sum_{i=1}^{M}\ \sum_{j=0}^{N}\ (-j\ C_{ij} + B_{ij})\ \sin\ \alpha_i x_a\ \sin\ \frac{j\pi}{2}\left.\right\} = 0 \tag{6b}$$

$$\left[D_B \left(1.7 \; \alpha_m \frac{n}{a} + \frac{n^3}{\alpha_m \, a^3} \right) + D_A \frac{n}{\alpha_m a} \right] B_{mn} - 0.3 \; D_A \; \dot{A}_{mn}$$

$$- \left[D_B \frac{a}{\alpha_m} \left(\alpha_m^2 + \frac{n^2}{a^2} \right)^2 + D_A \frac{L}{m\pi a} \right] C_{mn} + \omega^2 \left\{ 0.5 \; M_S \; C_{mn} \right.$$

$$+ m_a \left[\sin \alpha_m x_a \; \cos \frac{n\pi}{2} \sum_{i=1}^{M} \; \sum_{j=0}^{N} \; C_{ij} \sin \alpha_i x_a \; \cos \frac{j\pi}{2} \right.$$

$$- e \; \alpha_m \; \cos \; \alpha_m x_a \; \cos \frac{n\pi}{2} \sum_{i=1}^{M} \; \sum_{j=0}^{N} \; (A_{ij} - e \; \alpha_i \; C_{ij}) \cos \alpha_i x_a$$

$$\times \cos \frac{j\pi}{2} + \frac{1}{a} e \; n \; \sin \; \alpha_m x_a \; \sin \frac{n\pi}{2} \sum_{i=1}^{M} \; \sum_{j=0}^{N} \left(\frac{e}{a} \; j \; C_{ij} \right.$$

$$\left. + B_{ij} - \frac{e}{a} B_{ij} \right) \sin \alpha_i x_a \; \sin \frac{j\pi}{2} \Bigg] + I_\theta \left(\alpha_m \; \cos \; \alpha_m x_a \right.$$

$$\times \cos \frac{n\pi}{2} \sum_{i=1}^{M} \; \sum_{j=0}^{N} \; \alpha_i \; C_{ij} \cos \alpha_i x_a \; \cos \frac{j\pi}{2} \Bigg)$$

$$+ \frac{1}{a^2} I_x \left[- n \; \sin \; \alpha_m x_a \; \sin \frac{n\pi}{2} \sum_{i=1}^{M} \; \sum_{j=0}^{N} \; (B_{ij} - j C_{ij}) \right.$$

$$\left. \left. \sin \alpha_i x_a \; \sin \frac{j\pi}{2} \right] \right\} = 0$$

(6c)

Matrix iteration can then be applied, and computer programs can be conveniently written to solve for the natural frequencies and mode shapes. In the preceding study, the computer program was limited to only a few terms (M = N = 3). A solution with 33 natural frequencies was obtained by using a Jacobian subroutine and consumed a very short computer time. The analytical results appeared to be surprisingly accurate in comparison with experimental data and the results obtained by Arnold, Warburton, and Weingarten (References 29, 30, and 31). The interacted mode shape of shell motion associated with each frequency can be obtained by using the large number of Fourier coefficients, which are provided by the formulations. A general computer program which is capable of taking in any number of mn values will be developed in conjunction with the formulations.

The solutions presented are for the symmetric case. Similar frequency equations and solutions with only a few different terms and sign changes can be found for the antisymmetric case resulting from the substitution of the corresponding displacement function, Equation 2. .

FREE-VIBRATION ANALYSES BY FINITE-ELEMENT APPROACH

Matrix-iteration techniques can be applied in conjunction with many structural theories to solve dynamic problems. Examples are lumped-mass/stiffness matrix, finite-difference/matrix, lumped-mass/flexibility matrix, and grid-work/finite-element matrix. Because of the structural idealization assumed in these methods, added mass as well as the distributed mass of shell structures can be conveniently applied; however, difficulties may arise in costs and computer programming to solve extremely large matrices with available computers. Table 2 summarizes some classifications of finite-element methods in solid mechanics by comparing their models, theories, assumptions, boundary conditions, and unknowns. A number of computer programs have been written by various authors to solve many problems using finite-element techniques. Most of these are special-purpose programs aimed at effectively solving one class of problems using simple-element representation. There are also several general purpose computer programs either already available or being developed as outlined in Table 3.

In the application of finite-element method, conventional engineering structures are visualized as an assemblage of structural elements inter-connected at a discrete number of nodal points. If the force-displacement relationships for the individual elements are known, it is possible, by using the direct-stiffness method of structural analysis, to derive the properties and study the behavior of the assembled structure (References 24 through 27).

After a suitable mathematical model (discrete-elements) of the structural system has been adopted, equations relating nodal forces and nodal displacements for each type of structural element must be derived. These equations take the matrix form

$$\left| F \right| = [k] \left| u \right| \tag{7}$$

where $[k]$ is known as the element stiffness matrix. The derivation of theories and the detailed description of the methods for various element types and different structures are given in the references and by the individual descriptions of the general computer programs listed in Table 3. Instead of getting into the complex details of individual approaches, a brief description of a beam element to illustrate the finite-element method is presented in this section. Beam and plate are the two basic element types which may be used to solve the mass-loaded shell problem by the finite-element method.

Table 2. A Comparison of Finite-Element Methods

Model	Theory	Assumption in Each Element	Inter-Element Boundary	Unknown in Final Equations
Compatibility	Minimum potential energy	Continuous displacements	Displacement compatibility	Nodal displacement
Equilibrium	Minimum complementary energy	Equilibrating stresses	Equilibrium of boundary tractions	General nodal displacement
Hybrid (CE)	Modified complementary energy (CE)	Equilibrating stresses	Assume compatible displacements	Nodal displacement
Hybrid (PE)	Modified potential energy (PE)	Continuous displacements	Assume compatible displacements	Displacement and boundary forces
Mixed	Reissner's Principle	Continuous displacements and stresses	Displacement compatibility	Displacement and stresses

Table 3. General Computer Programs
of Finite-Elements Methods

No.	Program Name	Developed by	Description	Status
1	NASTRAN	NASA-CSC	Most recent and expensive program to date. Capable of 30,000 DOF. Can solve static, dynamic, and control problems.	Partial completion and operation.
2	ASKA	ARGYRIS – NR	Contains over 50 element types. Can be used for linear and piece-wise linear static analysis, stability and vibration studies. Capable of 20,000 DOF.	Static portion has been completed. Other capacities are in progress.
3	SAMIS	JPL	A matrix iteration system containing a series of programs which may be used to generate a variety of element stiffness and matrices. Static and dynamic problems then may be solved through manipulation. The capacity is large up to about 10,000 DOF but expensive and requiring formulations and bookkeeping.	Completed and in operation.
4	ELAS	Utku and Akyns-JPL	Modification to overcome samis problems for linear static analysis of moderate problems (600 DOF narrow band matrices). Solutions of problems can be performed within core memory. Two-element type.	Completed and in operation.
5	ICES-STRUDL	MIT	Integrated system consists of a large set of design and application programs. About 20,000 source statements. Various and mix element types. Can be used for linear and piecewise linear static analysis, stability, dynamic, and design studies.	Static portion complete; other option in progress.
6	STARDYNE	MRC	Static, stability, and dynamic analyses of moderate problems. Max. 4,000 DOF. Beam and plate elements.	Completed and in operation.

For the two-dimensional Euler beam element (Figure 2) the specific equations are as shown on the following page.
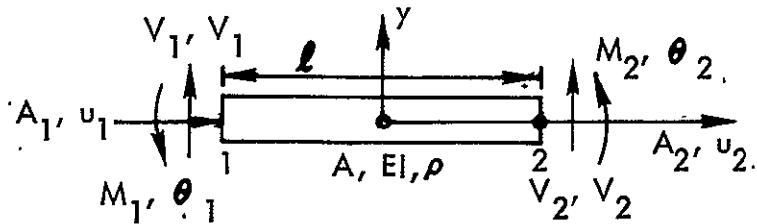
Figure 2.   Beam Element

$$
\begin{Bmatrix} A_1 \\ V_1 \\ M_1 \\ A_2 \\ V_2 \\ M_2 \end{Bmatrix}
=
\begin{bmatrix}
\dfrac{AE}{\ell} & 0 & 0 & -\dfrac{AE}{\ell} & 0 & 0 \\[2mm]
0 & \dfrac{12EI}{\ell^3} & \dfrac{6EI}{\ell^2} & 0 & -\dfrac{12EI}{\ell^3} & \dfrac{6EI}{\ell^2} \\[2mm]
0 & \dfrac{6EI}{\ell^2} & \dfrac{4EI}{\ell} & 0 & -\dfrac{6EI}{\ell^2} & \dfrac{2EI}{\ell} \\[2mm]
-\dfrac{AE}{\ell} & 0 & 0 & \dfrac{AE}{\ell} & 0 & 0 \\[2mm]
0 & \dfrac{-12EI}{\ell^3} & \dfrac{-6EI}{\ell^2} & 0 & \dfrac{12EI}{\ell^3} & -\dfrac{6EI}{\ell^2} \\[2mm]
0 & \dfrac{6EI}{\ell^2} & \dfrac{2EI}{\ell} & 0 & \dfrac{-6EI}{\ell^2} & \dfrac{4EI}{\ell}
\end{bmatrix}
\begin{Bmatrix} u_1 \\ v_1 \\ \theta_1 \\ u_2 \\ v_2 \\ \theta_2 \end{Bmatrix}
\tag{8}
$$

Dynamic response analysis requires a similar set of equations relating nodal forces and nodal accelerations.   These may be written

$$
\{F\} = [m] \{\ddot{u}\} \tag{9}
$$

where [m] is referred to as the element mass or inertia matrix.   For the beam, these equations become

$$\begin{Bmatrix} A_1 \\ V_1 \\ M_1 \\ A_2 \\ V_2 \\ M_2 \end{Bmatrix} = \frac{\rho \ell A}{g} \begin{bmatrix} \frac{1}{3} & 0 & 0 & \frac{1}{6} & 0 & 0 \\ 0 & \frac{13}{35} & \frac{11\ell}{210} & 0 & \frac{9}{70} & -\frac{13\ell}{420} \\ 0 & \frac{11\ell}{210} & \frac{\ell^2}{105} & 0 & \frac{13\ell}{420} & -\frac{\ell^2}{140} \\ \frac{1}{6} & 0 & 0 & \frac{1}{3} & 0 & 0 \\ 0 & \frac{9}{70} & \frac{13\ell}{420} & 0 & \frac{13}{35} & -\frac{11\ell}{210} \\ 0 & -\frac{13\ell}{420} & -\frac{\ell^2}{140} & 0 & -\frac{11\ell}{210} & \frac{\ell^2}{105} \end{bmatrix} \begin{Bmatrix} \ddot{u}_1 \\ \ddot{v}_1 \\ \ddot{\theta}_1 \\ \ddot{u}_2 \\ \ddot{v}_2 \\ \ddot{\theta}_2 \end{Bmatrix} \qquad (10)$$

The form of the mass matrix given here is referred to as a consistent mass matrix, since its derivation is based on the same displacement functions used for the stiffness matrix; therefore, there is no need for arbitrary mass lumping.

Structural element stiffness and mass properties are usually derived with respect to coordinate axes convenient to that element. Prior to assembly of the structural equations, it is necessary to transform each $[\bar{k}]$ and $[\bar{m}]$ so that forces, displacements, and accelerations are referred to a common structural coordinate system. If the barred quantities pertain to the common coordinate system, the transformations (Figure 3) required are
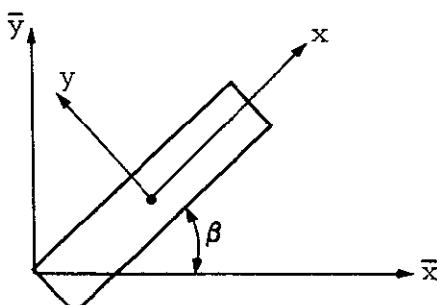
$$\{F\} = [B] \{\bar{F}\} \qquad (11)$$

$$\{u\} = [B] \{\bar{u}\} \qquad (12)$$

Figure 3. Coordinate Transformation

where

$$[B] = \begin{bmatrix} \cos\beta & \sin\beta & 0 & 0 & 0 & 0 \\ -\sin\beta & \cos\beta & 0 & 0 & 0 & 0 \\ 0 & 0 & 1 & 0 & 0 & 0 \\ 0 & 0 & 0 & \cos\beta & \sin\beta & 0 \\ 0 & 0 & 0 & -\sin\beta & \cos\beta & 0 \\ 0 & 0 & 0 & 0 & 0 & 1 \end{bmatrix} \tag{13}$$

Substitution into the force-displacement equations gives

$$[B] \left| \bar{F} \right| = [k] [B] \left| \bar{u} \right| \tag{14}$$

Since $[B]$ is an orthogonal matrix,

$$\left| \bar{F} \right| = [B]^T [k] [B] \left| \bar{u} \right| \tag{15}$$

The element stiffness matrix in structural coordinates is then identified as

$$[\bar{k}] = [B]^T [k] [B] \tag{16}$$

Similarly, the transformed element mass matrix is

$$[\bar{m}] = [B]^T [m] [B] \tag{17}$$

An overall structure stiffness and mass matrix may now be assembled by superimposing individual $[\bar{k}]$ and $[\bar{m}]$ in such a way that all matrix elements associated with the same nodal degree of freedom are added. This procedure, which is the essence of the direct stiffness method, is represented in equation form by

$$[k] = \sum_{i=1}^{n} [\bar{k}]_i \tag{18}$$

$$[M] = \sum_{i=1}^{n} [\bar{m}]_i \tag{19}$$

After forming the system free-free stiffness and mass matrices, all boundary conditions to be imposed are accounted for. In the case of zero constraint conditions, rows and columns of the system matrices corresponding to suppressed degrees of freedom are deleted.

There may also be degrees of freedom present in the system matrices associated with inertia forces which may be neglected in comparison to those that are more dominant. It is then preferable to remove these freedoms from the problem before proceeding with the solution. One such technique for eliminating excess unknowns from the system equations is given in Reference 28.

For modal analysis, the structural equations of the vibration take the form

$$[k] \ |u_o| = \omega^2 [M] \ |u_o| \tag{20}$$

where u_o is defined by: $u = u_o \sin \omega t$.

For structures not fully supported, $[k]$ will be singular; and it is preferable to invert $[M]$ to obtain equations in the standard eigenproblem form,

$$[M]^{-1} \ [k] \ |u_o| = \omega^2 \ |u_o| \tag{21}$$

It is a matter of numerical efficiency that the coefficient matrix $[M]^{-1} \ [k]$ be symmetric. This may be accomplished if $[M]^{-1}$ is obtained by a Choleski decomposition and new variables are adopted. Let

$$[M] = [F]^T \ [F] \tag{22}$$

where $[F]$ is an upper triangular matrix. Then,

$$[M]^{-1} = [F]^{-1} \left([F]^{-1} \right)^T \tag{23}$$

Next, introduce the variables $|q|$ so that

$$|q| = [F] \ |u_o| \tag{24}$$

Substitution and premultiplication by $[F]$ reduces to the form

$$\left([F]^{-1} \right)^T [k] [F]^{-1} \ |q| = [D] \ |q| = \omega^2 |q| \tag{25}$$

in which the dynamic matrix $[D]$ is symmetric. Solution of these equations gives the natural frequencies of the structure, and the modes are obtained by the inverse transformation

$$|u_o| = [F]^{-1} \ |q| \tag{26}$$

Mass-loaded and -unloaded shell structures, such as the present
study specimen, may be represented by a finite element model consisting of
two basic element types in which bar elements are used to model the flange
rings while triangle elements model the shell structure. Details of the model
are shown in Figure 4.
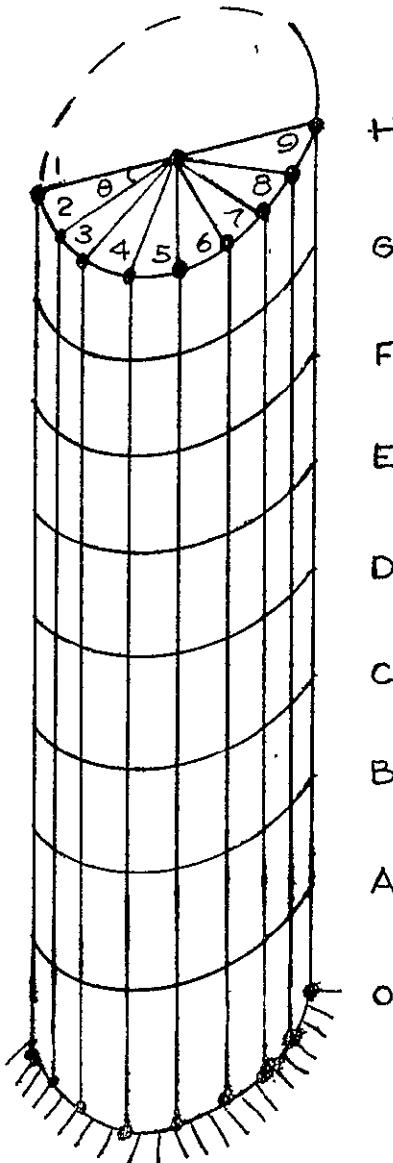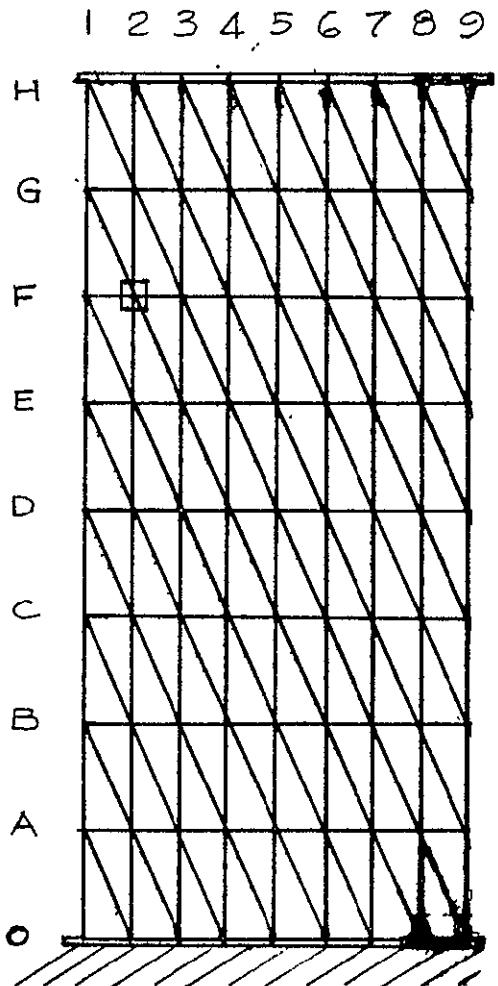
Typical Beam (Bar) Elements

Length = 3.81 inch
Width = 1-3/8 inch
Thickness = 1/4 inch
Weights = 0.131 pounds

Typical Right Triangular Plate Elements

Height = 9 inch
Base = 3.55 inch
Angle = 22.5 degrees
Thickness = 0.05 inch
Weight = 0.08 pounds

Discrete Mass

Length = 5 inch
Width = 4 inch
Thick = 1-1/2 inch (Sample Case)
Weight = 1.258 pounds (Sample Case)

Figure 4-A. Finite-Elements Representation of Mass-Loaded Shell

ORTHORTHORTHROJECTION IN X2-X3 PLANE

TEST CASE STU LEE ROTATE 45,45,45

Figure 4-B. **Three-Dimensional Finite-Element Model and Coordinates System**

- 24 -

SD 69-766

NO GERBER ID CARD, STANDARD OPTIONS USED.

H K K K K G

TEST CASE STU LEE ROTATE 45,45,45
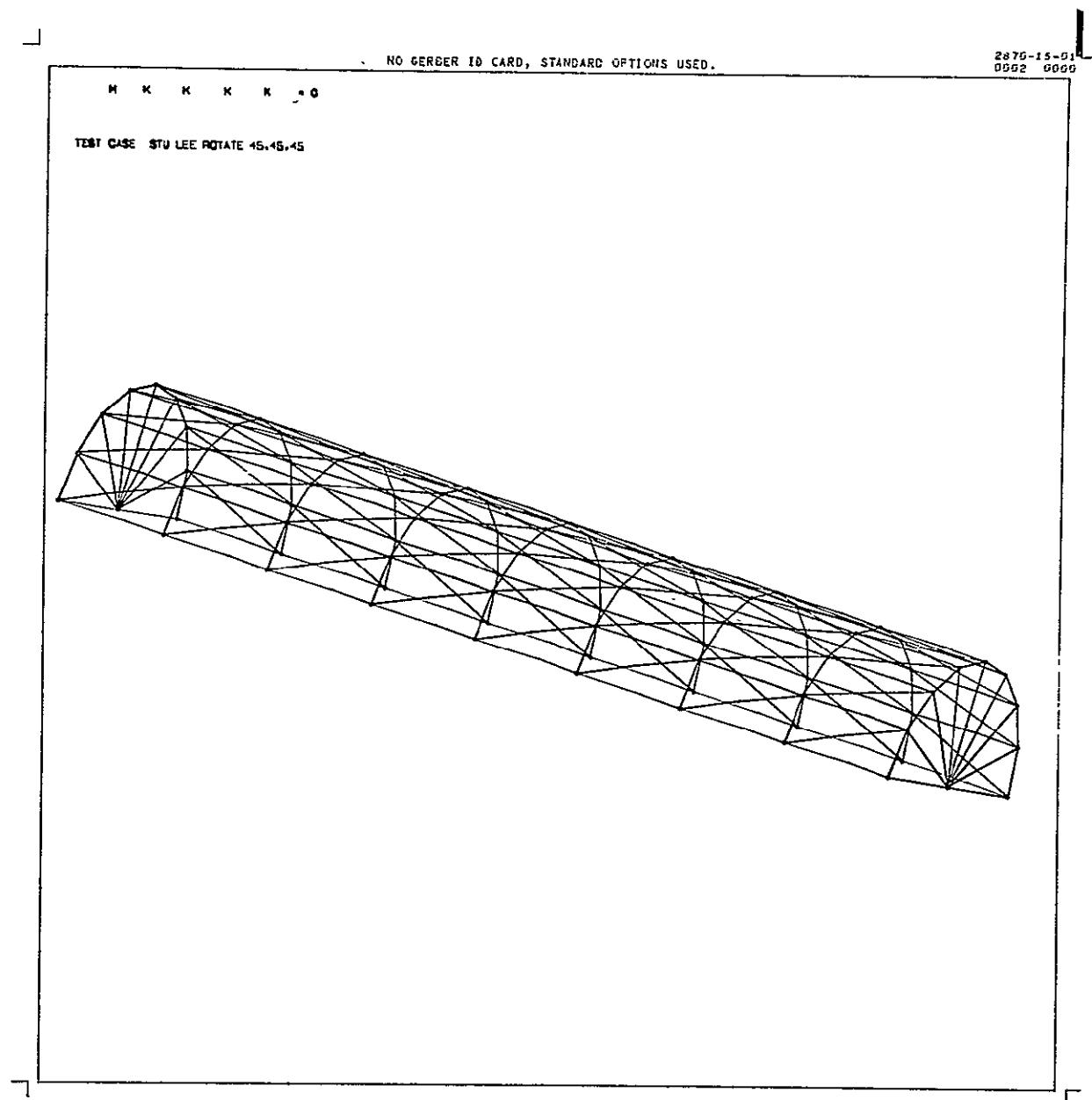
Figure 4-C. Three-Dimensional Finite-Element Model, Side View

- 25 -

SD 69-766

40 P   K • M   •

TEST CASE STU LEE ROTATE 45.45.45
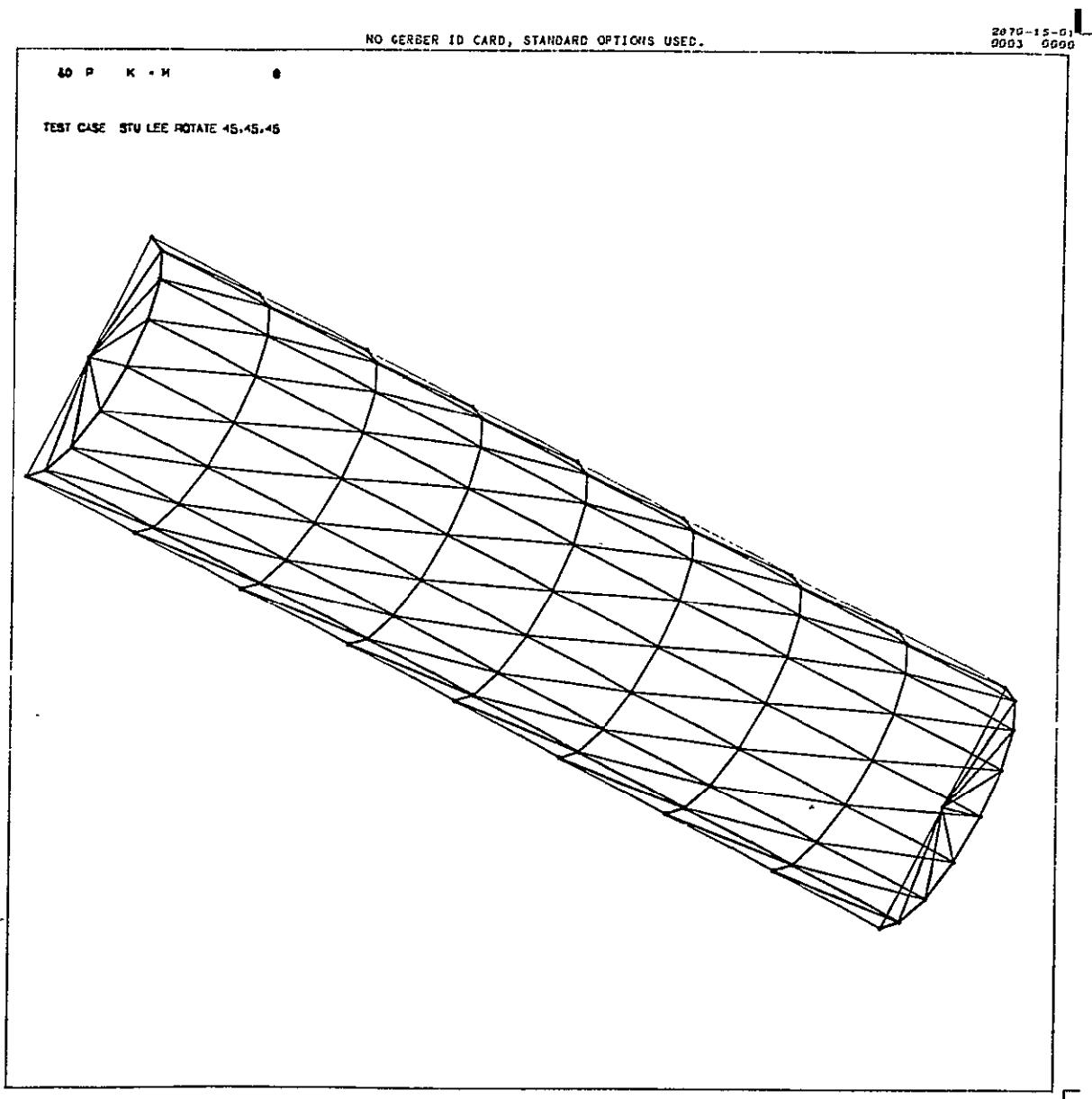
Figure 4-D. **Three-Dimensional Finite-Element Model, Top View**

ORTHORTHORTHPROJECTION IN X2-X3 PLANE

TEST CASE STU LEE NO ROTATE
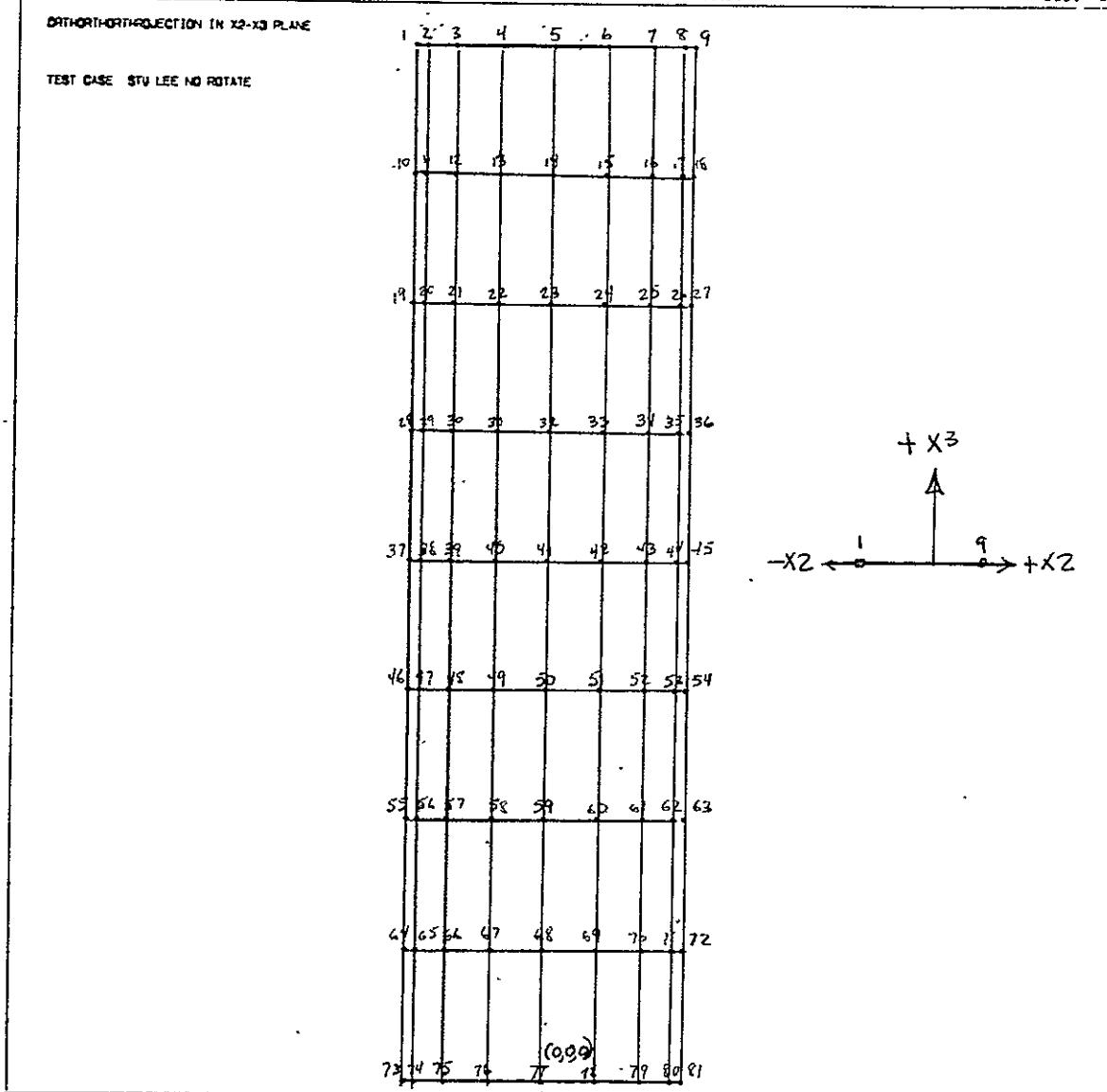
Figure 4-E.   Two-Dimensional Finite-Element Model and Nodal Points,
Front View

- 27 -

SD 69-766
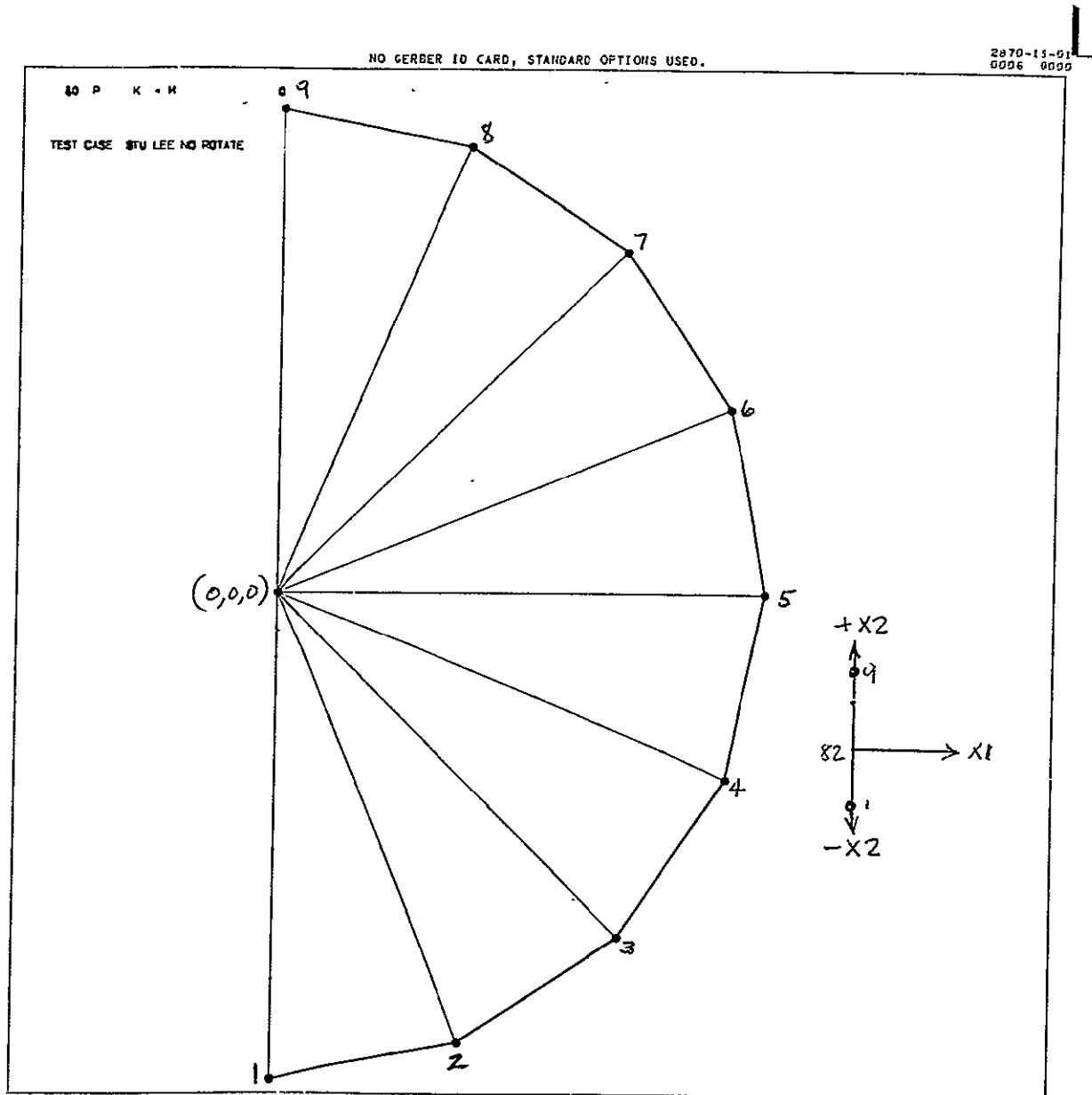
Figure 4-F. Two-Dimensional Finite-Element Model and Nodal Points, End View

SD 69-766

SHOCK AND FORCED VIBRATION ANALYSES

SHELL APPROACH

The dynamic response of mass-loaded and unloaded shells will be discussed in this section. Of particular interest in the study are the radial response of shells to three types of excitation: radial vibration, longitudinal oscillation and axial transient excitations.

The excitation produced by an electro-induction shaker is a form of forcing function with constant amplitude applied at one point. The problem of vibration response of unloaded, closed, cylindrical shells to such an excitation can be conveniently solved by the series-expansion methods. The following nomenclature applies:

a = mean radius of cylinder

b^2 = $\dfrac{D}{a^2 E h}$

A_{mn}, A'_{mn}, B'_{mn}, B''_{mn} = constants

c = $\dfrac{a^4 \rho h}{D}$

$C_{mn}(t)$, $S_{mn}(t)$ = time functions

D = flexural rigidity = $\dfrac{E h^3}{12(1 - \nu^2)}$

L = length of the cylinder

m = number of axial half-waves

M_{mn} = generalized mass

n = number of circumferential waves

p_z = forcing function

- 29 -

$P_{mn}(t)$, $Q_{mn}(t)$ = generalized forces

P_o = amplitude of the force $P(t)$

$P(t)$ = concentrated force excitation

w = displacements of shell in radial direction, with positive w outward

W_{mn} = radial mode shape (symmetric)

W_{mn}' = radial mode shape (antisymmetric)

x, y, z = axial, circumferential, and radial coordinates, respectively, with positive z outward

α_m = $\dfrac{m \pi a}{L}$

δ = Dirac delta function

θ = angular coordinate

ν = Poisson's ratio

ξ = $\dfrac{x}{a}$ = nondimensional coordinate in axial direction

ξ_p, θ_p location of the applied force

ρ = mass density of shell material

ϕ = stress function, related to radial displacement by $w = \nabla^4 \phi$

ω_{mn} = circular natural frequency

∇^4 = $\left(\dfrac{\partial^2}{\partial \xi^2} + \dfrac{\partial^2}{\partial \theta^2} \right)^2$

For a finite cylinder without surface tractions in the x and y directions, the equation of motion for forced vibration can be derived in terms of stress function as follows (References 30, 31, 34 and 35):

$$\nabla^8 \Phi + \frac{1}{b^2} \frac{\partial^4 \Phi}{\partial \xi^4} + c \nabla^4 \frac{\partial^2 \Phi}{\partial t^2} = \frac{a^4}{D} p_z \qquad (27)$$

where p_z = the forcing function in the z direction, positive if outward. If the concentrated force is radially applied at location (ξ_p, θ_p) on a cylinder having simply supported ends, p_z can be expressed in the form

$$p_z = P(t) \, \delta(\xi - \xi_p) \, \delta(\theta - \theta_p) \qquad (28)$$

where the Dirac delta function has the following properties:

$$\int \delta(\xi - \xi_p) d\xi = 1 \quad \text{at} \quad \xi = \xi_p$$

$$\int \delta(\theta - \theta_p) d\theta = 1 \quad \text{at} \quad \theta = \theta_p$$

and becomes zero elsewhere.

By series expansion, Equation 28 becomes

$$p_z = \sum_{m=1}^{\infty} \sum_{n=0}^{\infty} P_{mn}(t) \sin \alpha_m \xi \cos n\theta$$

$$+ \sum_{m=1}^{\infty} \sum_{n=1}^{\infty} Q_{mn}(t) \sin \alpha_m \xi \sin n\theta \qquad (29)$$

The time functions in Equation 29 are the generalized forces given by

$$P_{mn}(t) = \frac{2a}{\pi L} \int_0^{2\pi} \int_0^{L/a} P(t) \, \delta(\xi - \xi_p) \sin \alpha_m \xi \, \delta(\theta - \theta_p) \cos n\theta \, d\xi \, d\theta$$

$$= \frac{2a}{\pi L} P(t) \sin \alpha_m \xi_p \sin n \theta_p \qquad (30)$$

where

$$m = 1, 2, 3, \ldots, \qquad n = 0, 1, 2, 3, \ldots$$

$$Q_{mn}(t) = \frac{2a}{\pi L} \int_0^{2\pi} \int_0^{L/a} P(t)\, \delta(\xi - \xi_p) \sin \alpha_m \xi\, \delta(\theta - \theta_p) \sin n\theta\, d\xi d\theta$$

$$= \frac{2a}{\pi L}\, P(t) \sin \alpha_m \xi_p \sin n\theta_p \tag{31}$$

where

$$m = 1,\ 2,\ 3,\ \ldots,\qquad n = 1,\ 2,\ 3,\ \ldots$$

The solution of Equation 27, which also satisfies the boundary conditions of simply supported ends, is of the form

$$\Phi = \sum_{m=1}^{\infty} \sum_{n=0}^{\infty} C_{mn}(t) \sin \alpha_m \xi \cos n\theta$$

$$+ \sum_{m=1}^{\infty} \sum_{n=1}^{\infty} S_{mn}(t) \sin \alpha_m \xi \sin n\theta \tag{32}$$

where $C_{mn}(t)$ and $S_{mn}(t)$ are time functions to be determined.

If Equations 28 and 32 are substituted into Equation 27, two second-order differential equations are obtained:

$$\ddot{C}_{mn} + \omega_{mn}^2\, C_{mn} = \frac{P_{mn}(t)}{M_{mn}} \tag{33}$$

$$\ddot{S}_{mn} + \omega_{mn}^2\, S_{mn} = \frac{Q_{mn}(t)}{M_{mn}} \tag{34}$$

where $M_{mn} = \rho H \left(\alpha_m^2 + n^2\right)^2$ = generalized mass

$$\ddot{C}_{mn} = \frac{\partial^2 C_{mn}}{\partial t^2} \qquad\qquad \ddot{S}_{mn} = \frac{\partial^2 S_{mn}}{\partial t^2} \tag{35}$$

The general solution of Equation 33 can be found by a convolution integral:

$$C_{mn}(t) = A_{mn} \sin \omega_{mn} t + B_{mn} \cos \omega_{mn} t$$

$$+ \frac{1}{\omega_{mn} M_{mn}} \int_0^t P_{mn}(t') \sin \omega_{mn}(t-t') dt' \qquad (36)$$

where A_{mn} and B_{mn} are constants determined by initial conditions.

For sinusoidal excitation at frequency ω,

$$P(t) = P_0 \sin \omega t \quad \text{where} \quad P_0 = \text{constant} \qquad (37)$$

From Equation 30,

$$P_{mn}(t) = \frac{2a}{\pi L} P_0 \sin \omega t \sin \alpha_m \xi_p \cos n \theta_p \qquad (38)$$

Substituting Equation 36 into Equation 34 and integrating.

$$C_{mn}(t) = A_{mn} \sin \omega_{mn} t + B_{mn} \cos \omega_{mn} t$$

$$+ \frac{P_0 \sin \alpha_m \xi_p \sin n \theta_p}{M_{mn} \omega_{mn} \left(\omega^2 - \omega_{mn}^2\right)} \left[\omega \sin \omega_{mn} t - \omega_{mn} \sin \omega t \right] \qquad (39)$$

Similarly, the solution of Equation 34 is found as

$$S_{mn}(t) = A'_{mn} \sin \omega_{mn} t + B'_{mn} \cos \omega_{mn} t$$

$$+ \frac{P_0 \sin \alpha_m \xi_p \sin n \theta_p}{M_{mn} \omega_{mn} \left(\omega^2 - \omega_{mn}^2\right)} \left[\omega \sin \omega_{mn} t - \omega_{mn} \sin \omega t \right] \qquad (40)$$

where A'_{mn}, B'_{mn} = constants.

The response function $\Phi(\xi, \theta, t)$ is determined by substituting Equations 39 and 40 into Equation 32. The radial displacement response can then be found from the relation

$$w(\xi, \theta, t) = \nabla^4 \Phi(\xi, \theta, t) \qquad (41)$$

For transient excitation applied radially at (ξ_p, θ_p), all formulations from Equation 27 to Equation 36 are applicable. The forcing function $P(t)$ in Equation 28 then represents the shock input. The solutions $C_{mn}(t)$ and $S_{mn}(t)$ of Equations 33 and 34 can be evaluated according to Equation 36. In the previous study, "Axial Transmissibility Characteristics of Multi-Stage Rocket Vehicle Structures" (Contract NAS8-18124, Reference 3), detailed

- 33 -

methods were developed for the derivation of strucutral response to various types of shock input. The computer program generated in that study can be used to solve the present problem of radially applied transient excitation.

If the shell is loaded with component masses, all of the above discussions can still be applied, except that the frequencies ω_{mn} and mode shapes W_{mn} (ξ, θ) and W'_{mn} (ξ, θ) are replaced by the new values obtained from the free vibration analysis as outlined in the previous section, and that generalized forces are to be calculated by

$$P_{mn}(t) = \frac{\int_0^{2\pi} \int_0^{L/a} P(t)\, \delta(\xi - \xi_p)\, \delta(\theta - \theta_p)\, W_{mn}\,(\xi, \theta)\, d\xi\, d\theta}{\int_0^{2\pi} \int_0^{L/a} W_{mn}^2\,(\xi, \epsilon)\, d\xi\, d\theta} \qquad (42)$$

$$Q_{mn}(t) = \frac{\int_0^{2\pi} \int_0^{L/a} P(t)\, \delta(\xi - \xi_p)\, \delta(\theta - \theta_p)\, W'_{mn}\,(\xi, \theta)\, d\xi\, d\theta}{\int_0^{2\pi} \int_0^{L/a} W'^2_{mn}\,(\xi, \theta)\, d\xi\, d\theta} \qquad (43)$$

If the shock is applied axially at one end of the cylinder, the radial response cannot be obtained directly from the above analysis. It would be advantageous to use the three Lagrange equations given in the earlier section: "Frequency and Modal Analysis by Series-Expansion Technique."

Through a similar procedure for analyzing free vibration cases, as described previously, the solution for forced vibration response can be obtained directly by solving the equations of motion, which include the forcing function terms. Adding the generalized forces Q_x, Q_θ, and Q_w to Equation 3, the equations of motion for forced vibration are

$$\frac{d}{dt}\left(\frac{\partial T}{\partial \dot{A}_{mn}}\right) - \frac{\partial T}{\partial A_{mn}} + \frac{\partial V}{\partial A_{mn}} = Q_x \qquad (44)$$

$$\frac{d}{dt}\left(\frac{\partial T}{\partial \dot{B}_{mn}}\right) - \frac{\partial T}{\partial B_{mn}} + \frac{\partial V}{\partial B_{mn}} = Q_\theta \qquad (45)$$

$$\frac{d}{dt}\left(\frac{\partial T}{\partial \dot{C}_{mn}}\right) - \frac{\partial T}{\partial C_{mn}} + \frac{\partial V}{\partial C_{mn}} = Q_w \qquad (46)$$

where Q_x, Q_θ and Q_w represent the generalized forces in a function of time at their specified direction x, θ, or w distributed over a three-dimensional shell surface. The three equations of motion can be simply obtained by setting $Q_x = 0$ and $\theta = 0$ for the case of constant vibratory force excitation

which is applied at a station S(x, θ) with an amplitude Q, in a function of time t and on a direction w. By retaining only the axial generalized force Q_x ($Q_\theta = Q_w = 0$) in a function of time over a three-dimensional shell surface, these three equations of motion become applicable for axial and radial response analyses under a shock or vibration excitation. Then, matrix iteration techniques may be applied to obtain the forced response solutions.

If systems include damping, the strain energy is described in terms of a complex Modulus of Elasticity ($\overline{E}$) instead of the Young's modulus of elasticity (E), which is all that is required for undamped structures. Since the free-vibration characteristics have been solved and the frequencies and mode shapes have become available, the laborious computations may be substituted with simple textbook methods for solving forced vibrations of simple systems. The empirical information provided in later sections may be used for estimating the transmissibility characteristics of mass-loaded shell structures or for predicting the damping factors in conjunction with unloaded structures.

ANALYSIS OF THE EFFECTIVE FORCING AREA

The effective forcing area is referred to the mass-loading affected local area of the vibrating shell structure immediately around the attached discrete mass. These effective forcing areas may be numerically computed through the free-vibration and forced-response analyses or experimentally measured. These methods are discussed in separate sections, while the following alternative approach is presented here to provide a simple, direct insight of the problem.

The equation of motion for shallow cylindrical shell can be written as

$$\nabla^8 w + \frac{1 - \nu^2}{C^2} \frac{\partial^4 w}{\partial \xi^4} + \frac{R^4}{D} \mu \nabla^4 \frac{\partial^2 w}{\partial t^2} = 0 \tag{47}$$

where

$$\xi = \frac{X}{R}, \quad \mu = \rho h + M$$

ρ = mass density of shell

M = concentrated mass

$$\dot{C}^2 = \frac{h^2}{12R^2}, \quad \nabla^8 = \left(\frac{\partial^2}{\partial \xi^2} + \frac{\partial^2}{\partial \theta^2} \right)^4$$

Let

$$\beta^4 = \frac{3\,(1 - \nu^2)}{R^2 h^2} = \frac{1 - \nu^2}{4C^2 R^4} \tag{48}$$

and rewrite Equation 47 as

$$\nabla^8 w + 4\beta^4 R^4 \frac{\partial^4 w}{\partial \xi^4} + \frac{R^4 \mu}{D} \nabla^4 \frac{\partial^2 w}{\partial t^2} = 0 \tag{49}$$

Assume

$$w = W(\xi, \theta)\, e^{i\omega t} \tag{50}$$

Substituting Equation 50 into Equation 49 yields

$$\nabla^8 W + 4\beta^4 R^4 \frac{\partial^4 W}{\partial \xi^4} - \frac{R^4 \mu \omega^2}{D} \nabla^4 W = 0 \tag{51}$$

For a simply supported cylindrical shell, the radial displacement function may be written as

$$W(\xi, \theta) = \Sigma C_{mn} \sin k_m\, \xi \sin n\, \theta \tag{52}$$

where

$$k_m = \frac{m\pi R}{L} = R\alpha_m$$

$$\alpha_m = \frac{m\pi}{L}$$

$$\left(\text{note } \sin k_m \xi = \sin\left(\frac{m\pi R}{L} \cdot \frac{X}{R}\right) = \sin(\alpha_m X)\right)$$

When Equation 52 and Equation 51 are combined, the result is

$$(k_m^2 + n^2)^4 + 4\beta^4 R^4 k_m^4 = \frac{R^4 \mu \omega^2}{D} (k_m^2 + n^2)^2 \tag{53}$$

- 36 -

Solving for ω^2, the natural frequency formula is

$$\omega^2 = \frac{D}{R^4 \mu} \left[(k_m^2 + n^2)^2 + \frac{4\beta^4 R^4 k_m^4}{(k_m^2 + n^2)^2} \right] \tag{54}$$

In solving for β from Equation 53, the relation of β with the natural frequency and modal parameters, k_m and n, can be obtained by

$$\beta^4 = \frac{(k_m^2 + n^2)^2}{4R^4 k_m^4} \left[\frac{R^4 \mu \omega^2}{D} - (k_m^2 + n^2)^2 \right] \tag{55}$$

$$\beta = \frac{\sqrt{0.5\,(k_m^2 + n^2)}}{R k_m} \left[\frac{R^2 \omega^2\,(\rho h + M)}{D} - (k_m^2 + n^2)^2 \right]^{1/4} \tag{56}$$

As shown in Figure 5, the static deflection due to a concentrated load P, is

Figure 5. The Static Deflection Due to a Concentrated Load
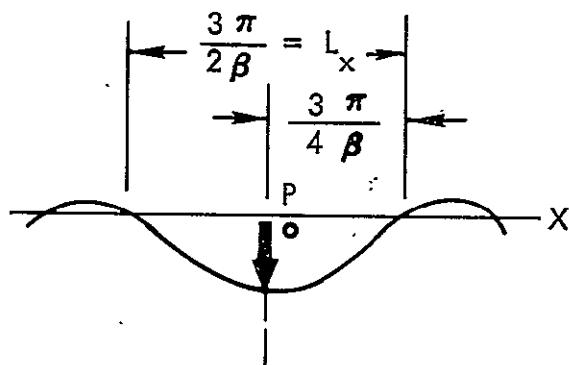
$$w = \frac{P}{8\beta^3 D} \phi(\beta X) \tag{57}$$

$$\phi(\beta X) = e^{-\beta X} (\sin \beta X + \cos \beta X) \tag{58}$$

where $\beta = \dfrac{3\,(1 - \nu^2)}{R^2 h^2}$

For a dynamic problem, Equation 58 can be used as an approximate mode shape with β computed from Equation 56. The concentrated force P is now replaced by the attached mass M.

The effective forcing length in the x-direction, becomes

$$L_x = \frac{3\pi}{2\beta}$$

$$= \frac{3\pi R k_m}{2\sqrt{0.5\,(k_m^2 + n^2)}} \left[\frac{R^4 \omega^2\,(\rho h + M)}{D} - (k_m^2 + n^2)^2 \right]^{-1/4} \tag{59}$$

Now for nonshallow cylindrical shells, the equation of motion is

$$(\nabla^2 + 1)\, \nabla^4 w - 2(1 - \nu)\left(\frac{\partial^4}{\partial\xi^4} - \frac{\partial^4}{\partial\xi^2\partial\theta^2}\right)\nabla^2 w$$

$$+ \frac{1 - \nu^2}{C^2}\frac{\partial^4 w}{\partial\xi^4} + \frac{R^4\mu}{D}\nabla^4\frac{\partial^2 w}{\partial t^2} = 0 \tag{60}$$

When Equation 50 is substituted into Equation 60:

$$(\nabla^2 + 1)\,\nabla^4 W = 2(1 - \nu)\left(\frac{\partial^4}{\partial\xi^4} - \frac{\partial^4}{\partial\xi^2\partial\theta^2}\right)\nabla^2 W$$

$$+ 4\beta^4 R^4\frac{\partial^4 W}{\partial\xi^4} - \frac{R^4\mu\omega^2}{D}\nabla^4 W = 0 \tag{61}$$

and

$$\nabla^8 W + \left(1 - \frac{R^4\mu\omega^2}{D}\right)\nabla^4 W + 4\beta^4 R^4\frac{\partial^4 W}{\partial\xi^4}$$

$$- 2(1 - \nu)\left(\frac{\partial^4}{\partial\xi^4} - \frac{\partial^4}{\partial\xi^2\partial\theta^2}\right)\nabla^2 W = 0 \tag{62}$$

When Equation 52 is substituted into Equation 62:

$$(k_m^2 + n^2)^4 + \left(1 - \frac{R^4\mu\omega^2}{D}\right)(k_m^2 + n^2)^2 + 4\beta^4 R^4 k_m^4$$

$$+ 2(1 - \nu)(k_m^2 + n^2)(k_m^4 - k_m^2 n^2) = 0 \tag{63}$$

or

$$- 4\beta^4 R^4 k_m^4 = p^4 + (1 - \Omega^2)\, p^2 + 2(1 - \nu)\, pq \tag{64}$$

where

$$p = k_m^2 + n^2$$

$$q = k_m^2 (k_m^2 - n^2)$$

$$\Omega^2 = \frac{R^4 \mu \omega 2}{D}$$

Solving for β^4 from Equation 64,

$$\beta^4 = - \frac{1}{4R^4 k_m^4} \cdot [p^4 + (1 - \Omega^2) p^2 + 2 (1 - \nu) p q]$$

$$= - \frac{p}{4R^4 k_m^4} [p (p^2 + 1 - \Omega^2) + 2 (1 - \nu) q]$$

$$= \frac{p}{4R^4 k_m^4} [p (\Omega^2 - p^2 - 1) - 2 (1 - \nu) q]$$

$$= \frac{0.707}{Rk_m} \left\{ p [p (\Omega^2 - p^2 - 1) - 2 (1 - \nu) q] \right\}^{\frac{1}{4}} \tag{65}$$

When Equation 62 is substituted into Equation 61, the effective forcing length can be obtained for a nonshallow shell.

BEAM APPROACH

For the prediction of axial shock transmissibility of typical rocket vehicle structures, the technique of normal mode expansion is employed, which is considered to be the most efficient and practical approach among many other available methods. For the application of this technique, it is necessary to find first the free vibration characteristics of the vehicle. This analysis can be accomplished by any one of the following methods:

1. Beam Continuous System—The vehicle is idealized as a beam with nonuniform cross sections.

2. Lumped-Masses or Finite-Element System—The vehicle is represented by a series of lumped masses and linear springs or by connecting a series of structural elements.

3. Three-Dimensional Shell-Like Structure—The vehicle is treated as a three-dimensional shell structure.

The beam approach is discussed briefly in this section; the shell and finite element methods have been previously presented. Both the lumped masses and beam approaches have been found in the preceding program to be sufficiently accurate for practical engineering application in predicting the axial shock transmissibility characteristics of the specific types of structures.

A shell structure may be treated as a beam in dynamic analysis providing that the shell structure behaves like a beam in the dynamic environment; this condition requires that a cylindrical shell under consideration be long, slender, isotropic, symmetrical, having negligible imperfections and Poisson's effects, and that the force applied be in an ideal condition.

To find the axial shock transmissibility along the vehicle structure, the axial responses at various locations of the vehicle are first calculated. Derivations of the forced responses to three types of shock pulses, namely halfsine, sawtooth, and arbitrary pulses, were presented in detail in the preceding study (Reference 13), by using the method of Laplace transformation or Duhamel integration in conjunction with the modal expansion technique. The axial shock transmissibility can then be calculated as the output to input acceleration ratio.

The items of nomenclature used in this section are as follows:

a_i = coefficient of the ith normal mode

(a) = column matrix with elements a_i

A = cross-sectional area of the vehicle structure

c_{ij} = coefficients of a_i

$[C]$ = square matrix with elements c_{ij}

$[D]$ = $[k]^{-1} (m)$ = dynamic matrix

E = modulus of elasticity

g = acceleration of gravity

$[I]$ = unit matrix

i, j = integer, subscript for mode numbers or mass number

k_{ij} = spring constant

$[k]$ = stiffness matrix with elements k_{ij}

$[k]^{-1}$ = inverse of $[k]$

L = axial length of the structure

m_i = lumped mass at location i

(m) = diagonal matrix of m_i

n = total number of lumped masses or modes

(0) = zero column matrix

p = angular natural frequency

t = time

u = axial displacement or deformation

(u) = column matrix of displacement

$(\ddot{u})$ = column matrix of acceleration

(U) = column matrix of mode shapes

$[W]$ = $(m)^{-1} [k]$ = inverse dynamic matrix

x = axial coordinate

X = mode shape

α = $(Eg/\gamma)^{1/2}$ = velocity of wave propagation of displacement or stress

γ = specific weight of material, weight per unit volume

λ = p^2 = eigenvalue of $[w]$

ϕ_i = the ith normal mode

θ = phase angle

dot = differentiation with respect to time

prime = differentiation with respect to x

If the vehicle is treated as a nonuniform beam with variable cross-sections, the equation of motion of free longitudinal vibration is as follows (Reference 13):

$$E \frac{d}{dx} \left[A(x) \frac{\partial u(x, t)}{\partial x} \right] - \frac{A(x)\gamma}{g} \frac{\partial^2 u}{\partial t^2} = 0 \qquad (66)$$

where $A(x)$ = cross-sectional area, a function of the axial coordinate, x. For a specially constructed section, a proper equivalent cross-sectional area should be used.

Expanding the differentiation, Equation 66 becomes

$$E \left[A \frac{\partial^2 u}{\partial x^2} + \frac{dA}{dx} \frac{\partial u}{\partial x} \right] - \frac{A\gamma}{g} \frac{\partial^2 u}{\partial t^2} = 0 \qquad (67)$$

or

$$u'' + \frac{A'}{A} u' - \frac{1}{\alpha^2} \ddot{u} = 0 \tag{68}$$

where

$$\alpha = (E_g/\gamma)^{1/2}$$

= velocity of propagation of displacement or stress waves

The primed quantities are derivatives with respect to x; and dotted quantities are derivatives with respect to time.

By assuming a solution of the form

$$u(x, t) = X(x) \cos pt \tag{69}$$

where

$$X(x) = \sum_{i=1}^{n} a_i \phi_i(x) \tag{70}$$

and $\phi_i(x)$ is the ith normal mode which satisfies the boundary conditions,

$X = 0$ for fixed end

$X' = 0$ for free end

By substituting Equation 69 into Equation 68 and applying Galerkin's method, the following equation is obtained:

$$\int_0^L \left[X'' + \frac{A'}{A} X' + \left(\frac{p}{\alpha}\right)^2 X \right] \phi_i(x) \, dx = 0 \tag{71}$$

By putting the series (Equation 70) into Equation 71 and integrating, a system of n equations in terms of the unknown coefficients, a_i, will be derived.

$$c_{11} a_1 + c_{12} a_2 + \ldots \ldots \ldots + c_{1n} a_n = 0$$

$$c_{21} a_1 + c_{22} a_2 + \ldots \ldots \ldots + c_{2n} a_n = 0$$

$$\cdot \quad \cdot \quad \cdot \quad \cdot \quad \cdot \quad \cdot \quad \cdot \quad \cdot \quad \cdot \quad \cdot \quad \cdot \quad \cdot \quad \cdot \quad \cdot \quad \cdot$$

$$c_{n1} a_1 + c_{n2} a_2 + \ldots \ldots \ldots + c_{nn} a_n = 0 \tag{72}$$

where

c_{ij} = coefficients of a_i obtained from the integration (Equation 71).

ij = 1, 2, 3 . . . n

In matrix form, Equation 72 becomes

$$[C] (a) = 0 \tag{73}$$

where

$[C]$ = square matrix of c_{ij}

(a) = column matrix of a_i

The frequency equation is obtained by setting the determinant $|C|$ equal to zero.

$$\det |C| = 0 \tag{74}$$

The frequency p_i for each mode is then determined from the polynomial of the nth order in p^2 derived by expansion of Equation 74. The modal coefficients, a_i, are found from Equations 72 or 73. The mode shape, $X(x)$, is given by Equation 70.

Equation 71 applies not only to the case in which the cross-sectional area A is a continuous function of x, but also to the case with piecewise continuous function $A(x)$. In the latter case, the integration will be performed step by step for each length interval within which the cross section $A(x)$ can be expressed as a continuous function.

For the prediction of axial transmissibility of typical vehicle structures, the technique of modal expansion plus Laplace transformation or Duhamel integration is employed to determine the transient response to various types of impulsive excitation (References 36 through 41).

New items of nomenclature are introduced as follows:

a_i = acceleration at time t_i

A_i = average acceleration in the time interval $(t_i - t_{i-1})$

A_o = maximum acceleration amplitude

$A(t)$ = acceleration input

$\overline{A}(s)$ = Laplace transform of $A(t)$

$b(t)$ = base displacement

$B_n(t)$ = generalized force

$\overline{B}_n$ = Laplace transform of $B_n(t)$

c = viscous damping coefficient

c_r = critical damping coefficient

C_n = mode participation factor

$H(t)$ = unit step function

i = time interval number; subscript for quantity at time t_i

K $= \dfrac{1 - 2\zeta^2}{(1 - \zeta^2)^{1/2}}$

n = mode number; subscript for quantity in the nth mode

N = total number of normal modes

$q(t)$ = generalized coordinate, response function of time

$\overline{q}$ = Laplace transform of q(t)

Q   = shock load factor

R   = total number of time intervals within pulse duration

s   = parameter of Laplace transform

t   = time

t' $= t - \tau = t - t_R$

$\overline{t}$ $= t - t_{R-1}$

β $= \tan^{-1}\left[2\zeta\dfrac{\omega}{\omega_n} \middle/ \left(1 - \dfrac{\omega^2}{\omega_n^2} \right) \right]$

ζ $= c/c_r =$ damping factor

η = dummy variable of time

θ $= \tan^{-1}\dfrac{2\zeta(1 - \zeta^2)^{1/2}}{1 - \zeta^2}$

ξ $= t - t_{i-1}$

ξ' $= t - t_i$

ρ = mass density

τ = shock duration

ϕ $= \tan^{-1}\dfrac{\zeta}{(1 - \zeta^2)^{1/2}}$

SD 69-766

$$\psi = \tan^{-1}\left[2\zeta(1-\zeta^2)^{1/2}\middle/\left(1 - \frac{\omega^2}{\omega_n^2} - 2\zeta^2\right)\right]$$

$\omega \quad = \pi/\tau = $ angular frequency of forcing function

$\omega_d \quad = \omega_n(1-\zeta^2)^{1/2} = $ damped angular frequency

$\omega_n \quad = $ angular natural frequency of the nth mode

Equation of Motion

To illustrate the application of the modal expansion method to shock response problems, the structure is considered to be a slender, cantilevered beam with shock input at the fixed end, as shown in Figure 6.

For a uniform beam, the equation of motion of free axial vibration can be written from Equation 66 as

$$\frac{\partial^2 u}{\partial t^2} - \alpha^2 \frac{\partial^2 u}{\partial x^2} = 0 \tag{75}$$
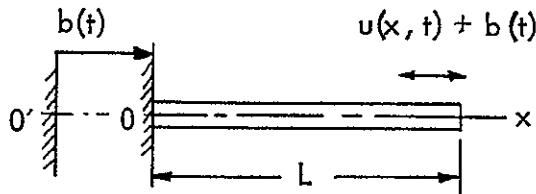
Figure 6.   Axial Vibration of A Beam Excited at the Base

If the beam is excited at its fixed end by base displacement b(t), the equation of motion of forced vibration is derived by replacing u(x, t) of Equation 75 by u(x, t) + b(t), which is the displacement of the beam with respect to a fixed reference point $0'$ (Figure 6).

$$\frac{\partial^2}{\partial t^2}\left[u(x,\ t) + b(t)\right] - \alpha^2 \frac{\partial^2}{\partial x^2}\left[u(x,\ t) + b(t)\right] = 0 \tag{76}$$

or

$$\ddot{u} - \alpha^2 u'' = - b(t) \tag{77}$$

where

$$\ddot{b}(t) = \frac{d^2}{dt^2} b(t)$$

$$= \text{acceleration input at the base}$$

Let

$$A(t) \equiv - \ddot{b}(t) \tag{78}$$

The equation becomes

$$\ddot{u} - \alpha^2 u'' = A(t) \tag{79}$$

Applying modal expansion technique, the solution of Equation 79 can be assumed as

$$u(x, t) = \sum_{n=1}^{\infty} X_n(x) \, q_n(t) \tag{80}$$

where

$$X_n(x) = \text{the } n^{th} \text{ normal mode}$$

The base acceleration can also be expressed in a similar form:

$$A(x, t) = \sum_{n=1}^{\infty} X_n(x) \, B_n(t) \tag{81}$$

where $B_n(t)$ is the generalized force defined by the following equation:

$$B_n(t) = C_n A(t) \tag{82}$$

- 48 -

where C_n is the mode participation factor given by

$$C_n = \frac{\int_0^L X_n(x)\ dx}{\int_0^L X_n^2(x)\ dx}$$

Substituting Equations 80 and 81 into Equation 79 and using the equation of free vibration,

$$X_n{''} = \frac{-\omega_n^2}{\alpha^2} X_n \tag{83}$$

the following equation of motion in terms of the generalized coordinate is obtained:

$$\ddot{q}_n(t) + \omega_n^2\, q_n(t) = B_n(t) \tag{84}$$

If damping is considered, the equation of forced vibration becomes

$$\ddot{q}_n + 2\zeta\,\omega_n\,\dot{q}_n + \omega_n^2\, q_n = B_n \tag{85}$$

where

$$\zeta = \frac{c}{c_r} = \text{damping factor}$$

Through Duhamel integration or Laplace transformation, solutions for beam type structural response to various shock forces were obtained in the preceding study (Reference 13).

A. Sawtooth Pulse (Figure 7A, B, C)

A. Sawtooth Pulse

$$A(t) = A_o \frac{t}{\tau}$$

B. Half-Sine Pulse

$$A(t) = A_o \sin \omega t$$

C. Arbitrary Pulse

$$A_i = \frac{1}{2}\left(a_{i-1} + a_i\right)$$
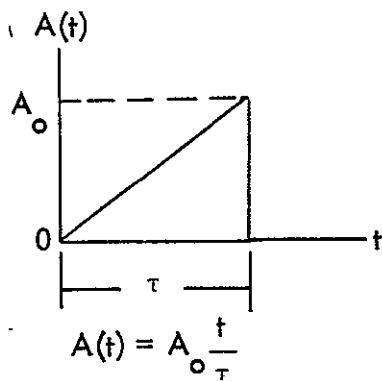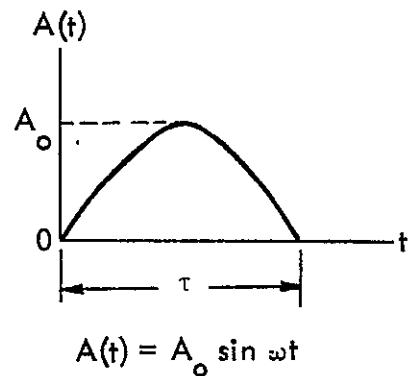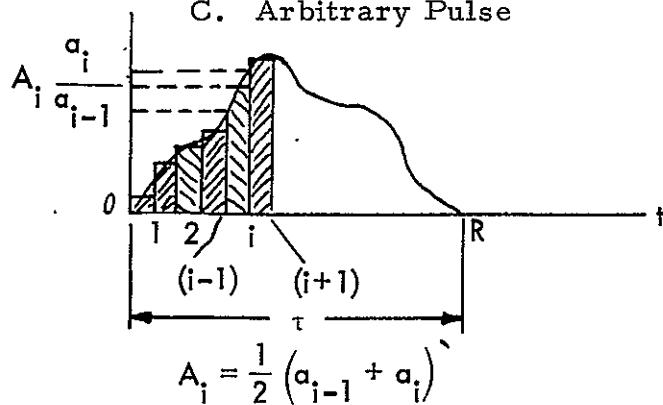
Figure 7. Three Types of Shock Pulse

For $0 < t \le \tau$,

$$\ddot{q}_n(t) = \frac{-C_n A_o}{\tau}\left[t - \frac{2\zeta}{\omega_n} + \frac{1}{\omega_d}e^{-\zeta\omega_n t}\sin(\omega_d t - \theta)\right] \tag{86}$$

and for $t > \tau$,

$$\ddot{q}_n(t) = +\frac{C_n A_o}{\tau\omega_d}\left\{e^{-\zeta\omega_n t}\sin(\omega_d t - \theta) - e^{-\zeta\omega_n t'}\left[\sin(\omega_d t' - \theta) + \omega_n\tau\cos(\omega_d t' - \phi)\right]\right\} \tag{87}$$

50 -

Introducing

$$L_n(t) = -\frac{1}{\tau}\left[t = \frac{2\zeta}{\omega_n} - \frac{1}{\omega_d} e^{-\zeta\omega_n t} \sin(\omega_d t - \theta)\right] \tag{88}$$

$$L_n^*(t) = +\frac{1}{\tau\omega_d}\left\{e^{-\zeta\omega_n t} \sin(\omega_d t - \theta) - e^{-\zeta\omega_n t'}\left[\sin(\omega_d t' - \theta) + \omega_n \tau \cos(\omega_d t' - \phi)\right]\right\} \tag{89}$$

Equations 86 and 87 are simplified as

$$\ddot{q}_n(t) = C_n A_o L_n(t) \quad \text{for } 0 < t \leq \tau \tag{90}$$

$$\ddot{q}_n(t) = C_n A_o L_n^*(t) \quad \text{for} \quad t > \tau \tag{91}$$

Then, the acceleration responses are

$$\ddot{u}(x, t) = A_o \sum_{n=1}^{N} C_n X_n(x) L_n(t), \quad 0 < t \leq \tau \tag{92}$$

$$\ddot{u}(x, t) = A_o \sum_{n=1}^{N} C_n X_n(x) L_n^*(t), \quad t > \tau \tag{93}$$

For numerical evaluation of the acceleration responses, a computer program based on Equations 88 through 93 can be written. To find the maximum response at any location x, it is only necessary to let the computer search for the maximum value among all calculations. Designating the maximum value as $\ddot{u}_{max}$, namely, $\ddot{u}_{max} = \ddot{u}(x, t_{max})$, the shock load factor Q is expressed as

$$Q = \frac{\ddot{u}_{max}}{A_o} = \frac{\text{maximum acceleration response}}{\text{maximum acceleration input}} \tag{94}$$

This dimensionless factor, then, represents shock transmissibility in the system. The computed values of Q can be plotted versus the axial stations by the computer while it calculates the numerical values.

B. Response to Half-Sine Pulse (Figure 7B)

The response at $t > \tau$ is as follows:

$$q_n(t) = \frac{C_n A_o}{\omega_n^2} \left\{ \left[1 - \left(\frac{\omega}{\omega_n}\right)^2 \right]^2 + \left(2\zeta \frac{\omega}{\omega_n}\right)^2 \right\}^{-1/2}$$

$$\left[\sin(\omega t - \beta) - \frac{\omega}{\omega_d} e^{-\zeta \omega_n t} \sin(\omega_d t - \psi) \right.$$

$$\left. + \sin(\omega t' - \beta) - \frac{\omega}{\omega_d} e^{-\zeta \omega_n t'} \sin(\omega_d t' - \psi) \right] \qquad (95)$$

where

$$t' = t - \tau$$

In another form,

$$q_n(t) = \frac{C_n A_o \omega}{\omega_n^2 \omega_d} \left\{ \left[1 - \left(\frac{\omega}{\omega_n}\right)^2 \right]^2 + \left(2\zeta \frac{\omega}{\omega_n}\right)^2 \right\}^{-1/2} \left[e^{-\zeta \omega_n t} \sin(\omega_d t - \psi) + \right.$$

$$\left. e^{-\zeta \omega_n t'} \sin(\omega_d t' - \psi) \right] \qquad (96)$$

and the acceleration responses become

$$\ddot{q}_n(t) = C_n A_o S_n(t) \quad \text{for} \quad 0 \le t \le \tau \qquad (97)$$

$$\ddot{q}_n(t) = C_n A_o S_n^*(t) \quad \text{for} \quad t > \tau \qquad (98)$$

where

$$S_n(t) = \left\{ \left[1 - \left(\frac{\omega}{\omega_n}\right)^2 \right]^2 + \right.$$

$$\left. \left(2\zeta \frac{\omega}{\omega_n}\right)^2 \right\}^{-1/2} \left[\frac{\omega}{\omega_d} e^{-\zeta\omega_n t} \sin(\omega_d t - \psi) - \sin(\omega t - \beta) \right]$$

$$S_n^*(t) = \frac{\omega}{\omega_d} \left\{ \left[1 - \left(\frac{\omega}{\omega_n}\right)^2 \right]^2 + \right.$$

$$\left. \left(2\zeta \frac{\omega}{\omega_n}\right)^2 \right\}^{-1/2} \left[e^{-\zeta\omega_n t} \sin(\omega_d t - \psi) + e^{-\zeta\omega_n t'} \sin(\omega_d t' - \psi) \right]$$

or, for $0 \le t \le \tau$,

$$\ddot{u}(x, t) = A_o \sum_{n=1}^{N} C_n X_n(x) S_n(t)$$

For $t > \tau$,

$$\ddot{u}(x, t) = A_o \sum_{n=1}^{N} C_n X_n(x) S_n^*(t) \tag{99}$$

The shock load factor is given by Equation 94, as in the case of sawtooth impulse.

Response to Arbitrary Pulse

An arbitrary acceleration impulse can be represented by a series of constant acceleration inputs acting one after another as shown in Figure 7C.

The response to the step input for $t > t_i$ is:

$$q_{n_i}(t) = \frac{C_n A_i}{\omega_n^2}\left\{\left[1 - \frac{\omega_n}{\omega_d} e^{-\zeta\omega_n\xi} \cos(\omega_d\xi - \phi)\right] - \left[1 - \frac{\omega_n}{\omega_d} e^{-\zeta\omega_n\xi'} \cos(\omega_d\xi' - \phi)\right]\right\}$$

$$= \frac{C_n A_i}{\omega_n \omega_d}\left[e^{-\zeta\omega_n\xi'} \cos(\omega_d\xi' - \phi) - e^{-\zeta\omega_n\xi'} \cos(\omega_d\xi - \phi)\right] \tag{100}$$

where

$$\xi' = t - t_i$$

The acceleration responses are found as $t_{i-1} \le t \le t_i$,

$$\ddot{q}_{n_i}(t) = C_n A_i P(t) \tag{101}$$

where

$$P(t) = \frac{\omega_n}{\omega_d} e^{-\zeta\omega_n\xi} \cos(\omega_d\xi - \phi) - 1$$

For $t > t_i$,

$$\ddot{q}_{n_i}(t) = C_n A_i P^*(t) \tag{102}$$

where

$$p^*(t) = \frac{\omega_n}{\omega_d}\left[e^{-\zeta\omega_n\xi} \cos(\omega_d\xi - \phi) - e^{-\zeta\omega_n\xi'} \cos(\omega_d\xi' - \phi)\right]$$

The structural acceleration responses to the ith step input are then determined

$$\ddot{u}_i(x, t) = A_i \sum_{n=1}^{N} C_n X_n(x) P(t), \quad t_{i-1} \le t \le t_i \qquad (103)$$

$$\ddot{u}_i(x, t) = A_i \sum_{n}^{N} C_n X_n(x) P^*(t), \qquad t > t_i \qquad (104)$$

Equations 101 through 104 are the basic equations for the determination of shock responses to the ith step input. The calculation starts with the first step input, A_1, to find the responses, $\ddot{u}_1$, for all the time concerned. They then go on to find the responses $\ddot{u}_2$, $\ddot{u}_3$ ... $\ddot{u}_R$ corresponding to the second, third, ... and R^{th} step inputs, respectively. The response to the complete pulse is equal to the summation of all $\ddot{u}_i$'s, namely,

$$\ddot{u}(x, t) = \sum_{i=1}^{R} \ddot{u}_i(x, t) \qquad (105)$$

The shock load factor Q for any station is then determined in the same manner as in the case of sawtooth or half-sine pulse.

Based on this discussion, a computer program can be written for the calculation of acceleration responses to an arbitrary pulse.

If the system has an initial displacement, q_0, and an initial velocity, $\dot{q}_0$, the total displacement response will be the summation of both. Thus,

$$q_{n_i}(t) = e^{-\zeta\omega_n\xi_i} \left[q_{n_{i-1}} \cos\omega_d\xi_i + \frac{1}{\omega_d} \left(\dot{q}_{n_{i-1}} + \zeta\omega_n q_{n_{i-1}} \right) \sin\omega_d\xi_i \right]$$

$$+ \frac{C_n A_i}{\omega_n^2} \left[1 - \frac{\omega_n}{\omega_d} e^{-\zeta\omega_n\xi_i} \cos(\omega_d\xi_i - \phi) \right] \qquad (106)$$

where

$$\xi_i = t_i - t_{i-1} = \text{time interval for the } i^{th} \text{ step input}$$

By differentiation,

$$\dot{q}_{n_i}(t) = e^{-\zeta \omega_n \xi_i} \left\{ \dot{q}_{n_{i-1}} \cos \omega_d \xi_i - \frac{1}{\omega_d} \left[\omega_n^2 q_{n_{i-1}} + \zeta \omega_n \dot{q}_{n_{i-1}} \right] \sin \omega_d \xi_i \right.$$

$$\left. + \frac{C_n A_i}{\omega_n} \left[\sin(\omega_d t - \phi) + \frac{\zeta \omega_n}{\omega_d} \cos(\omega_d \xi_i - \phi) \right] \right\} \qquad (107)$$

$$\ddot{q}_{n_i}(t) = e^{-\zeta \omega_n \xi_i} \left\{ \frac{\omega_n^2}{\omega_d} \left[\left[\zeta \omega_n q_{n_{i-1}} + (2\zeta^2 - 1)\dot{q}_{n_{i-1}} \right] \sin \omega_d \xi_i \right. \right.$$

$$\left. - \omega_d \left(q_{n_{i-1}} + \frac{2\zeta}{\omega_n} \dot{q}_{n_{i-1}} \right) \cos \omega_d \xi_i \right]$$

$$\left. - C_n A_i \left[K \cos(\omega_d \xi_i - \phi) - 2\zeta \sin(\omega_d \xi_i - \phi) \right] \right\} \qquad (108)$$

where

$$K = \frac{1 - 2\zeta^2}{(1 - \zeta^2)^{1/2}}$$

Starting with q_0 and $\dot{q}_0$ as known initial conditions and using Equations 106, 107 and 108, the responses q_{n_1}, $\dot{q}_{n_1}$ and $\ddot{q}_{n_1}$ at the end of the first time-interval, ξ_1, are found. Then, using these values as new initial conditions, the responses q_{n_2}, $\dot{q}_{n_2}$ and $\ddot{q}_{n_2}$ to the second step input at the end of the second interval ξ_2 are determined. The responses to the other step inputs can be calculated in the same way by setting $i = 1, 2, 3 \cdots R$ in the three equations above. The procedure above applies only to the responses within the shock duration.

For $t > \tau$, the responses are obtained by superposition of responses to the last step input, A_R, at $t = t_{R-1}$, and those to a negative step input, $-A_R$, at $t = \tau$. The result has been given by Equation 102 for the case of zero initial conditions. The complete solution for a general case at $t > \tau$ is

$$q_n(t) = e^{-\zeta \omega_n \bar{t}} \left[q_{n_{R-1}} \cos \omega_d \bar{t} + \frac{1}{\omega_d} \left(\dot{q}_{n_{R-1}} + \zeta \omega_n q_{n_{R-1}} \right) \sin \omega_d \bar{t} \right]$$

$$+ \frac{C_n A_R}{\omega_n \omega_d} \left[e^{-\zeta \omega_n t} \cos(\omega_d t - \phi) - e^{-\zeta \omega_n \bar{t}} \cos(\omega_d \bar{t} - \phi) \right] \qquad (109)$$

where

$$\bar{t} \qquad = t - t_{R-1}$$

$$t' \qquad = t - t_R$$

$$t \qquad = \text{actual time from start}$$

$q_{n_{R-1}}$

$\dot{q}_{n_{R-1}}$

quantities obtained previously by Equations 106 and 107 at $t = t_{R-1}$.

Differentiating Equation 109 twice, the acceleration at $t > \tau$ is

$$\ddot{q}_n(t) = \frac{\omega_n^2}{\omega_d} e^{-\zeta \omega_n \bar{t}} \left\{ \left[\zeta \omega_n q_{n_{R-1}} + (2\zeta^2 - 1) \dot{q}_{n_{R-1}} \right] \sin \omega_d \bar{t} - \omega_d \left(q_{n_{R-1}} + \frac{\zeta}{\omega_n} \dot{q}_{n_{R-1}} \right) \cos \omega_d \bar{t} \right\}$$

$$+ C_n A_R \left\{ e^{-\zeta \omega_n \bar{t}} \left[K \cos(\omega_d \bar{t} - \phi) - 2\zeta \sin(\omega_d \bar{t} - \phi) \right] \right.$$

$$\left. - e^{-\zeta \omega_n t'} \left[K \cos(\omega_d t' - \phi) - 2 \sin(\omega_d t' - \phi) \right] \right\} \qquad (110)$$

The structural acceleration response, therefore, can be computed from the above equation.

N70-31065

EXPERIMENTAL INVESTIGATION

DESIGN AND FABRICATION

A specimen was designed and fabricated for the experimental investigation: an aluminum cylindrical shell of 18-inch OD, 0.050-inch thickness, and 72-inch length with a 1/4-inch-thick flange welded to the upper end and a 1/2-inch-thick flange welded to the lower end. This is one of the three shell models previously fabricated for the Axial Transmissibility contract, NAS8-18124.

A total of eighteen aluminum or steel blocks of various sizes (nine new) were also fabricated; their properties are given in Tables 4 and 5. By mounting one or more of these solid blocks on the ring or shell, the mass-loaded test specimens were obtained.

Table 4. Properties of Attached Masses, Model Shells I, II and III

Mass No.	Material	Thickness (Inches)	Weight (Grams)	Length of 1/4-Inch Bolt (Inches)	Weight of 4 Bolts (Grams)
K	Alum.	1/4	64.5	--	--
J	Alum.	3/8	94	--	--
b_1	Alum.	1/2	127	--	--
b_2	Alum.	1/2	127	--	--
H_1	Steel	1/4	181	1/2	19
G_1	Steel	3/8	280	3/4	25
G_2	Steel	3/8	283	3/4	25
F_1	Steel	1/2	365	3/4	25
E_2	Steel	5/8	480	1	29
C_1	Steel	1	740	1-1/2	40.5
B_2	Steel	1-1/4	890	1-1/2	40.5
A_1	Steel	1-1/2	1110	2	63
A_2	Steel	1-1/2	1110	2	63

Note: All masses are rectangular blocks 2 inches wide and 3 inches long.

Table 5. Properties of Attached Masses, Model Shell IV

M_2 Mass No.	Mass Ratio M_2/M_1	M_2 Thickness (Inches)	M_2 Weight (Grams)	M_2 Weight (Pounds)
1	0.		2	0.004
2	0.025	0.034	10	0.022
3	0.05	0.074	20	0.044
4	0.075	0.11	30	0.066
5	0.10	0.15	40	0.089
7	0.32	0.50	127	0.280
8 (B)	0.60	0.875	240	0.530
9 (BH)	0.82	0.75	327	0.722
10 (BD)	1.7	1.25	677	1.495

Note: All masses are rectangular blocks 2 inches wide and 3 inches long. M_1 = 400 grams = weight of a 3-inch shell section = 0.883 pounds.

RADIAL VIBRATION TEST SET-UP

Since a considerable amount of information is available from the previous program, a vibration test utilizing constant force excitation was performed to supplement the available test data. The test was conducted in a similar way as in the previous program on mass-loaded shells (Reference 1).

An electro-induction shaker was used to provide constant and concentrated force excitation. The general arrangement of the vibration test of the shell is shown in Figure 8. The shell was placed upright on a rigid floor with its lower flange fastened by bolts. The electro-induction shaker was set up at a Level F, 54 inches above the lower end. The proximity gauge set-up used in the ring test was suspended above the cylinder with the gauge extended downward inside the shell to survey the mode shape as shown in Figure 9. Miniature accelerometers were used to measure the acceleration responses and evaluate the proximity measurements. A proximity gauge was used to map the shell m-n mode shapes continuously defining the effective forcing area, shell imperfection shape and displacement responses revolving around the circumferential levels and along the longitudinal lines automatically (Figure 10).
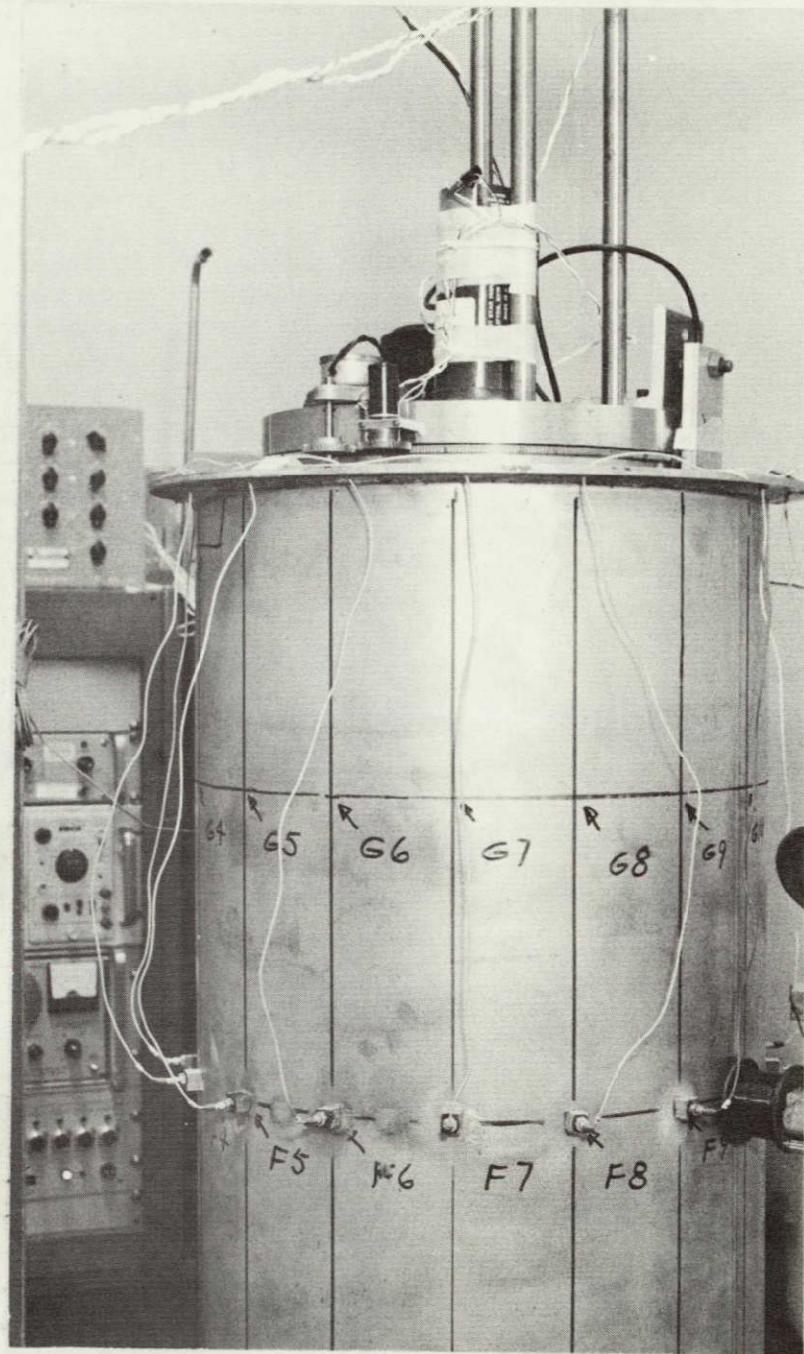
Figure 8.   Radial Vibration Test Set-Up

SD 69-766
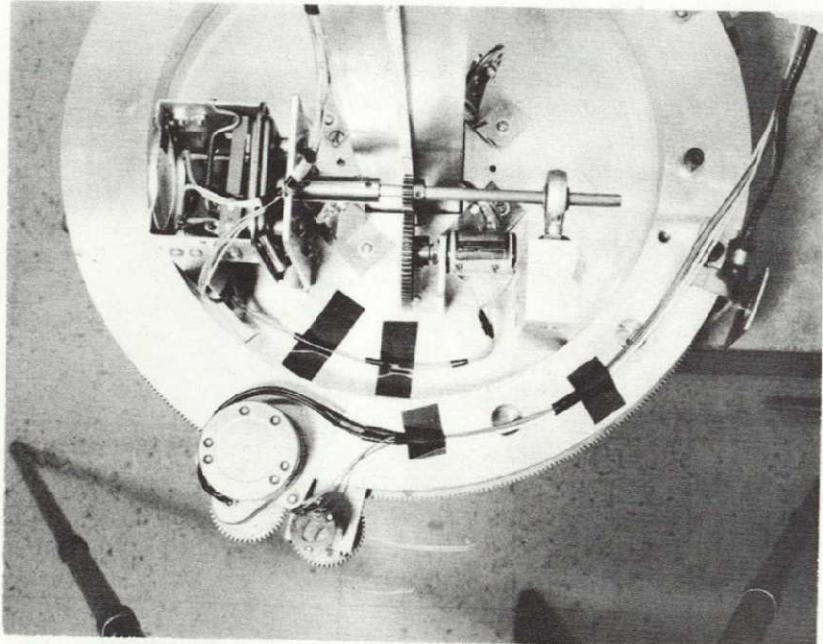
Figure 9. Proximity Gauge Set-Up for Plotting Radial-Mode Shapes of Shell

Other test equipment used in both ring and shell test included the following:

1. Driving amplifier

2. Band spread oscillator

3. Electronic counter

4. Dual beam oscilloscope

5. Voltmeter

6. 100-channel switch box

7. Visicorder

8. X-Y plotter

Some of the equipment listed are shown in Figure 11 and 12.

RADIAL VIBRATION TEST OF MODELS I, II AND III

Three sets of vibration tests using the electro-induction shaker were performed for the mass-loaded and unloaded shell Models I, II, and III. The first set of tests was for cases having only one accelerometer on the shell at the mass location F2 (Figure 10). The shell was called Shell I in these cases. The second set of tests was for the cases with 20 accelerometers on the shell, 16 of which were equally spaced on the shell circumference at level F and 4 were placed in the same column, 2, as the mass but at different levels (C, D, E and G) as shown in Figure 10. In these cases, the test specimen was called Shell II. The third set was for the cases with 15 accelerometers attached to the shell in a single column, 2 and equally spaced at 15 levels, plus 5 accelerometers at 5 levels in Column 14, 90 degrees apart from Column 2. In these cases the test model was called Shell III. All test runs for Model Shells I, II and III are listed in Table 6. All the discrete masses had concave contours on one side to match the outer shell surface. They were all cemented to the shell at location F-2. One exception is that the mass b_2 was cemented on the inner surface of the shell at the mass location to reduce rocking motion of the heavy masses which were cemented and bolted outside the cylinder. In Table 6, the test run numbers are also identified by mass ratios M_2/M_1. The quantity M_1 is defined as the mass of the unloaded shell section whose length is the same as the attached mass, 3 inches in the present cases. This shell section

- 63 -

RADIAL ACCELEROMETERS
MODELS I, II, III (16)

4 (F4)

3

22-1/2° TYP

RADIAL
EXCITATION
FORCE

10 (F10)

2

1

ATTACHED MASS

RADIAL
EXCITATION
FORCE

(F2)

9 IN.

17 — G

MASS

9 IN. TYP

F

18 — E

19 — D

FOR MODEL IV

1. F2 OR 2F
2. F4 OR 2D
3. F10 OR 2B

20 — C

ADDITIONAL
ACCELEROMETERS
MODELS I, II, III (4)

(B2) — B

A
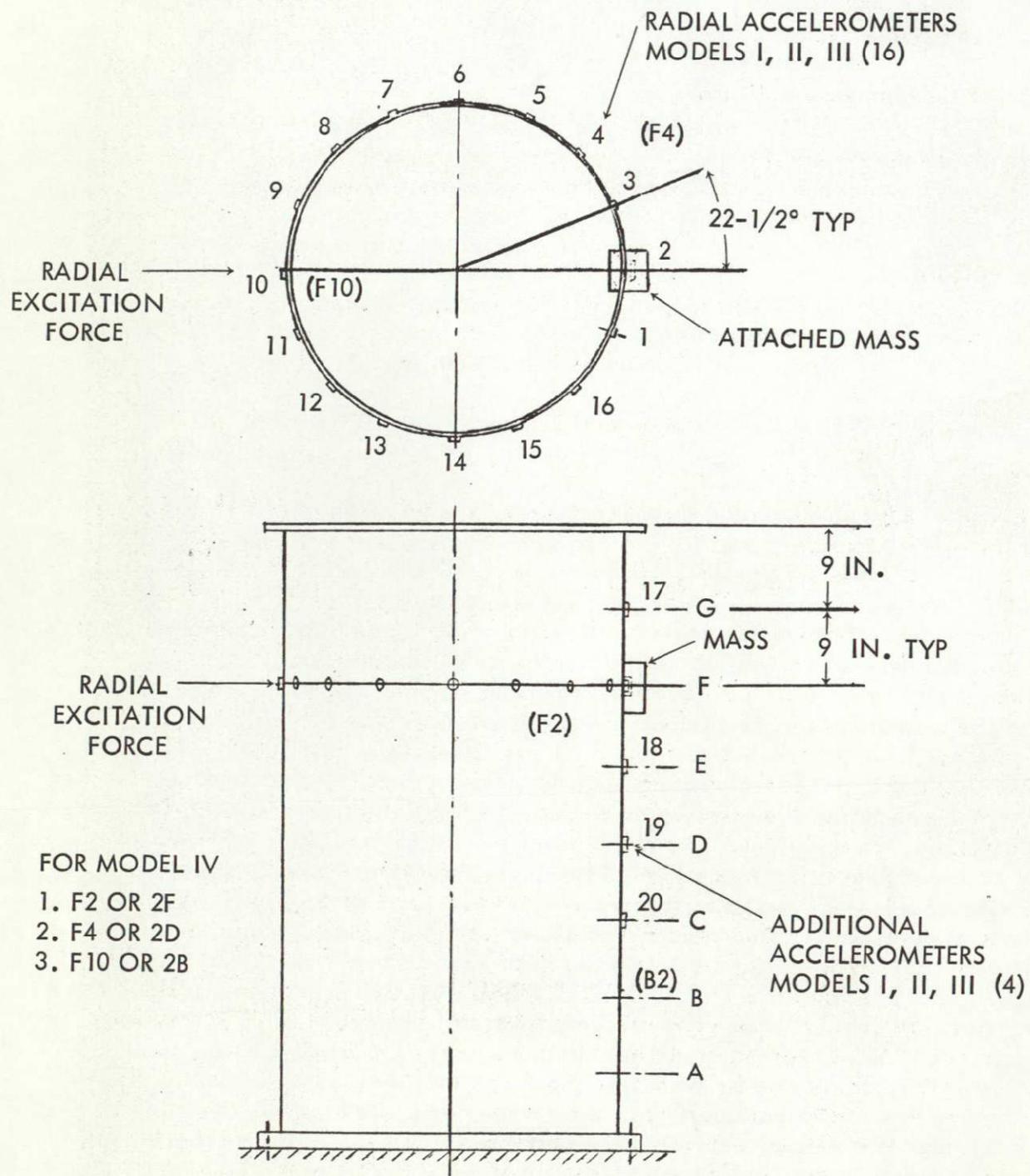
Figure 10. Accelerometers Set-Up for Vibration Test of
Mass-Loaded Shell
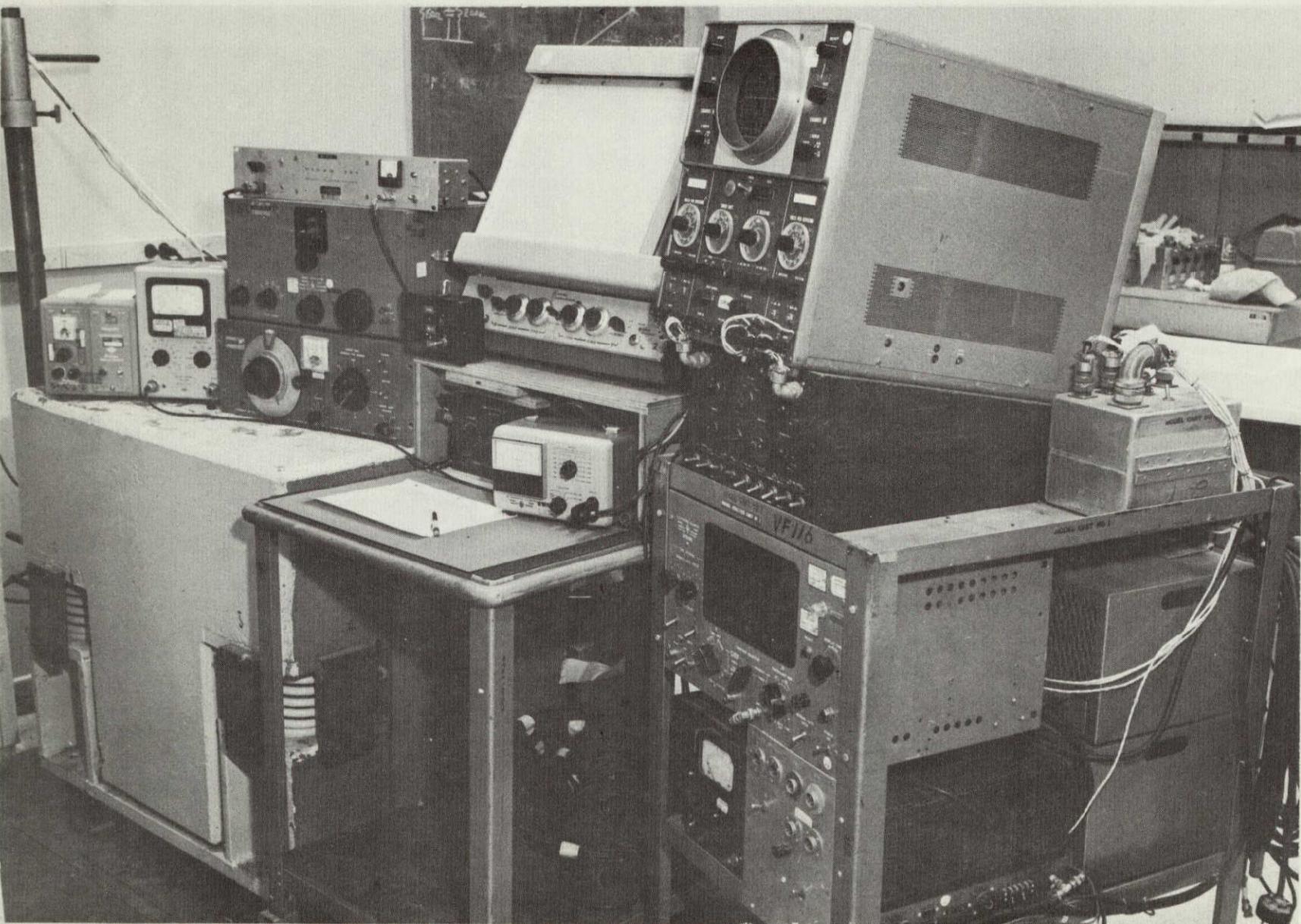
Figure 11. Instrumentation Set-Up for Vibration Tests of Shell, Part I
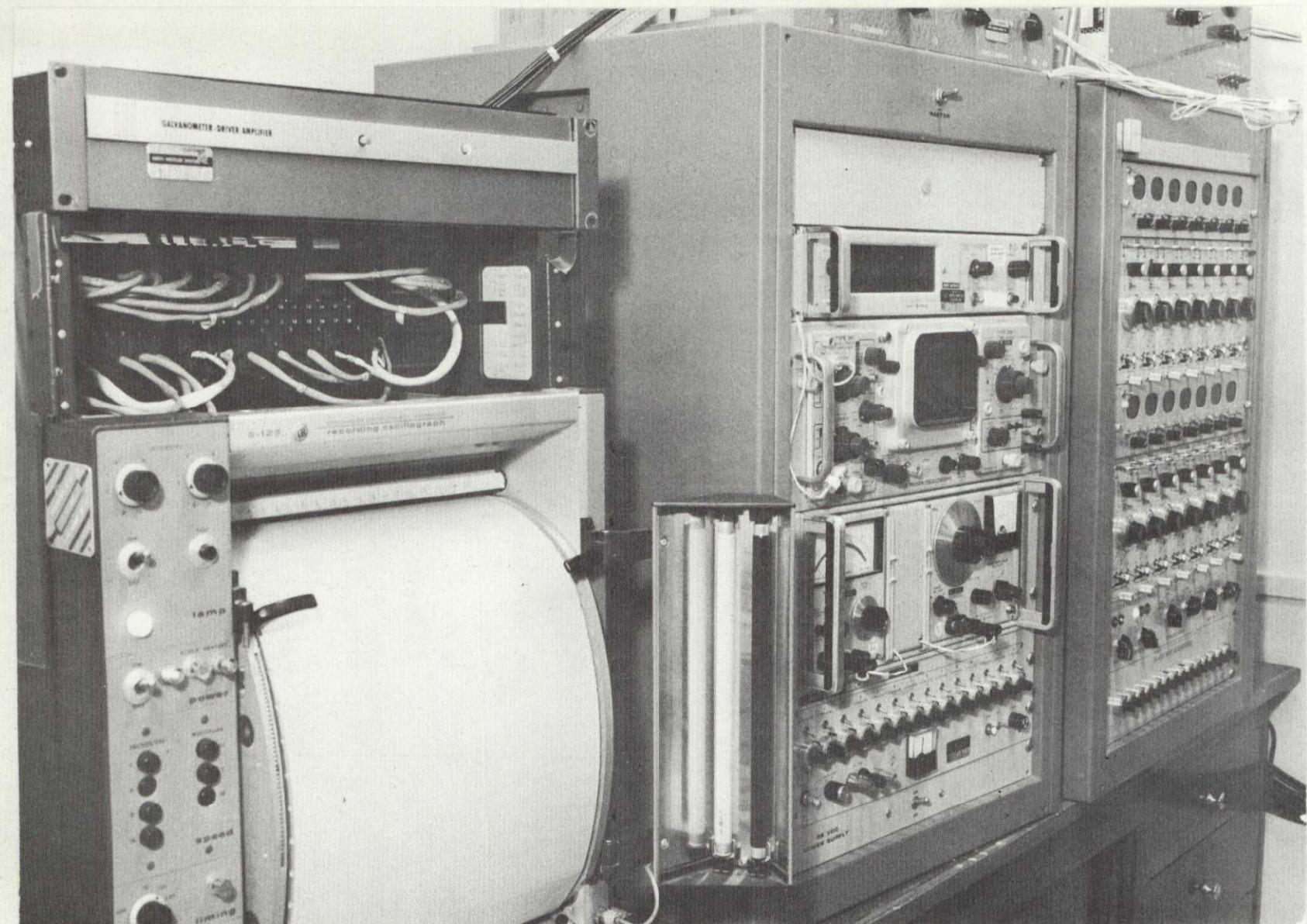
Figure 12. Instrumentation Set-Up for Vibration Tests of Shell, Part II

Table 6. Vibration Test Runs for Unloaded and Mass-Loaded Shell.
Models I, II, and III Excited by Electroinduction Shaker

Run Number	Mass Number	Weight of Mass (Grams)	Weight of 4 Bolts (Grams)	Total Weight M_2 (Grams)	Mass Ratio M_2/M_1
0, 0-2, 0-3	0	0	0	0	0
1a-2	K	64.5	0	64.5	0.16
1, 1-2, 1-3	b_1	127	0	127	0.32
1.2-2	$b_1 + J$	221	19	240	0.60
2-2	$b_1 + H_1$	308	19	327	0.82
3, 3-2, 3-3	$b_1 + b_2$	245	0	245	0.61
4, 4-2, 4-3	$b_1 + b_2 + G_1$	525	25	550	1.40
5, 5-2, 5-3	$b_1 + b_2 + H_1 + G_2$	709	44	753	1.90
7, 7-2, 7-3	$b_1 + b_2 + E_2 + F_1$	1090	54	1144	2.86
8, 8-2, 8-3	$b_1 + b_2 + C_1 + E_2$	1465	69.5	1534.5	3.84
9, 9-2, 9-3	$b_1 + b_2 + B_2 + C_1$	1875	81	1956	4.9

Notes:
1. Runs 0, 1, 3, 4, 5, 7, 8, and 9 are the cases with 16 accelerometers around the shell at the same Level F. Run numbers with -2 are the cases with only one accelerometer at the mass location. Run numbers with -3 are the cases with 15 accelerometers in one Column No. 2 along the shell.
2. All solid masses except b_2 are mounted on the outer surface of the shell.
3. $M_1 = 400$ gm = weight of unloaded shell section of 3 inches long.

Space Division
North American Rockwell

under the attached mass was then identical to the ring test model. Therefore M_1 is taken to be 400 gm or 0.883 lb. The test operations for the unloaded and mass-loaded Shells I and II were as follows:

1. Unloaded Shell

   a. Performed a resonance survey using a sinusoidal sweep at one minute per octave from 5 to 3800 cps. Maintained a constant voltage of 6 volts input to the shaker for all test runs. Repeated the sweep from 5 to 760 cps for detailed and resonance dwell check only.

   b. Obtained X-Y plots for the accelerometer output at the mass location during the above sweeps to determine the natural frequencies and maximum responses.

   c. At the first five natural frequencies obtained the following data:

   > Mode shape plots from the proximity gauge.
   > Oscillograph records for all accelerometer responses.
   > Meter readings for all accelerometer outputs.

2. Mass-Loaded Shell

   a. Mounted the solid mass (or masses) on the shell according to the test runs plan.

   b. Performed sinusoidal test as in Steps A-1 to A-3.

On Shell III the radial accelerometers were placed in two columns to measure lateral bending modes. Only oscillographs and meter readings were taken during each resonance. No X-Y plots were made.

RADIAL VIBRATION TEST OF MODEL IV

Objective

The test objective was to investigate the mass loading effect phenomena of very small masses on the radial vibration transmissibility characteristics of shell structure. Emphasis is placed on mass attenuation and amplification, continuous mapping of the shell m-n modes, effective forcing areas (mapping around the discrete mass), shell imperfection shapes (statics) and resonance disappearance.

Specimens

The unloaded shell consisted of an aluminum cylindrical shell 0. 05 inch thick, 18 inches outer diameter by 72 inches long. The mass-loaded shell consisted of the unloaded shell plus eight solid masses with a mass ratio (M_2/M_1) less than 0. 8 as compared to a ratio of 5 for Models I, II, and III. Table 5 lists the properties of these small masses.

The electro-induction shaker was placed at location F10, 54 inches above the lower end. The gap between the shell and the shaker remained constant for all test runs.

The automatic proximity gauge was used for continuous mapping of mode shape and the effective forcing area. The setup enabled the proximity gauge to travel either around the circumference or up and down the cylinder with a controlled speed.

Two sets of three miniature accelerometers were cemented on the outer surface of the shell as shown in Figure 10.

Test Operation

Sine Sweep

A sine sweep test was performed on both the mass-loaded and unloaded shells. For test run 1, on the unloaded shell, a resonance survey was performed using a sinusoidal sweep at one minute per octave from 5 to 3000 cps. A constant voltage of 0. 06 volts input to the shaker was maintained for all test runs. X-Y plots (acceleration-response versus frequency) were obtained for the accelerometer output at the mass location during the sine sweep to determine the natural frequencies and maximum responses.

For test runs 2 through 9 on mass-loaded shells, the solid mass (or masses) was mounted on the shell at location F2 according to Table 5. Sinusoidal sweep were performed for each case as for the unloaded shell. Wherever possible, the same scale was used on all X-Y plots. All X-Y plots were compared to determine the first 16 significant frequencies and maximum responses; and some resonance dwelling was performed for evaluation of further amplification.

Proximity Gauge Calibration

Before plotting the mode shapes of the shell, the proximity gauge output was calibrated for linear evaluation.

Mode Shape Plots

Mode shapes (m and n modes) were plotted for each test run at 16 selected frequencies. The procedure was as follows:

1. Starting from test run 1, time the shell to the first resonance with a constant force excitation (input voltage = 0.06 volt).

2. Use proximity gauge to plot m and n mode shapes through the mass location F2. Also, obtain meter readings for accelerometers 1 and 2.

3. Tune to the next frequency and repeat step 2.

4. Continue the plot for all other frequencies.

5. Repeat steps 1 through 4 for the mass-loaded cases, test runs 2 through 9.

DATA ANALYSIS

The following sets of data were assembled for further analysis:

1. X-Y plots - acceleration response of accelerometer 1 versus frequency from 5 to 3000 cps, one plot per each run.

2. Proximity calibration.

3. Mode-shape plots - one m mode and one n mode for each frequency.

4. Shell imperfection plot - Static plot of the gap variation between the shell and proximity gage, one for m mode, one for n mode.

5. Meter readings obtained at 16 frequencies per each test run for evaluation.

LONGITUDINAL SHOCK TEST OF UNLOADED SHELL

Shock tests on the unloaded shell model were performed on an electro-mechanical shaker which could produce the required shock pulses of various forms and with extremely short duration. Ordinary shock test machines were found inadequate for the generation of short duration pulses. It is also convenient and economic to perform both shock and vibration test on the same setup.

The test setup is shown in Figure 13. Twelve screws of 1/4-inch diameter were used to fasten the bottom flange of the model to the armature of the shaker. The instrumentations for measuring responses are shown in Figure 14. Miniature accelerometers and strain gauges were attached to the shells to measure axial and radial responses. The number of pickups for each model are listed in Table 7.

Table 7. Number of Pickups on Test Models

Model Number	1	2	3
Axial accelerometers	5	4	11
Radial accelerometers	7	0	0
Axial strain gauges	3	3	8
Total pickups	15	7	19

The following test equipment was used:

Ling 246, power amplifier and shaker
6 Endevco accelerometers, Type 2227
1 Endevco accelerometer, Type 2217
6 Endevco accelerometers, Type 101
5 Endevco dynamonitor amplifiers 2702 (13 channels)
2 CEC carrier amplifiers 1-127 (8 channels)
8 Budd Instrumentation strain gauges C9-141 -
120-ohm
1 CEC 1-inch tape recorder
1 Ampex 1-inch tape recorder
1 K/H band-pass filter
1 H/P scope
1 Exact signal generator
1 CEC scope camera

Test equipment is shown in Figure 15.

After a complete calibration of all accelerometers and strain gauges, test operation began with several trial runs to see if valid input and output data could be obtained. Shock pulses were shaped to the desired forms, half-sine or sawtooth wave. Figure 11 shows two typical input shock pulses as seen on the oscilloscope.

- 71 -
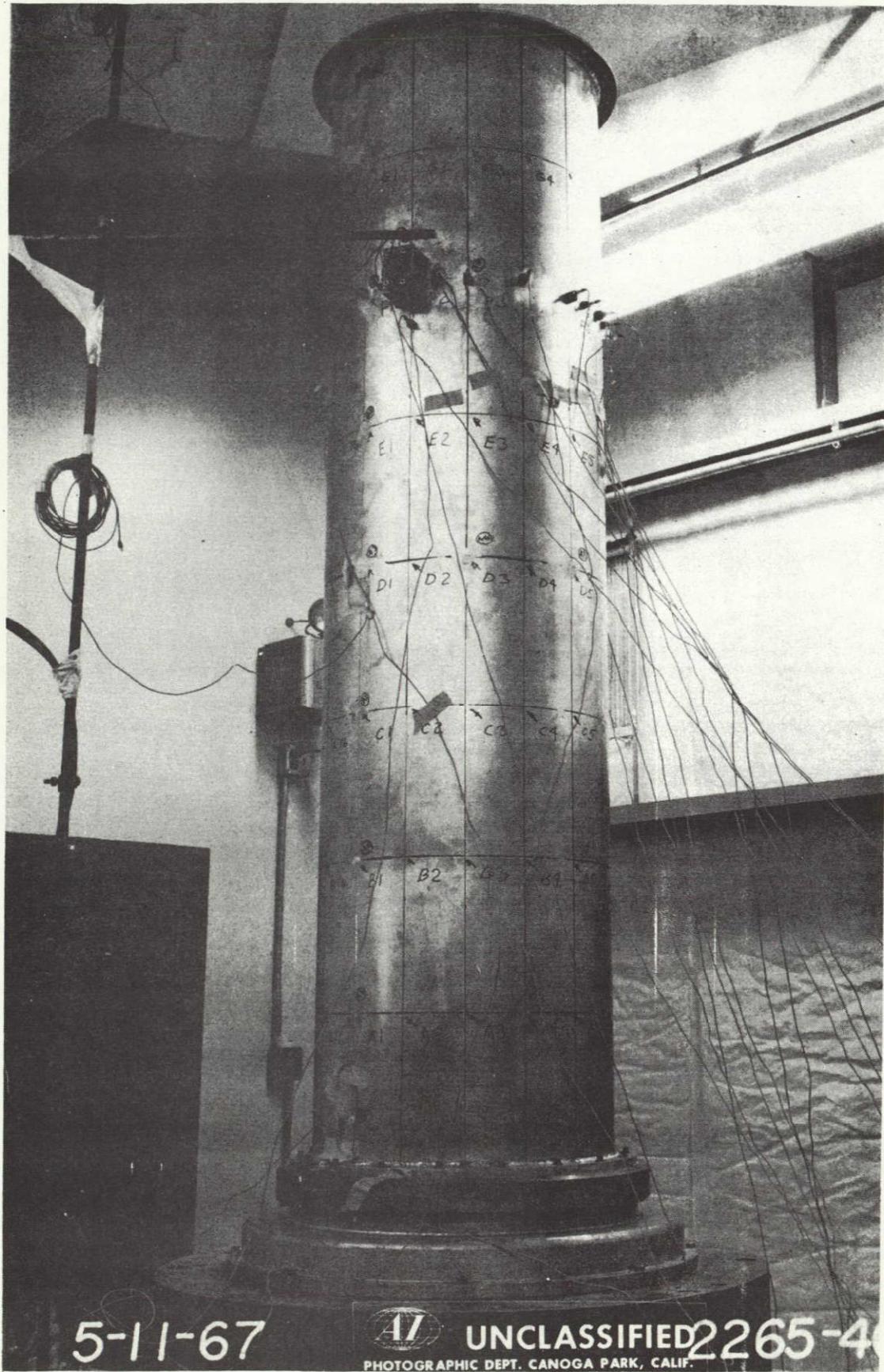
Figure 13.   Test Set-Up for Longitudinal Vibration and
Shock Tests

- 72 -

MASS-LOADED CASES

LOCATION	DIRECTIONS		INSTRUMENTATIONS
A-2	U		ACCELEROM
B-2	U W		ACCELEROM
D-2	UVW		ACCELEROM
F-2	UVW		ACCELEROM
G-2	U		ACCELEROM
4-F	VW		ACCELEROM
6-F	W		ACCELEROM
10-F	UVW		ACCELEROM
14-F	VW		ACCELEROM
D-2	U	(ALREADY ON)	STRAIN GAUGE
O-2	UV	(ALREADY ON)	STRAIN GAUGE
T-2	U	(ALREADY ON)	STRAIN GAUGE
P	2^+_-, 10^+_-, F^L_R, D^L_R		AUTOMATIC PROXIMITY G_1
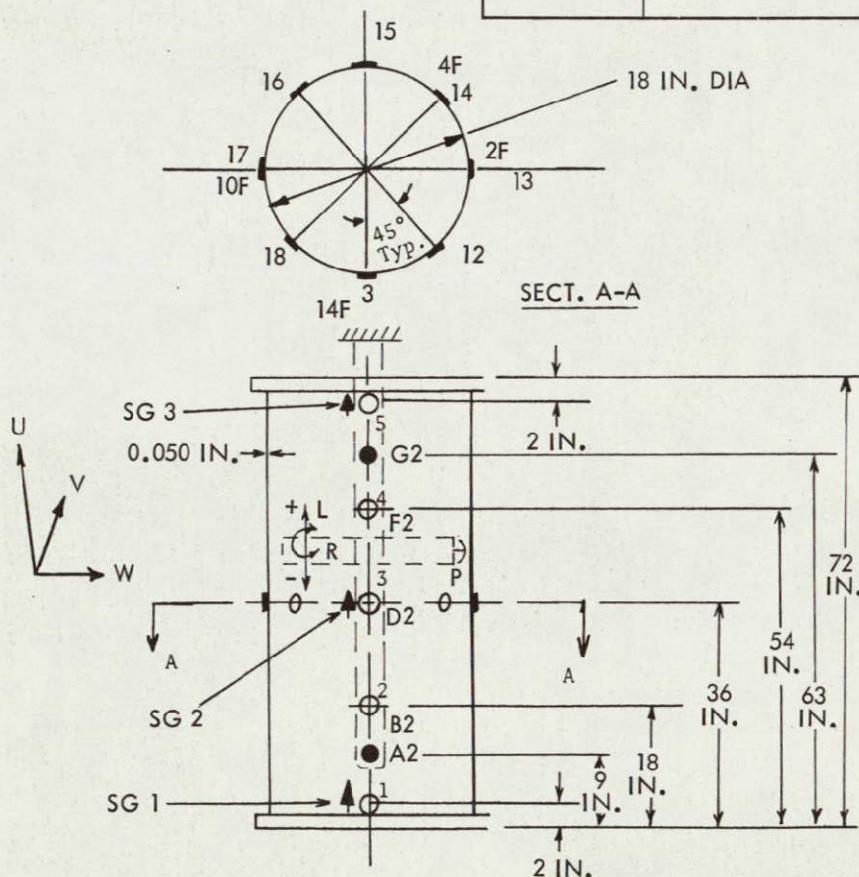
Note: O ── ACCELEROMETER FOR UNLOADED CASES

▲ ── STRAIN GAUGE FOR UNLOADED CASES

Figure 14. Instrumentation for Longitudinal Vibration and Shock Tests
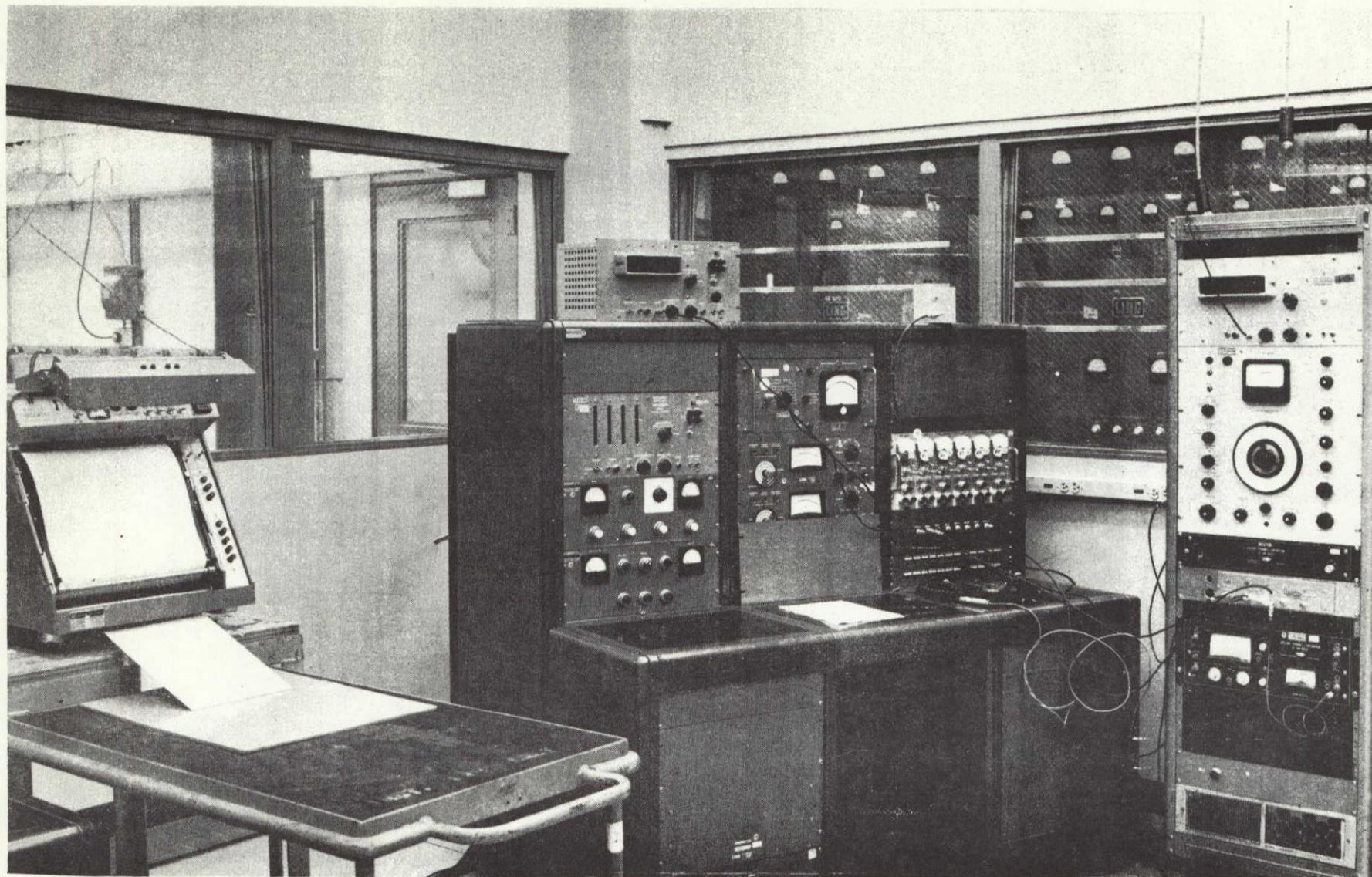
Figure 15.   Equipment for Longitudinal Vibration and Shock Tests

The test procedure was as follows:

1. Applied shock pulse to the specimen (Table 8).

2. Recorded the input pulse and all output responses on two magnetic tapes

3. Obtained oscillographs of the input and a part of the output signals for a "quick-look" survey. If the data were not satisfactory, the test was rerun.

Table 8. Shock Test Specification

Test Run Number	Model Number	Shock Form*	Shock Duration Milliseconds	Acceleration Level g's
1	1	H	0.8	20
2	1	H	1.2	20
2R	1	H	1.2	20
2A	1	H	2.0	20
3	2	H	1.5	20
4	2	H	1.0	20
5	3	H	1.2	20
5A	3	H	3.0	20
5B	3	H	5.0	20
6	3	H	6.0	20
7	3	S	5.0	-20
8	3	S	1.0	20

*S = terminal sawtooth; H = half-sine-wave

DATA REDUCTION

Upon completion of all tests, data were reduced from the tape. The required plots are as follows:

Sanborn Plots

Table 9 shows the number of Sanborn plots (response versus time) needed for each test.

Table 9. Sanborn Plots Requirement

Test Number	Model Number	Total Number of Channels	Number of Tests	Number of Plots	Remarks
1, 2	1	15	2	30	
3, 4	2	7	2	14	
5, 6	3	19	2	38	
7, 8	3	12	2	24	Axial pickups only
Total				106	

Spectral Plots

Only accelerometer measurements were needed. The number of spectral plots (acceleration response versus frequency) needed for three test runs are given in Table 10.

Table 10. Spectral-Density Plots Requirement

Test Run Number	Model Number	Number of Accelerometers	Number of Plots	Remarks
1	1	3	3	
4	2	3	3	
5	3	10	10	10 axial accelerometers only
Total		16	16	

Damping Plots

The required number of damping plots (amplitude versus time) are given in Table 11.

Table 11. Damping Plots Requirement

Test Number	Model Number	Number of Accelerometers	Number of Modes	Number of Plots
1	1	12	2	24
4	2	4	2	8
5	3	11	2	22
Total				54

LONGITUDINAL VIBRATION AND SHOCK TEST OF MASS-LOADED SHELL

Objective

The objective of this test was to determine radial and axial responses of a mass-loaded and unloaded shell subjected to an axial shock load.

Specimen and Test Runs

The unloaded shell specimen consisted of an aluminum cylindrical shell of 0.05 inch thick by 18 inch outside diameter. For the mass-loaded shell specimen, five different solid masses were attached, one at a time, to the outer surface of the unloaded shell. Test runs and mass descriptions are given in Table 12. For each test run, shock loads of half-sine wave with a duration of about one millisecond were input to the specimen.

Table 12. Test Runs and Mass Descriptions

Mass Description	Run Number					
	1	2	3	4	5	6
Mass no.		3	5	b_1	$b_1 + H_1$	$b_1 + D_1$
M_2 (gm)	0	20	40	127	327	677
M_2/M_1	0	0.05	0.10	0.32	0.82	1.7
Shock form	H	H	H	H	H	H

Notes:

   M_1 = 400 grams = weight of unloaded shell section three inches long

   M_2 = weight of solid mass.

   H = half-sine shock form.

- 77 -

Test Set-Up

The bottom flange of the shell was fastened to the shaker by 12 screws of 1/4-inch diameter as shown in Figure 13. Eighteen miniature accelerometers and four strain gauges were attached to the outer surface of the shell around the cylinder at different levels, different angular locations, and different directions. The automatic proximity-gauge mechanism was used for measuring the displacement response and mode shape for the modal survey studies. Other important equipment included the following:

Tape recorder	Frequency counter
Visicorder	Scope camera
Signal generator	Voltmeter
Oscilloscope	Dual X-Y plotter

Test Operation

The sequence of the test operation was as follows:

1. In accordance with the sequence of test runs given in Table 12, the shock pulse was generated with proper shape and duration. The maximum amplitude of the pulse was 20 g's.

2. Shock pulse was applied to the specimen.

3. View-o-graphs (apply no filter) of the input and output signals were obtained for a "quick-look" survey.

4. If the View-o-graph data were satisfactory, Step 2 was repeated and all input and output data were recorded on magnetic tape.

5. No automatic proximity-gauge device or X-Y plotter operation was required for the shock tests. They were required only for the survey test.

Resonance and Modal Survey

A longitudinal vibration sweep test was performed to survey resonant frequencies and mode shapes prior to each shock test. Vibratory input of 1 or 1/2 g was applied longitudinally through a frequency range from 5 to 2000 cps at a sweep rate of 2 minutes per octave. The sweep outputs were emphasized on 2-F and 4-F locations only; the outputs, peak accelerations versus frequencies, were recorded on the dual X-Y plotter.

Other outputs of accelerometers and strain gauges were recorded on magnetic tape. No View-o-graph operation was required.

At the major resonances below 2000 cps, the mode shapes were surveyed by turn on the automatic mapping device plotting the mode shapes on the X-Y plotter (displacement versus station) on AC output. Before the survey, the shell imperfection was plotted by DC output. All accelerometers and strain gauges were recorded on View-o-graph for a very short duration at each resonance.

SD 69-766
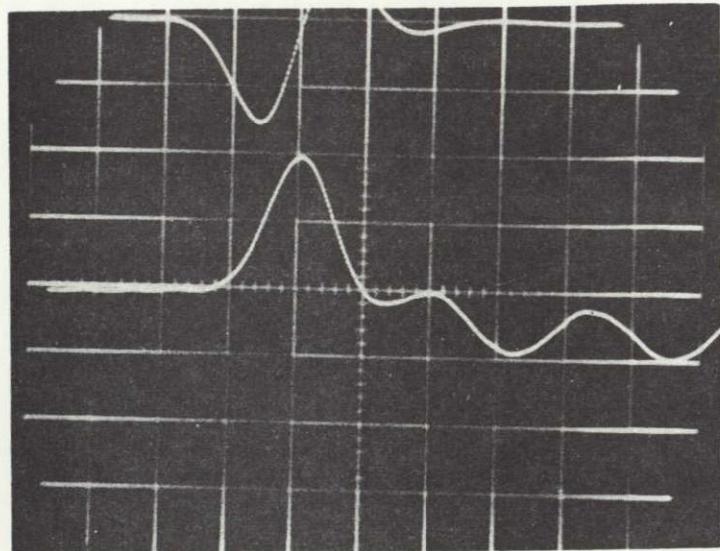
HALF-SINE PULSE
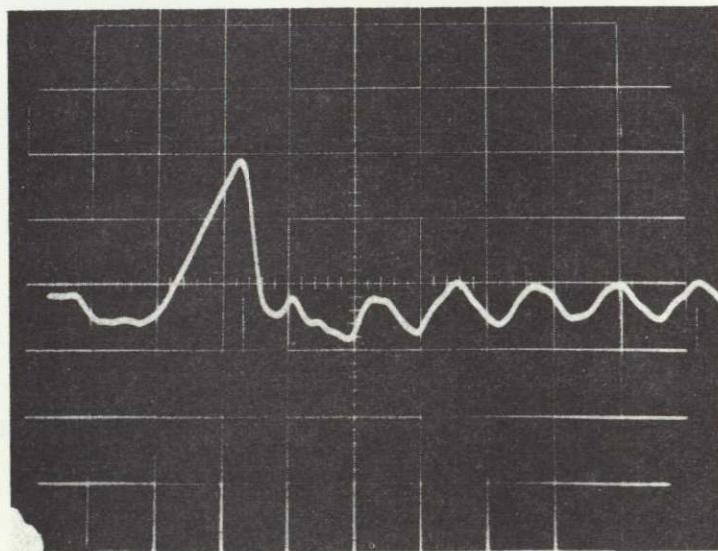
SAWTOOTH PULSE

Figure 16.   Typical Shock Pulses

N70-31066

COMPARISON AND CORRELATION OF
EXPERIMENTAL RESULTS

In accordance with the specific program requirements, the subject study emphasized an empirical evaluation and comparison of the following four types of test data:

1. Modal characteristics of mass-loaded and unloaded shells and the variation of mode shapes and effective forcing area due to the incremental addition of mass-loads.

2. Radial response and effective forcing area associated with each of the first 16 modes excited by radial force input.

3. Mass-loading effects on radial response and attenuation characteristics for mass ratios less than 0.1 (very small masses).

4. Correlation of longitudinally excited shock responses to mass-loading effects or vibration of mass-loaded shells under radial excitations.

In these specific areas, all test data were analyzed, tabulated and/or graphically presented in Appendixes under individual headings. In addition to these program requirements, the following items are added:

1. Comparison of theoretical and experimental solutions

2. Longitudinal vibration test/axial shock and radial excitations

3. Investigation of shell imperfections

4. Extension of 16 mode study to cover 23 modes

5. Increase in the number of mass-loaded cases to include studies beyond a mass ratio of 0.1.

6. Effects of the number of m-n waves on theoretical results.

7. Presentation of series expansion technique and finite element method in computing analytical solutions.

The following notations are used in the Appendixes, tables and diagrams, from which the subsequent discussions will be referenced.

f = natural frequency in cps, or Hz

G = maximum acceleration response in g's measured at the discrete mass mounting location

M = mass

m = number of axial half-waves in shell

n = number of circumferential waves in ring or shell

MS = milliseconds

MV = acceleration or displacement in millivolts

Subscripts:

1 = unloaded structure

2 = mass-loaded structure

Vibration test data of mass-loaded and unloaded shells are presented in Appendixes so that empirical results can be conveniently used for practical applications. For shell I with only one miniature accelerometer mounted, there are nine mass-loaded cases having a mass ratio M_2/M_1, ranging from 0.16 to 4.9 in addition to one unloaded case. For shell II with 20 miniature accelerometers attached, there are eight mass-loaded cases with M_2/M_1, ranging from 0.32 to 4.9 in addition to one unloaded case. The rearrangement of the 20 miniature accelerometers of shell II to form a longitudinal line, constitutes the model shell III specifically for M-mode evaluation. Shell IV model is used for an extended study, emphasizing cases of very small masses ranging from 0.004 to 0.722 and 1.495 pounds.

Included in the following discussion or presented in appendixes, figures, or tables are: general characteristics of mass-loading effects, a comparison of the shell vibration to ring and plate cases, theoretical results and their comparisons with experimental data, frequencies and attenuation characteristics of shell IV, a comparison of theoretical solutions computed by using a different number of m-n waves, theoretical results by finite element method, survey of effective forcing areas, evaluation of shell imperfections, calibration and linearity checks, mass-loading effects characteristics

of shell I and II, comparison of shock responses, longitudinal vibration characteristics, M-mode investigations and mapping of n-modes.

GENERAL CHARACTERISTICS OF MASS-LOADING EFFECTS ON SHELL VIBRATIONS

A discrete mass, even a small one, attached to a shell structure may have significant effects upon the shell vibration characteristics. These effects include the shift of natural frequencies, elimination of resonances, response attenuation, change of mode shapes and an unusual case of acceleration response amplification. This type of amplification was not observed in any of the previous studies and did not occur with heavier mass-loaded cases at any time thus far; it seems to appear only in a special case of the small mass-loaded range.

Appendix I. Mass-loading effects on the vibration transmissibility of shells are shown by the X-Y plots in Appendix I. These plots are the acceleration responses at the mass location demonstrating the significance of mass-loading effects on shell vibration induced by radial excitation. In comparison to the experimental data, the first graph shows that mass-loading effects rapidly alter shell vibrations along with the nine incremental additions of discrete masses. These cases included only the very small masses (0.004, 0.022, 0.044, 0.066, 0.089, 0.28, 0.53, 0.722 and 1.495 pounds). The second graph of Appendix I indicates substantial mass-loading effects attenuating the high intensity vibration levels of the unloaded shell to negligible amplitudes when 4.15 pounds of mass were attached to the unloaded shell structure.

The first plot of Appendix II presents a comparison of the raw vibration data of mass-loaded and unloaded plates. These raw test data reveal a simplified and concise indication of the basic mass-loading effects: (1) the mass attenuation of amplitude of the major resonance by 80 percent, (2) the elimination of the higher mode resonant frequencies, and (3) the lowering of the major natural frequency.

The second diagram of the Appendix II presents four mass-loaded and unloaded ring cases which generate more complicated mass-loading effects but possess the significances found by mass-loaded plate studies.

The presentation of the two graphs of Appendix II provides a simple and clear view describing the general characteristics of mass-loading effects. It also reveals the relationship of mass-loading effects among plate, ring, and shell structures. Note that all three types of structures have the basic characteristics of mass loading effects, but in different degrees of attenuation and complexity.

Mass-loaded shells demonstrate the simple amplitude attenuation, frequency shift, elimination of resonances like plates, but more frequencies are affected and the characteristics are more complicated than the plate cases. With some similarity in general characteristics, there is a difference in the pattern of amplitude attenuation and resonance elimination between the shell and ring cases. For the shell case, resonance elimination is not limited to higher modes as in the cases of ring and plate, but applied to some lower modes as well; also, frequency shifts are not as significant as the cases of plate and beam.

The details of the important features of mass-loading effects will be further studied and discussed individually in later sections, with the referenced test data presented in Appendixes.

COMPARISON OF FREQUENCIES AND ATTENUATION CHARACTERISTICS, SHELL IV

Vibration test data of the mass loaded and unloaded shell IV and a comparison of the frequencies and attenuation characteristics are presented in Appendix III. Listed in these tables are the natural frequencies and acceleration responses (at the mass location) for the first 23 modes, of which 7 modes are beyond the program requirement of the shell IV Model. Frequency ratios f_2/f_1 and acceleration ratios (G_2/G_1) are also given. There are nine very lightly mass-loaded cases with M_2/M_1 being 0.004, 0.025, 0.05, 0.075, 0.1, 0.32, 0.60, 0.82, and 1.7.

Through an observation and comparison of the data presented in Appendix III, it is observed that mass-loading effects exist with smaller mass cases as well as heavier masses, and that the experimental data obtained for shell IV tests are in general, compatible with the earlier investigations in prior programs. Also, these data are consistent with the study results for the cases of beams, plates, honeycomb plates, rings and shell structures as previously reported in the related studies listed in references.

It can be seen from Appendixes I and II that response amplitudes decrease rapidly, natural frequencies lower slowly and many resonances in higher as well as lower frequency regions disappear completely while the attached mass M_2 increases. These results constitute the most important phenomena of mass-loading effects on shell vibrations. The details of Appendix III indicate that natural frequencies of a shell structure mounted with very light weight masses follow the earlier study results for different mass-loaded structures to shift to lower values. However, the lowering of frequency values were in a much slower manner with a gradual change of few cycles per second until an abrupt change to negligible amplitude. This abrupt reduction of amplitude resulted in the phenomena of the frequencies disappearance (or resonances elimination) process.

The reduction of the response amplitude (mass attenuation) was as pronounced and significant with these shell IV tests as the already established test results of other structures. There was one exception (and it may be an important one) in this test series of lightly mass-loaded shell models; an unusual amplification in response instead of attenuation was recorded. This unusual amplification case occurred only at the transition from the merge of resonances to resonance disappearance. The data was detected only by a prolonged resonant dwell beyond the specified time for sweep vibration testing. Immediately before and after the evolution of merging frequencies (or resonant elimination) the mass attenuation process became predominantly effective, over-ruling the action of amplification and rapidly reducing the response. The special case that introduced an amplification rather than the established attenuation process, was essentially with Mass Number 8 which weighed 0 53 pounds, having a mass ratio of $\frac{M_2}{M_1} = 0.6$ and a resonant frequency of 118 Hz for the mode m=1 and n=2. The peak responses by the unified sweep excitation are listed in Appendix III and are marked with an arrowhead sign ($<$) in Appendix I, while the amplified peaks which resulted from the prolonged dwelling of the merged resonances, are listed in parenthesis ( ) in Appendix III. By a detailed study of the raw data reported in Appendix I and the reduced data in Appendix III, many resonances disappear or almost disappear in some low frequency regions and are overwhelmingly eliminated in the high frequency range.

MASS LOADING EFFECTS OF SHELLS I AND II

Vibration test data of the mass-loaded and unloaded shells I and II are presented in Appendix IV. For shell I, with only one miniature accelerometer, there are nine mass-loaded cases with a mass ratio M_2/M_1 ranging from 0.16 to 4.9 in addition to one unloaded case. For shell II with 20 miniature accelerometers, there are eight mass loaded cases with M_2/M_1 ranging from 0.32 to 4.9 in addition to one unloaded case.

The mass-loading effect on radial acceleration response at the mass location of shell I can be seen from two typical X-Y plots in Appendix I; the upper curve is for the unloaded case while the lower one is for the heaviest mass-loaded case. The frequency shift and response attenuation between the two cases are apparent. On these X-Y plots, there are numerous resonant frequencies. For the purposes of systematic analysis and comparison, the frequencies are so chosen that they are for the corresponding mode. For example, in Tables 11 and 13, Mode 1 has been chosen to have m = 1 and n = 3. For the other modes, however, the values of m or n are not identical because the effects of mass attenuation, merging frequencies and resonance disappearance have caused some changes in modal response and some difficulties in the modal survey. Some clarification of these

complications are accomplished through an extensive study in conjunction with the shell IV series, the results of which are presented in Appendixes III, XV and XVI.

The data for frequency ratios, f_2/f_1, and those of acceleration response ratios, G_2/G_1, for the shell I and II study series are also plotted and presented in Appendix IV.

COMPARISON OF THEORETICAL SOLUTIONS AND EXPERIMENTAL RESULTS

The technical effort of this study emphasizes a theoretical work on free vibration of the mass-loaded shell structure, a shock response analysis, and a basic research of the transmissibility characteristics. The theoretical work leads to a closed form and a finite-element solution of the free vibration problems, while the basic research results in a fundamental basis for a theoretical solution of the mass loading effect mechanism and provides some urgently needed empirical transmissibility information for practical applications in the fields of environmental dynamics and vibratory loads. The information includes attenuation, amplification, input-output relation, quality factor "Q", damping ratio "ζ" or transmission function H. The shock response analysis is intended to evaluate a simple method and its relation to vibration analyses. Theoretical methods in computing other forced vibration responses for important resonances become routine and are given in textbooks, when the free vibration characteristics have been computed and the transmissibility parameters (such as Q, ζ or H) are known.

The free vibration characteristics of the mass-loaded shell were theoretically analyzed by a series expansion technique and again by a finite-element method. Twenty sets of computations were performed covering symmetrical and unsymmetrical cases for each of the nine mass-loaded shell models. Each of these 20 cases was theoretically analyzed by letting M = 4 and n = 4 in the series expansion formulations, resulting in 56 frequencies for each mass-loaded model. The theoretical analyses require the generation of the stiffness matrices [K] and mass matrices [M] from formulations which were developed by a series expansion technique in an earlier chapter. These numerical solutions of frequencies and mode shapes in terms of eigenvalues and eigenvectors are then obtained through computer iteration using Jacobian and Cholesky techniques. These computed frequencies are presented in Appendix V. A close agreement is found between these analytical solutions for all cases in Appendix V and the experimentally measured data listed in Appendix III. A comparison of the analytical and experimental results is tabulated in Appendix VIII.

In order to describe the possible refined effects of the mass M_2 on the modal pattern, multiple m-waves and n-waves with variable coefficients were applied in conjunction with the series expansion technique. Appendix VI shows the frequency values as affected by three sets of m-n waves.

The mass-loaded shell problems are again solved by a finite-element technique using 144 plate elements with 80 node points and 8 bar elements. The finite-element solutions are shown in Appendix VII. A comparison of the finite-element solutions, series expansion solutions, and the test results is presented in Appendix VIII. It can be seen by the comparison that the finite element solution is in general agreement with both the series expansion solution and test data; however, the finite element solutions in this particular case are comparably less elaborate and consume more computer iteration time.

Another comparison of the theoretical and experimental results shown in Appendix VIII is for model shell I, on which heavier masses were mounted.

A group of mode shapes extracted from the computer solutions through series expansion techniques are presented in Appendix XVII. These theoretical mode shapes agree with experimental results, indicating that the presence of any one of these small discrete masses does not cause a local dip on the mode shapes of the shell structure. This suggests that modal area could be used to define a local forcing area.

Theoretical analysis of the shock waves propagated along the shell structure including the shock peaks, durations and decaying oscillation can also be accomplished by series expansion and finite-element techniques as discussed previously. To demonstrate an application of the technique and compare its results with experimental data, an extensive study using series extension technique in conjunction with a one dimensional system was made in an earlier investigation of the shell structure. The computed natural frequencies for the first six modes and their comparison with the experimental frequencies are given in Appendix VIII. It is seen from the comparison that both analytical and experimental frequencies agree very closely with each other. The maximum error of the analytical values is only 4.8 percent, occurring in the third mode of Model 1. All other deviations are less than 3 percent. The axial shock responses calculated by the computer program and their experimental counterparts are all shown in Appendix VIII. A portion of the results on two similar shells, Models 2 and 3 (See Reference 13) are also illustrated in the Appendix for comparison. In these figures, the time-histories of experimental data and analytical solutions are arranged in pairs corresponding to a particular axial location. The close resemblance in wave forms between analytical and experimental results proves the correctness of the theoretical prediction. In fact, it has been shown by

repeated computations that the shape of the computed response can be almost identical to the test results if the input pulses in both cases have the same form. If only the major portion of the test pulse is used for computation, the wave form of the analytical response will deviate somewhat; however, the maximum response remains unaffected. Shock response in other directions may be computed from the axial response using force-displacement and stress-strain relationships, or by a three-dimensional shell approach.

The analytical solutions of axial shock transmissibility in terms of shock load factors versus axial stations have been plotted by computer and are presented in the same Appendix. From these plots, it can be seen how the shock loads transmit along the axial direction of the vehicle structure. The experimental data of shock transmissibility are also given in the figures of the Appendix and show a close agreement with the theoretical solutions.

AXIAL SHOCK RESPONSE.

Upon a review of the many interesting test data, including acceleration density spectrum and time histories of the axial shock response cases for the unloaded shell (Model No. 1) which were reported separately in Reference 13, some results directly related to this study were extracted and are listed in Appendix XIV. The shock load factor, defined as the ratio of maximum response to maximum input, is obtained by dividing the maximum acceleration response at each location of the test model by the maximum acceleration input. The test data of maximum shock responses are tabulated and the shock load factors from testing are listed in the Appendix. It can be observed from these tables how the axial shock loads transmit along the test models. The shock load factor serves as an indicator for shock magnification; thus, it is called shock magnification factor or shock transmissibility. During the four test runs on Model No. 1, shell motions in the radial direction were also observed and recorded. The maximum responses to axial shock loads are listed in Table 13.

LONGITUDINAL AND RADIAL OSCILLATION BY AXIAL EXCITATION

. Vibration characteristics of mass-loaded and unloaded shell models were first studied by radial input and again by axial excitation. Appendix XII shows that the longitudinal oscillation of shell IV resulted from axial excitations. These test data indicated that there are only two major longitudinal resonances within the frequency band 50-3000 Hz. Both resonances were higher than 500 Hz while other frequencies were not excited having very low amplitudes near the noise level. Radial shell vibrations induced by axial excitation follow the trend of longitudinal oscillation as shown in Appendix XIII. From these data plots, it can be seen that radial responses also had only two major resonances corresponding to the longitudinal oscillation. Amplitudes of other frequencies (radial or axial) in the band 50-3000 Hz were much lower than the two major radial resonances.

In comparison of the axially induced longitudinal and radial vibration characteristics, it is found that both longitudinal and radial vibrations resemble each other in the response pattern, having two major resonances at their corresponding frequencies. The amplitudes of these major frequencies are governed by the structural and damping characteristics and the transmissibility of force from longitudinal to radial direction which excites the radial modes.

A comparison of shell vibration excited axially and radially shows a compatibility between the two cases, although the two axially excited frequencies may not be the major ones in a radially excited resonant spectrum. Also, many radially induced significant resonances are not outstandingly excited by axial inputs. However, other frequencies may be excited by either one or both excitations, depending on structural properties, imperfections and the condition of excitation.

RADIAL AND LONGITUDINAL SHOCK RESPONSE

Shell motions in both radial and longitudinal directions excited by an axial impulse were experimentally measured in both time and frequency domains (shock wave propagation plots and acceleration spectral density plots) and are shown in Appendix XIV. Test results indicated that the shock waves propagated longitudinally and radially along the shell structures with amplifications only at frequencies near the major resonances as expected. These shock tests agree with the transient dynamic response theory, showing no amplification of shock waves other than those of critical frequencies. Mass-loading effects had no significant influences on shock wave responses with the shell IV tests since the major frequencies changed only slightly with the light weight masses (M2); however, there were some primary shock peaks attenuated by the coupling of two resonances (beating).

STUDY OF IMPERFECTION, CALIBRATION AND LINEARITY

An automatic setup of a proximity gage was used to survey the geometrical and physical imperfections of the shell structure and to calibrate the measurements for linearity checking. These experimental data are shown in Appendixes X and XI. A plot of the force responses for different modes under incrementally increased excitation levels shows a favorable linearity in the experimental measurements.

EFFECTIVE FORCING AREA AND MODAL STUDIES

Refined measurements of the localized shell response around the attached mass (M2) were made to investigate the possible abrupt change of the vibratory pattern and to determine the effective forcing area induced by the added mass (M2). The data are shown in Appendix IX, indicating no . localized abrupt change. A mapping of the m-n modes for almost all of the significant frequencies was conducted and is presented in Appendixes XV and XVI. Appendix XVII shows the theoretically computed modes and frequencies. These studies all indicate that no significant localized abrupt change by these light weight masses was found on the response mode. It is, hence, believed that vibration mode shape may be used to determine the effective forcing area for shell IV type of structure..

CONCLUSION AND RECOMMENDATION

Radial and axial transmissibility characteristics of typical rocket vehicle structures, is an important problem for the design of advanced aerospace systems, modification of current vehicles, shock and vibration analyses, and establishing environmental dynamic requirements. An investigation of the transmissibility characteristics and the related problems requires a comprehensive and unusual experimental and analytical study which is somewhat beyond the specified program effort; such a study program and additional effort has been successfully completed and the results can be concluded as follows:

1. Without a study of the transmissibility characteristics, dynamic analyses become incomplete and have little practicability.

2. A discrete mass, even a small one, attached to a shell structure may have significant effects upon the shell vibration characteristics. These significant effects include the shift of natural frequencies, eliminations of resonances, attenuation in responses and change of mode shapes.

3. Efficient methods have been developed for analyzing vibration of mass-loaded and unloaded shell structures in addition to beam, plate, honeycomb plate, and ring structures.

4. Theoretical solutions by a series expansion technique, finite-element method, and a beam approach are favorably agreeable with test data

5. An unusual case of amplification in acceleration response instead of attenuation was found in this study with the particular mass-loaded (very light weight masses) shell series. This unusual case was recorded by prolonged resonance dwell at merging frequencies.

6. The shell imperfection survey and the proof of linearity in measurement can be easily accomplished by a special set-up of instrumentation.

7. The theoretical analysis and test data indicated that the mass affected, localized area (the effective forcing area) may be defined through modal investigations for lightweight mass-loaded cases.

8. Frequency-shifts for mass-loaded shells differed somewhat from those previously obtained for the cases of beams, plates and rings. Because of the motion of the mass interacted with the three-dimensional motions of the support structures, the effect of mass loading on shells caused a decrease in natural frequencies as expected; however, the frequency shifts became less significant as the attached mass increased. This information is presented in this report in the form of equations, tables, plots, and non-dimensional graphs for various applications.

9. Transmissibilities and attenuations followed a trend similar to that of beams, plates and rings but possessed special character-istics; beam and plate cases provided a simple and concise mass-loading effect while ring and shell cases resulted in a more complicated phenomenum.

10. Mass-loading also caused changes in mode shapes and disappear-ance of some modes at the mass mounting location; however, these phenomena of shells deviated from that of beams, plates and rings and were demonstrated by test data and computer solutions in this report.

11. The free vibration characteristics of mass-loaded shells can be solved analytically by the Fourier series-expansion technique, which gives closed-form and nearly exact solution, depending on the shell equations used. This method required the use of four summations of the m n i j terms rather than two summations of m n terms to describe the interacted motion.

12. The finite-element method can be a convenient tool in solving the free vibration problem of a complicated mass-loaded shell structure; however, the method requires an elaborate element-model, very large matrix iteration process and a high cost in computer operation.

13. Application of the series expansion technique to a beam approach in computing the shock responses resulted in a surprisingly accurate solution in comparison with experimental shock wave propagation data.

14. The developed experimental and instrumentation techniques per-mitted continuous plotting of mode shapes and produced meaningful data for immediate evaluation during the test. This special setup permitted study accomplishment beyond program requirements.

15. Sufficient data has been obtained for smaller mass ratios to better define the mass-loading phenomena for shell structures.

16. Transmission and attenuation characteristics (y) follow the equation $y = A + \dfrac{B}{X^n}$ which was previously established in the related programs (References 11 and 12). The coefficients A, B and n can be determined from the transmissibility plots in conjunction with firing test data and some consideration for design safety.

As a general conclusion to the study, a general trend of mass-loading effects on shock and vibration of beam, plate, honeycomb plate, ring and shell structures has been established and the prediction methods have been developed empirically and theoretically wherever possible. It essentially provided urgently needed empirical information for practical applications and developed a basis toward the further understanding of the thus far theoretically unsolvable problem in dynamics. Some further investigations and refined studies are needed and recommended as follows:

1. An impedance study in conjunction with this program.

2. Further theoretical development of the forced response problems and the mass-loading effects mechanism.

3. Application of the results in conjunction with static firing and flight tests data to develop environmental dynamic requirements for advanced systems.

4. A forced response study for further development in defining the effective forcing areas.

5. Refinement of the closed-form exact-solution approach and finite-element technique for shock and vibration analyses of typical rocket vehicle structures.

6. Application of results to solve bracketry problems, definition of support structures, design of local structures, and test and evaluation of components.

REFERENCES

1. Lee, S.Y. Shock and Vibration Analysis of Structures. Mechanical Engineering Department, University of Southern California, Research Report ME 590 (1959).

2. Lee, S.Y. Sonic Induced Vibration and Control for Advanced Spacecraft. Presented at the 65th Meeting of Acoustical Society of America, May 15-18, 1963, New York.

3. Lee, S.Y. Vibration Environment and Design Development Program. Space Division, North American Rockwell Corporation. Report SD 62-74 (May 1962).

4. Lee, S.Y. Test Results of Mass-Loading and Coupling Investigation. Space Division, North American Rockwell Corporation, Dynamic Sciences Internal Report (June 1963).

5. Lee, S.Y. and M. Chapman. Technical Proposal for a Study of Mass Loading Effects on Localized Vibratory Environments of Rocket Vehicles. Space Division, North American Rockwell Corporation, Report SID 64-2180-1 (December 1964).

6. Lee, S.Y. The Mass-Loading and Mass-Coupling Effects on Vibration Response. University of Southern California, Research Report AE590 (1959-1962).

7. Lee, S.Y. Extension of Study of Mass Loading Effects on Localized Vibratory Rocket Vehicle Environments. Space Division, North American Rockwell Corporation, Report SID 66-319 (March 1966).

8. Lee, S.Y. Further Study of Mass-Loading Effects of Localized Vibratory Rocket Vehicle Environments. Space Division, North American Rockwell Corporation, SID 66-1284 (5 August 1966).

9. Lee, S.Y. Analytical and Experimental Determination of Localized Structure to be Used in Laboratory Testing of Shell Structure Mounted Components. Space Division, North American Rockwell Corporation, Report SID 64-2081 (7 December 1964).

10. Lee, S. Y. A Study of Axial Transmissibility Characteristics for Typical Rocket Vehicle Structures. Space Division, North American Rockwell Corporation, Report SID 63-1496 (7 January 1964).

11. Lee, S. Y. Mass Loading Effects on Vibration of Honeycomb Plates, (Contract NAS8-20019-II). Space Division, North American Rockwell Corporation, Report SD 67-605 (21 June 1967).

12. Lee, S. Y. and S. S. Tang. Mass Loading Effects on Localized Vibratory Environments of Rocket Vehicles, (Contract NAS8-20019I). Space Division, North American Rockwell Corporation, Report SID 66-1201 (20 July 1966).

13. Lee, S. Y., and Tang, S. S. and J. G. Liyeos. Axial Transmissibility Characteristics of Typical Multi-Stage Rocket Vehicle Structures, (Contract NAS8-18124). Space Division, North American Rockwell Corporation, Report SID 67-604 (28 June 1967).

14. Lee, S. Y., Tang, S. S. and J. G. Liyeos. Mass-Loading Effects on Vibration of Ring and Shell Structures, (Contract NAS8-20019 III). Space Division, North American Rockwell Corporation, Report SD 68-29 (February 1968).

15. Lee, S. Y., et al., Axial Transmissibility Characteristics for Typical Rocket Vehicle Structures (Contract NAS8-11162). Space Division, North American Rockwell Corporation, Report SID 65-1435 (29 November 1965).

16. Franken, P. "Sound Induced Vibration of Cylindrical Vehicles," J. Acou. Soci. of America, Vol. 34 No. 4 (April 1962).

17. MIL-STD-810 Dynamic Conference; USAF-ASD Wright-Patterson Air Force Base, Ohio (September 1960).

18. Schock, R. W., et al. Vibration, Acoustic, and Shock Environmental Specifications for Saturn Vehicles. NASA Internal Notes (1964-1966).

19. Barrett, R. E. Statistical Techniques for Describing Localized Vibratory Environments of Rocket Vehicles. NASA/MSFC, NASA TN D-2158 (July 1964).

20. Jewell, R. E. "A Technique for Predicting Localized Vibration Environments in Rocket Vehicles and Spacecraft," Shock and Vibration Bulletin No. 33, Part II (March 1964), pp. 26-33.

21. Lifer, C.E. "Design of Space Vehicle Structures for Vibration and Acoustic Environments," Shock and Vibration Bulletin No. 33, Part IV (March 1964), pp. 201-207.

22. Barrett, R.E. Techniques for Predicting Localized Vibratory Environments of Rocket Vehicles. NASA TN D-1836 (Oct. 1963).

23. MAC Staff. Summary of Random Vibration Prediction Procedures. NASA-CR, NASA/MSFC, Huntsville, Alabama, 1968.

24. Pestel, E.C., and F.A. Leckie. Matric Methods in Elasto Mechanics. McGraw-Hill Book Co. (1963).

25. Martin, H.D. Introduction to Matrix Methods of Structural Analysis, McGraw-Hill Book Company (1966).

26. Zienkiewicz, O.C. The Finite Element Method in Structural and Continuum Mechanics. McGraw-Hill Book Company (1967).

27. Przemieniecki, J.S. Theory of Matrix Structural Analysis. McGraw-Hill Book Company (1968).

28. Guyan, R.J. "Reduction of Stiffness and Mass Matrices," J. AIAA, 3, No. 2 (1965) p. 380.

29. Arnold, R.N. and G.B. Warburton. "Flexural Vibrations of the Walls of Thin Cylindrical Shells Having Freely Supported Ends." Proc. Roy. Soc. A197 (1949).

30. Arnold, R.N. and G.B. Warburton. "The Flexural Vibration of Thin Cylinders," Proc. Inst. Med. Engr. A 167 (1953).

31. Weingarten, V.I. "Free Vibration of Thin Cylindrical Shells," AIAA J., V2N4 (April 1964).

32. Mahaffey, P.T., and K.W. Smith. "Methods for Predicting Environmental Vibration Levels in Jet Powered Vehicles," Noise Control, (July-August 1960).

33. Eldred, K., W. Roberts, and R. White. Structural Vibrations in Space Vehicles, WADD TR 61-62 (December 1961).

34. Kraus, H. Thin Elastic Shells. New York: John Wiley and Sons, Inc. (1967).

35. Yu, Y. Y. "Free Vibration of Thin Cylindrical Shells Having Finite Lengths With Freely Supported and Clamped Edges," Jour. App. Mech. (December 1955).

36. Timoshenko, S., Vibration Problems in Engineering, D. Van Nostrand Co., 1964.

37. Jacobson, L.S., and Ayre, R.S., Engineering Vibrations, McGraw-Hill, 1958.

38. Harris, C.M., and C.E. Crede. Shock and Vibration Handbook, McGraw-Hill, 1961.

39. Macduff, J.N., and J.R. Curreri. Vibration Control, McGraw-Hill, 1958.

40. Flugge, W., Handbook of Engineering Mechanics, McGraw-Hill, 1962.

41. Korn, G., and T.M. Korn. Mathematical Handbook, McGraw-Hill, 1961.

I. MASS-LOADING EFFECTS ON SHELL VIBRATION
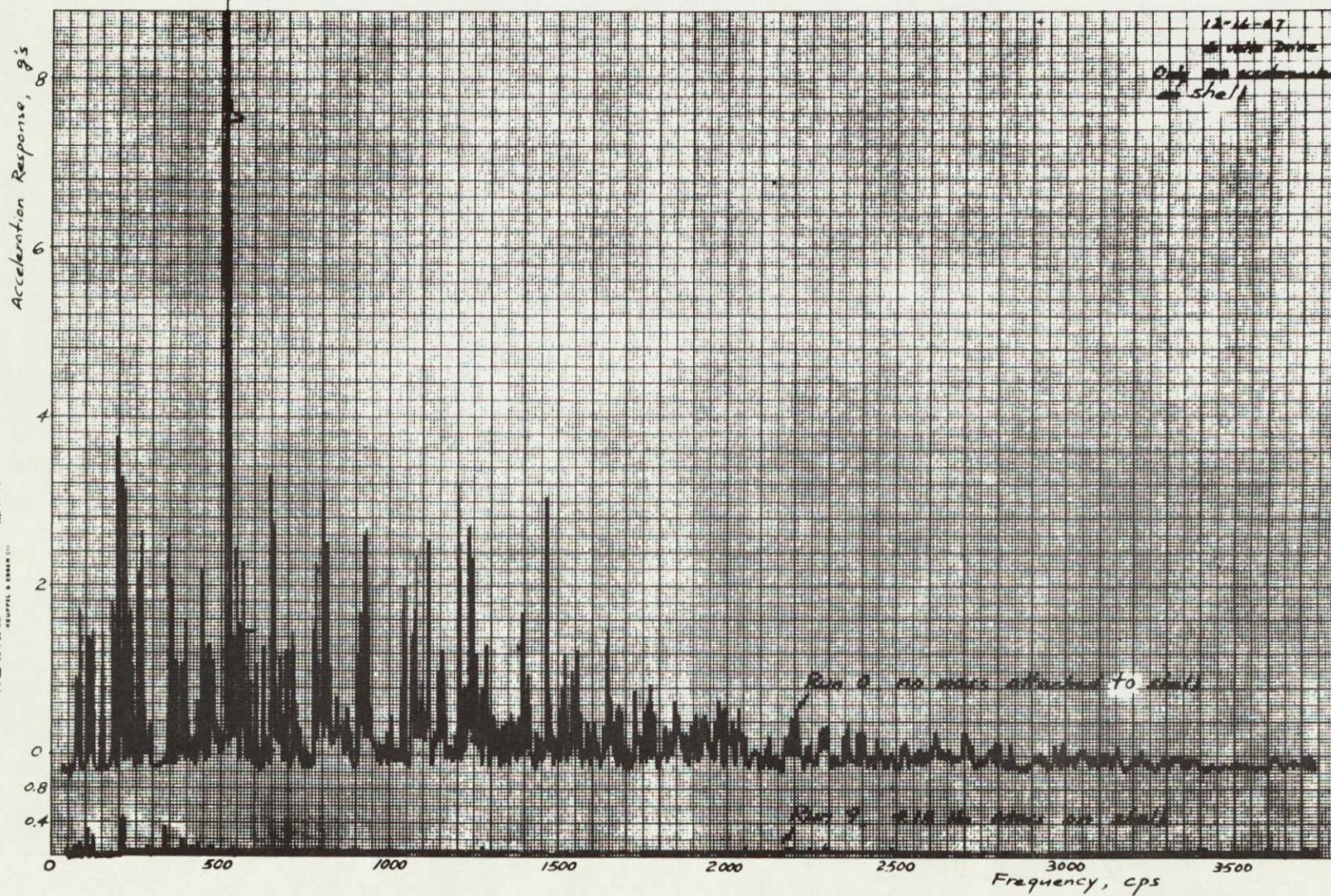
Figure I-2.   Mass-Loading Effect on Radial Shell Vibration,
Heavier Mass Cases

II. MASS-LOADING EFFECTS ON PLATE VIBRATION AND
RING VIBRATION
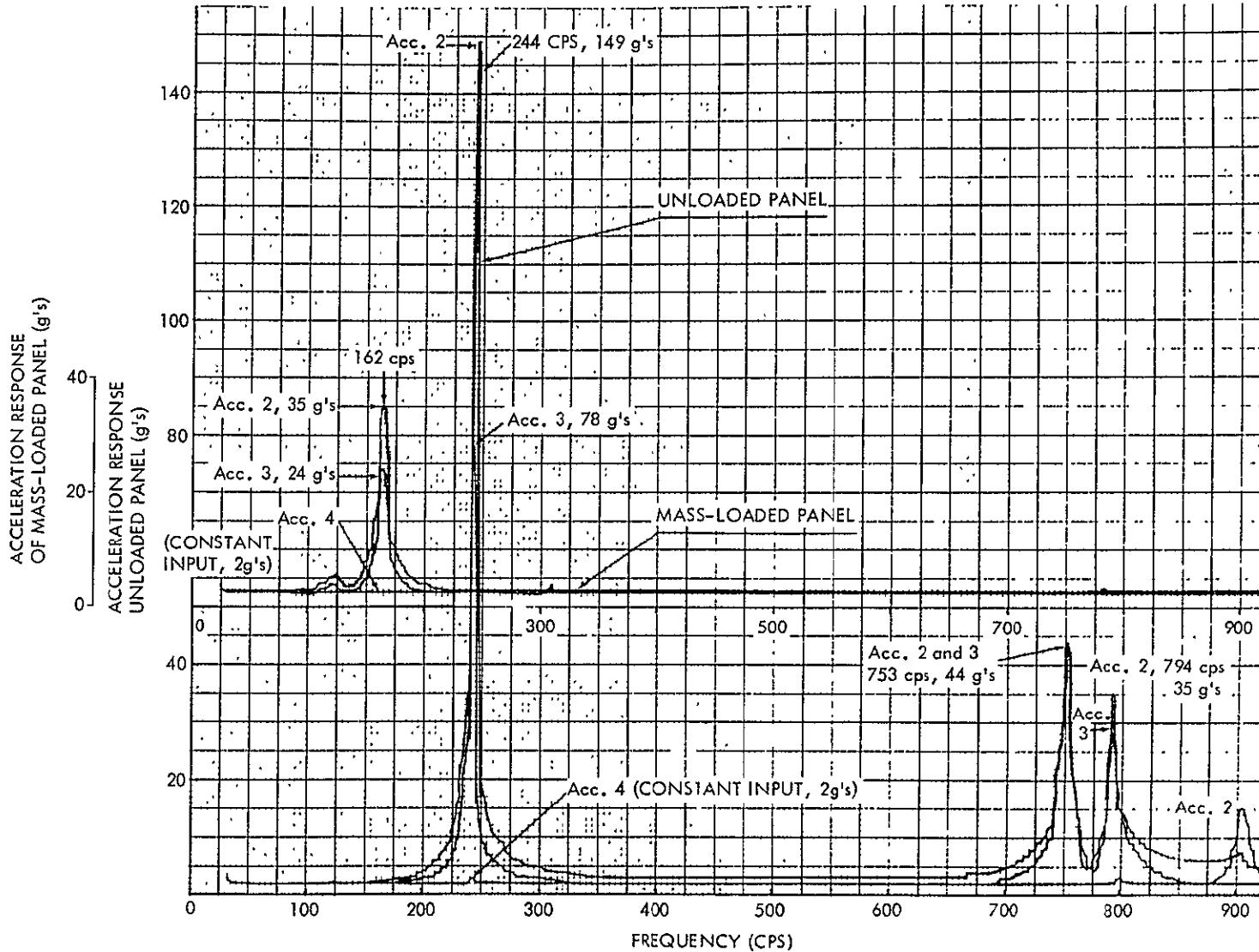
Figure II-1. Mass-Loading Effect on Plate Vibration - Attenuation of
Response and Higher Modes of Mass-Loaded Plate
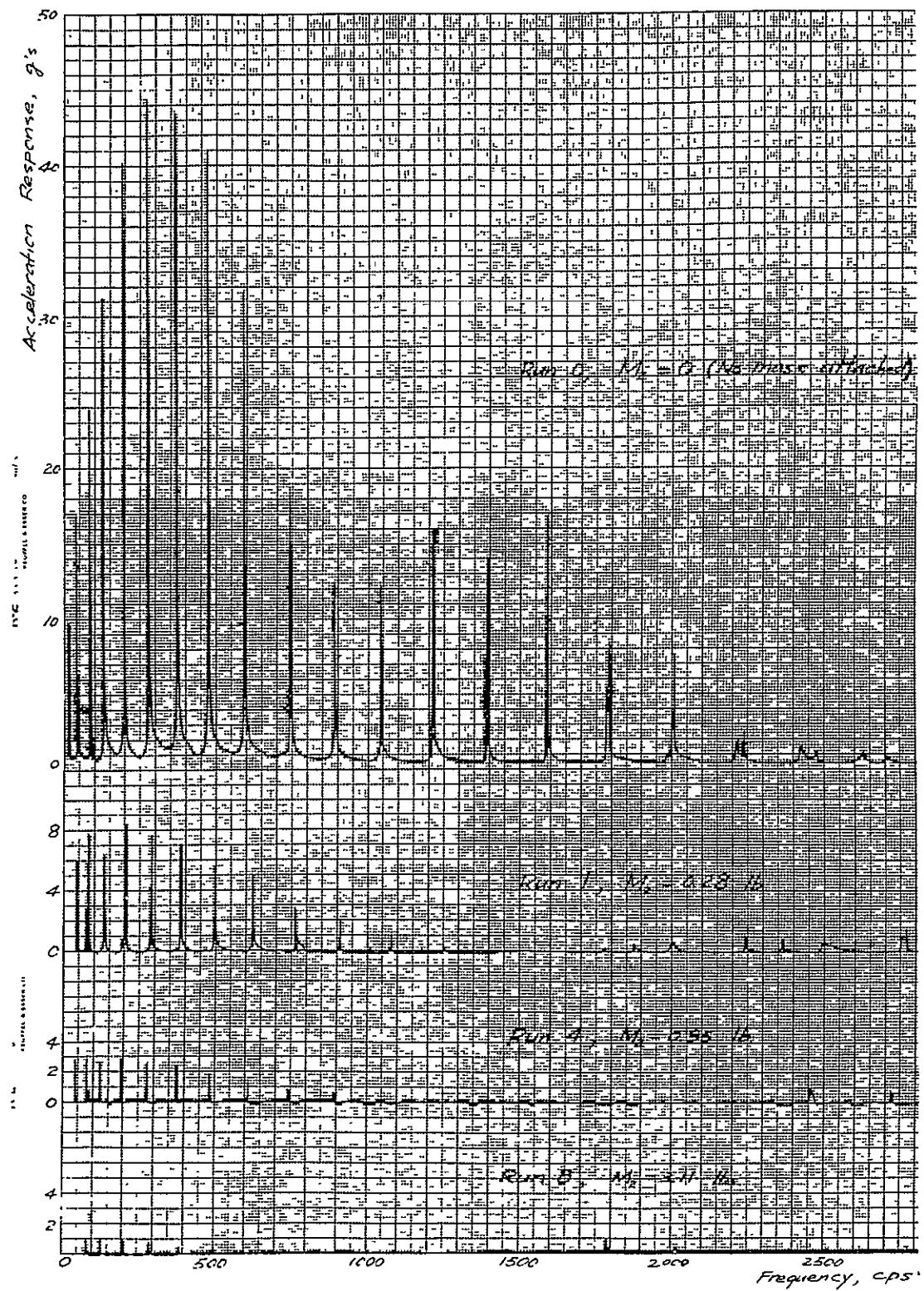
Figure II-2. Mass-Loading Effect on Ring Vibration

III. COMPARISON OF FREQUENCIES AND ATTENUATION
CHARACTERISTICS, SHELL IV

Table III-1. Comparison of Frequencies and Attenuation Characteristics, Radial Vibration Test Data of Shell IV

Run No		0-1-R	2-3-R	3-3-R	4-3-R	5-3-R	7-3-R	8-3-R	9-3-R	10-3-R
M_2/M_1		0.006	0.025	0.05	0.075	0.1	0.32	0.60	0.82	1.7
Mode 1, n=3, m=1	Freq (cps)	86.8	86.4	86.1	86.0	85.9	84.9	82.5	81.1	76.3
	f_2/f_1	1.0	0.995	0.992	0.991	0.989	0.978	0.95	0.935	0.88
	Accel (g's)	3.3 (3.8)	2.2 (2.2)	1.9 (2.0)	1.9 (3.1)	1.7 (2.9)	1.6 (2.8)	1.4 (2.7)	1.5 (1.6)	1.4 --
	G_2/G_1	1.0	0.7 (0.58)	0.57 (0.528)	0.57 (0.82)	0.515 (0.763)	0.485 (0.738)	0.424 (0.738)	0.455 (0.71)	0.424 (0.42)
Mode 2, n=2, m=1	Freq (cps)	124.1 (125.5)	124.0 (125.3)	124.0 (125.0)	123.8 (124.7)	123.3 (124.0)	120.3 (120.6)	118.0 --	117.6 --	113.4 --
	f_2/f_1	1.0	0.999	0.999	0.996	0.995	0.97	0.95	0.942	0.913
	Accel (g's)	5.0 --	2.2 --	2.1 --	2.2 (2.6)	1.9 (3.2)	1.2 (5.0)	2.1 (5.8)	1.5 (5.0)	1.0 (2.3)
	G_2/G_1	1.0	0.44	0.42	0.44 (0.52)	(0.38) (0.64)	(0.24) (1.0)	(0.42) (1.16)	0.3 (1.0)	0.2 (0.46)
Mode 3, n=5, m=1	Freq (cps)	142.0	141.5	141.4	141.0	141.0	140.6	139.0	138.1	134.8
	f_2/f_1	1.0	0.995	0.994	0.992	0.992	0.99	0.98	0.972	0.95
	Accel (g's)	3.4 --	2.7 --	2.6 --	2.2 --	2.2 (2.4)	1.9 (2.5)	1.7 (2.8)	1.1 (2.9)	0.9 --
	G_2/G_1	1.0	0.784	0.765	0.647	0.647	0.558	0.5	0.324	0.265
Mode 4, n=4, m=2	Freq (cps)	170.0	167.5	165.0	164.0	163.0	162.0	160.0	157.9	152.6
	f_2/f_1	1.0	0.989	0.971	0.965	0.96	0.951	0.942	0.929	0.898
	Accel (g's)	5.4	5.0	4.7	3.4	3.3 (4.3)	2.9	2.0	1.4	0.6
	G_2/G_1	1.0	0.925	0.87	0.63	0.61	0.537	0.37	0.26	0.111
Mode 5, n=6, m=1	Freq (cps)	212.0	211.0	210.0	209.0	208.0	205.0	201.0	198.4	193.5
	f_2/f_1	1.0	0.995	0.99	0.985	0.981	0.967	0.95	0.936	0.912
	Accel (g's)	5.62	4.75	4.6	4.3	4.3	3.4	2.9	2.4	1.2
	G_2/G_1	1.0	0.845	0.82	0.765	0.765	0.605	0.516	0.428	0.214
Mode 6, n=3, m=2	Freq (cps)	229.0	228.4	228.1	227.9	227.6	225.7	224.	222.0	210.0
	f_2/f_1	1.0	0.998	0.997	0.994	0.993	0.984	0.98	0.97	0.92
	Accel (g's)	14.2	12.6	13.1	6.5	6.9	5.8	3.4	2.6	1.1
	G_2/G_1	1.0	0.89	0.92	0.458	0.486	0.409	0.24	0.183	0.078
Mode 7, n=3, m=2	Freq (cps)	279.9	279.7	279.5	279.2	279.0	278.0	276.7	275.7	270.0
	f_2/f_1	1.0	0.999	0.999	0.998	0.997	0.994	0.99	0.975	0.96
	Accel (g's)	6.5	6.2	5.3	4.4	3.5	3.1	2.4	1.9	1.0
	G_2/G_1	1.0	0.955	0.815	0.677	0.54	0.478	0.37	0.293	0.154
Mode 8, n=4, m=3	Freq (cps)	303.0	302.2	302.0	301.8	301.6	300.3	299.5	299.0	294.0
	f_2/f_1	1.0								
	Accel (g's)	9.0	7.5	7.2	3.9	5.1	2.6	2.6	1.2	0
	G_2/G_1	1.0	0.834	0.8	0.434	0.566	0.289	0.289	0.133	0
Mode 9, n=8, m=1	Freq (cps)	368.0	367.7	366.5	365.5	364.5	363.0	360.0	358.7	350.0
	f_2/f_1	1.0	0.996	0.995	0.994	0.993	0.99	0.98	0.975	0.951
	Accel (g's)	9.6	6.7	6.0	4.6	5.3	4.3	3.8	2.8	1.2
	G_2/G_1	1.0	0.695	0.625	0.48	0.55	0.447	0.396	0.292	0.125
Mode 10, n=9, m=2	Freq (cps)	468.0	467.8	467.5	467.2	466.9	466.0	462.5	457.0	453.0
	f_2/f_1	1.0	0.999	0.999	0.998	0.997	0.996	0.988	0.976	0.969
	Accel (g's)	11.7	4.9	4.0	3.4	3.8	2.0	0.9	0.8	0.6
	G_2/G_1	1.0	0.418	0.342	0.29	0.325	0.171	0.077	0.068	0.051

III-1

Table III-1. Comparison of Frequencies and Attenuation Characteristics, Radial Vibration Test Data of Shell IV (Cont)

Run No		0-1-R	2-3-R	3-3-R	4-3-R	5-3-R	7-3-R	8-3-R	9-3-R	10-3-R
M_2/M_1		0.006	0.025	0 05	0.075	0.1	0 32	0 60	0 82	1.7
Mode 11, n=8, m=6	Freq (cps)	499 0	498 0	497.0	496 0	495.0	495.0	495 0	495 0	490.0
	f_2/f_1	1.0	0.998	0 995	0 994	0.992	0.992	0.992	0.992	0.984
	Accel (g's)	7.3	4.4	3 9	3.2	2.9	2 3	1.3	1 1	0.5
	G_2/G_1	1.0	0.603	0 535	0.44	0.398	0 315	0.178	0 151	0.0685
Mode 12, n=6, m=6	Freq (cps)	538.5	538 1	537.7	537 6	537.1	534.7	531.0	529.4	530 0
	f_2/f_1	1 0	0 999	0 998	0 998	0.997	0.992	0.986	0.983	0.984
	Accel (g's)	13 15	9.5	9.4	6.5	5 6	3.0	0 9	0.7	0
	G_2/G_1	1.0	0.724	0.715	0 495	0.426	0.228	0.0685	0.532	0
Mode 13, n=10, m=6	Freq (cps)	579 0	579.0	578 8	578.6	578 5	578.3	578.0	577 5	0
	f_2/f_1	1 0	1.0	0.999	0.999	0.999	0 998	0 998	0 998	--
	Accel (g's)	13 3	6 5	5 6	5.4	4.7	1.5	0 6	0.3	0
	G_2/G_1	1 0	0 49	0 42	0 406	0 353	0 112	0.045	0 023	0
Mode 14, n=10, m=6	Freq (cps)	645 0	645.0	645 0	644.5	642.0	640 0	640 0	0	0
	f_2/f_1	1 0	1 0	1.0	0 999	0.995	0.992	0.992	0	0
	Accel (g's)	6.9	3.6	3 8	3 3	2.0	0.4	0.1	0	0
	G_2/G_1	1.0	0.522	0 55	0.48	0 29	0 058	0 016	0	0
Mode 15, n=11, m=3	Freq (cps)	704 0	703 9	703 9	703 3	703 4	702.6	701 0	699.2	700.0
	f_2/f_1	1.0	1 0	1 0	0 999	0.999	0 998	0 995	0 993	0.994
	Accel (g's)	15 3	6.3	4.5	3.9	3 3	2 0	0 9	0 65	0.15
	G_2/G_1	1.0	0 412	0 294	0.255	0 216	0.13	0 059	0 0425	0.009
Mode 16, n=10, m=9	Freq (cps)	806.0	805.0	804.0	804 0	803 0	801.0	800 0	0	0
	f_2/f_1	1.0	0 998	0 997	0 997	0 996	0 992	0 991	0	0
	Accel (g's)	12.3	6.3	4.85	3.6	3.5	1 8	0 2	0	0
	G_2/G_1	1 0	0.512	0.394	0.293	0.284	0.146	0 016	0	0
Mode 17, n=10, m=9	Freq (cps)	830.0	830 0	829 4	829.6	828 9	823 0	822 5	822 0	814 6
	f_2/f_1	1 0	1.0	0.999	0 999	0.998	0.991	0.989	0 989	0 981
	Accel (g's)	19.4	4 5	2.0	2.6	2 6	1.5	0.6	0 55	0.25
	G_2/G_1	1 0	0 232	0 103	0 134	0.134	0 077	0 031	0.028	0 013
Mode 18, n=10, m=5	Freq (cps)	889 0	889 0	889 0	889.0	889.0	887.0	0	0	0
	f_2/f_1	1 0	1 0	1 0	1.0	1.0	0 997	0	0	0
	Accel (g's)	4 9	3 8	3 4	2 3	1 8	0.8	0	0	0
	G_2/G_1	1.0	0 775	0 694	0.47	0 367	0 163	0	0	0
Mode 19, n=13, m=5	Freq (cps)	983 0	983 0	983.0	983 0	983.0	982.0	981.0	981 0	980.0
	f_2/f_1	1.0	0 1	0 1	0 1	0 1	0 998	0 997	0.997	0 996
	Accel (g's)	16 1	3 8	1 9	1 9	1 5	0 9	0.4	0.2	0.1
	G_2/G_1	1 0	0 236	0 118	0.118	0 093	0 056	0 025	0 012	0 006
Mode 20, n=13, m=9	Freq (cps)	1139 0	1138 0	1137 0	1136.0	1132 0	1125 0	1125.0	1125 0	1124.0
	f_2/f_1	1 0	0 999	0 998	0 997	0.993	0.989	0 989	0.989	0 988
	Accel (g's)	13.6	3 2	1 6	1.3	. 0 8	0 8	0 5	0 4	0 1
	G_2/G_1	1.0	0.236	0.118	0 095	0.059	0 058	0 037	0.029	0 007

SD 69-766

Table III-1. Comparison of Frequencies and Attenuation Characteristics, Radial Vibration Test Data of Shell IV (Cont)

| Run No		0-1-R	2-3-R	3-3-R	4-3-R	5-3-R	7-3-R	8-3-R	9-3-R	10-3-R
	M_2/M_1	0.006	0.025	0.05	0.075	0 1	0 32	0.60	0 82	1.7
Mode 21, n=7, m=7	Freq (cps)	1202.0	1201 0	1200 0	1200.0	1200 0	1200 0	1199.0	1200.0	0
	f_2/f_1	1 0	0 999	0 998	0.998	0.998	0.998	0 997	0 998	0
	Accel (g's)	8 3	5.1	4 7	4.4	3 8	1 5	0.6	0 4	0
	G_2/G_1	1.0	0 615	0 566	0.53	0.458	0.18	0.072	0.048	0
Mode 22, n=10, m=5	Freq (cps)	1295 0	1295.0	1295.0	1295 0	1295 0	1294.0	1294 0	1294 0	0
	f_2/f_1	1 0	1.0	1.0	1.0	1.0	0 999	0 999	0 999	0
	Accel (g's)	10.4	2 4	1 2	0 9	0.6	0.5	0.5	0.1	0
	G_2/G_1	1 0	0.231	0.115	0.086	0 057	0 048	0 048	0.009	0
Mode 23, n=15, m=6	Freq (cps)	1311 5	1311.0	1311.0	1309.0	1307.0	1305.0	0	0	0
	f_2/f_1	1 0	0.999	0 999	0 998	0 996	0 995	0	0	0
	Accel (g's)	10.6	2.2	1.0	0 6	0.5	0.5	0	0	0
	G_2/G_1	1.0	0.208	0 094	0 056	0.047	0.047	0	0	0
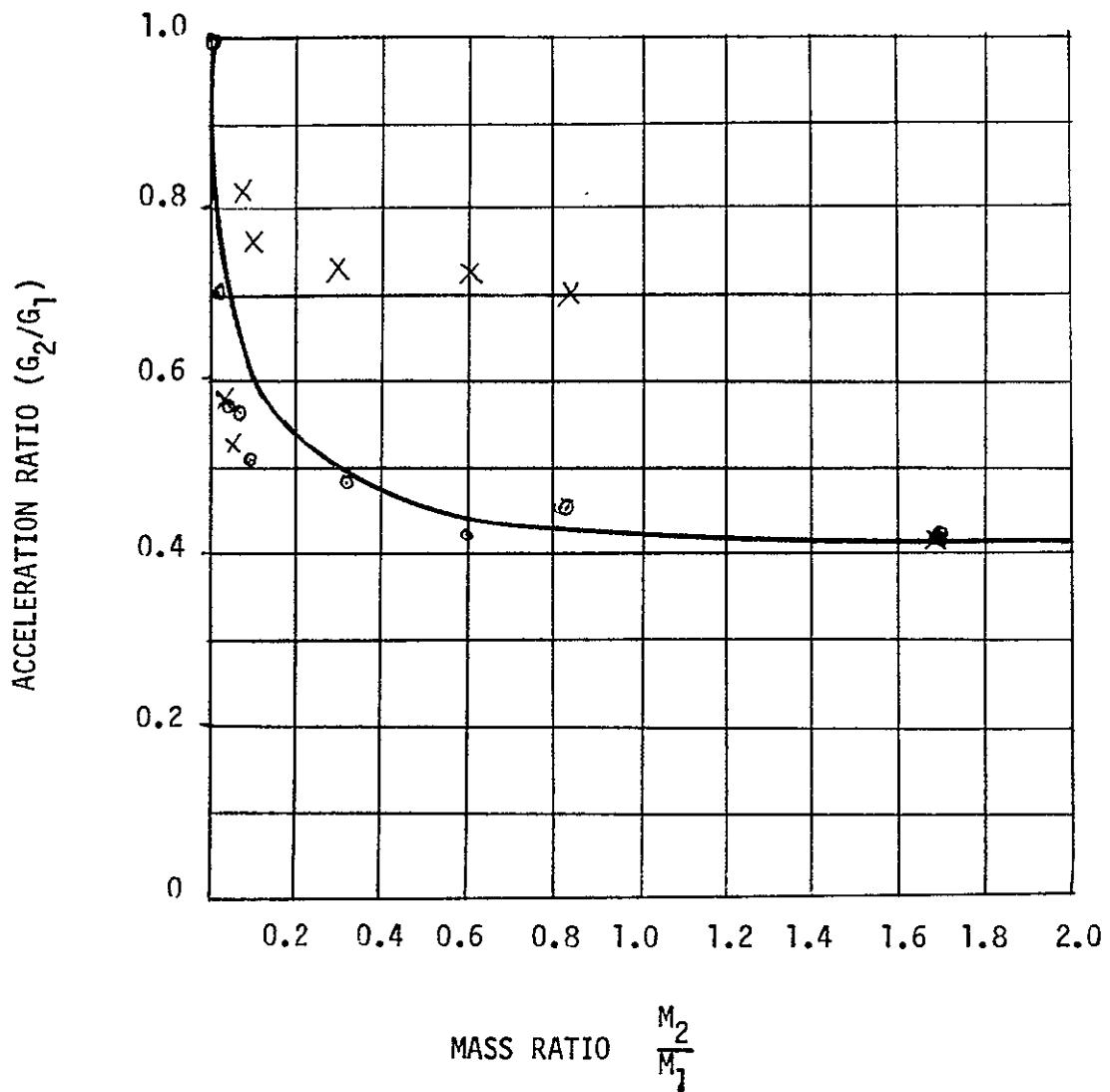
Figure III-1. Mass-Loading Effect on Acceleration Response of Shell IV, Mode 1 (m=1, n=3)
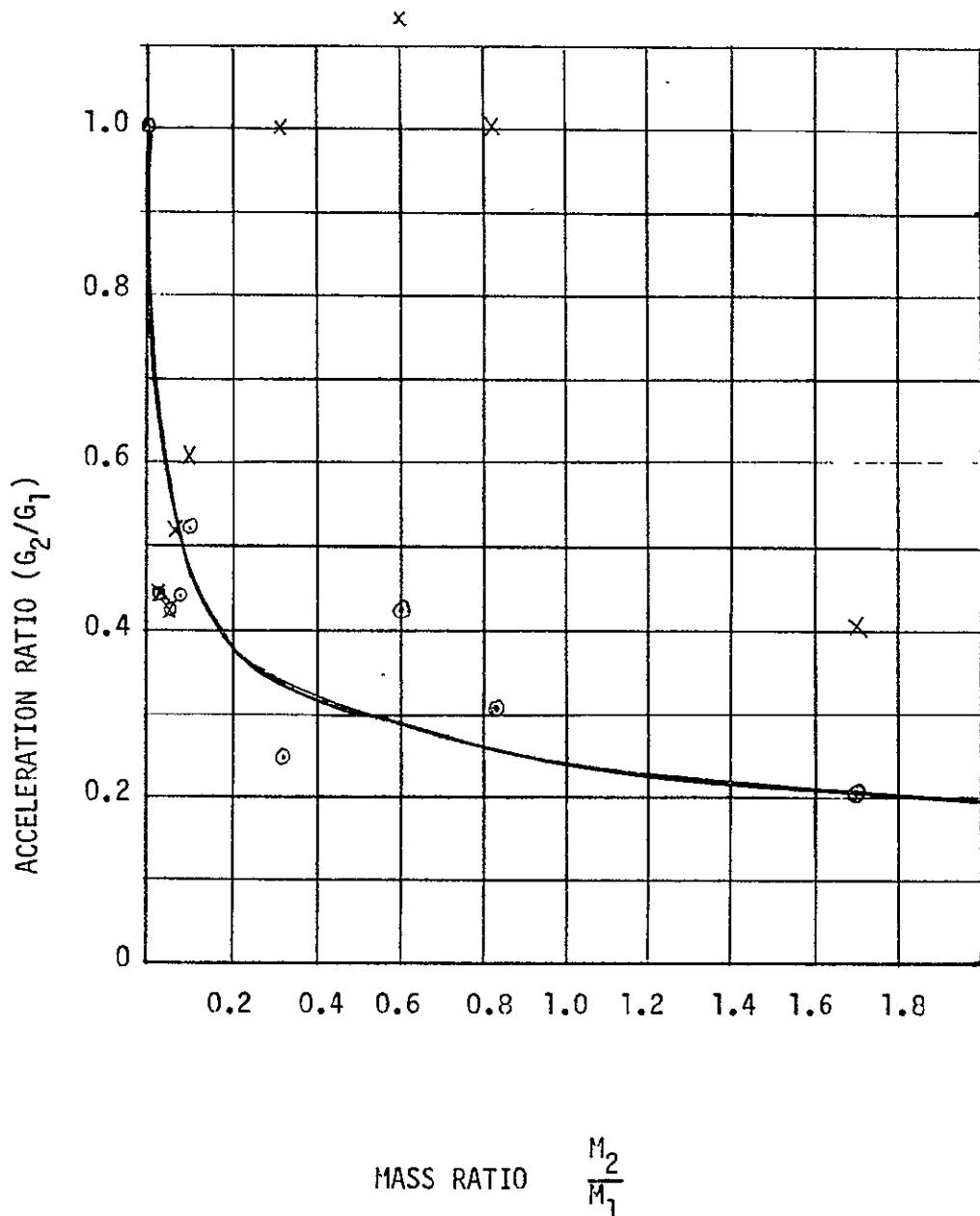
Figure III-2. Mass-Loading Effect on Acceleration Response of
Shell IV, Mode 2 (m=1, n=2)
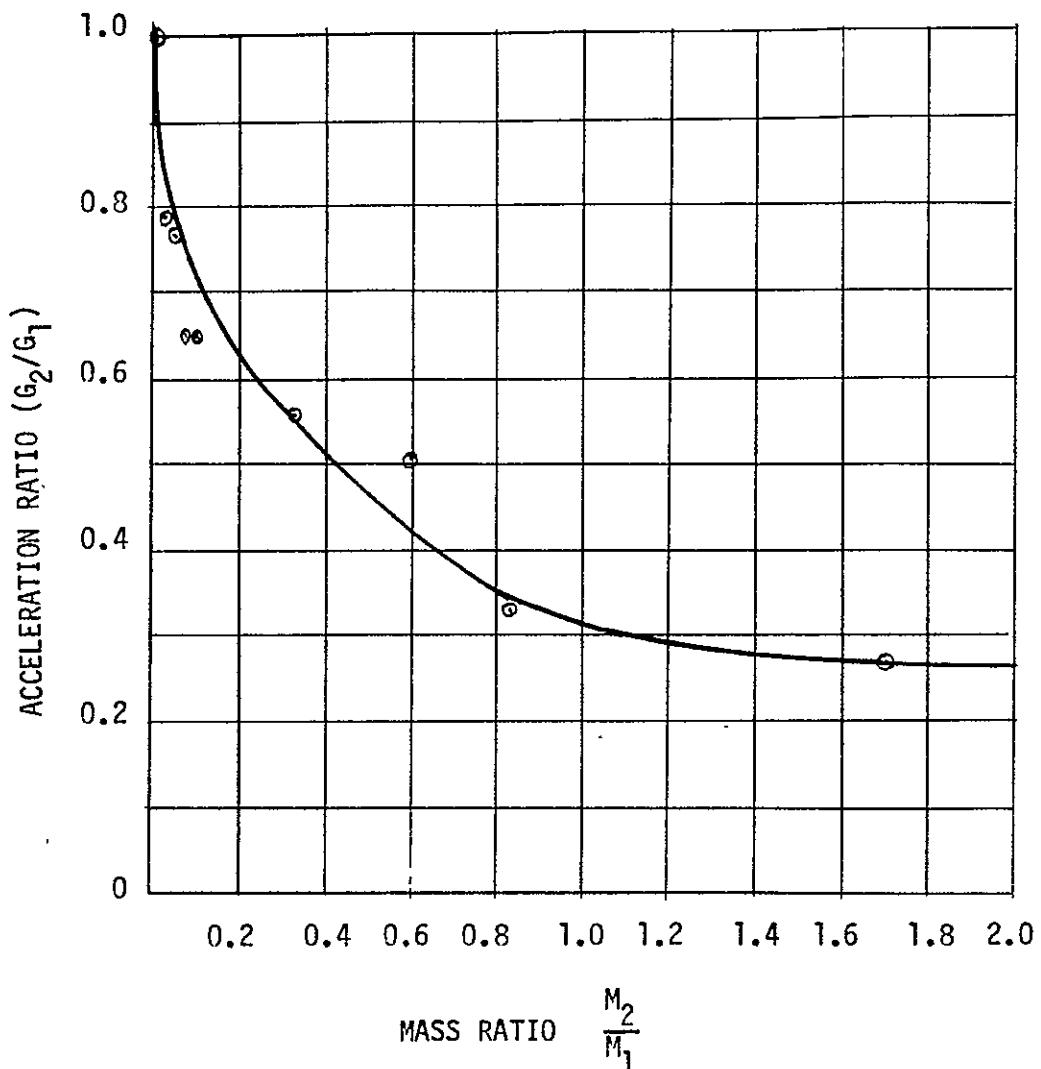
Figure III-3. Mass-Loading Effect on Acceleration Response of
Shell IV, Mode 3 (m=1, n=5)
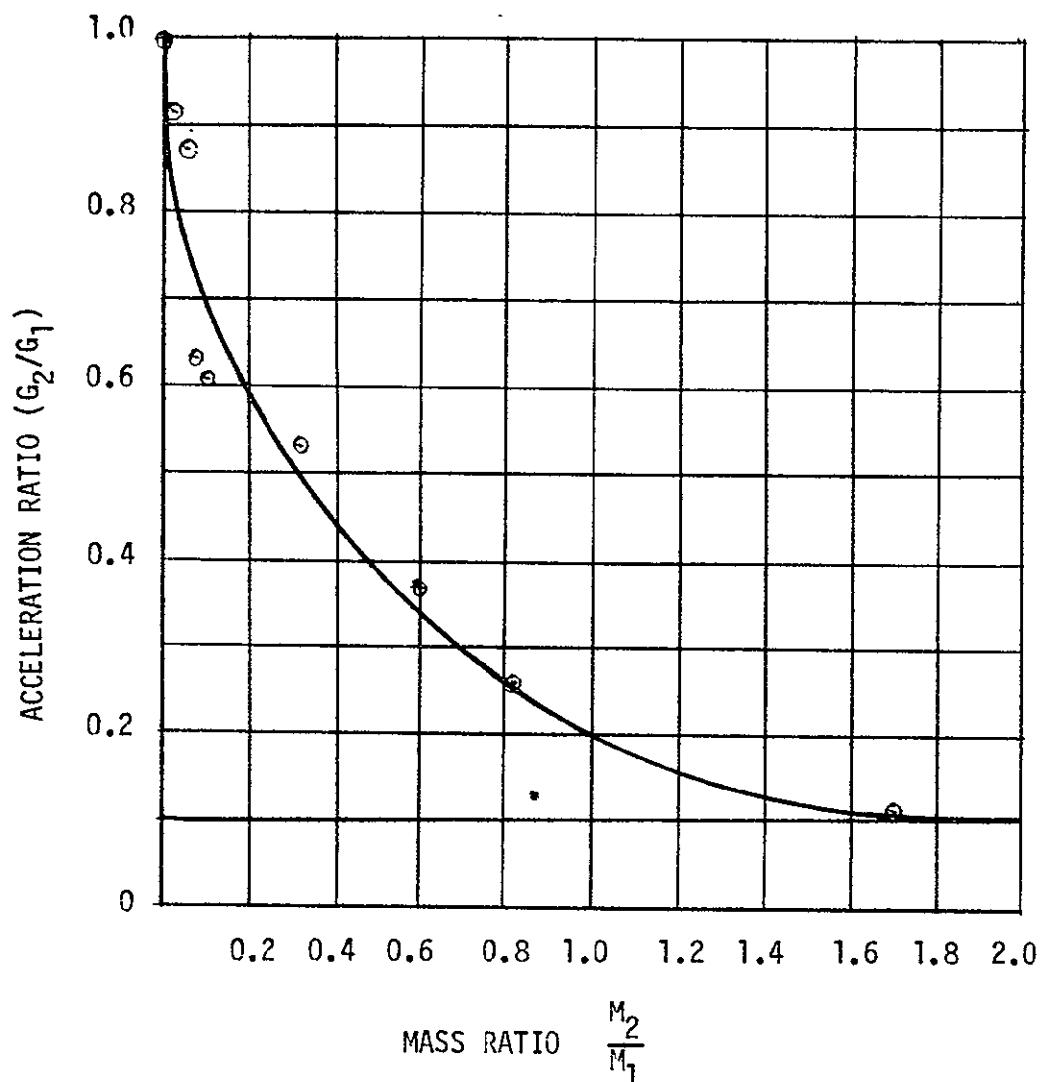
Figure III-4. Mass-Loading Effect on Acceleration Response of
Shell IV, Mode 4, (m=2, n=4)
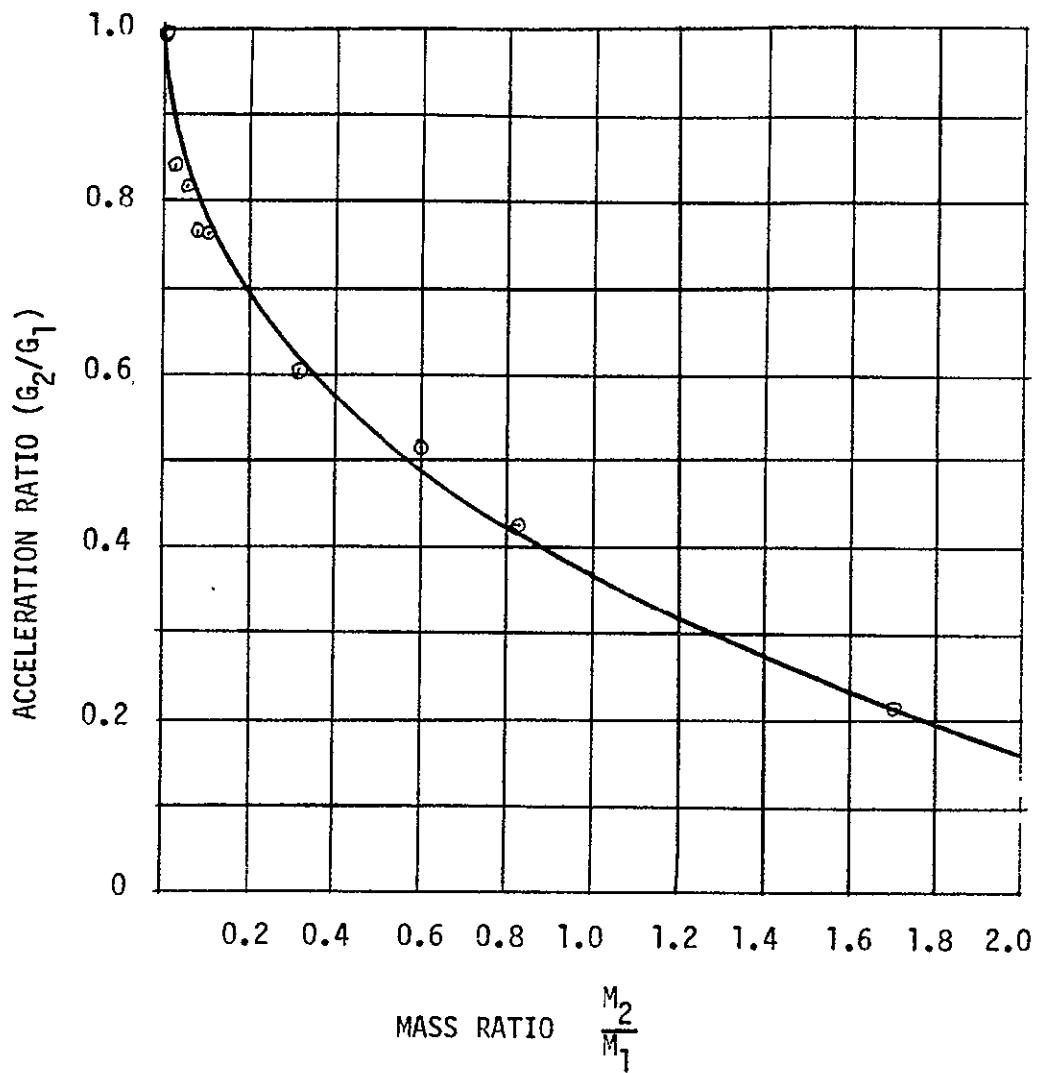
Figure III-5. Mass-Loading Effect on Acceleration Response of Shell IV, Mode 5, (m=1, n=6)
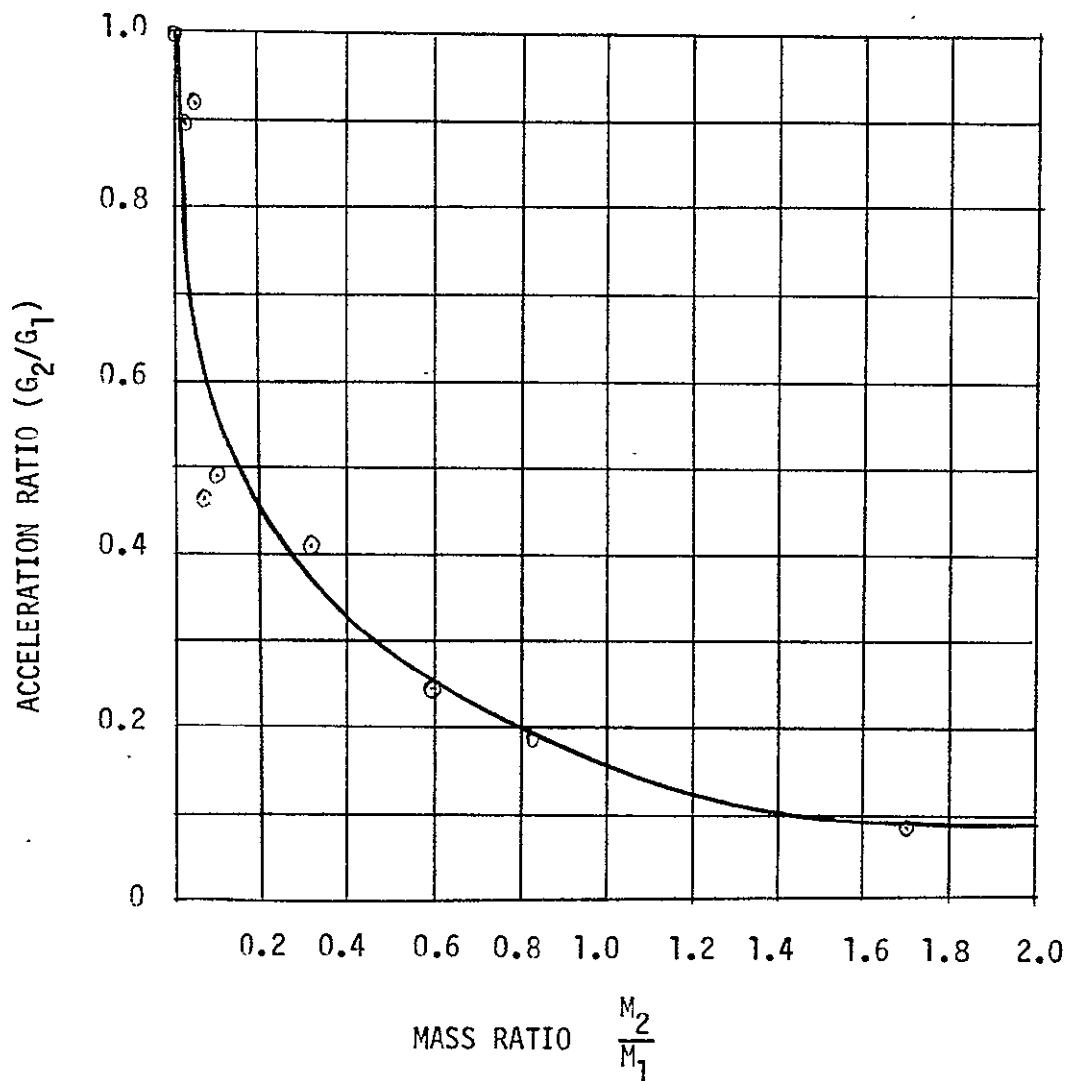
Figure III-6.   Mass-Loading Effect on Acceleration Response of
Shell IV, Mode 6, (m=2, n=3)
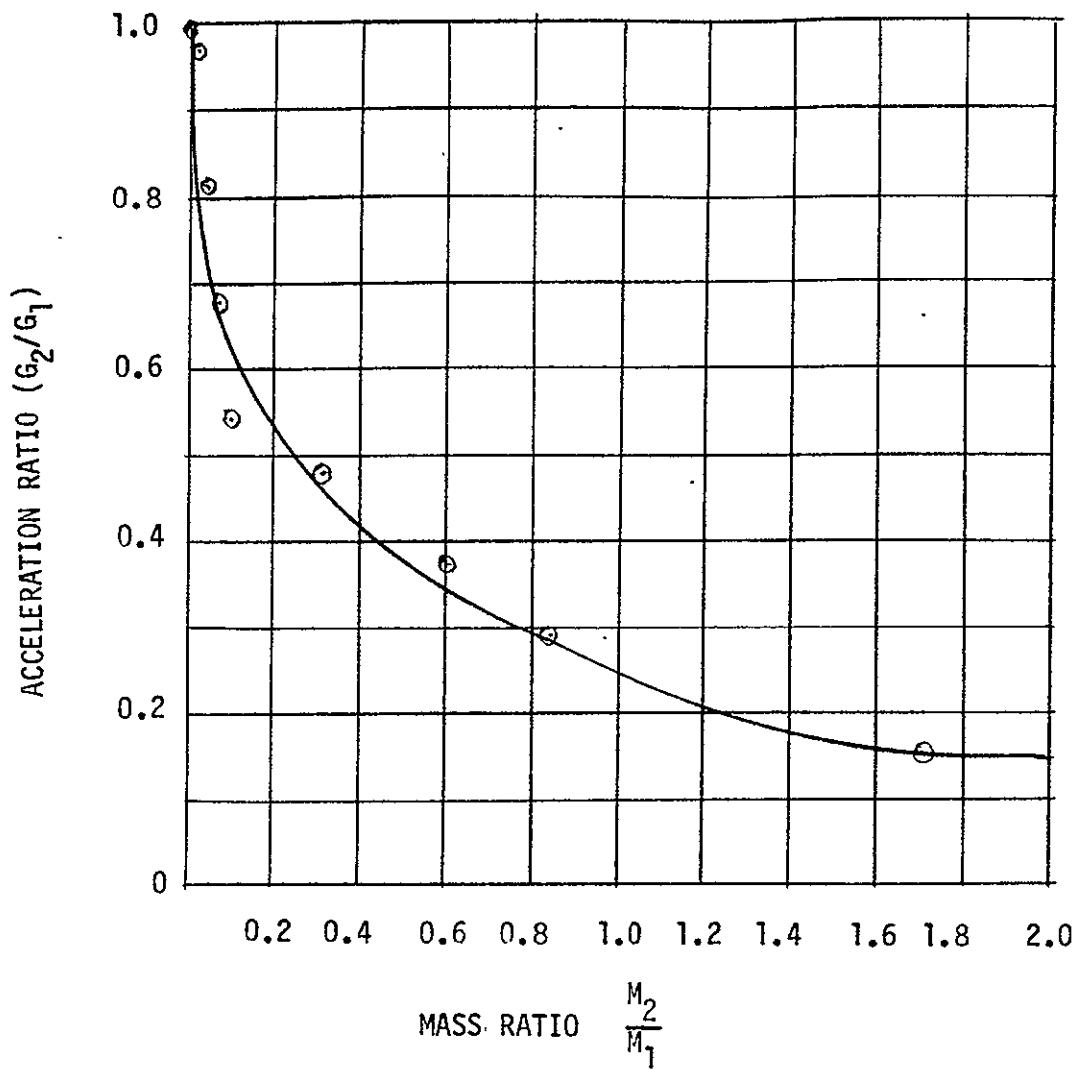
Figure III-7. Mass-Loading Effect on Acceleration Response of Shell IV, Mode 7, (m=2, n=3)
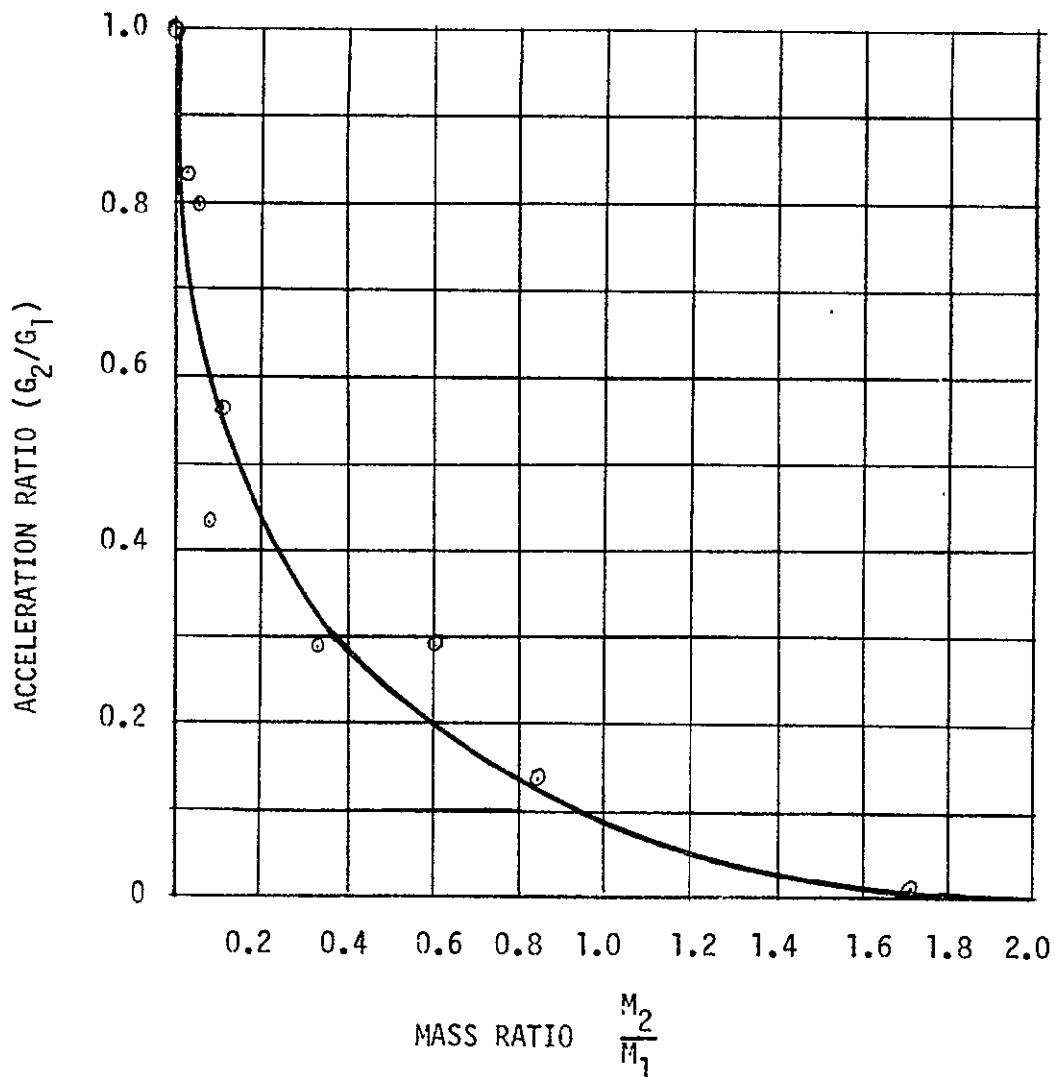
III-10

Figure III-8. Mass-Loading Effect on Acceleration Response of
Shell IV, Mode 8, (m=3, n=4)
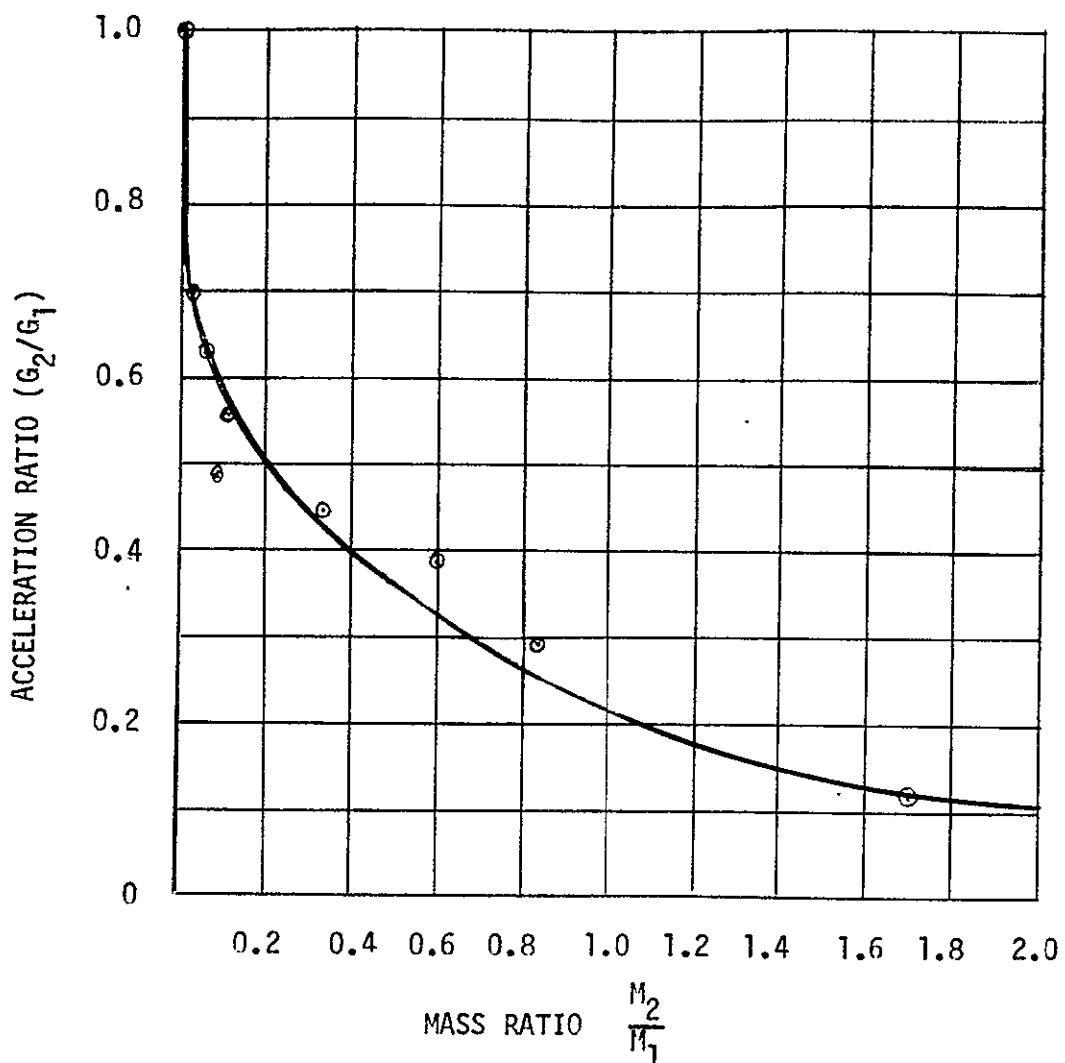
Figure III-9.   Mass-Loading Effect on Acceleration Response of
Shell IV, Mode 9, (m=1, n=8)
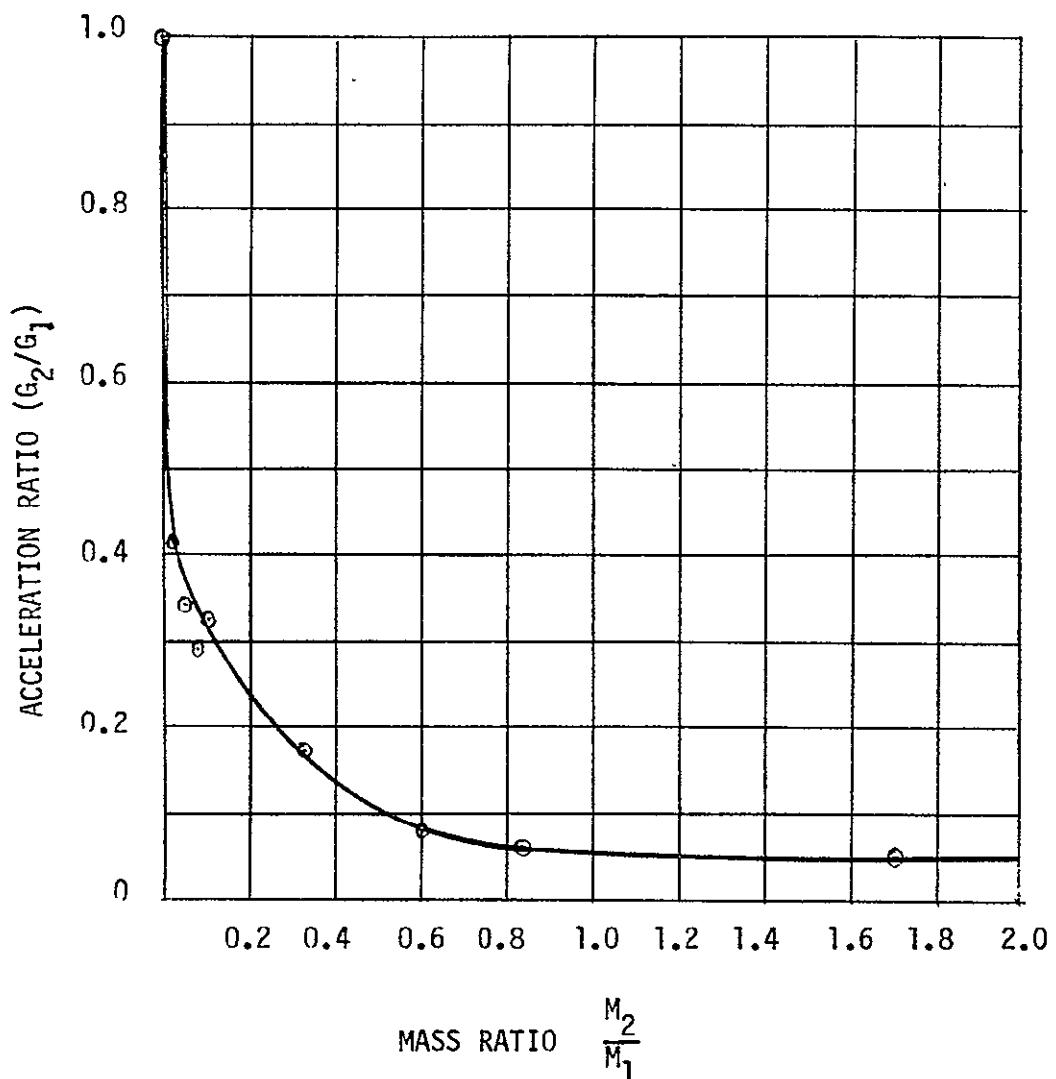
Figure III-10. Mass-Loading Effect on Acceleration Response of
Shell IV, Mode 10, (m=2, n=9)
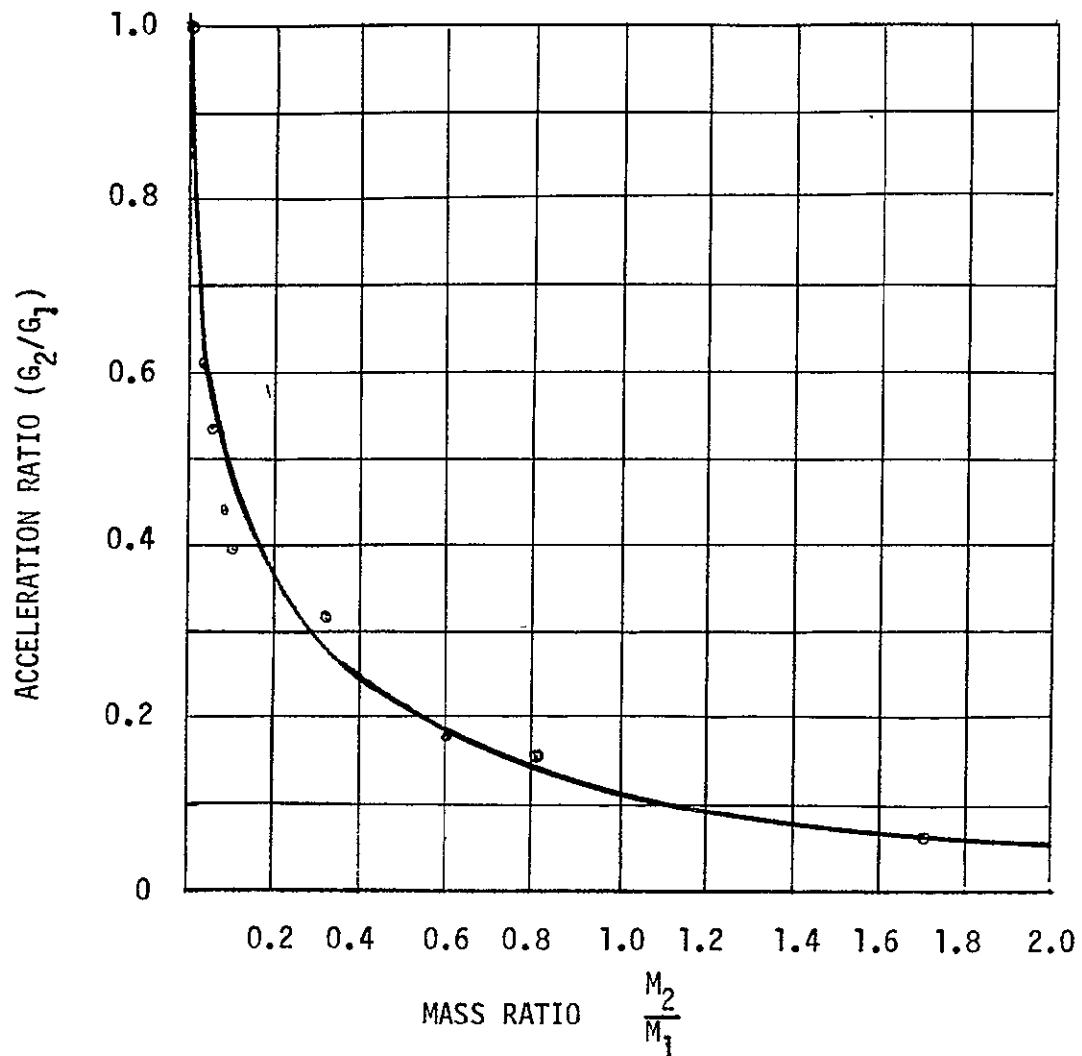
Figure III-11. Mass-Loading Effect on Acceleration Response of Shell IV, Mode 11, (m=6, n=8)
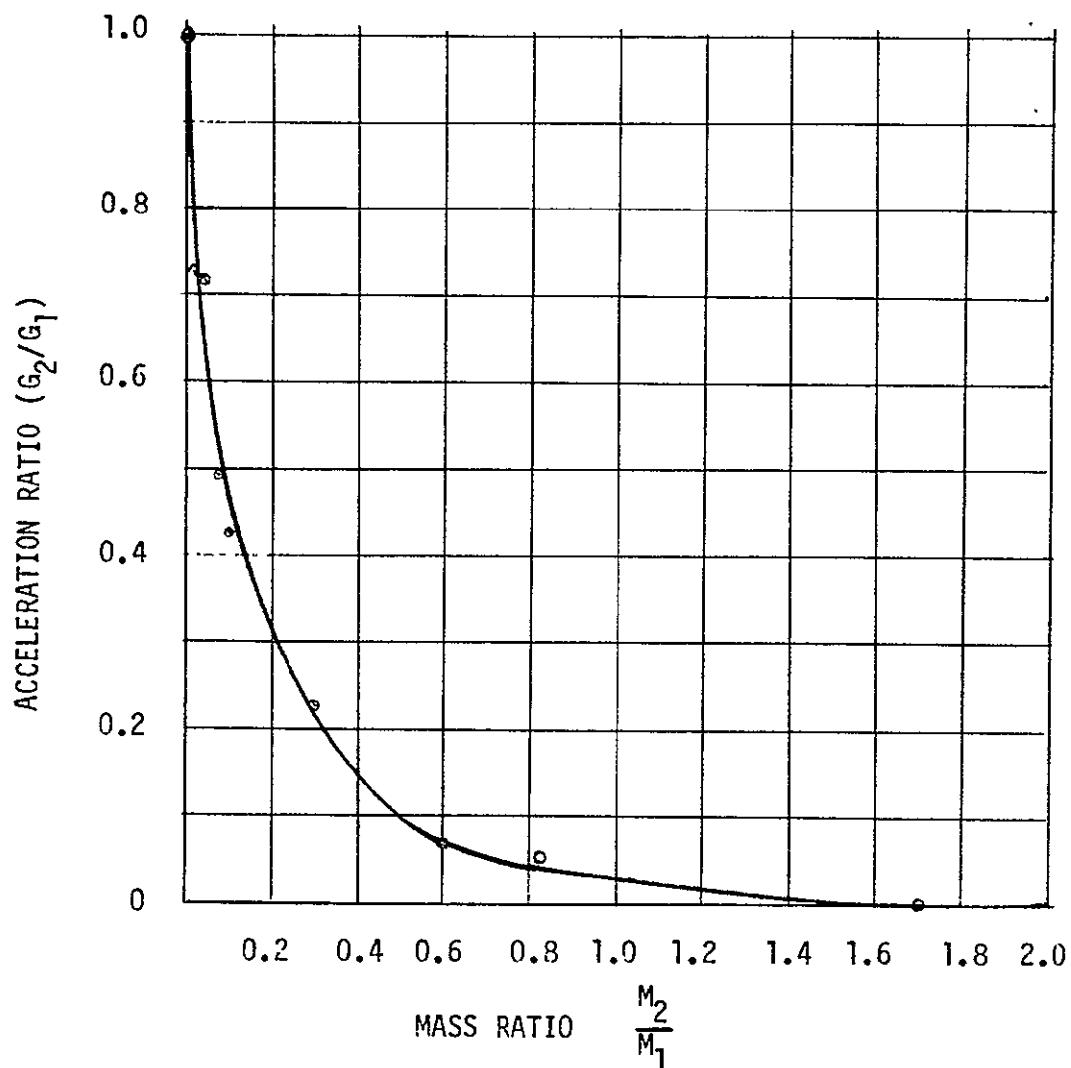
Figure III-12. Mass-Loading Effect on Acceleration Response of
Shell IV, Mode 12, (m=6, n=6)
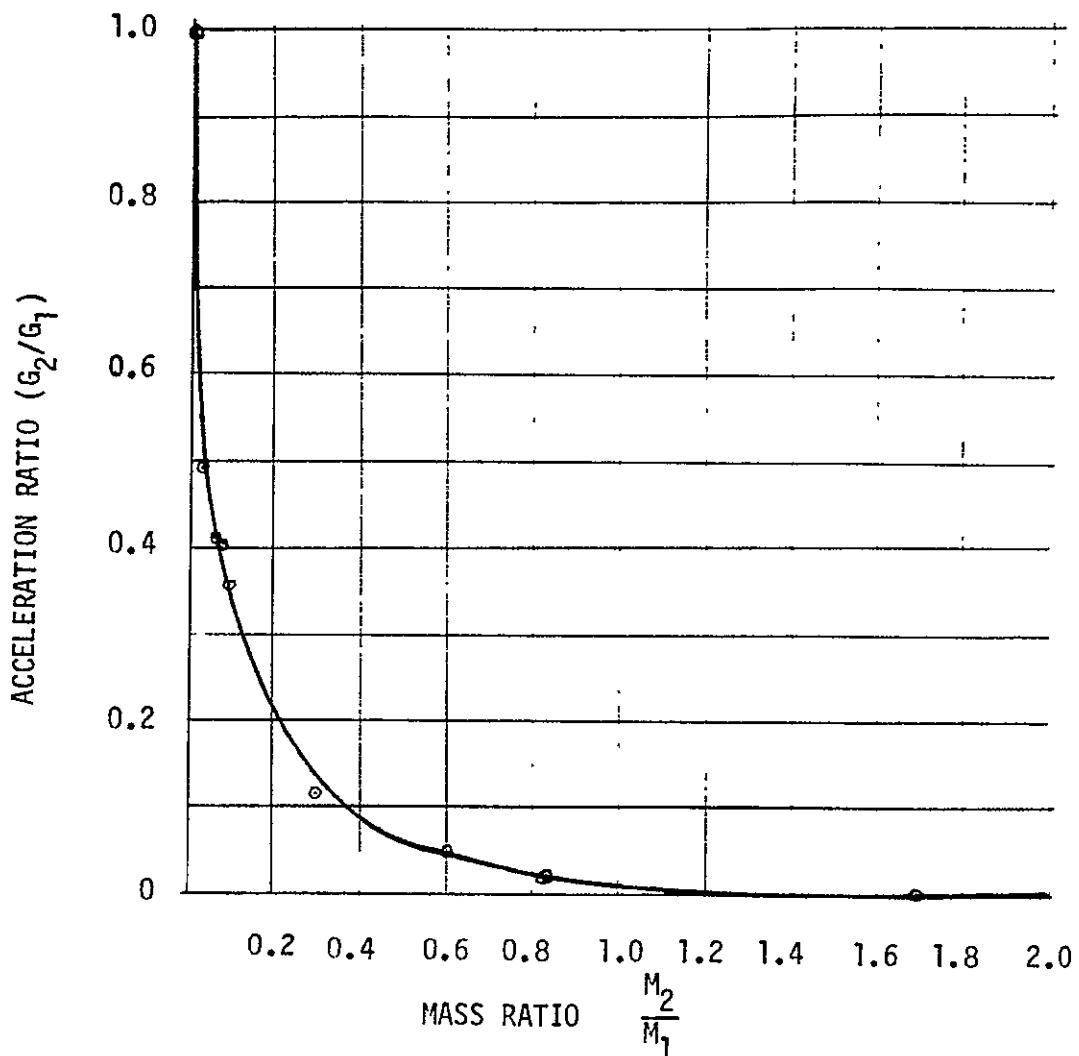
Figure III-13. Mass-Loading Effect on Acceleration Response of Shell IV, Mode 13, (m=6, n=10)
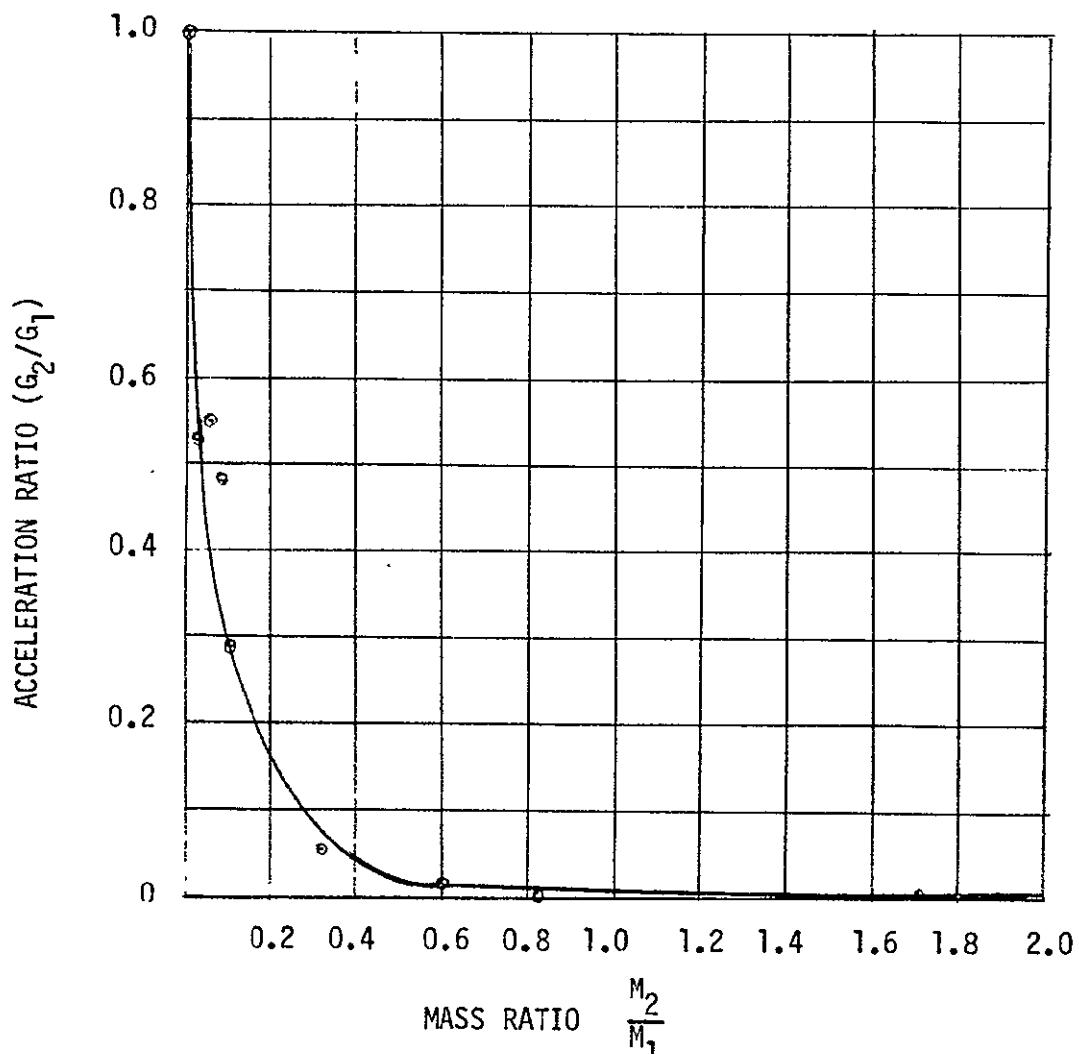
Figure III-14. Mass-Loading Effect on Acceleration Response of
Shell IV, Mode 14, (m=6, n=10)
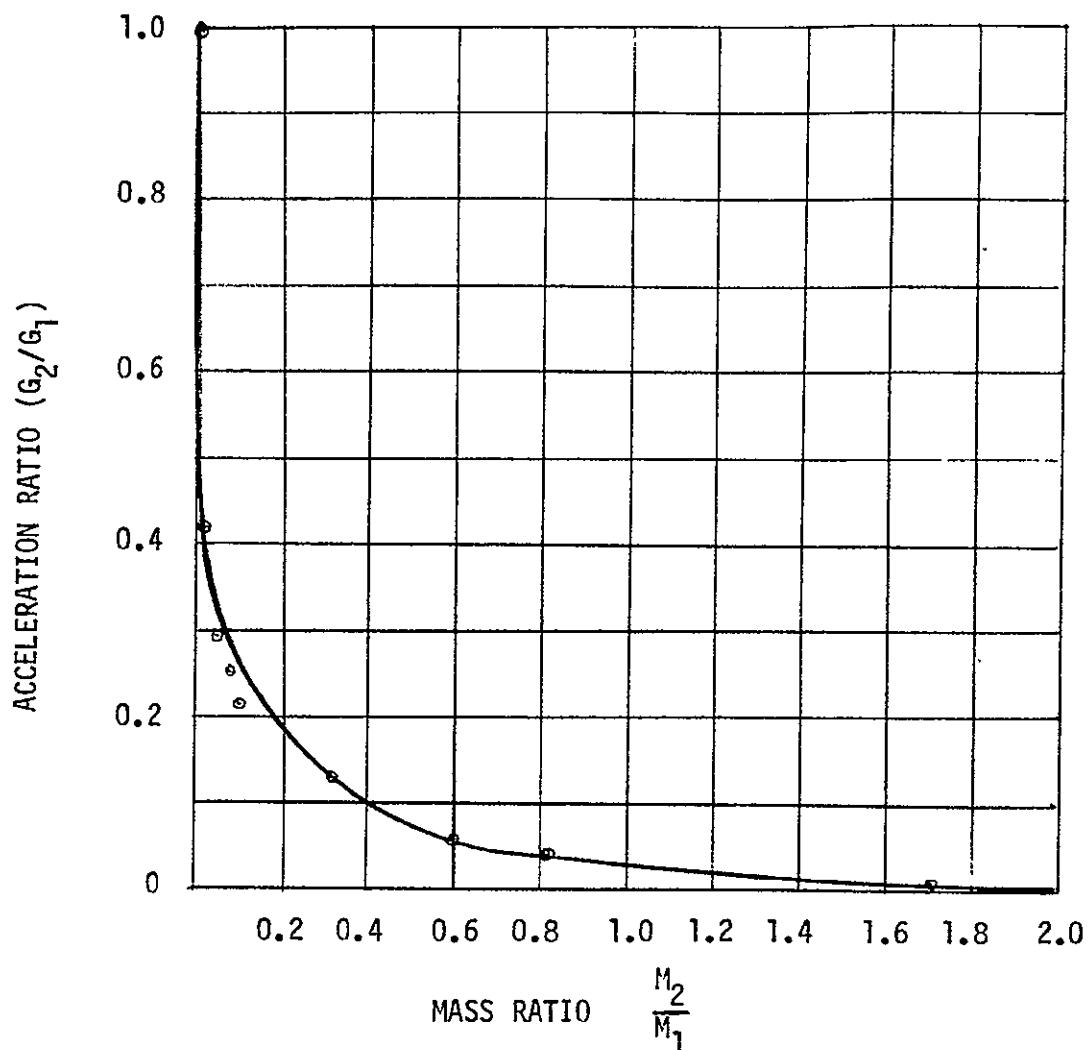
Figure III-15.   Mass-Loading Effect on Acceleration Response of
Shell IV, Mode 15, (m=3, n≈11)
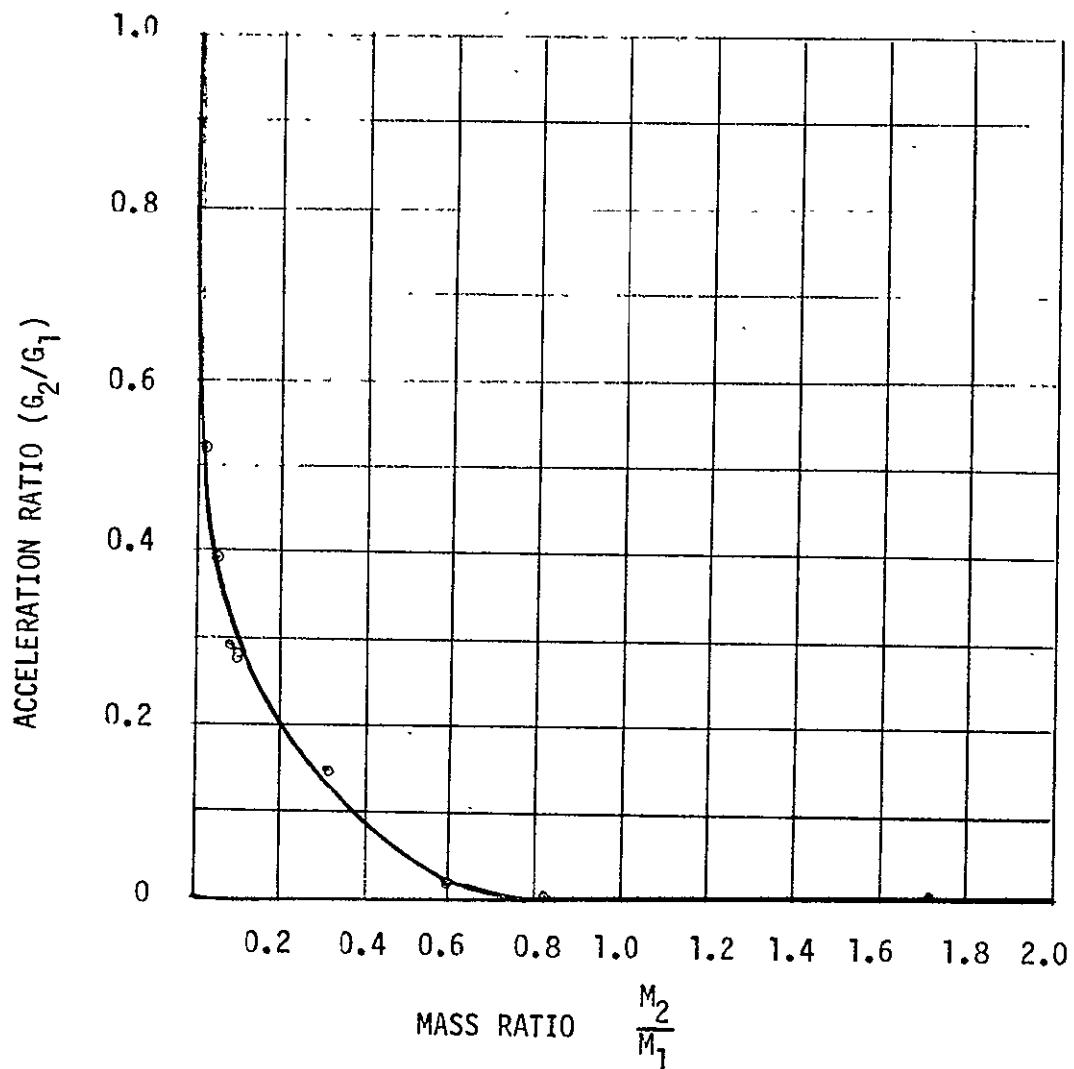
Figure III-16. Mass-Loading Effect on Acceleration Response of
Shell IV, Mode 16, (m=9, n=10)
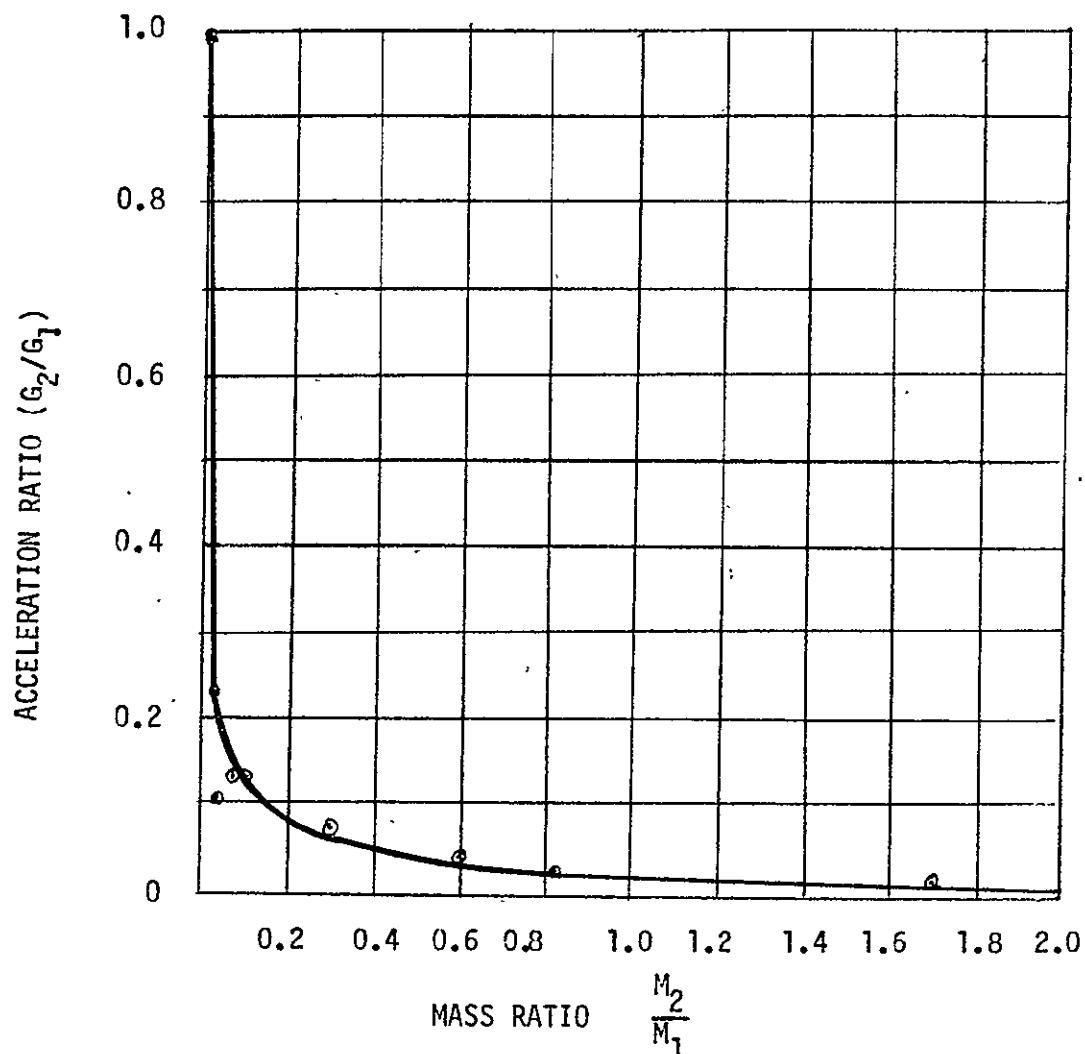
Figure III-17.   Mass-Loading Effect on Acceleration Response of
Shell IV, Mode 17, (m=9, n=10)
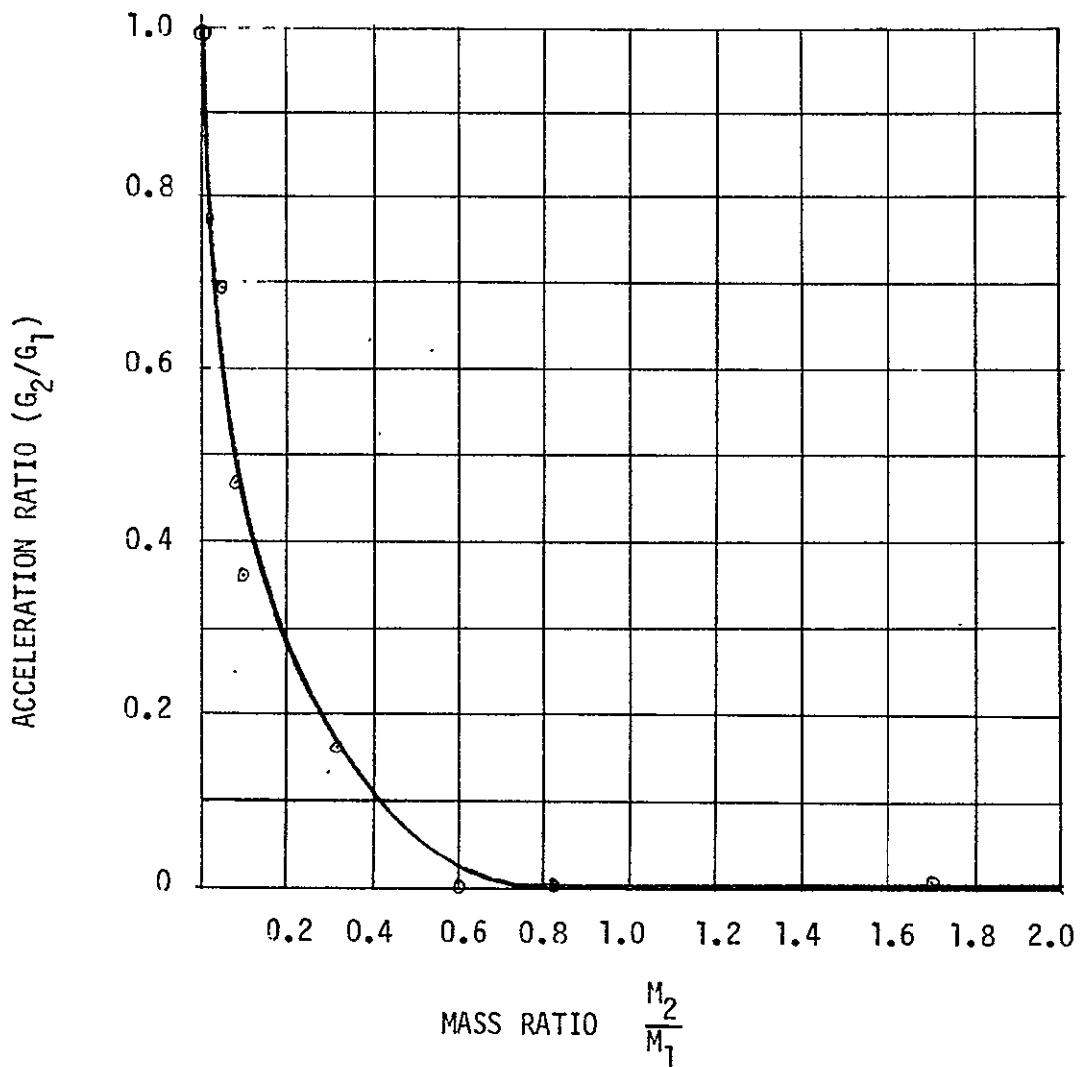
Figure III-18. Mass-Loading Effect on Acceleration Response of Shell IV, Mode 18, (m=9, n=10)
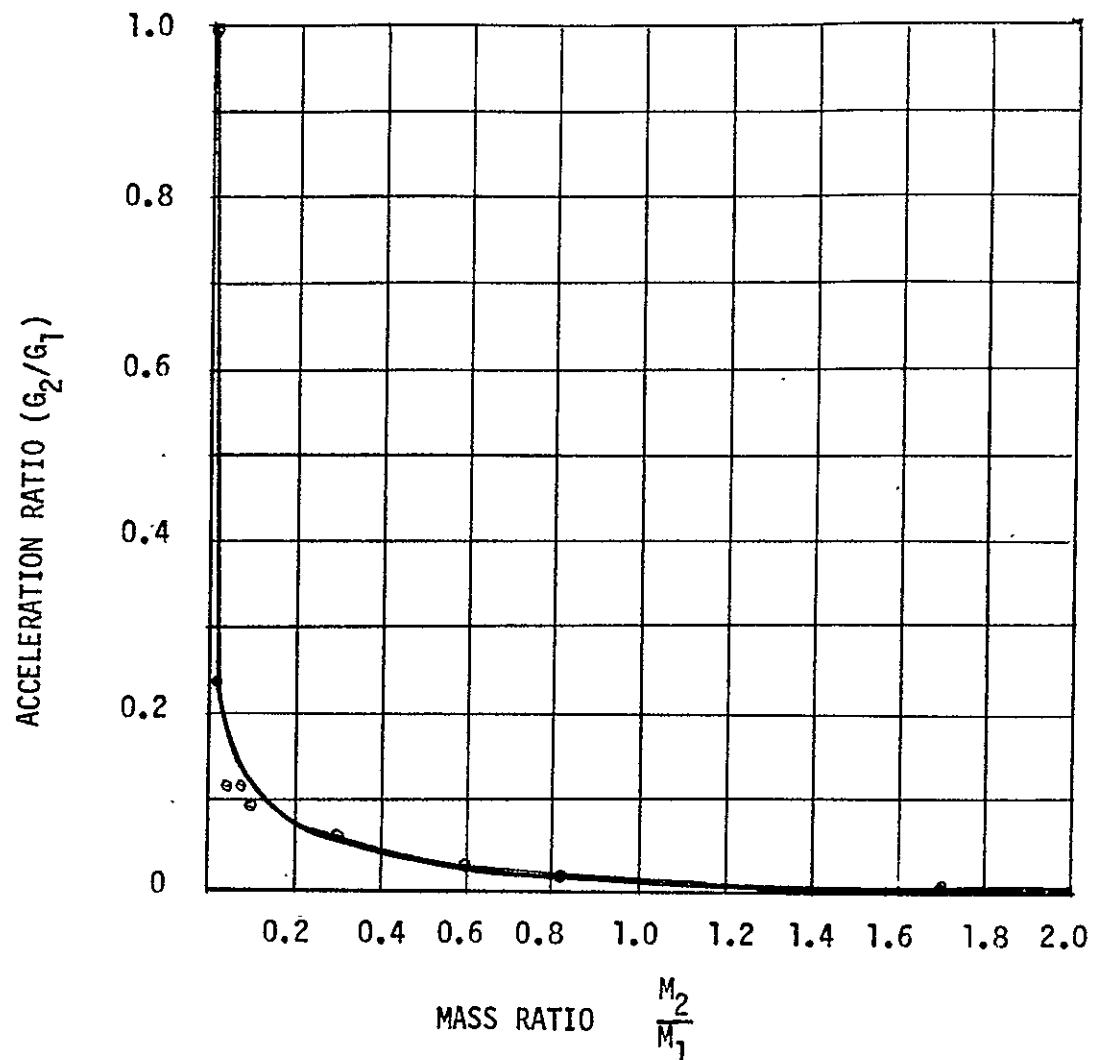
Figure III-19. Mass-Loading Effect on Acceleration Response of
Shell IV, Mode 19, (m=5, n=13)
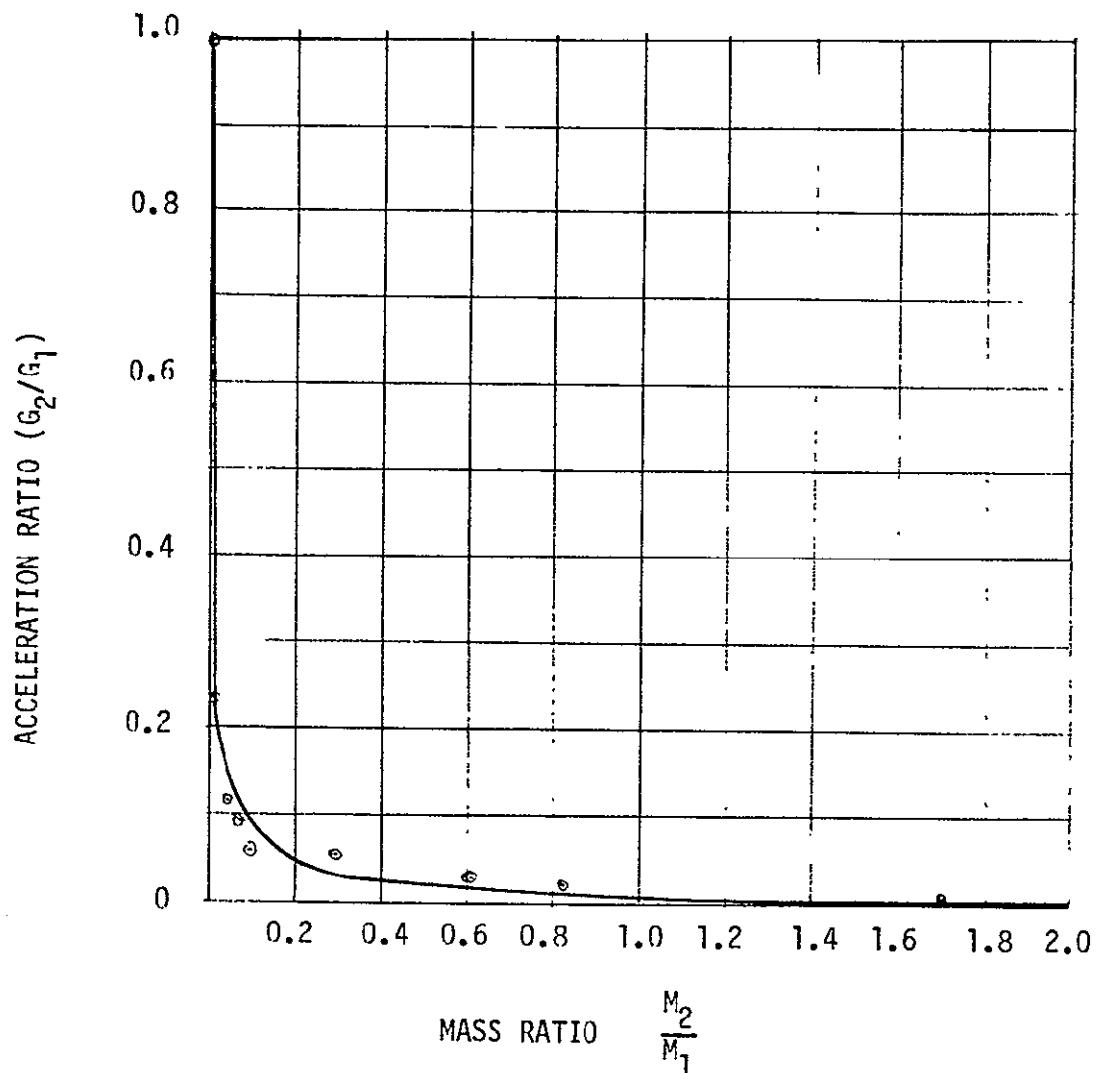
Figure III-20. Mass-Loading Effect on Acceleration Response of
Shell IV, Mode 20, (m=9, n=13)
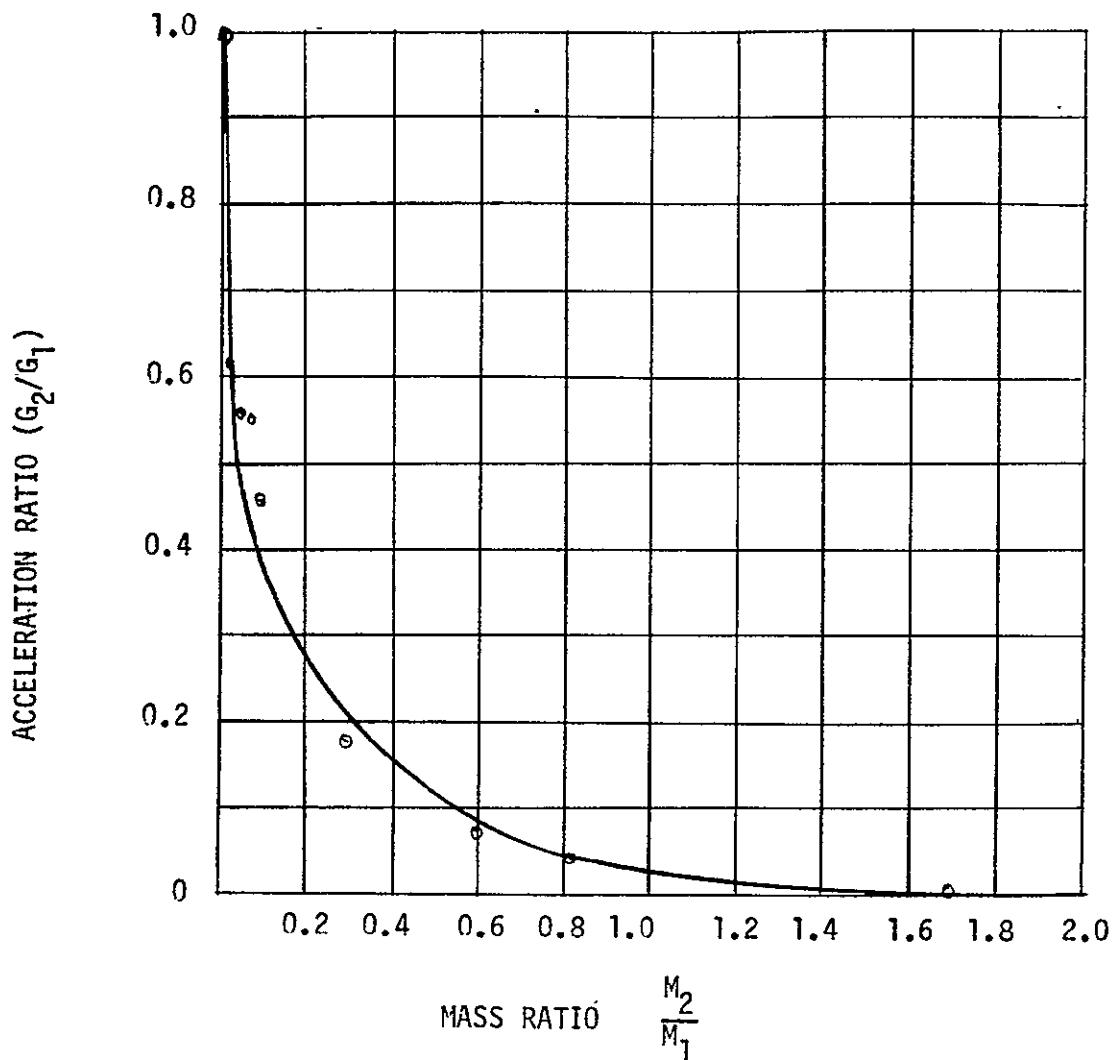
Figure III-21. Mass-Loading Effect on Acceleration Response of
Shell IV, Mode 21, (m=7, n=7)
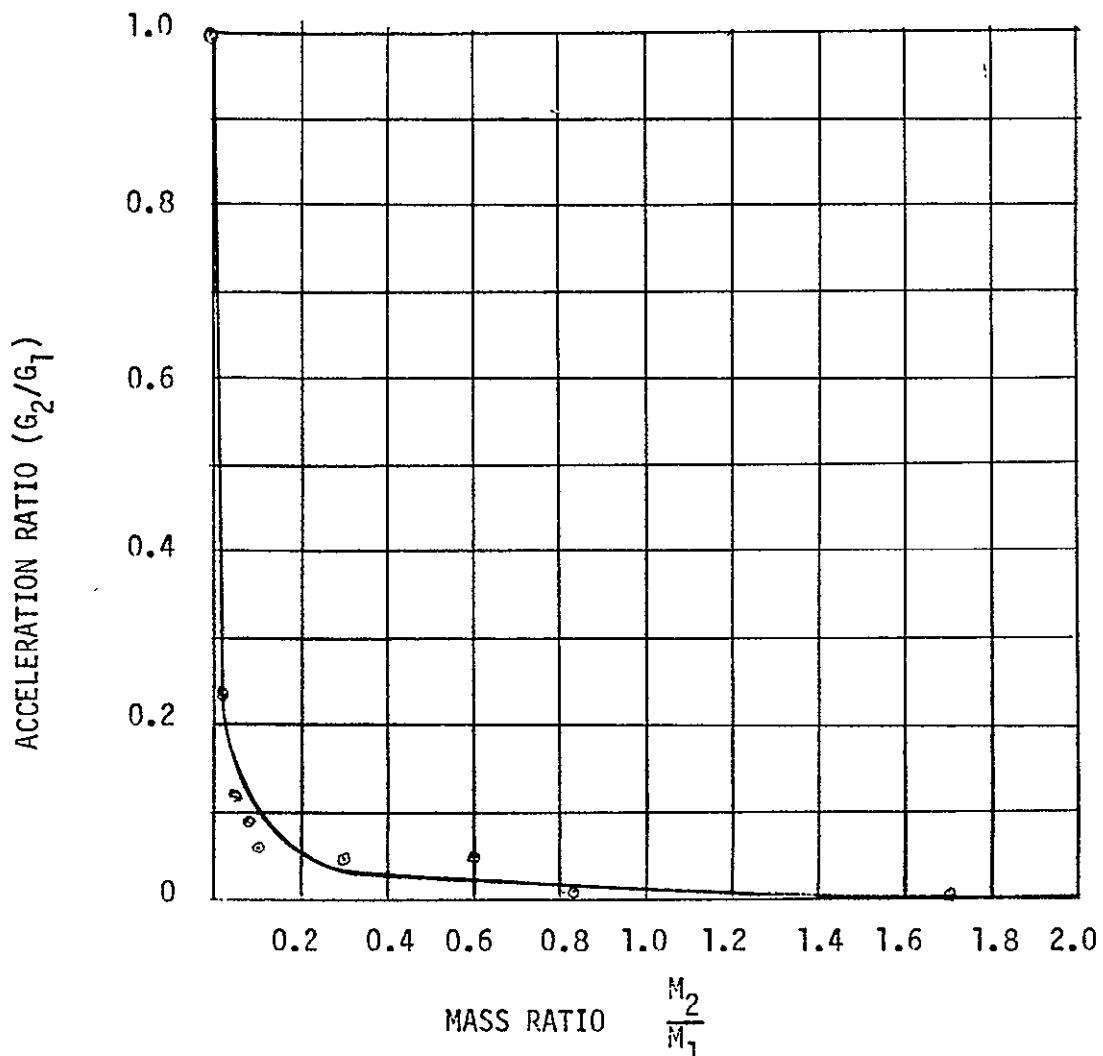
Figure III-22.   Mass-Loading Effect on Acceleration Response of
Shell IV, Mode 22, (m=5, n=10)
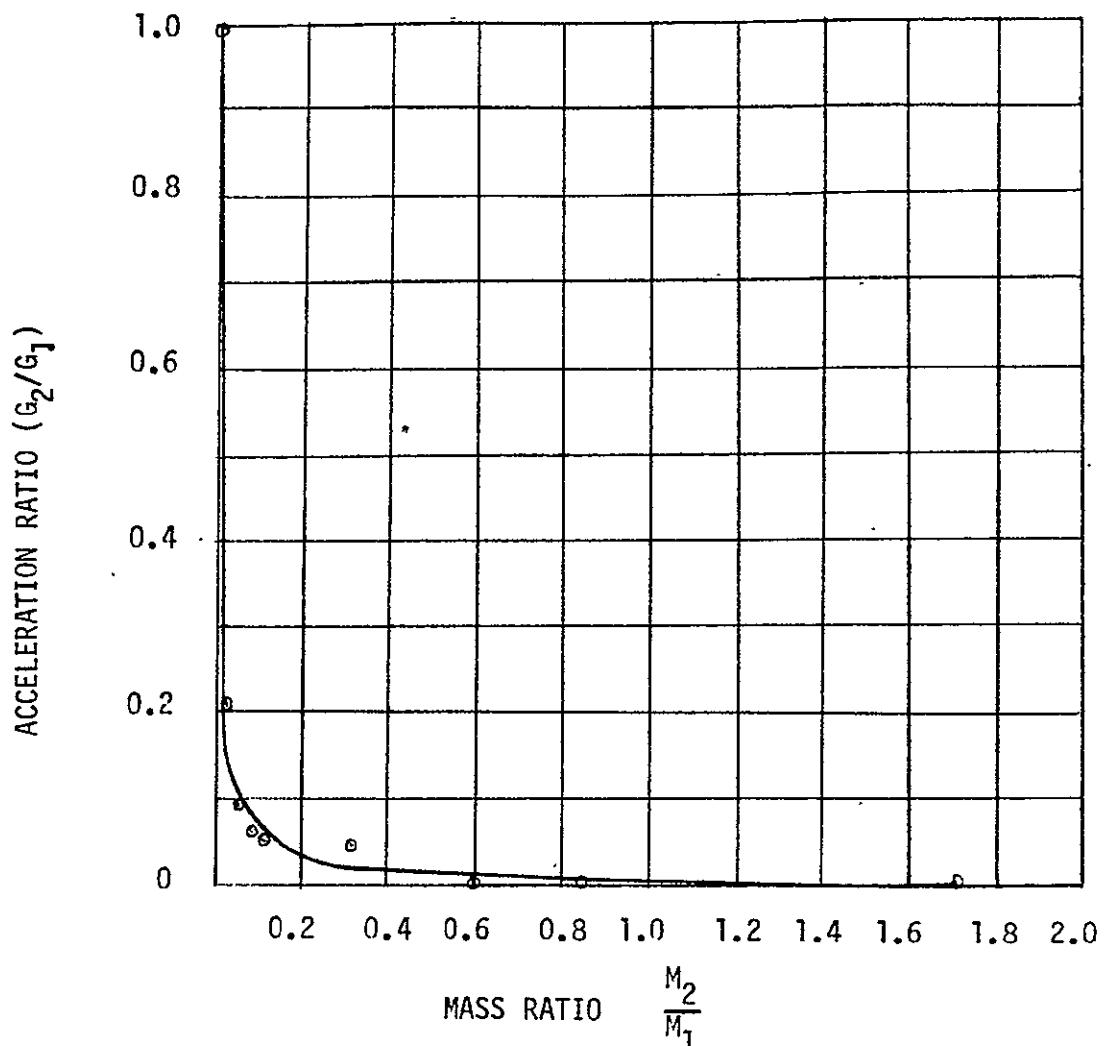
Figure III-23. Mass-Loading Effect on Acceleration Response of
Shell IV, Mode 23, (m=6, n=15)
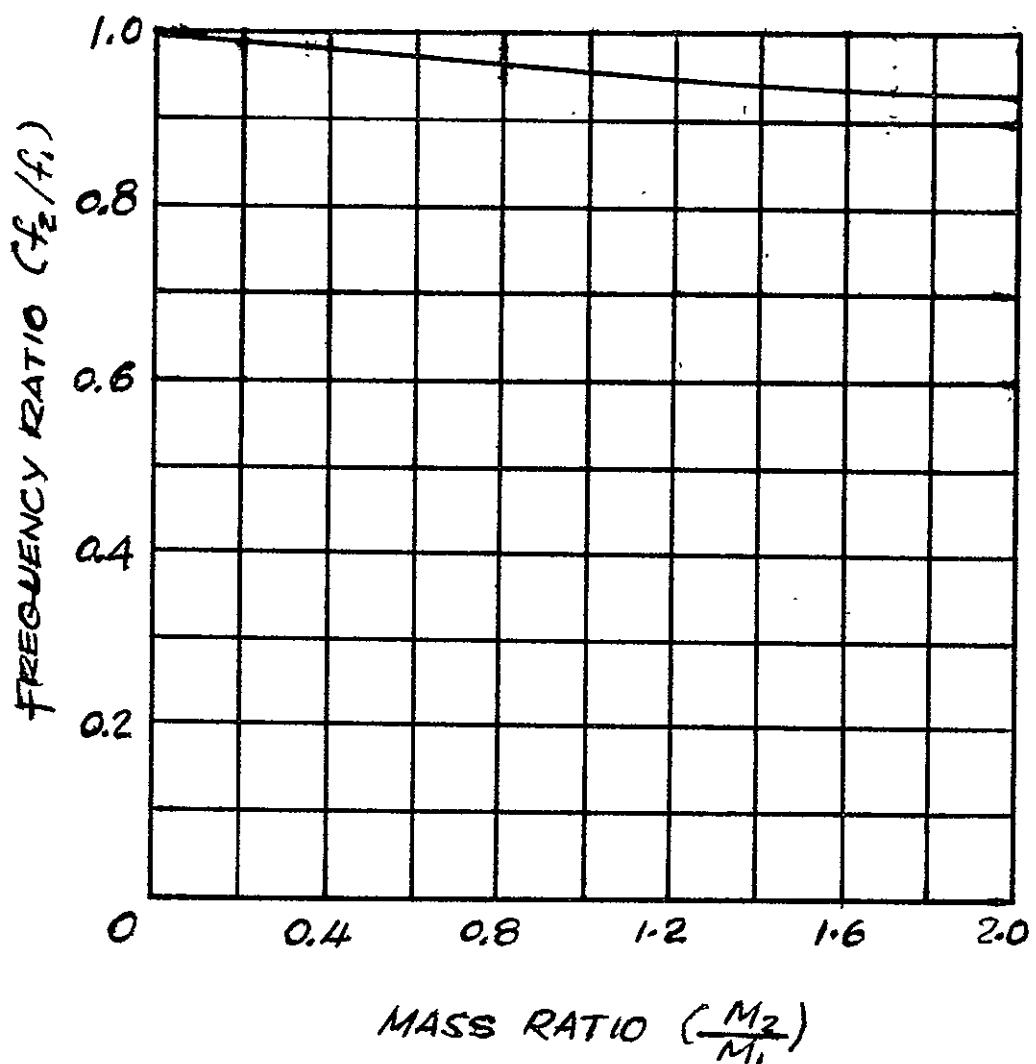
Figure III-24. Mass-Loading Effect on Acceleration Response of
Shell IV (23 Modes)

IV. MASS-LOADING EFFECTS ON FREQUENCY AND ATTENUATION
CHARACTERISTICS OF SHELLS I AND II

Table IV-1. Vibration Test Data of Shell I Excited by Electroinductance Shaker, One Accelerometer on Shell

	Run Number	0-2	1a-2	1-2	2-2	3-2	4-2	5-2	6-2	7-2	8-2
	M_2/M_1	0	0.16	0.32	0.60	0.82	1.40	1.90	2.86	3.84	4.90
Mode 1	m	1	1	1	1	1	1	1	1	1	1
	n	3	3	3	3	3	3	3	3	3	3
	Freq. cps	87.5	87.1	86.4	84.2	82.6	76.5	71.5	63.7	57.4	52.1
	f_2/f_1	1.0	0.995	0.987	0.962	0.944	0.875	0.817	0.728	0.655	0.596
	Accel. g's	2.50	2.40	2.25	2.10	1.98	1.52	1.28	0.87	0.57	0.43
	G_2/G_1	1.0	0.96	0.90	0.84	0.791	0.608	0.512	0.348	0.228	0.172
Mode 2	m	1	1	1	1	1	2	2	2	2	2
	n	2	2	2	2	2	4	4	4	4	4
	Freq. cps	128.6	128.0	127.0	124.5	123.1	119.6	118.0	115.4	114.4	113.8
	f_2/f_1	1.0	0.995	0.986	0.968	0.958	0.930	0.918	0.897	0.890	0.885
	Accel. g's	4.62	3.7	3.4	3.05	2.86	1.58	1.28	0.57	0.44	0.34
	G_2/G_1	1.0	0.800	0.735	0.660	0.619	0.342	0.277	0.123	0.095	0.074
Mode 3	m	1	1	1	1	1	3	3	3	3	3
	n	5	5	5	5	5	5	5	5	5	5
	Freq. cps	141.5	141.0	140.3	139.4	138.7	137.7	136.1	136.8	136.5	136.2
	f_2/f_1	1.0	0.995	0.991	0.985	0.980	0.972	0.962	0.966	0.965	0.963
	Accel. g's	1.75	1.64	1.55	1.35	1.23	0.99	0.47	0.46	0.34	0.27
	G_2/G_1	1.0	0.936	0.885	0.772	0.702	0.565	0.268	0.263	0.194	0.154

Table IV-1. Vibration Test Data of Shell I Excited by Electroinductance
Shaker, One Accelerometer on Shell (Cont)

	Run Number	0-2	1a-2	1-2	2-2	3-2	4-2	5-2	6-2	7-2	8-2
	M_2/M_1	0	0.16	0.32	0.60	0.82	1.40	1.90	2.86	3.84	4.90
Mode 4	·m	2	2	3	3	3	3	3	3	3	3
	n	3	3	3	3	3	6	6	6	6	6
	Freq. cps	233.9	232.2	230.7	228.5	228.1	226.7	226.1	223.2	226.7	226.3
	f_2/f_1	1.0	0.993	0.987	0.977	0.975	0.970	0.967	0.954	0.970	0.968
	Accel. (g's)	7.0	6.1	4.95	3.93	3.3	1.72	1.24	0.46	0.46	0.54
	G_2/G_1	1.0	0.870	0.707	0.561	0.471	0.246	0.177	0.066	0.066	0.077
Mode 5	m	1	1	1	1	1	2	2	3	3	3
	n	7	7	7	7	7	7	7	7	7	7
	Freq. cps.	279.0	278.6	278.2	277.3	276.1	274.9	274.3	275.1	274.9	273.0
	f_2/f_1	1.0	0.998	0.997	0.993	0.990	0.985	0.983	0.986	0.985	0.978
	Accel. (g's)	2.51	1.51	1.42	1.0	0.97	0.52	0.40	0.20	0.20	0.14
	G_2/G_1	1.0	0.601	0.561	0.398	0.386	0.207	0.160	0.080	0.080	0.056

Table IV-2. Vibration Test Data of Shell II Excited by Electroinductance
Shaker, 20 Accelerometers on Shell

	Run Number	0	1	2	3	4	5	6	7	8
	M_2/M_1	0	0.32	0.60	0.82	1.40	1.90	2.86	3.84	4.90
Mode 1	m	1	1	1	1	1	1	1	1	1
	n	3	3	3	3	3	3	3	3	3
	Freq. (cps)	86.7	85.5	82.7	81.1	74.2	70.1	62.0	55.8	49.5
	f_2/f_1	1.0	0.986	0.955	0.935	0.856	0.809	0.715	0.644	0.571
	Accel. (g's)	2.34	1.96	1.67	1.52	1.10	0.94	0.77	0.51	0.34
	G_2/G_1	1.0	0.837	0.714	0.65	0.47	0.401	0.329	0.218	0.145
Mode 2	m	1	1	1	1	2	2	2	2	2
	n	2	2	2	2	4	4	4	4	4
	Freq. (cps)	126.7	125.5	123.7	122.0	118.3	116.8	114.9	113.4	112.5
	f_2/f_1	1.0	0.990	0.976	0.963	0.935	0.922	0.907	0.895	0.888
	Accel. (g's)	2.84	2.68	2.36	2.00	1.27	1.00	0.48	0.34	0.29
	G_2/G_1	1.0	0.865	0.75	0.675	0.526	0.432	0.365	0.29	0.27
Mode 3	m	1	1	1	1	3	3	3	3	3
	n	5	5	5	5	5	5	5	5	5
	Freq. (cps)	140.9	132.9	137.6	137.4	135.8	136.0	134.9	134.7	134.5
	f_2/f_1	1.0	0.989	0.976	0.975	0.963	0.965	0.957	0.955	0.954
	Accel. (g's)	1.48	1.28	1.11	1.00	0.78	0.64	0.54	0.43	0.40
	G_2/G_1	1.0	0.865	0.75	0.675	0.526	0.432	0.365	0.29	0.27

Table IV-2. Vibration Test Data of Shell II Excited by Electroinductance
Shaker, 20 Accelerometers on Shell (Cont)

	Run Number	0	1	2	3	4	5	6	7	8
	M_2/M_1	0	0.32	0.60	0.82	1.40	1.90	2.86	3.84	4.90
Mode 4	m	2	3	3	3	3	3	3	3	3
	n	3	3	3	3	6	6	6	6	6
	Freq. (cps)	230.9	228.1	225.6	225.0	223.8	222.9	225.9	225.5	224.1
	f_2/f_1	1.0	0.988	0.975	0.974	0.968	0.965	0.977	0.975	0.970
	Accel. (g's)	5.45	4.25	2.25	1.85	1.04	0.94	0.53	0.55	0.47
	G_2/G_1	1.0	0.78	0.413	0.34	0.191	0.172	0.097	0.101	0.086
Mode 5	m	1	1	1	1	2	2	3	3	3
	n	7	7	7	7	7	7	7	7	7
	Freq. (cps)	275.9	274.1	271.6	271.0	268.7	267.6	269.4	268.6	268.2
	f_2/f_1	1.0	0.993	0.983	0.982	0.974	0.969	0.976	0.973	0.972
	Accel. (g's)	2.78	1.48	1.02	0.62	0.28	0.16	0.11	0.08	0.07
	G_2/G_1	1.0	0.532	0.367	0.223	0.101	0.058	0.040	0.029	0.025
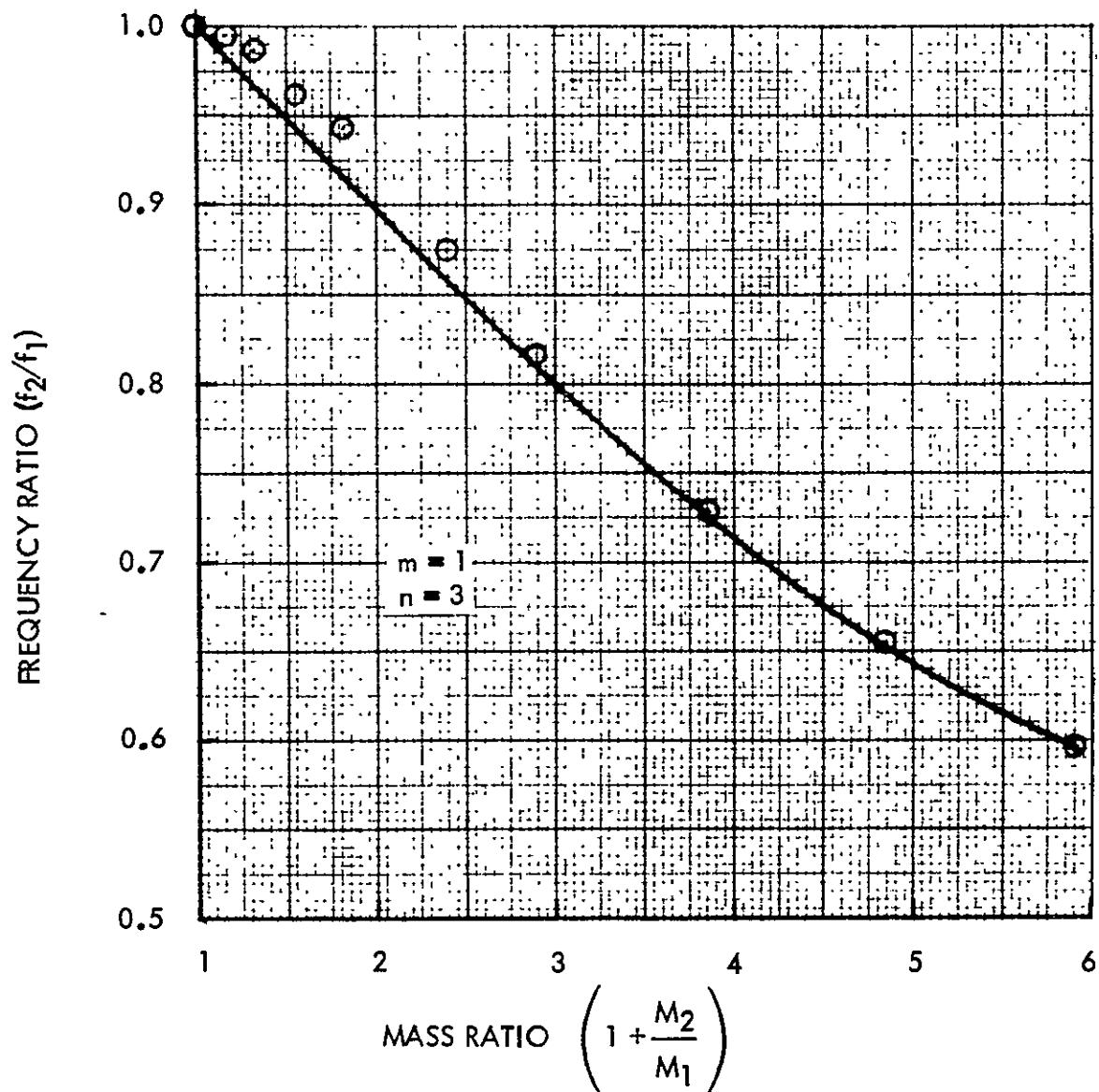
Figure IV-1. Mass-Loading Effect on Natural Frequencies of
Shell I, Mode 1
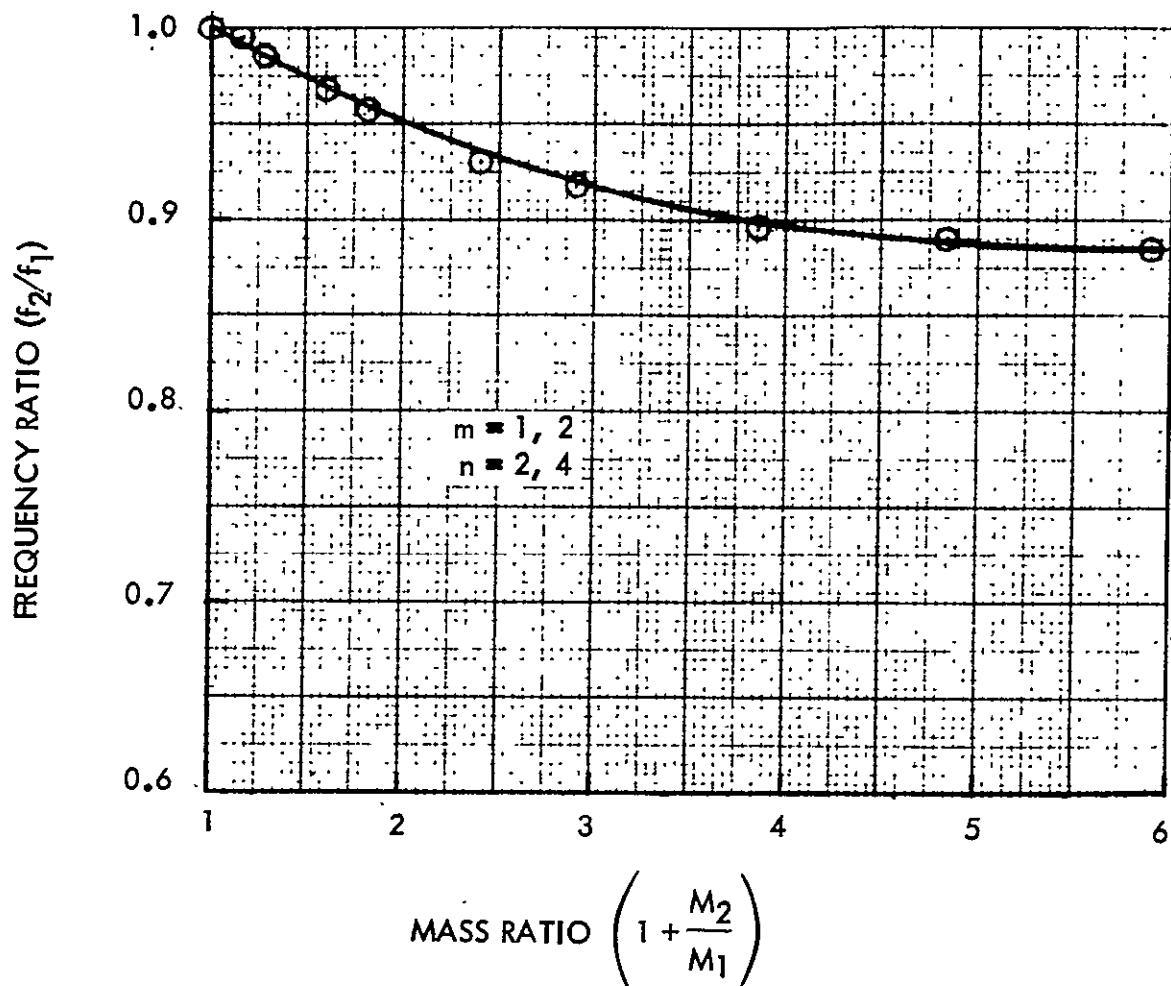
Figure IV-2. Mass-Loading Effect on Natural Frequencies of
Shell I, Mode 2
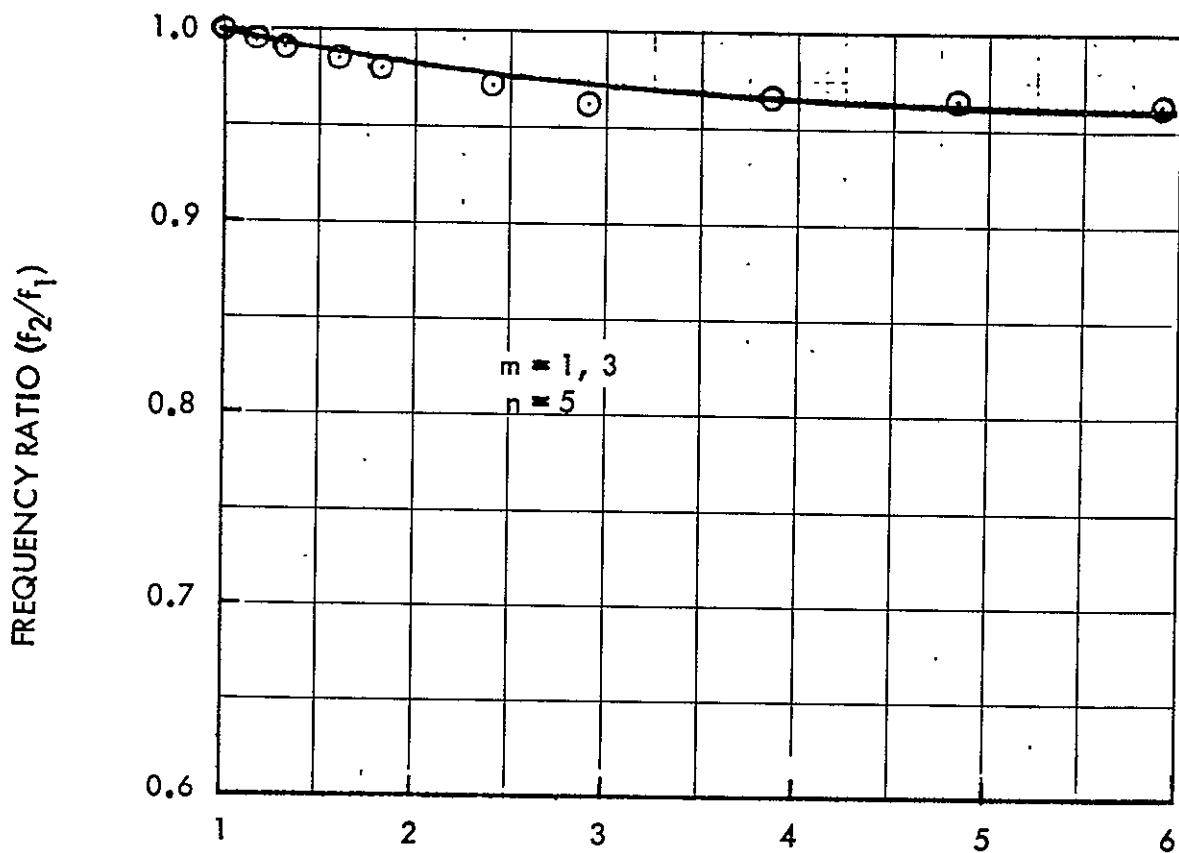
Figure IV-3. Mass-Loading Effect on Natural Frequencies of
Shell I, Mode 3
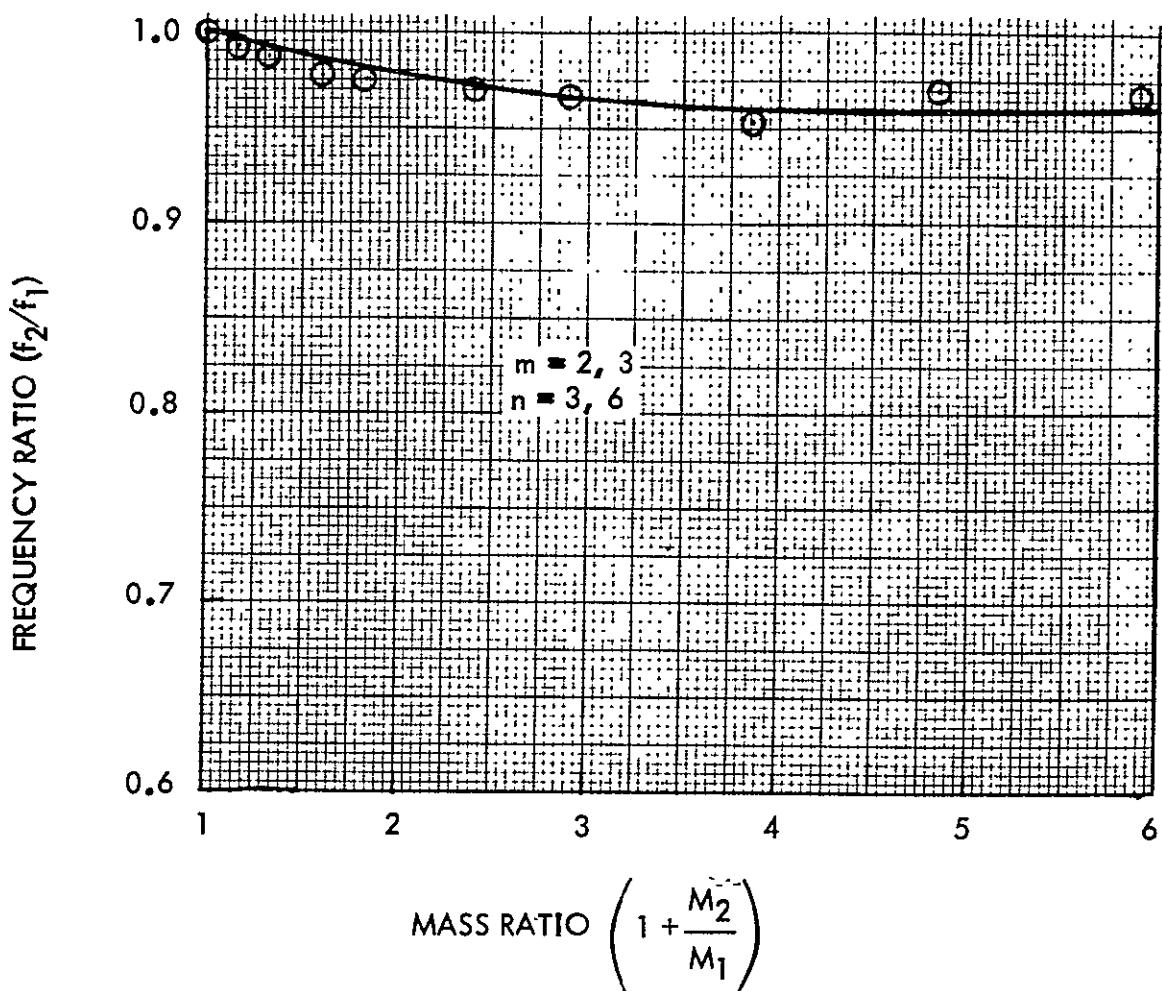
Figure IV-4. Mass-Loading Effect on Natural Frequencies of
Shell I, Mode 4
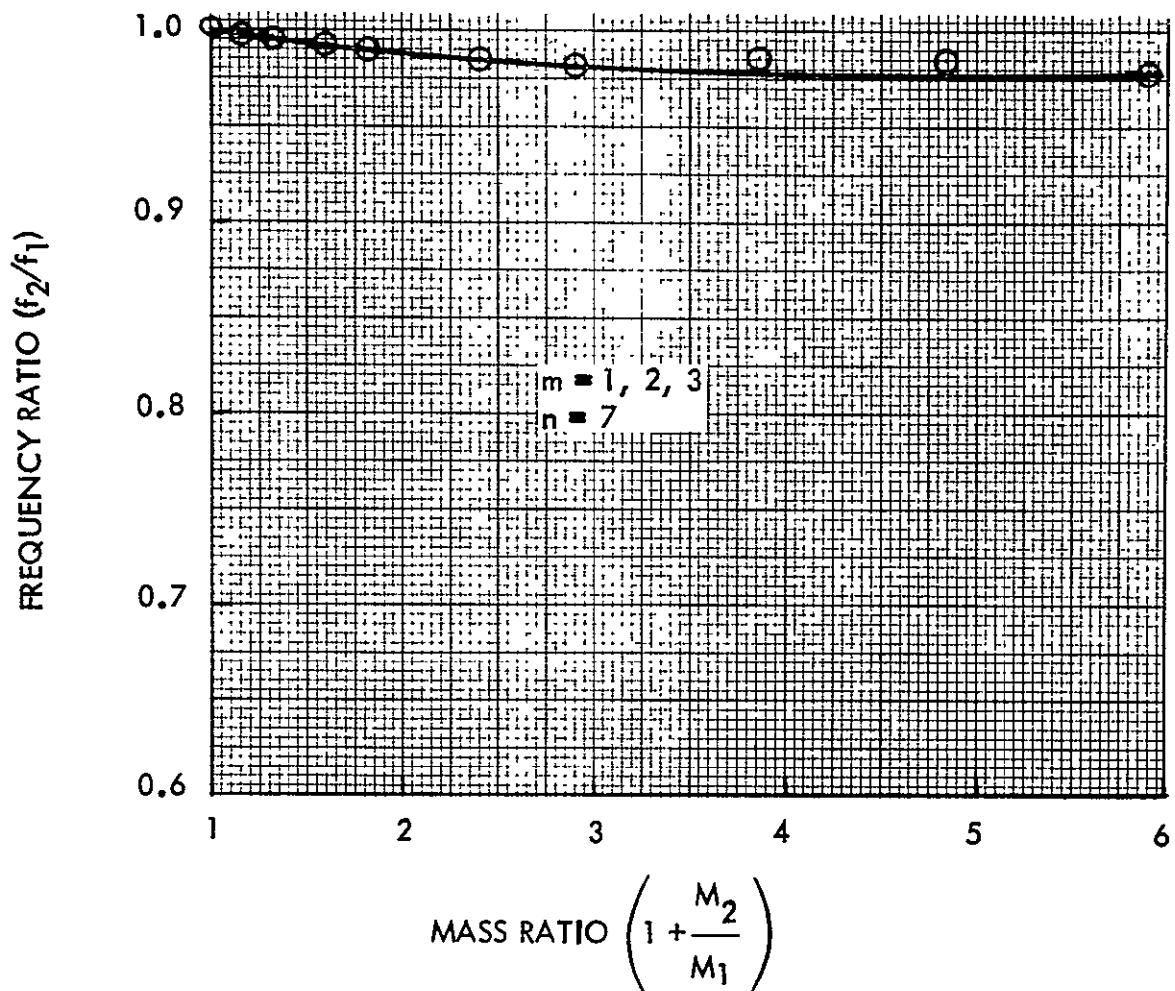
Figure IV-5. Mass-Loading Effect on Natural Frequencies of
Shell I, Mode 5
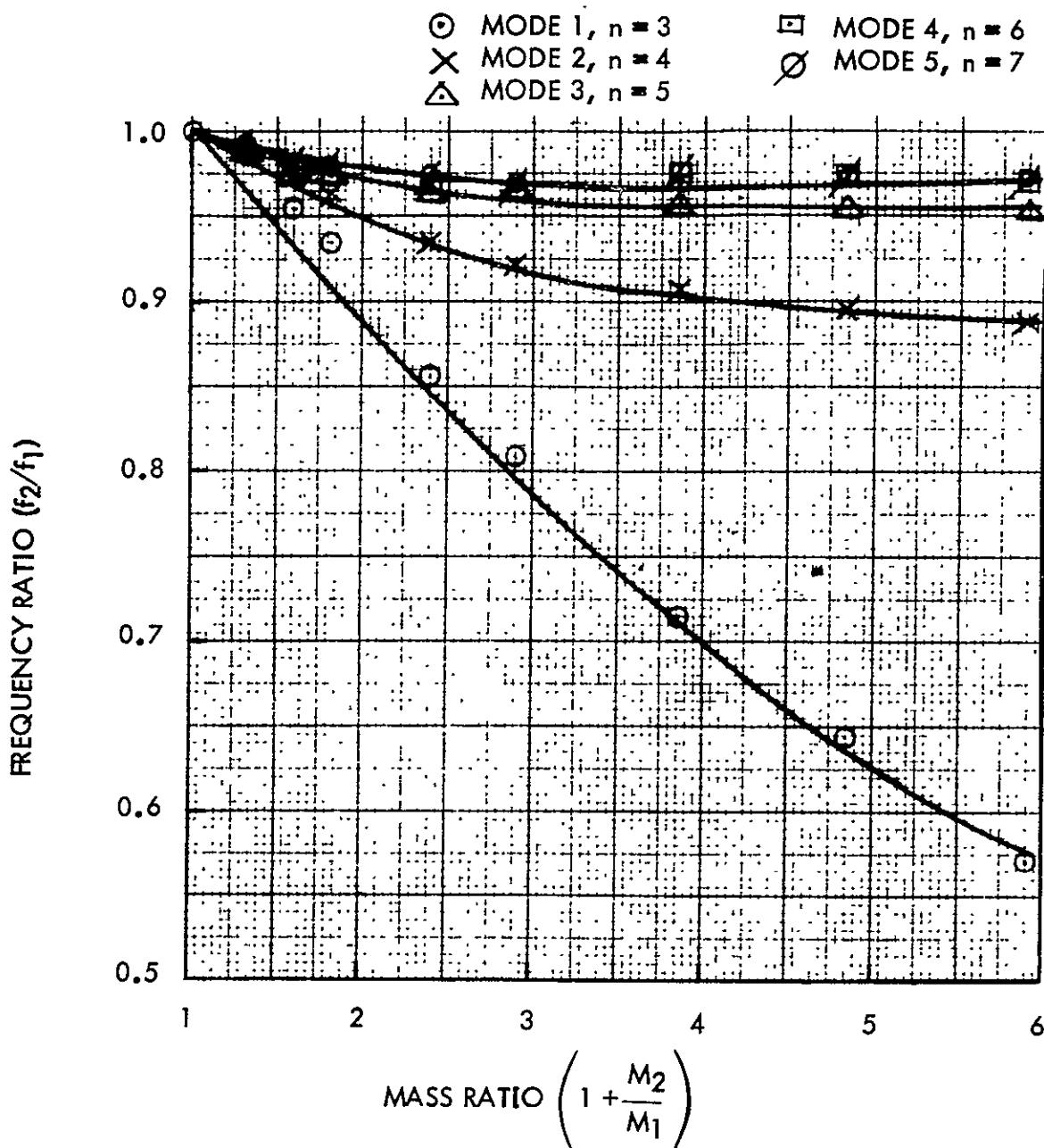
Figure IV-6. Mass-Loading Effect on Natural Frequencies of Shell II
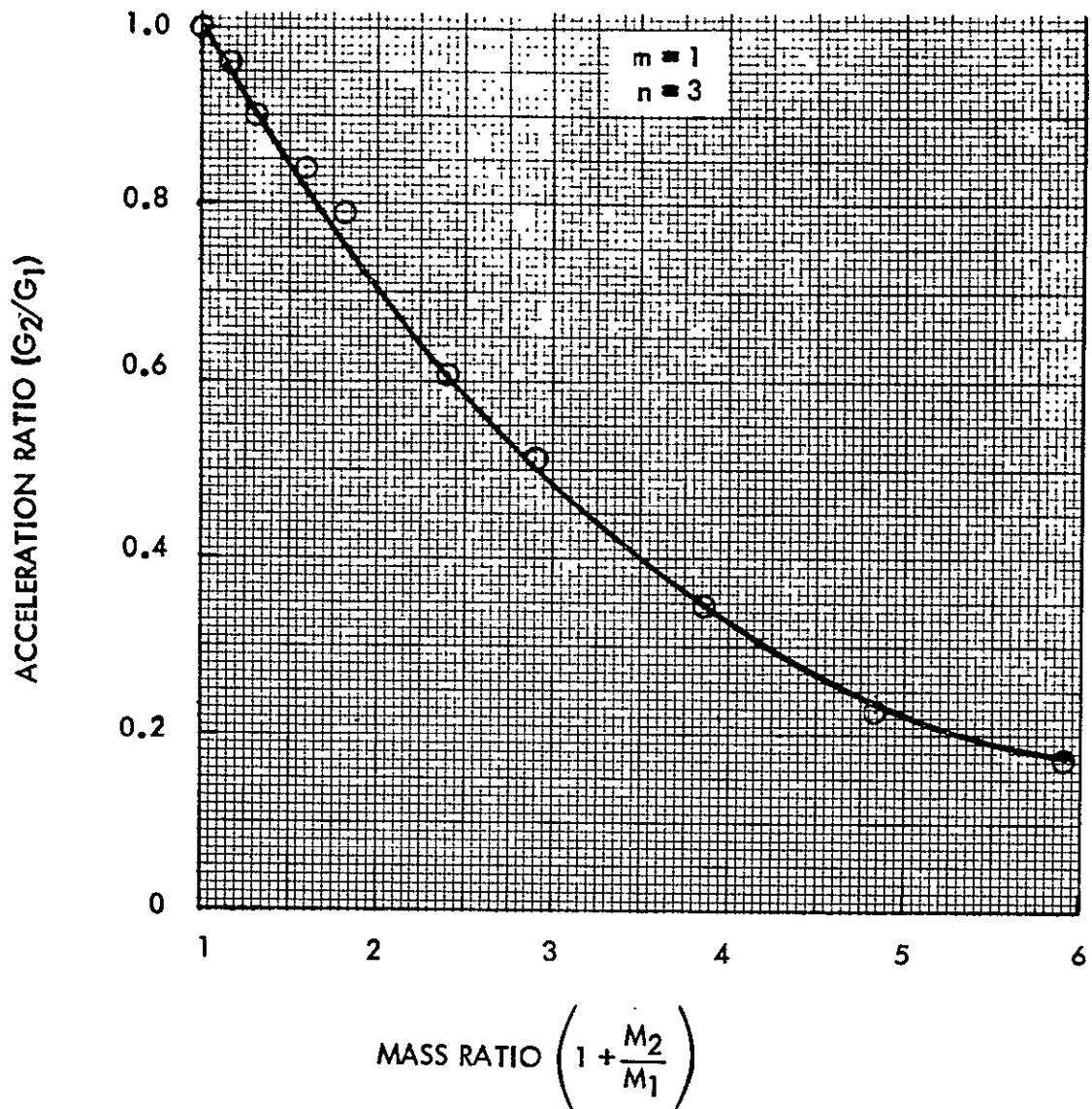
Figure IV-7.   Mass-Loading Effect on Acceleration Response of
Shell I, Mode 1
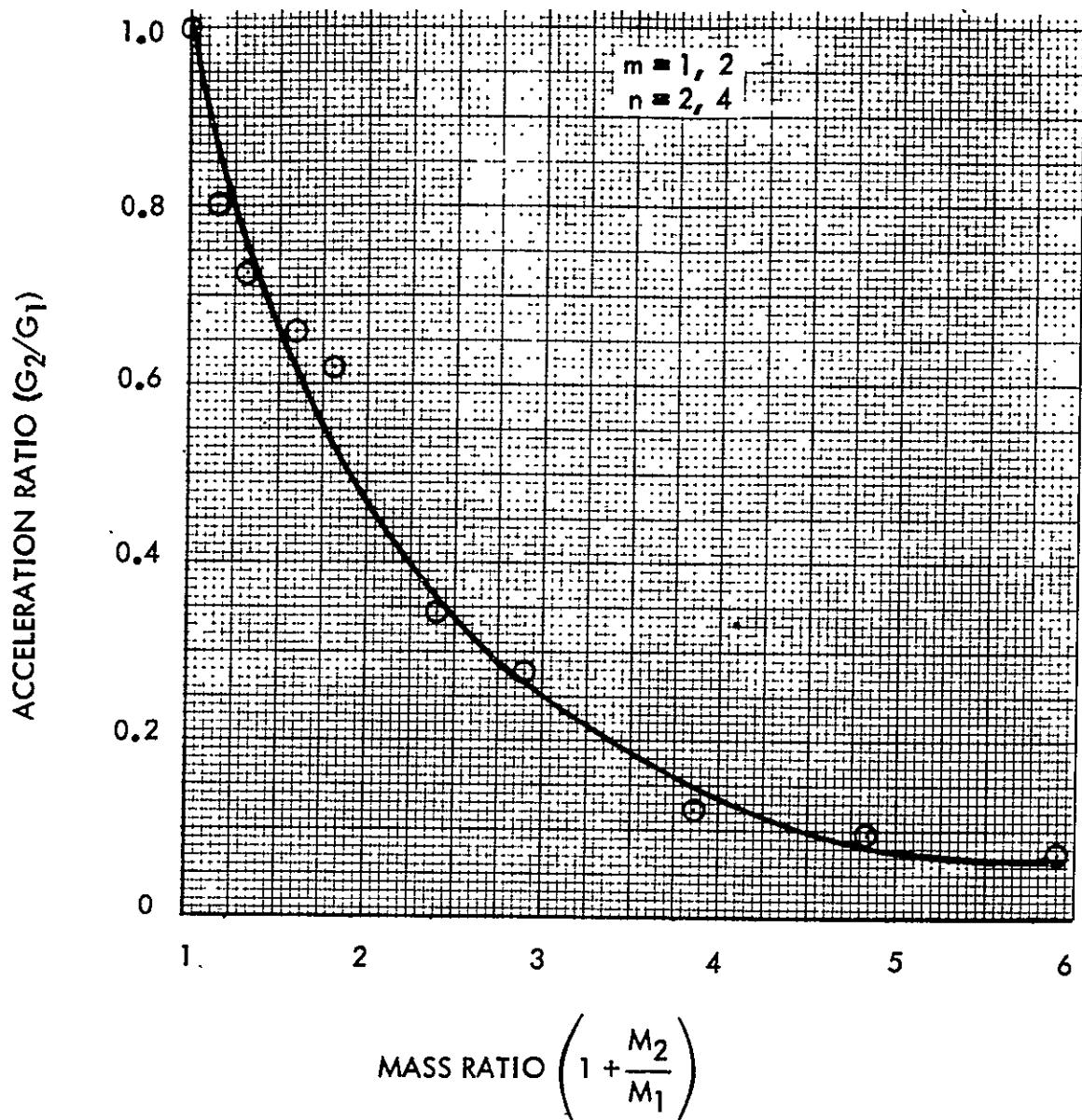
Figure IV-8. Mass-Loading Effect on Acceleration Response of
Shell I, Mode 2
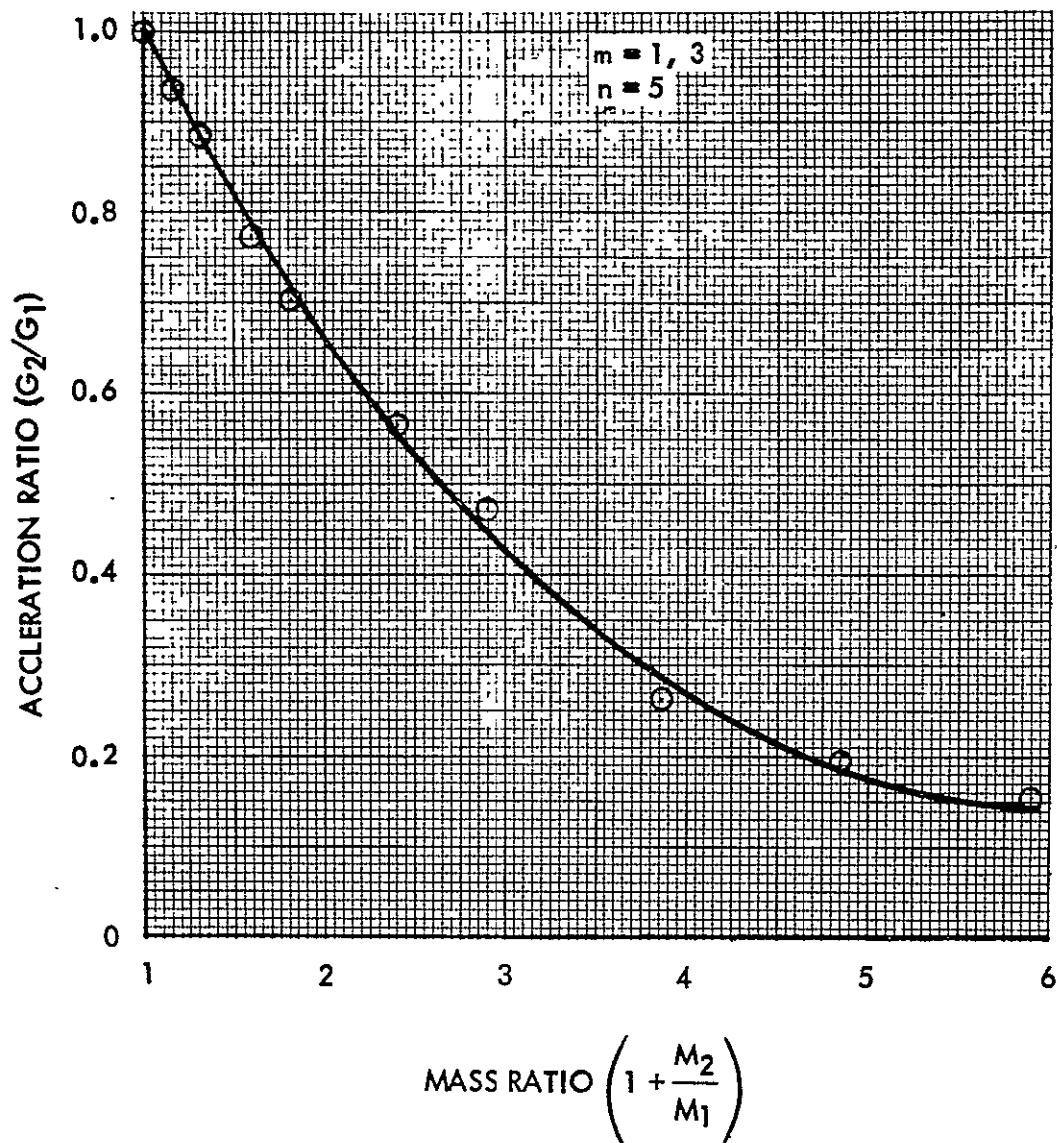
Figure IV-9. Mass-Loading Effect on Acceleration Response of
Shell I, Mode 3
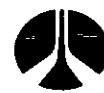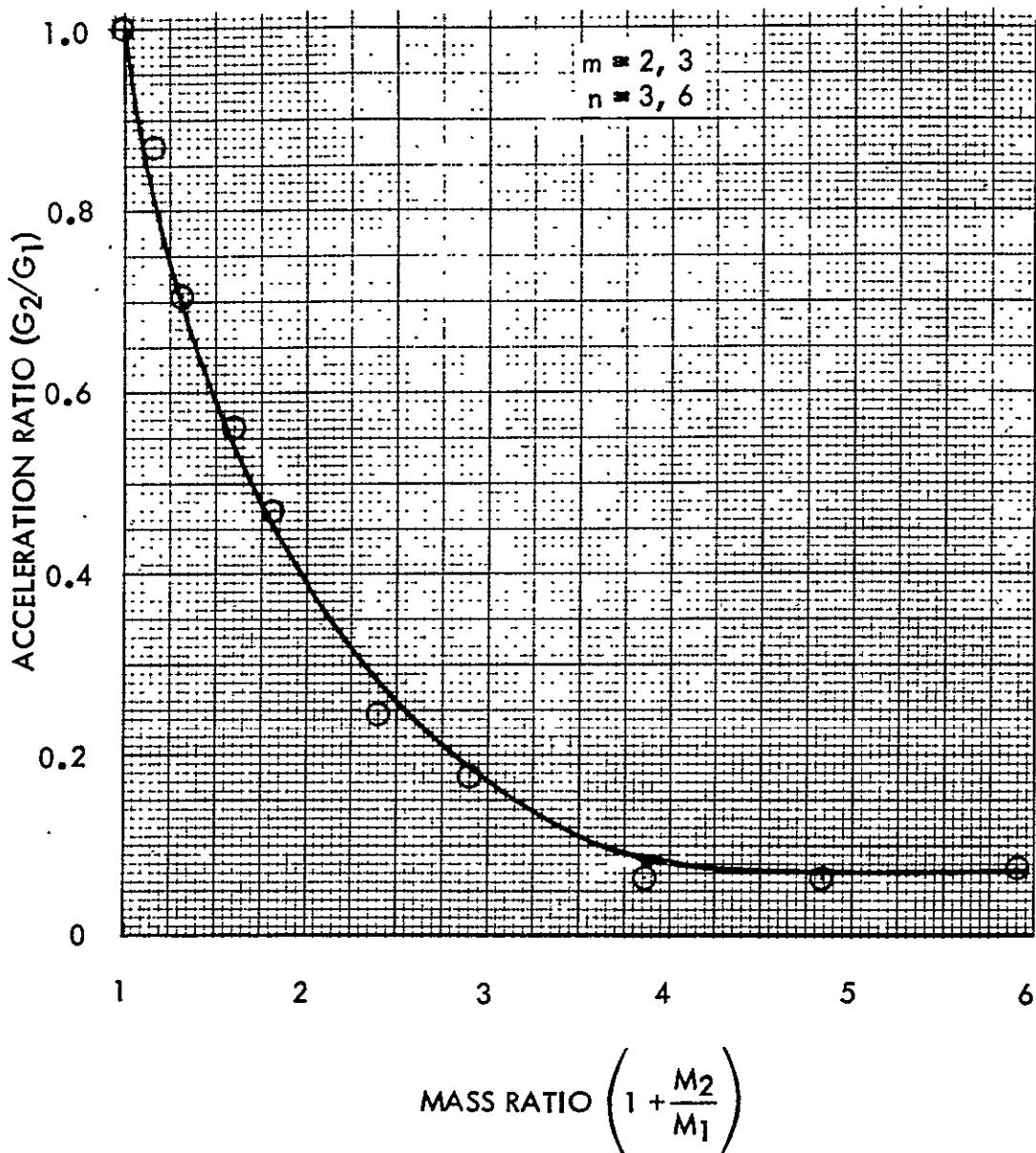
Figure IV-10. Mass-Loading Effect on Acceleration Response of
Shell I, Mode 4
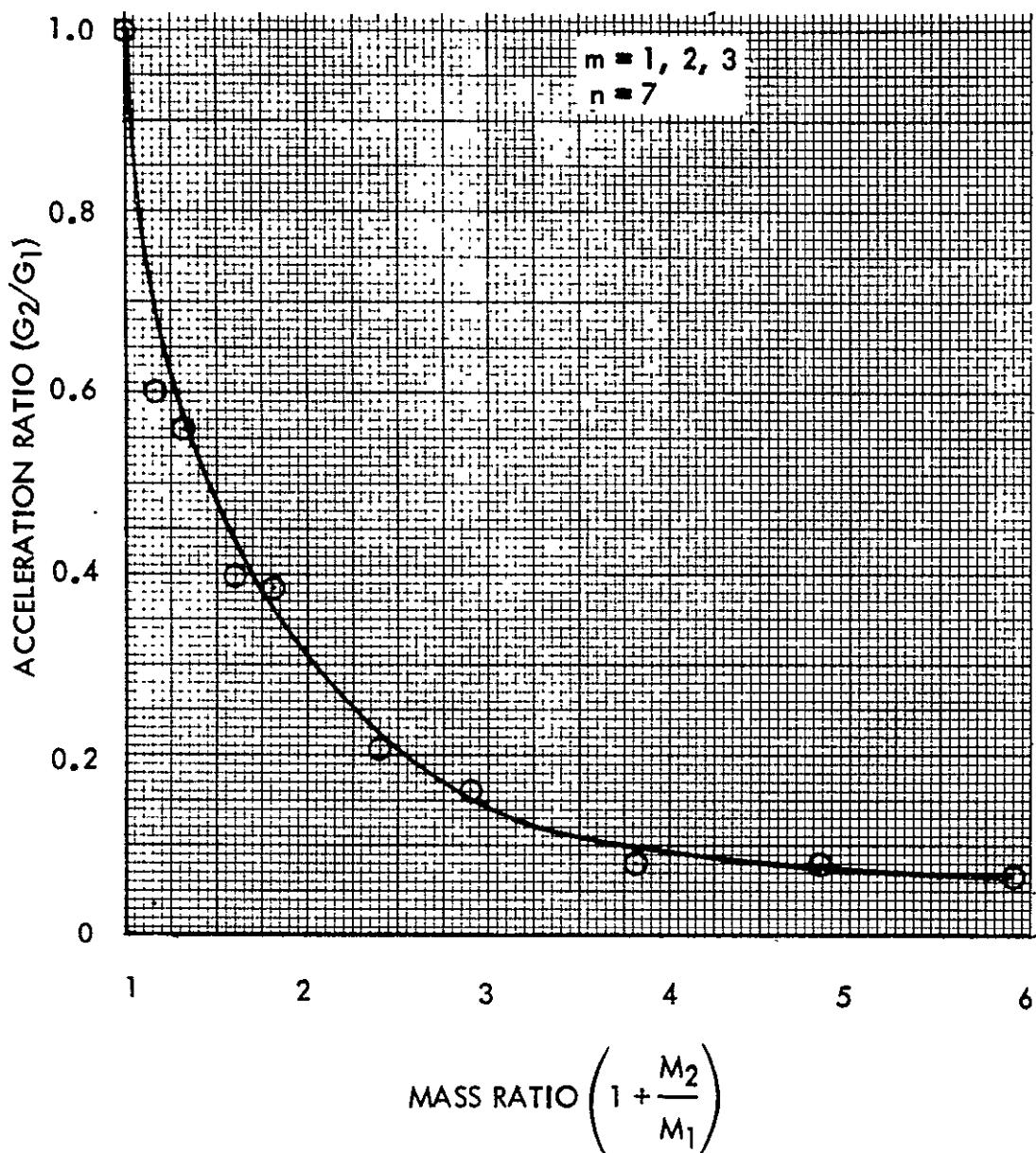
Figure IV-11. Mass-Loading Effect on Acceleration Response of
Shell I, Mode 5
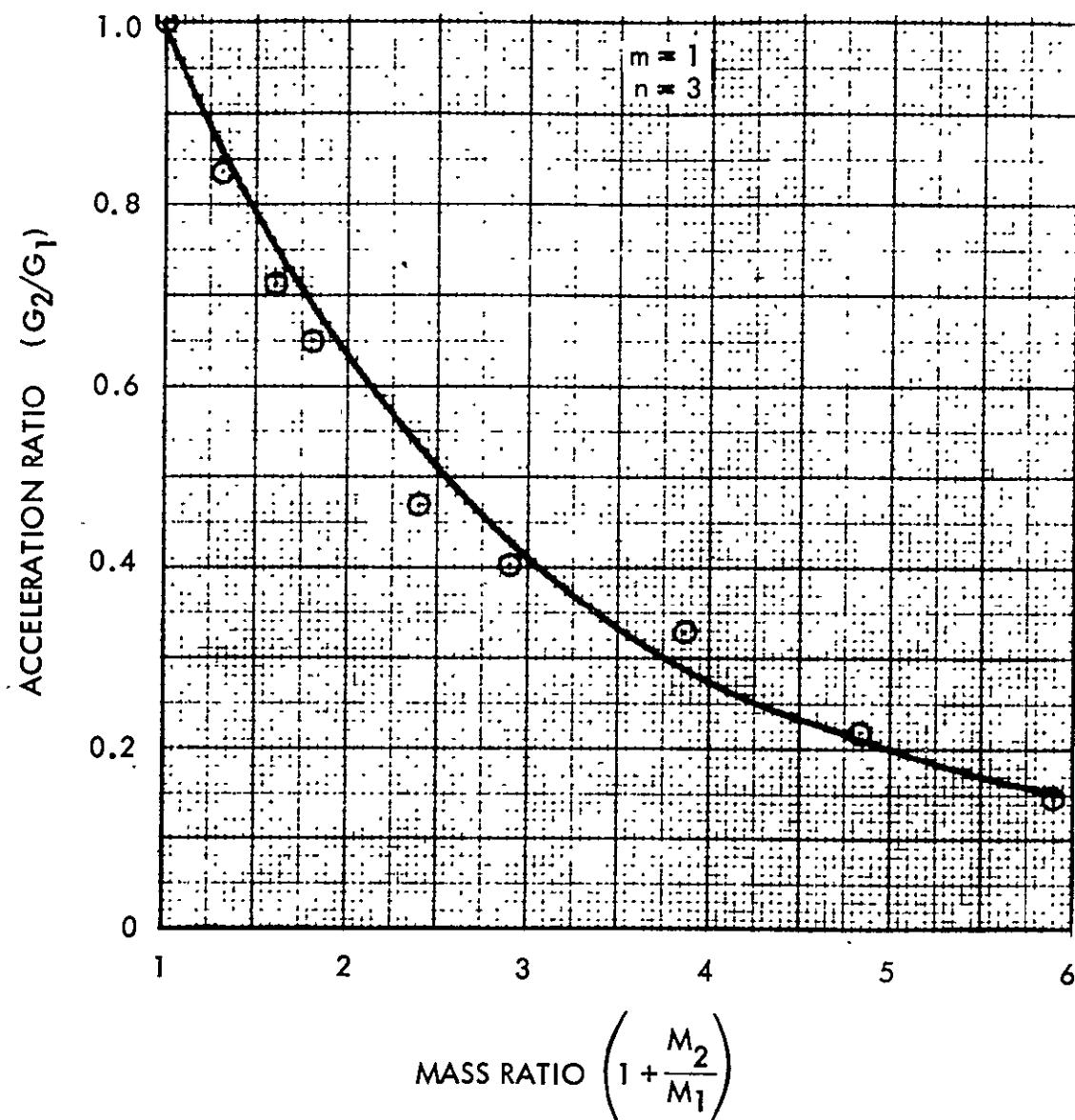
Figure IV-12. Mass-Loading Effect on Acceleration Response of Shell II, Mode 1
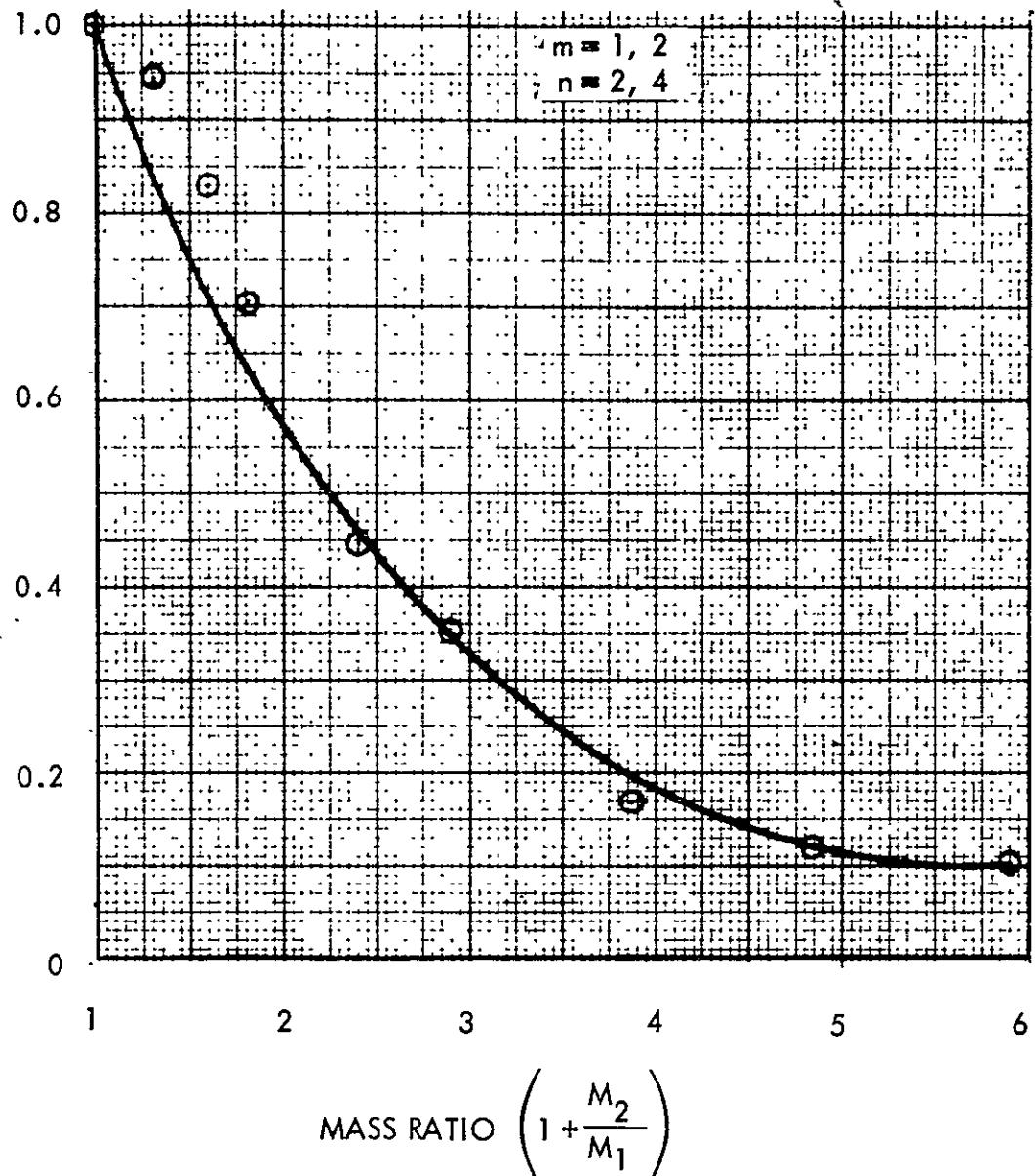
Figure IV-13. Mass-Loading Effect on Acceleration Response of
Shell II, Mode 2
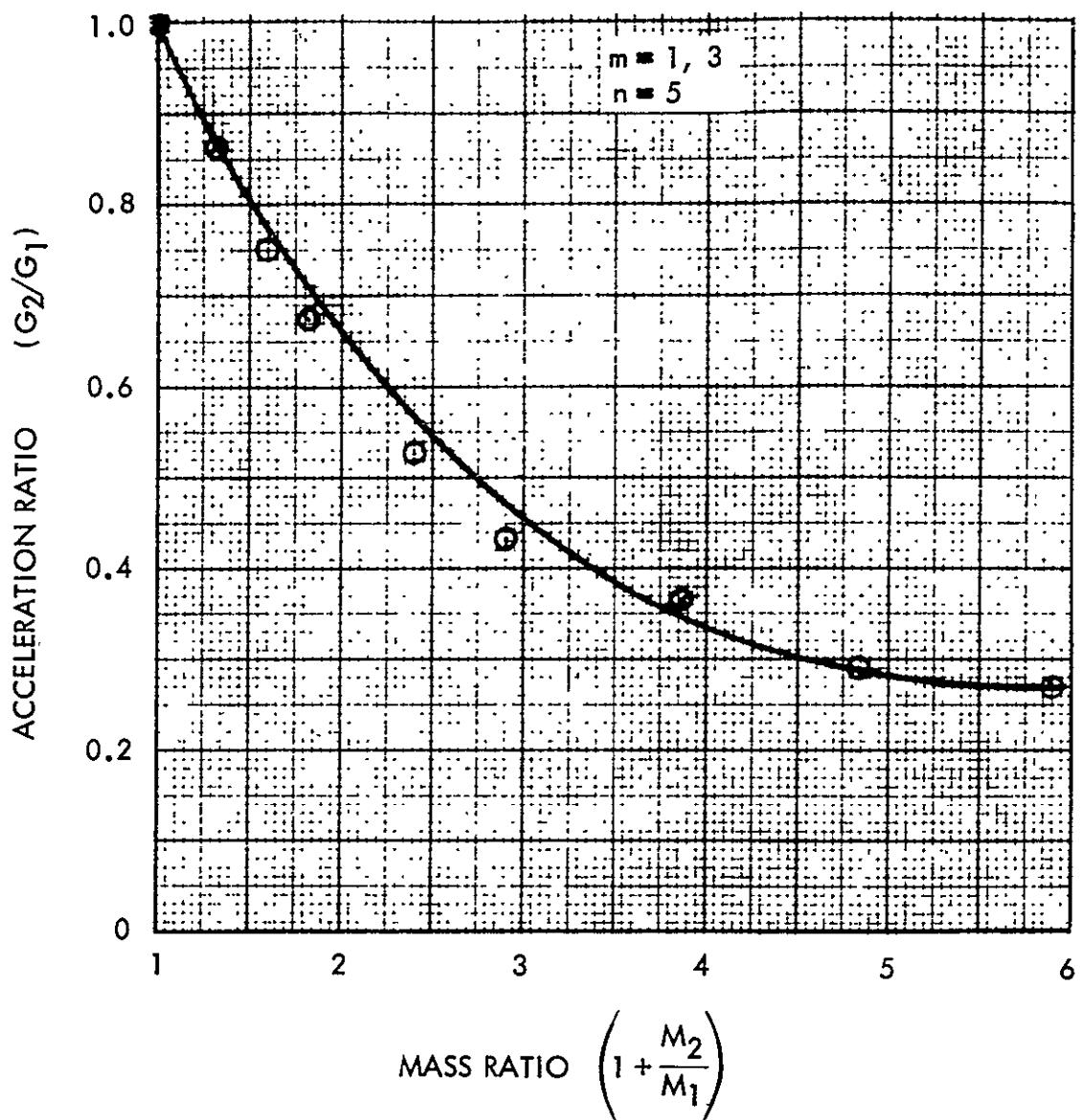
Figure IV-14.   Mass-Loading Effect on Acceleration Response of Shell II, Mode 3

IV-18
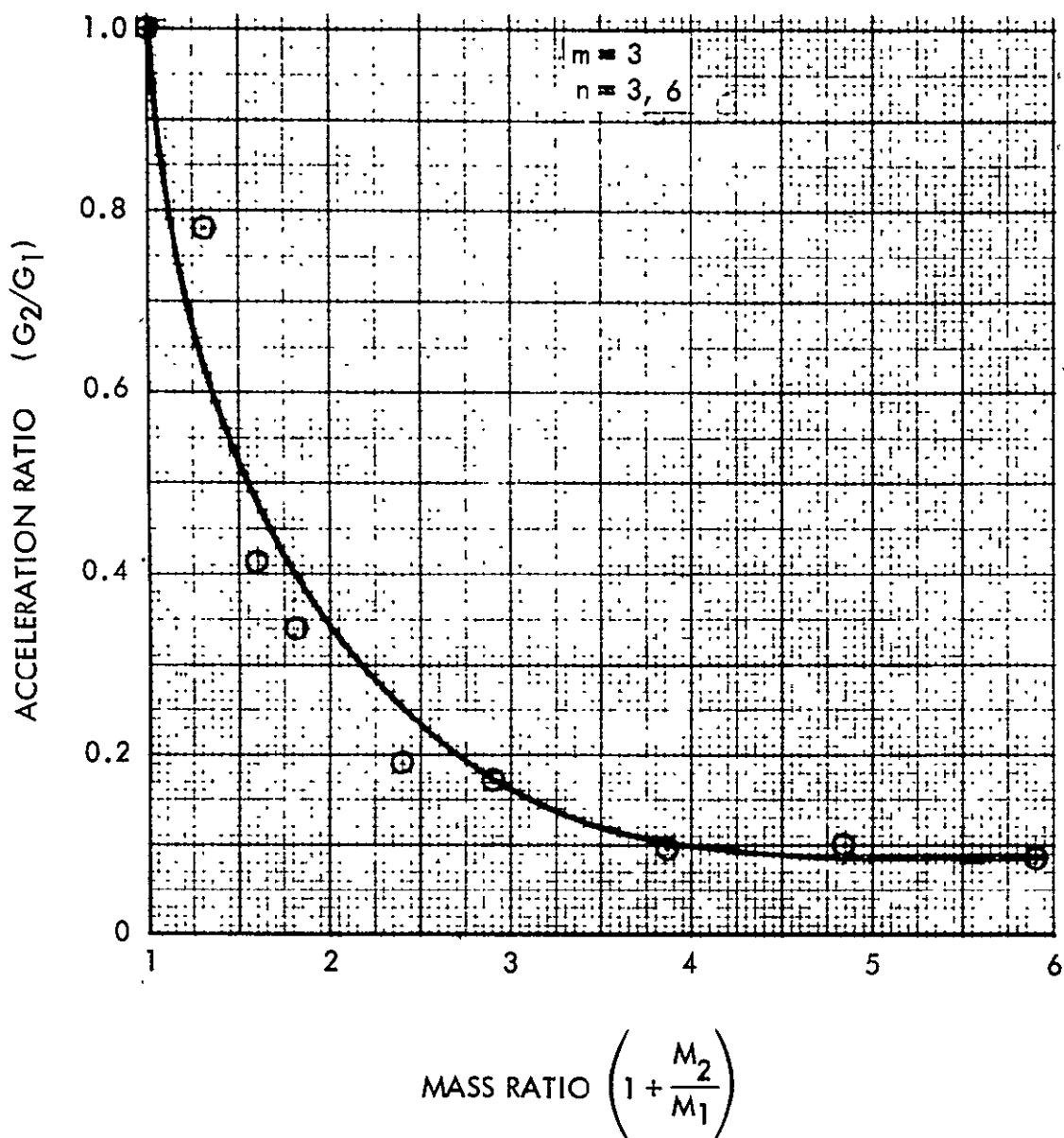
Figure IV-15.   Mass-Loading Effect on Acceleration Response of
Shell II, Mode 4
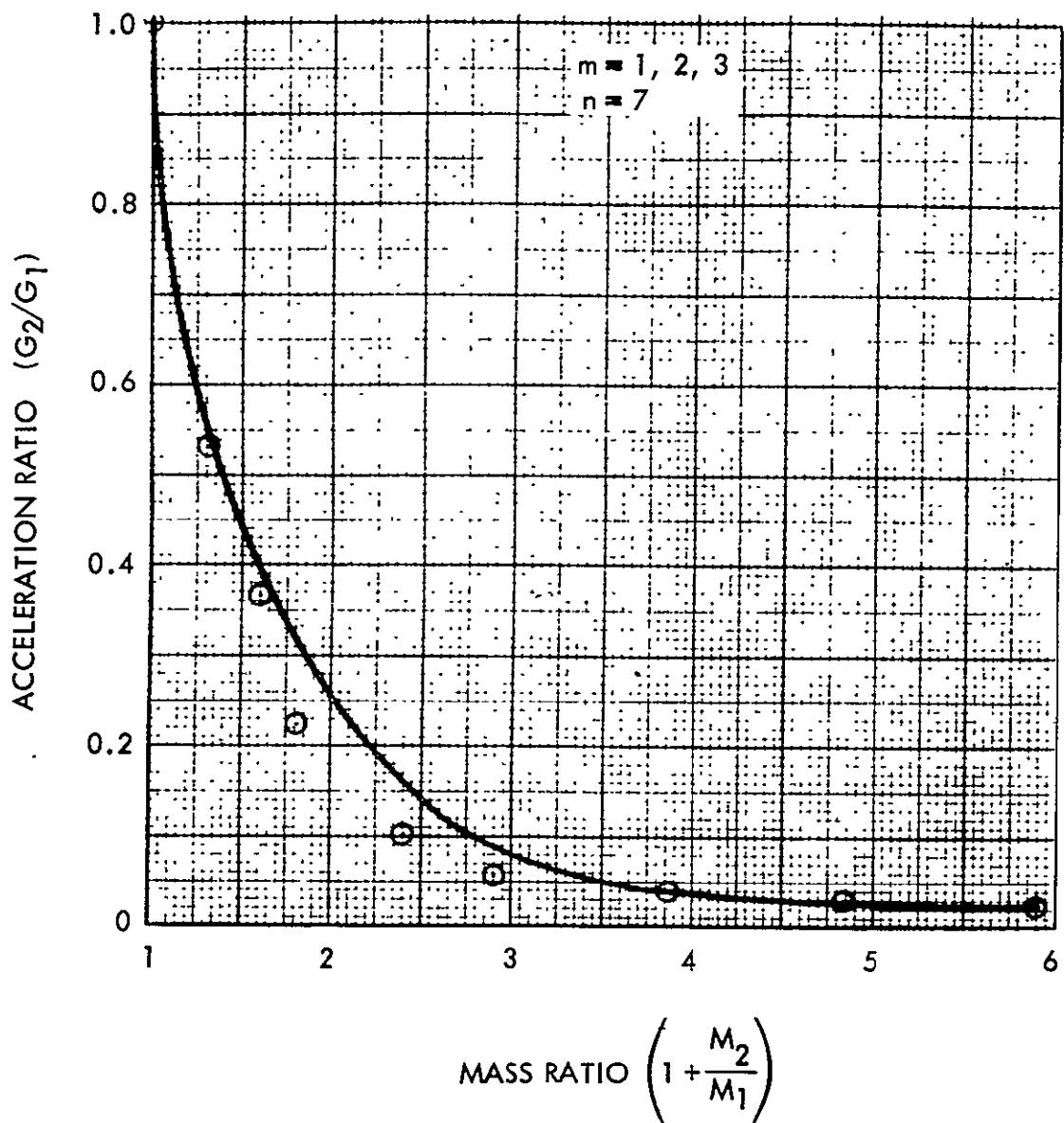
Figure IV-16. Mass-Loading Effect on Acceleration Response of Shell II, Mode 5

IV-20

V. THEORETICAL SOLUTIONS BY SERIES-EXPANSION
TECHNIQUE

Table V-1. Theoretical Solutions, Symmetrical Case, M2 = 0.004 Pound

FREQUENCIES

	(RADIANS2 PER SECCNC2)	(RADIANS PER SECOND)	(CYCLES PER SECOND)
1	1.0955156E 05	3.3098560E 02	5.2679040E 01
2	1.6643850E 05	4.0796875E 02	6.4930298E 01
3	2.8024487E 05	5.2938159E 02	8.4253760E 01
4	4.7019400E 05	6.8570679E 02	1.0913373E 02
5	9.3223362E 05	9.6552246E 02	1.5366782E 02
6	1.5732160E 06	1.2542791E 03	1.9962489E 02
7	1.9812430E 06	1.4075662E 03	2.2402132E 02
8	3.2941010E 06	1.8149658E 03	2.8886084E 02
9	3.7884050E 06	1.9463823E 03	3.0977461E 02
10	4.0035020E 06	2.0008752E 03	3.1844946E 02
11	9.6707140E 06	3.1097771E 03	4.9493677E 02
12	1.2079298E 07	3.4755283E 03	5.5314705E 02
13	1.6708976E 07	4.0986523E 03	6.5232129E 02
14	2.6692224E 07	5.1664492E 03	8.2226660E 02
15	3.4974416E 07	5.9139141E 03	9.4122949E 02
16	4.6373888E 07	6.8098359E 03	1.0838701E 03
17	8.3096944E 07	9.1157500E 03	1.4508179E 03
18	1.2109683E 08	1.1004398E 04	1.7514060E 03
19	1.2787546E 08	1.1308203E 04	1.7997581E 03
20	1.9926974E 08	1.4116293E 04	2.2466799E 03
21	1.9993203E 08	1.4139730E 04	2.2504099E 03
22	2.1329038E 08	1.4604461E 04	2.3243743E 03
23	2.5696682E 08	1.6030184E 04	2.5512854E 03
24	2.8134682E 08	1.6773395E 04	2.6695710E 03
25	2.9626829E 08	1.7212445E 04	2.7394482E 03
26	3.7744742E 08	1.9428004E 04	3.0920657E 03
27	3.9510477E 08	1.9877242E 04	3.1635642E 03
28	4.0335693E 08	2.0083746E 04	3.1964304E 03
29	4.4161613E 08	2.1014664E 04	3.3445908E 03
30	5.2448614E 08	2.2901660E 04	3.6449158E 03
31	5.3548237E 08	2.3140492E 04	3.6829272E 03
32	5.8887757E 08	2.4266797E 04	3.8621843E 03
33	6.4965043E 08	2.5488238E 04	4.0565928E 03
34	6.5806746E 08	2.5652824E 04	4.0827776E 03
35	7.2653107E 08	2.6954238E 04	4.2899023E 03
36	8.1627750E 08	2.8570570E 04	4.5471484E 03
37	8.7118285E 08	2.9515805E 04	4.6975898E 03
38	9.5821645E 08	3.0955070E 04	4.9266562E 03
39	9.5997286E 08	3.0983426E 04	4.9311680E 03
40	1.0729900E 09	3.2756523E 04	5.2133672E 03
41	1.2948516E 09	3.5984643E 04	5.7270430E 03
42	1.3860083E 09	3.7229129E 04	5.9252031E 03
43	1.4342715E 09	3.7871773E 04	6.0274844E 03
44	1.4845778E 09	3.8530219E 04	6.1322773E 03
45	1.5450081E 09	3.9306590E 04	6.2584437E 03
46	1.5656712E 09	3.9568562E 04	6.2975352E 03
47	1.6755535E 09	4.0933523E 04	6.5147773E 03
48	1.7805256E 09	4.2196273E 04	6.7157500E 03
49	2.5649160E 09	5.0645000E 04	8.0604062E 03
50	2.6668559E 09	5.1641609E 04	8.2190234E 03
51	2.8409213E 09	5.3300293E 04	8.4830117E 03
52	3.0896581E 09	5.5584691E 04	8.8465859E 03
53	4.3391959E 09	6.5872562E 04	1.0483053E 04
54	4.4471337E 09	6.6686812E 04	1.0613543E 04
55	4.6263869E 09	6.8017500E 04	1.0825328E 04
56	4.8781804E 09	6.9843937E 04	1.1116016E 04

V-1

Table V-2. Theoretical Solutions, Symmetrical Case, M2 = 0.022 Pound

FREQUENCIES

	(RADIANS2 PER SECOND2)	(RADIANS PER SECOND)	(CYCLES PER SECOND)
1	1.0917287E 05	3.3041309E 02	5.2586914E 01
2	1.6573250E 05	4.0710254E 02	6.4792435E 01
3	2.7912756E 05	5.2832520E 02	8.4085632E 01
4	4.6941119E 05	6.8513574E 02	1.0904283E 02
5	9.3153531E 05	9.6516064E 02	1.5361023E 02
6	1.5267900E 06	1.2356370E 03	1.9665791E 02
7	1.9802930E 06	1.4072288E 03	2.2396762E 02
8	3.2897830E 06	1.8137750E 03	2.8867163E 02
9	3.6257040E 06	1.9041279E 03	3.0305151E 02
10	2.7882010E 06	1.9463301E 03	3.0976831E 02
11	9.6709040E 06	3.1098076E 03	4.9494165E 02
12	1.1777286E 07	3.4318049E 03	5.4618921E 02
13	1.6785072E 07	4.0969570E 03	6.5205151E 02
14	2.4492592E 07	4.9489961E 03	7.8765771E 02
15	3.4941264E 07	5.9111133E 03	9.4079369E 02
16	4.6356464E 07	6.8085547E 03	1.0836160E 03
17	8.3096976E 07	9.1157539E 03	1.4508186E 03
18	1.2109658E 08	1.1004387E 04	1.7514041E 03
19	1.2783520E 08	1.1306422E 04	1.7994746E 03
20	1.9322206E 08	1.3900434E 04	2.2123247E 03
21	1.9441449E 08	1.3943258E 04	2.2191404E 03
22	1.9992549E 08	1.4139500E 04	2.2503733E 03
23	2.5585664E 08	1.5995516E 04	2.5457476E 03
24	2.8096256E 08	1.6761937E 04	2.6677476E 03
25	2.9623322E 08	1.7211426E 04	2.7392859E 03
26	3.7708390E 08	1.9418645E 04	3.0905762E 03
27	3.9510477E 08	1.9877242E 04	3.1635642E 03
28	4.0000333E 08	2.0000082E 04	3.1831147E 03
29	4.4157133E 08	2.1013598E 04	3.3444211E 03
30	5.2425242E 08	2.2896559E 04	3.6441038E 03
31	5.3351091E 08	2.3097855E 04	3.6761414E 03
32	5.8836531E 08	2.4256242E 04	3.8605044E 03
33	6.4168346E 08	2.5331469E 04	4.0316323E 03
34	6.5257882E 08	2.5545621E 04	4.0657156E 03
35	7.2625860E 08	2.6949187E 04	4.2890977E 03
36	8.1626982E 08	2.8570434E 04	4.5471289E 03
37	8.7112627E 08	2.9514848E 04	4.6974375E 03
38	9.5914886E 08	3.0953977E 04	4.9264805E 03
39	9.5997338E 08	3.0983434E 04	4.9311680E 03
40	1.0729900E 09	3.2756523E 04	5.2133672E 03
41	1.2937551E 09	3.5968805E 04	5.7246172E 03
42	1.3856256E 09	3.7223992E 04	5.9243867E 03
43	1.4330094E 09	3.7855109E 04	6.0248320E 03
44	1.4845581E 09	3.8529961E 04	6.1322383E 03
45	1.5387436E 09	3.9226820E 04	6.2431445E 03
46	1.5636265E 09	3.9542715E 04	6.2934219E 03
47	1.6693263E 09	4.0857387E 04	6.5026602E 03
48	1.7643622E 09	4.2004312E 04	6.6851992E 03
49	2.5628416E 09	5.0624516E 04	8.0571484E 03
50	2.6630036E 09	5.1604297E 04	8.2130959E 03
51	2.8390359E 09	5.3282605E 04	8.4801053E 03
52	3.0896584E 09	5.5584695E 04	8.8465859E 03
53	4.3380654E 09	6.5863937E 04	1.0482578E 04
54	4.4467159E 09	6.6683687E 04	1.0613047E 04
55	4.6190223E 09	6.7963375E 04	1.0816715E 04
56	4.8567788E 09	6.9690562E 04	1.1091605E 04

V-2

Table V-3. Theoretical Solutions, Symmetrical Case, M2 = 0.044 Pound

FREQUENCIES

	(RADIANS2 PER SECOND2)	(RADIANS PER SECOND)	(CYCLES PER SECOND)
1	1.0943631E 05	3.3081152E 02	5.2650330E 01
2	1.6510562E 05	4.0633179E 02	5.4669760E 01
3	2.7821119E 05	5.2745728E 02	8.3947510E 01
4	4.6877212E 05	6.8466919E 02	1.0896859E 02
5	9.3169700E 05	9.6524438E 02	1.5362355E 02
6	1.4723300E 06	1.2133960E 03	1.9311915E 02
7	1.9791970E 06	1.4068394E 03	2.2390564E 02
8	3.2470140E 06	1.8019473E 03	2.8678906E 02
9	3.2845290E 06	1.9123269E 03	2.9844092E 02
10	3.7874380E 06	1.9461340E 03	3.0973706E 02
11	9.6708480E 06	3.1097986E 03	4.9494019E 02
12	1.1424909E 07	3.3900752E 03	5.3795605E 02
13	1.6768549E 07	4.0949417E 03	6.5173071E 02
14	2.2288832E 07	4.7147461E 03	7.5037573E 02
15	3.4809792E 07	5.9076016E 03	9.4022485E 02
16	4.6335594E 07	6.8070234E 03	1.0833723E 03
17	8.3096976E 07	9.1157539E 03	1.4509186E 03
18	1.2109638E 08	1.1004379E 04	1.7514029E 03
19	1.2778645E 08	1.1304266E 04	1.7991313E 03
20	1.7295376E 08	1.3151187E 04	2.0930784E 03
21	1.8859600E 08	1.3733023E 04	2.1856904E 03
22	1.9991731E 08	1.4139211E 04	2.2503274E 03
23	2.5450371E 08	1.5953172E 04	2.5390286E 03
24	2.8051277E 08	1.6748512E 04	2.6655108E 03
25	2.9619046E 08	1.7210184E 04	2.7390884E 03
26	3.7661414E 08	1.9406547E 04	3.0886506E 03
27	3.9510477E 08	1.9877242E 04	3.1635642E 03
28	3.9639910E 08	1.9909773E 04	3.1687417E 03
29	4.4152243E 08	2.1012434E 04	3.3442359E 03
30	5.2396314E 08	2.2890238E 04	3.6430079E 03
31	5.3111578E 08	2.3045949E 04	3.6678901E 03
32	5.8775296E 08	2.4243617E 04	3.8584951E 03
33	6.3324211E 08	2.5164301E 04	4.0050266E 03
34	6.4762957E 08	2.5448566E 04	4.0502688E 03
35	7.2593459E 08	2.6943172E 04	4.2891406E 03
36	8.1626138E 08	2.8570285E 04	4.5471055E 03
37	8.7106330E 08	2.9513781E 04	4.6972656E 03
38	9.5806771E 08	3.0952668E 04	4.9262734E 03
39	9.5997338E 08	3.0983434E 04	4.9311680E 03
40	1.0729902E 09	3.2756527E 04	5.2133672E 03
41	1.2974413E 09	3.5950539E 04	5.7217109E 03
42	1.3851727E 09	3.7217906E 04	5.9234180E 03
43	1.4314099E 09	3.7833977E 04	6.0214687E 03
44	1.4845356E 09	3.8529668E 04	6.1321914E 03
45	1.5316636E 09	3.9136473E 04	6.2287656E 03
46	1.5610824E 09	3.9510531E 04	6.2883008E 03
47	1.6625516E 09	4.0774398E 04	6.4894531E 03
48	1.7487916E 09	4.1818555E 04	6.6556328E 03
49	2.5601039E 09	5.0597469E 04	8.0528437E 03
50	2.6584922E 09	5.1560565E 04	8.2061250E 03
51	2.8369096E 09	5.3262645E 04	8.4770195E 03
52	3.0896584E 09	5.5584695E 04	8.8465859E 03
53	4.3367096E 09	6.5853687E 04	1.0480949E 04
54	4.4462203E 09	6.6679937E 04	1.0612449E 04
55	4.6106706E 09	6.7901875E 04	1.0806926E 04
56	4.8357949E 09	6.9539875E 04	1.1067625E 04

Table V-4.   Theoretical Solutions, Symmetrical Case, M2 = 0.066 Pound

FREQUENCIES

	(RADIANS2 PER SECOND2)	(RADIANS PER SECOND)	(CYCLES PER SECOND)
1	1.0989050E 05	3.3149731E 02	5.2750476E 01
2	1.6465950E 05	4.0578247E 02	6.4582336E 01
3	2.7688700E 05	5.2620044E 02	8.3747467E 01
4	4.6780087E 05	6.8395947E 02	1.0985562E 02
5	9.3099237E 05	9.6487939E 02	1.5356546E 02
6	1.4215170E 06	1.1922737E 03	1.8975642E 02
7	1.9782150E 06	1.4064902E 03	2.2385008E 02
8	2.9355750E 06	1.7133518E 03	2.7268948E 02
9	3.2795550E 06	1.8109541E 03	2.8822241E 02
10	3.7868890E 06	1.9459929E 03	3.0971460E 02
11	9.6710640E 06	3.1098335E 03	4.9494580E 02
12	1.0988312E 07	3.3299116E 03	5.2997217E 02
13	1.6752251E 07	4.0929512E 03	6.5141382E 02
14	2.0320112E 07	4.5077812E 03	7.1743628E 02
15	3.4857792E 07	5.9040469E 03	9.3965894E 02
16	4.6315712E 07	6.8055625E 03	1.0831399E 03
17	8.3096960E 07	9.1157500E 03	1.4508179E 03
18	1.2109616E 08	1.1004367E 04	1.7514009E 03
19	1.2773792E 08	1.1302117E 04	1.7987893E 03
20	1.5619576E 08	1.2497828E 04	1.9890930E 03
21	1.8293208E 08	1.3525238E 04	2.1526104E 03
22	1.9990926E 08	1.4138926E 04	2.2502820E 03
23	2.5314890E 08	1.5910652E 04	2.5322612E 03
24	2.8007885E 08	1.6735555E 04	2.6635486E 03
25	2.9614694E 08	1.7208918E 04	2.7388870E 03
26	2.7610880E 08	1.9393523E 04	3.0865779E 03
27	3.9324902E 08	1.9830504E 04	3.1561257E 03
28	3.9510477E 08	1.9877242E 04	3.1635642E 03
29	4.4147405E 08	2.1011281E 04	3.3440522E 03
30	5.2367155E 08	2.2883871E 04	3.6420845E 03
31	5.2874035E 08	2.2994355E 04	3.6596687E 03
32	5.8714803E 08	2.4231137E 04	3.8565088E 03
33	6.2597094E 08	2.5019410E 04	3.9819666E 03
34	6.4389453E 08	2.5375074E 04	4.0385723E 03
35	7.2561818E 08	2.6937301E 04	4.2872070E 03
36	8.1625395E 08	2.8570156E 04	4.5470859E 03
37	8.7099776E 08	2.9512668E 04	4.6970898E 03
38	9.5798810E 08	3.0951383E 04	4.9260664E 03
39	9.5997235E 08	3.0983418E 04	4.9311680E 03
40	1.0729900E 09	3.2756523E 04	5.2133672E 03
41	1.2911411E 09	3.5932440E 04	5.7188320E 03
42	1.3847319E 09	3.7211984E 04	5.9224766E 03
43	1.4297618E 09	3.7812187E 04	6.0180000E 03
44	1.4845151E 09	3.8529402E 04	6.1321484E 03
45	1.5251284E 09	3.9052891E 04	6.2154648E 03
46	1.5584991E 09	3.9477828E 04	6.2830937E 03
47	1.6566003E 09	4.0701352E 04	6.4778242E 03
48	1.7364521E 09	4.1670758E 04	6.6321133E 03
49	2.5571144E 09	5.0567918E 04	8.0481406E 03
50	2.6542126E 09	5.1519051E 04	8.1995156E 03
51	2.8349655E 09	5.3244395E 04	8.4741133E 03
52	3.0896584E 09	5.5584695E 04	8.8465859E 03
53	4.3353702E 09	6.5843500E 04	1.0479328E 04
54	4.4457533E 09	6.6676437E 04	1.0611895E 04
55	4.6029087E 09	6.7844687E 04	1.0797824E 04
56	4.8189071E 09	6.9418312E 04	1.1048277E 04

Table V-5. Theoretical Solutions, Symmetrical Case, M2 = 0.089 Pound

FREQUENCIES

	(RADIANS2 PER SECOND2)	(RADIANS PER SECOND)	(CYCLES PER SECOND)
1	1.0956019E 05	3.3099854E 02	5.2680099E 01
2	1.6323956E 05	4.0402905E 02	6.4303268E 01
3	2.7570687E 05	5.2507788E 02	8.3568817E 01
4	4.6660662E 05	6.8308594E 02	1.0871660E 02
5	9.3068C00E 05	9.6471753E 02	1.5353970E 02
6	1.3705240E 06	1.1706936E 03	1.8632184E 02
7	1.9772520E 06	1.4061479E 03	2.2379561E 02
8	2.6622800E 06	1.6316494E 03	2.5968530E 02
9	3.2740520E 06	1.8094341E 03	2.8798047E 02
10	3.7862230E 06	1.9458218E 03	3.0968726E 02
11	9.6710360E 06	3.1098289E 03	4.9494507E 02
12	1.0749923E 07	3.2787075E 03	5.2182300E 02
13	1.6735580E 07	4.0909143E 03	6.5108984E 02
14	1.8607856E 07	4.3136797E 03	6.8654395E 02
15	3.4813072E 07	5.9002578E 03	9.3905591E 02
16	4.6294800E 07	6.8040273E 03	1.0828955E 03
17	8.3096912E 07	9.1157500E 03	1.4508179E 03
18	1.2109589E 08	1.1004355E 04	1.7513992E 03
19	1.2768755E 08	1.1299891E 04	1.7984351E 03
20	1.4142661E 08	1.1892289E 04	1.8927193E 03
21	1.7712715E 08	1.3308910E 04	2.1181807E 03
22	1.9990018E 08	1.4138605E 04	2.2502310E 03
23	2.5171870E 08	1.5865645E 04	2.5250981E 03
24	2.7964288E 08	1.6722523E 04	2.6614746E 03
25	2.9610086E 08	1.7207578E 04	2.7386736E 03
26	3.7553050E 08	1.9378605E 04	3.0842036E 03
27	3.9038003E 08	1.9758035E 04	3.1445918E 03
28	3.9510426E 08	1.9877227E 04	3.1635618E 03
29	4.4142566E 08	2.1010129E 04	3.3438689E 03
30	5.2336282E 08	2.2877125E 04	3.6410110E 03
31	5.2624922E 08	2.2940121E 04	3.6510371E 03
32	5.8652390E 08	2.4218254E 04	3.8544585E 03
33	6.1932826E 08	2.4886305E 04	3.9607820E 03
34	6.4088602E 08	2.5315727E 04	4.0291267E 03
35	7.2529510E 08	2.6931301E 04	4.2862500E 03
36	8.1624602E 08	2.8570020E 04	4.5470625E 03
37	8.7093043E 08	2.9511527E 04	4.6969062E 03
38	9.5790541E 08	3.0950047E 04	4.9259555E 03
39	9.5997363E 08	3.0983437E 04	4.9311719E 03
40	1.0729902E 09	3.2756527E 04	5.2133672E 03
41	1.2897815E 09	3.5913527E 04	5.7158203E 03
42	1.3842819E 09	3.7205937E 04	5.9215117E 03
43	1.4279654E 09	3.7788430E 04	6.0142187E 03
44	1.4844938E 09	3.8529129E 04	6.1321055E 03
45	1.5188019E 09	3.8971809E 04	6.2025586E 03
46	1.5557583E 09	3.9443102E 04	6.2775703E 03
47	1.6511529E 09	4.0634379E 04	6.4671680E 03
48	1.7260588E 09	4.1545863E 04	6.6122344E 03
49	2.5537155E 09	5.0534301E 04	8.0427891E 03
50	2.6500047E 09	5.1478195E 04	8.1930156E 03
51	2.8331036E 09	5.3226926E 04	8.4713320E 03
52	3.0896584E 09	5.5584695E 04	9.8465859E 03
53	4.3340063E 09	6.5833125E 04	1.0477676E 04
54	4.4452700E 09	6.6672812E 04	1.0611316E 04
55	4.5953597E 09	6.7789062E 04	1.0788073E 04
56	4.8044851E 09	6.9314375E 04	1.1031734E 04

V-5

Table V-6. Theoretical Solutions, Symmetrical Case, M2 = 0.28 Pound

FREQUENCIES

	(RADIANS2 PER SECOND2)	(RADIANS PER SECOND)	(CYCLES PER SECOND)
1	1.0943425E 05	3.3080835E 02	5.2649926E 01
2	1.5529931E 05	3.9408032E 02	6.2719879E 01
3	2.6387187E 05	5.1368457E 02	8.1755508E 01
4	4.5946475E 05	6.7783813E 02	1.0788139E 02
5	9.2867331E 05	9.6367676E 02	1.5337405E 02
6	1.0020239E 06	1.0010112E 03	1.5931602E 02
7	1.3555360E 06	1.1642747E 03	1.8530023E 02
8	1.9693750E 06	1.4033442E 03	2.2334938E 02
9	3.2319150E 06	1.7977527E 03	2.8612134E 02
10	3.7814810E 06	1.9446030E 03	3.0949341E 02
11	8.1890470E 06	2.8616511E 03	4.5544629E 02
12	9.6711520E 06	3.1098477E 03	4.9494300E 02
13	9.9457960E 06	3.1536956E 03	5.0192651E 02
14	1.6608750E 07	4.0753833E 03	6.4861792E 02
15	3.4400688E 07	5.8652070E 03	9.3347754E 02
16	4.6140032E 07	6.7926445E 03	1.0810840E 03
17	7.0992832E 07	8.4257227E 03	1.3409964E 03
18	8.3097089E 07	9.1157578E 03	1.4508191E 03
19	1.2109354E 08	1.1004250E 04	1.7513923E 03
20	1.2717306E 08	1.1277102E 04	1.7948081E 03
21	1.3168869E 08	1.1475566E 04	1.8263948E 03
22	1.9981605E 08	1.4135629E 04	2.2497573E 03
23	2.3774384E 08	1.5418941E 04	2.4540029E 03
24	2.7642035E 08	1.6625891E 04	2.6460950E 03
25	2.9571994E 08	1.7196508E 04	2.7369116E 03
26	3.6835072E 08	1.9192465E 04	3.0545784E 03
27	3.7844326E 08	1.9453617E 04	3.0961421E 03
28	3.9510477E 08	1.9877242E 04	3.1635642E 03
29	4.4106342E 08	2.1001508E 04	3.3424968E 03
30	5.0695654E 08	2.2515695E 04	3.5834875E 03
31	5.2057754E 08	2.2816168E 04	3.6313093E 03
32	5.8161434E 08	2.4116680E 04	3.8382922E 03
33	5.9027328E 08	2.4295539E 04	3.8667588E 03
34	6.3424691E 08	2.5184258E 04	4.0082029E 03
35	7.2281165E 08	2.6885156E 04	4.2789062E 03
36	8.1617920E 08	2.8568848E 04	4.5468750E 03
37	8.7036877E 08	2.9502012E 04	4.6953945E 03
38	9.5721933E 08	3.0938961E 04	4.9240898E 03
39	9.5997389E 08	3.0983445E 04	4.9311719E 03
40	1.0729900E 09	3.2756523E 04	5.2133672E 03
41	1.2769864E 09	3.5734945E 04	5.6873984E 03
42	1.3809316E 09	3.7160887E 04	5.9143437E 03
43	1.4121213E 09	3.7578199E 04	5.9807617E 03
44	1.4778117E 09	3.8442316E 04	6.1182891E 03
45	1.4843666E 09	3.8527477E 04	6.1318437E 03
46	1.5409646E 09	3.9255121E 04	6.2476523E 03
47	1.6367227E 09	4.0456426E 04	6.4388437E 03
48	1.6883896E 09	4.1090016E 04	6.5396836E 03
49	2.5155876E 09	5.0155633E 04	7.9825234E 03
50	2.6259927E 09	5.1244441E 04	8.1558125E 03
51	2.8223529E 09	5.3125820E 04	8.4552422E 03
52	3.0896584E 09	5.5584695E 04	8.8465859E 03
53	4.3226726E 09	6.5747000E 04	1.0463969E 04
54	4.4416532E 09	6.6645687E 04	1.0607000E 04
55	4.5462077E 09	6.7425562E 04	1.0731121E 04
56	4.7487754E 09	6.8911312E 04	1.0967586E 04

V-6

Table V-7. Theoretical Solutions, Symmetrical Case, M2 = 0.53 Pound

FREQUENCIES

	(RADIANS2 PER SECONC2)	(RADIANS PER SECOND)	(CYCLES PER SECOND)
1	1.1002644E 05	3.3170215E 02	5.2792084E 01
2	1.4076312E 05	3.7518408E 02	5.9712448E 01
3	2.4255212E 05	4.9249561E 02	7.8393179E 01
4	4.5000525E 05	6.7082422E 02	1.0676509E 02
5	6.4145762E 05	8.0091040E 02	1.2746896E 02
6	6.6671800E 05	8.1652783E 02	1.2995454E 02
7	9.2450925E 05	9.6151392E 02	1.5302983E 02
8	1.9603440E 06	1.4001228E 03	2.2283667E 02
9	3.1810280E 06	1.7835435E 03	2.8385986E 02
10	3.7735150E 06	1.9425537E 03	3.0916724E 02
11	5.0135150E 06	2.2390879E 03	3.5636206E 02
12	5.4734340E 06	2.3395371E 03	3.7234912E 02
13	9.6706610E 06	3.1097847E 03	4.9493799E 02
14	1.6463414E 07	4.0575132E 03	6.4577368E 02
15	3.3425440E 07	5.7814727E 03	9.2015063E 02
16	3.4928560E 07	5.9100352E 03	9.4061206E 02
17	4.5965552E 07	6.7797891E 03	1.0790378E 03
18	8.3096960E 07	9.1157500E 03	1.4508179E 03
19	8.4375536E 07	9.1856133E 03	1.4619370E 03
20	1.2108830E 08	1.1004012E 04	1.7513445E 03
21	1.2682339E 08	1.1261586E 04	1.7923386E 03
22	1.9967181E 08	1.4130527E 04	2.2489453E 03
23	2.1115787E 08	1.4531270E 04	2.3127256E 03
24	2.7254170E 08	1.6508836E 04	2.6274553E 03
25	2.9517670E 08	1.7180707E 04	2.7343970E 03
26	3.6294016E 08	1.9050988E 04	3.0320618E 03
27	3.7526272E 08	1.9371695E 04	3.0831040E 03
28	3.9510477E 08	1.9877242E 04	3.1635642E 03
29	4.4065485E 08	2.0991777E 04	3.3409482E 03
30	4.9738957E 08	2.2302230E 04	3.5495134E 03
31	5.1626982E 08	2.2721570E 04	3.6162537E 03
32	5.7590605E 08	2.3998043E 04	3.8194106E 03
33	5.9209523E 08	2.4333008E 04	3.8727222E 03
34	6.8808934E 08	2.6231457E 04	4.1748672E 03
35	7.2001664E 08	2.6833125E 04	4.2706250E 03
36	8.1609395E 08	2.8567355E 04	4.5466367E 03
37	8.6963405E 08	2.9489555E 04	4.6934102E 03
38	9.5634611E 08	3.0924844E 04	4.9218437E 03
39	9.5997363E 08	3.0983437E 04	4.9311719E 03
40	1.0729905E 09	3.2756531E 04	5.2133672E 03
41	1.2524861E 09	3.5390480E 04	5.6325742E 03
42	1.3770783E 09	3.7109004E 04	5.9060859E 03
43	1.4003351E 09	3.7421051E 04	5.9557500E 03
44	1.4407112E 09	3.7956699E 04	6.0410000E 03
45	1.4841856E 09	3.8525133E 04	6.1314687E 03
46	1.5522703E 09	3.9398859E 04	6.2705273E 03
47	1.6493455E 09	4.0612133E 04	6.4636250E 03
48	1.8791493E 09	4.3349156E 04	6.8992383E 03
49	2.4524283E 09	4.9521996E 04	7.8816758E 03
50	2.6135404E 09	5.1122797E 04	8.1364531E 03
51	2.8150551E 09	5.3057094E 04	8.4443047E 03
52	3.0896586E 09	5.5584695E 04	8.8465859E 03
53	4.3119616E 09	6.5665500E 04	1.0450996E 04
54	4.4378317E 09	6.6617000E 04	1.0602434E 04
55	4.5121659E 09	6.7172625E 04	1.0690863E 04
56	4.8184975E 09	6.9415375E 04	1.1047809E 04

Table V-8. Theoretical Solutions, Symmetrical Case, M2 - 0.722 Pound

FREQUENCIES

	(RADIANS2 PER SECOND2)	(RADIANS PER SECOND)	(CYCLES PER SECOND)
1	1.0974512E 05	3.3127783E 02	5.2724548E 01
2	1.3566825E 05	3.6833154E 02	5.8621841E 01
3	2.3522662E 05	4.8500146E 02	7.7190445E 01
4	4.4312556E 05	6.6567676E 02	1.0594585E 02
5	5.5977444E 05	7.4818066E 02	1.1907675E 02
6	5.6694550E 05	7.5295776E 02	1.1983705E 02
7	9.2292150E 05	9.6068799E 02	1.5289838E 02
8	1.9524900E 06	1.3973152E 03	2.2238983E 02
9	3.1452490E 06	1.7734849E 03	2.8225903E 02
10	3.7699590E 06	1.9416382E 03	3.0902148E 02
11	4.2337870E 06	2.0576167E 03	3.2747299E 02
12	4.8658400E 06	2.2058647E 03	3.5107446E 02
13	9.6710670E 06	3.1098340E 03	4.9494580E 02
14	1.6338004E 07	4.0420295E 03	6.4330957E 02
15	2.8942224E 07	5.3797969E 03	8.5622192E 02
16	3.3552928E 07	5.7924883E 03	9.2190381E 02
17	4.5817312E 07	6.7688477E 03	1.0772064E 03
18	7.4430464E 07	8.6273086E 03	1.3730801E 03
19	8.3097072E 07	9.1157578E 03	1.4508191E 03
20	1.2108696E 08	1.1003949E 04	1.7513345E 03
21	1.2647256E 08	1.1246000E 04	1.7898582E 03
22	1.9959586E 08	1.4127836E 04	2.2485168E 03
23	2.0239446E 08	1.4226539E 04	2.2642261E 03
24	2.7003904E 08	1.6432863E 04	2.6153738E 03
25	2.9479475E 08	1.7169586E 04	2.7326270E 03
26	3.5800730E 08	1.8921078E 04	3.0113860E 03
27	3.7449574E 08	1.9351891E 04	3.0799519E 03
28	3.9510502E 08	1.9877246E 04	3.1635649E 03
29	4.4039219E 08	2.0985523E 04	3.3399529E 03
30	4.9451520E 08	2.2237695E 04	3.5392424E 03
31	5.1267968E 08	2.2642430E 04	3.6036590E 03
32	5.7223782E 08	2.3921492E 04	3.8072273E 03
33	5.9171712E 08	2.4325234E 04	3.9714849E 03
34	6.9930214E 08	2.6444320E 04	4.2087461E 03
35	7.1816576E 08	2.6798613E 04	4.2651328E 03
36	8.1604582E 08	2.8566516E 04	4.5465039E 03
37	8.6921472E 08	2.9482445E 04	4.6922812E 03
38	9.5582797E 08	3.0916465E 04	4.9205117E 03
39	9.5997440E 08	3.0983453E 04	4.9311719E 03
40	1.0729902E 09	3.2756527E 04	5.2133672E 03
41	1.2444434E 09	3.5276668E 04	5.6144609E 03
42	1.3744151E 09	3.7073102E 04	5.9003711E 03
43	1.3883791E 09	3.7260957E 04	5.9302695E 03
44	1.4326446E 09	3.7850289E 04	6.0240625E 03
45	1.4840855E 09	3.8523828E 04	6.1312617E 03
46	1.5510925E 09	3.9383910E 04	6.2681484E 03
47	1.6476754E 09	4.0591566E 04	6.4603516E 03
48	1.9406067E 09	4.4052316E 04	7.0111484E 03
49	2.4054310E 09	4.9045195E 04	7.8057891E 03
50	2.6094769E 09	5.1083039E 04	8.1301250E 03
51	2.8117955E 09	5.3026363E 04	8.4394141E 03
52	3.0896591E 09	5.5584703E 04	8.8465859E 03
53	4.3069645E 09	6.5627437E 04	1.0444937E 04
54	4.4353577E 09	6.6598437E 04	1.0599480E 04
55	4.5034373E 09	6.7107625E 04	1.0680520E 04
56	4.8408494E 09	6.9576187E 04	1.1073402E 04

4

Table V-9. Theoretical Solutions, Symmetrical Case, M2 = 1.495 Pounds

FREQUENCIES

	(RADIANS2 PER SECOND2)	(RADIANS PER SECOND)	(CYCLES PER SECOND)
1	−2.6127587E 05	5.1115137E 02	8.1352341E 01
2	2.8031785E 04	1.6742696E 02	2.6646851E 01
3	7.7105187E 04	2.7767798E 02	4.4193863E 01
4	1.0796712E 05	3.2843115E 02	5.2271484E 01
5	1.1413706E 05	3.3784155E 02	5.3769196E 01
6	4.2331119E 05	6.5062354E 02	1.0355005E 02
7	5.2428256E 05	7.2407349E 02	1.1523997E 02
8	9.0384994E 05	9.5071021E 02	1.5131036E 02
9	9.6913775E 05	9.8444775E 02	1.5667987E 02
10	1.9270170E 06	1.3881704E 03	2.2093439E 02
11	3.0124000E 06	1.7356267E 03	2.7623364E 02
12	3.7352090E 06	1.9326687E 03	3.0759309E 02
13	9.6706780E 06	3.1097712E 03	4.9493579E 02
14	9.9582750E 06	3.1556733E 03	5.0224146E 02
15	1.5947540E 07	3.9934370E 03	6.3557569E 02
16	2.9545776E 07	5.4356016E 03	8.6510352E 02
17	3.2717520E 07	5.7199219E 03	9.1035449E 02
18	4.5367184E 07	6.7355156E 03	1.0719915E 03
19	8.3096816E 07	9.1157422E 03	1.4508167E 03
20	1.2106253E 08	1.1002840E 04	1.7511580E 03
21	1.2430508E 08	1.1149258E 04	1.7744612E 03
22	1.3561547E 08	1.1645402E 04	1.8534250E 03
23	1.9901203E 08	1.4107160E 04	2.2452263E 03
24	2.5940501E 08	1.6106055E 04	2.5633606E 03
25	2.9285658E 08	1.7113051E 04	2.7236292E 03
26	3.4870810E 08	1.8673727E 04	2.9720186E 03
27	3.7222938E 08	1.9293246E 04	3.0706184E 03
28	3.9510451E 08	1.9877234E 04	3.1635630E 03
29	4.3948570E 08	2.0963914E 04	3.3365137E 03
30	4.8673434E 08	2.2062055E 04	3.5112883E 03
31	4.9396966E 08	2.2225426E 04	3.5372896E 03
32	5.6166682E 08	2.3699512E 04	3.7718979E 03
33	5.9240627E 08	2.4339395E 04	3.8737385E 03
34	7.1241754E 08	2.6691148E 04	4.2480312E 03
35	8.1583283E 08	2.8562785E 04	4.5459102E 03
36	8.6739430E 08	2.9451559E 04	4.6873633E 03
37	9.2550707E 08	3.0422145E 04	4.8418359E 03
38	9.5372365E 08	3.0882414E 04	4.9150898E 03
39	9.5997312E 08	3.0983430E 04	4.9311680E 03
40	1.0729905E 09	3.2756531E 04	5.2133672E 03
41	1.1101681E 09	3.3319184E 04	5.3029141E 03
42	1.3566876E 09	3.6833238E 04	5.8621953E 03
43	1.3660268E 09	3.6959797E 04	5.8823398E 03
44	1.3866668E 09	3.7237973E 04	5.9266094E 03
45	1.4837422E 09	3.8519371E 04	6.1305508E 03
46	1.5507213E 09	3.9379195E 04	6.2673984E 03
47	1.6371756E 09	4.0462023E 04	6.4397344E 03
48	2.2453187E 09	4.7384793E 04	7.5415312E 03
49	2.6037117E 09	5.1026578E 04	8.1211367E 03
50	2.8056704E 09	5.2968578E 04	8.4302187E 03
51	3.0896581E 09	5.5584691E 04	8.8465859E 03
52	4.0881075E 09	6.3938309E 04	1.0176105E 04
53	4.1344348E 09	6.4299570E 04	1.0233602E 04
54	4.4223775E 09	6.6500937E 04	1.0583961E 04
55	4.4475474E 09	6.6689875E 04	1.0614031E 04
56	1.1732443E 12	1.0831640E 06	1.7239106E 05

V-9

Table V-10. Theoretical Solutions, Antisymmetrical Case, M2 = 0.004 Pound

FREQUENCIES

	(RADIANS2 PER SECOND2)	(RADIANS PER SECOND)	(CYCLES PER SECOND)
1	1.0031662E 05	3.3063062E 02	5.2621536E 01
2	1.6690900E 05	4.0862184E 02	6.5035828E 01
3	2.8236512E 05	5.2049512E 02	8.4271835E 01
4	4.7046244E 05	6.8590259E 02	1.0916489E 02
5	9.3161725E 05	9.6520213E 02	1.5361699E 02
6	1.5836470E 06	1.2594302E 03	2.0028557E 02
7	1.0905260E 06	1.4073115E 03	2.2398079E 02
8	3.2950410E 06	1.8152246E 03	2.8890210E 02
9	3.7630470E 06	1.9400894E 03	3.0877490E 02
10	4.0981350E 06	2.0243850E 03	3.2219116E 02
11	9.4576540E 06	3.0753298E 03	4.8945435E 02
12	1.2147954E 07	3.4853014E 03	5.5471777E 02
13	1.6700216E 07	4.0986836E 03	6.5222617E 02
14	2.7234090E 07	5.2186250E 03	8.3057056E 02
15	3.4981696E 07	5.9145312E 03	9.4132764E 02
16	4.6104304E 07	6.7966367E 03	1.0817102E 03
17	8.1745120E 07	9.0413008E 03	1.4389690E 03
18	1.2106660E 08	1.1003027E 04	1.7511877E 03
19	1.2788437E 08	1.1308594E 04	1.7998293E 03
20	1.9992083E 08	1.4139326E 04	2.2503472E 03
21	2.0036728E 08	1.4155113E 04	2.2528584E 03
22	2.1828498E 08	1.4774469E 04	2.3514319E 03
23	2.5721426E 08	1.6037898E 04	2.5525132E 03
24	2.8143409E 08	1.6776020E 04	2.6699888E 03
25	2.9571405E 08	1.7196336E 04	2.7368843E 03
26	3.7752453E 08	1.9430039E 04	3.0923896E 03
27	3.9269376E 08	1.9816500E 04	3.1538967E 03
28	4.0415770E 08	2.0103672E 04	3.1996018E 03
29	4.4161869E 08	2.1014723E 04	3.3446001E 03
30	5.2429722E 08	2.2897535E 04	3.6442593E 03
31	5.3591450E 08	2.3149824E 04	3.6844124E 03
32	5.8891110E 08	2.4267488E 04	3.8622042E 03
33	6.5158554E 08	2.5526172E 04	4.0626201E 03
34	6.5953050E 08	2.5681324E 04	4.0873135E 03
35	7.2542285E 08	2.6933672E 04	4.2866289E 03
36	8.1611853E 08	2.8567785E 04	4.5467070E 03
37	8.7118874E 08	2.9515906E 04	4.6976055E 03
38	9.5718389E 08	3.0938484E 04	4.9240156E 03
39	9.5787008E 08	3.0949473E 04	4.9257656E 03
40	1.0713819E 09	3.2731965E 04	5.2094570E 03
41	1.2948974E 09	3.5984680E 04	5.7271445E 03
42	1.3856934E 09	3.7224902E 04	5.9245312E 03
43	1.4345454E 09	3.7875391E 04	6.0280586E 03
44	1.4845647E 09	3.8530047E 04	6.1322500E 03
45	1.5462572E 09	3.9322473E 04	6.2583711E 03
46	1.5661048E 09	3.9574039E 04	6.2984062E 03
47	1.6770455E 09	4.0951746E 04	6.5176758E 03
48	1.7846519E 09	4.2245137E 04	6.7235273E 03
49	2.5651064E 09	5.0646879E 04	8.0607070E 03
50	2.6676401E 09	5.1649203E 04	8.2202305E 03
51	2.8397460E 09	5.3289266E 04	8.4812578E 03
52	3.0847150E 09	5.5540211E 04	8.8395039E 03
53	4.3395593E 09	6.5868500E 04	1.0483305E 04
54	4.4456837E 09	6.6675937E 04	1.0611812E 04
55	4.6273249E 09	6.8024437E 04	1.0826434E 04
56	4.8836035E 09	6.9892750E 04	1.1122195E 04

Table V-11. Theoretical Solutions, Antisymmetrical Case, M2 = 0.022 Pound

FREQUENCIES

	(RADIANS2 PER SECOND2)	(RADIANS PER SECOND)	(CYCLES PER SECOND)
1	1.0938931E 05	3.3074048E 02	5.2639023E 01
2	1.6656162E 05	4.0811938E 02	6.4954269F 01
3	2.8047044E 05	5.2959448E 02	8.4287659F 01
4	4.7046481E 05	6.8590430E 02	1.0916516E 02
5	9.3019475E 05	9.6446704E 02	1.5349983E 02
6	1.5835890E 06	1.2584072E 03	2.0029192F 02
7	1.9762190E 06	1.4057805E 03	2.2372712E 02
8	3.2935970E 06	1.8148269E 03	2.8883887E 02
9	3.6578350E 06	1.9125466E 03	3.0439136E 02
10	4.0978450E 06	2.0243132E 03	3.2217969E 02
11	8.6029530E 06	2.9330791E 03	4.6681445E 02
12	1.2145429E 07	3.4850293E 03	5.5466016E 02
13	1.6785648E 07	4.0970273E 03	6.5206274E 02
14	2.7234144E 07	5.2186328E 03	8.3057178E 02
15	3.4981680E 07	5.9145312E 03	9.4132764E 02
16	4.5382816E 07	6.7366758E 03	1.0721763E 03
17	7.6107856E 07	8.7239805E 03	1.3884658E 03
18	1.2092891E 08	1.0996766E 04	1.7501912E 03
19	1.2788419E 08	1.1308586E 04	1.7998188E 03
20	1.9986490E 08	1.4137355E 04	2.2500320E 03
21	2.0036686E 08	1.4155098E 04	2.2528557E 03
22	2.1828498E 08	1.4774469E 04	2.3514319E 03
23	2.5721331E 08	1.6037871E 04	2.5525088E 03
24	2.8143334E 08	1.6775973E 04	2.6699814E 03
25	2.9322675E 08	1.7123863E 04	2.7253501E 03
26	3.7752243E 08	1.9429934E 04	3.0923728E 03
27	3.8308710E 08	1.9572609E 04	3.1150803E 03
28	4.0415693E 08	2.0103652E 04	3.1995986E 03
29	4.4158413E 08	2.1013902E 04	3.3444695E 03
30	5.2321894E 08	2.2873977E 04	3.6405098E 03
31	5.3586355E 08	2.3148727E 04	3.6842375E 03
32	5.8854912E 08	2.4260031E 04	3.8611074E 03
33	6.5158554E 08	2.5526172E 04	4.0626201E 03
34	6.5953050E 08	2.5681324E 04	4.0873135E 03
35	7.2041190E 08	2.6840488E 04	4.2717969E 03
36	8.1539046E 08	2.8555043E 04	4.5446797E 03
37	8.7116160E 08	2.9515445E 04	4.6975312E 03
38	9.4656205E 08	3.0766246E 04	4.8966016E 03
39	9.5608115E 08	3.0920559E 04	4.9211641E 03
40	1.0647557E 09	3.2630594E 04	5.1933242E 03
41	1.2939873E 09	3.5972035E 04	5.7251289E 03
42	1.3839060E 09	3.7200887E 04	5.9207070E 03
43	1.4345364E 09	3.7875273E 04	6.0280391E 03
44	1.4844966E 09	3.8529164E 04	6.1321094E 03
45	1.5453542E 09	3.9310992E 04	6.2565430E 03
46	1.5660321E 09	3.9573121E 04	6.2982617E 03
47	1.6770455E 09	4.0951746E 04	6.5176758E 03
48	1.7846518E 09	4.2245137E 04	6.7235273E 03
49	2.5639985E 09	5.0635941E 04	8.0589648E 03
50	2.6672366E 09	5.1645297E 04	8.2196094E 03
51	2.8327818E 09	5.3223883E 04	8.4708516E 03
52	3.0652260E 09	5.5364480E 04	8.8115391E 03
53	4.3348050E 09	6.5839187E 04	1.0478641E 04
54	4.4389376E 09	6.6625312E 04	1.0603758E 04
55	4.6240973E 09	6.8000687E 04	1.0822652E 04
56	4.8836035E 09	6.9882750E 04	1.1122195E 04

Table V-12. Theoretical Solutions, Antisymmetrical Case, M2 = 0.044 Pound

FREQUENCIES

	(RADIANS2 PER SECOND2)	(RADIANS PER SECOND)	(CYCLES PER SECOND)
1	1.0863012E 05	3.2960449E 02	5.2458221E 01
2	1.6685450E 05	4.0847827E 02	6.5011399E (1
3	2.8047381E 05	5.2959766E 02	8.4288162E 01
4	4.7012956E 05	6.8565991E 02	1.0912627E 02
5	9.2839062E 05	9.6353027E 02	1.5335074E 02
6	1.5933080E 06	1.2582957E 03	2.0026414E 02
7	1.9713130E 06	1.4040344E 03	2.2345923E 02
8	3.2918150E 06	1.8143359E 03	2.8876074E 02
9	3.5345450E 06	1.8800383E 03	2.9921753E 02
10	4.0980600E 06	2.0243687E 03	3.2218848E 02
11	7.7305230E 06	2.7810998E 03	4.4276929E 02
12	1.2143176E 07	3.4847061E 03	5.5460864E 02
13	1.6769730E 07	4.0950859E 03	6.5175365E 02
14	2.7234048E 07	5.2186250E 03	8.3057056E 02
15	3.4981680E 07	5.9145312E 03	9.4132764E 02
16	4.4417856E 07	6.6646719E 03	1.0607163E 03
17	7.0058816E 07	8.3701133E 03	1.3321460E 03
18	1.2075522E 08	1.0988867E 04	1.7489341E 03
19	1.2788400E 08	1.1308578E 04	1.7998176E 03
20	1.9979779E 08	1.4134984E 04	2.2496548E 03
21	2.0036619E 08	1.4155074E 04	2.2528521E 03
22	2.1828501E 08	1.4774469E 04	2.3514319E 03
23	2.5721218E 08	1.6037832E 04	2.5525027E 03
24	2.8143104E 08	1.6775906E 04	2.6699709E 03
25	2.9025664E 08	1.7036918E 04	2.7115122E 03
26	3.7347251E 08	1.9325434E 04	3.0757412E 03
27	3.7751834E 08	1.9429828E 04	3.0923560E 03
28	4.0415667E 08	2.0103645E 04	3.1995974E 03
29	4.4154470E 08	2.1012965E 04	3.3443203E 03
30	5.2191946E 08	2.2845535E 04	3.6359832E 03
31	5.3580314E 08	2.3147422E 04	3.6840630E 03
32	5.8811930E 08	2.4251172E 04	3.8596975E 03
33	6.5158528E 08	2.5526168E 04	4.0626196E 03
34	6.5953024E 08	2.5681320E 04	4.0873130E 03
35	7.1480141E 08	2.6735770E 04	4.2551328E 03
36	8.1446989E 08	2.8538918E 04	4.5421133E 03
37	8.7112806E 08	2.9514875E 04	4.6974414E 03
38	9.3643162E 08	3.0601168E 04	4.8703281E 03
39	9.5394022E 08	3.0885922E 04	4.9156484E 03
40	1.0576991E 09	3.2522285E 04	5.1760859E 03
41	1.2928346E 09	3.5956008E 04	5.7225781E 03
42	1.3817659E 09	3.7172109E 04	5.9161289E 03
43	1.4345262E 09	3.7875137E 04	6.0280195E 03
44	1.4844183E 09	3.8528148E 04	6.1319492E 03
45	1.5442875E 09	3.9297422E 04	6.2543828E 03
46	1.5659525E 09	3.9572117E 04	6.2981016E 03
47	1.6770458E 09	4.0951746E 04	6.5176758E 03
48	1.7846520E 09	4.2245141E 04	6.7235273E 03
49	2.5626673E 09	5.0622793E 04	8.0568750E 03
50	2.6667497E 09	5.1640582E 04	8.2188594E 03
51	2.8248832E 09	5.3149629E 04	8.4590312E 03
52	3.0461885E 09	5.5192258E 04	8.7841328E 03
53	4.3294106E 09	6.5798250E 04	1.0472125E 04
54	4.4312699E 09	6.6567750E 04	1.0594594E 04
55	4.6206198E 09	6.7975125E 04	1.0818586E 04
56	4.8836035E 09	6.9882750E 04	1.1122195E 04

Table V-13. Theoretical Solutions, Antisymmetrical Case, M2 = 0.066 Pound

FREQUENCIES

	(RADIANS2 PEP SECOND2)	(RADIANS PER SECOND)	(CYCLES PER SECOND)
1	1.0798531E 05	3.2861108E 02	5.2300125E 01
2	1.6708969E 05	4.0876587E 02	6.5057159E 01
3	2.8017725E 05	5.2931763E 02	8.4243591E 01
4	4.7025762E 05	6.8575317E 02	1.0914110E 02
5	9.2643769E 05	9.6251611E 02	1.5318933E 02
6	1.5832590E 06	1.2582761E 03	2.0026105E 02
7	1.9663420E 06	1.4022632E 03	2.2317732E 02
8	3.2905370E 06	1.8139836E 03	2.8870459E 02
9	3.4177060E 06	1.8487030E 03	2.9423047E 02
10	4.0980370E 06	2.0243608E 03	3.2218726E 02
11	7.0233190E 06	2.6501545E 03	4.2178540E 02
12	1.2130941E 07	3.4842417E 03	5.5453467E 02
13	1.6753098E 07	4.0931646E 03	6.5144775E 02
14	2.7234080E 07	5.2186250E 03	8.3057056E 02
15	3.4981680E 07	5.9145312E 03	9.4132764E 02
16	4.3477280E 07	6.5937266E 03	1.0494250E 03
17	6.4769568E 07	8.0479531E 03	1.2808724E 03
18	1.2057600E 08	1.0980711E 04	1.7476360E 03
19	1.2788378E 08	1.1308570E 04	1.7998164E 03
20	1.9973162E 08	1.4132641E 04	2.2492817E 03
21	2.0036552E 08	1.4155051E 04	2.2528484E 03
22	2.1828501E 08	1.4774469E 04	2.3514319E 03
23	2.5721115E 08	1.6037801E 04	2.5524976E 03
24	2.8142899E 08	1.6775844E 04	2.6699609E 03
25	2.8736333E 08	1.6951793E 04	2.6979641E 03
26	3.6560742E 08	1.9120863E 04	3.0431826E 03
27	3.7751424E 08	1.9429723E 04	3.0923394E 03
28	4.0415616E 08	2.0103633E 04	3.1995955E 03
29	4.4150195E 08	2.1011945E 04	3.3441580E 03
30	5.2062604E 08	2.2817250E 04	3.6314814E 03
31	5.3574298E 08	2.3146121E 04	3.6838230E 03
32	5.8770022E 08	2.4242527E 04	3.8583215E 03
33	6.5158528E 08	2.5526168E 04	4.0626196E 03
34	6.5953024E 08	2.5681320E 04	4.0873130E 03
35	7.0964349E 08	2.6639508E 04	4.2398125E 03
36	8.1350938E 08	2.8522086E 04	4.5394336E 03
37	8.7109555E 08	2.9514324E 04	4.6973516E 03
38	9.2843136E 08	3.0470168E 04	4.8494805E 03
39	9.5183411E 08	3.0851809E 04	4.9102187E 03
40	1.0515940E 09	3.2428133E 04	5.1611016E 03
41	1.2916244E 09	3.5939176E 04	5.7199023E 03
42	1.3796659E 09	3.7143852E 04	5.9116228E 03
43	1.4345172E 09	3.7875020E 04	6.0280000E 03
44	1.4843356E 09	3.8527074E 04	6.1317773E 03
45	1.5432643E 09	3.9284398E 04	6.2523086E 03
46	1.5658819E 09	3.9571223E 04	6.2979609E 03
47	1.6770458E 09	4.0951746E 04	6.5176758E 03
48	1.7846520E 09	4.2245141E 04	6.7235273E 03
49	2.5613458E 09	5.0609738E 04	8.0547969E 03
50	2.6662712E 09	5.1635949E 04	8.2181211E 03
51	2.8175537E 09	5.3080633E 04	8.4480508E 03
52	3.0308879E 09	5.5053500E 04	8.7620430E 03
53	4.3232092E 09	6.5751062E 04	1.0464613E 04
54	4.4243354E 09	6.6515625E 04	1.0586297E 04
55	4.6175846E 09	6.7952750E 04	1.0815023E 04
56	4.8836035E 09	6.9882750E 04	1.1122195E 04

Table V-14. Theoretical Solutions, Antisymmetrical Case, M2 = 0.089 Pound

FREQUENCIES

	(RADIANS² PER SECOND²)	(RADIANS PER SECOND)	(CYCLES PER SECOND)
1	1.0754004E 05	3.2793286E 02	5.2192184E 01
2	1.6682125E 05	4.0843750E 02	6.5004998E 01
3	2.8032875E 05	5.2946069E 02	8.4266357E 01
4	4.7002650E 05	6.8558472E 02	1.0911429E 02
5	9.2478944E 05	9.6165067E 02	1.5305302E 02
6	1.5829860E 06	1.2591255E 03	2.0023720E 02
7	1.9611130E 06	1.4003970E 03	2.2288031E 02
8	3.2892190E 06	1.8136204E 03	2.8864673E 02
9	3.3009810E 06	1.8168601E 03	2.8914235E 02
10	4.0980240E 06	2.0243577E 03	3.2218677E 02
11	6.3997500E 06	2.5277054E 03	4.0231129E 02
12	1.2137100E 07	3.4838481E 03	5.5447217E 02
13	1.6737890E 07	4.0911975E 03	6.5113477E 02
14	2.7234048E 07	5.2186250E 03	8.3057056E 02
15	3.4981664E 07	5.9145273E 03	9.4132715E 02
16	4.2511552E 07	6.5200859E 03	1.0377048E 03
17	5.9880656E 07	7.7382578E 03	1.2315830E 03
18	1.2038176E 08	1.0971859E 04	1.7462273E 03
19	1.2788354E 08	1.1308559E 04	1.7998147E 03
20	1.9966366E 08	1.4130238E 04	2.2488094E 03
21	2.0364090E 08	1.4155031E 04	2.2528452E 03
22	2.1828501E 08	1.4774460E 04	2.3514319E 03
23	2.5720982E 08	1.6037762E 04	2.5524915E 03
24	2.8142643E 08	1.6775766E 04	2.6690485E 03
25	2.8438323E 08	1.6863664E 04	2.6839380E 03
26	3.5872543E 08	1.8940051E 04	3.0144055E 03
27	3.7750012E 08	1.9429594E 04	3.0922188E 03
28	4.0415565E 08	2.0103621E 04	3.1995925E 03
29	4.4145766E 08	2.1010891E 04	3.3430902E 03
30	5.1927782E 08	2.2797668E 04	3.6267734E 03
31	5.3567770E 08	2.3144711E 04	3.6835986E 03
32	5.8726912E 08	2.4233637E 04	3.8569067E 03
33	6.5158528E 08	2.5526169E 04	4.0626196E 03
34	6.5953024E 08	2.5681320E 04	4.0873130E 03
35	7.0472218E 08	2.6546602E 04	4.2250234E 03
36	8.1245670E 08	2.8503625E 04	4.5364961E 03
37	8.7106202E 08	2.9513758E 04	4.6972617E 03
38	9.2168422E 08	3.0359250E 04	4.8318291E 03
39	9.4965402E 08	3.0816453E 04	4.9045937E 03
40	1.0459622E 09	3.2341336E 04	5.1472852E 03
41	1.2902950E 09	3.5920676E 04	5.7169570E 03
42	1.3775124E 09	3.7114852E 04	5.9070156E 03
43	1.4346093E 09	3.7874914E 04	6.0279844E 03
44	1.4842537E 09	3.8526012E 04	6.1316004E 03
45	1.5422354E 09	3.9271305E 04	6.2502266E 03
46	1.5658173E 09	3.9570406E 04	6.2978281E 03
47	1.6770460E 09	4.0951750E 04	6.5176797E 03
48	1.7846520E 09	4.2245141E 04	6.7235273E 03
49	2.5599800E 09	5.0596246E 04	8.0526484E 03
50	2.6657777E 09	5.1631168E 04	8.2173633E 03
51	2.8104090E 09	5.3013289E 04	8.4373320E 03
52	3.0177951E 09	5.4934461E 04	8.7430977E 03
53	4.3158323E 09	6.5694937E 04	1.0455684E 04
54	4.4179087E 09	6.6467312E 04	1.0578609E 04
55	4.6148157E 09	6.7932375E 04	1.0811781E 04
56	4.8836035E 09	6.9882750E 04	1.1122195E 04

**Table V-15. Theoretical Solutions, Antisymmetrical Case,
M2 = 0.28 Pound**

FREQUENCIES

	(RADIANS2 PER SECOND2)	(RADIANS PER SECOND)	(CYCLES PER SECOND)
1	1.0204806E 05	3.1944946E 02	5.0841005E 01
2	1.6679487E 05	4.0840527E 02	6.4990771E 01
3	2.7961094E 05	5.2878247E 02	8.4159417E 01
4	4.6865062E 05	6.8458057E 02	1.0895449E 02
5	9.1122712E 05	9.5458203E 02	1.5192459E 02
6	1.5806080E 06	1.2572222E 03	2.0009321E 02
7	1.9133860E 06	1.3832520E 03	2.2015160E 02
8	2.4438460E 06	1.5632805E 03	2.4880405E 02
9	3.2791520E 06	1.8108428E 03	2.8820483E 02
10	3.3079980E 06	1.8187900E 03	2.8946949E 02
11	4.0981030E 06	2.0243770E 03	3.2218970E 02
12	1.2113937E 07	3.4805081E 03	5.5394043E 02
13	1.6618885E 07	4.0766233E 03	6.4881510E 02
14	2.7233824E 07	5.2186016E 03	8.3056689E 02
15	3.3265584E 07	5.7676289E 03	9.1794751E 02
16	3.4537664E 07	5.8768750E 03	9.3533447E 02
17	3.4981600E 07	5.9145234E 03	9.4132642E 02
18	1.1844720E 08	1.0883344E 04	1.7321394E 03
19	1.2788038E 08	1.1308418E 04	1.7997922E 03
20	1.9914390E 08	1.4111832E 04	2.2459700E 03
21	2.0035509E 08	1.4154684E 04	2.2527890E 03
22	2.1928493E 08	1.4774469E 04	2.3514319E 03
23	2.5719296E 08	1.6037234E 04	2.5524075E 03
24	2.6080272E 08	1.6149387E 04	2.5702571E 03
25	2.8139597E 08	1.6774859E 04	2.6698042E 03
26	3.2723174E 08	1.8089547E 04	2.8790435E 03
27	3.7746995E 08	1.9428586E 04	3.0921584E 03
28	4.0414925E 08	2.0103461E 04	3.1995681E 03
29	4.4104806E 08	2.1001145E 04	3.3424390E 03
30	5.0677786E 08	2.2511727E 04	3.5828560E 03
31	5.3511270E 08	2.3132504E 04	3.6816558E 03
32	5.8407245E 08	2.4167590E 04	3.8463050E 03
33	6.5158528E 08	2.5526168E 04	4.0626196E 03
34	6.5952998E 08	2.5681316E 04	4.0873123E 03
35	6.7442278E 08	2.5969648E 04	4.1331992E 03
36	8.0174720E 08	2.8315141E 04	4.5064061E 03
37	8.7079322E 08	2.9509203E 04	4.6965391E 03
38	8.9837261E 08	2.9972863E 04	4.7703320E 03
39	9.3377997E 08	3.0557812E 04	4.8634297E 03
40	1.0207442E 09	3.1949086E 04	5.0848594E 03
41	1.2766049E 09	3.5729605E 04	5.6865469E 03
42	1.3619011E 09	3.6903941E 04	5.8734492E 03
43	1.4344499E 09	3.7874729E 04	6.0278594E 03
44	1.4836152E 09	3.8517723E 04	6.1302891E 03
45	1.5351544E 09	3.9181047E 04	6.2358504E 03
46	1.5654477E 09	3.9565738E 04	6.2970859E 03
47	1.6770458E 09	4.0951746E 04	6.5176758E 03
48	1.7846518E 09	4.2245137E 04	6.7235273E 03
49	2.5483658E 09	5.0481340E 04	8.0343594E 03
50	2.6618870E 09	5.1593477E 04	8.2113673E 03
51	2.7634486E 09	5.2568512E 04	8.3665430E 03
52	2.9652255E 09	5.4453883E 04	8.6666094E 03
53	4.2310193E 09	6.5046285E 04	1.0352445E 04
54	4.3906744E 09	6.6262125E 04	1.0545953E 04
55	4.6009426E 09	6.7830187E 04	1.0795520E 04
56	4.8836116E 09	6.9882812E 04	1.1122203E 04

Table V-16. Theoretical Solutions, Antisymmetrical Case,
M2 = 0.53 Pound

FREQUENCIES

	(RADIANS2 PER SECOND2)	(RADIANS PER SECOND)	(CYCLES PER SECOND)
1	9.3101562E 04	3.0512524E 02	4.8542225E 01
2	1.6613194E 05	4.0759277E 02	6.4870453E 01
3	2.7905544E 05	5.2825684E 02	8.4074753E 01
4	4.6486794E 05	6.8181201E 02	1.0851395E 02
5	8.9554369E 05	9.4634204E 02	1.5061516E 02
6	1.5556500E 06	1.2472568E 03	1.9850729E 02
7	1.6037960E 06	1.2664106E 03	2.0155569E 02
8	1.6421180E 06	1.2814514E 03	2.0394951E 02
9	1.8294490E 06	1.3525710E 03	2.1526857E 02
10	3.2666020E 06	1.8073743E 03	2.8765250E 02
11	4.0982800E 06	2.0244231E 03	3.2219702E 02
12	1.2079330E 07	3.4753904E 03	5.5312503E 02
13	1.6501622E 07	4.0622187E 03	6.4652271E 02
14	1.7039808E 07	4.1279297E 03	6.5698096E 02
15	2.4597872E 07	4.9596211E 03	7.8934899E 02
16	2.7234176E 07	5.2186367E 03	8.3057251E 02
17	3.4981520E 07	5.9145156E 03	9.4132520E 02
18	1.1526119E 08	1.0735973E 04	1.7086846E 03
19	1.2797224E 08	1.1308059E 04	1.7997351E 03
20	1.9857766E 08	1.4091758E 04	2.2427749E 03
21	2.0033120E 08	1.4153840E 04	2.2526555E 03
22	2.1828501E 08	1.4774469E 04	2.3514312E 03
23	2.3847392E 08	1.5442598E 04	2.4577481E 03
24	2.5715022E 08	1.6035902E 04	2.5521956E 03
25	2.8131635E 08	1.6772484E 04	2.6694253E 03
26	3.1484544E 08	1.7743883E 04	2.8240293E 03
27	3.7740595E 08	1.9426937E 04	3.0918960E 03
28	4.0412928E 08	2.0102965E 04	3.1994893E 03
29	4.4035738E 08	2.0984691E 04	3.3398206E 03
30	4.8399181E 08	2.1999812E 04	3.5013821E 03
31	5.3418138E 08	2.3112363E 04	3.6784502E 03
32	5.8086016E 08	2.4101039E 04	3.8359030E 03
33	6.5158323E 08	2.5526129E 04	4.0626133E 03
34	6.5328307E 08	2.5559402E 04	4.0679089E 03
35	6.5953050E 08	2.5681324E 04	4.0873135E 03
36	7.9016371E 08	2.8109848E 04	4.4738242E 03
37	8.7048448E 08	2.9503973E 04	4.6957070E 03
38	9.1769523E 08	3.0293484E 04	4.8213594E 03
39	9.2951347E 08	3.0487922E 04	4.8523047E 03
40	1.0461330E 09	3.2343977E 04	5.1477070E 03
41	1.2519800E 09	3.5383328E 04	5.6314336E 03
42	1.3479749E 09	3.6714777E 04	5.8433437E 03
43	1.4343923E 09	3.7873371E 04	6.0277383E 03
44	1.4928603E 09	3.8507922E 04	6.1287305E 03
45	1.5286797E 09	3.9098332E 04	6.2226953E 03
46	1.5651438E 09	3.9561898E 04	6.2964766E 03
47	1.6770455E 09	4.0951746E 04	6.5176758E 03
48	1.7846518E 09	4.2245137E 04	6.7235273E 03
49	2.5320622E 09	5.0320547E 04	8.0102031E 03
50	2.6573916E 09	5.1549895E 04	8.2044258E 03
51	2.7260989E 09	5.2212059E 04	8.3098125E 03
52	2.9826967E 09	5.4614070E 04	8.6921055E 03
53	4.1095775E 09	6.4105984E 04	1.0202793E 04
54	4.3805737E 09	6.6185875E 04	1.0533916E 04
55	4.5926441E 09	6.7769000E 04	1.0785781E 04
56	4.8836035E 09	6.9882750E 04	1.1122195E 04

Table V-17. Theoretical Solutions, Antisymmetrical Case, M2 = 0.722 Pound

FREQUENCIES

	(RADIANS² PER SECOND²)	(RADIANS PER SECOND)	(CYCLES PER SECOND)
1	8.9522562E 04	2.9920313E 02	4.7619690E 01
2	1.6614844E 05	4.0761304E 02	6.4873688E 01
3	2.7849137E 05	5.2771313E 02	8.3988220E 01
4	4.6345062E 05	6.8077197E 02	1.0834823E 02
5	8.8478175E 05	9.4062817E 02	1.4970576E 02
6	1.3775620E 06	1.1736958E 03	1.8679967E 02
7	1.3985080E 06	1.1825852E 03	1.8821445E 02
8	1.5816140E 06	1.2576223E 03	2.0015700E 02
9	1.7980590E 06	1.3409172E 03	2.1341380E 02
10	3.2567200E 06	1.8046384E 03	2.8721729E 02
11	4.0980190E 06	2.0243562E 03	3.2218652E 02
12	1.2046121E 07	3.4707522E 03	5.5238770E 02
13	1.4420663E 07	3.7974546E 03	6.0438403E 02
14	1.6438912E 07	4.0544927E 03	6.4529797E 02
15	2.2175084E 07	4.7091367E 03	7.4948291E 02
16	2.7234080E 07	5.2186250E 03	8.3057056E 02
17	3.4981504E 07	5.9145156E 03	9.4132520E 02
18	1.1365371E 08	1.0660848E 04	1.6967280E 03
19	1.2787034E 08	1.1307977E 04	1.7997219E 03
20	1.9822640E 08	1.4079289E 04	2.2407905E 03
21	2.0032542E 08	1.4153633E 04	2.2526224E 03
22	2.1828485E 08	1.4774465E 04	2.3514312E 03
23	2.3379045E 08	1.5290207E 04	2.4335142E 03
24	2.5714030E 08	1.6035594E 04	2.5521462E 03
25	2.8129792E 08	1.6771937E 04	2.6693391E 03
26	3.1281536E 08	1.7686586E 04	2.8149102E 03
27	3.7736832E 08	1.9425969E 04	3.0917417E 03
28	4.0412495E 08	2.0102855E 04	3.1994717E 03
29	4.3982464E 08	2.0971996E 04	3.3377998E 03
30	4.7643981E 08	2.1827500E 04	3.4729578E 03
31	5.3346944E 08	2.3096957E 04	3.6759983E 03
32	5.7911782E 08	2.4064867E 04	3.8300461E 03
33	6.4732970E 08	2.5442676E 04	4.0493313E 03
34	6.5158426E 08	2.5526148E 04	4.0626165E 03
35	6.5952998E 08	2.5681316E 04	4.0873123E 03
36	7.8054733E 08	2.7938277E 04	4.4465156E 03
37	8.7027482E 08	2.9500418E 04	4.6951406E 03
38	9.1721318E 08	3.0285527E 04	4.8200937E 03
39	9.2958082E 08	3.0472770E 04	4.8498945E 03
40	1.0516352E 09	3.2428922E 04	5.1612266E 03
41	1.2302804E 09	3.5075352E 04	5.5824180E 03
42	1.3416960E 09	3.6629168E 04	5.8297148E 03
43	1.4343729E 09	3.7873113E 04	6.0276953E 03
44	1.4824820E 09	3.8503023E 04	6.1279492E 03
45	1.5252554E 09	3.9054516E 04	6.2157227E 03
46	1.5650609E 09	3.9560848E 04	6.2963086E 03
47	1.6770455E 09	4.0951746E 04	6.5176758E 03
48	1.7846520E 09	4.2245141E 04	6.7235273E 03
49	2.5268260E 09	5.0267543E 04	8.0003320E 03
50	2.6543465E 09	5.1520352E 04	8.1997227E 03
51	2.7161137E 09	5.2116348E 04	8.2945820E 03
52	2.9822804E 09	5.4610258E 04	8.6915000E 03
53	4.0263567E 09	6.3453578E 04	1.0098957E 04
54	4.3777475E 09	6.6164500E 04	1.0530414E 04
55	4.5894697E 09	6.7745625E 04	1.0782059E 04
56	4.8836076E 09	6.9882812E 04	1.1122203E 04

Table V-18. Theoretical Solutions, Antisymmetrical Case, M2 = 1.495 Pounds

FREQUENCIES

	(RADIANS2 PER SECOND2)	(RADIANS PER SECOND)	(CYCLES PER SECOND)
1	-2.0344320E 06	1.7130183E 03	2.7263550E 02
2	-4.9330075E 05	7.0235352E 02	1.1178313E 02
3	6.0593875E 04	2.4613791E 02	3.9174088E 01
4	2.7615200E 05	5.2550146E 02	8.3636230E 01
5	2.8774212E 05	5.3641577E 02	8.5373291E 01
6	4.8829700E 05	6.9877515E 02	1.1121342E 02
7	5.6299931E 05	7.5032666E 02	1.1941830E 02
8	9.6090397E 05	9.2784889E 02	1.4767187E 02
9	1.5012740E 06	1.2252646E 03	1.9500711E 02
10	3.2157780E 06	1.7931475E 03	2.8538943E 02
11	4.2870527E 06	2.0707371E 03	3.2956812E 02
12	5.0700000E 06	2.2536636E 03	3.5868199E 02
13	1.0149480E 07	3.1856692E 03	5.0701538E 02
14	1.1917779E 07	3.4522136E 03	5.4943726E 02
15	1.6293020E 07	4.0364612E 03	6.4242334E 02
16	2.7233568E 07	5.2185781E 03	8.3056323E 02
17	3.4980896E 07	5.9144648E 03	9.4131714E 02
18	1.0479118E 08	1.0236266E 04	1.6291538E 03
19	1.2783320E 08	1.1306281E 04	1.7994521E 03
20	1.9691021E 08	1.4032469E 04	2.2333399E 03
21	2.0021936E 08	1.4149887E 04	2.2520264E 03
22	2.1828480E 08	1.4774461E 04	2.3514307E 03
23	2.2143780E 08	1.4880780E 04	2.3683533E 03
24	2.5693933E 08	1.6029324E 04	2.5511484E 03
25	2.8092595E 08	1.6760844E 04	2.6675735E 03
26	3.1734554E 08	1.7814191E 04	2.8352192E 03
27	3.7711283E 08	1.9419391E 04	3.0906948E 03
28	4.0403379E 08	2.0100590E 04	3.1991111E 03
29	4.2044083E 08	2.0504652E 04	3.2634197E 03
30	4.3898599E 08	2.0951992E 04	3.3346162E 03
31	5.2897152E 08	2.2999379E 04	3.6604683E 03
32	5.7420954E 08	2.3962668E 04	3.8137805E 03
33	6.3760819E 08	2.5250902E 04	4.0188096E 03
34	6.5158118E 08	2.5526086E 04	4.0626064E 03
35	6.5953050E 08	2.5681324E 04	4.0873135E 03
36	7.6858675E 08	2.7723395E 04	4.4123164E 03
37	8.6939750E 08	2.9485547E 04	4.6927734E 03
38	9.0044896E 08	3.0157070E 04	4.7996484E 03
39	9.5823334E 08	3.0955344E 04	4.9266992E 03
40	1.1323110E 09	3.3649828E 04	5.3555391E 03
41	1.3286098E 09	3.6450098E 04	5.8012187E 03
42	1.4342559E 09	3.7871570E 04	6.0274531E 03
43	1.4741832E 09	3.8395090E 04	6.1107734E 03
44	1.5150216E 09	3.8923277E 04	6.1948359E 03
45	1.5477865E 09	3.9341914E 04	6.2614648E 03
46	1.6770463E 09	4.0951754E 04	6.5176797E 03
47	1.7846467E 09	4.2245078E 04	6.7235156E 03
48	2.1179858E 09	4.6021578E 04	7.3245664E 03
49	2.5306634E 09	5.0305699E 04	8.0064062E 03
50	2.6421466E 09	5.1401812E 04	8.1808594E 03
51	2.7051116E 09	5.2010687E 04	8.2777656E 03
52	3.6955162E 09	6.0790754E 04	9.6751562E 03
53	4.3171840E 09	6.5705250E 04	1.0457324E 04
54	4.4177367E 09	6.6466000E 04	1.0578402E 04
55	4.8835912E 09	6.9882687E 04	1.1122194E 04
56	1.9185323E 12	1.3851100E 06	2.2044731E 05

VI.   EFFECTS OF m-n WAVES ON THEORETICAL SOLUTIONS

Table VI-1. Theoretical Results by Series-Expansion Technique Using
2-and-2 Waves, Symmetrical Case

FREQUENCIES

	(RADIANS2 PER SECOND2)	(RADIANS PER SECOND)	(CYCLES PER SECOND)
1	2.9803887E 05	5.4592920E 02	8.6887405E 01
2	4.0610080E 06	2.0151941E 03	3.2072827E 02
3	5.8424960E 06	2.4171255E 03	3.8469775E 02
4	3.2717200E 07	5.7198945E 03	9.1035034E 02
5	6.2173472E 07	7.8850156E 03	1.2549402E 03
6	2.4850598E 08	1.5764070E 04	2.5089319E 03
7	2.6599467E 08	1.6309340E 04	2.5957144E 03
8	2.7893914E 08	1.6701469E 04	2.6581238E 03
9	4.3561600E 08	2.0871414E 04	3.3217917E 03
10	5.2907366E 08	2.3001602E 04	3.6608220E 03
11	7.2221926E 08	2.6874137E 04	4.2771523E 03
12	9.6263680E 08	3.1026387E 04	4.9380039E 03
13	1.0099162E 09	3.1779176E 04	5.0578164E 03
14	1.2201825E 09	3.4931109E 04	5.5594609E 03
15	2.5576374E 09	5.0573090E 04	8.0489648E 03
16	2.9634816E 09	5.4437867E 04	8.6640625E 03

Table VI-2. Theoretical Results by Series-Expansion Technique Using
3-and-3 Waves, Symmetrical Case

FREQUENCIES

	(RADIANS2 PER SECOND2)	(RADIANS PER SECOND)	(CYCLES PER SECOND)
1	2.325370CF 05	4.8222070F 02	7.6747979E 01
2	2.9836369F 05	5.4622656F 02	8.6934738F 01
3	1.9283990CF 06	1.3886680F 03	2.2101358E 02
4	2.7873980F 06	1.6695500F 03	2.6571729E 02
5	4.0779050F 06	2.0193823F 03	3.2139478E 02
6	5.865344CF 06	2.4218472F 03	3.8544922F 02
7	8.1120610F 06	2.8481680F 03	4.5330029E 02
8	3.2843744F 07	5.7309453F 03	9.1210913E 02
9	4.0623020F 07	6.3736875F 03	1.0144048F 03
10	6.2523840F 07	7.9071992F 03	1.2584709E 03
11	9.7364992F 07	9.8673672F 03	1.5704417E 03
12	2.4123331F 08	1.5531684F 04	2.4719465F 03
13	2.6600024F 08	1.6309512F 04	2.5957417F 03
14	2.7354394F 08	1.6539160F 04	2.6322915E 03
15	4.3524096F 08	2.0862426F 04	3.3203613F 03
16	5.2585982E 08	2.2931609F 04	3.6496824E 03
17	6.3361766F 08	2.5171762E 04	4.0062141E 03
18	7.0613760F 08	2.6573250F 04	4.2292656E 03
19	8.8567680F 08	2.9760320F 04	4.7365039F 03
20	9.6241971F 08	3.1022887F 04	4.9374492E 03
21	9.8976810F 08	3.1460578F 04	5.0071094E 03
22	1.2150208F 09	3.4857148F 04	5.5476914E 03
23	1.2161065F 09	3.4872715F 04	5.5501680F 03
24	1.5497389F 09	3.9366719F 04	6.2654102F 03
25	1.7924004F 09	4.2336750F 04	6.7381094F 03
26	1.9017295E 09	4.3608812F 04	6.9405625F 03
27	2.0904550F 09	4.5721492F 04	7.2768047F 03
28	2.5794273F 09	5.0788062F 04	8.0831758E 03
29	2.9610260F 09	5.4415309F 04	8.6604727F 03
30	3.2900710F 09	5.7437530F 04	9.1414766E 03
31	4.4558746F 09	6.6752312F 04	1.0623969F 04
32	5.7156035F 09	7.5601562F 04	1.2032371F 04
33	6.1565420F 09	7.8463625F 04	1.2487983F 04

Table VI-3. Theoretical Results by Series-Expansion Technique Using 4-and-4 Waves, Symmetrical Case

FREQUENCIES

	(RADIANS2 PER SECOND2)	(RADIANS PER SECOND)	(CYCLES PER SECOND)
1	-8.8332375E 04	2.9720752E 02	4.7302078E 01
2	5.3197008E 04	2.3064476E 02	3.6708282E 01
3	1.8887437E 05	4.3459668E 02	6.9168274E 01
4	2.3238781E 05	4.8206616E 02	7.6723282E 01
5	3.9698919E 05	6.3007056E 02	1.0027893E 02
6	7.1456662E 05	8.4532031E 02	1.3453703E 02
7	1.3793840E 06	1.1744717E 03	1.8692314E 02
8	1.9285200E 06	1.3887117E 03	2.2102054E 02
9	4.0779220E 06	2.0193865E 03	3.2139551E 02
10	6.1100870E 06	2.4718589E 03	3.9340894E 02
11	8.1120470E 06	2.8481655E 03	4.5330005E 02
12	1.2564801E 07	3.5446863E 03	5.6415479E 02
13	2.1252256E 07	4.6100156E 03	7.3370728E 02
14	3.2843728E 07	5.7309414E 03	9.1210840E 02
15	4.0414592E 07	6.3572461E 03	1.0117891E 03
16	6.1488720E 07	7.8414727E 03	1.2480103E 03
17	9.7365024E 07	9.8673711E 03	1.5704424E 03
18	1.8261427E 08	1.3513484E 04	2.1507397E 03
19	1.8727363E 08	1.3684793E 04	2.1780044E 03
20	2.2137170E 08	1.4878562E 04	2.3679990E 03
21	2.6599931E 08	1.6309484E 04	2.5957373E 03
22	2.7137229E 08	1.6473379E 04	2.6218220E 03
23	4.3524147E 08	2.0862441E 04	3.3203638E 03
24	5.3604480E 08	2.3152641E 04	3.6848606E 03
25	6.3361715E 08	2.5171750E 04	4.0062122E 03
26	6.9887181E 08	2.6436184E 04	4.2074531E 03
27	8.1368166E 08	2.8525105E 04	4.5399141E 03
28	8.6828237E 08	2.9466629E 04	4.6897617E 03
29	9.6322611E 08	3.1035883E 04	4.9395156E 03
30	9.8976819E 08	3.1460578E 04	5.0071094E 03
31	1.0585175E 09	3.2534863E 04	5.1780859E 03
32	1.2150185E 09	3.4857113E 04	5.5476836E 03
33	1.3014927E 09	3.6076207E 04	5.7417109E 03
34	1.5497398E 09	3.9366734E 04	6.2654141E 03
35	1.7924009E 09	4.2336754E 04	6.7381094E 03
36	1.9017298E 09	4.3608824E 04	6.9405664E 03
37	2.0625518E 09	4.5415324E 04	7.2280781E 03
38	2.0904538E 09	4.5721480E 04	7.2768047E 03
39	2.1096376E 09	4.5930789E 04	7.3101172E 03
40	2.3215388E 09	4.8182348E 04	7.6684648E 03
41	2.3580001E 09	4.8559242E 04	7.7284492E 03
42	2.7818263E 09	5.2743020E 04	8.3943203E 03
43	2.9693565E 09	5.4491801E 04	8.6726445E 03
44	3.0310956E 09	5.5055387E 04	8.7623437E 03
45	3.2598185E 09	5.7094820E 04	9.0869297E 03
46	3.4002770E 09	5.8311891E 04	9.2806328E 03
47	3.5969298E 09	5.9974406E 04	9.5452305E 03
48	4.4558582E 09	6.6752187E 04	1.0623949E 04
49	5.7156035E 09	7.5601562E 04	1.2032371E 04
50	6.1565256E 09	7.8463000E 04	1.2487863E 04
51	6.7898081E 09	8.2400250E 04	1.3114418E 04
52	8.9513656E 09	9.4611625E 04	1.5057922E 04
53	9.1526758E 09	9.5669562E 04	1.5226297E 04
54	9.6831365E 09	9.8402875E 04	1.5661316E 04
55	9.7501716E 09	9.8742937E 04	1.5715441E 04
56	7.0252478E 13	8.3816750E 06	1.3339860E 06

VI-3

VII.   PARTIAL THEORETICAL RESULTS BY
       FINITE-ELEMENT METHOD

Table VII-1. Partial Theoretical Results by Finite-Element Method

Number	Frequency (cps)	Number	Frequency (cps)
1	100.0771	37	2058.8291
2	126.9309	38	2161.4058
3	222.0947	39	2635.6746
4	275.3350	40	3111.8683
5	293.9966	41	3357.9205
6	346.2781	42	3941.1907
7	399.8242	43	4010.1134
8	421.9558	44	4424.3725
9	423.4841	45	4574.8056
10	476.1563	46	4751.6628
11	563.7197	47	4913.0827
12	580.4711	48	4977.1049
13	628.1904	49	5068.8489
14	667.2099	50	5117.4123
15	734.3760	51	5341.0851
16	767.2533	52	5578.4356
17	864.4956	53	5896.8323
18	874.1940	54	6158.6119
19	948.2020	55	6318.6493
20	975.6170	56	6875.2379
21	983.8023	57	7896.6878
22	1028.1057	58	8165.1817
23	1106.9605	59	8235.4334
24	1157.8791	60	8259.5258
25	1210.9138	61	8275.9963
26	1245.2667	62	8283.7203
27	1296.9220	63	8295.8899
28	1406.9971	64	8313.4963
29	1441.4703	65	8367.6961
30	1456.2856	66	8529.9496
31	1569.3106	67	8891.9360
32	1605.9887	68	8960.3282
33	1685.4192	69	9205.9339
34	1765.1616	70	9337.6633
35	1840.8007	71	9391.6738
36	1888.7098	72	10733.6480

VIII.   COMPARISON OF ANALYTICAL AND EXPERIMENTAL
RESULTS, MAJOR RESONANCES

Table VIII-1. Comparison of Theoretical and Experimental Frequency Density (Mass Number 0)

Freq No.	Theo Freqs (Hz), Series Expansion Tech		Major Resonances (Hz), Experimental		
	Symmetrical	Antisymmetrical	Lower Freq	Center Freq	Higher Freq
1	52.68	52.62			
2	64.93	65.04			
3	84.25	84.27	83.9	84	86.8
4	109.13	109.16	97.3	120	124.1
5	153.67	153.62	141.	142	160
6	199.62	200.29	198.	204	205
7	224.02	223.98	218.	223	229
8	288.86	288.90	279.	280	288
9	309.78	308.77	297.	303	308
10	318.45	322.19			
11	494.94	489.45	468.	492	499
12	553.15	554.72	538.5	550	560
13	652.32	652.33	645.	646	660
14	822.27	830.57	819.	828	819
15	941.23	941.33	902.	925	983
16	1083.82	1081.72	1050	1110	1139
17	1450.81	1438.97	1420	1445	1460
18	1751.41	1751.19	1715	1729	1780
19	1799.76	1799.82	1790	1810	1830
20	2246.68	2250.35	2220	2240	
21	2250.41	2252.86		2250	
22	2324.37	2351.43	2320	2340	2350
23	2551.29	2552.51	2540	2545	2560
24	2669.57	2669.99	2620	2650	2690
25	2739.45	2736.88	2720	2730	2750
26	3092.07	3092.39	3060	3070	3095
27	3163.56	3153.90	3150	3160	3170

Table VIII-2. Comparison of Theoretical and Experimental Frequency Density (Mass Number 7)

Theo Freqs (Hz) by Series Expansion Tech*	Major Resonances (Hz) by Exp Measurement*	Theo Freqs (Hz) by Finite-Elements Method*
50.84		
52.65		
65.00		
62.72		
81.76		
84.16	83, 84, 85, 86	100.08
107.88	98, 99	
109.00	109, 115, 120	126.93
151.93	140, 141	
153.37	154	
159.32	159, 162, 170	
185.30	200, 205	
220.15	217	222.09
223.35	226	
248.80	256	
	278, 282	275.34
286.12	286	
288.20	288	
289.47	290	294
309.49	300, 302, 309, 310	
322.19	315	346.28
	363, 372, 385	399.82
	403, 422	421.96
455.44	455	423.48
494.95	466, 472, 488	476.16
501.92	495, 501	
	535, 540	
553.94	554, 555, 578	563.72
	590	580.47
648.62, 648.82	640, 648, 655	628.19
	660, 670	667.21
	701, 702	734.38
	760, 762	767.25
830.57	801, 823, 838	864.50
	887, 890	874.19
917.95	910	
933.48	933	
935.33	935	
941.33	941	948.20
	960, 970	975.62
	982	983.80
	1035	1028.11
1081.08	1090	

*NOTE: The missing frequencies are due to the limitation of (1) the number of m-n waves used with the series expansion technique, (2) the number of the elements and the degrees of freedom employed with the finite-element method, or (3) the instrumentation set-up and orientation in experimental measurement.

Table VIII-3. Comparison of Natural Frequencies of Shell I

Case Number	Test Run No.	M_2/M_1	Freq. (cps) / Mode	1	2	3
0	0-2	0	Comp. Test	75.8 87.5	121.3 128.6	221.2 233.9
1	1a-2	0.16	Comp. Test	75.7 87.1	117.9 128.0	220.6 232.2
2	1-2	0.32	Comp. Test	75.6 86.4	114.1 127.0	219.8 230.7
3	2-2	0.60	Comp. Test	75.2 84.2	105.7 124.5	217.7 228.5
4	3-2	0.82	Comp. Test	75.0 82.6	102.7 123.1	216.9 228.1
5	4-2	1.40	Comp. Test	74.7 76.5	94.6 119.6	214.7 226.7
6	5-2	1.90	Comp. Test	73.7 71.5	83.7 118.0	209.5 226.1

Table VIII-4. Comparison of Axial
Model Frequencies

Mode Number	Analytical (cps)	Experimental (cps)
1	621.8	610
2	1870.0	1893
3	3126.4	3285
4	4384.5	4396
5	5631.7	--
6	6853.5	--

Experimental   Analytical
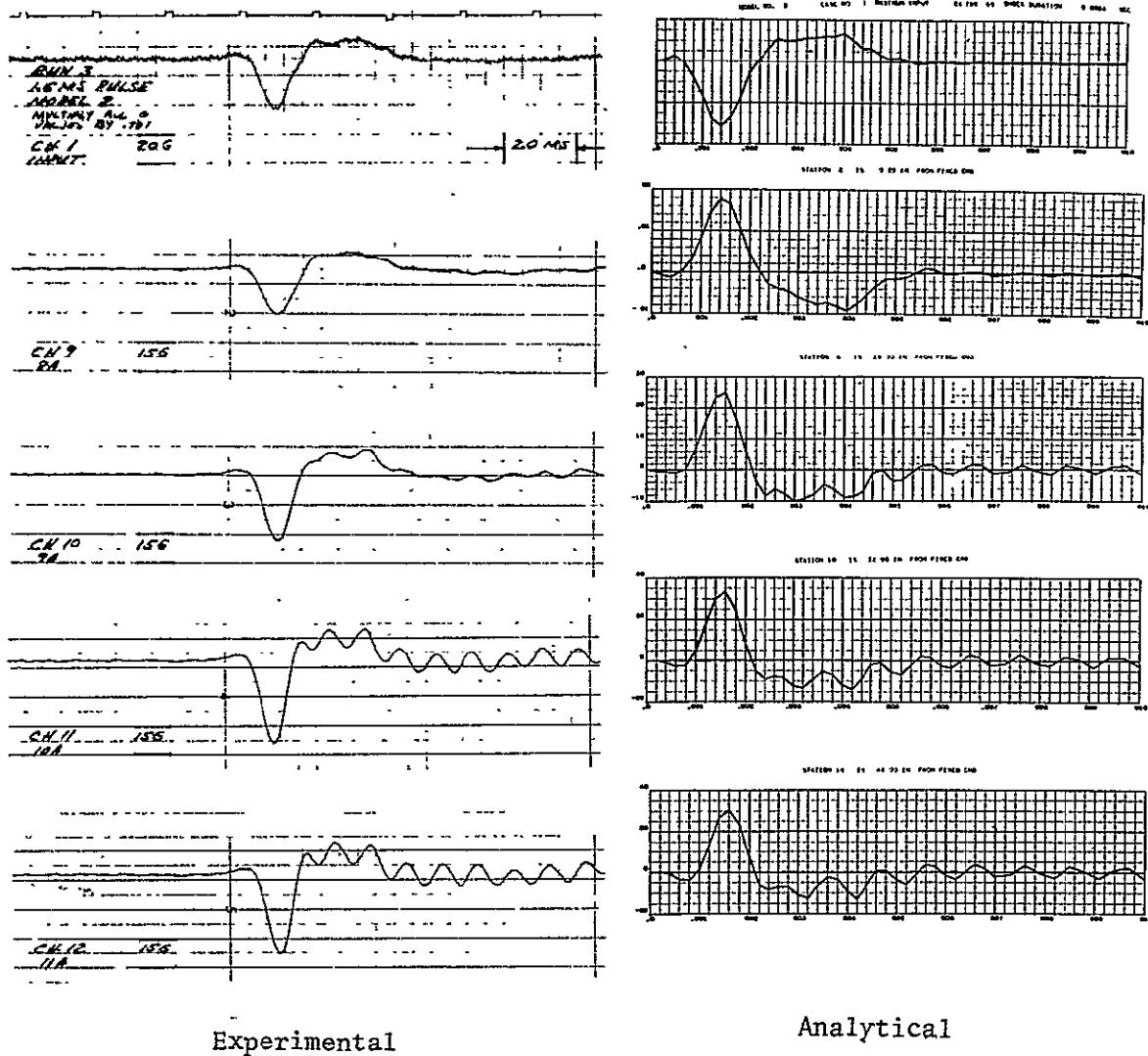
Figure VIII-1. Comparison of Analytical and Experimental Results,
Model 2, Run 3
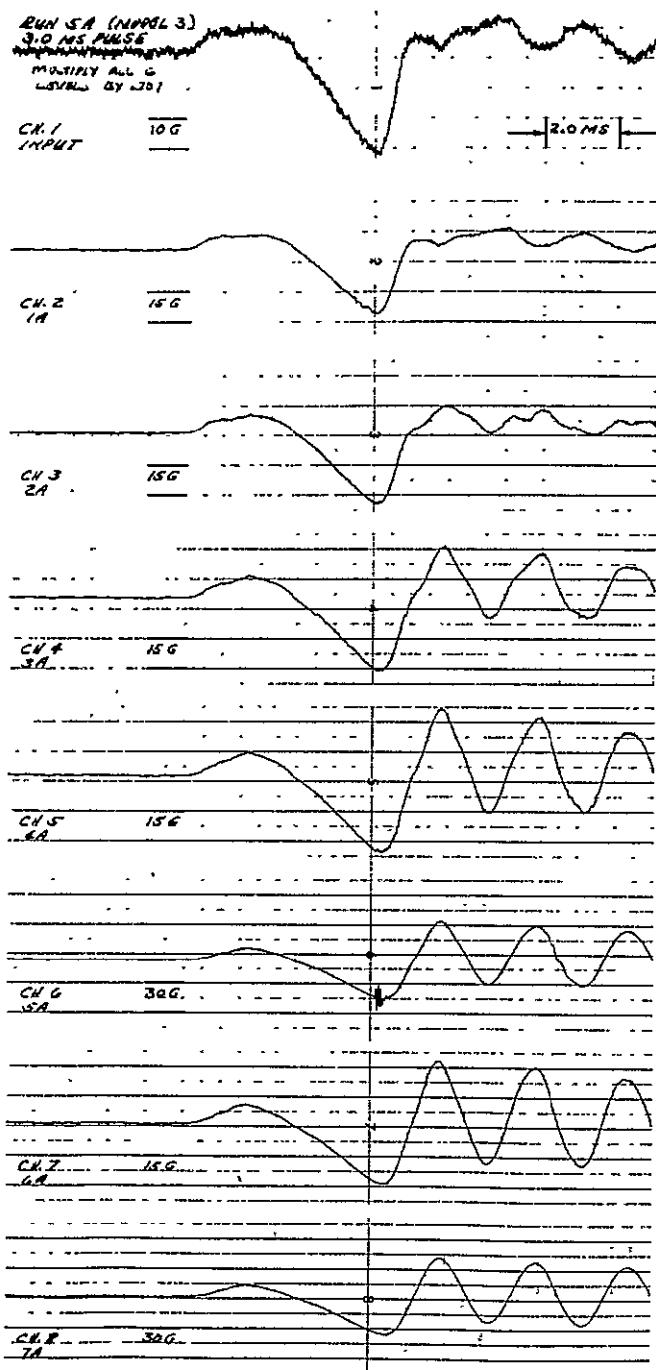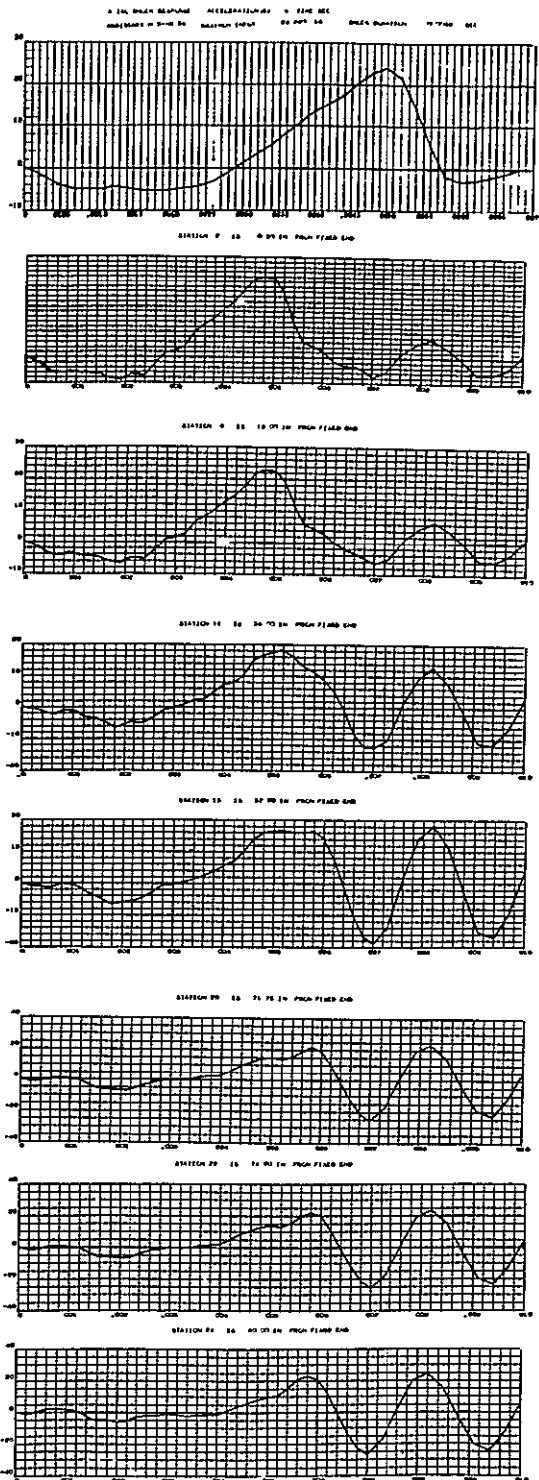
Experimental   Analytical

Figure VIII-2.   Comparison of Analytical and Experimental Results,
Model 3, Run 5A

Experimental
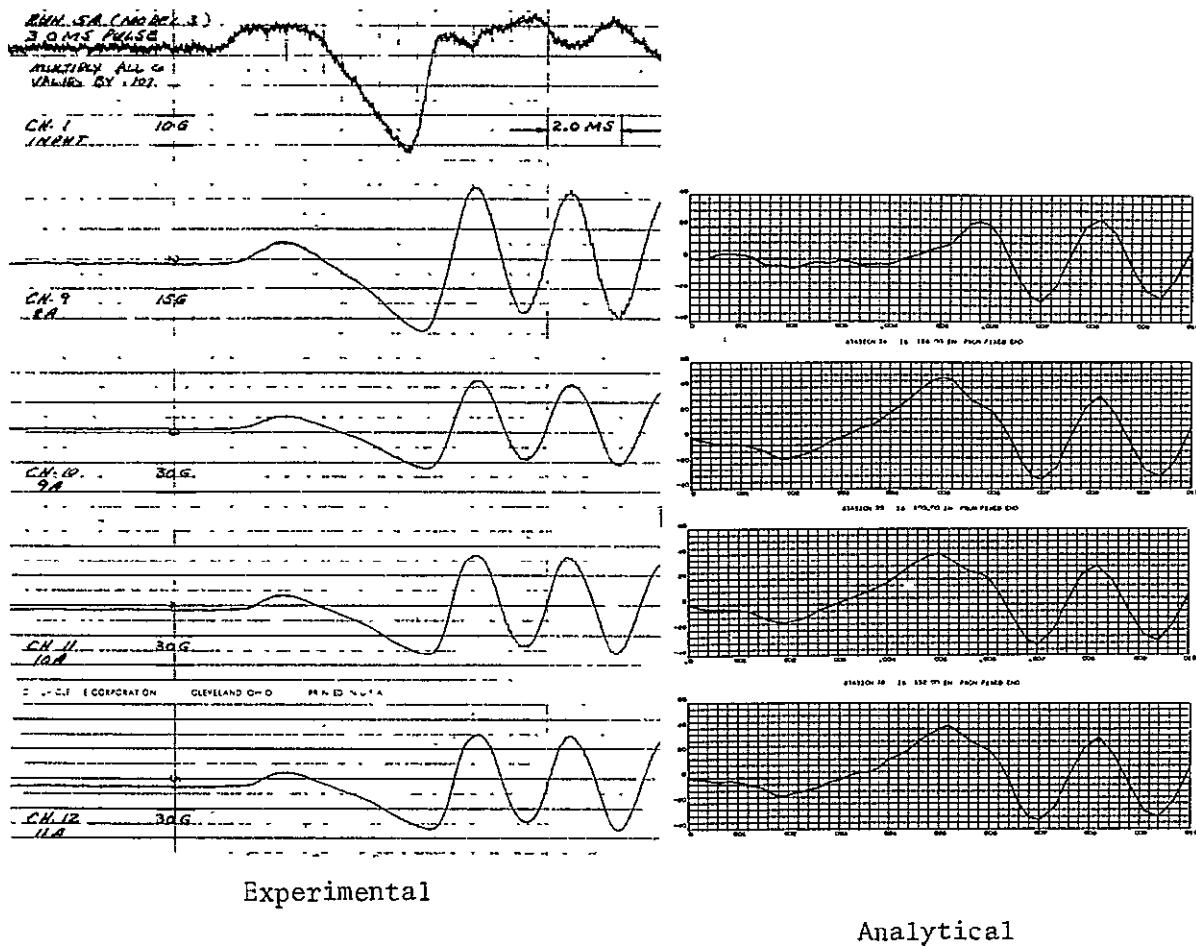
Analytical

Figure VIII-3. Comparison of Analytical and Experimental Results, Model 3, Run 5A (Continued)
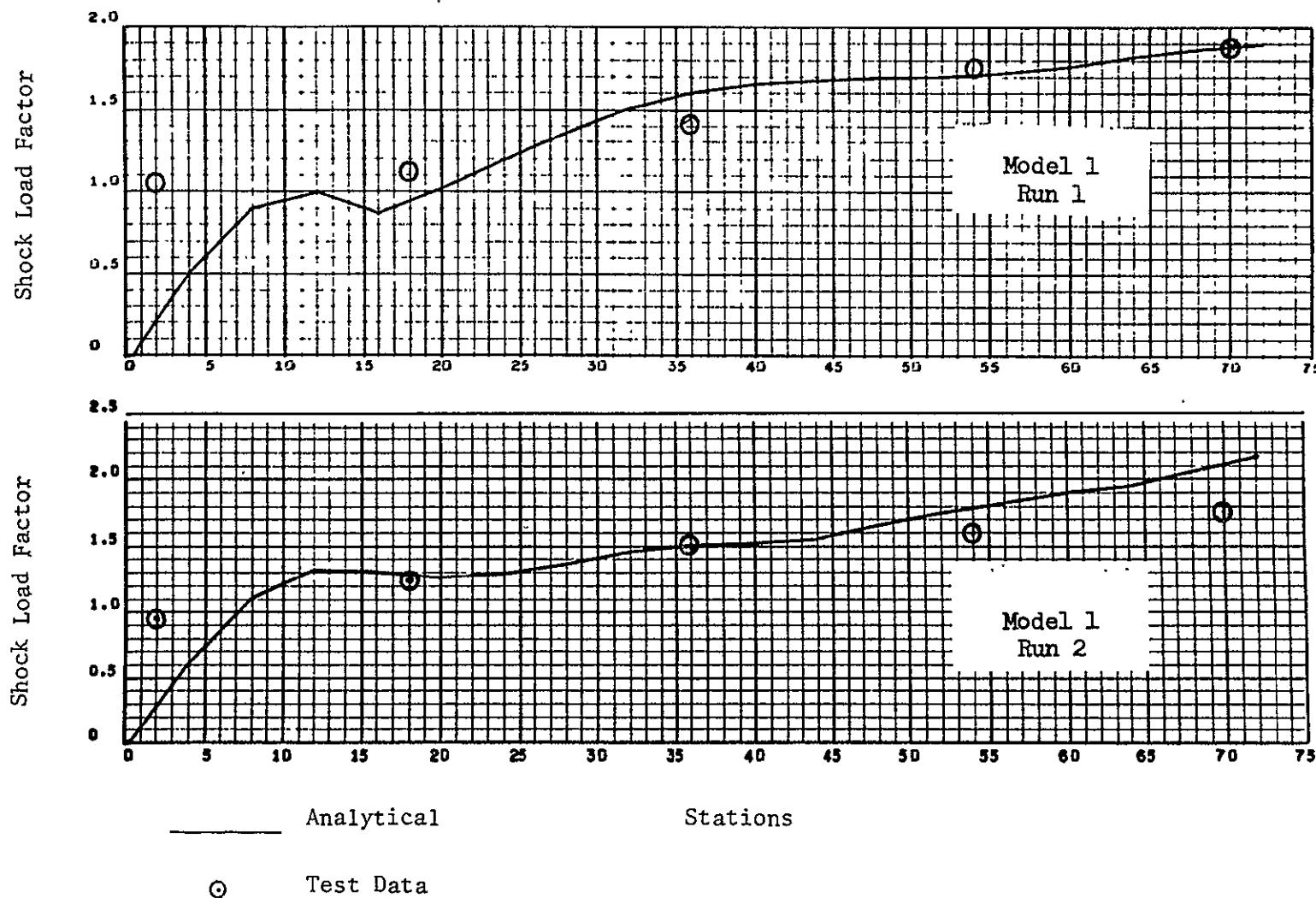
Figure VIII-4. Comparison of Shock Transmissibility for Model 1,
Runs 1 and 2
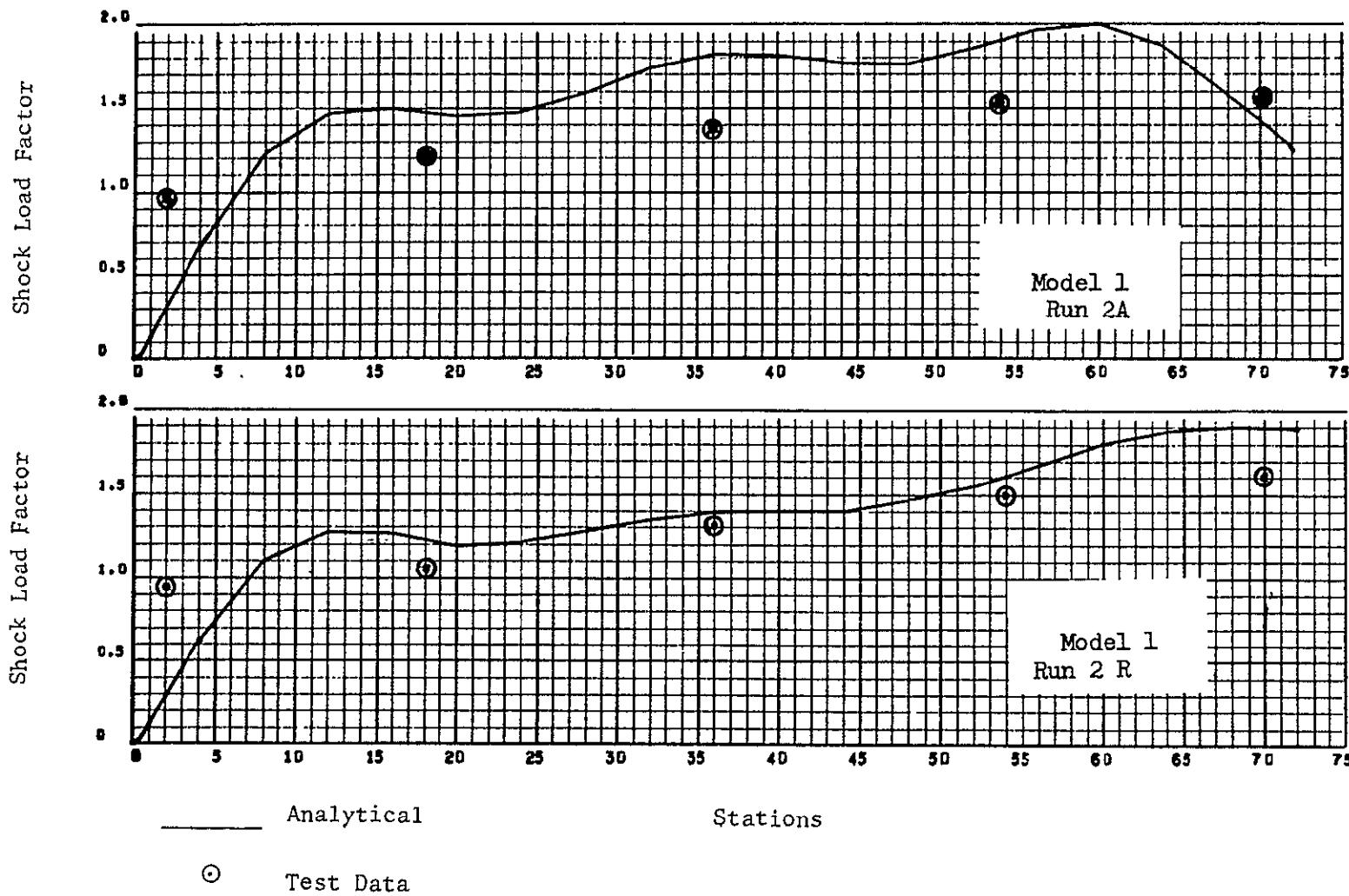
Figure VIII-5. Comparison of Shock Transmissibility for Model 1,
Runs 1 and 2

IX. SURVEY OF EFFECTIVE FORCING AREAS
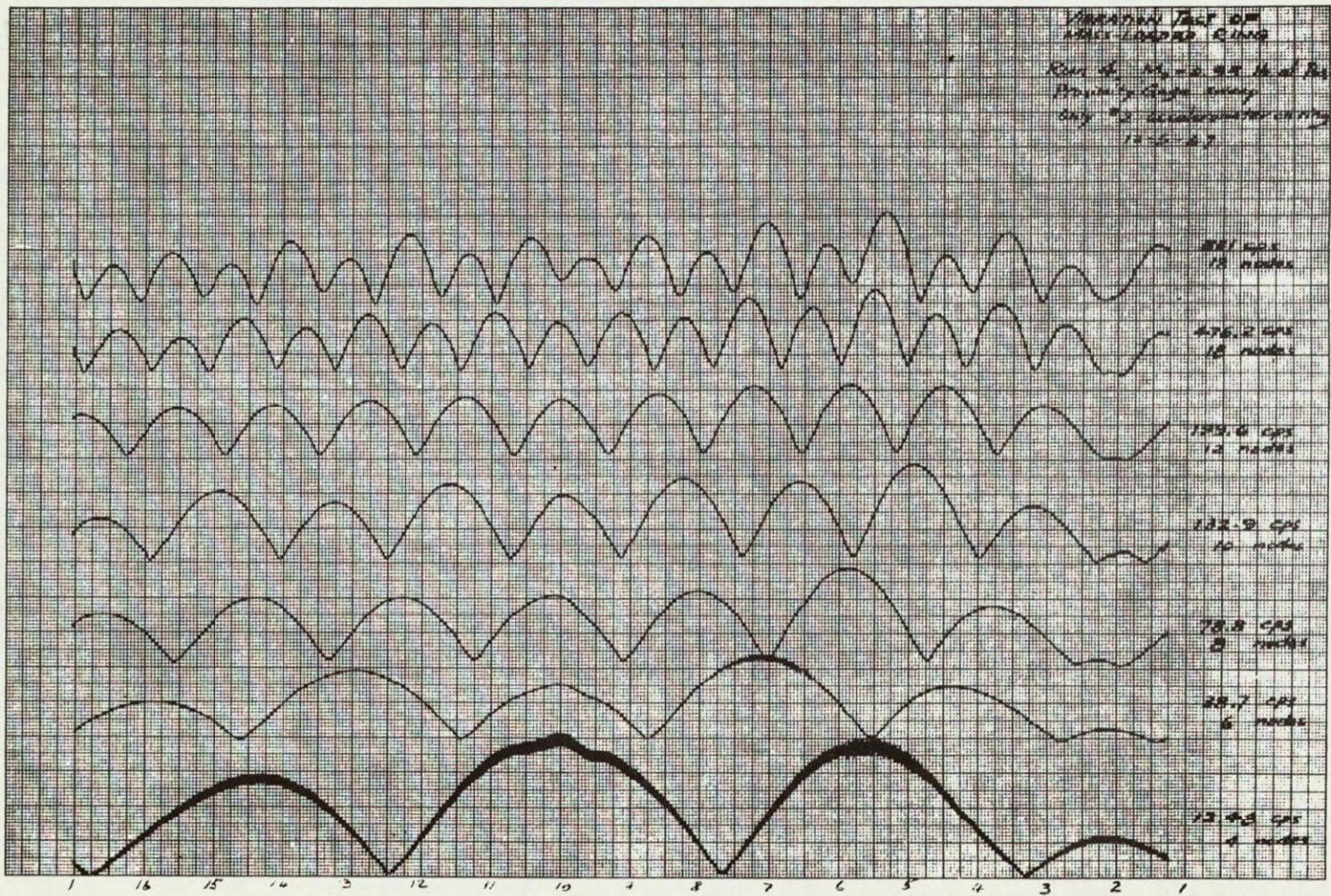
Figure IX-1.   Effective Vibratory Forcing Areas of Mass-Loaded Ring
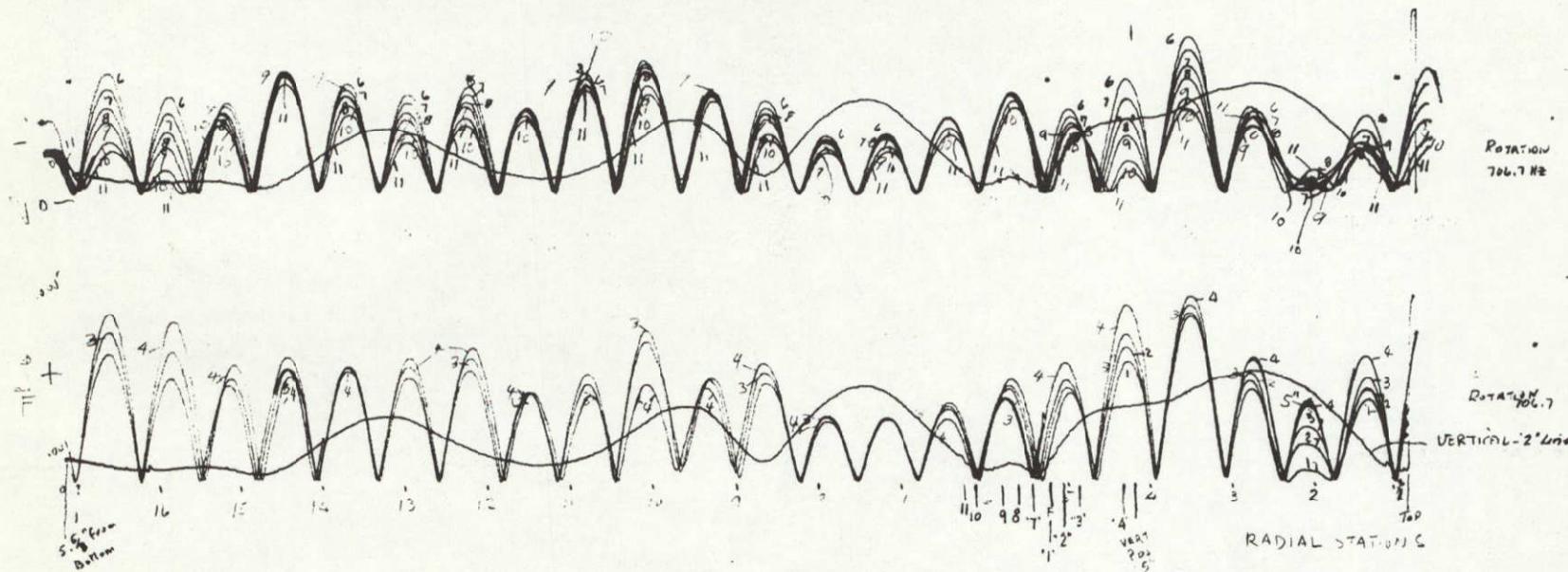
TEST RUN 8-3-V-P-"2"
            8-3-R-P-F
20V   3-26-69

ROTATIONAL
TEST RUNS   1 2 3 4 5 6 7 8 9 10 11
LOCATIONS "F 3¾"1·5 3 5 4½" F ⅞ 1½ 2⅜ 3⅜ 4¾"
           UP UP UP UP   DN DN DN DN DN
           0 + + + + 0 - - - - -

VERT
706.7 HZ

ROTATION
706.7 HZ

ROTATION
706.7

VERTICAL-2" Line

RADIAL STATIONS

Figure IX-2. Effective Vibratory Forcing Areas of Mass-Loaded Shell IV, 707 Hertz
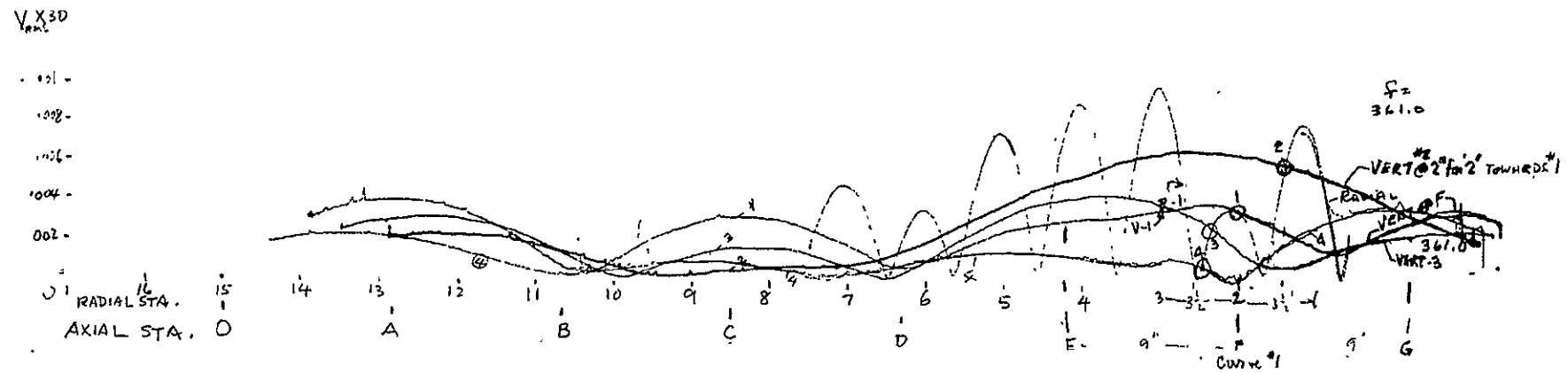
Figure IX-3. Effective Vibratory Forcing Areas of Mass-Loaded
Shell IV, 361 Hertz

VER7 82.5 HZ
. Sweep

82.5 HZ
RADIAL
C.P

RADIAL STATIONS
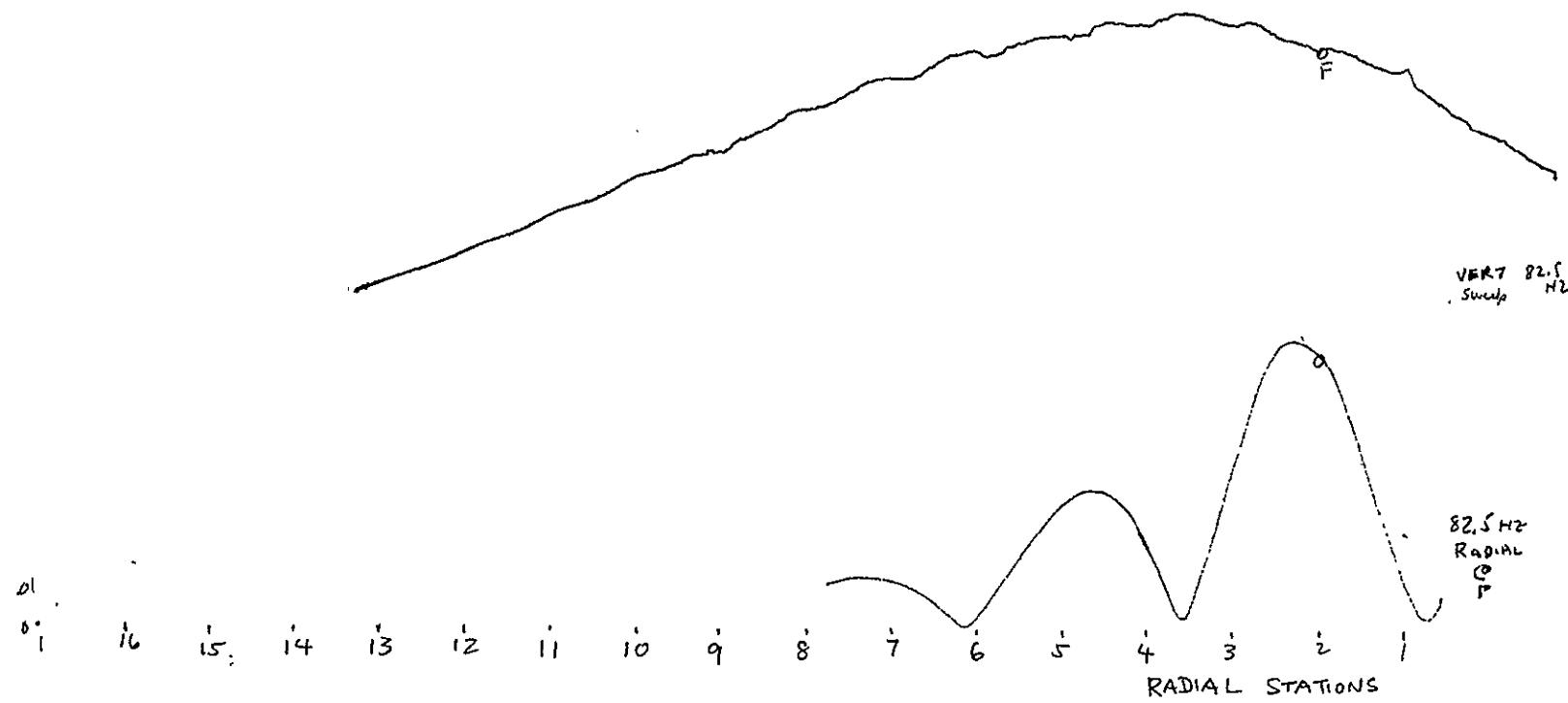
**Figure IX-4. Effective Vibratory Forcing Areas of Mass-Loaded
Shell IV, 82.5 Hertz**

Space Division
North American Rockwell

X. EVALUATION OF SHELL IMPERFECTIONS
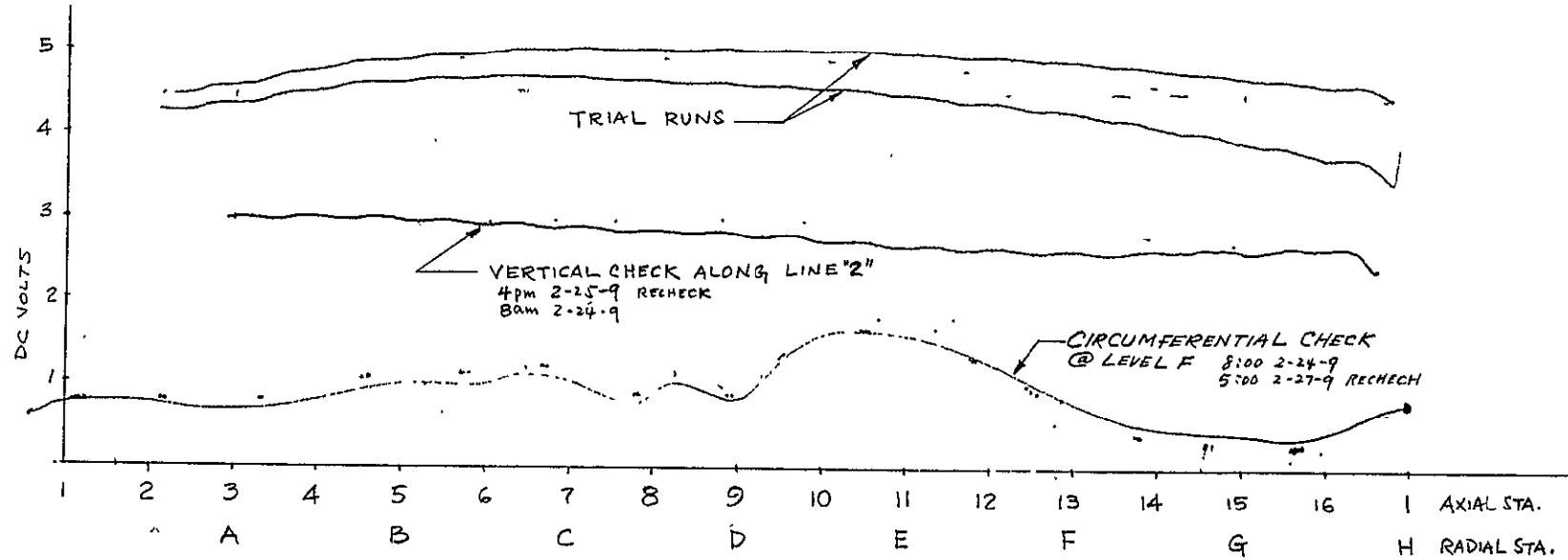
Figure X-1. Two-Dimensional (m, n) Imperfection of Mass-Loaded Shell
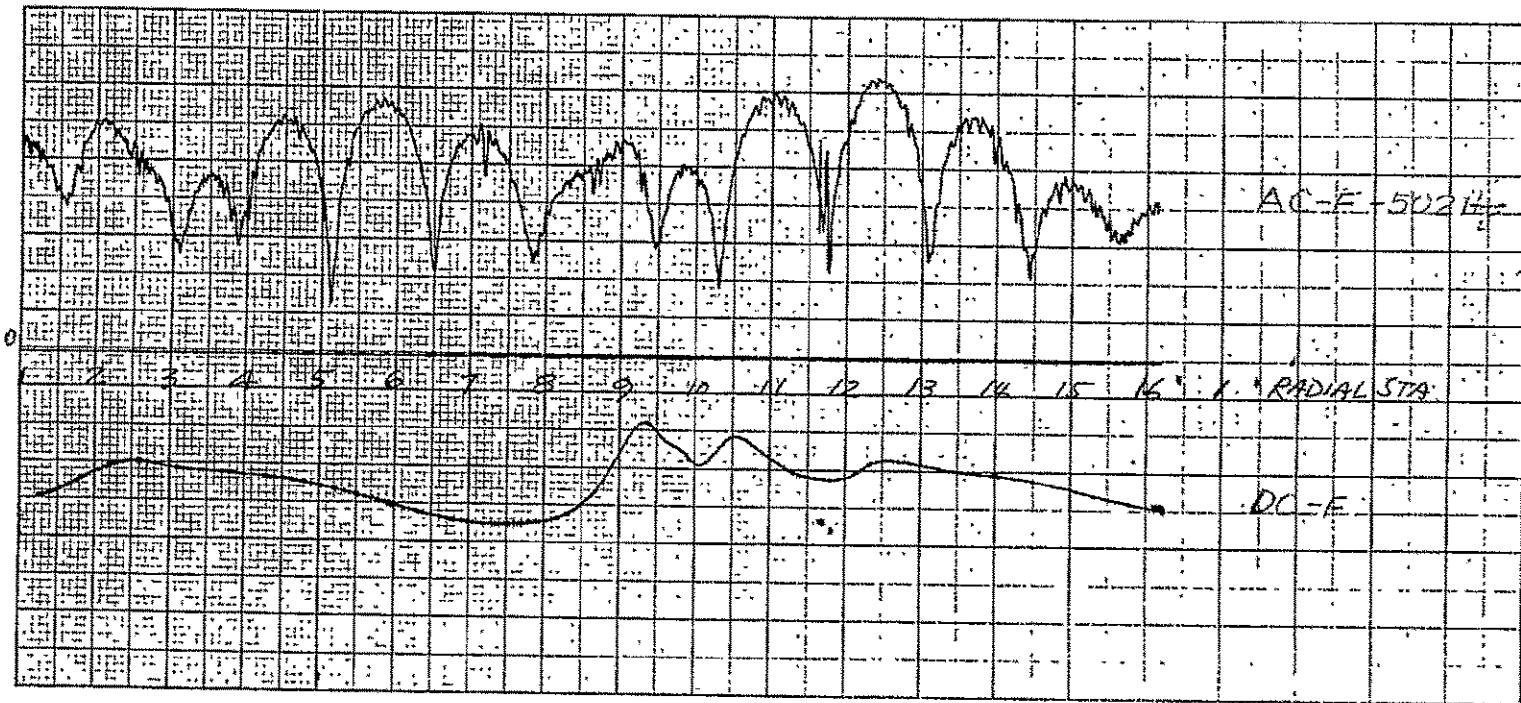
Figure X-2. Imperfection Shape (DC) Versus Vibratory Shape (AC)

Figure X-3. Circumferential and Longitudinal Imperfection

DC *F LEVEL
(CIRCUMFERENTIAL)

RADIAL STA

DC *B LEVEL
(CIRCUMFERENTIAL)

RADIAL STA

DC *10 LINE
(LONGITUDINAL)

VERT. STA.

G   F   E   D   C   B   A
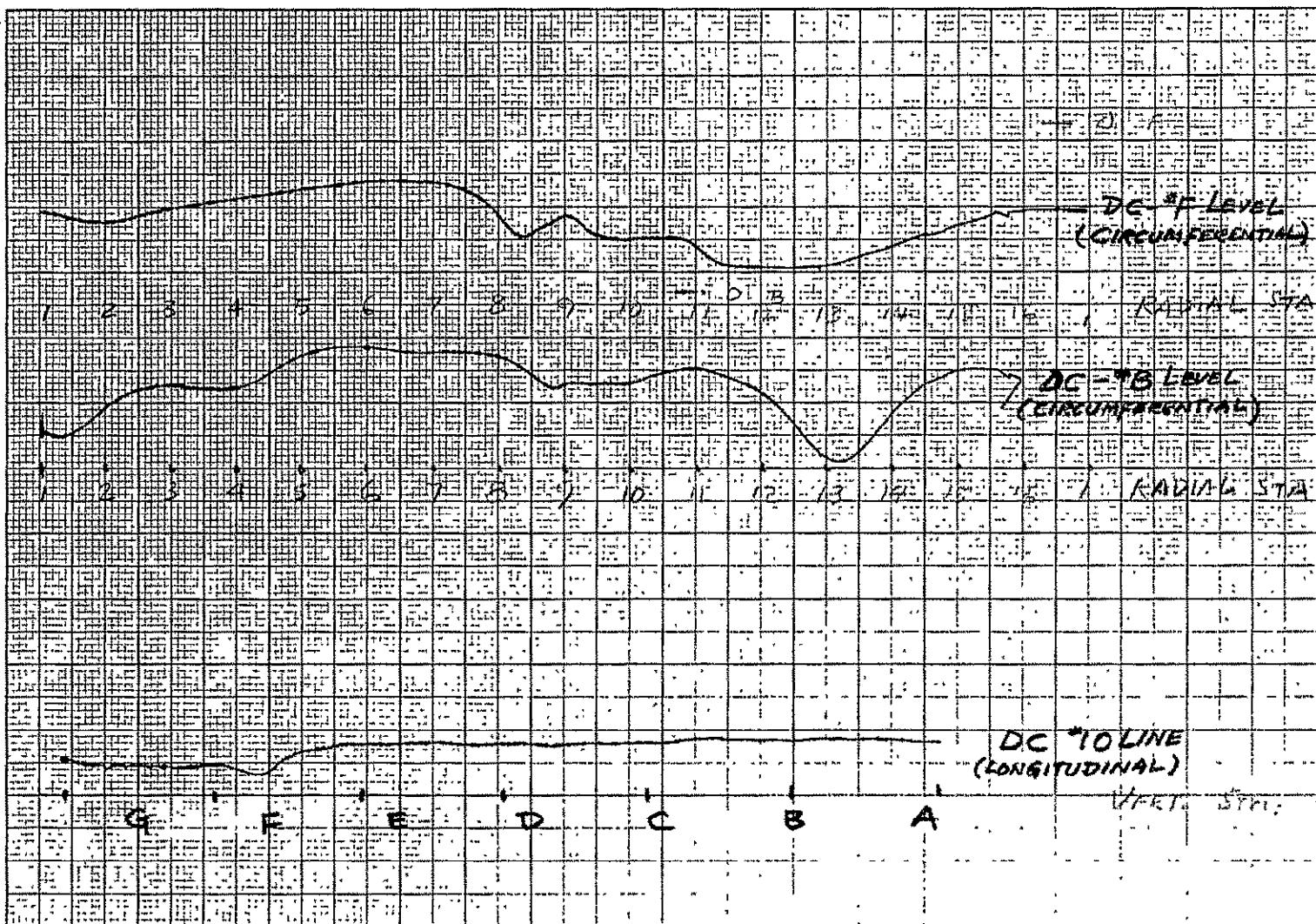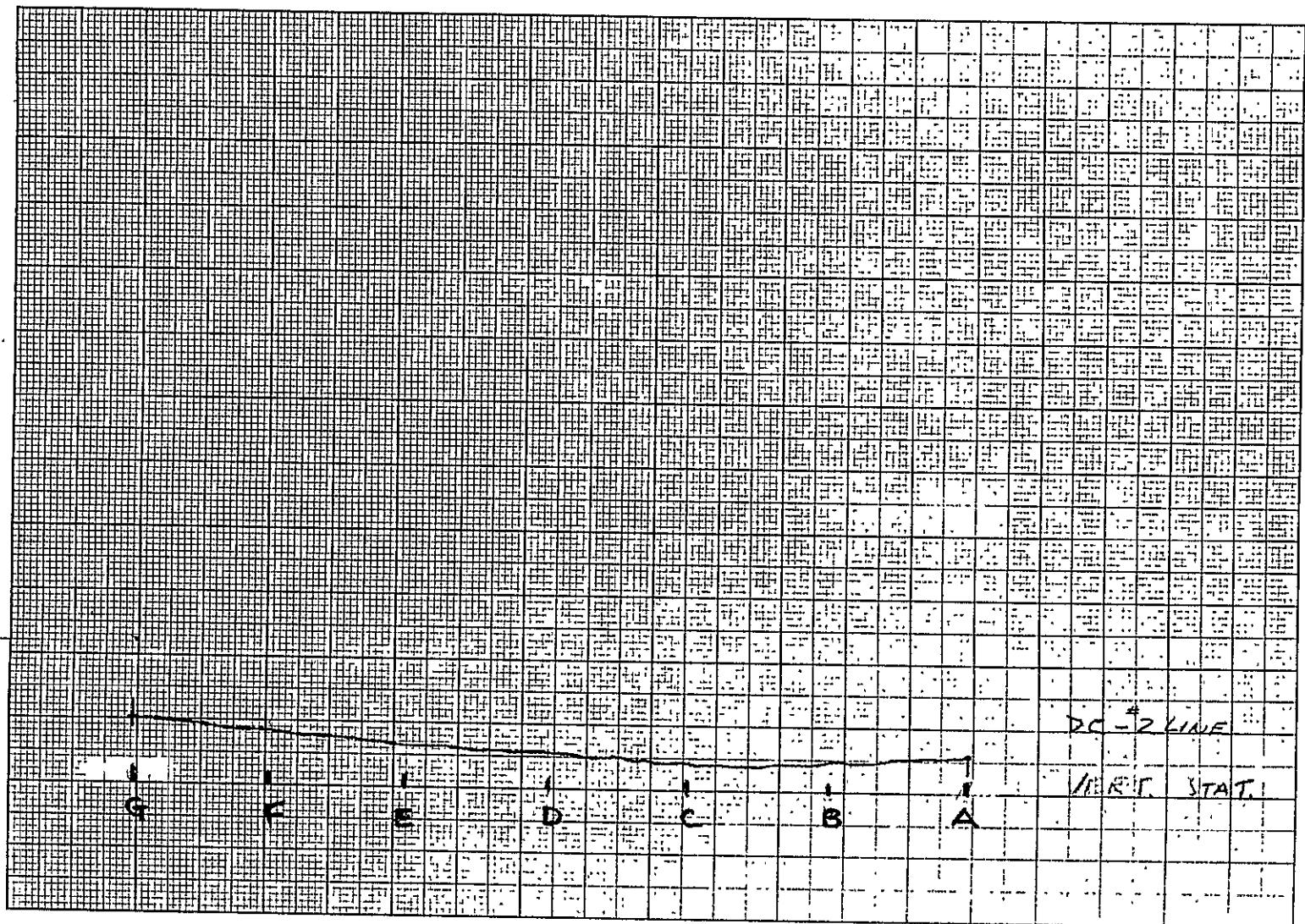
Figure X-4. Longitudinal Imperfection Line No. 2

XI. CALIBRATION AND LINEARITY CHECK

O-1-R-F-141.9
3/4/69
NO MASS CASE
N-MODE SURVEY AT "F" LEVEL
& LINEARITY CHECK
141.9 Hz

OUTPUT VOLTS

INPUTS
22 V
20 V
16 V
12 V
8 V
4 V

RADIAL STATIONS

Space Division
North American Rockwell
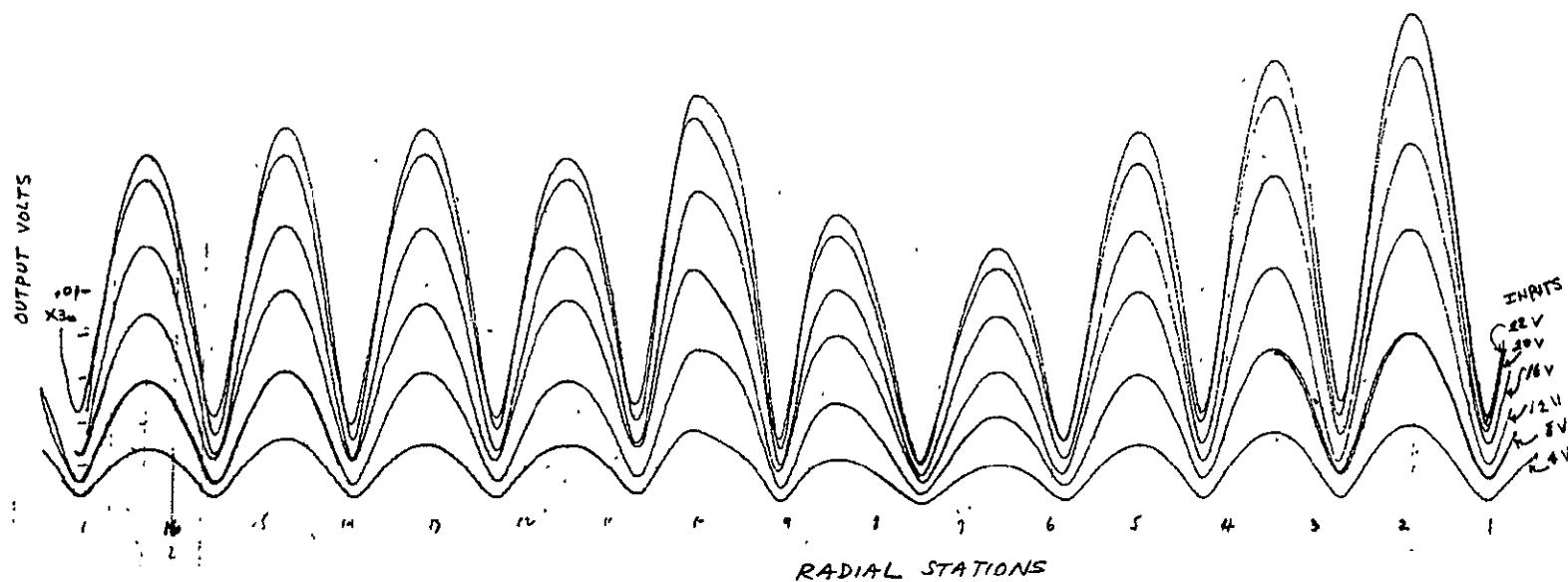
Figure XI-1. Calibration and Linearity Plot, 142 Hertz, n = 5

0-1-R-F-124.2
3/4/7

NO MASS CASE
N- MODE SURVEY &
LINEARITY CHECK
124.2 Hz
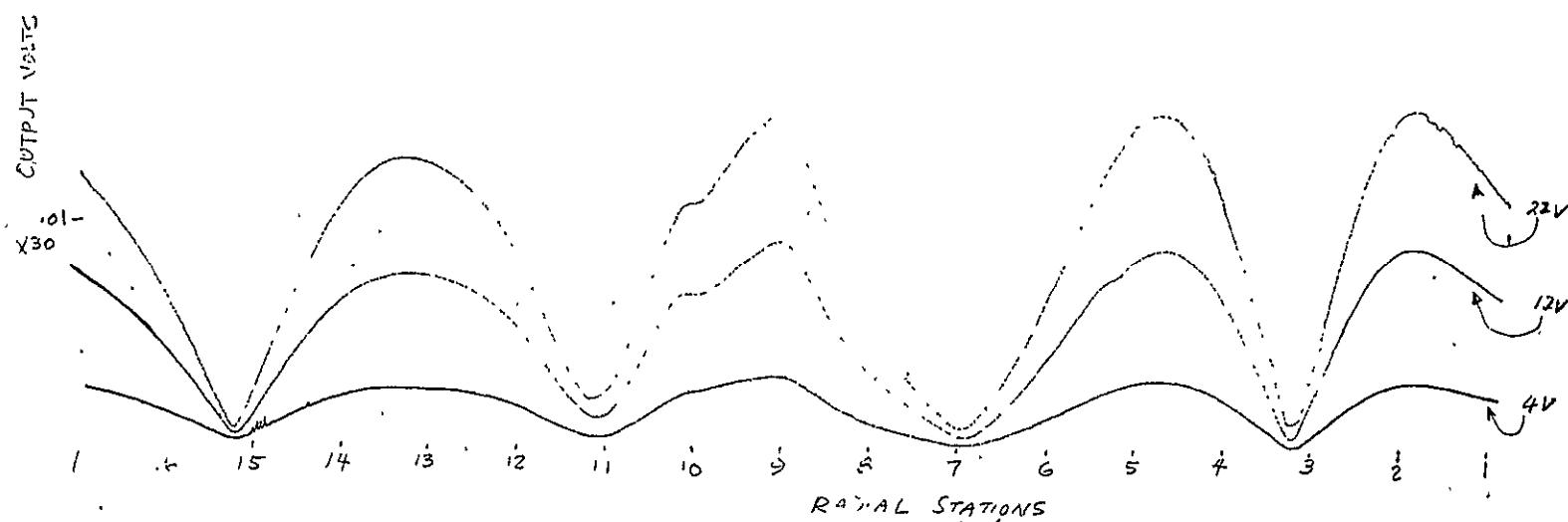
Figure XI-2. Calibration and Linearity Plot, 124 Hertz, n = 4

"N" mode 22 V
NO MASS, ROTATIONAL, 5 ACC, "F" LEVEL
O-5-R-F-141Hz
2/27/9
N-MODE SURVEY &
LINEARITY CHECK 141Hz

22V(INPUTS)

20V

16V

12V

8V

4V

RADIAL STATIONS
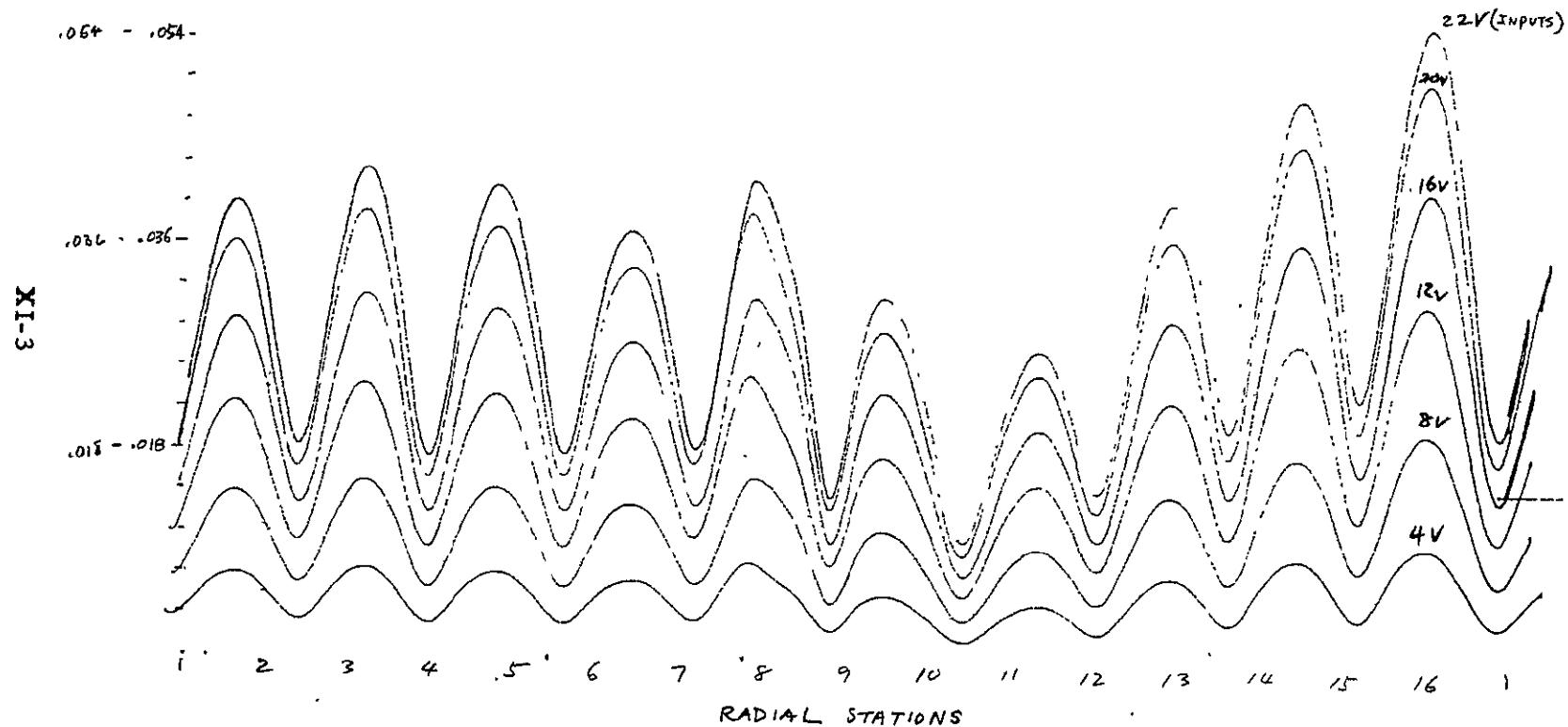
Figure XI-3. Calibration and Linearity Plot, 141 Hertz; n = 5

"N" mode Survey @ "D","F", & "B" level
O-5-R-D-141.5
NO MASS CASE 141.5 Hz

"D"-22 V

"F"-22 V

"B"-22 V

VOLTS OUTPUT

.054 .054

.036 .036

.018 .018

1 2 3 4 5 6 7 8 9 10 11 12 13 14 15 16

RADIAL STATIONS
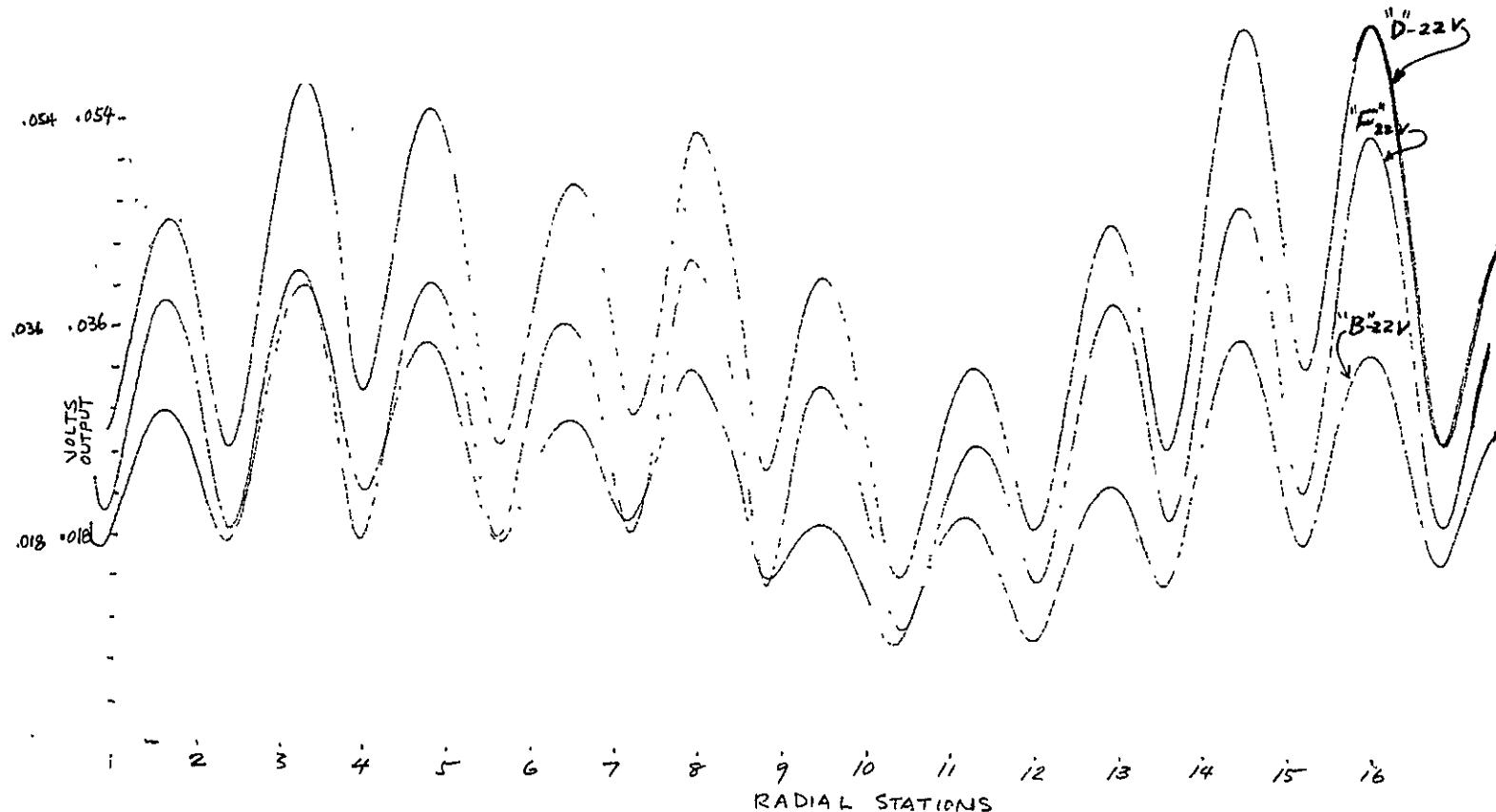
Figure XI-4. Calibration and Linearity Plot, Levels F, D, and B

Space Division
North American Rockwell
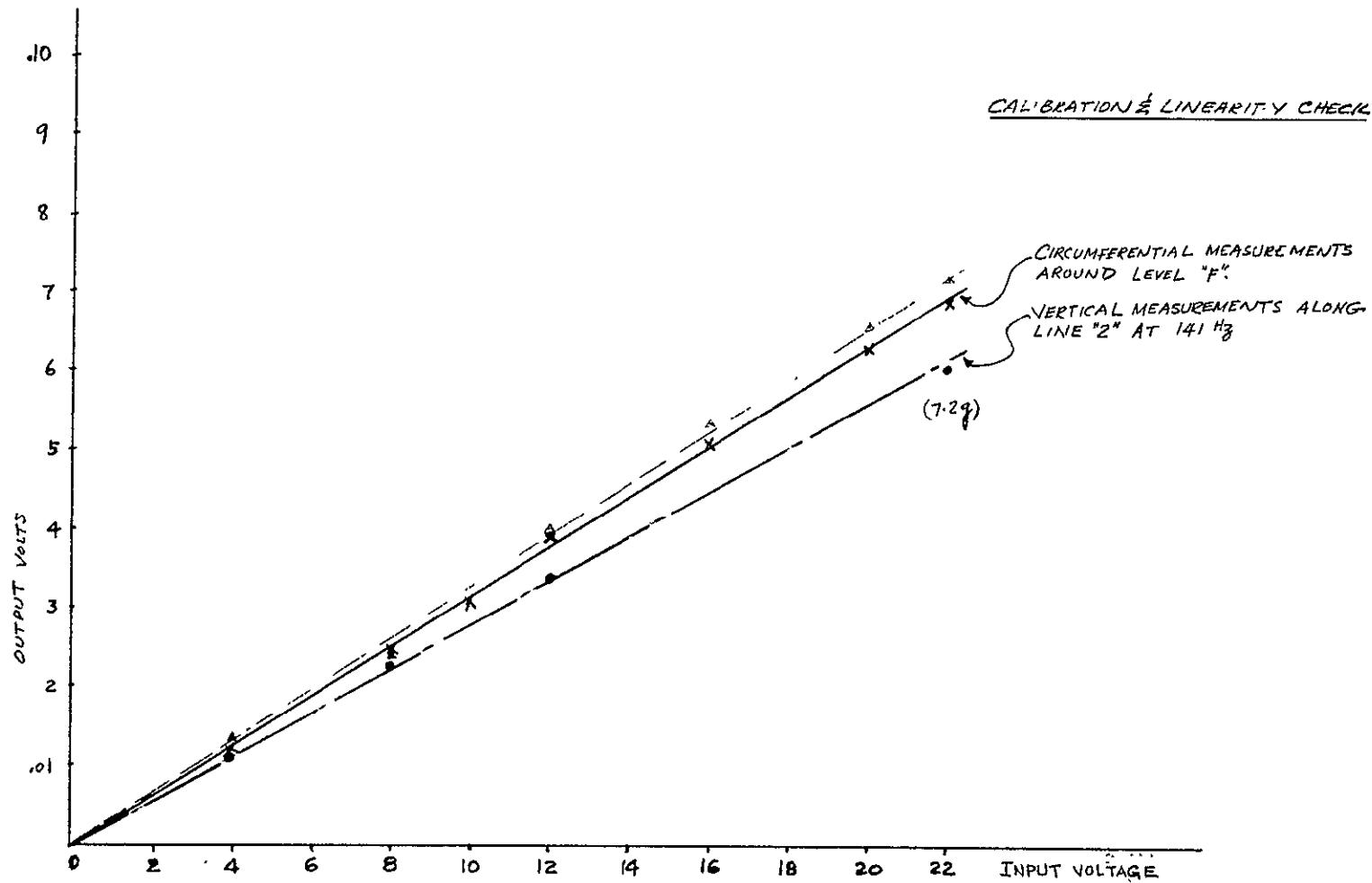
Figure XI-5. Linearity Between Input and Output Relations

0 - 5 - V - 141.5 Hz

2 - 26 - 9

NO MASS VERTICAL SURVEY
M-MODE 5 ACCEL.
FREQ 141.5 Hz

M - MODE SURVEY
&
LINEARITY CHECK

.07

.06

.05

.04

03

.02

.01

O

VOLTAGE OUTPUT

22V (INPUT)

20V (INPUT)

16L (INPUT)

12V (INPUT)

8V (INPUT)

4 VOLTS (INPUT)

2 V (INPUT)

141.5 Hz

22V

A   B   C   D   E   F   G   AXIAL STATIONS ~ #2 LINE
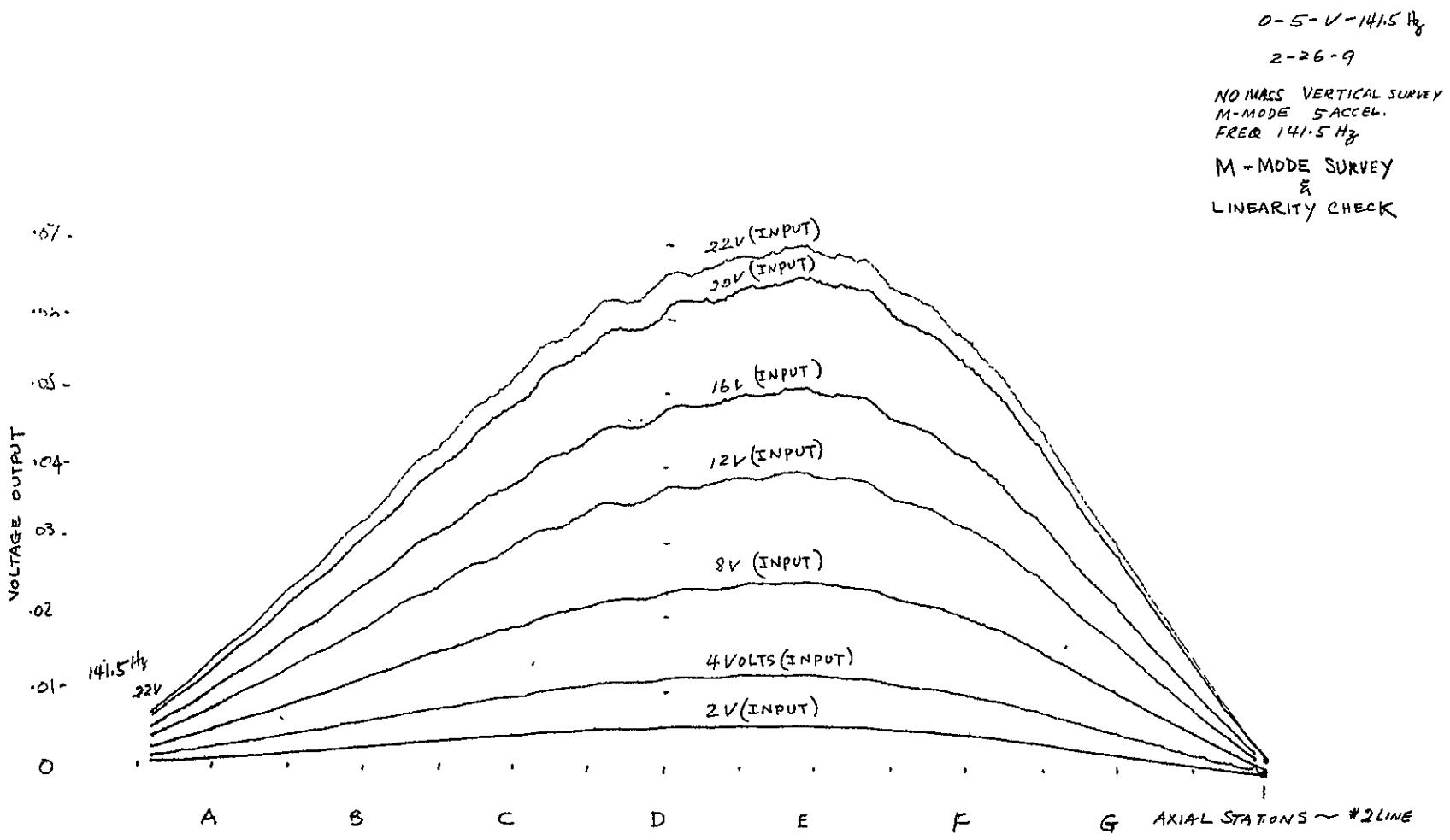
Figure XI-6. **M-Mode Linearity Plot 5 Accelerometers**
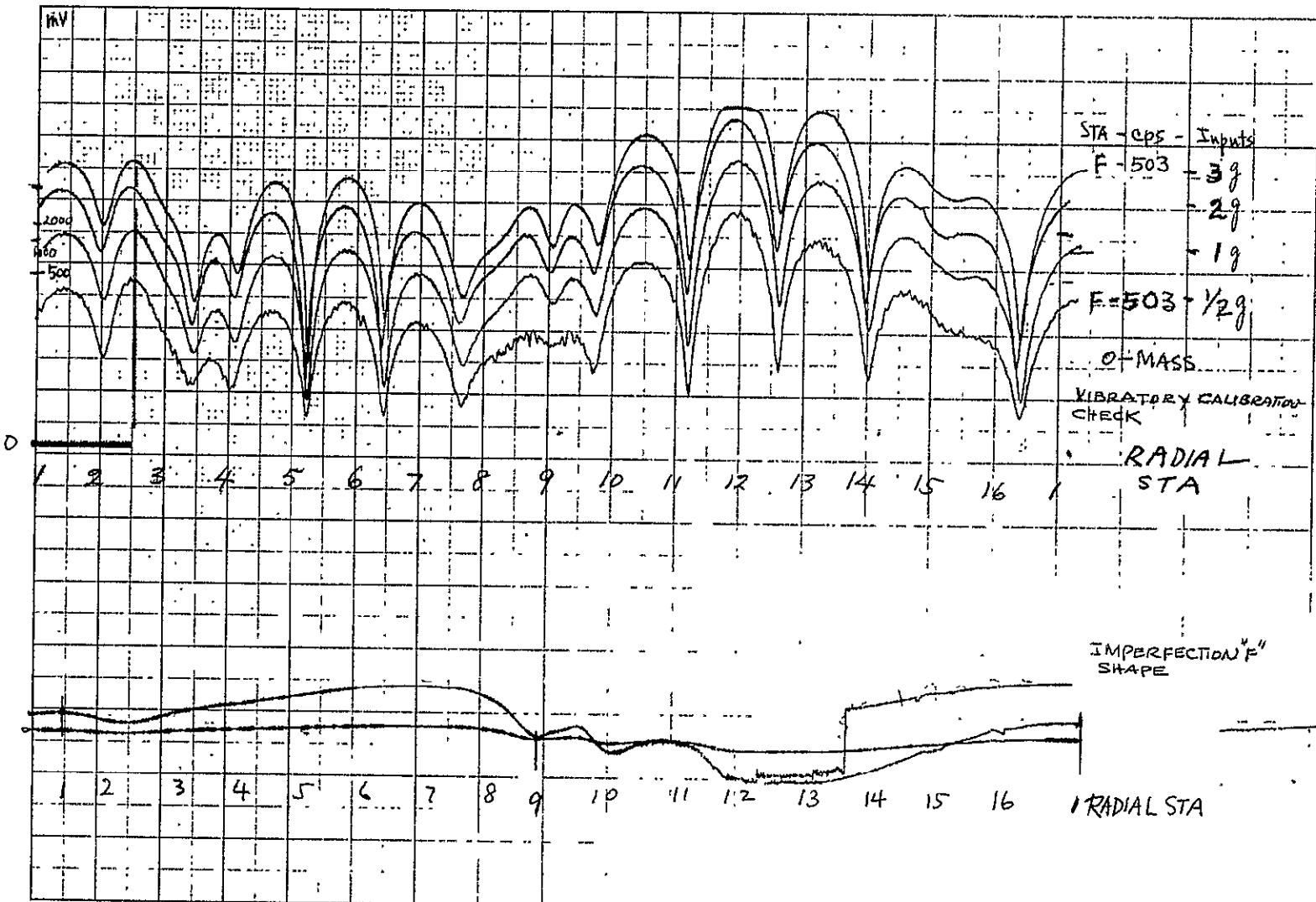
Figure XI-7. Imperfection and Vibratory Calibration

XII. LONGITUDINAL VIBRATION CHARACTERISTICS

SINUSOIDAL

LR _____ MEASUREMENT NUMBER __CH #8__ RUN NUMBER _S-1-C-½-#8_

TR _____ CONTROL ( ), RESPONSE (V) AXIS __AXIAL (LONGIT)__ DATE _____ 19 _____

TEST TITLE __LONGITUDINAL VIBRATION TEST__

FULL SCALE __100__ PK SWEEP· UP (V) DOWN ( )

OPERATOR __S. Y. LEE__ SPECIMEN P/N __NO MASS, SHELL IV__

REMARKS __0.5 g input__ S/N _____

ACCELERATION g's PEAK

FREQUENCY CPS
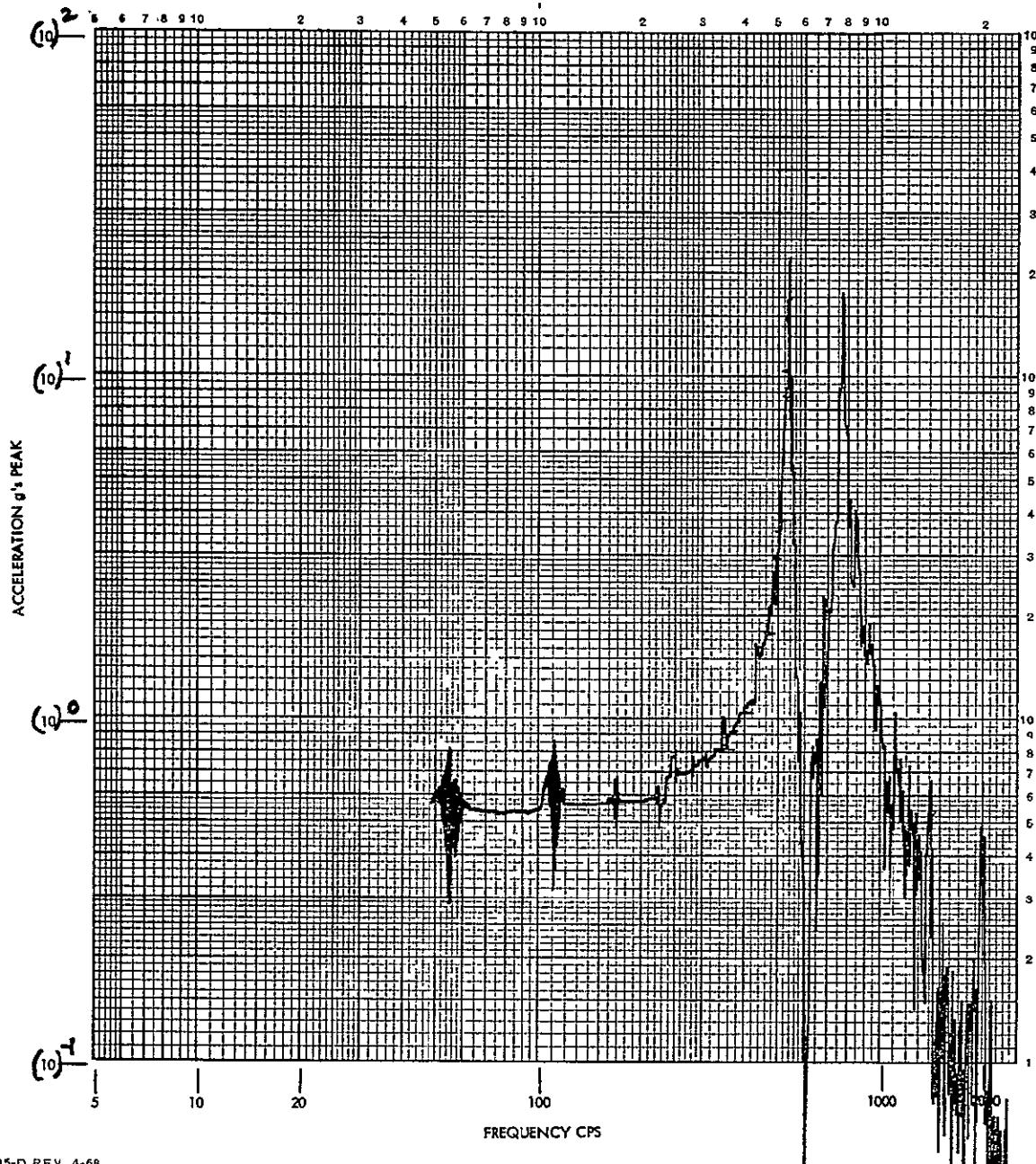
FORM 735-D REV. 4-68

Figure XII-I. Axial Response to Longitudinal Vibratory Excitations,
No-Mass Case

XII-1

SINUSOIDAL

LR _____ MEASUREMENT NUMBER *CH* #/*8* _____ RUN NUMBER *S-I-O-I-#IO*

TR _____ CONTROL ( ), RESPONSE (✓) AXI- *RADIAL* _____ DATE _____ 19 _____

TEST TITLE *LONGITUDINAL VIBRATION TEST* _____

FULL SCALE *IOOO* · _____ PK SWEEP· UP (✓) DOWN ( )

OPERATOR _____ SPECIMEN P/N *NO MASS,* _____ *SHELL II*

REMARKS _____ *I g input* _____ S/N _____
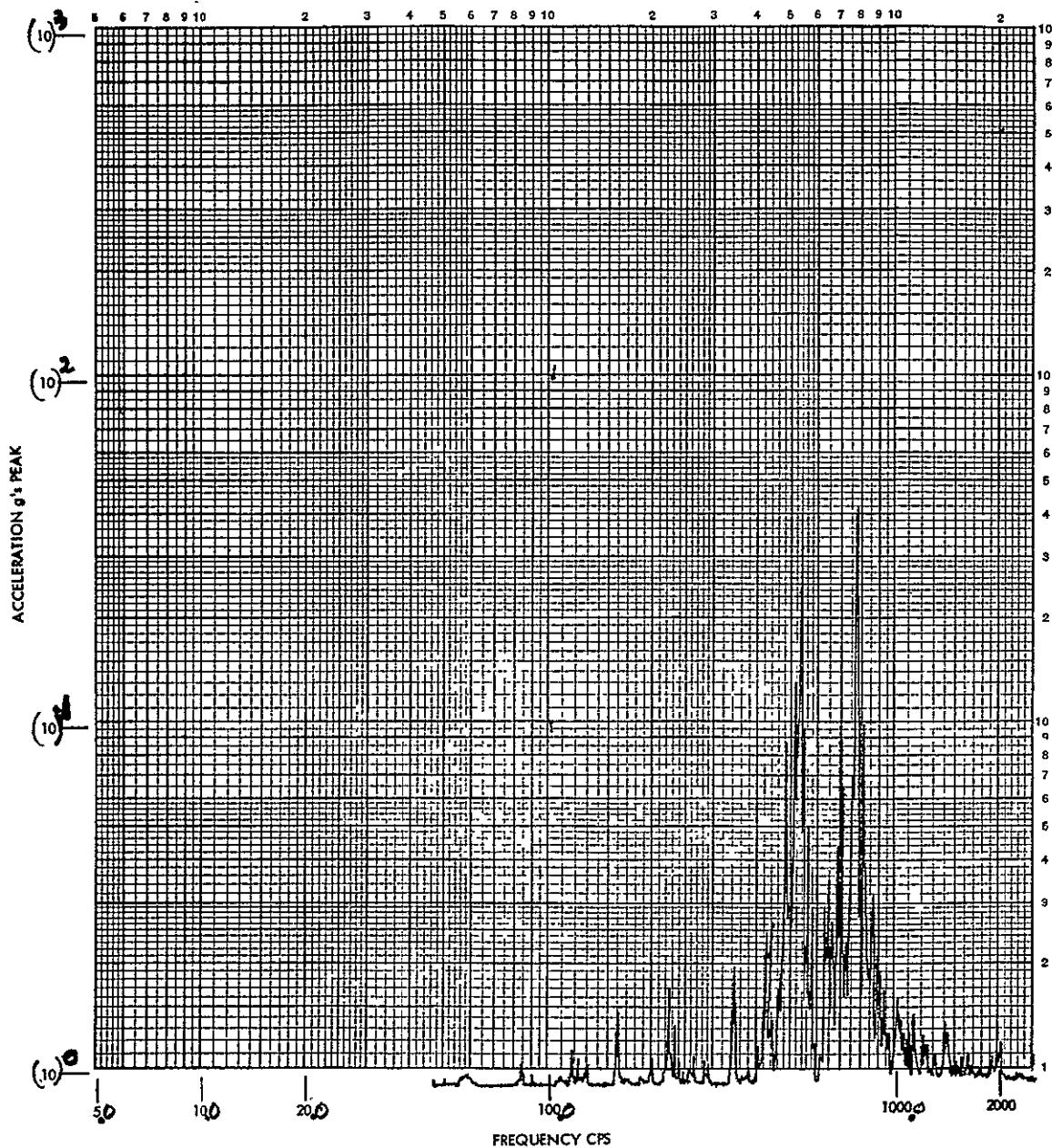
Figure XII-2. Radial Response to Longitudinal Vibratory Excitations,
No-Mass Case, 1-g Input

XII-2

SINUSOIDAL

LR _____ MEASUREMENT NUMBER _CH #8_ _____ RUN NUMBER S-1-0-½-#8

TR _____ CONTROL ( ), RESPONSE (V) AXI- _LONGITUDINAL_ DATE _____ 19 _____

TEST TITLE _LONGITUDINAL VIBRATION TEST, AXIAL TRANSMISSIBILITY STUDY_

FULL SCALE _100_ _____ PK SWEEP: UP (V) DOWN ( )

OPERATOR _S.Y. LEE_ _____ SPECIMEN P/N _NO MASS, SHELL IV_

REMARKS _0.5 g input_ _____ S/N _____

FORM 735-D REV. 4-66
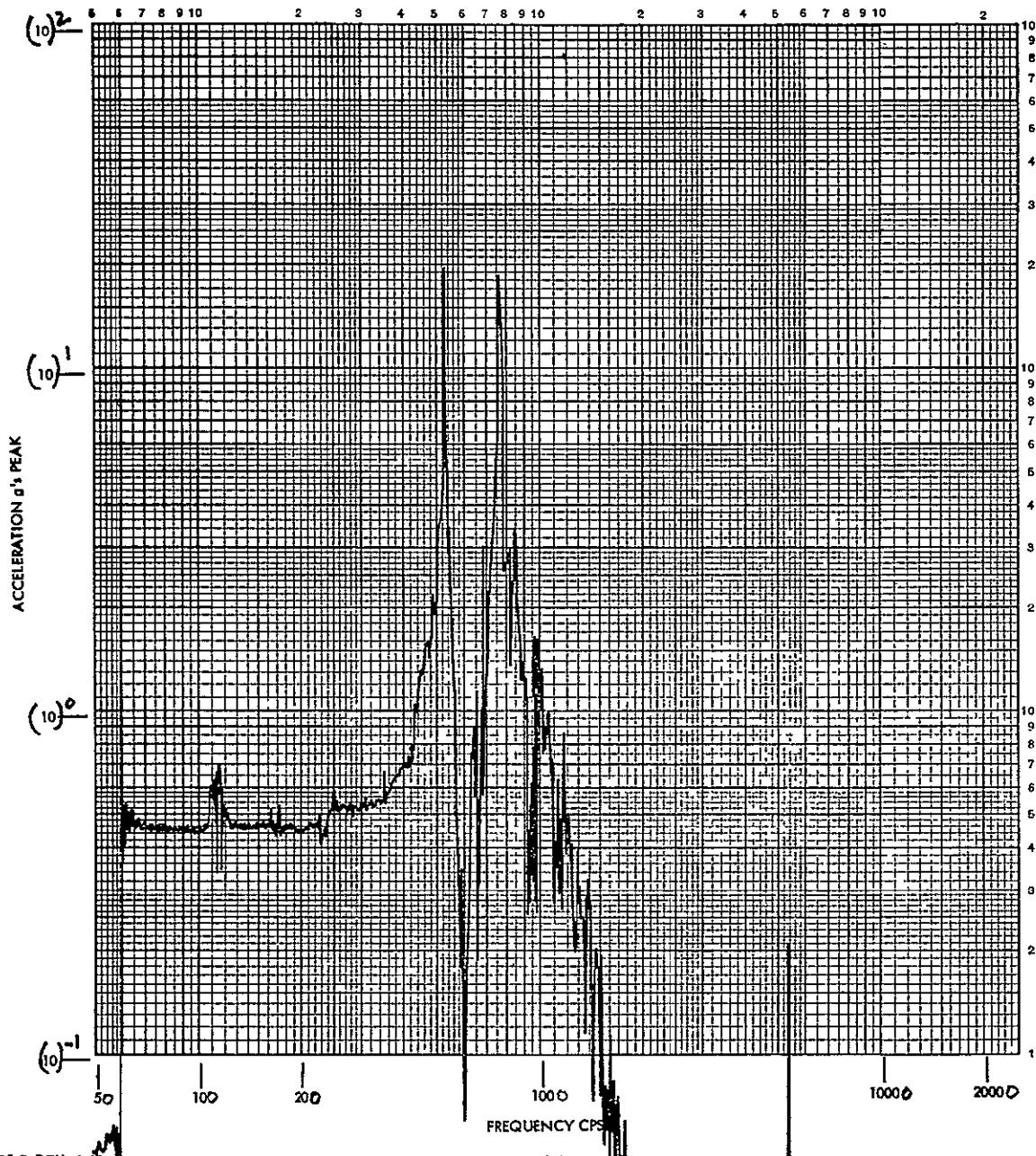
Figure XII-3. Axial Response to Longitudinal Vibratory Excitations, No-Mass Case, Broad Spectrum

XII-3

SD 69-766

LR_____ MEASUREMENT NUMBER _C H_ _#10_____ RUN NUMBER _S-1-0-½-#10_

TR_____ CONTROL ( ), RESPONSE (✔) AXI- _RADIAL_____ DATE _____ 19 _____

TEST TITLE _LONGITUDINAL VIBRATION TEST_____

FULL SCALE _____ _100_____ PK¹ SWEEP· UP (✔) DOWN ( )

OPERATOR _LEE_____ SPECIMEN P/N _No MASS, SHELL IV_

REMARKS _0.5 g INPUT_____ S/N_____
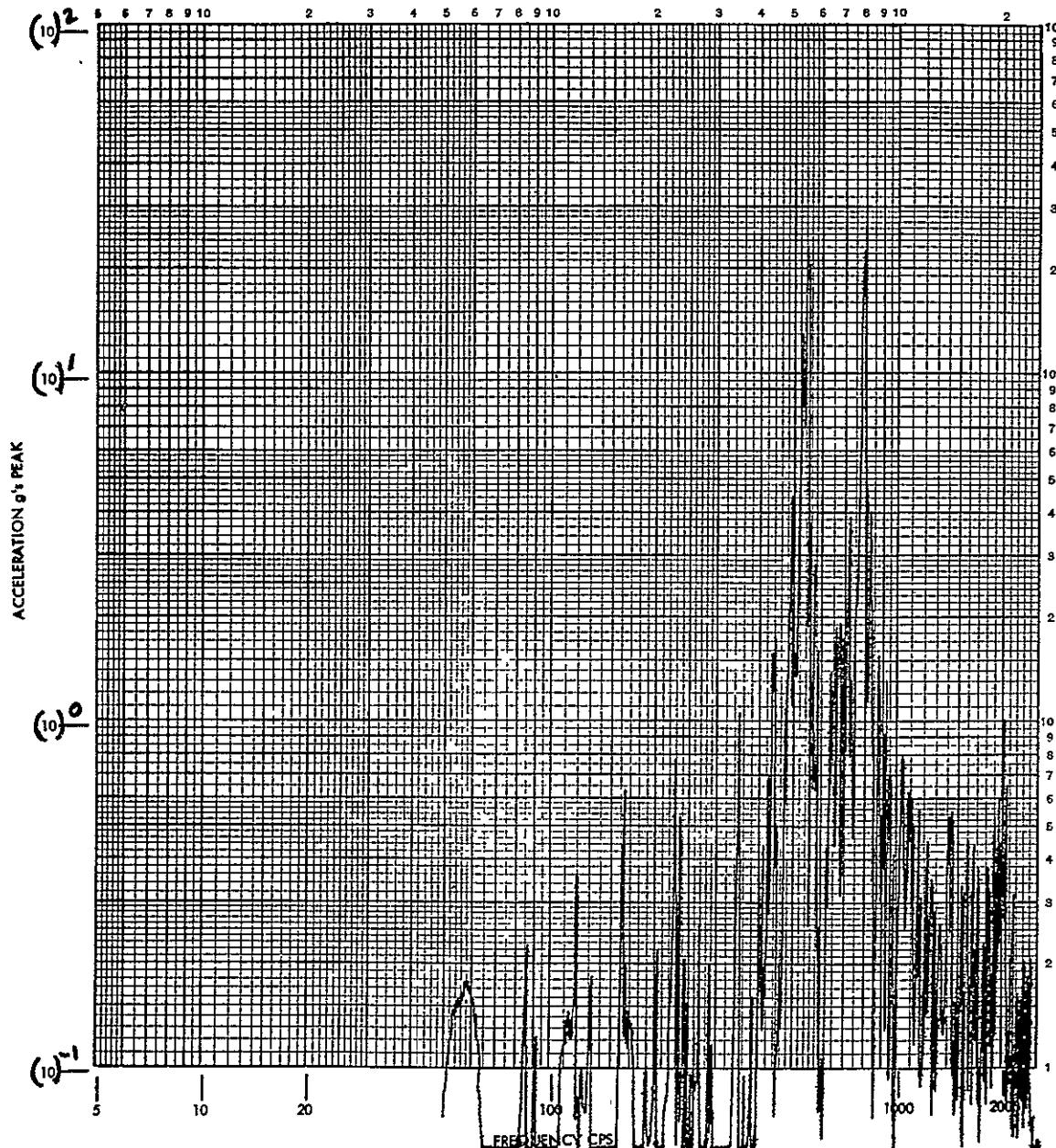
Figure XII-4. Radial Response to Longitudinal Vibratory Excitations, No-Mass Case, 0.5-g Input

FORM 735-D REV. 4-68

SINUSOIDAL

LR _____ MEASUREMENT NUMBER _CH #8_ _____ RUN NUMBER _S-2-3-½-#8_

TR _____ CONTROL ( ), RESPONSE (✓) AXI⁻ _LONGITUDINAL_ DATE _____ 19 _____

TEST TITLE _LONGITUDINAL VIBRATION TEST_

FULL SCALE _100_ _____ PK SWEEP· UP (✓ DOWN ( )

OPERATOR _LEE_ _____ SPECIMEN P/N _MASS #3 (0.044/LB) SHELL IV_

REMARKS _0.5g input, M₂/M₁ = 0.05_ _____ S/N _____
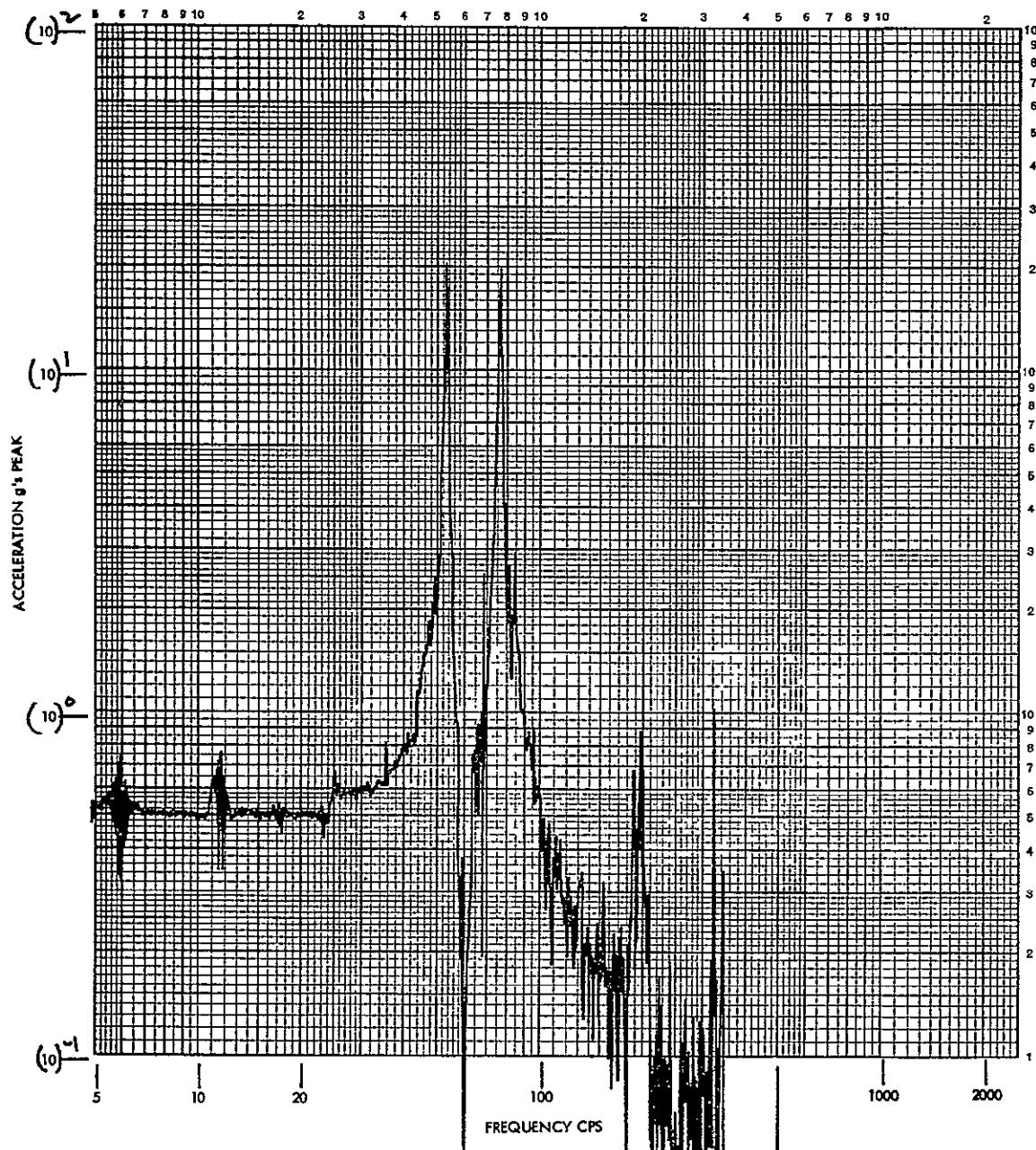
Figure XII-5. Axial Response to Longitudinal Vibratory Excitations, Mass-3 Case

FORM 735-D REV. 4-68

XII-5

SINUSOIDAL

LR_____ MEASUREMENT NUMBER __CH #10_____ RUN NUMBER S-1-3-½-#10

TR_____ CONTROL ( ), RESPONSE (V) AXI- RADIAL_____ DATE _____ 19 _____

TEST TITLE LONGITUDINAL VIBRATION TEST

FULL SCALE 100 _____ PK SWEEP: UP (V) DOWN ( )

OPERATOR LEE _____ SPECIMEN P/N MASS #3 (0.0441 LB) SHELL IV

REMARKS 0.5 g input, M2/M1 = 0.05 _____ S/N _____
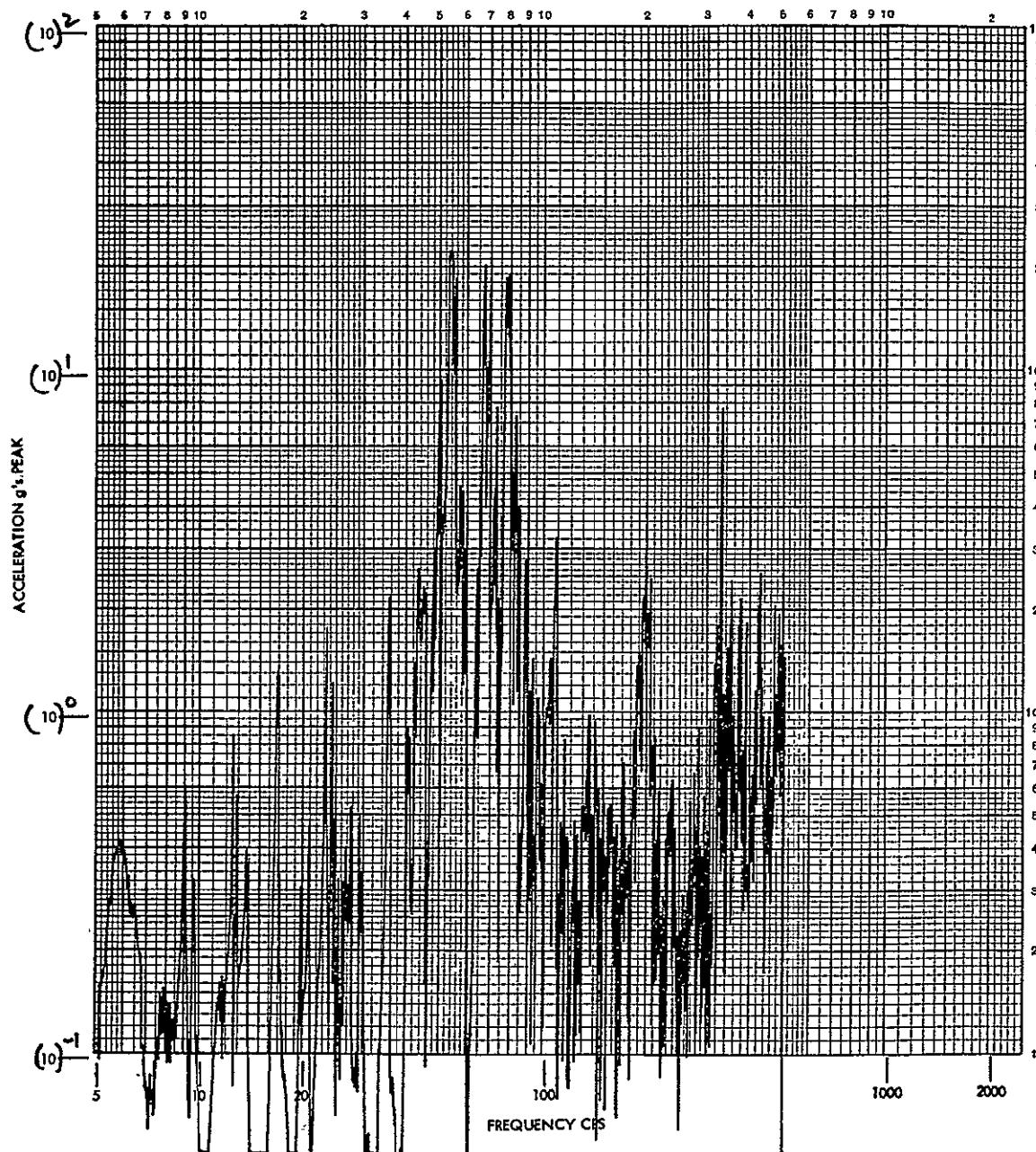
Figure XII-6. Radial Response to Longitudinal Vibratory
Excitations, Mass-5 Case

XII-6

FORM 735-D REV. 4-68

SINUSOIDAL

LR _____ MEASUREMENT NUMBER C H #8 _____ RUN NUMBER S-1-5-½-#8

TR _____ CONTROL ( ), RESPONSE (✓) AXIⁱ LONGITUDINAL DATE _____ 19 _____

TEST TITLE LONGITUDINAL VIBRATION TEST

FULL SCALE 100 _____ PK SWEEP: UP (✓) DOWN ( )

OPERATOR LEE _____ SPECIMEN P/N MASS #5 (0.0885ᴸᴮ) SHELL IV

REMARKS 0.5 g input, M₂/M₁ = 0.1 S/N _____
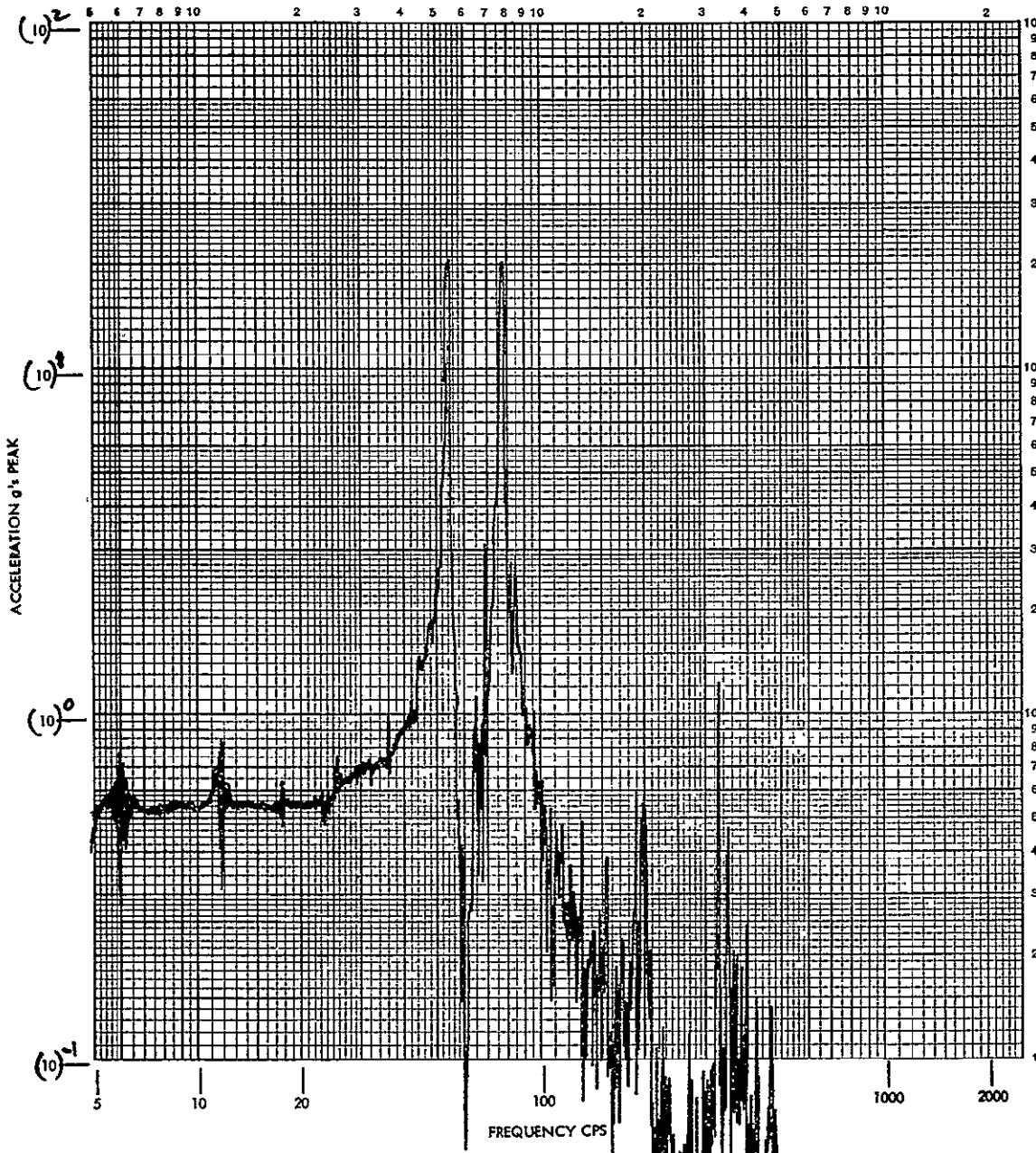
Figure XII-7. Axial Response to Longitudinal Vibratory
Excitations, Mass-5 Case

XII-7

FORM 735-D REV. 4-68

SD 69-766

SINUSOIDAL

LR_____ MEASUREMENT NUMBER *CH #10*_____ RUN NUMBER *S-2-5-½-#10*

TR_____ CONTROL ( ), RESPONSE (✓) AXIS *RADIAL*_____ DATE _____ 19 _____

TEST TITLE *LONGITUDINAL VIBRATION TEST*

FULL SCALE *100*_____ PK SWEEP: UP (✓) DOWN ( )

OPERATOR *LEE*_____ SPECIMEN P/N *MASS #5,*   *SHELL IV*

REMARKS *0.5 g input, M₂/M₁ = 0.1*_____ S/N_____
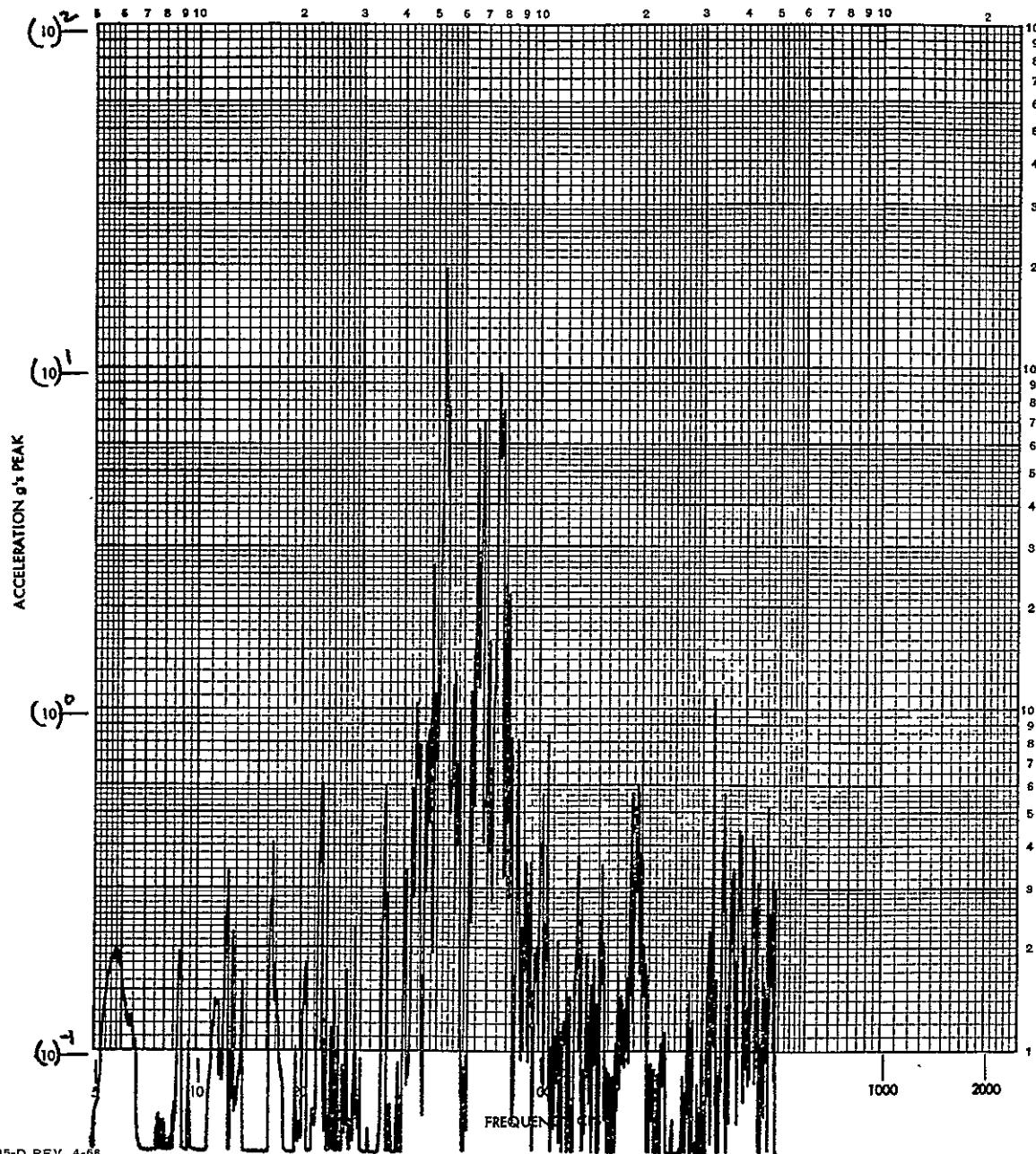
Figure XII-8.   Radial Response to Longitudinal Vibratory
Excitations, Mass-B Case

XII-8

SINUSOIDAL

LR _____ MEASUREMENT NUMBER _CH #8_____ RUN NUMBER S-2-R-½-#?

TR _____CONTROL ( ), RESPONSE (V) AXI- LONGITUDINAL DATE _____ 19 _____

TEST TITLE LONGITUDINAL VIBRATION TEST

FULL SCALE _100_____ PK SWEEP: UP (V) DOWN ( )

OPERATOR LEE_____ SPECIMEN P/N MASS #B₁ , SHELL IV

REMARKS ___0.5 g INPUT, M2/M₁=0.32 S/N (0.28LB)

ACCELERATION g's PEAK

FREQUENCY CPS
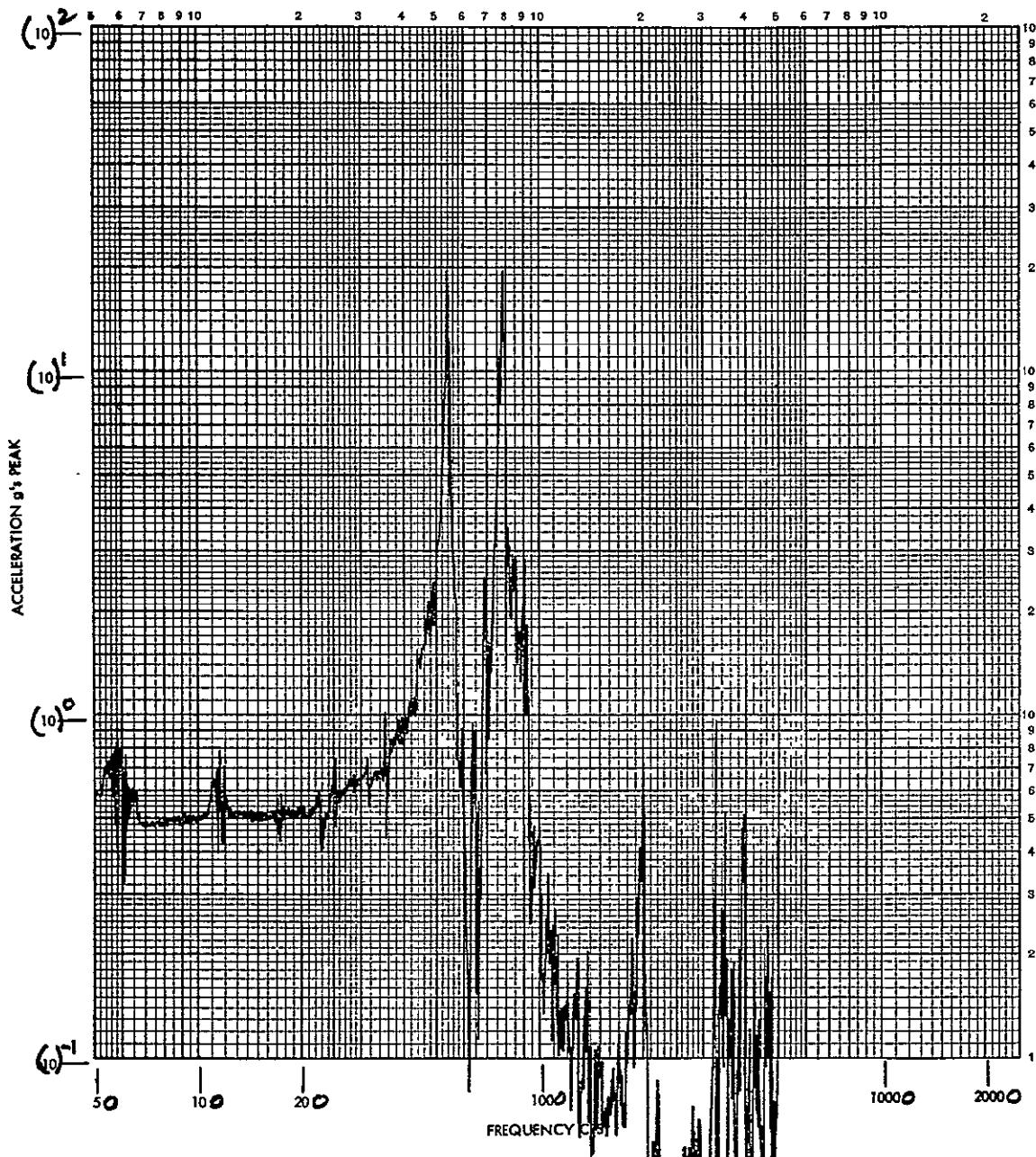
FORM 735-D REV. 4-68

Figure XII-9. Axial Response to Longitudinal Vibratory
Excitations, Mass-B Case

XII-9

SINUSOIDAL

LR _____ MEASUREMENT NUMBER __ CH 10 _____ RUN NUMBER S-2-B₁-½-#10

TR _____ CONTROL ( ), RESPONSE (✓) AXI⁻ RADIAL _____ DATE _____ 19 _____

TEST TITLE LONGITUDINAL VIBRATION TEST

FULL SCALE 100 _____ PK SWEEP- UP (✓) DOWN ( )

OPERATOR LEE _____ SPECIMEN P/N MASS #B₁, SHELL IV

REMARKS 0.5 g INPUT, M₂/M₁ = 0.32 S/N (0.28 LB)
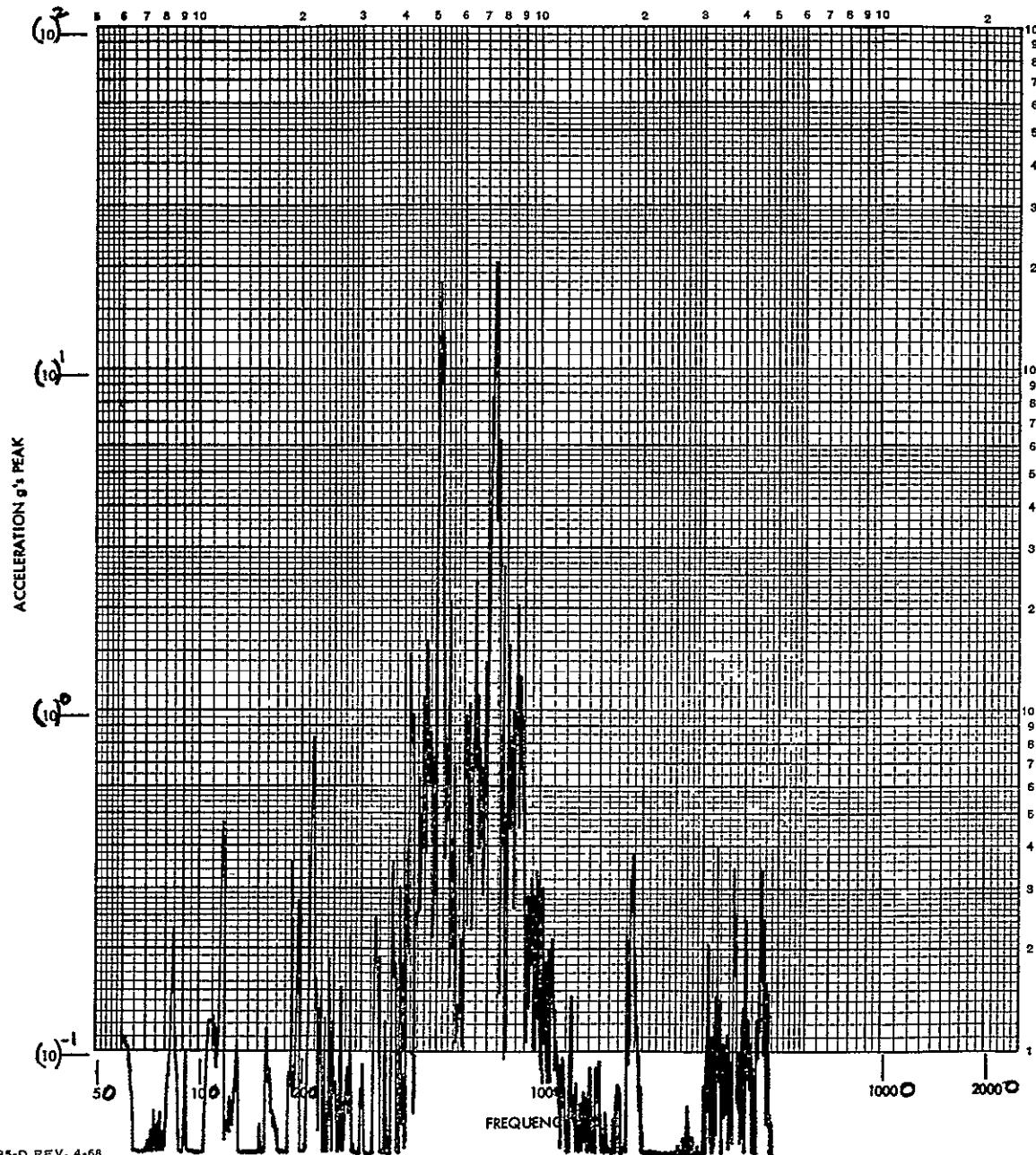
FORM 735-D REV. 4-68

Figure XII-10. Radial Response to Longitudinal Vibratory
Excitations, Mass-BH Case

XII-10

SINUSOIDAL

LR _____ MEASUREMENT NUMBER **#8** _____ RUN NUMBER S-2-BH-½-#8

TR _____ CONTROL ( ), RESPONSE (✓) AXI- **LONGITUDINAL** DATE _____ 19 _____

TEST TITLE **LONGITUDINAL VIBRATION TEST**

FULL SCALE **100** PK SWEEP: UP (✓) DOWN ( )

OPERATOR **LEE** SPECIMEN P/N **MASS #BH , SHELL IV**
(0.722 LB)

REMARKS **0.5 g input, M2/M1 = 0.82** S/N _____
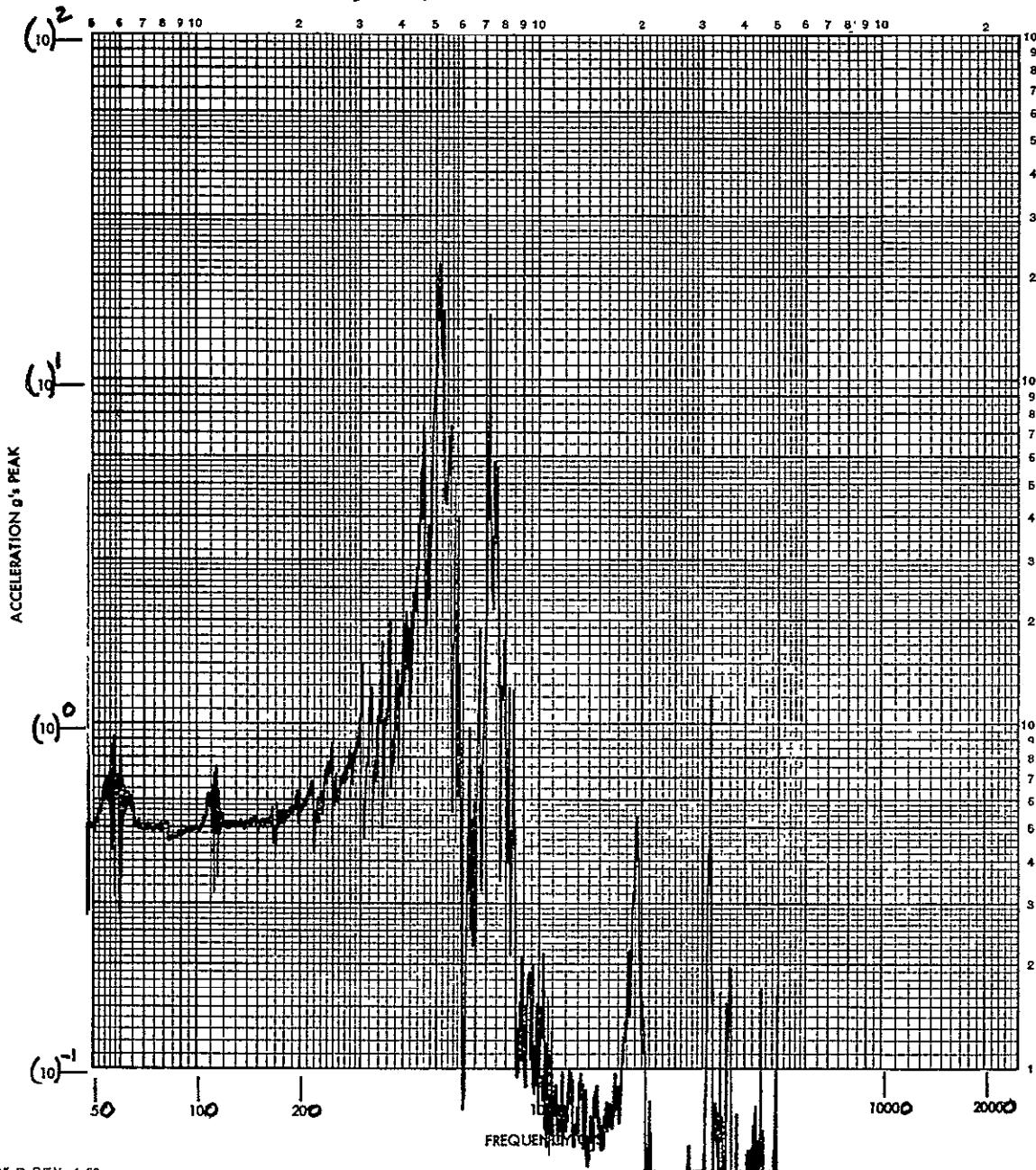
Figure XII-11. Axial Response to Longitudinal Vibratory Excitations, Mass-BH Case

XII-11

SD 69-766

FORM 735-D REV. 4-68

SINUSOIDAL

LR _____ MEASUREMENT NUMBER **Ch # 10** _____ RUN NUMBER **S-2-BH-½-#10**

TR _____ CONTROL ( ), RESPONSE (✓) AXI⁻ **RADIAL** _____ ·DATE _____ 19 ____

TEST TITLE **LONGITUDINAL VIBRATION TEST** _____

FULL SCALE **100** _____ PK SWEEP: UP (✓) DOWN ( )

OPERATOR **LEE** _____ SPECIMEN P/N **MASS # BH, SHELL IV**

REMARKS **0.5 g input, M₂/M₁ = 0.82** S/N **(0.722 LB)**
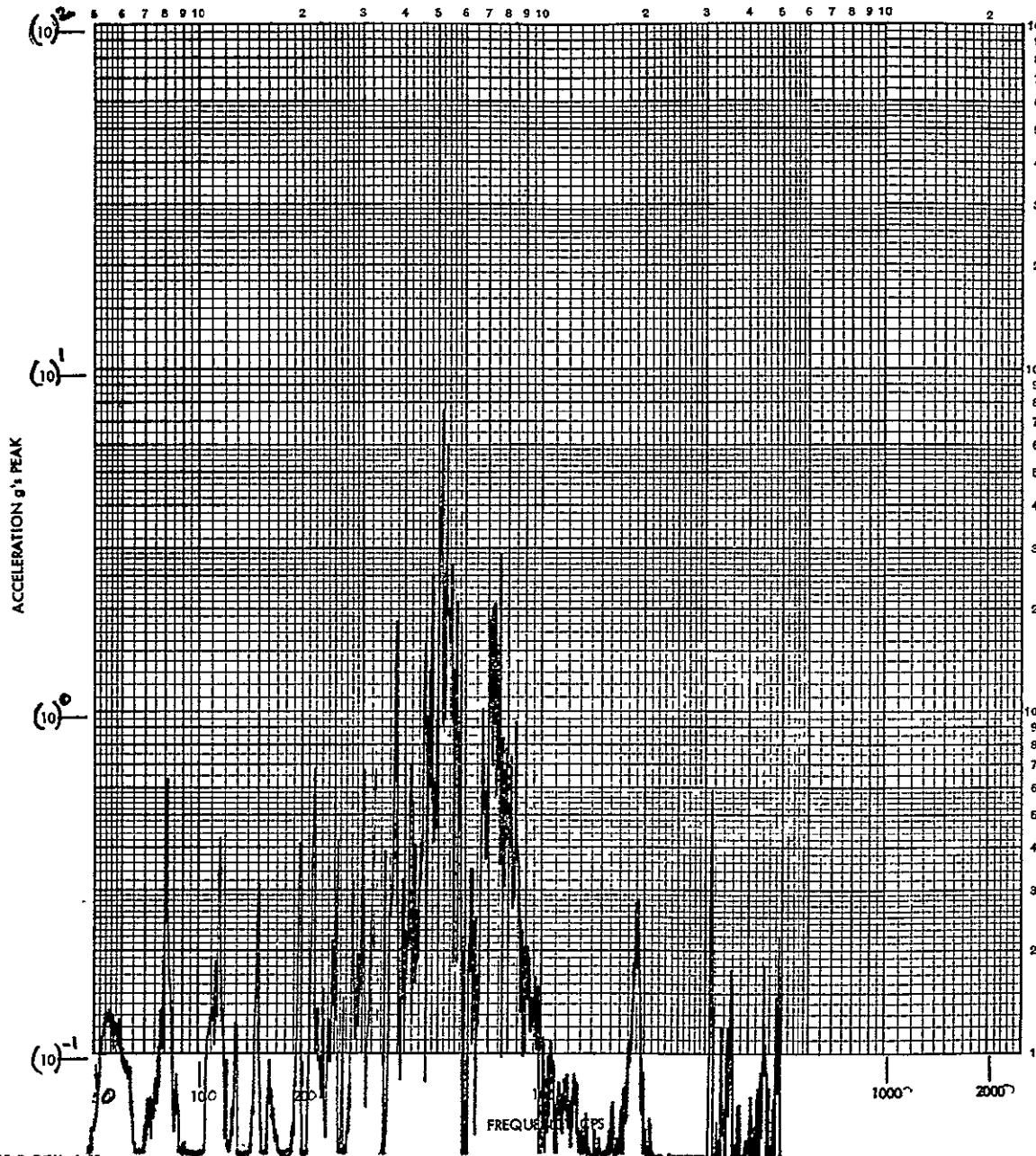
Figure XII-12. Radial Axial Response to Longitudinal Vibratory
Excitations, Mass-BD Case

XII-12

SINUSOIDAL

LR _____ MEASUREMENT NUMBER **CH # 8** _____ RUN NUMBER **S-3-BD-½-#8**

TR _____ CONTROL ( ), RESPONSE (✓) AXI- **LONGITUDINAL** DATE _____ 19 ____

TEST TITLE **LONGITUDINAL VIBRATION TEST** _____

FULL SCALE **100** _____ PK SWEEP: UP (✓) DOWN ( )

OPERATOR **LEE** _____ SPECIMEN P/N **MASS #BD**

REMARKS **0.5 g input, M₂/M₁ = 1.7** S/N **(1.495 LB)**
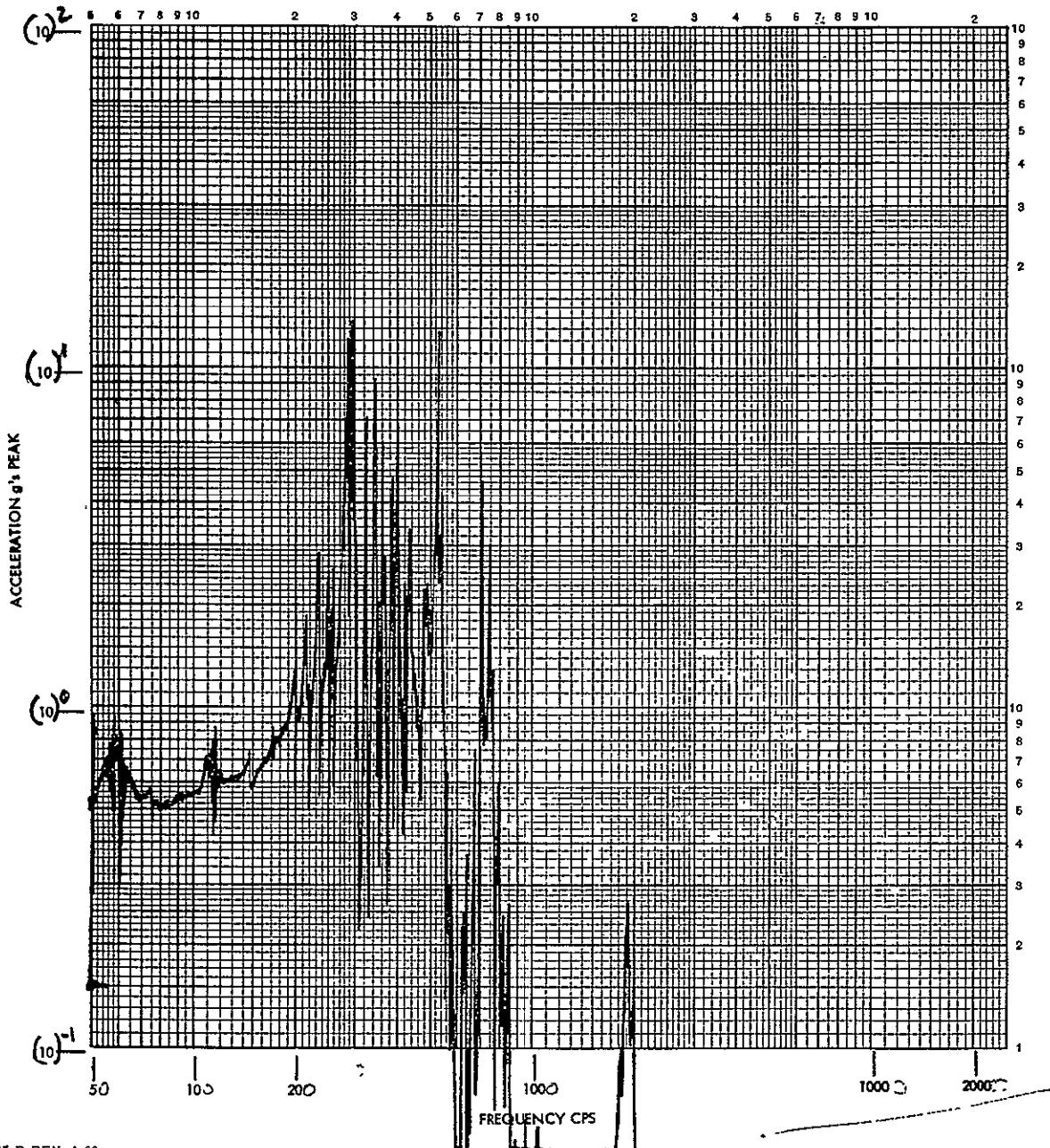
FORM 735-D REV. 4-68

Figure XII-13. Axial Response to Longitudinal Vibratory
Excitations, Mass-BD Case

XII-13

SINUSOIDAL

LR _____ MEASUREMENT NUMBER _CH #10_ _____ RUN NUMBER _S-3-BD-½-#10_

TR _____ CONTROL ( ), RESPONSE (V) AXI _RADIAL_ _____ DATE _____ 19 ____

TEST TITLE _LONGITUDINAL VIBRATION TEST_

FULL SCALE _100_ _____ PK SWEEP: UP (V) DOWN ( )

OPERATOR _LEE_ _____ SPECIMEN P/N _MASS #BD, SHELL IV_

REMARKS _0.5 g input, M2/M1 =1.7_ S/N _(1.495 LB)_

ACCELERATION g's PEAK
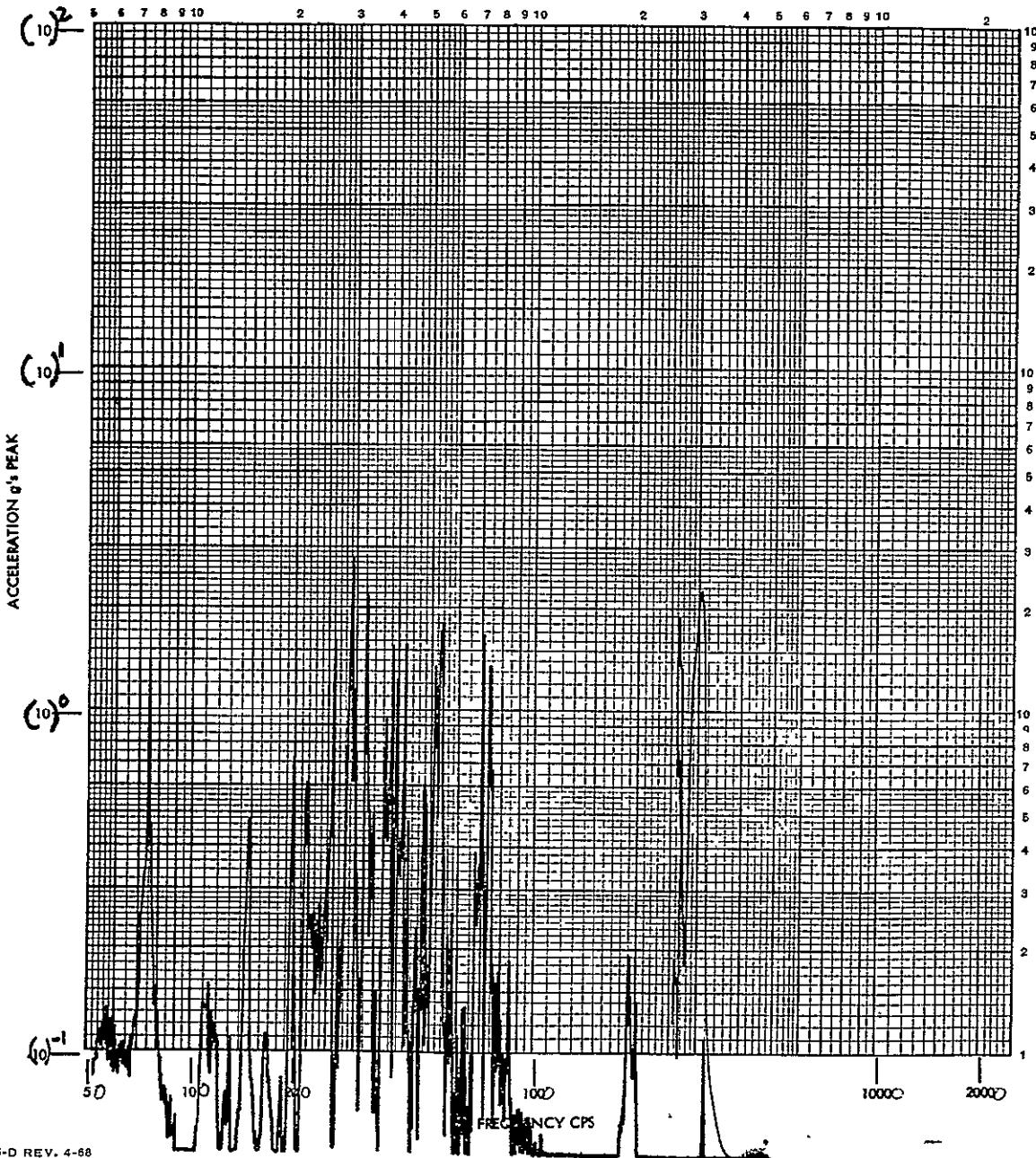
Figure XII-14. Radial Response to Longitudinal Vibratory
Excitations, MASS-BD Case

FORM 735-D REV. 4-68

XII-14

SD 69-766

XIII.   RADIAL m-n MODES INDUCED BY AXIAL EXCITATIONS
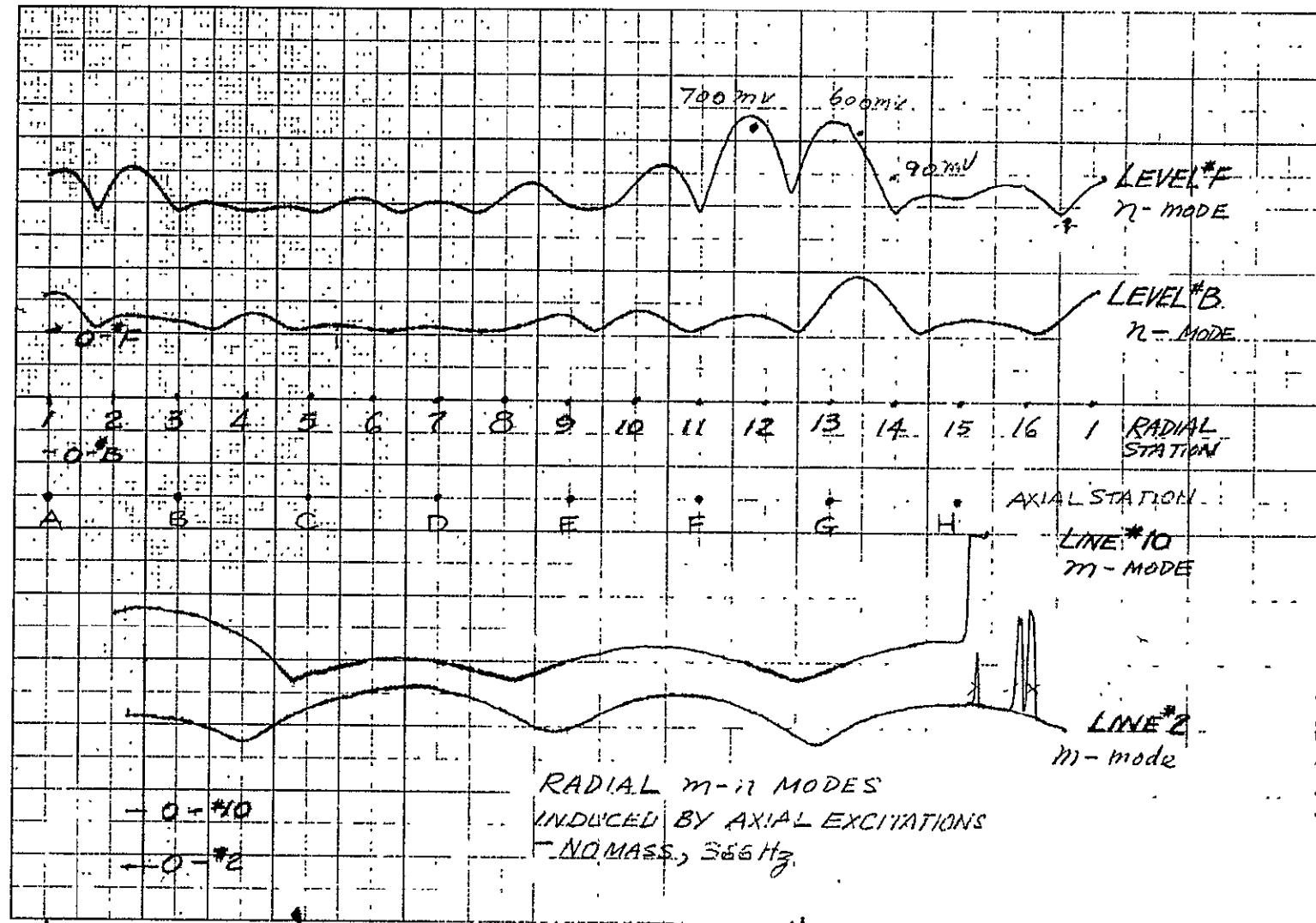
Figure XIII-1.   Radial m-n Modes Induced by Axial Excitations,
No Mass, 366 Hertz
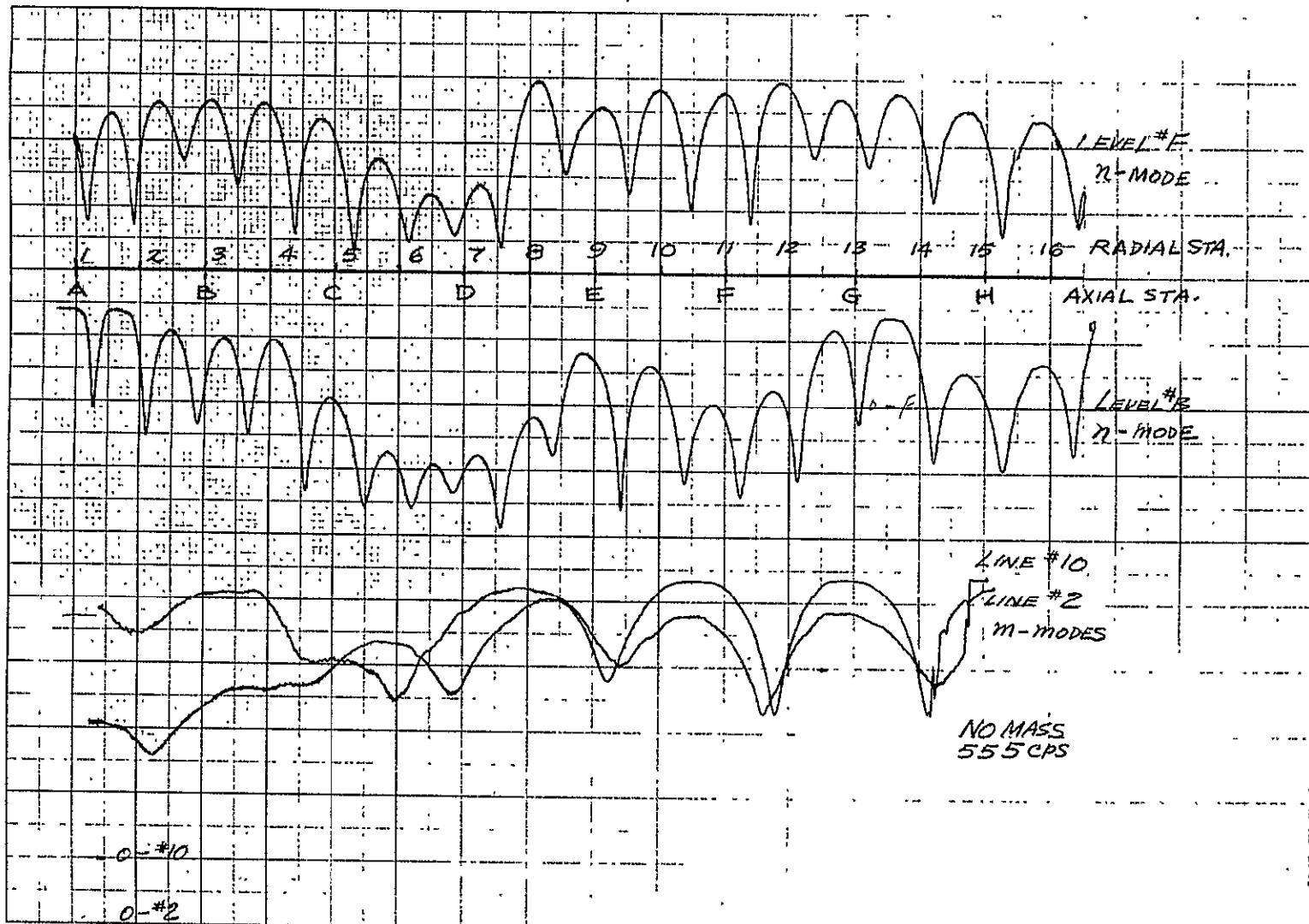
Figure XIII-2. Radial m-n Modes Induced by Axial Excitations, No Mass, 555 Hertz
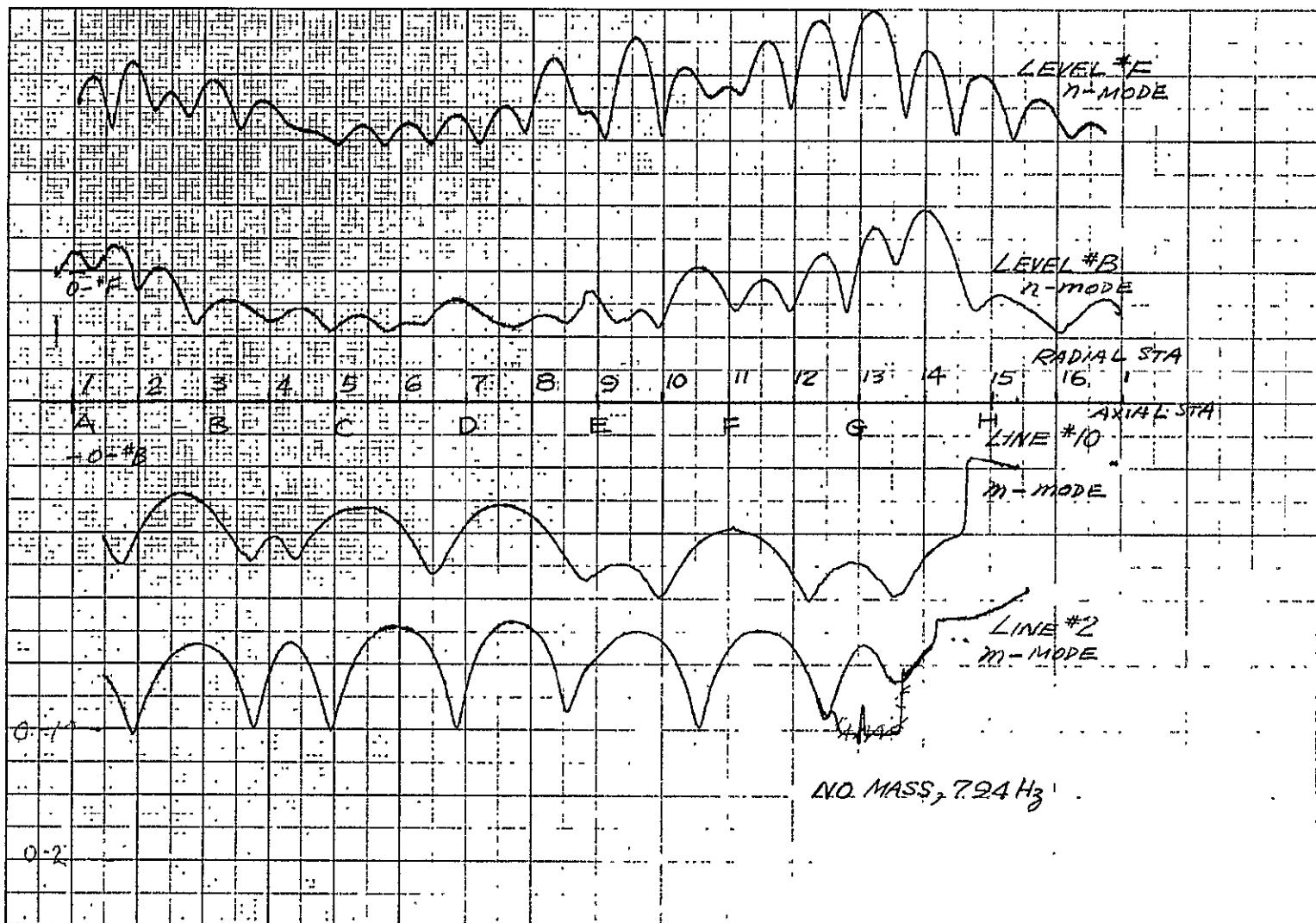
Figure XIII-3. Radial m-n Modes Induced by Axial Excitations,
No Mass, 794 Hertz
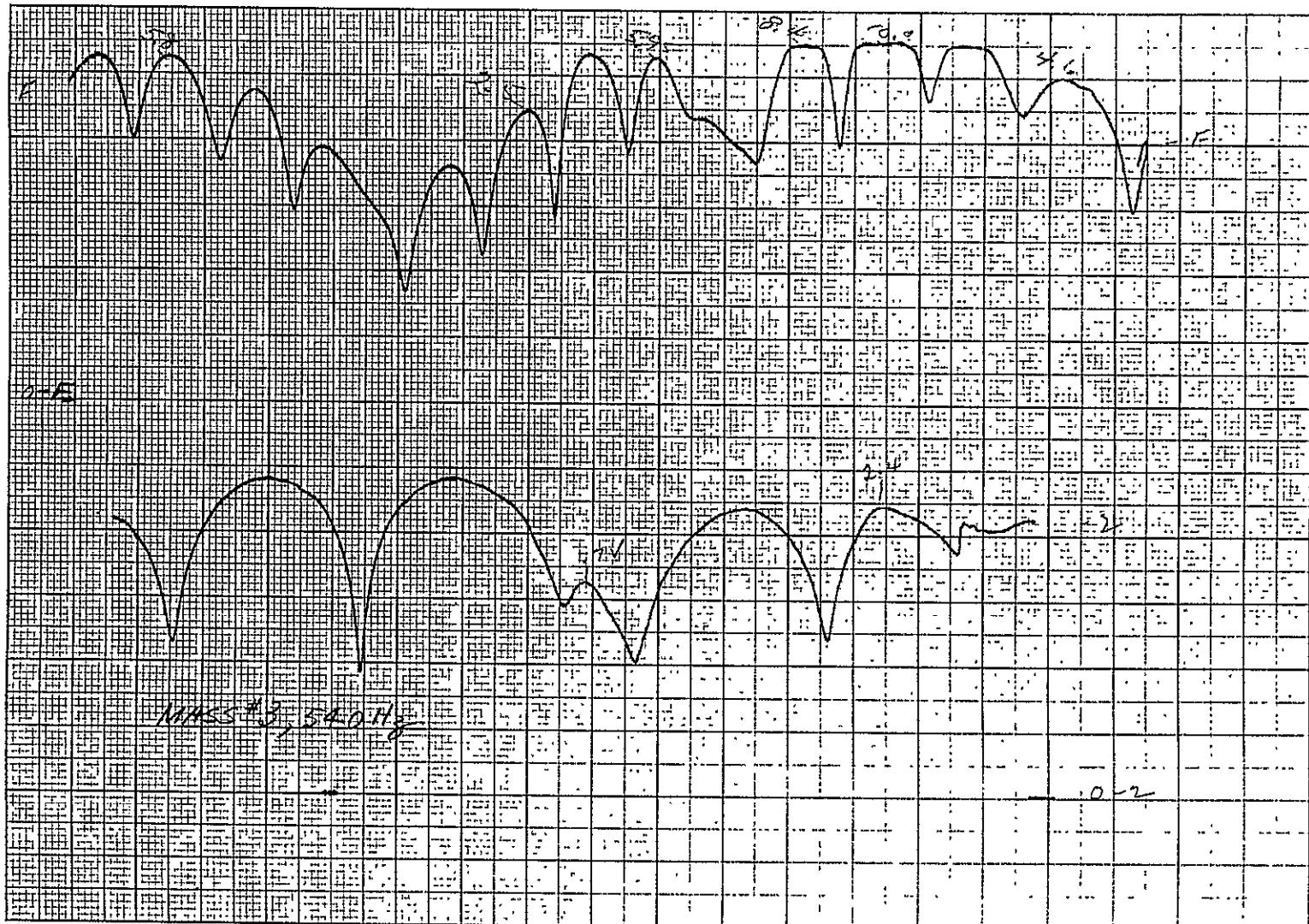
Figure XIII-4. Radial m-n Modes Induced by Axial Excitations, Mass 3, 540 Hertz
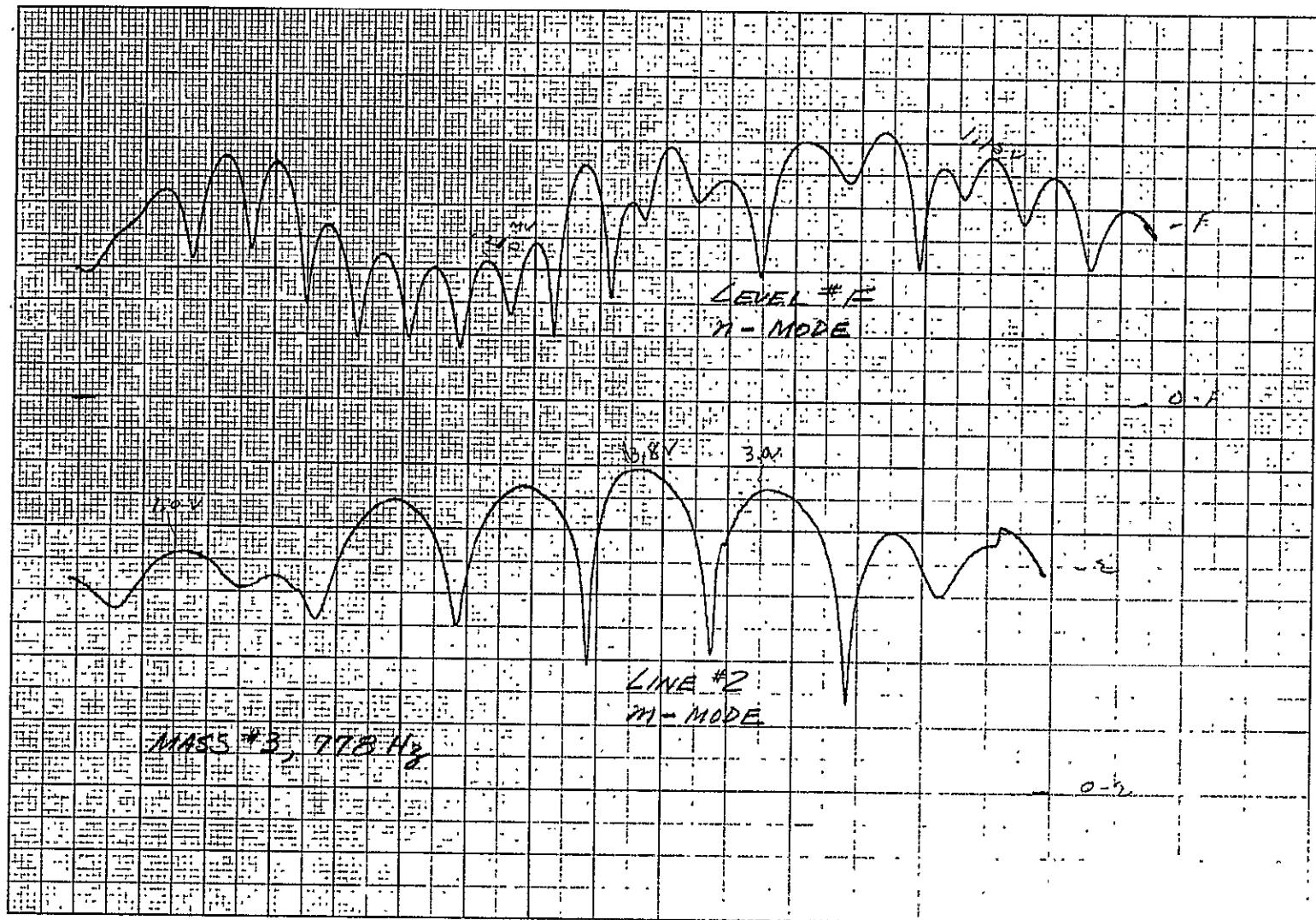
Figúre XIII-5.   Radial m-n Modes Induced by Axial Excitations,
Mass 3, 778 Hertz
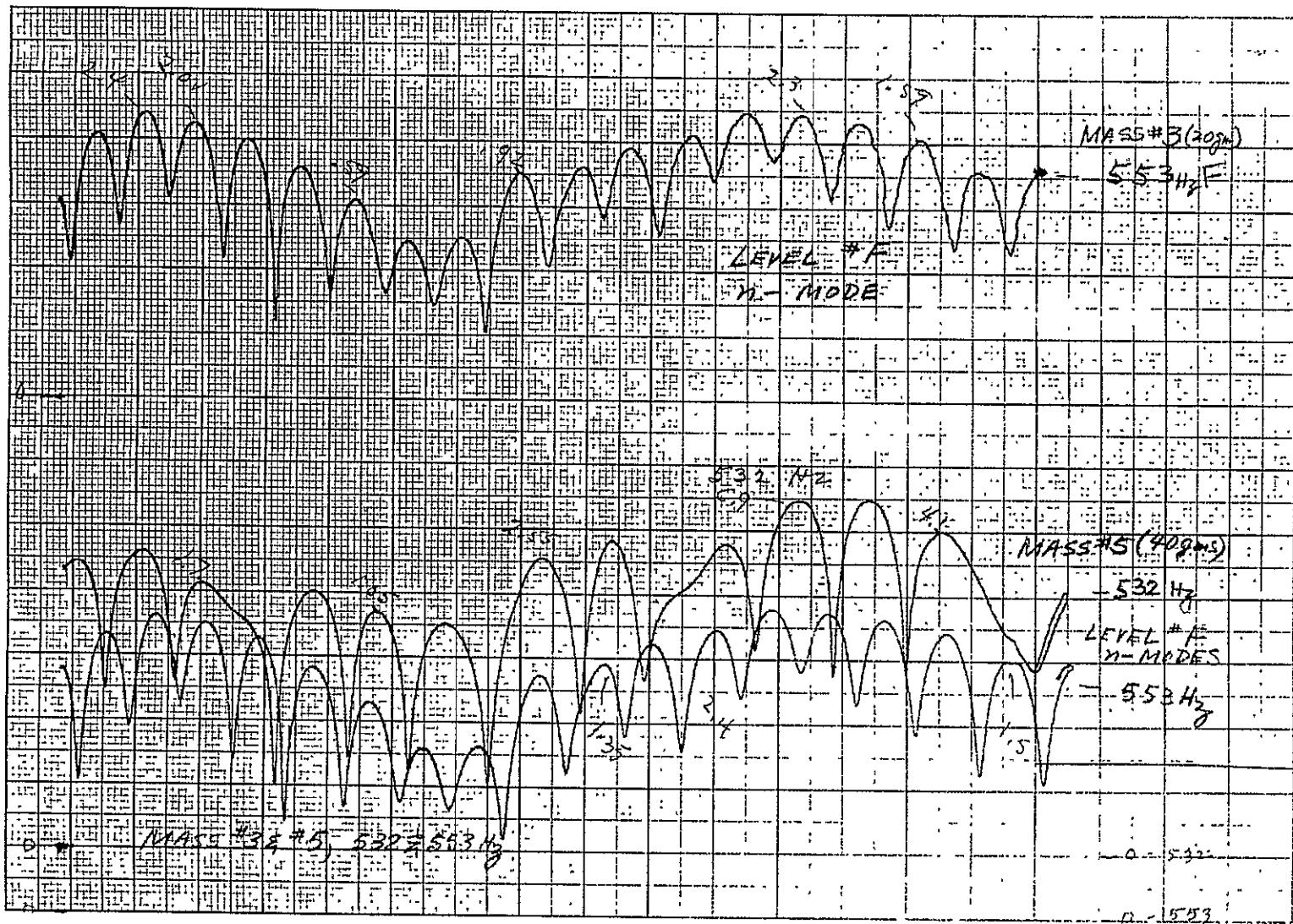
Figure XIII-6. Radial m-n Modes Induced by Axial Excitations, Masses 3 and 5, 532 and 553 Hertz
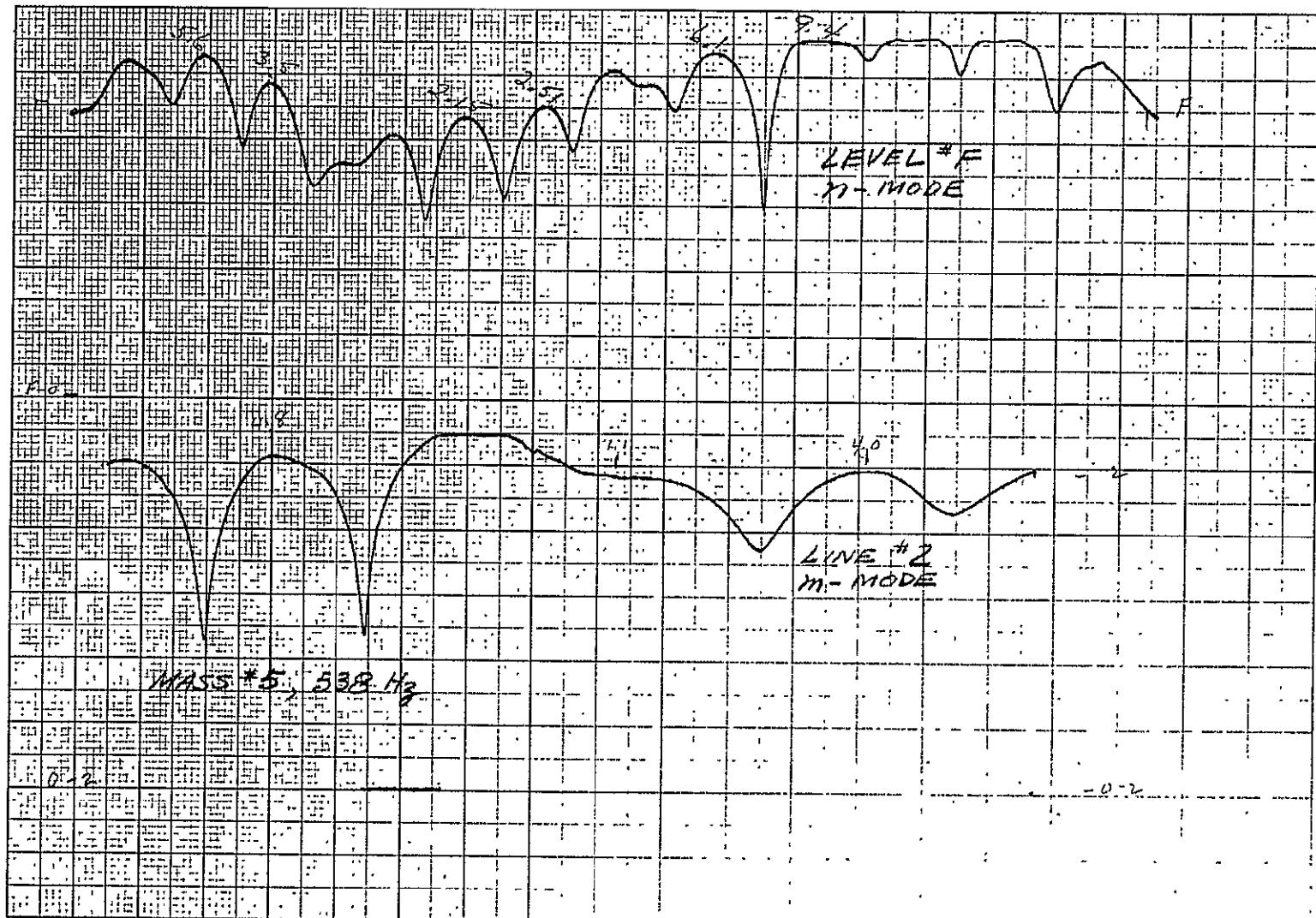
Figure XIII-7.   Radial m-n Modes Induced by Axial Excitations,
Mass 5, 538 Hertz
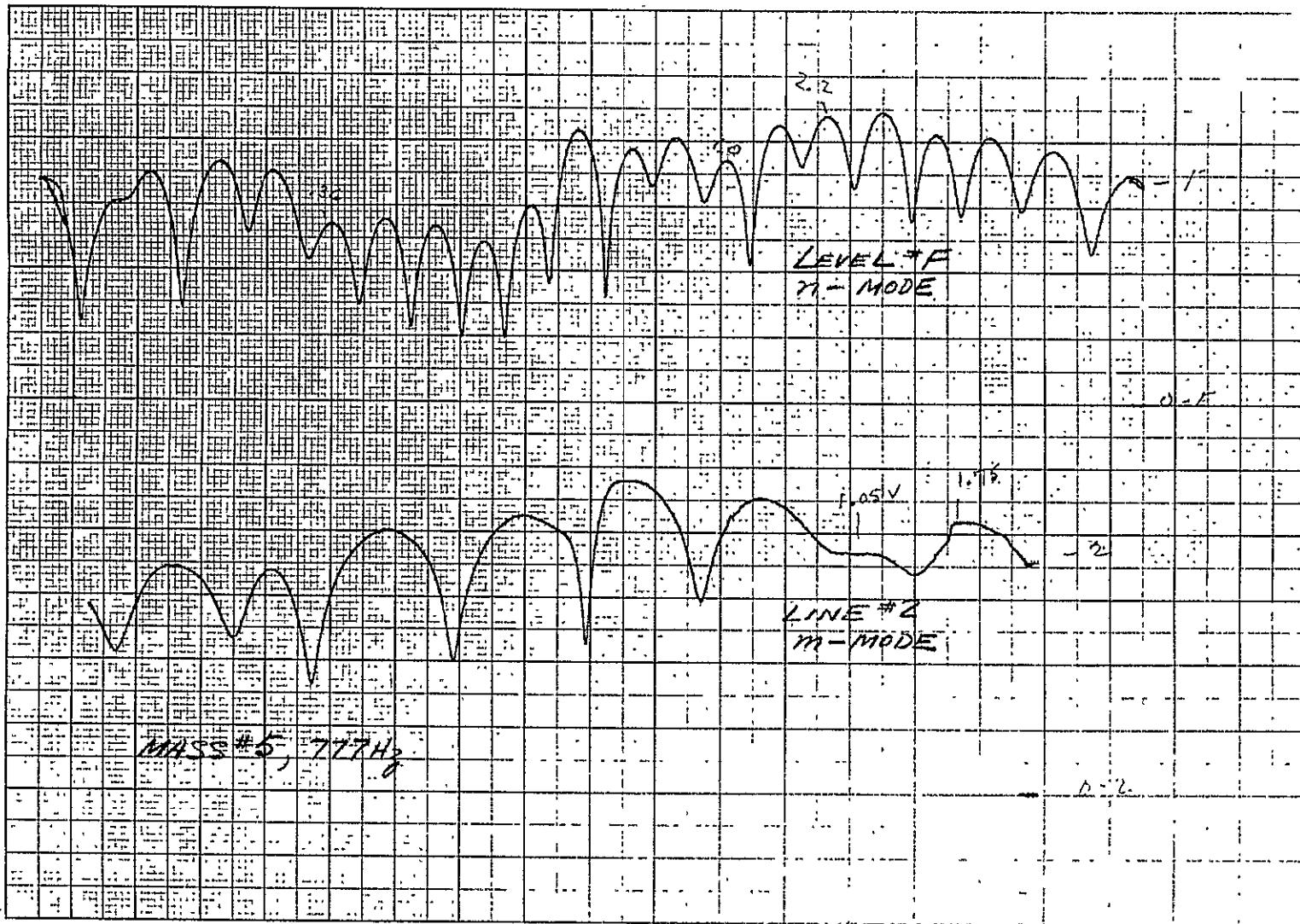
Figure XIII-8. Radial m-n Modes Induced by Axial Excitations,
Mass 5, 777 Hertz
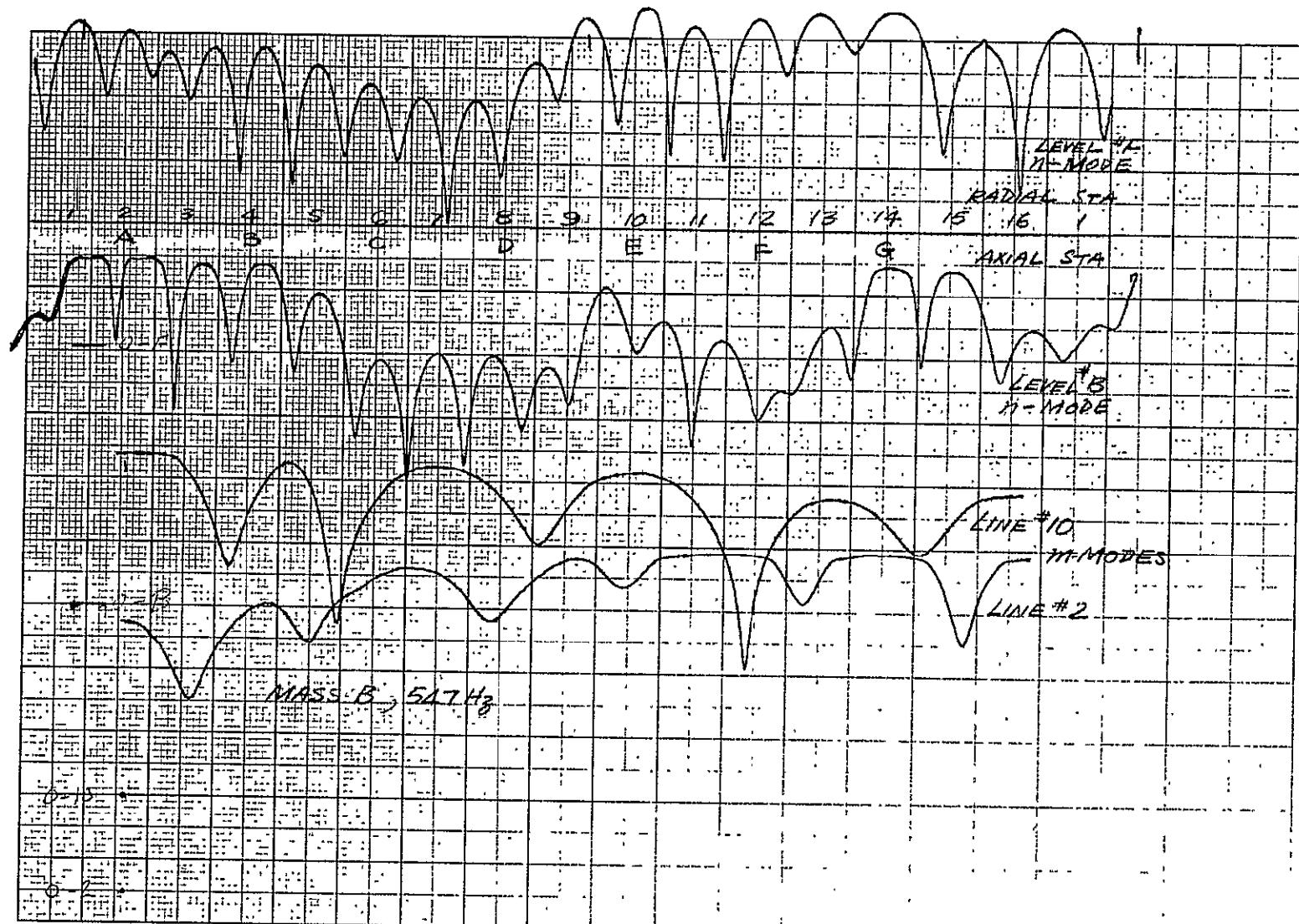
Figure XIII-9. Radial m-n Modes Induced by Axial Excitations,
Mass B, 547 Hertz
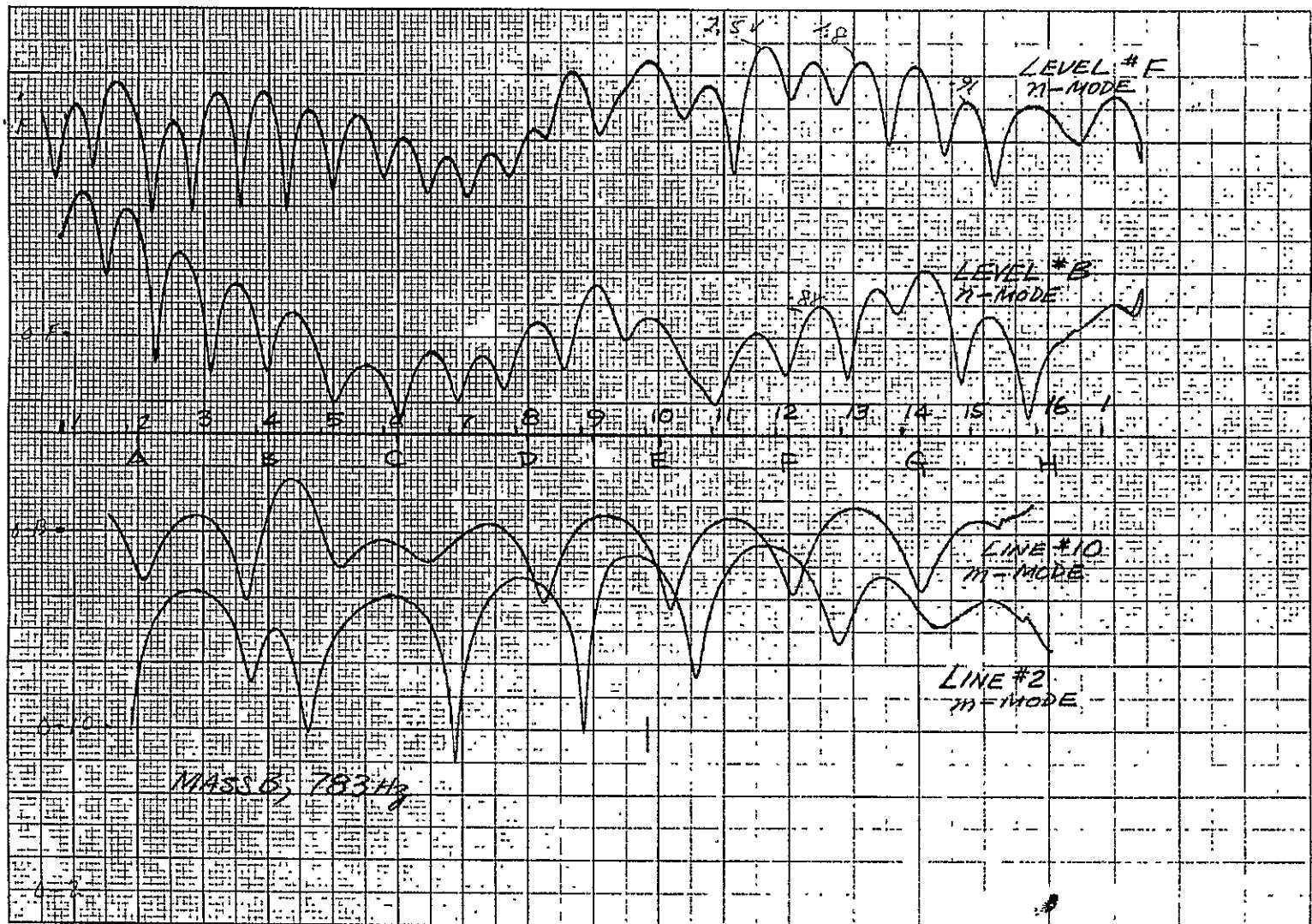
Figure XIII-10. Radial m-n Modes Induced by Axial Excitations, Mass B, 783 Hertz
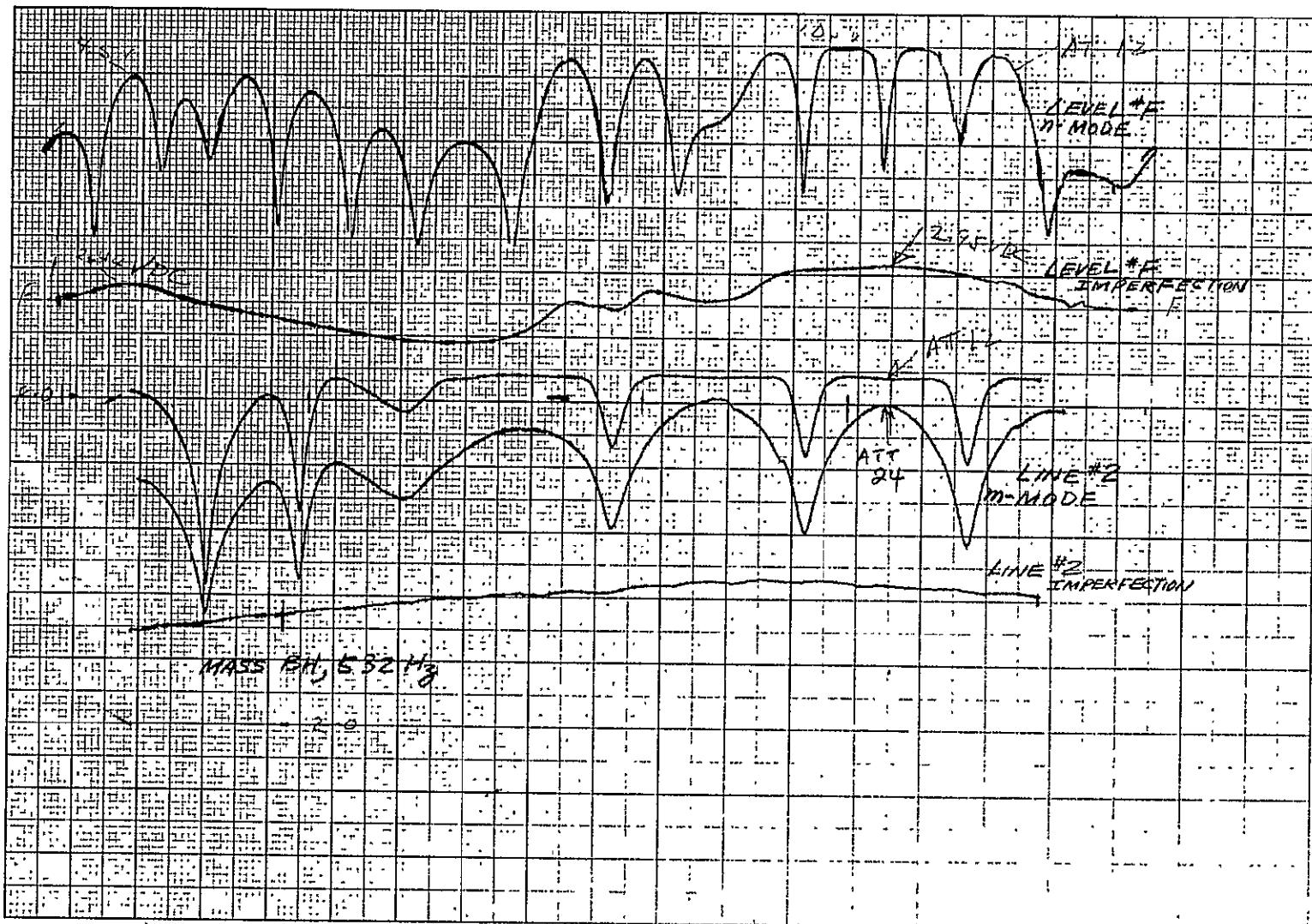
Figure XIII-11.   Radial m-n Modes Induced by Axial Excitations,
Mass BH, 532 Hertz
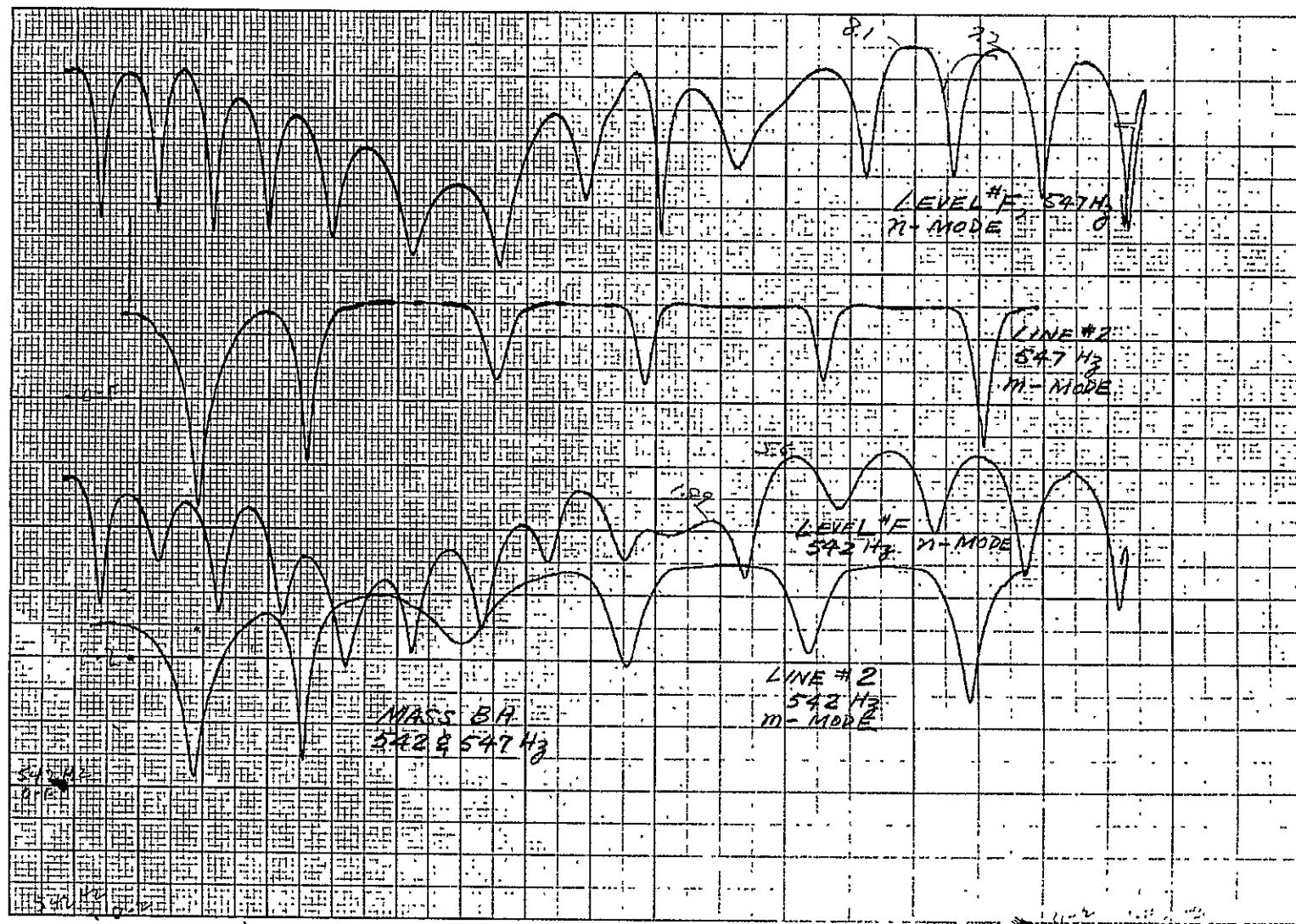
Figure XIII-12. Radial m-n Modes Induced by Axial Excitations, Mass BH, 542 and 547 Hertz
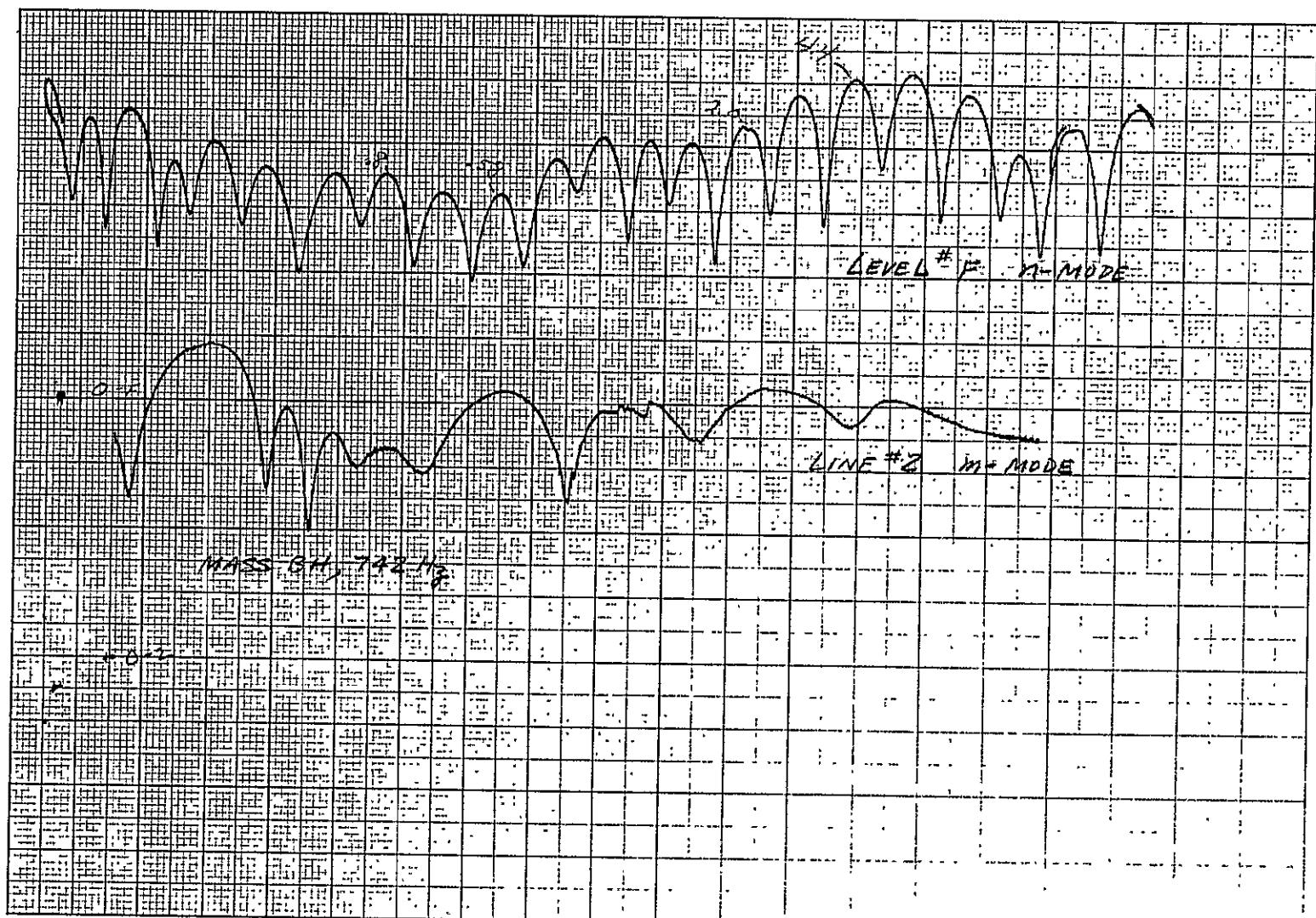
Figure XIII-13. Radial m-n Modes Induced by Axial Excitations, Mass BH, 742 Hertz

Space Division
North American Rockwell
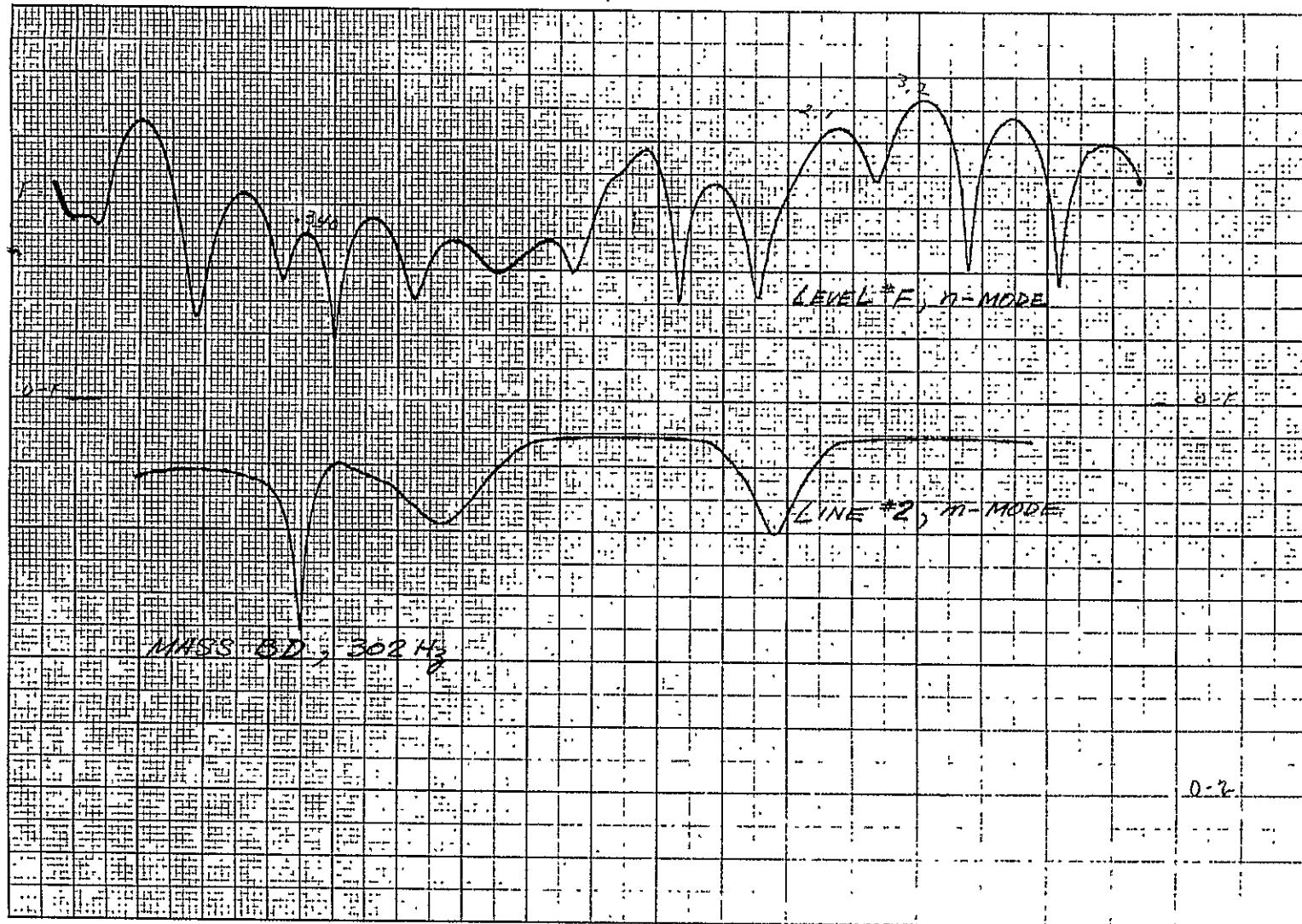
Figure XIII-14.   Radial m-n Modes Induced by Axial Excitations,
Mass BD, 302 Hertz
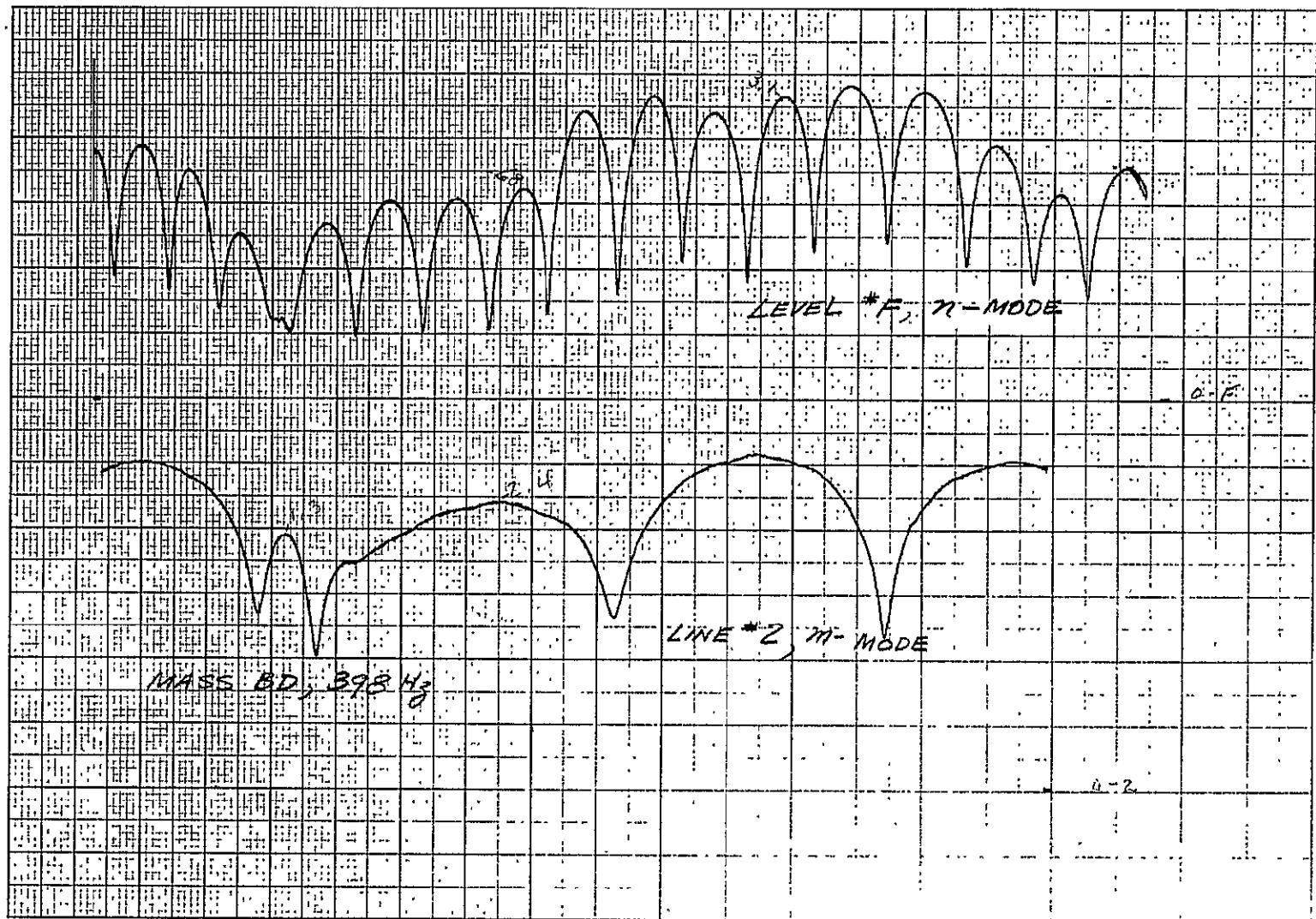
Figure XIII-15.   Radial m-n Modes Induced by Axial Excitations,
Mass BD, 398 Hertz
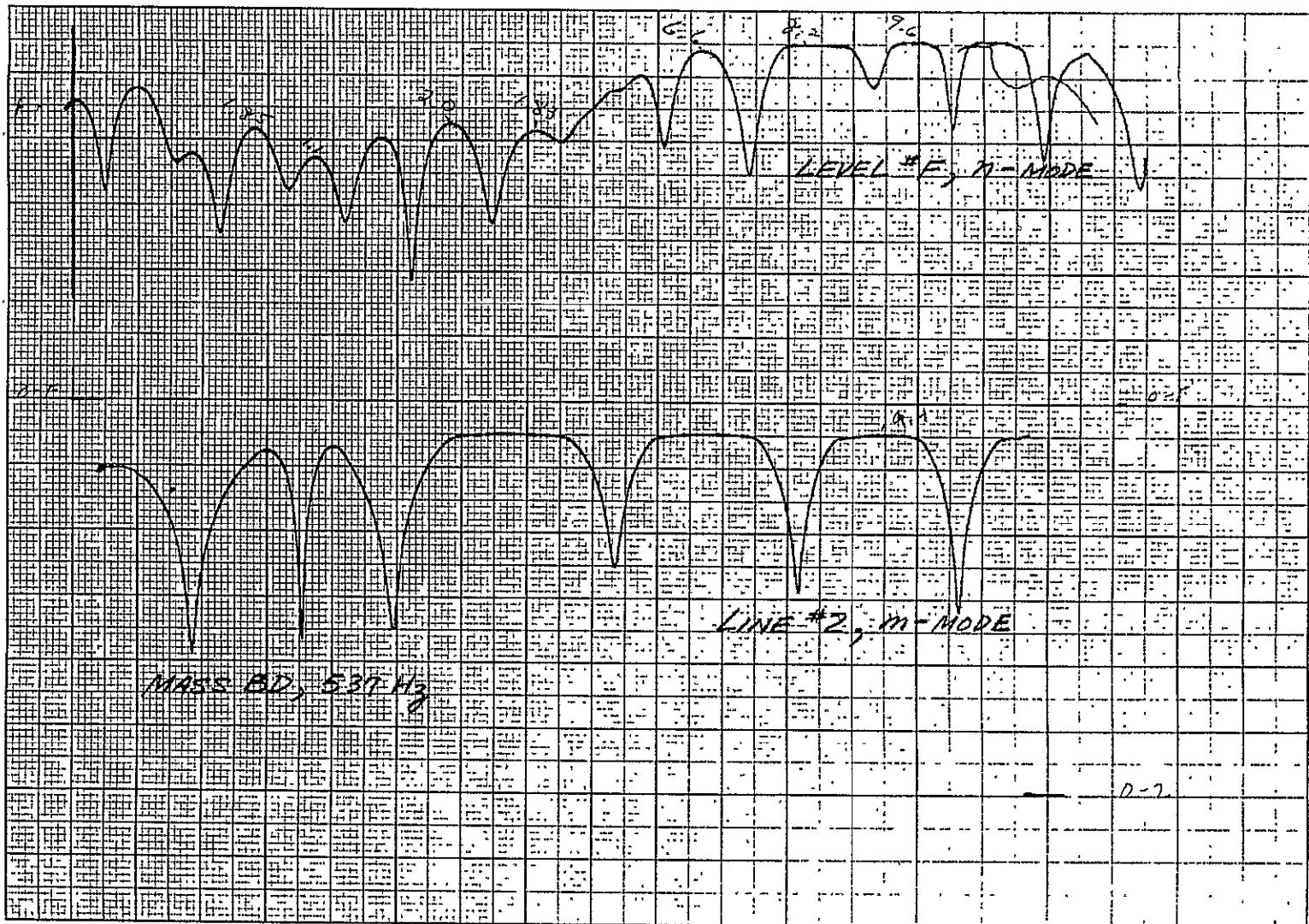
Figure XIII-16. Radial m-n Modes Induced by Axial Excitations,
Mass BD, 537 Hertz

XIV. SHOCK SPECTRAL DENSITY AND RESPONSE
CHARACTERISTICS
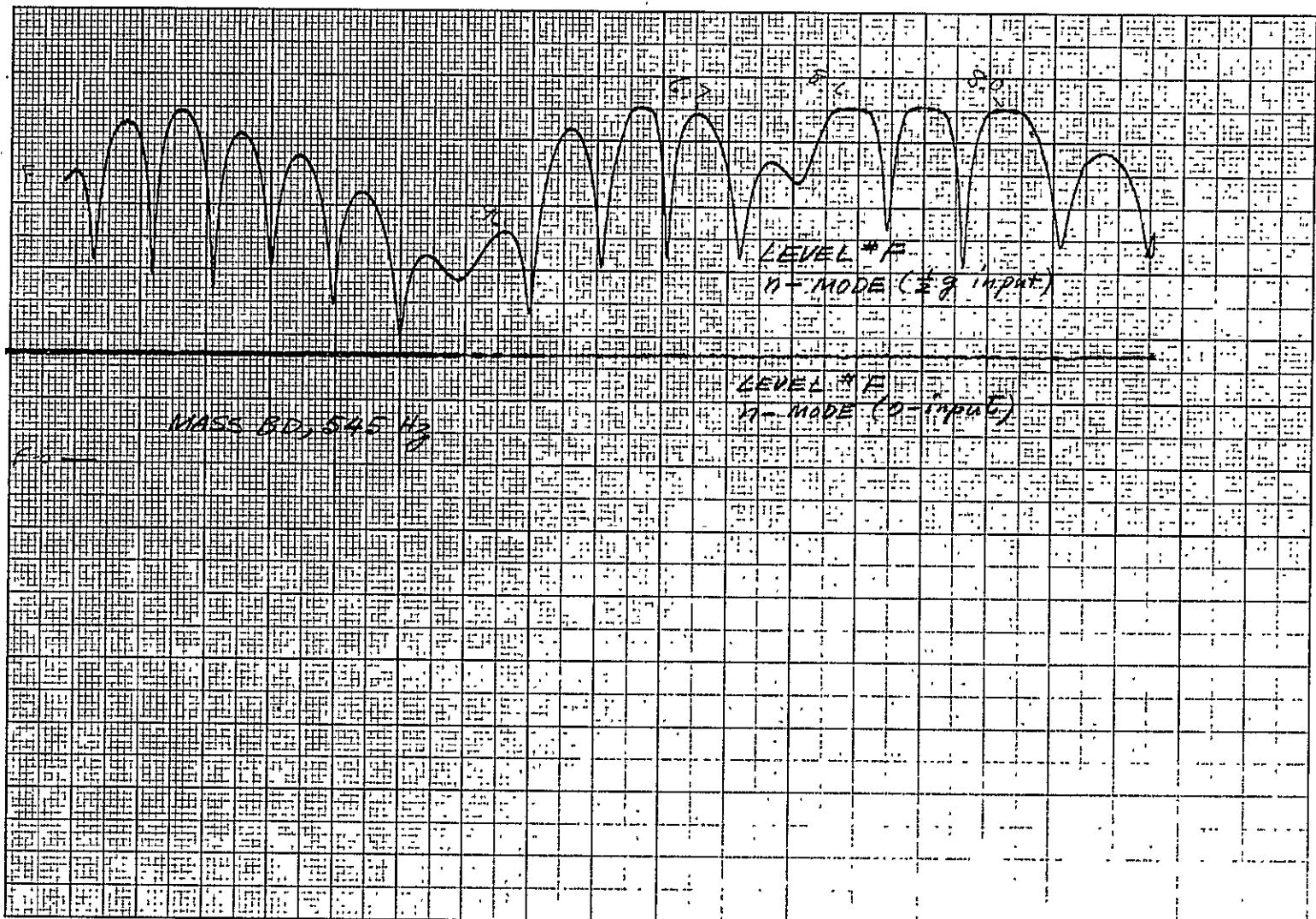
Figure XIII-17. Radial m-n Modes Induced by Axial Excitations, Mass BD, 545 Hertz
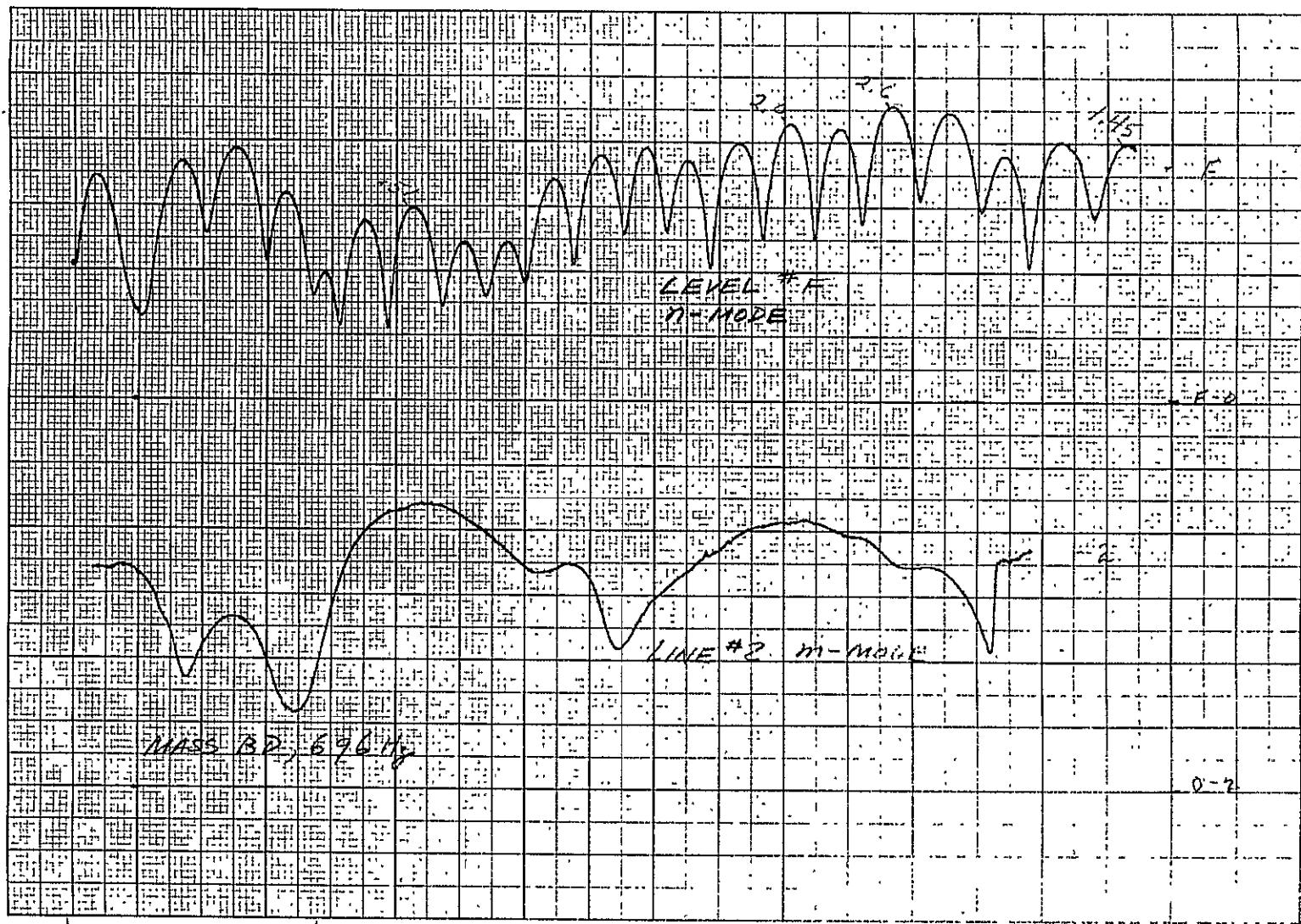
Figure XIII-18. Radial m-n Modes Induced by Axial Excitations, Mass BD, 696 Hertz
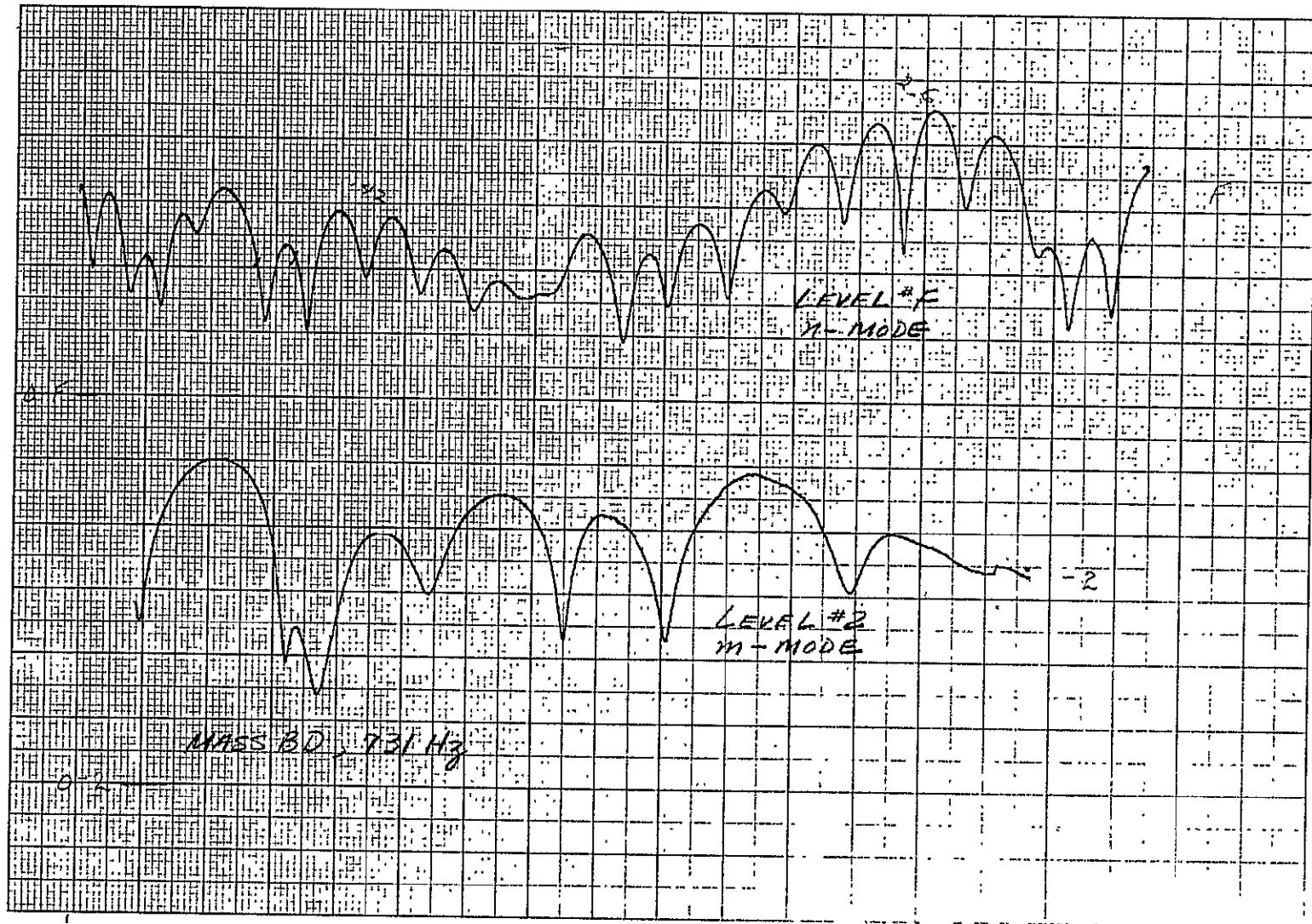
Figure XIII-19. Radial m-n Modes Induced by Axial Excitations,
Mass BD, 731 Hertz
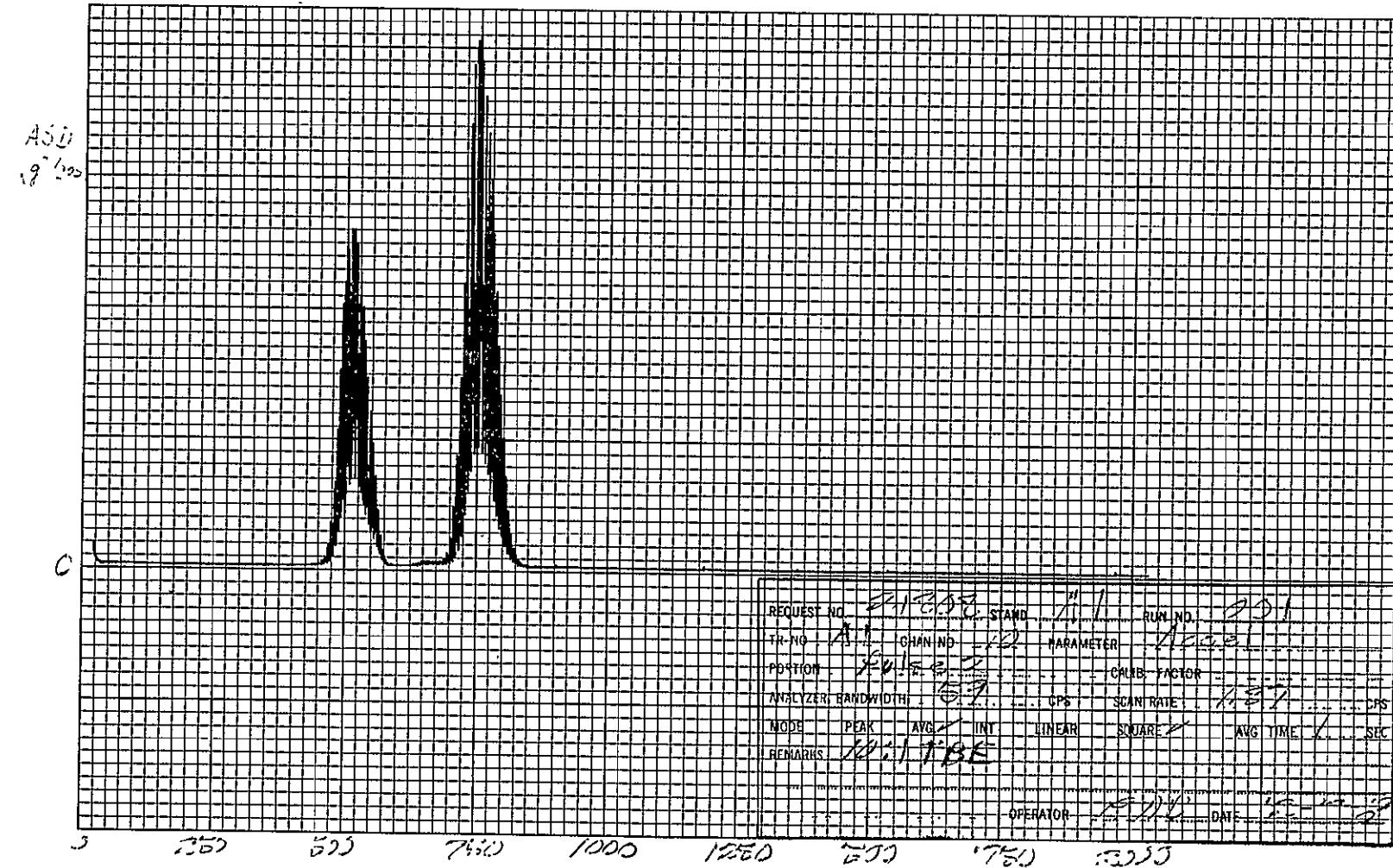
Figure XIV-1. Acceleration Spectral Density Representation of the Shock
Response, Test Run 1, Pulse 1 (0.9 milliseconds)
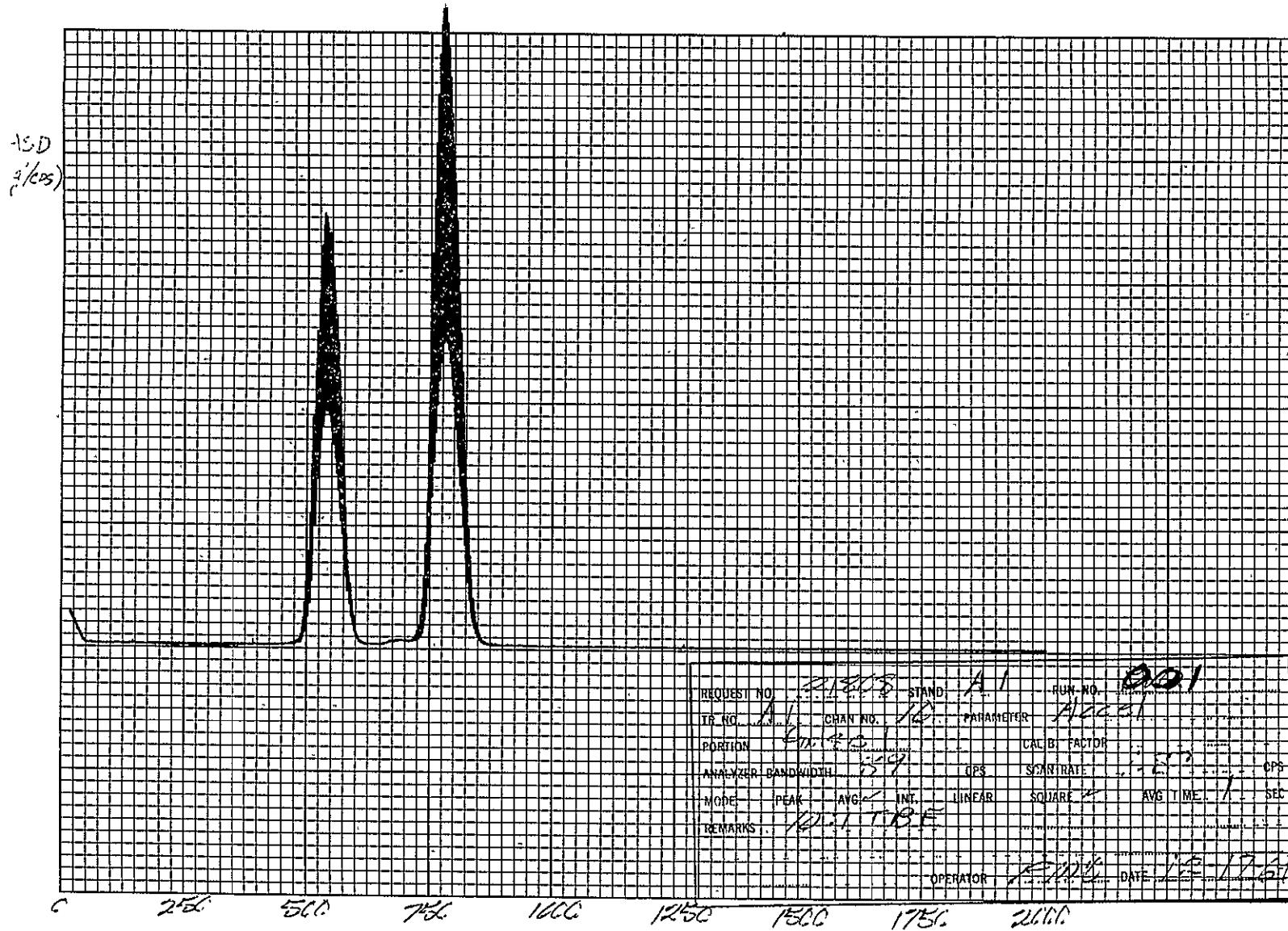
Figure XIV-2. Acceleration Spectral Density Representation of the Shock Response, Test Run 1, Pulse 2 (0.6 milliseconds)

Figure XIV-3. Acceleration Spectral Density Representation of the Shock Response, Test Run 2, Pulse 1 (0.9 milliseconds)

Figure XIV-4. Acceleration Spectral Density Representation of the Shock Response, Test Run 2, Pulse 2 (0.6 milliseconds)
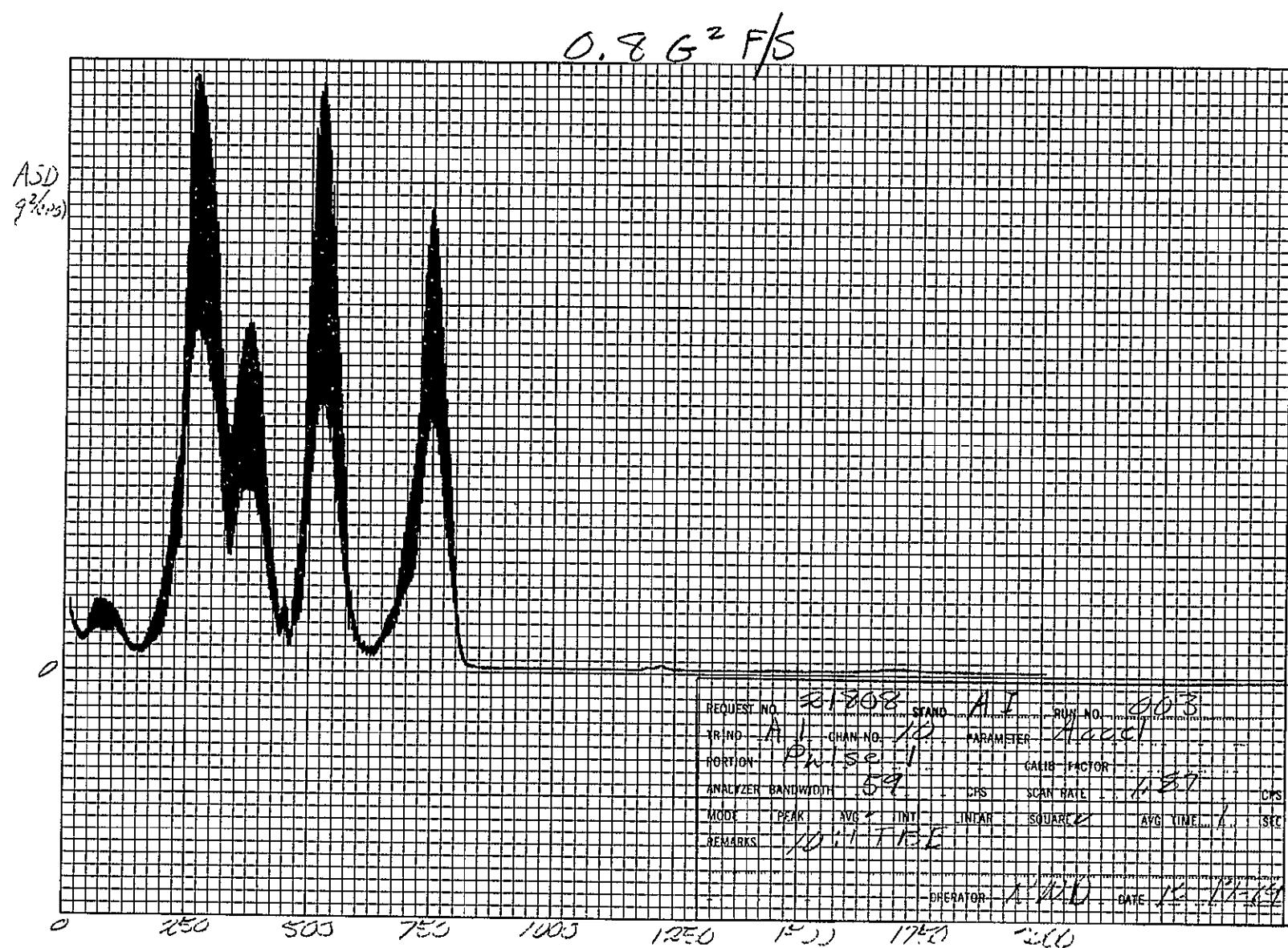
Figure XIV-5. Acceleration Spectral Density Representation of the Shock Response, Test Run 2, Pulse 3 (0.9 milliseconds)
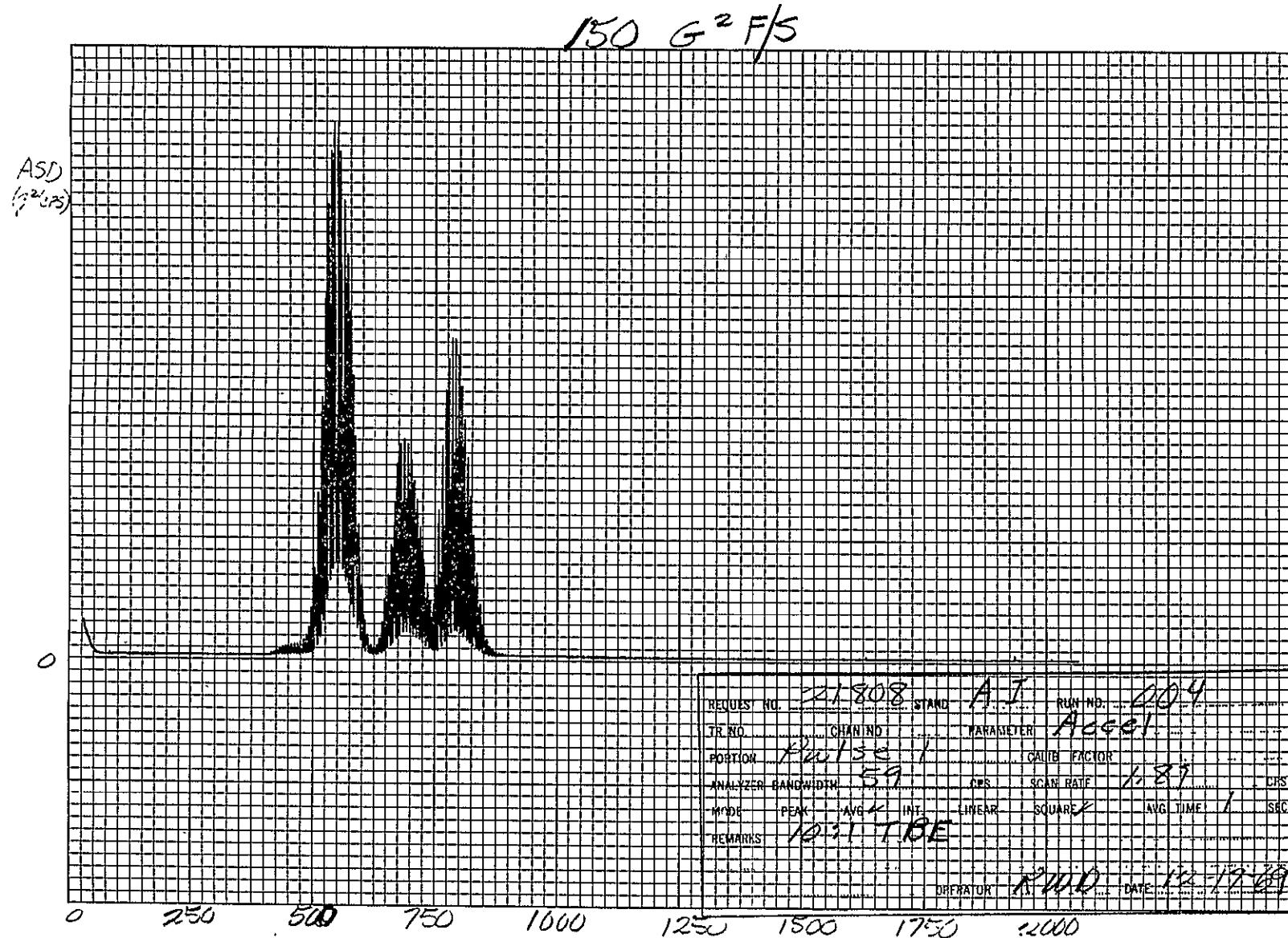
Figure XIV-6. Acceleration Spectral Density Representation of the Shock Response, Test Run 3, Pulse 1 (0.8 milliseconds)

$25G^2 F/S$

ASD (g^2/cps)

Figure XIV-7. Acceleration Spectral Density Representation of the Shock
Response, Test Run 4, Pulse (0. 9 milliseconds)
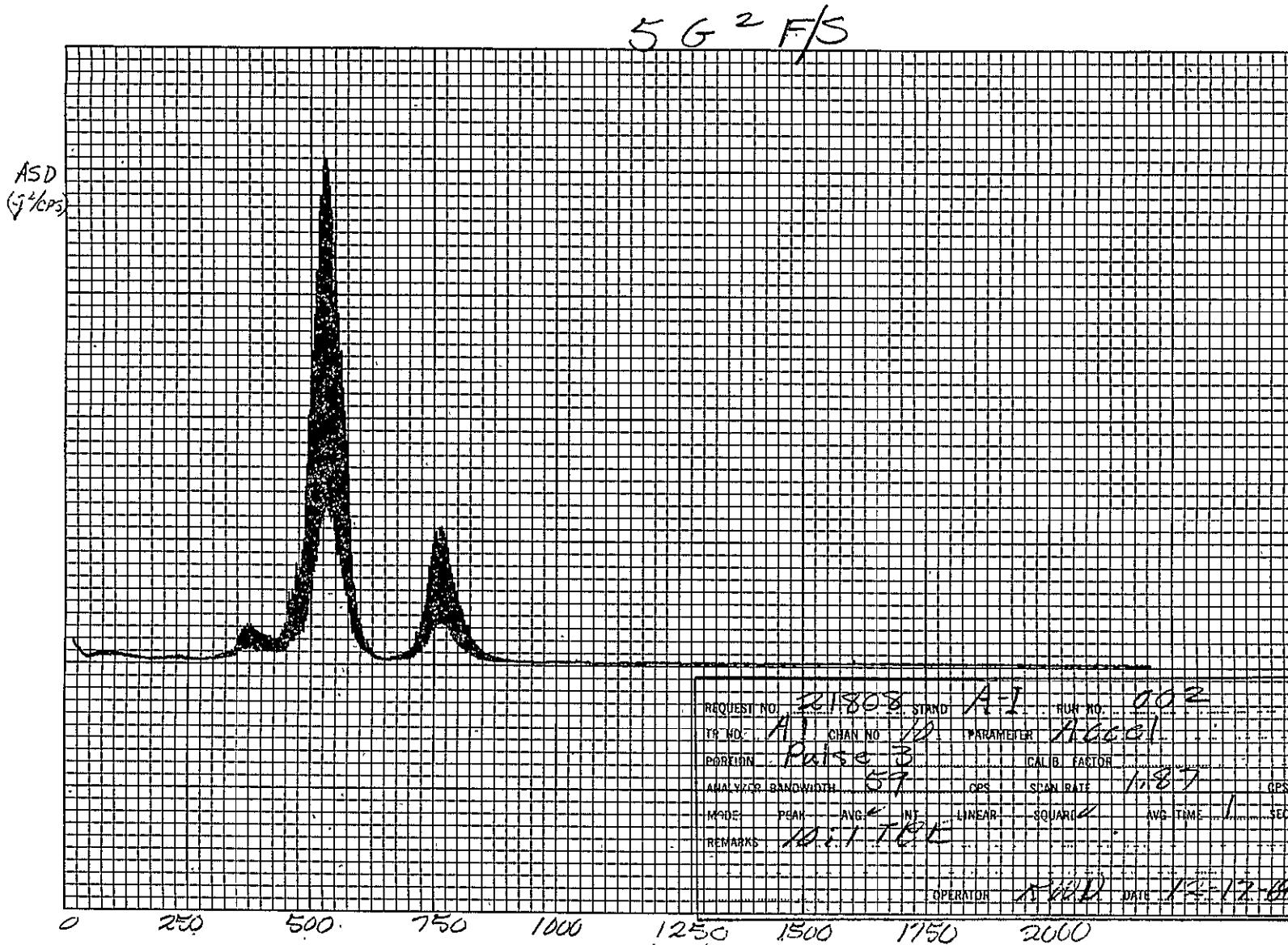
Figure XIV-8. Acceleration Spectral Density Representation of the Shock Response, Test Run 5, Pulse (0.9 milliseconds)

Space Division
North American Rockwell
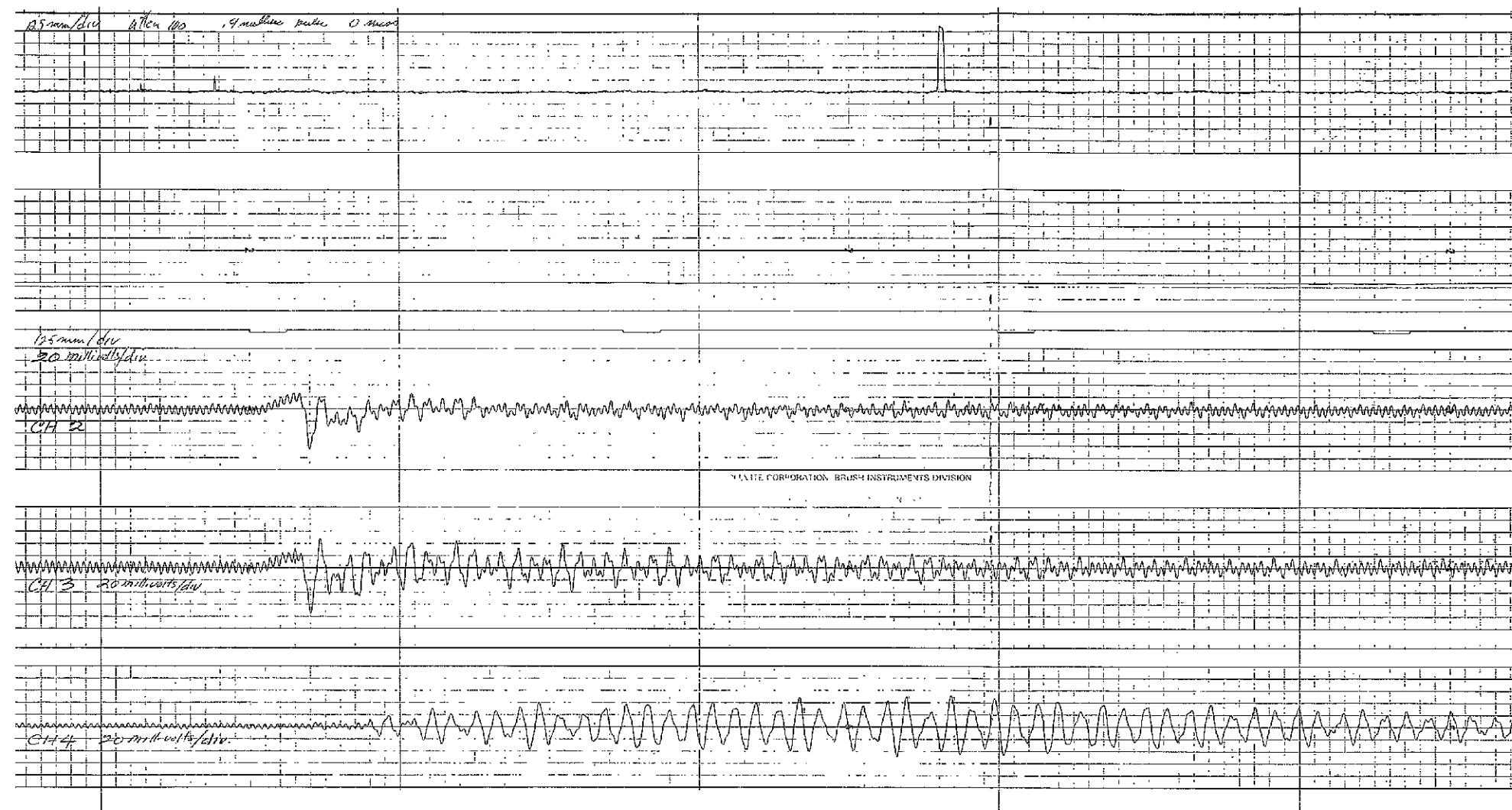
Figure XIV-9. Axial and Radial Shell Response Characteristics Induced by Longitudinal Shock Loads, No Mass, Pulse 1 (Sheet 1 of 4)
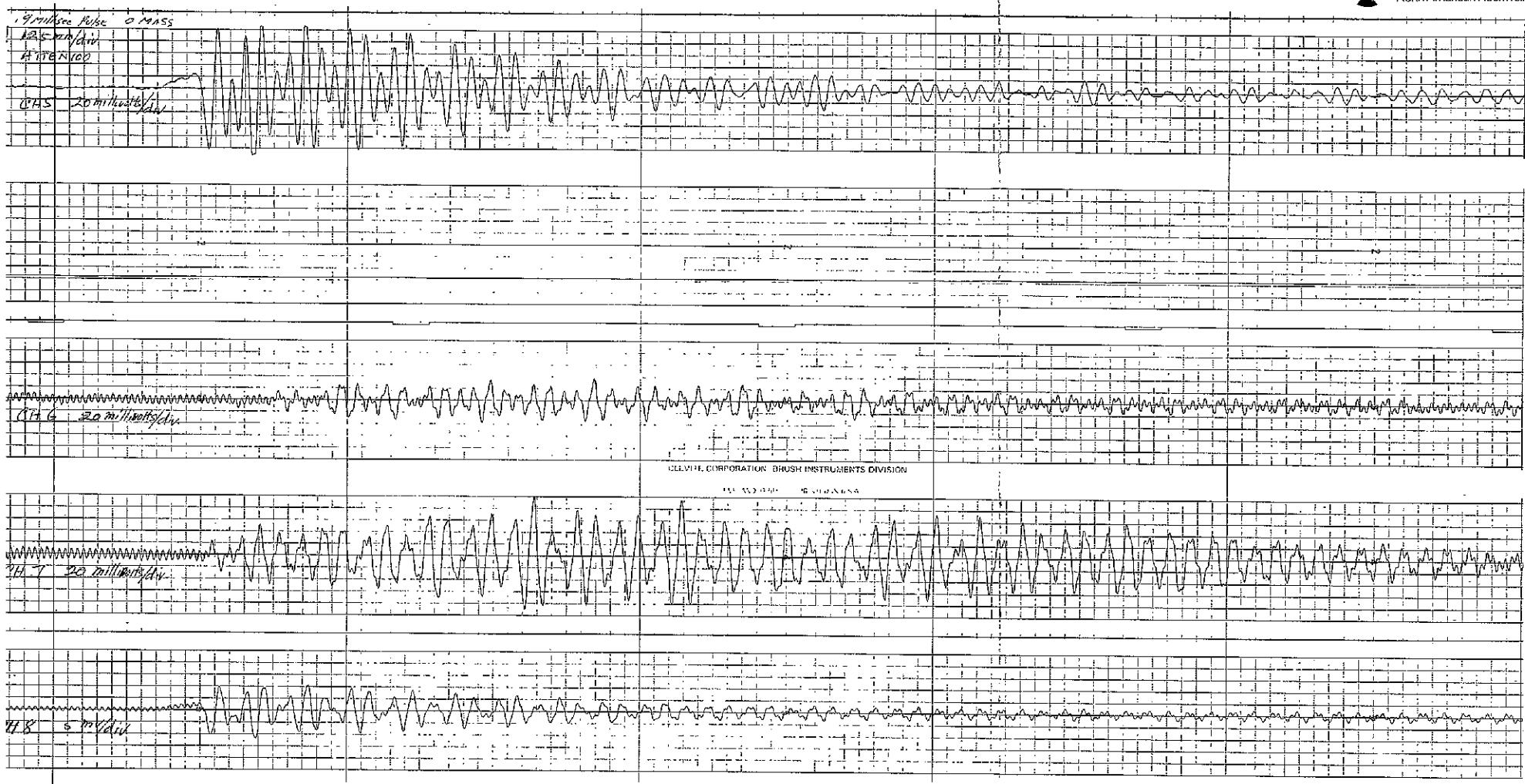
Figure XIV-9. Axial and Radial Shell Response Characteristics Induced by Longitudinal Shock Loads, No Mass, Pulse 1 (Sheet 2 of 4)

XIV-11, XIV-12

SD 69-766

FOLDOUT FRAME 2
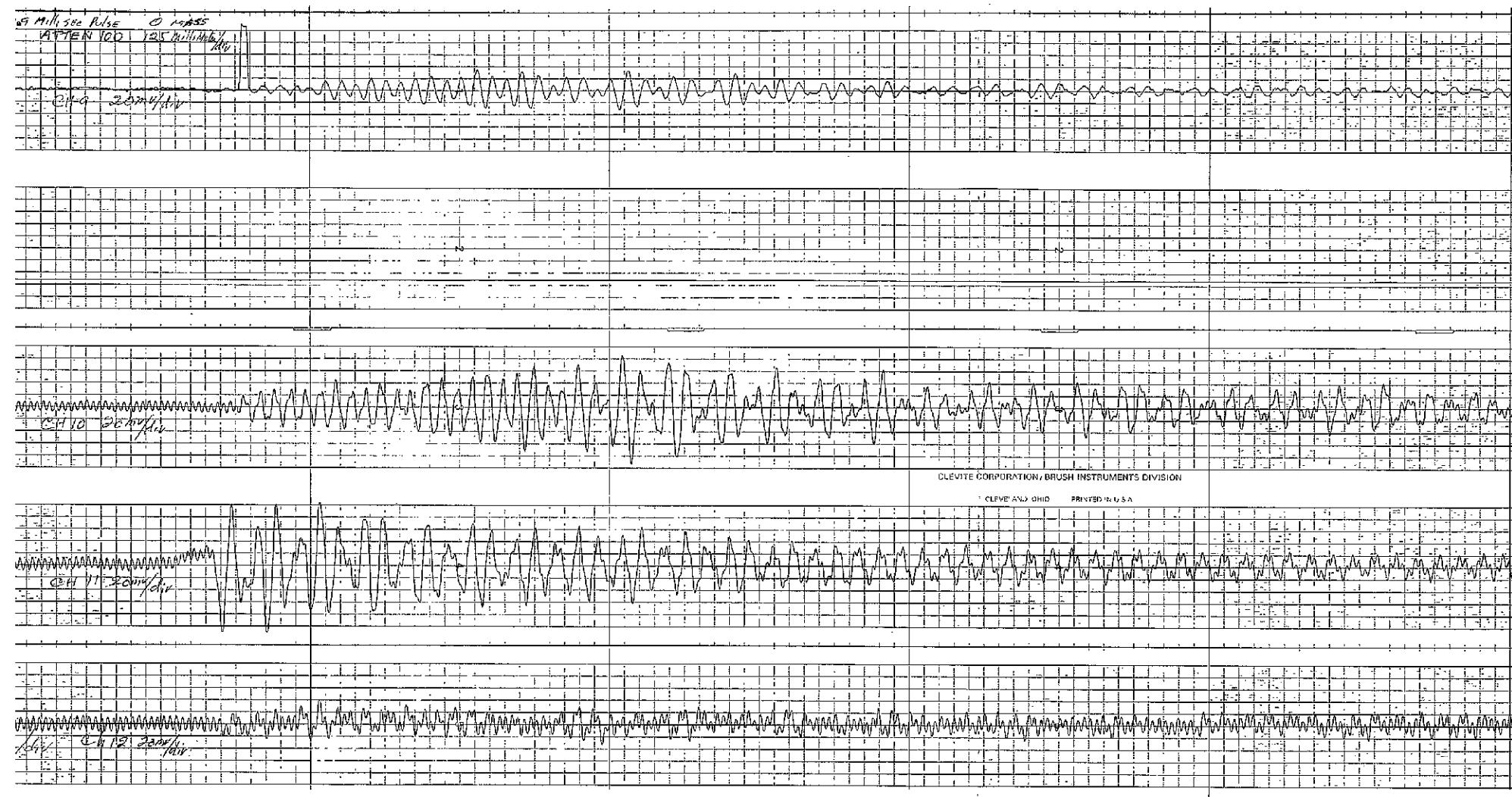
Figure XIV-9. Axial and Radial Shell Response Characteristics Induced by Longitudinal Shock Loads, No Mass, Pulse I (Sheet 3 of 4)
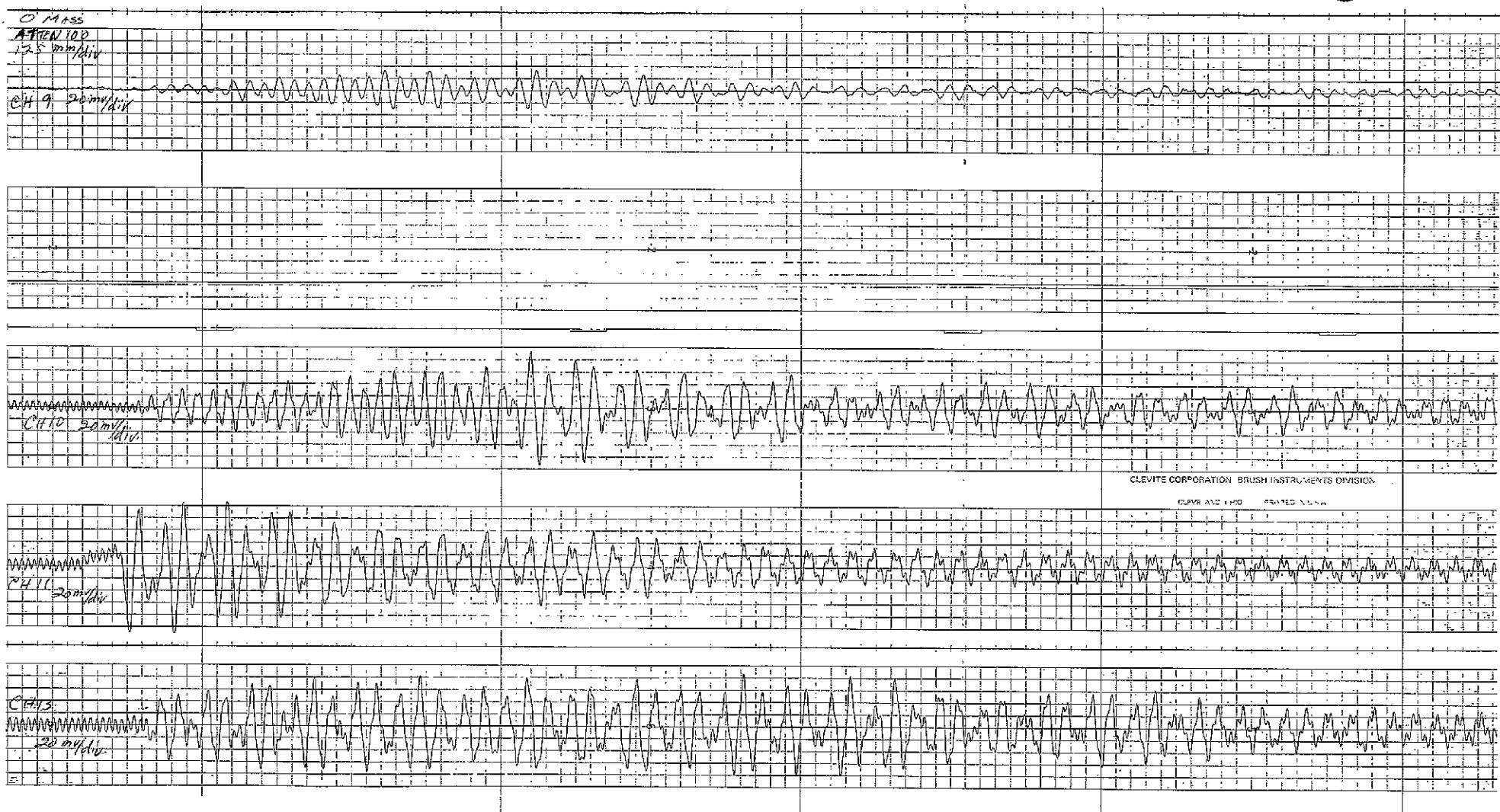
Figure XIV-9. Axial and Radial Shell Response Characteristics Induced by
Longitudinal Shock Loads, No Mass, Pulse 1 (Sheet 4 of 4)
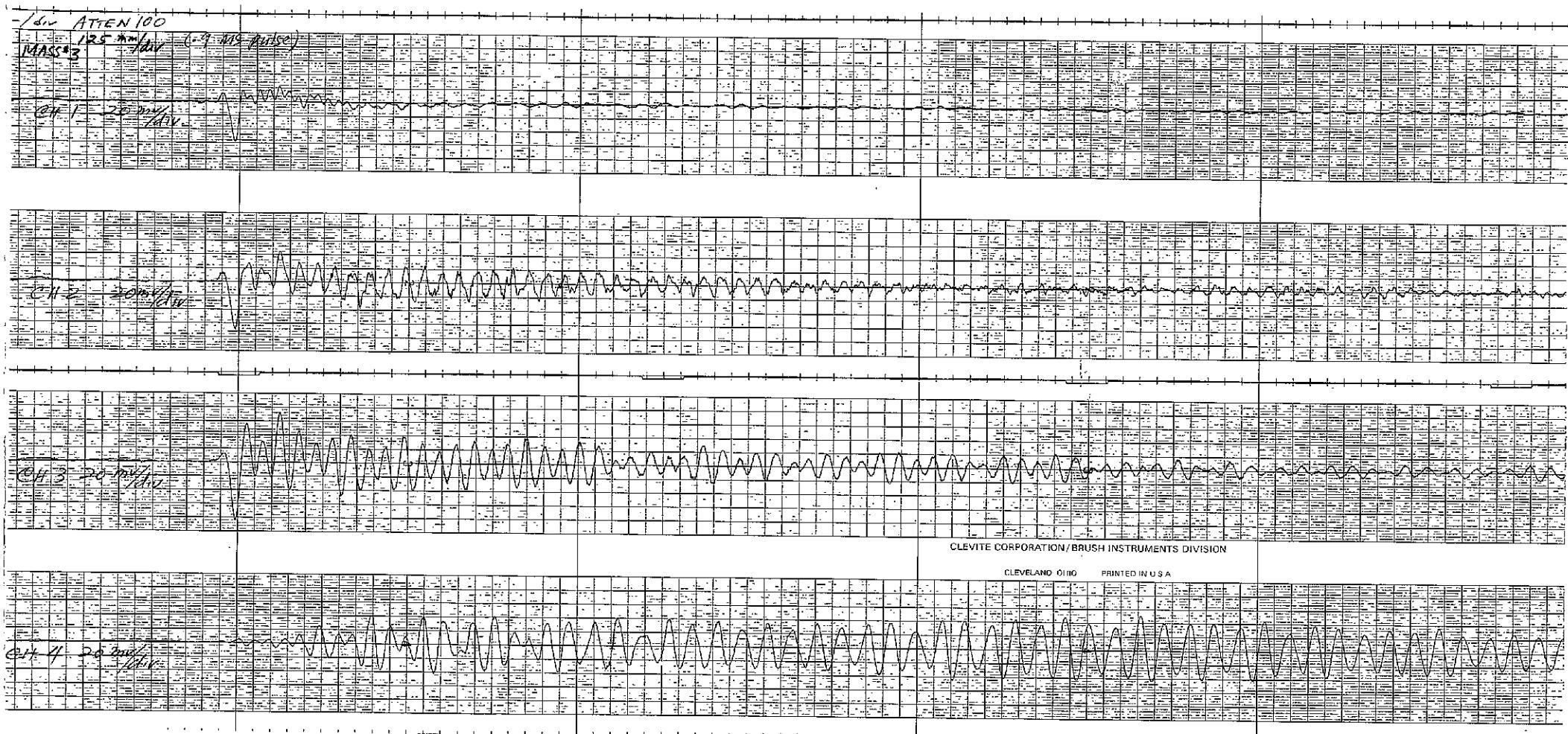
Figure XIV-10. Axial and Radial Shell Response Characteristics Induced by Longitudinal Shock Loads, Mass 3, Pulse 1 (Sheet 1 of 4)

FOLDOUT FRAME 1

FOLDOUT FRAME 2

XIV-17, XIV-18

FOLDOUT FRAME 3

Figure XIV-10. Axial and Radial Shell Response Characteristics Induced by Longitudinal Shock Loads, Mass 3, Pulse 1 (Sheet 2 of 4)
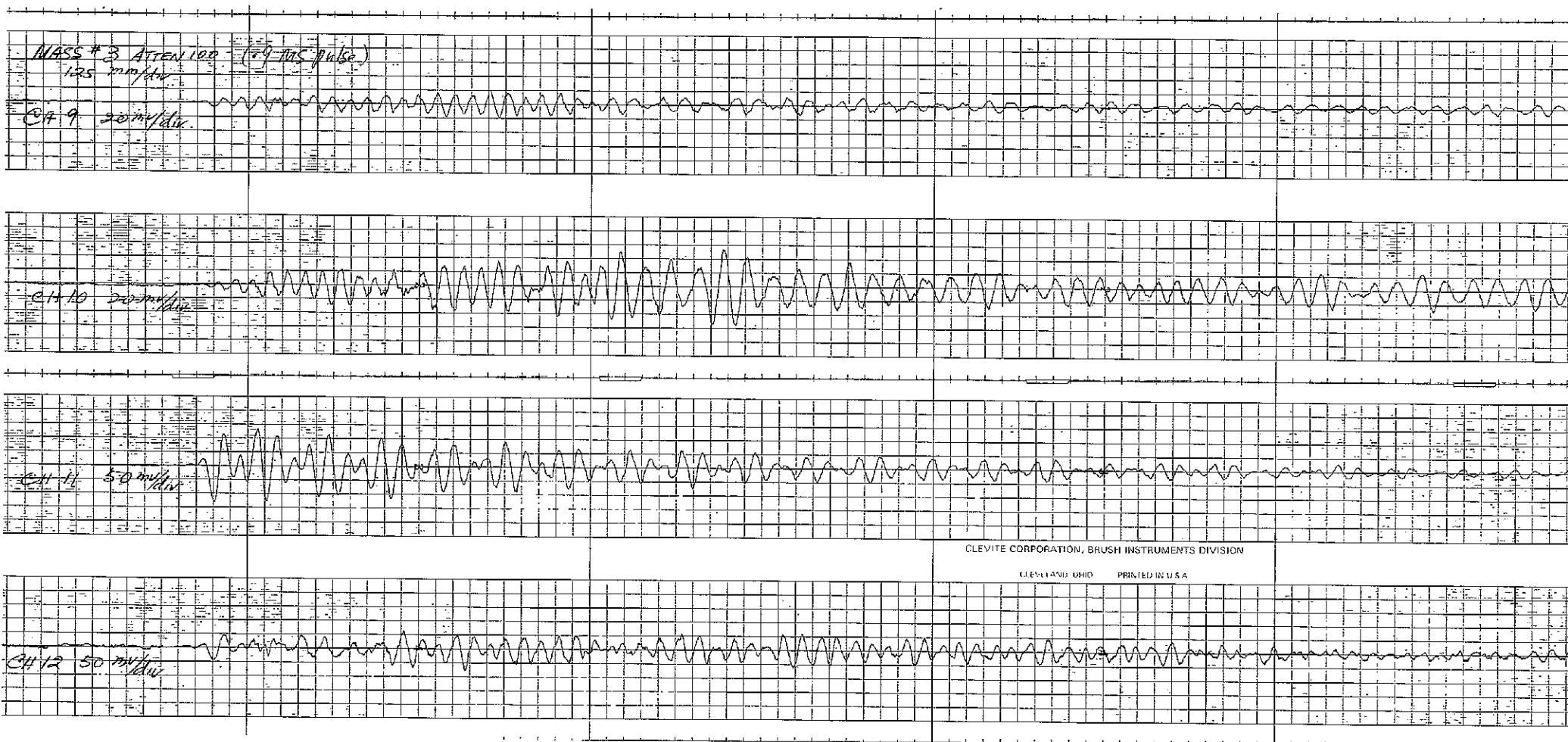
Figure XIV-10. Axial and Radial Shell Response Characteristics Induced by Longitudinal Shock Loads, Mass 3, Pulse 1 (Sheet 3 of 4)

CLEVITE CORPORATION/BRUSH INSTRUMENTS DIVISION

CLEVELAND OHIO   PRINTED IN U.S.A.

MASS #3 ATTEN-100 (.9 ms pulse)
12.5 mm/div

CH 3 10 mv/div

Figure XIV-10. Axial and Radial Shell Response Characteristics Induced by
Longitudinal Shock Loads, Mass 3, Pulse 1 (Sheet 4 of 4)
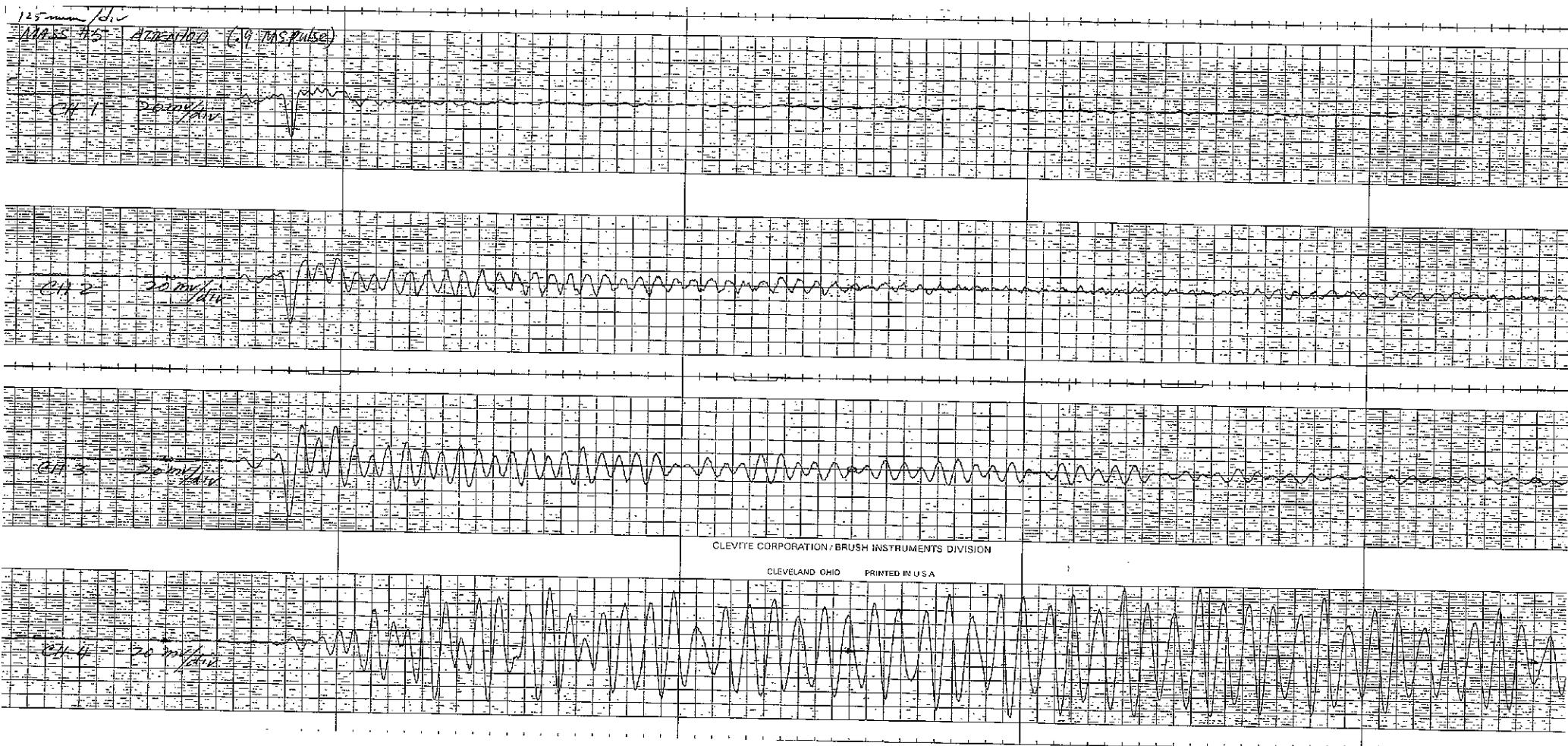
Figure XIV-11. Axial and Radial Shell Response Characteristics Induced by Longitudinal Shock Loads, Mass 5, Pulse 1 (Sheet 1 of 4)

CLEVITE CORPORATION / BRUSH INSTRUMENTS DIVISION

CLEVELAND OHIO   PRINTED IN U.S.A.

FOLDOUT FRAME 1

FOLDOUT FRAME 2

XIV-25, XIV-26
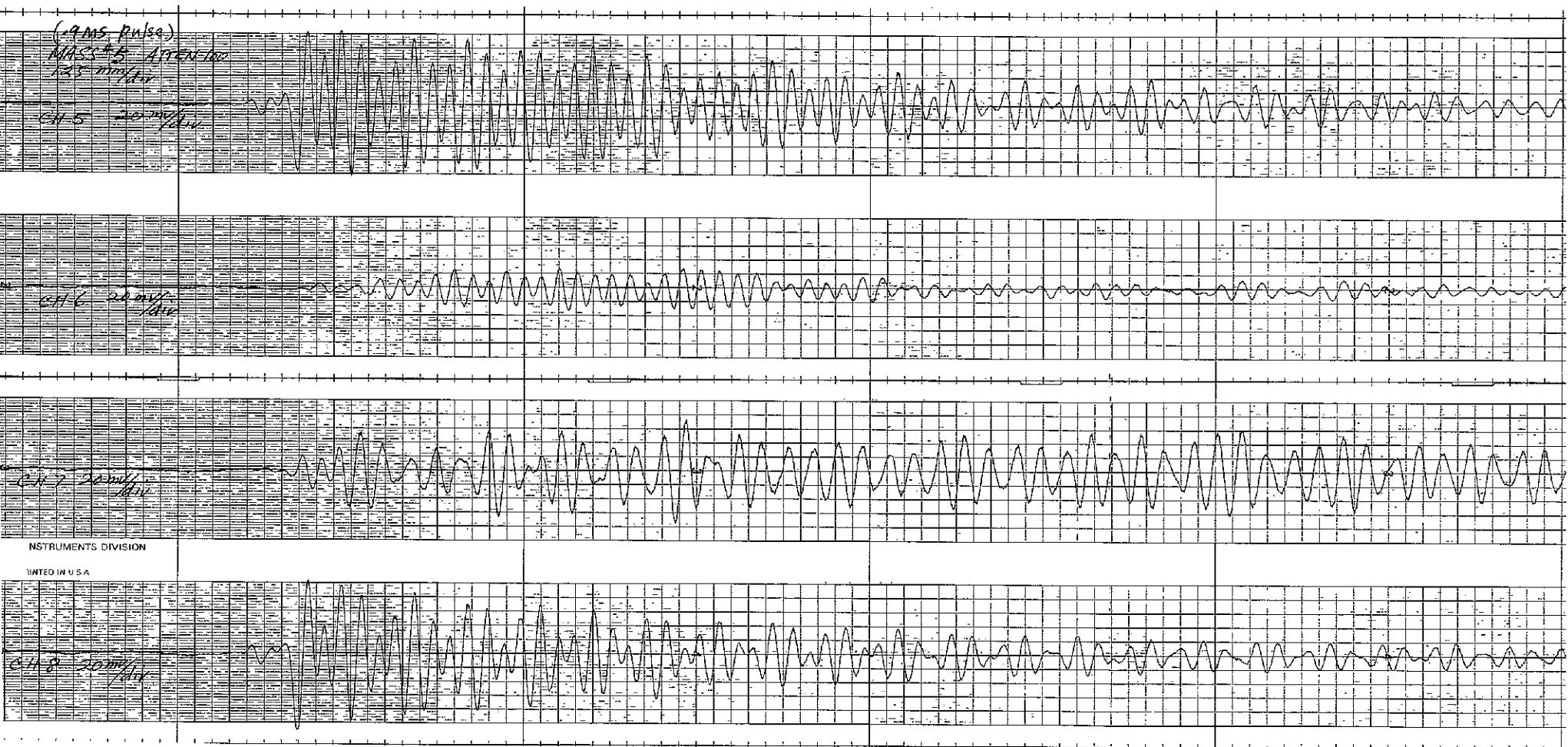
FOLDOUT FRAME 3

SD 69-766

Figure XIV-11. Axial and Radial Shell Response Characteristics Induced by Longitudinal Shock Loads, Mass 5, Pulse I (Sheet 2 of 4)
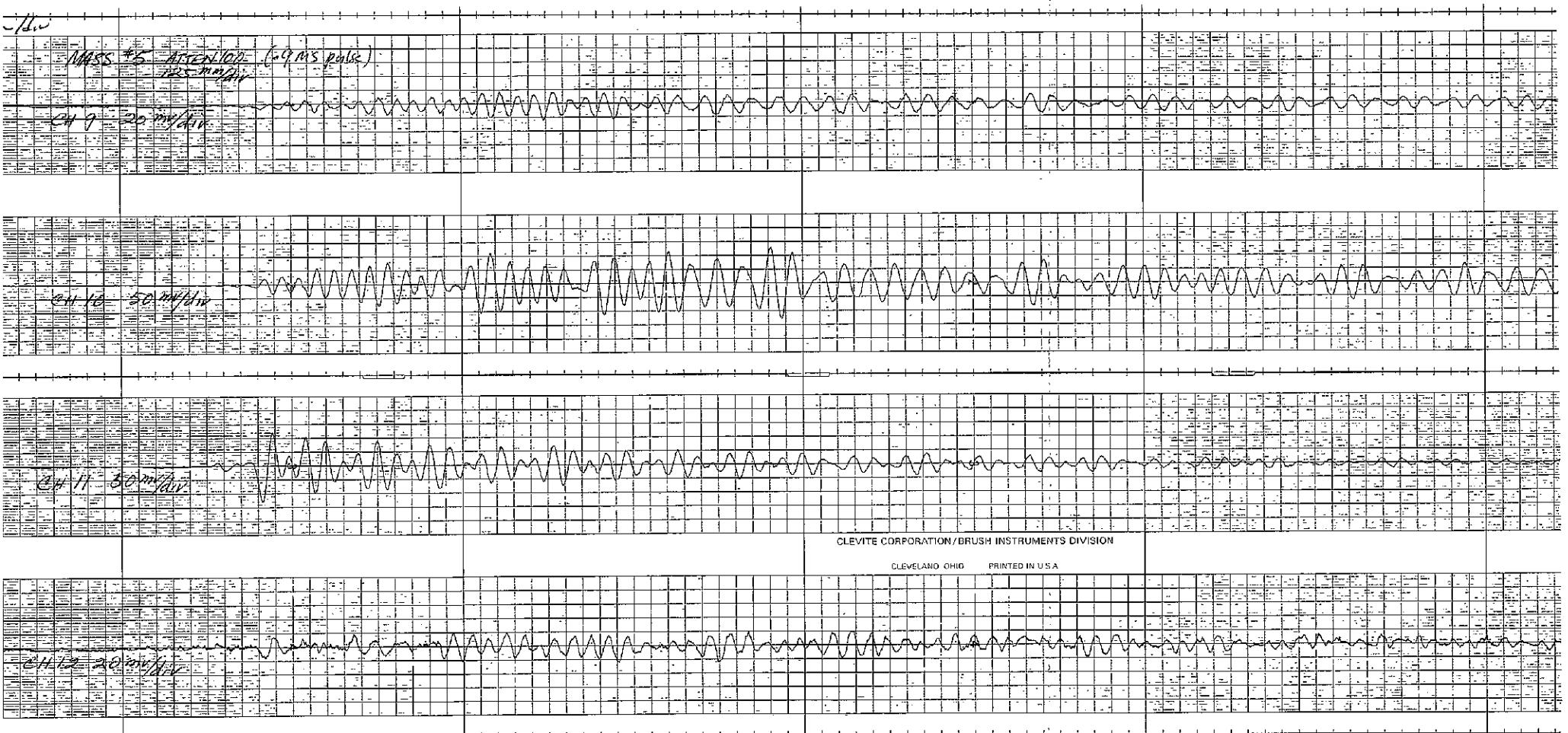
Figure XIV-11. Axial and Radial Shell Response Characteristics Induced by Longitudinal Shock Loads, Mass 5, Pulse 1 (Sheet 3 of 4)
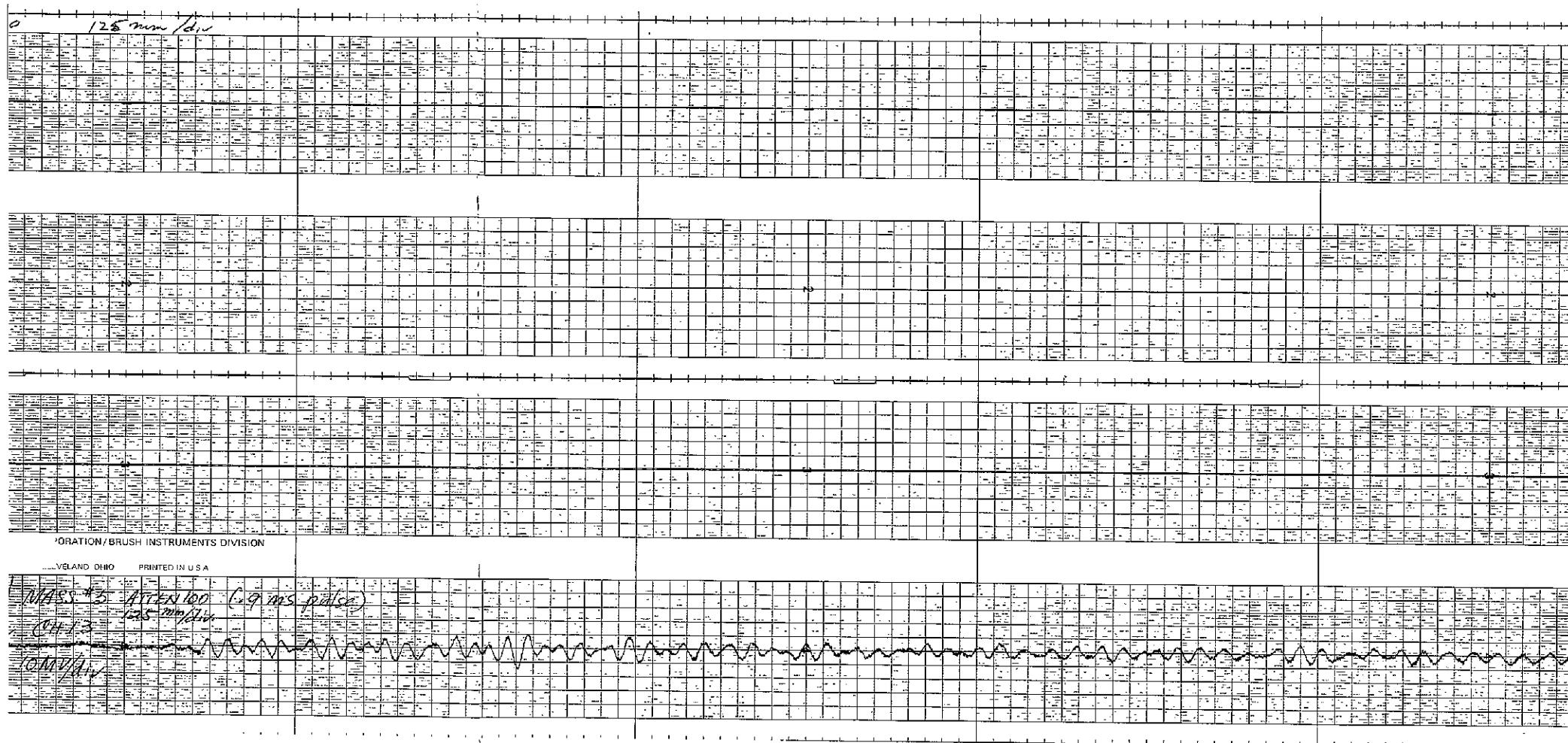
125 mm/div

'ORATION/BRUSH INSTRUMENTS DIVISION

...VELAND OHIO   PRINTED IN U.S.A.

MASS #5 ATTEN 100 (.9 ms pulse)
CH 13
125 mm/div
10 MV/A.7

Figure XIV-11. Axial and Radial Shell Response Characteristics Induced by
Longitudinal Shock Loads, Mass 5, Pulse 1 (Sheet 4 of 4)
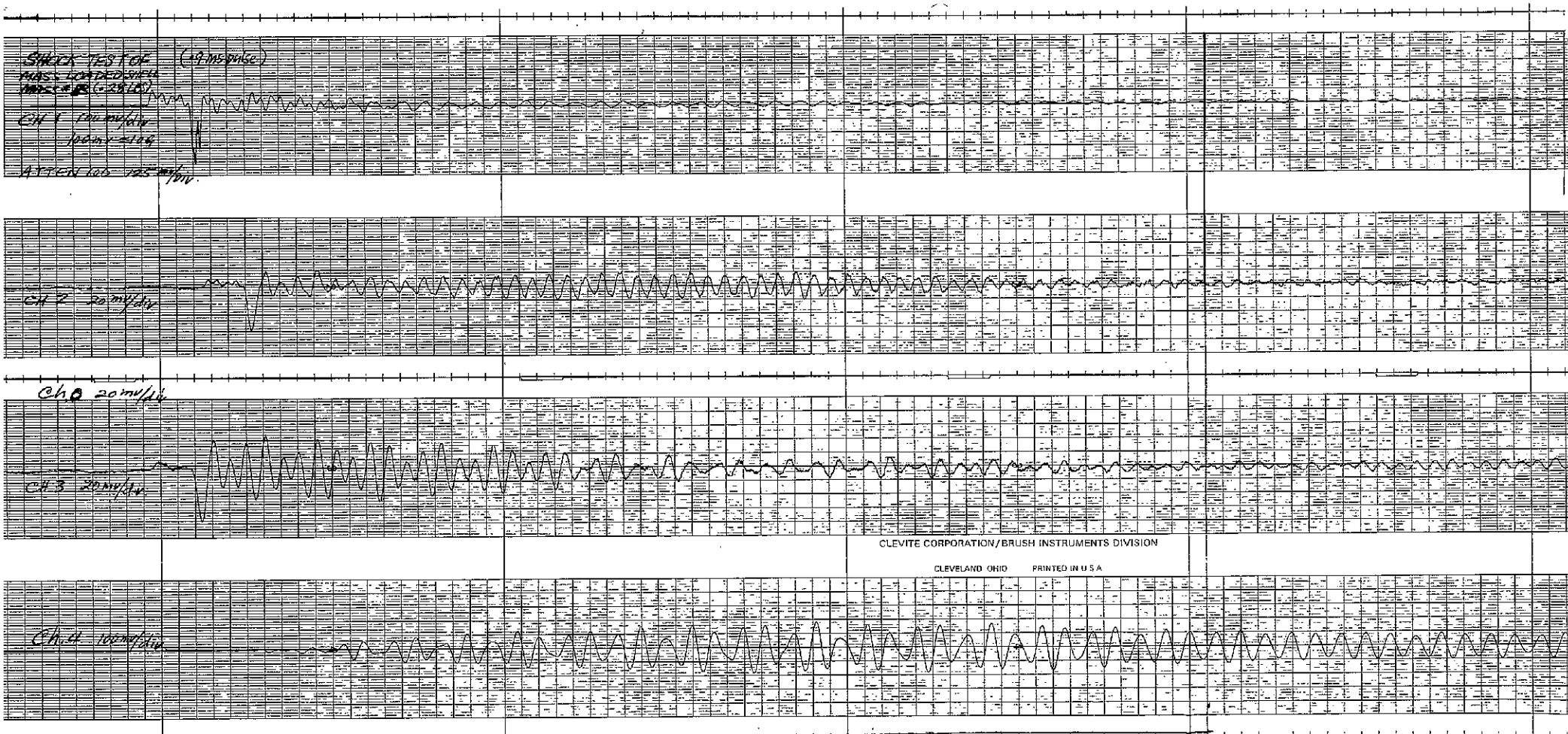
Figure XIV-12. Axial and Radial Shell Response Characteristics Induced by
Longitudinal Shock Loads, Mass B, Pulse 1 (Sheet 1 of 4)

CLEVITE CORPORATION / BRUSH INSTRUMENTS DIVISION

CLEVELAND, OHIO.   PRINTED IN U S A
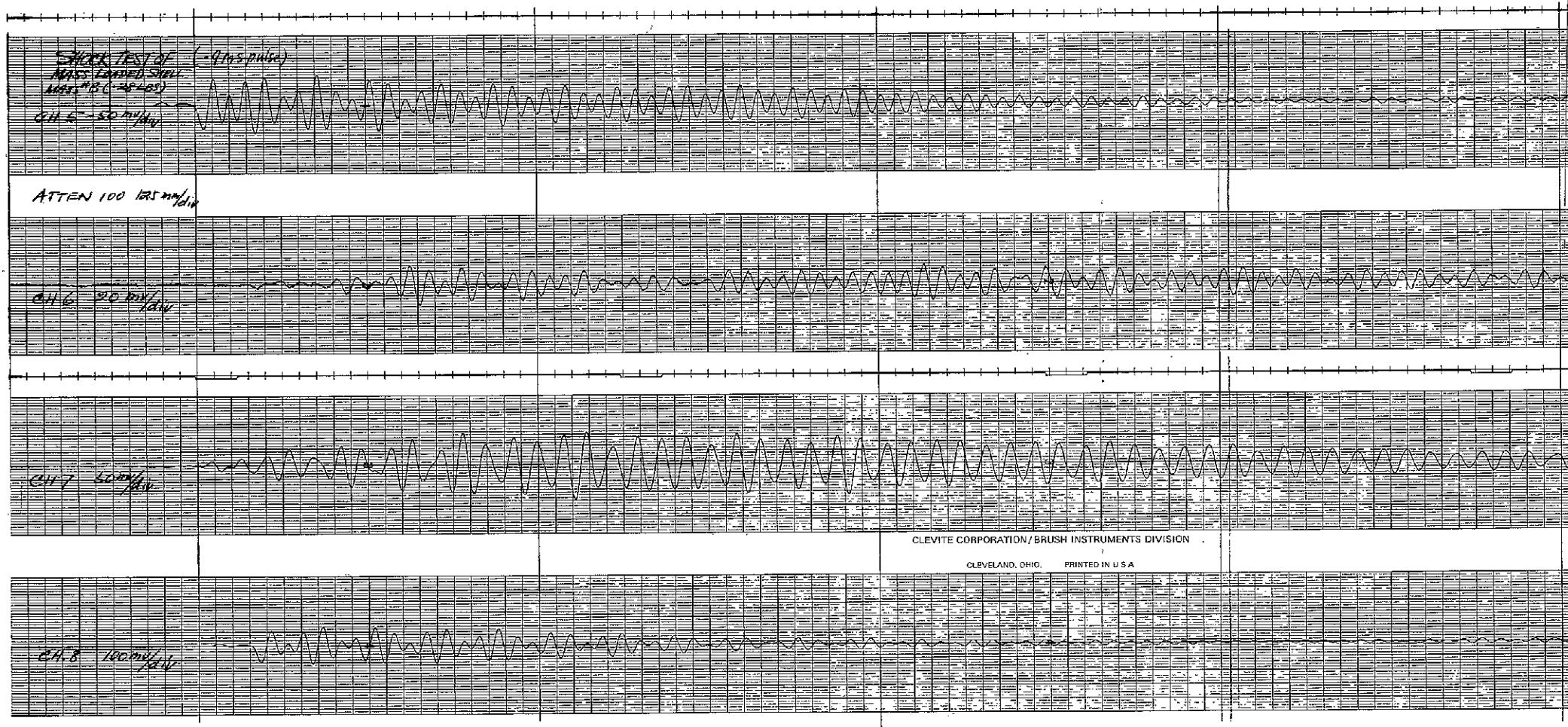
Figure XIV-12. Axial and Radial Shell Response Characteristics Induced by
Longitudinal Shock Loads, Mass B, Pulse I (Sheet 2 of 4)

Figure XIV-12. Axial and Radial Shell Response Characteristics Induced by Longitudinal Shock Loads, Mass B, Pulse 1 (Sheet 3 of 4)
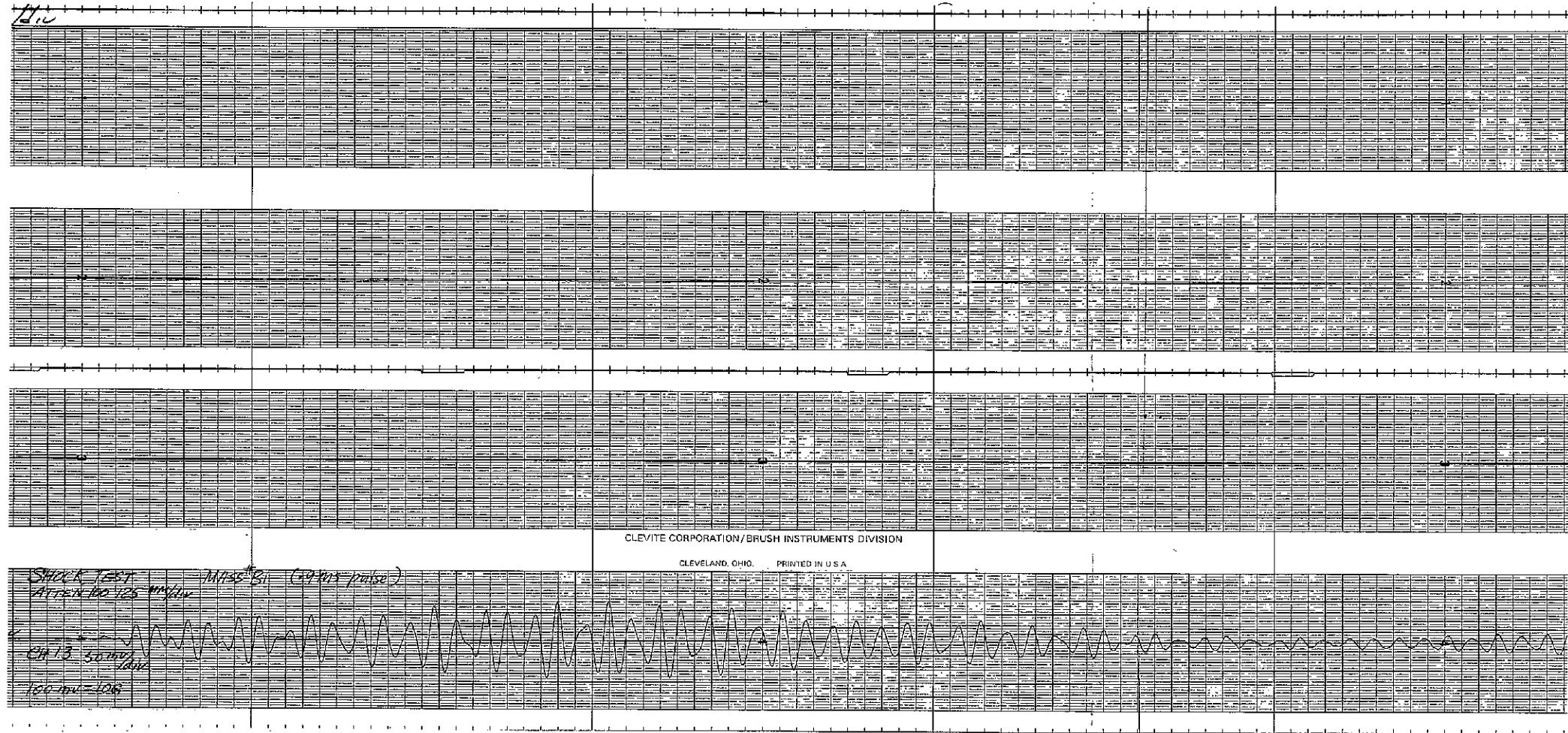
CLEVITE CORPORATION/BRUSH INSTRUMENTS DIVISION

CLEVELAND, OHIO.   PRINTED IN U.S.A.

SHOCK TEST   MASS B₁ (.9 ms pulse)
ATTEN 100-125 mm/div

CH 13 50 mv/div

100 mv = 100

Figure XIV-12. Axial and Radial Shell Response Characteristics Induced by
Longitudinal Shock Loads, Mass B, Pulse 1 (Sheet 4 of 4)

FOLDOUT FRAME 1

FOLDOUT FRAME 2

FOLDOUT FRAME 3

XIV-39, XIV-40
SD 69-766

Figure XIV-13. Axial and Radial Shell Response Characteristics Induced by Longitudinal Shock Loads, Mass BH, Pulse 1 (Sheet 1 of 4)

Figure XIV-13. Axial and Radial Shell Response Characteristics Induced by Longitudinal Shock Loads, Mass BH, Pulse 1 (Sheet 2 of 4)

FOLDOUT FRAME 1

FOLDOUT FRAME 2

XIV-43, XIV-44

FOLDOUT FRAME

SD 69-766

Figure XIV-13. Axial and Radial Shell Response Characteristics Induced by Longitudinal Shock Loads, Mass BH, Pulse 1 (Sheet 3 of 4)

Figure XIV-13. Axial and Radial Shell Response Characteristics Induced by Longitudinal Shock Loads, Mass BH, Pulse 1 (Sheet 4 of 4)

CLEVITE CORPORATION/BRUSH INSTRUMENTS DIVISION

CLEVELAND OHIO   PRINTED IN U.S.A.

100   125 mm/div

MASS #BH
SHOCK #1   (.2 ms pulse)
APPROX N.O. 125 mV/div

CH 13 50 mV/div

Figure XIV-14. Axial and Radial Shell Response Characteristics Induced by Longitudinal Shock Loads, Mass BD, Pulse I (Sheet 1 of 4)

Figure XIV-14. Axial and Radial Shell Response Characteristics Induced by
Longitudinal Shock Loads, Mass BD, Pulse 1 (Sheet 2 of 4)
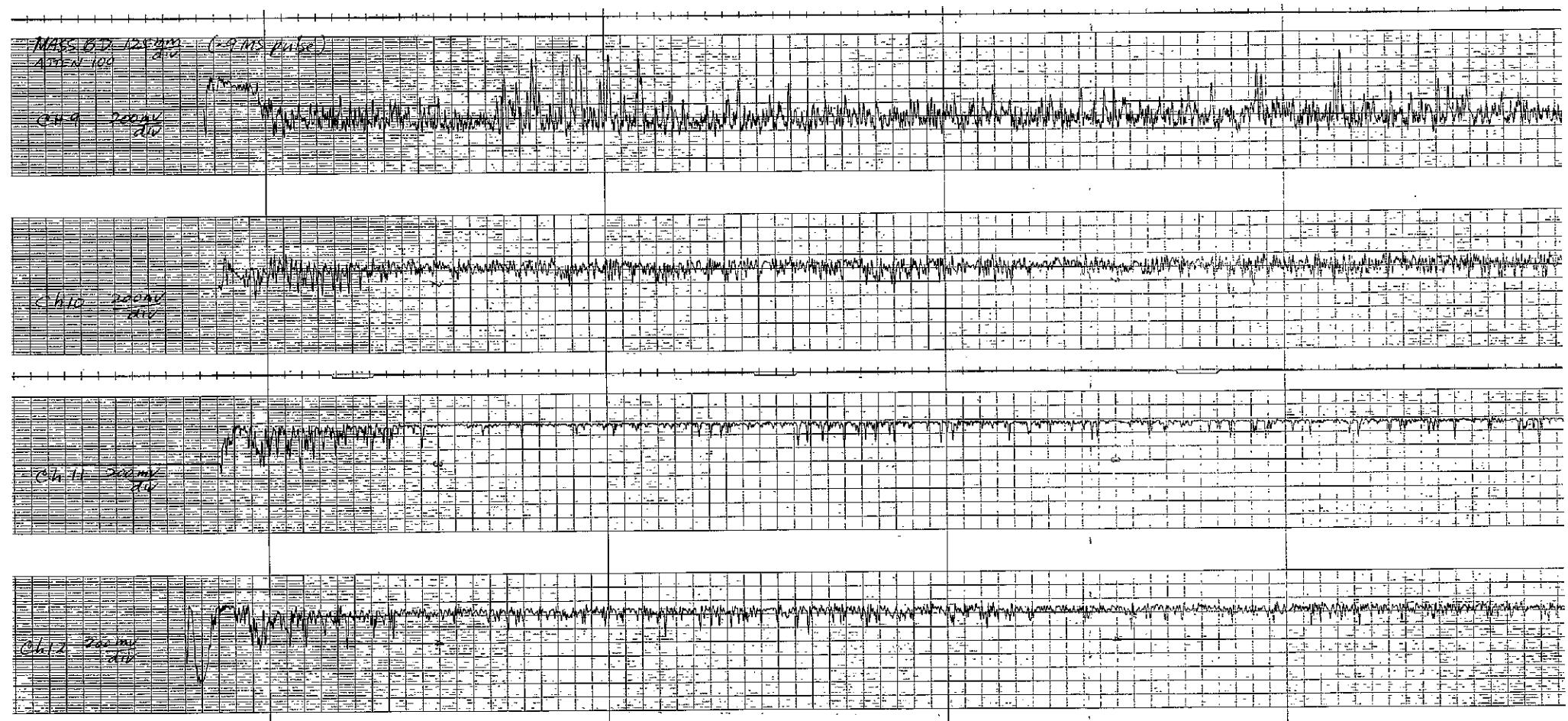
Figure XIV-14. Axial and Radial Shell Response Characteristics Induced by Longitudinal Shock Loads, Mass BD, Pulse 1 (Sheet 3 of 4)

Figure XIV-14. Axial and Radial Shell Response Characteristics Induced by Longitudinal Shock Loads, Mass BD, Pulse I (Sheet 4 of 4)

ON/BRUSH INSTRUMENTS DIVISION

), OHIO   PRINTED IN U.S.A

MASS BD   (.9 ms pulse)
ATTEN 100 12.5 m/dw

CH 13   200 mv/dw

Space Division
North American Rockwell

Figure XIV-15. Axial and Radial Shell Response Characteristics Induced by Longitudinal Shock Loads, No Mass, Pulse 2 (Sheet 1 of 4)
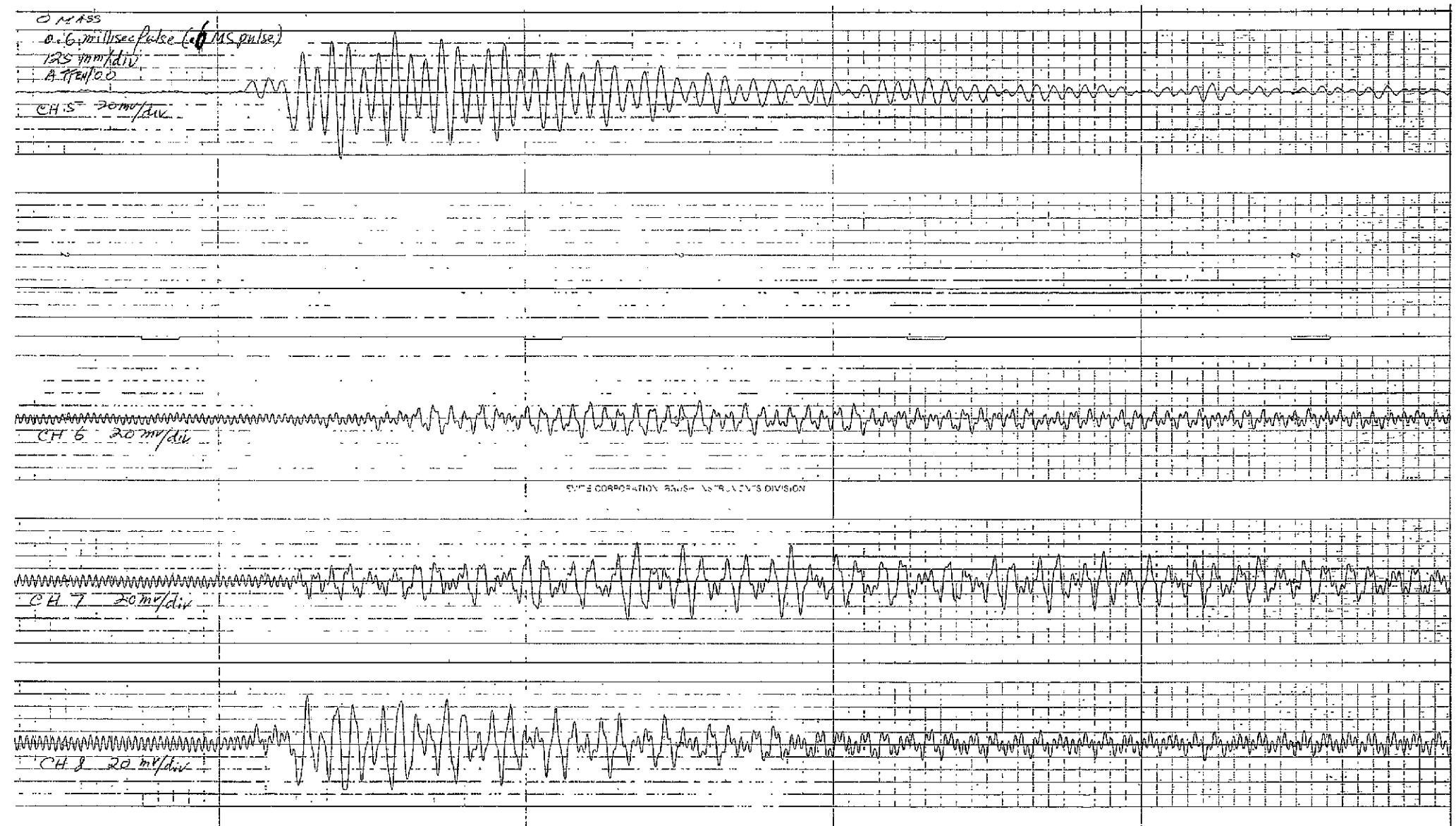
O MASS
0.6 millisec Pulse (of MS pulse)
125 mm/div
ATTEN 0.0

CH.5 20mv/div

CH 6 20 mv/div

SVTE CORPORATION BRUSH INSTRUMENTS DIVISION

CH 7 20 mv/div

CH 8 20 mv/div

Figure XIV-15. Axial and Radial Shell Response Characteristics Induced by
Longitudinal Shock Loads, No Mass, Pulse 2 (Sheet 2 of 4)

FOLDOUT FRAME 1

FOLDOUT FRAME 2

XIV-59, XIV-60
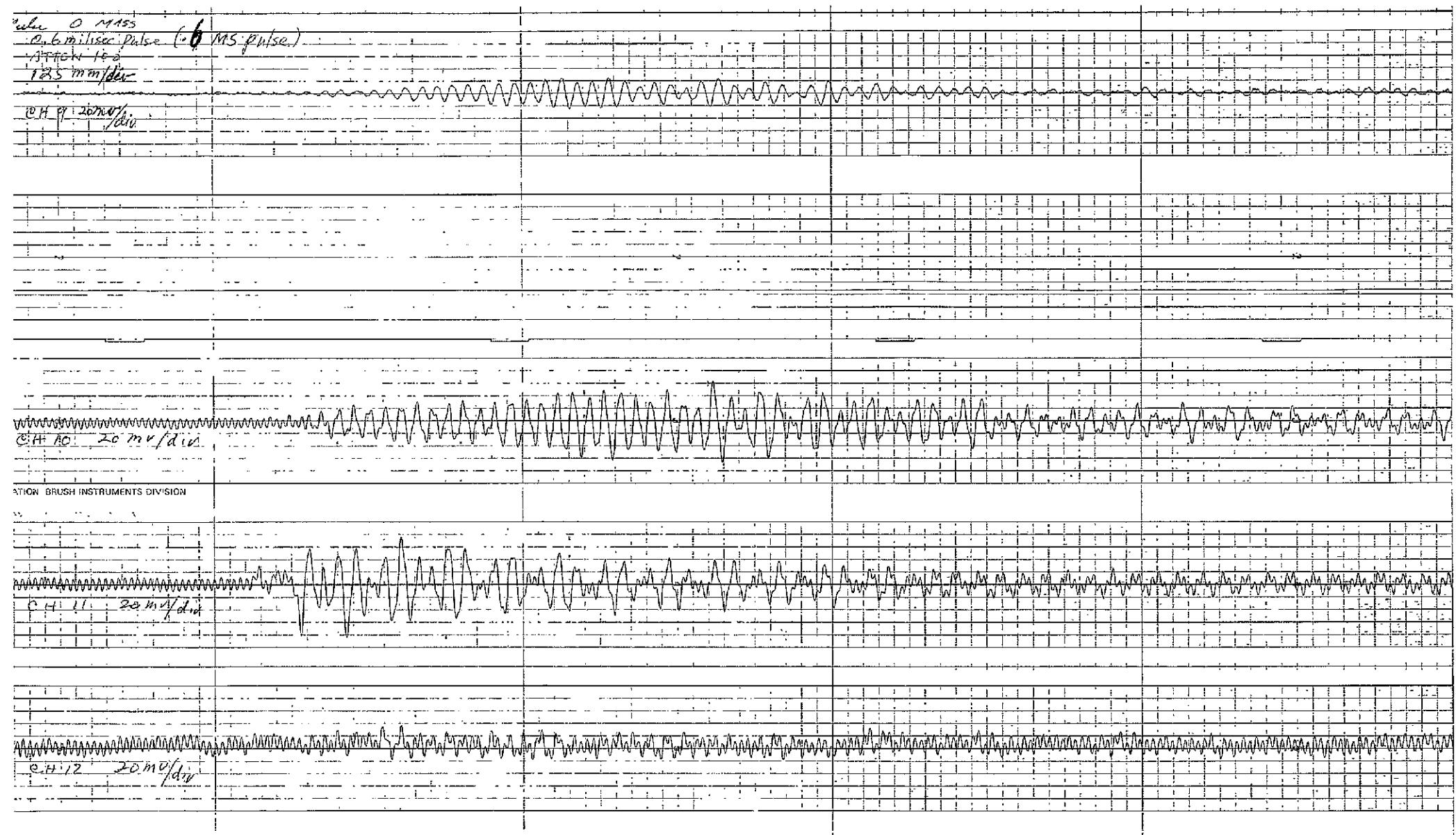
FOLDOUT FRAME

SD 69-766

Pulse 0 MASS
0.6 milisec Pulse (.6 MS pulse)
ATTCH 100
125 mm/div

CH 9 20mv/div

CH 10 20 mv/div

ATION BRUSH INSTRUMENTS DIVISION

CH 11 20 mv/div

CH 12 20 mv/div

Figure XIV-15. Axial and Radial Shell Response Characteristics Induced by
Longitudinal Shock Loads, No Mass, Pulse 2 (Sheet 3 of 4)

O - MASS (.6 ms pulse)
0.6 millisec pulse
125 mm/div
ATTEN 10.0

CLEVITE CORPORATION/BRUSH I

CLEVELAND OHIO   PR

CH 15
2.0 m/div
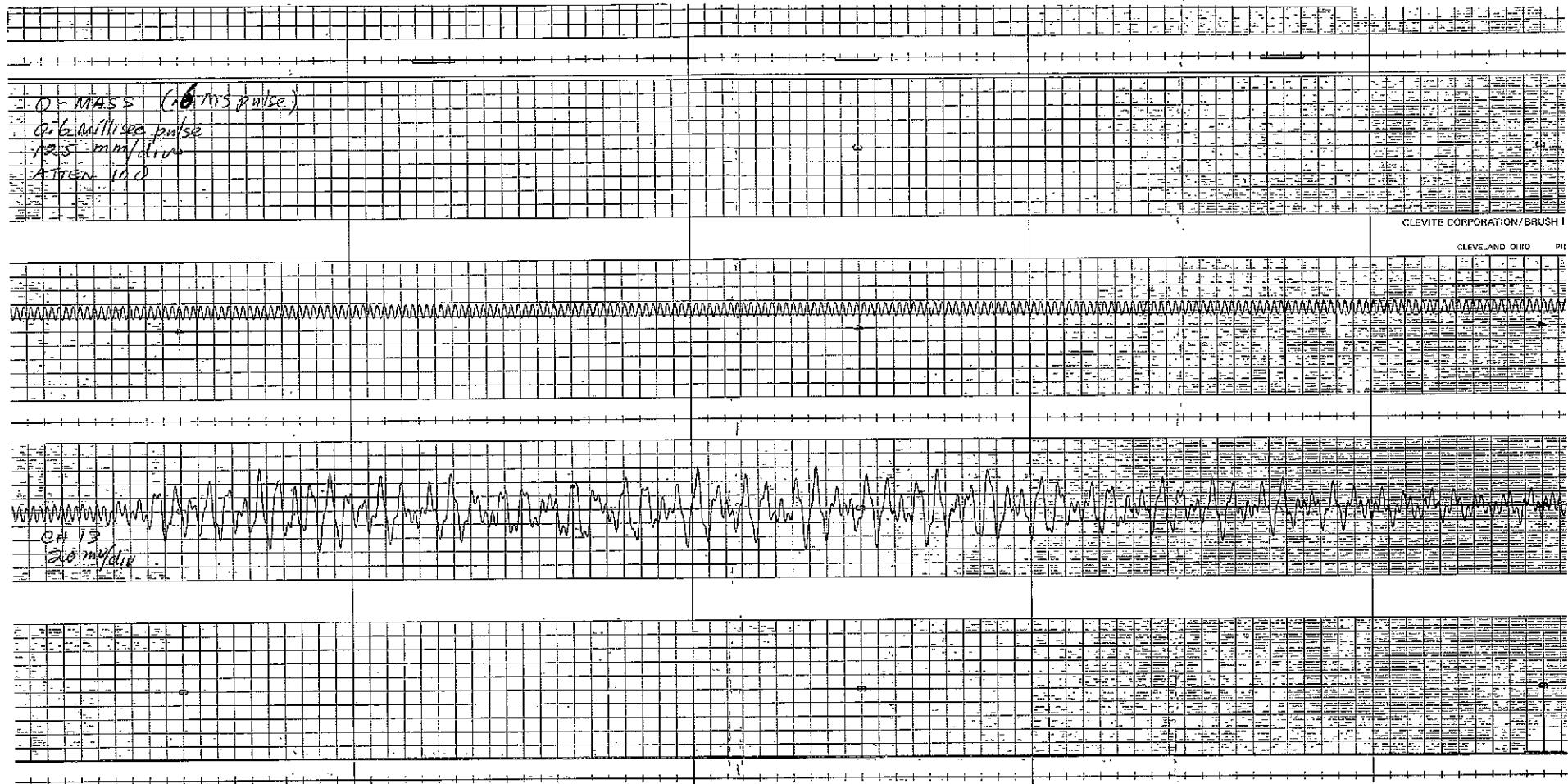
Figure XIV-15. Axial and Radial Shell Response Characteristics Induced by
Longitudinal Shock Loads, No Mass, Pulse 2 (Sheet 4 of 4)

FOLDOUT FRAME 1

FOLDOUT FRAME 2

XIV-63, XIV-64

SD 69-766
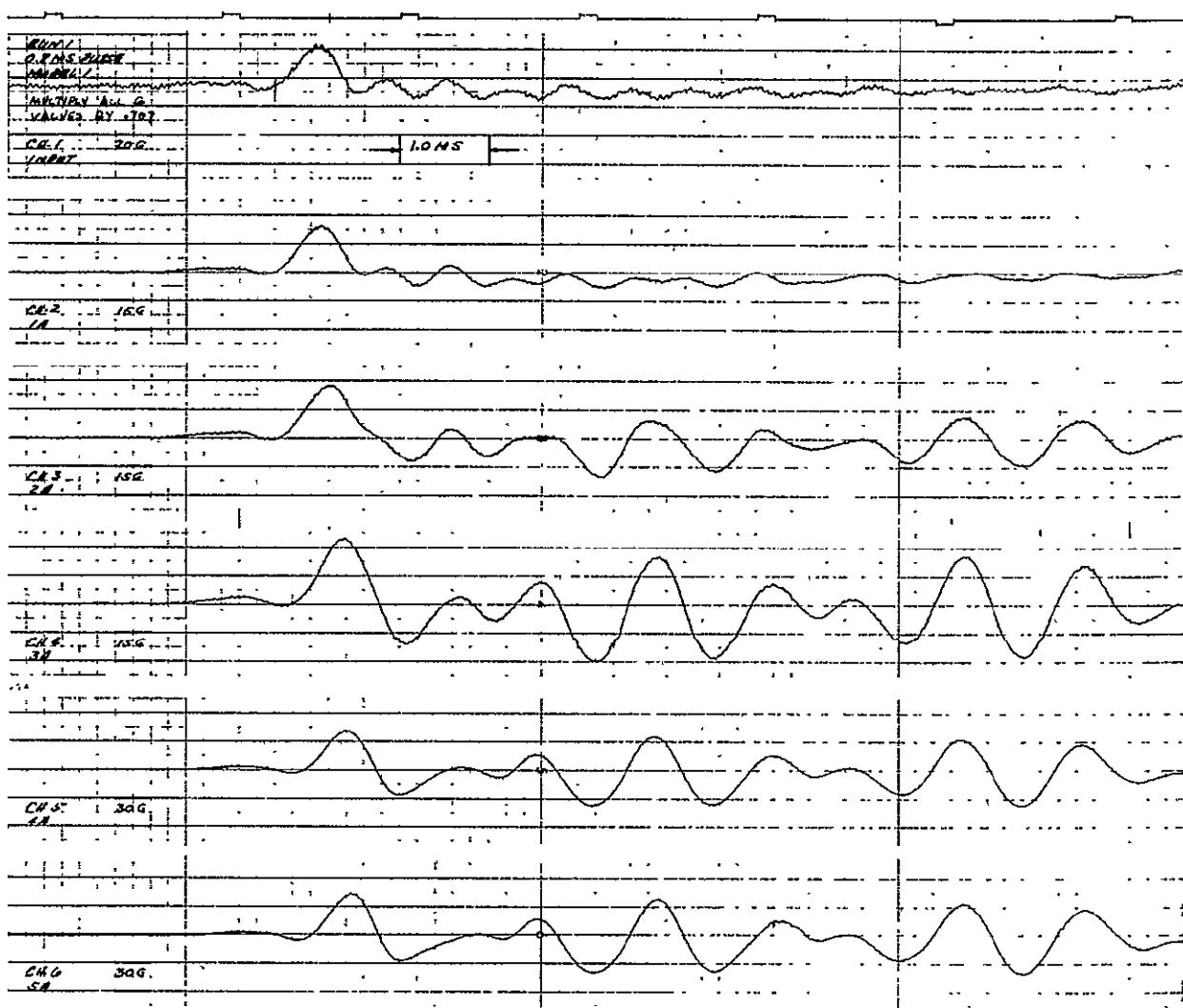
Figure XIV-16. Axial Acceleration Data, Model 1, Run 1
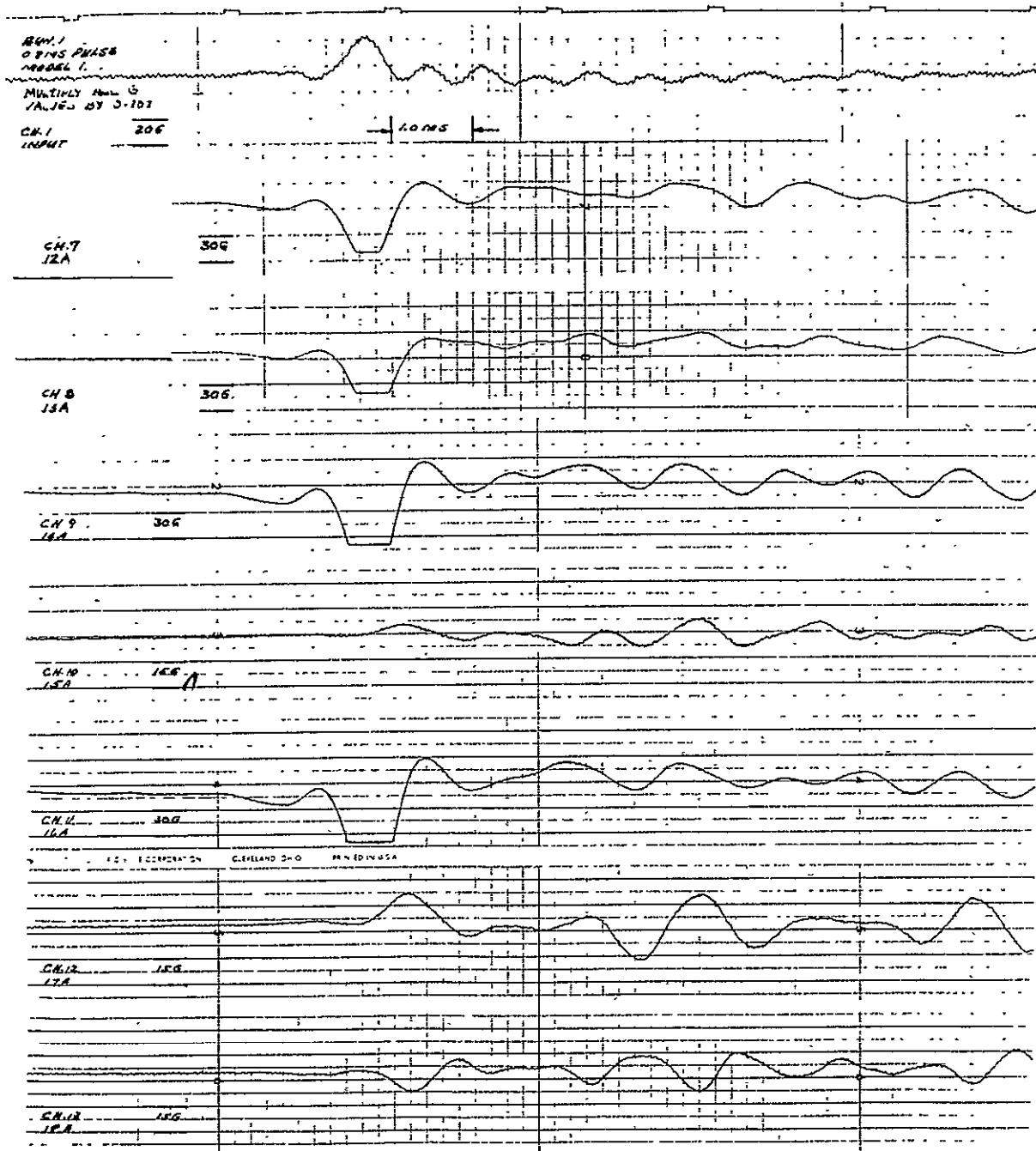
Figure XIV-17. Radial Acceleration Data, Model 1, Run 1
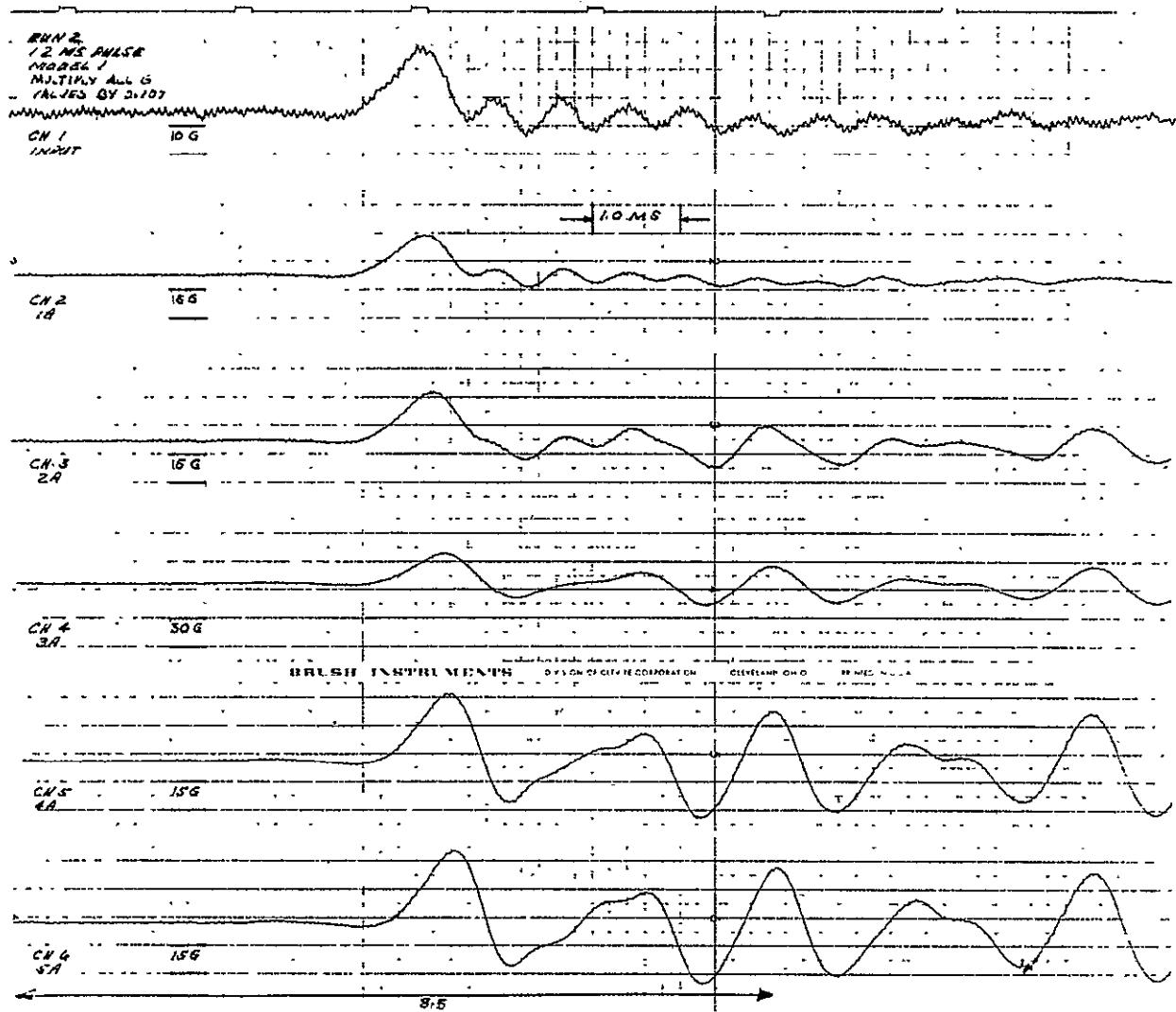
Figure XIV-18. Axial Acceleration Data, Model 1, Run 2
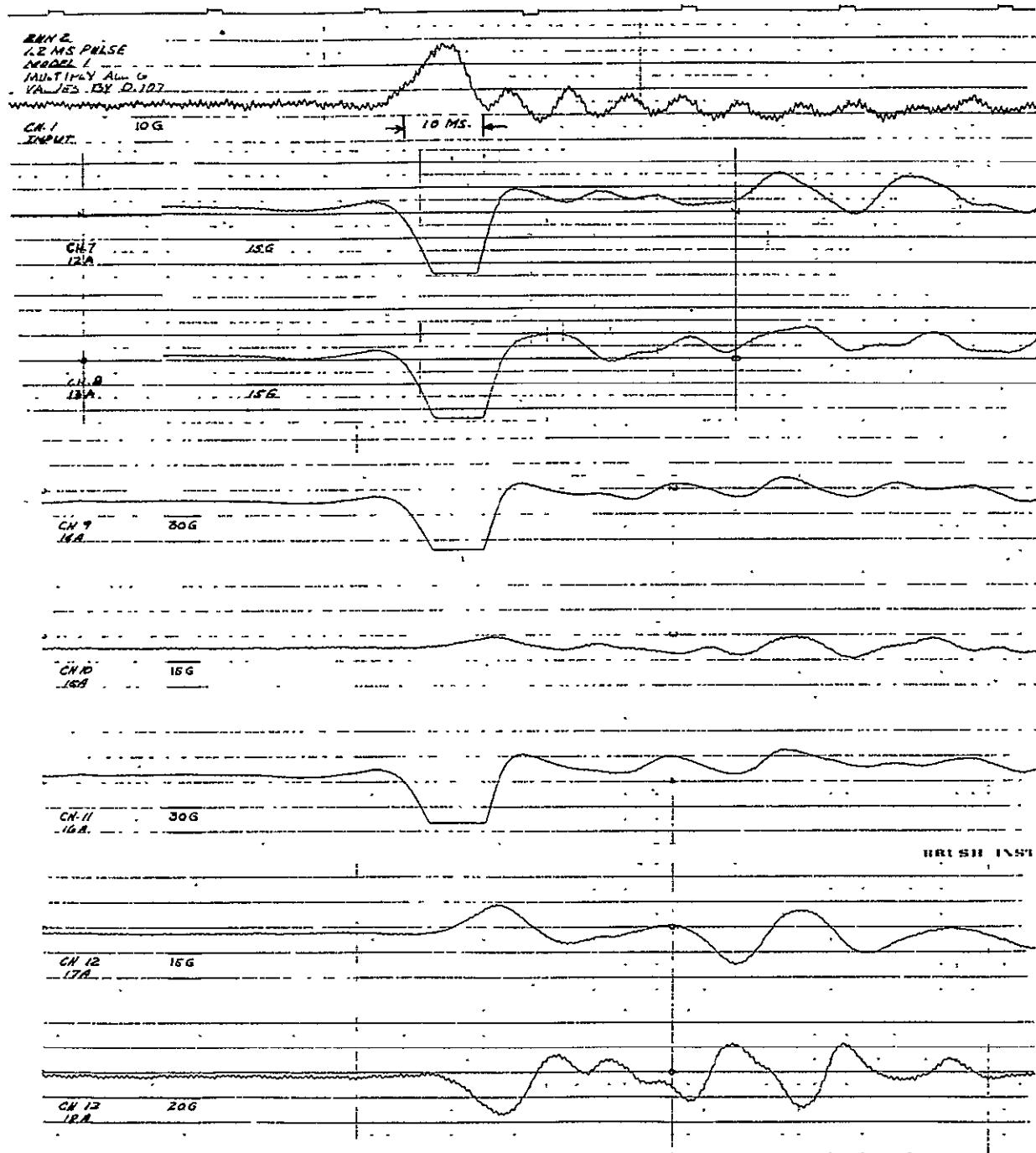
Figure XIV-19. Radial Acceleration Data, Model 1, Run 2
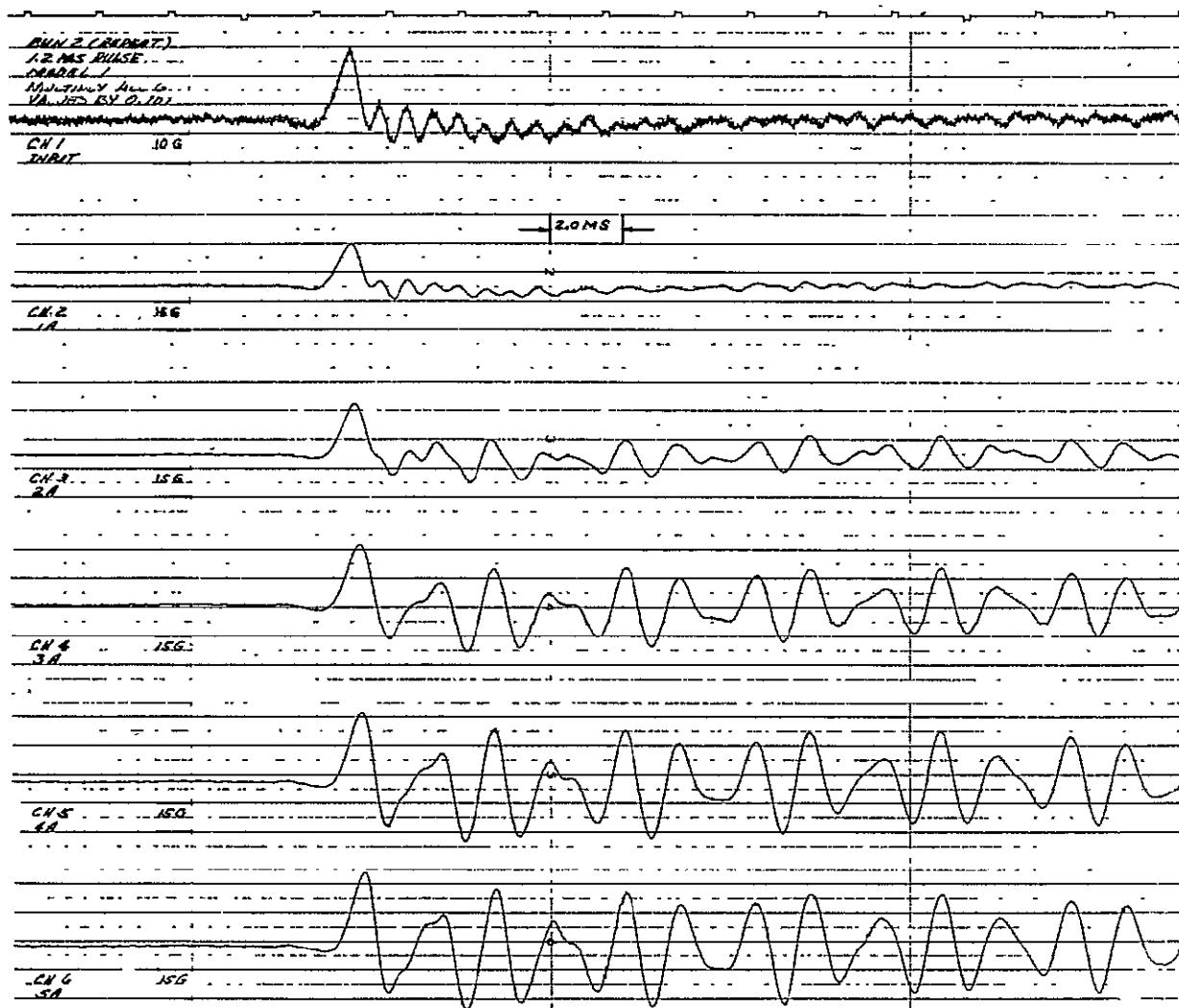
Figure XIV-20; Axial Acceleration Data, Model 1, Run 2R
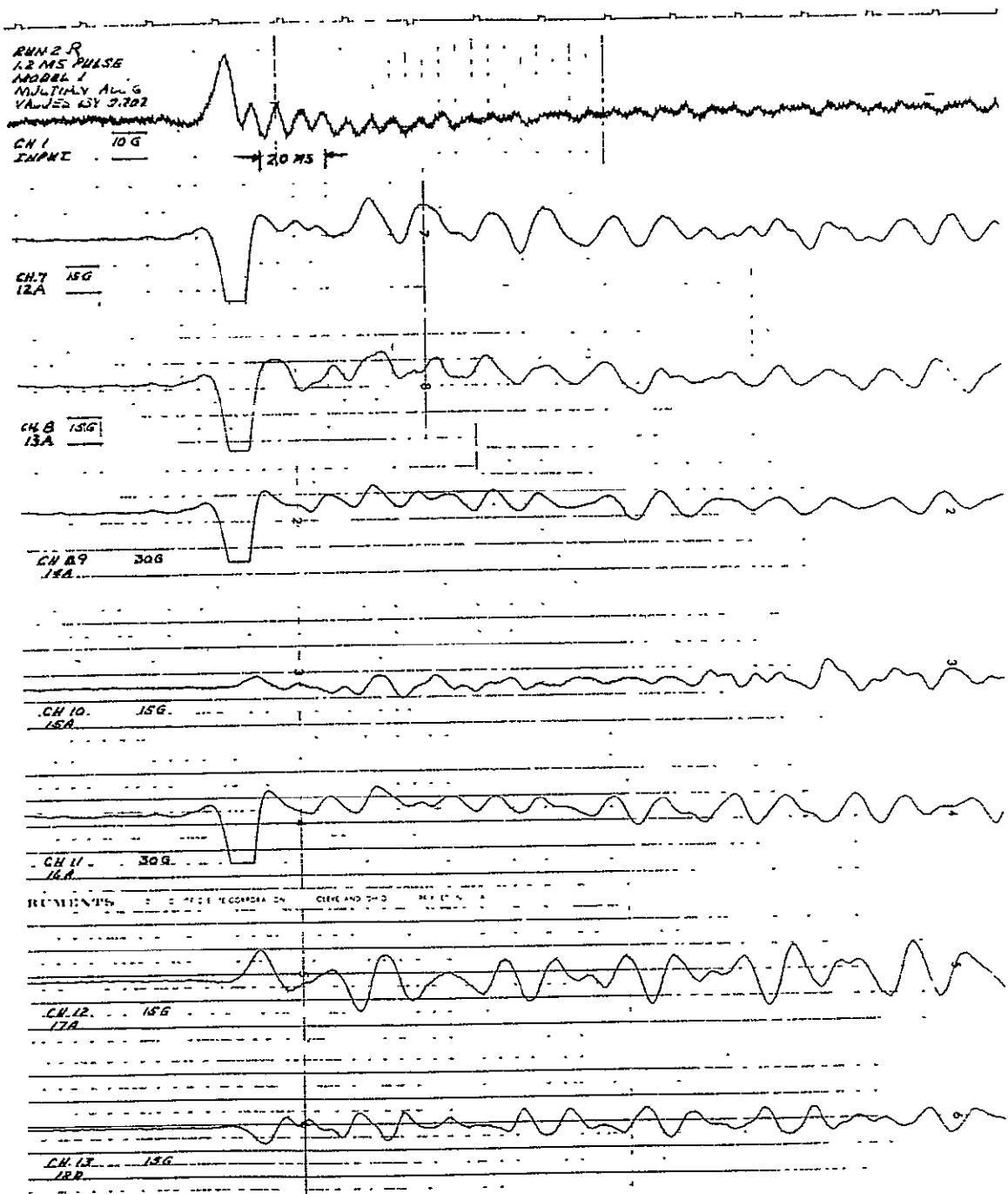
Figure XIV-21. Radial Acceleration Data, Model 1, Run 2R
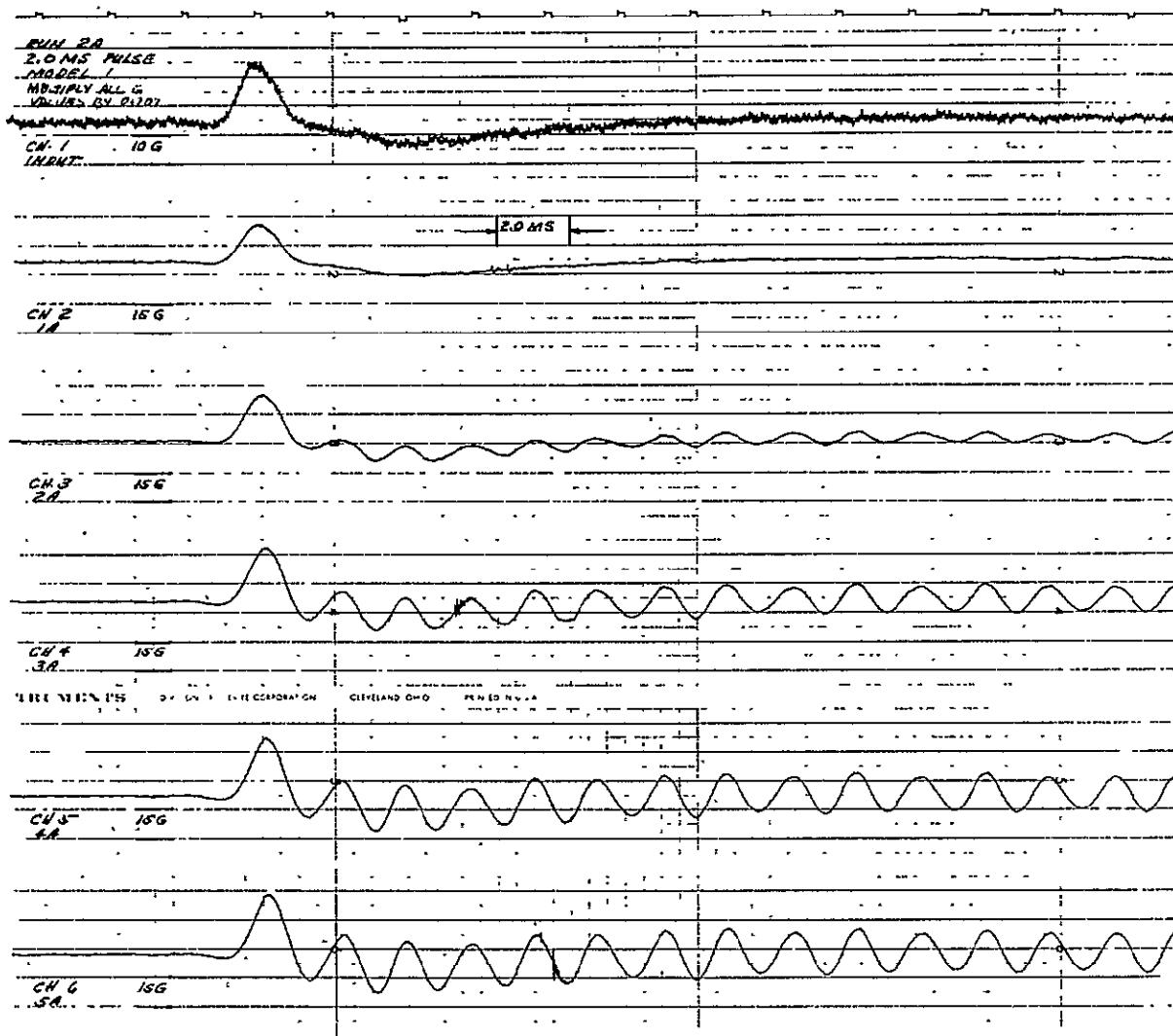
Figure XIV-22. Axial Acceleration Data, Model 1, Run 2A

RUN 2A
2.0 MS PULSE
MODEL 1
MULTIPLY ALL G
VALUES BY .101

CN 1   10 G
INPUT

2.0 MS

CH. 7
12A   30 G

CH. 8
13A   30 G

CH. 9
14A   30 G

CH 10
15A   6 G

CH 11
16A   30 G

CH 12
17A   6 G

CH 13
18A   6 G
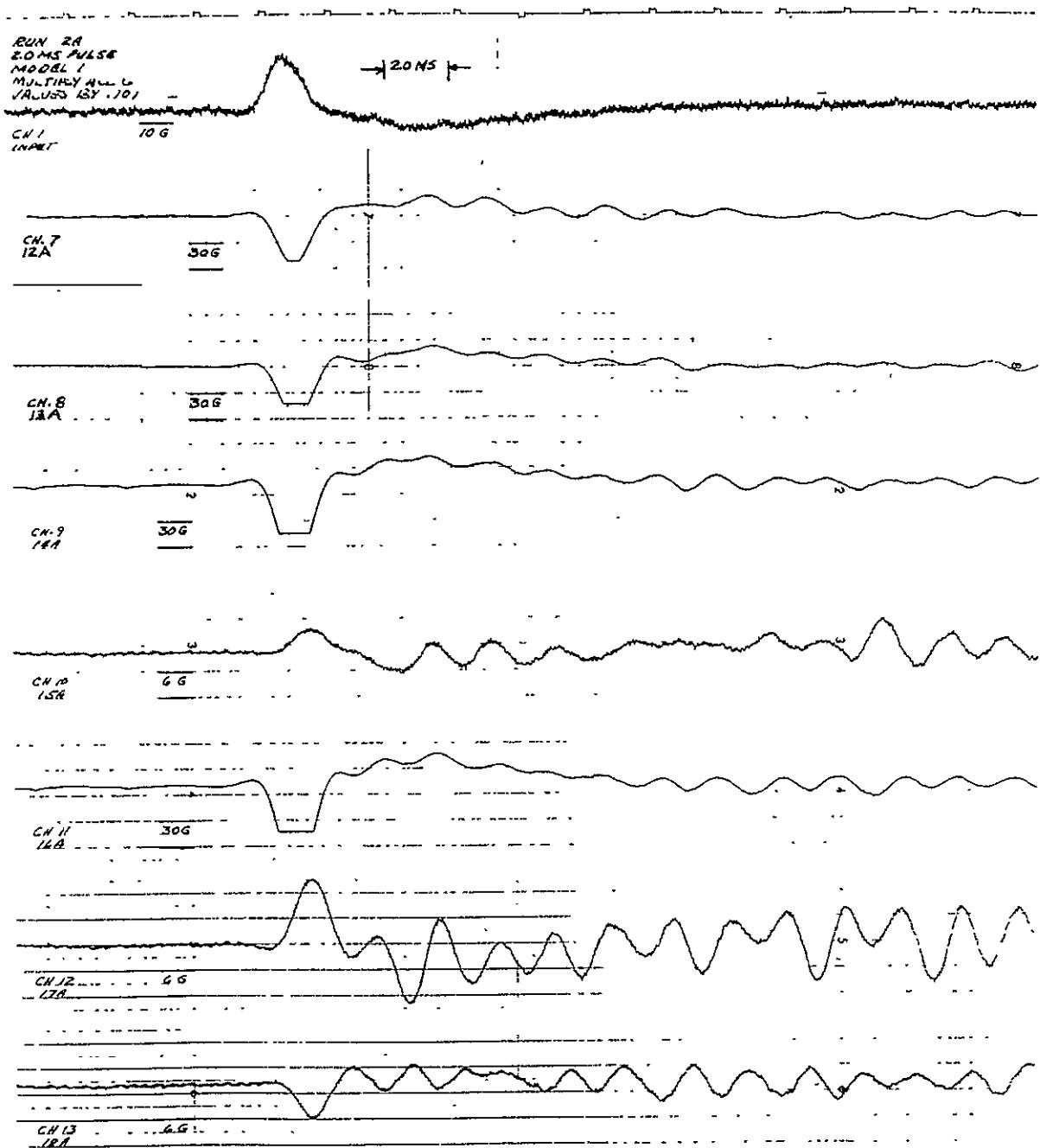
Figure XIV-23.   Radial Acceleration Data, Model 1, Run 2A

Table XIV-1. Test Data of Model No. 1
Maximum Responses

	RUN NO.		1	2	2R	2A
DATA						
	SHOCK FORM		H*	H	H	H
INPUT	MAX. ACCEL. g's		18.05	16.35	18.56	14.59
	DURATION M.S.		0.8	1.2	1.2	2.0
ACCELERO-METER & ITS LOCATION FROM FIXED END (g's)	5	70"	34.08	27.3	27.0	22.00
	4	54"	31.29	24.9	25.4	21.22
	3	36"	25.19	23.3	22.25	19.10
	2	18"	20.16	19.1	18.0	16.95
	1	2"	18.56	14.8	15.90	13.77
STRAIN GAGE 10^{-6} in/in	3	70"	10.0	10.8	10.0	9.0
	2	36"	15.0	15.0	15.0	12.5
	1	2"	20.0	17.5	17.5	15.0

*H = halfsine

Table XIV-2. Shock Load Factors From
Tests Model No. 1

	RUN NO.	1	2	2R	2A
ACCEL. NO.					
5	70"	1.89	1.75	1.60	1.57
4	54"	1.73	1.60	1.50	1.51
3	36"	1.40	1.50	1.31	1.36
2	18"	1.12	1.23	1.06	1.21
1	2"	1.03	0.95	0.94	0.98

Table XIV-3. Test Data of Radial Motion of Model 1

TEST RUN NUMBER		1	2	2R	2A
Input Shock	Form	*H	H	H	H
	Duration M.S.	0.8	1.2	1.2	2.0
	Max. g's	21.21	17.68	17.68	21.25
Accel. No. & Response (g's)	#12	42.70	28.11	26.52	38.45
	13	31.82	26.52	27.85	31.82
	14	45.08	42.43	42.43	39.78
	15	15.91	14.59	15.25	7.42
	16	45.08	41.11	40.31	38.72
	17	21.22	29.17	15.25	10.61
	18	9.28	31.82	7.03	5.30

*H - Halfsine

XV. MAPPING OF N MODES
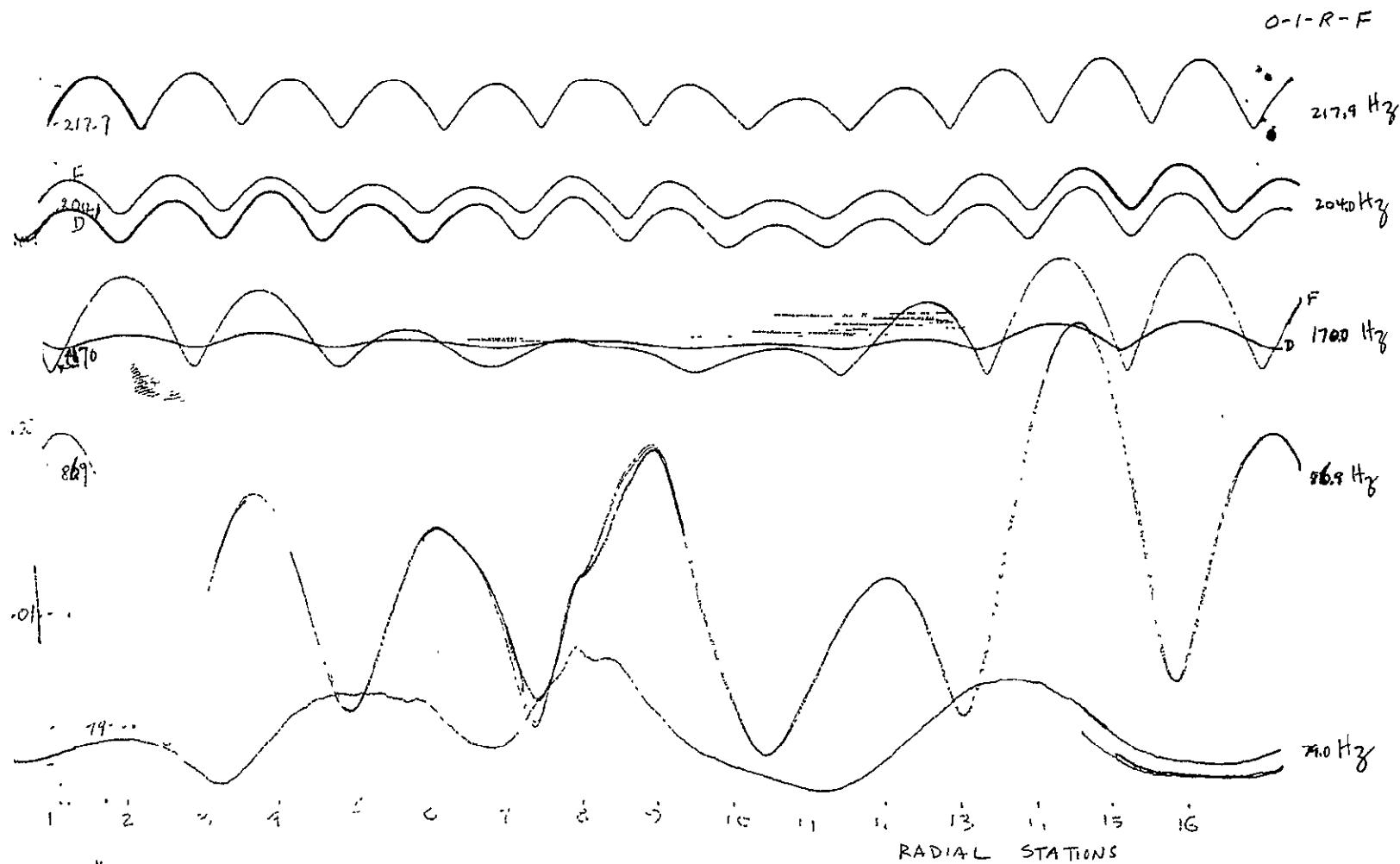
Figure XV-1. Mapping of N Modes (Sheet 1 of 26)

Space Division
North American Rockwell

Figure XV-1. Mapping of N Modes (Sheet 2 of 26)

Space Division
North American Rockwell

O-1-R-F
10V 3/4/9

279.9 Hz

141.9 Hz

0

01 3°

0
1

16

15

14

13

12

11

10

9

8

7

6

5

4

3

2

1

RADIAL STATIONS

Space Division
North American Rockwell
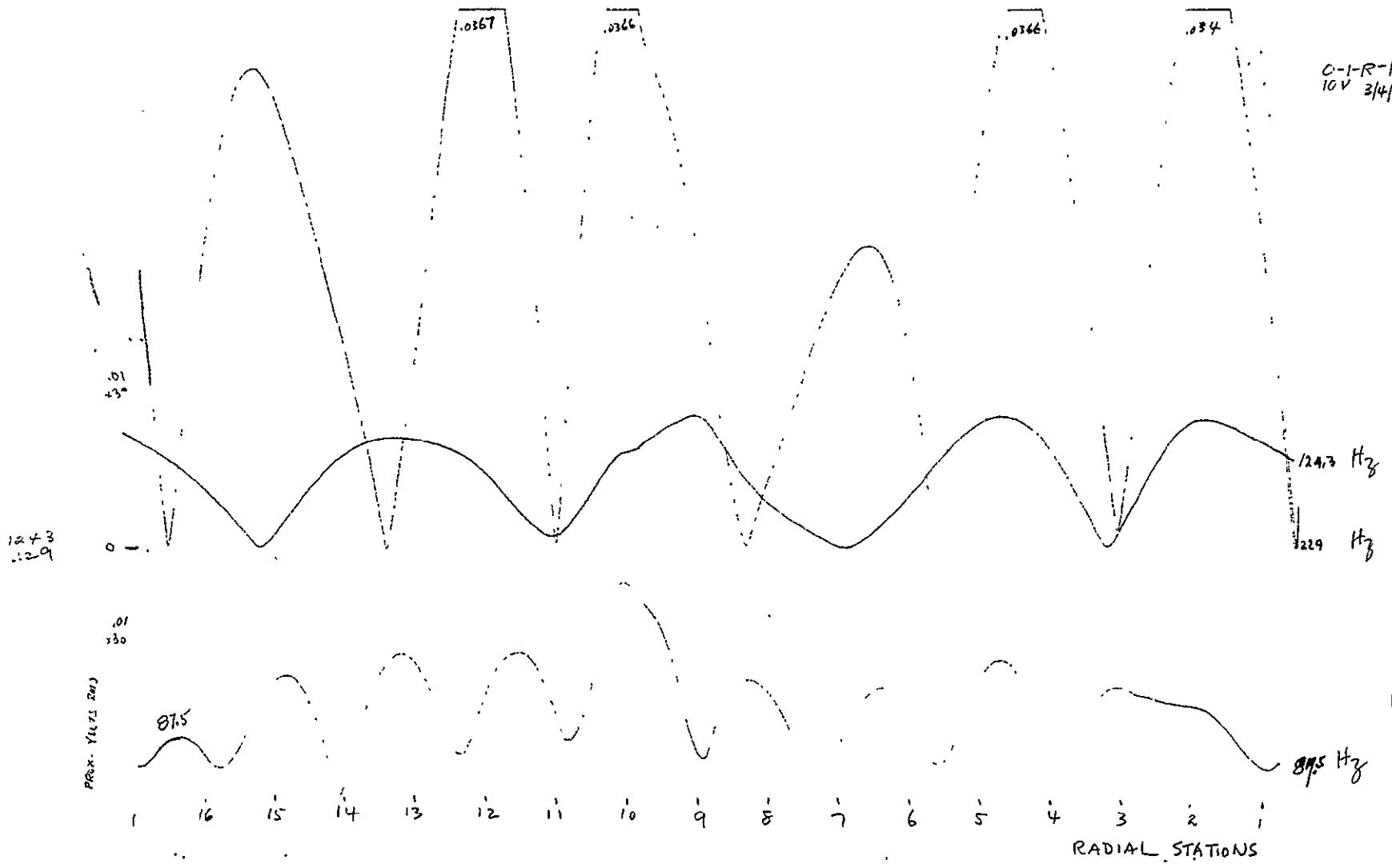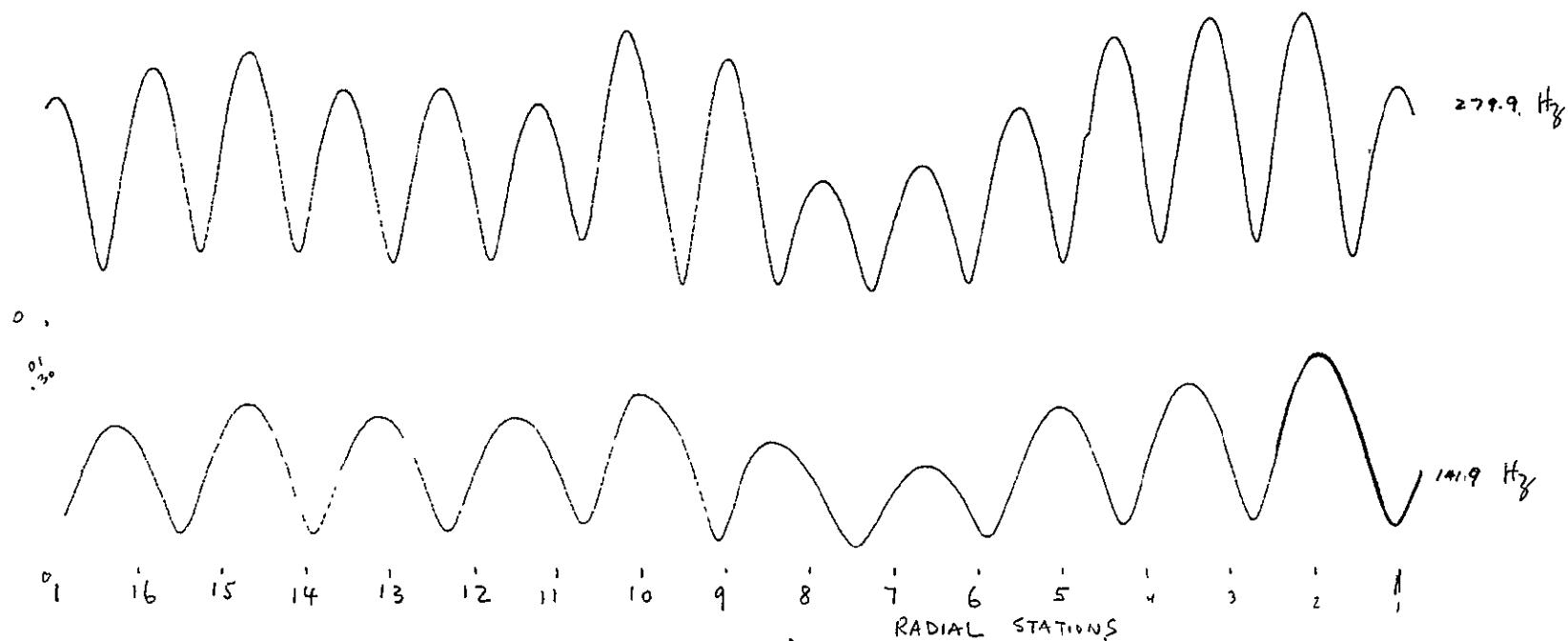
Figure XV-1. Mapping of N Modes (Sheet 3 of 26)
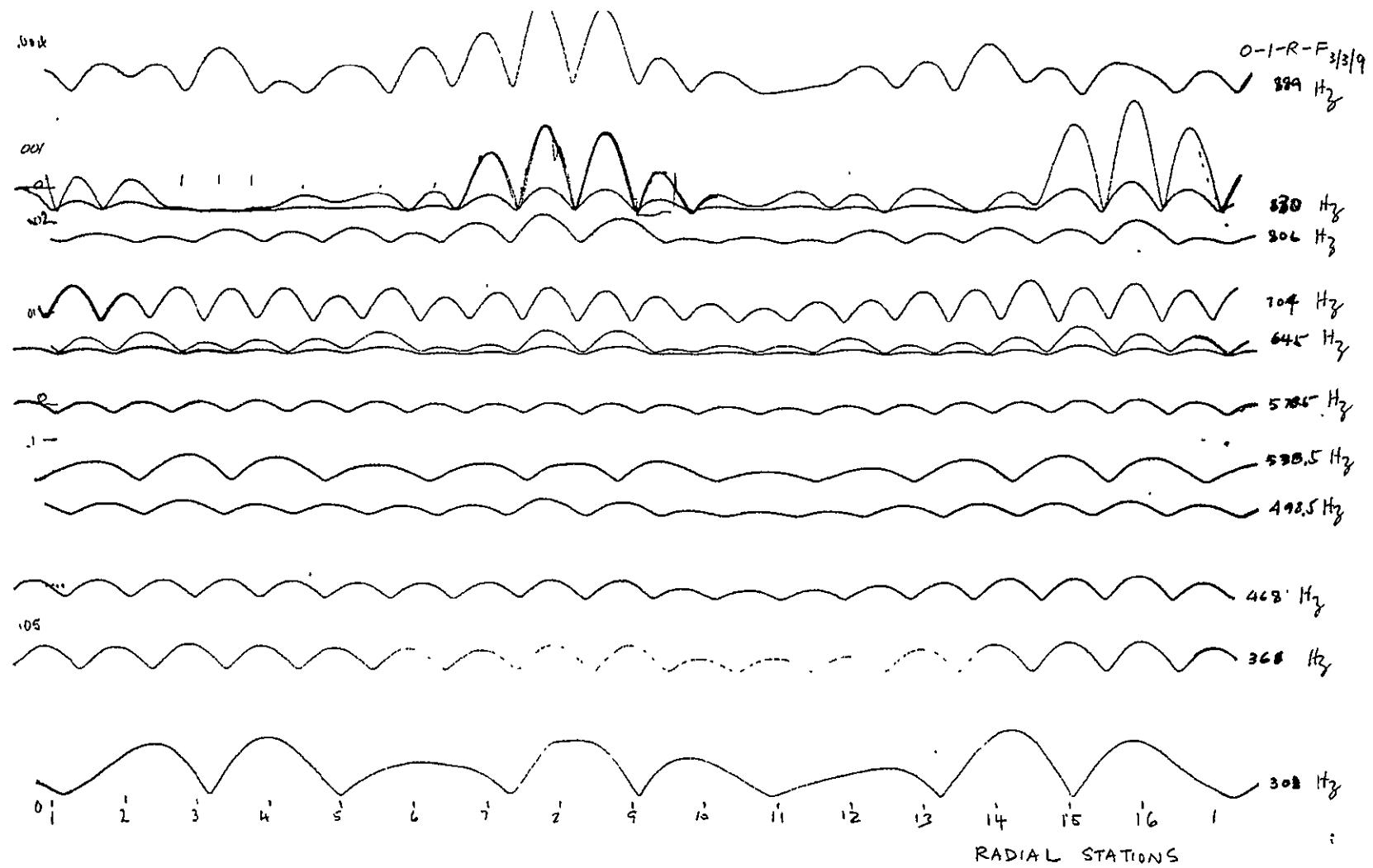
Figure XV-1. Mapping of N Modes (Sheet 4 of 26)

Space Division
North American Rockwell
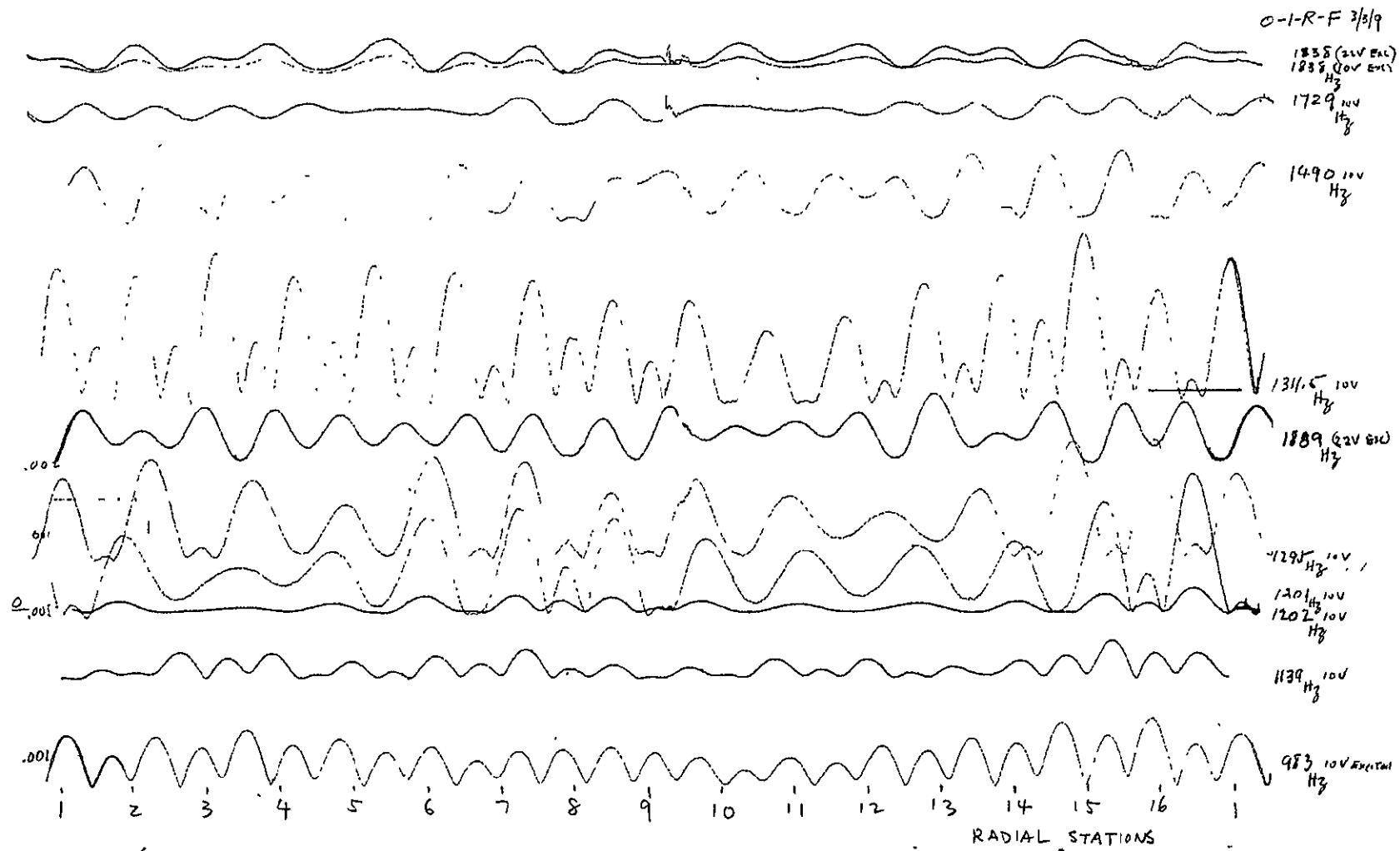
Figure XV-1. Mapping of N Modes (Sheet 5 of 26)

O-5-R-F
228 Hz 7.85V
2/27/9

n=3

RADIAL STATIONS
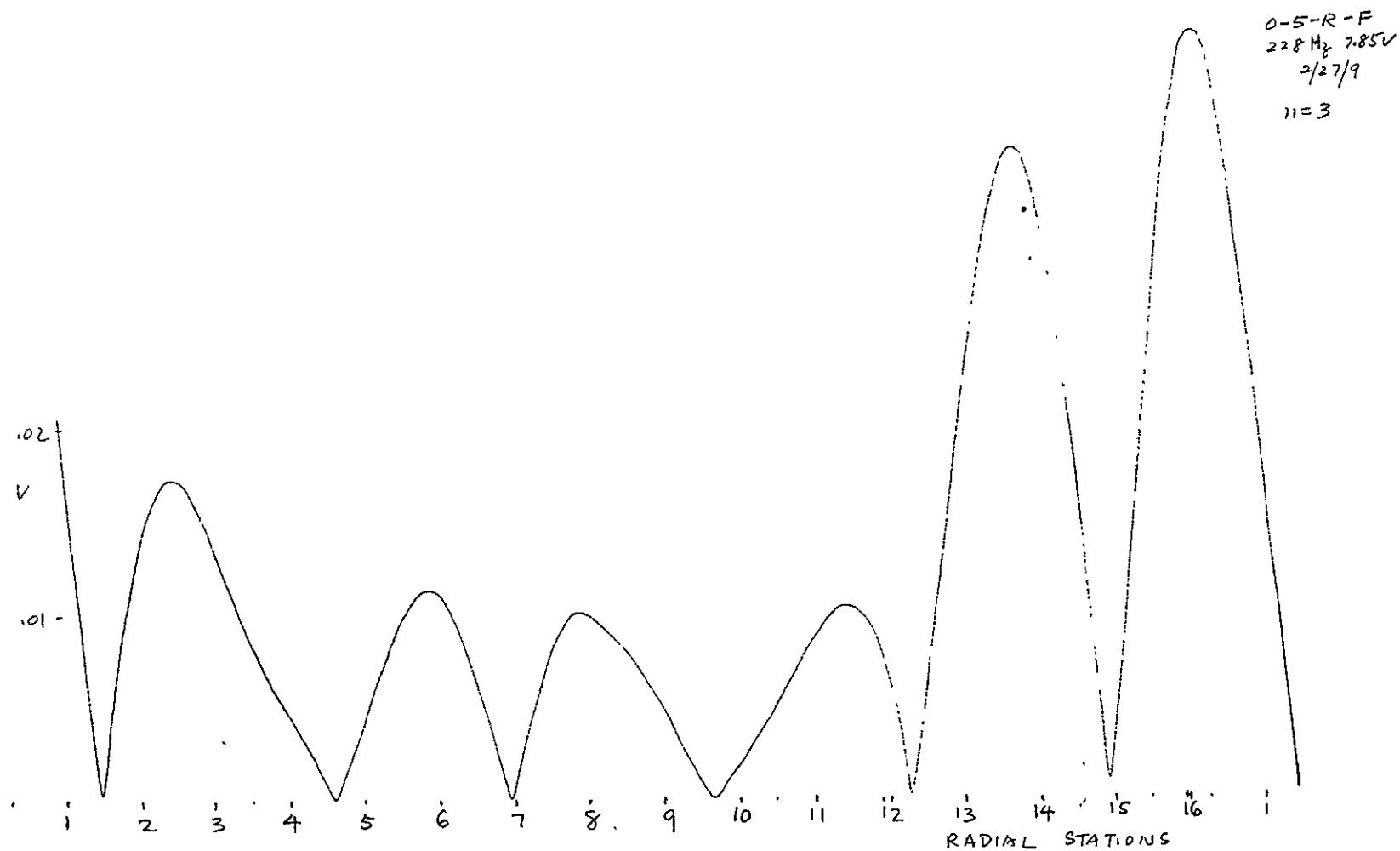
Figure XV-1. Mapping of N Modes (Sheet 6 of 26)

Space Division
North American Rockwell
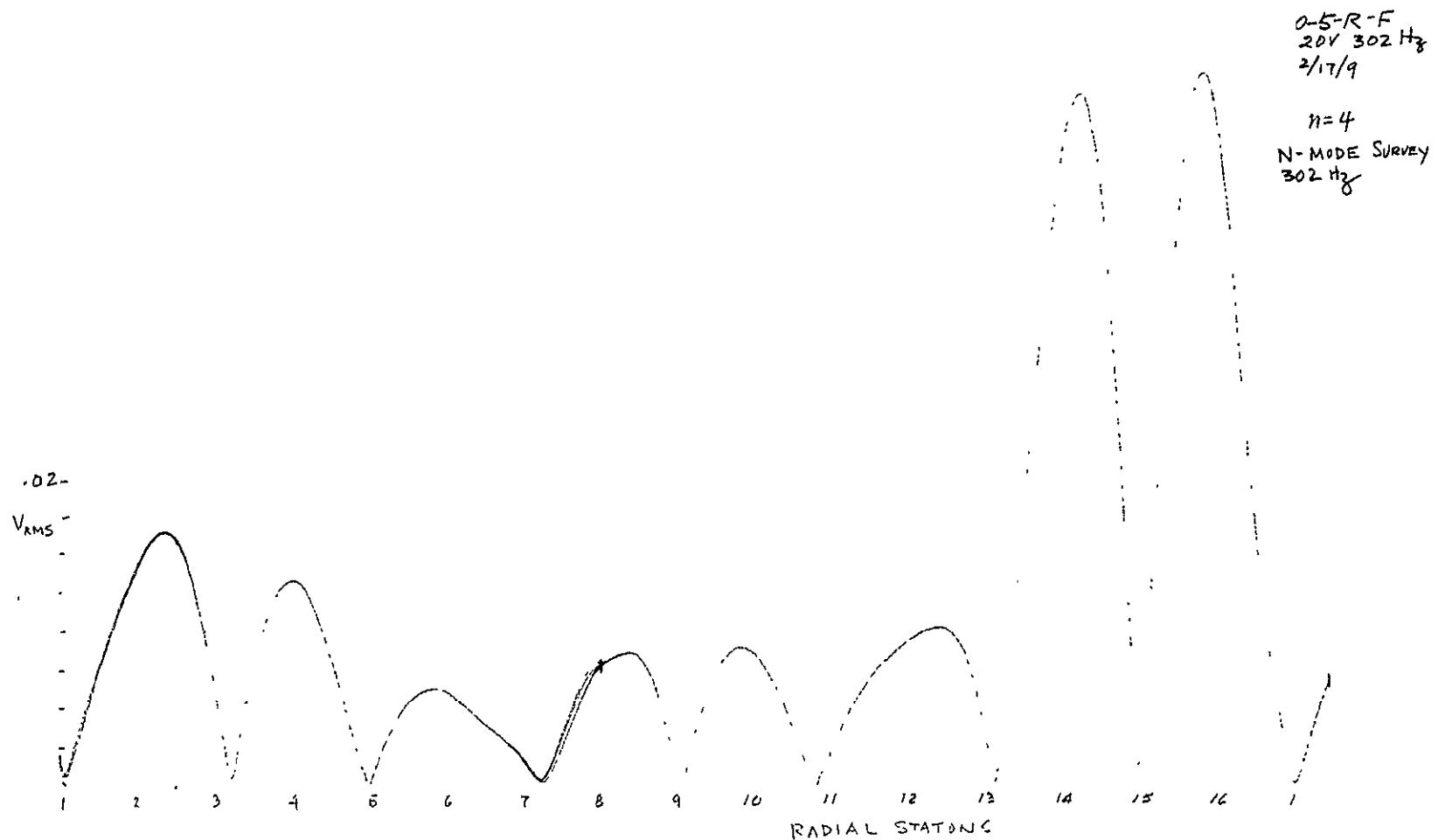
Figure XV-1. Mapping of N Modes (Sheet 7 of 26)
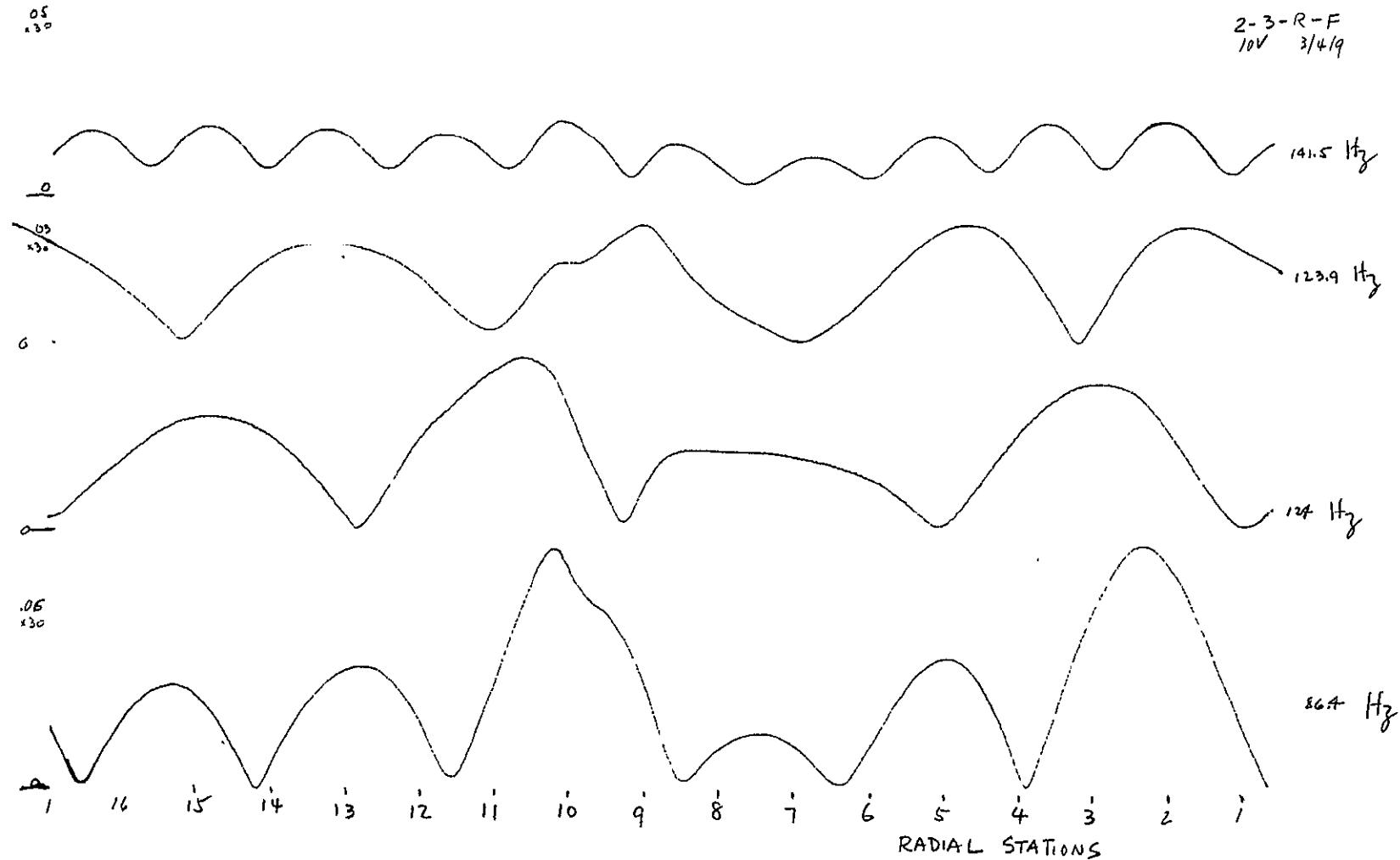
Figure XV-1.   Mapping of N Modes (Sheet 8 of 26)
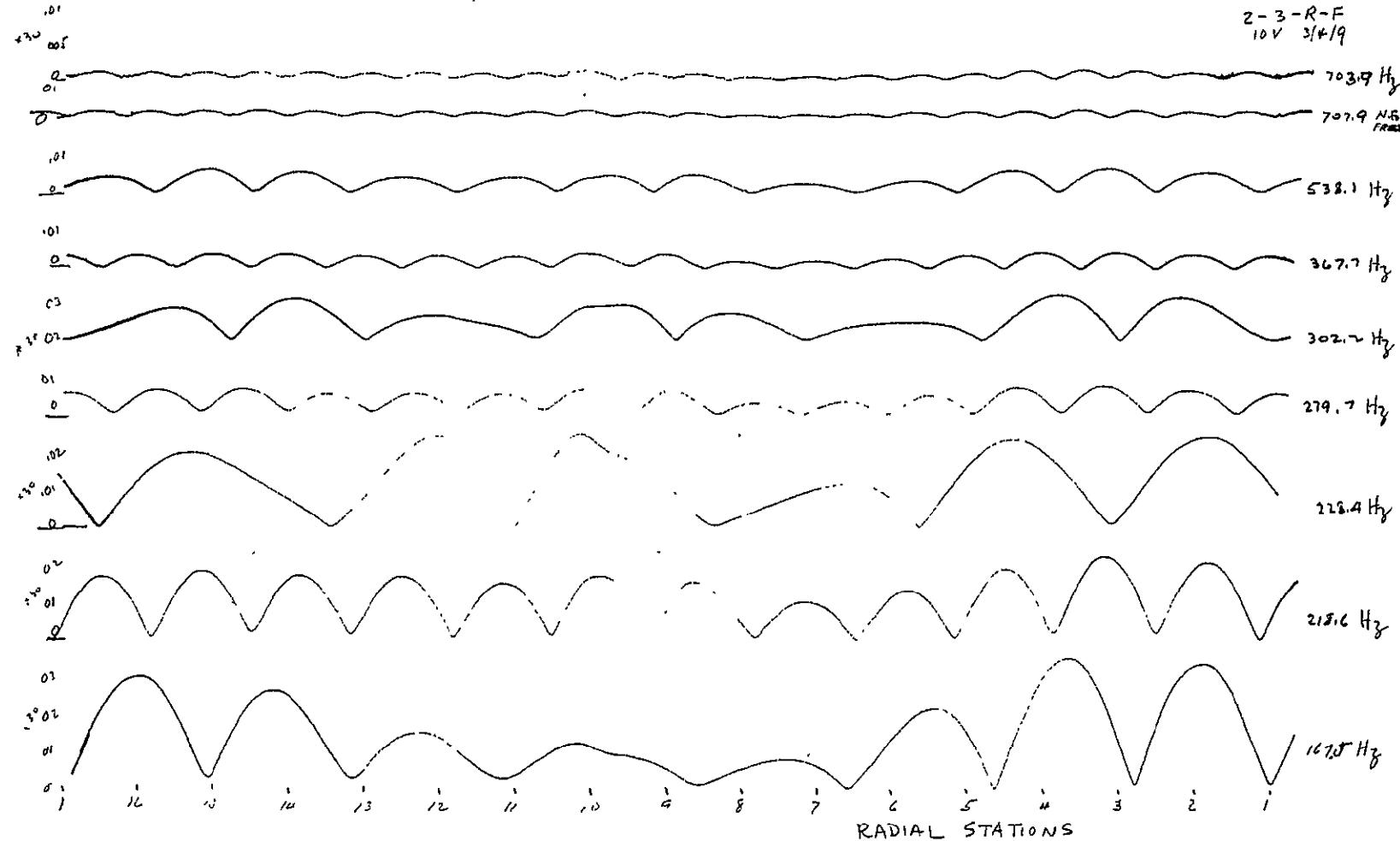
Figure XV-1. Mapping of N Modes (Sheet 9 of 26)
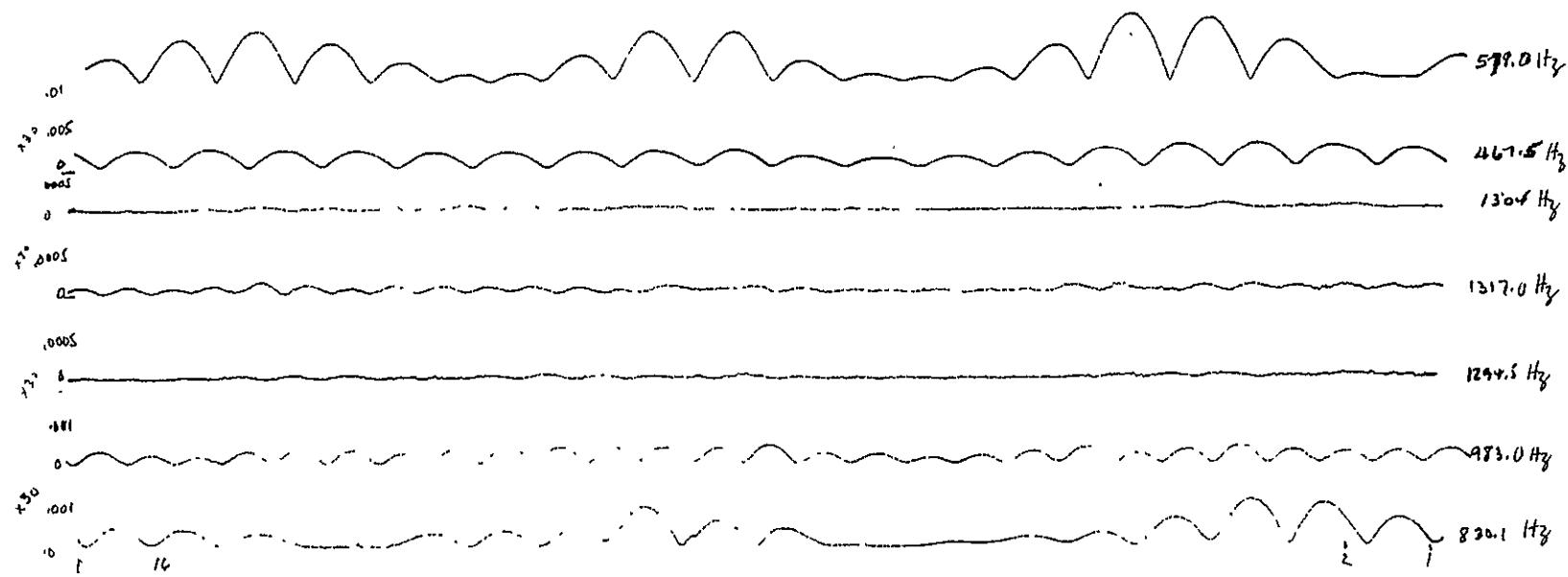
Figure XV-1.   Mapping of N Modes (Sheet 10 of 26)
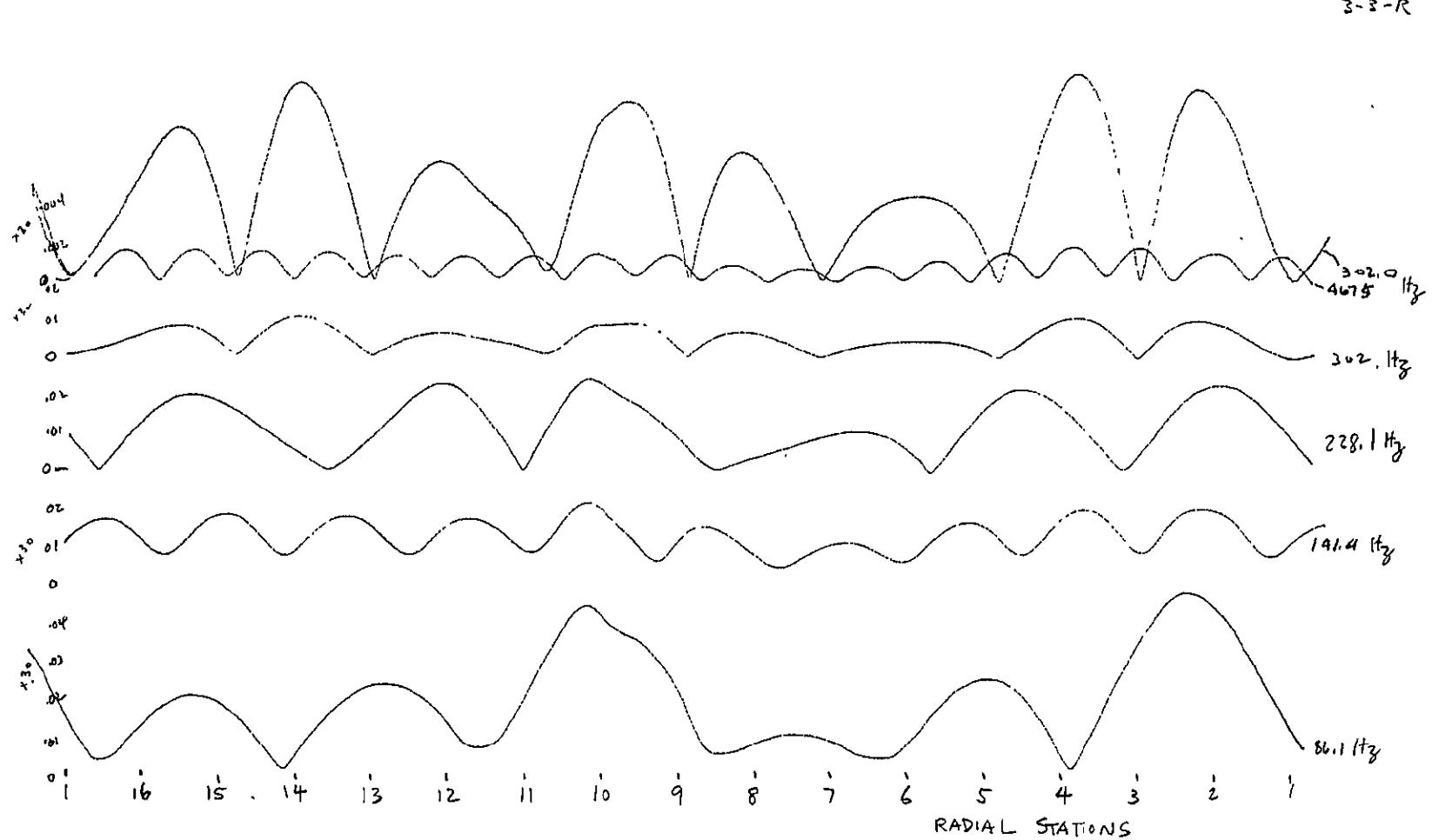
Figure XV-1.   Mapping of N Modes (Sheet 11 of 26)

Space Division
North American Rockwell

XV-12

SD 69-766

829.4 Hz

703.9 Hz

709.1 Hz

537.7 Hz

RADIAL STATIONS

Space Division
North American Rockwell
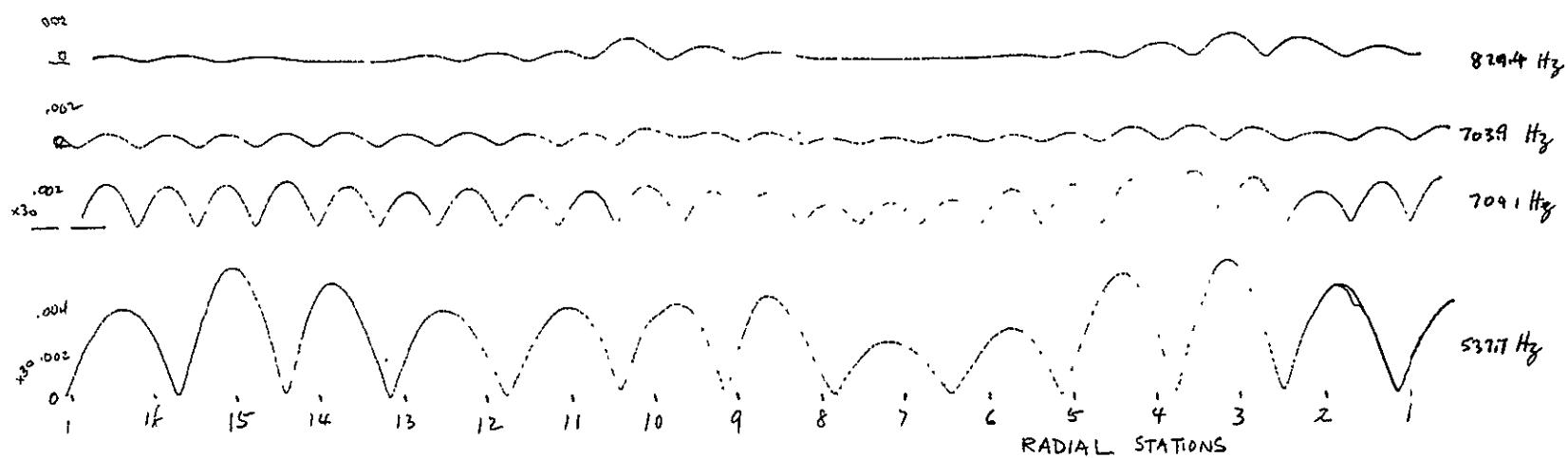
Figure XV-1. Mapping of N Modes (Sheet 12 of 26)

4-3-R-F
10V 3/5/9

301.8 Hz

227.9 Hz

141.0 Hz

123.8 Hz

86.0 Hz

RADIAL STATIONS

Space Division
North American Rockwell
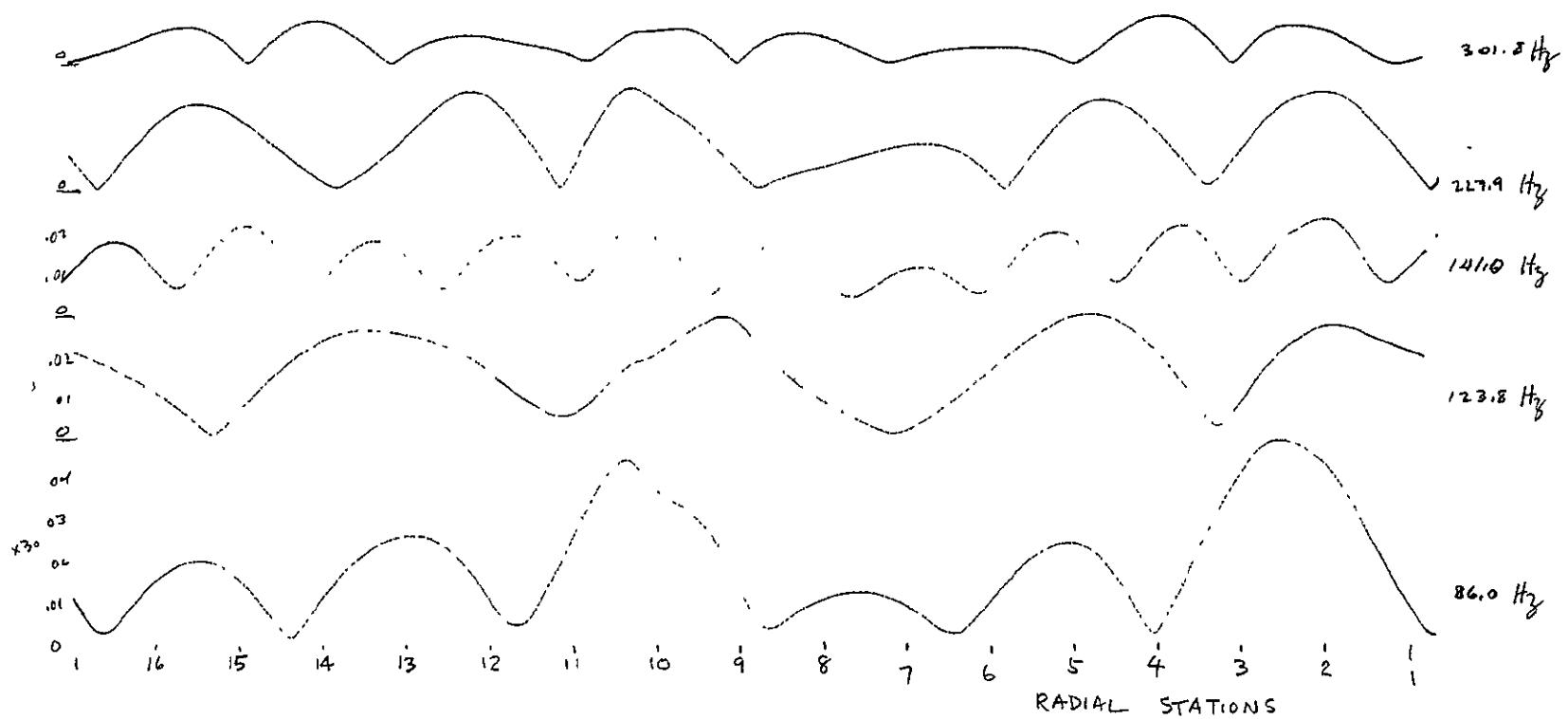
Figure XV-1. Mapping of N Modes (Sheet 13 of 26)

4-3-R-F
10 V 3/5/9

829.6 Hz

703.3 Hz

537.6 Hz

301.8 Hz

225.0 Hz

RADIAL STATIONS
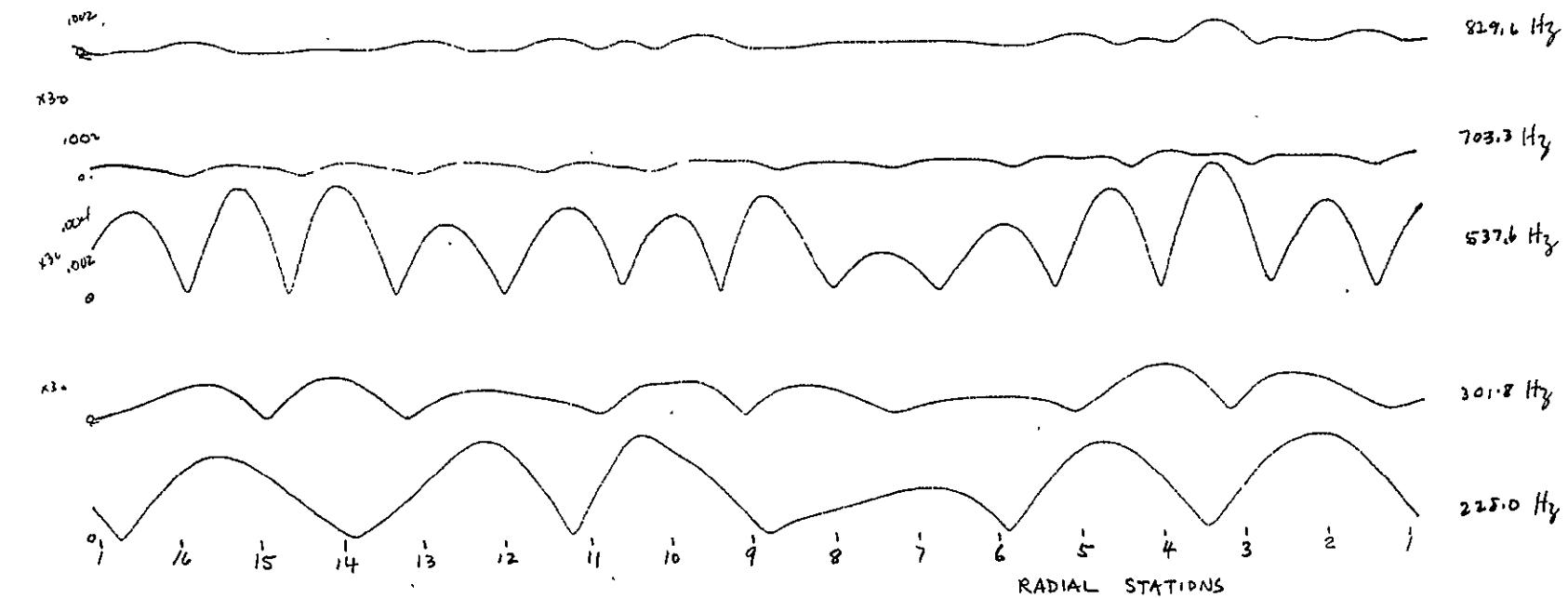
Figure XV-1. Mapping of N Modes (Sheet 14 of 26)
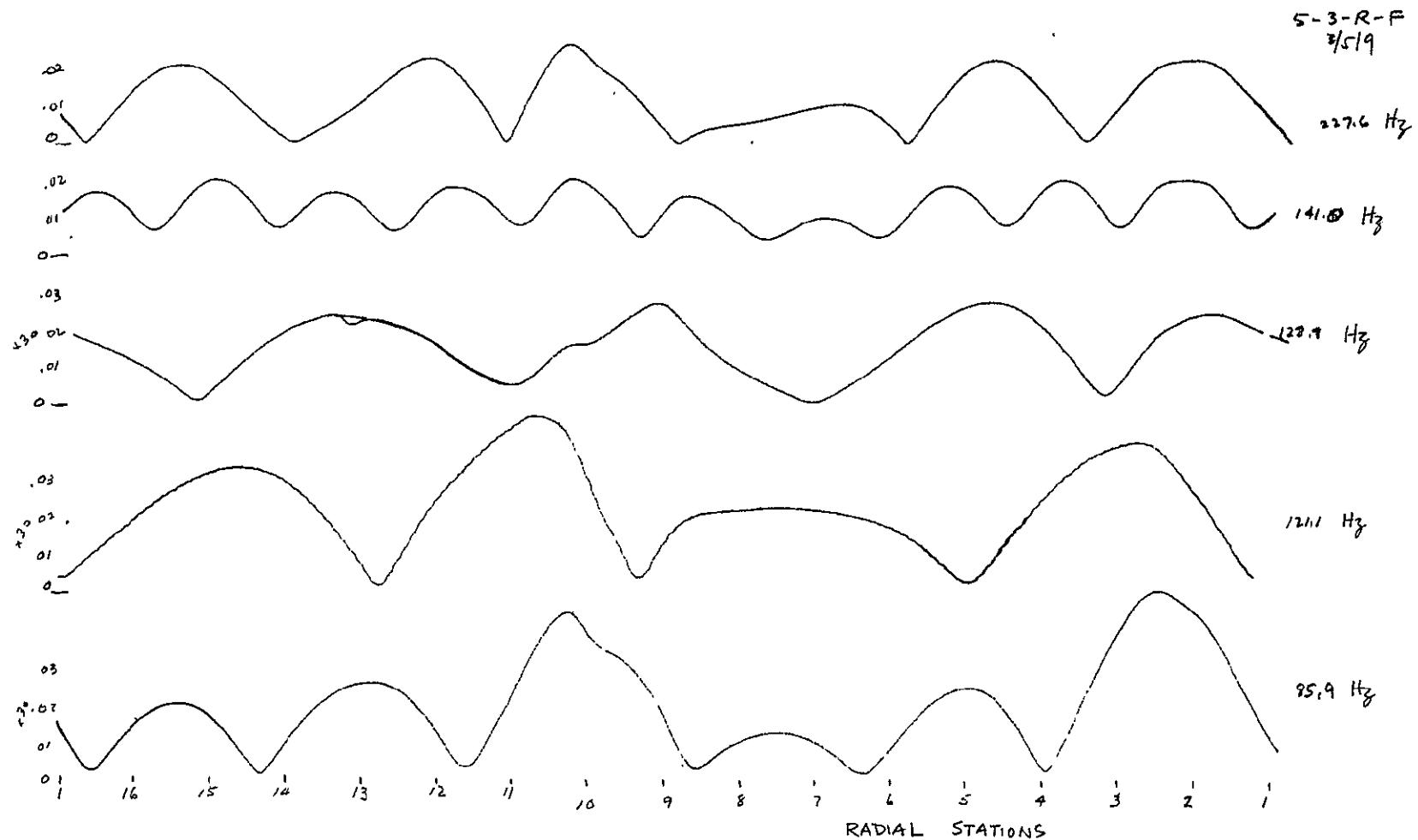
Figure XV-1.   Mapping of N Modes (Sheet 15 of 26)

5-3-R-F
10 V   3/5/9

829.9 Hz

703.4 Hz

537.1 Hz

301.6 Hz

RADIAL STATIONS
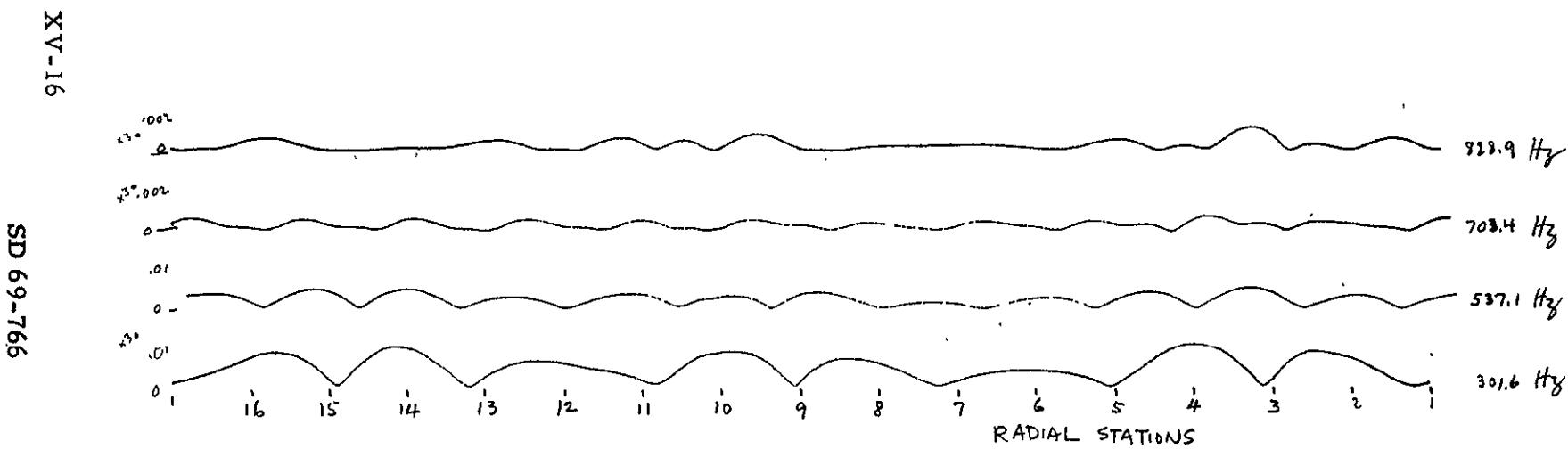
Figure XV-1.   Mapping of N Modes (Sheet 16 of 26)
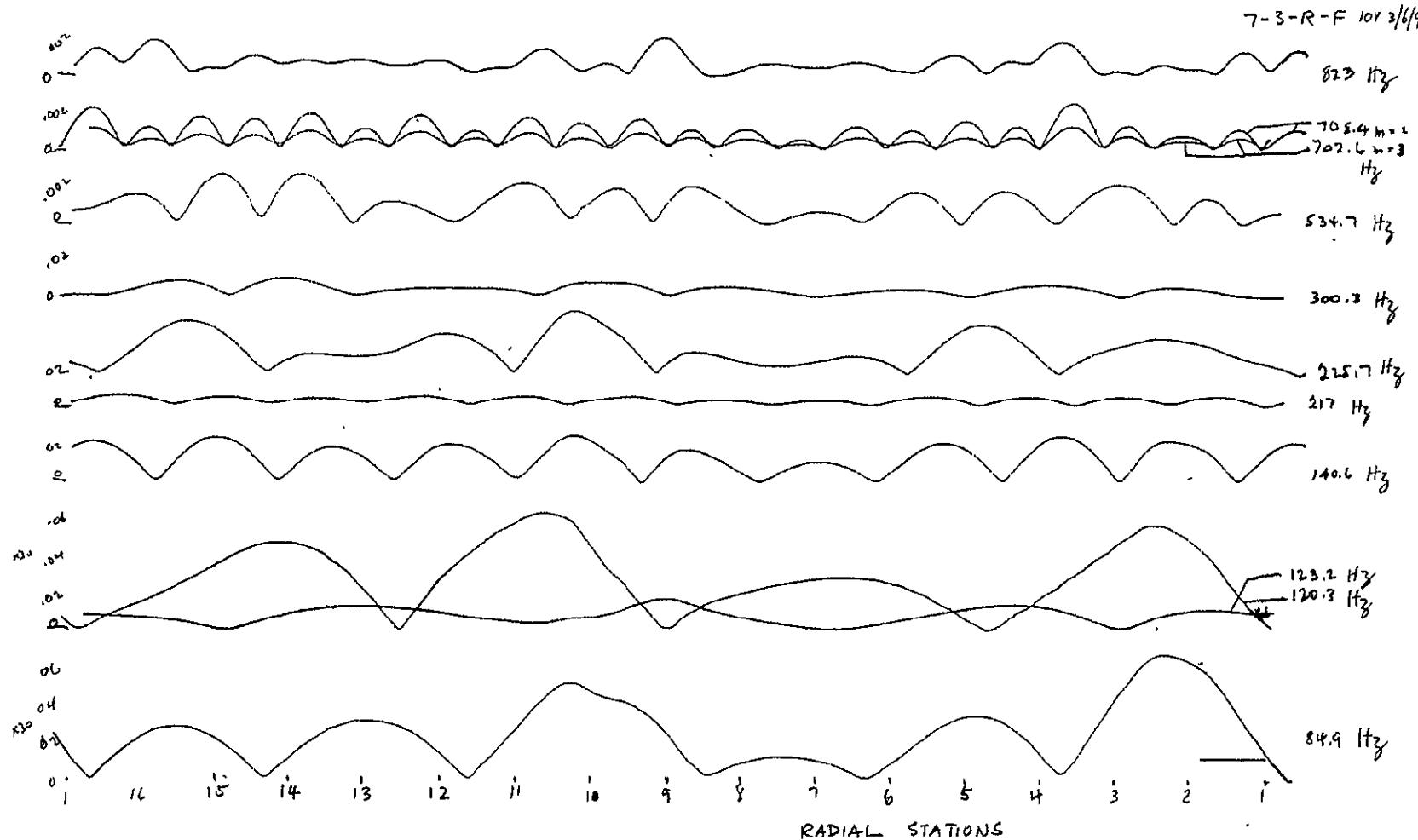
Figure XV-1.   Mapping of N Modes (Sheet 17 of 26)
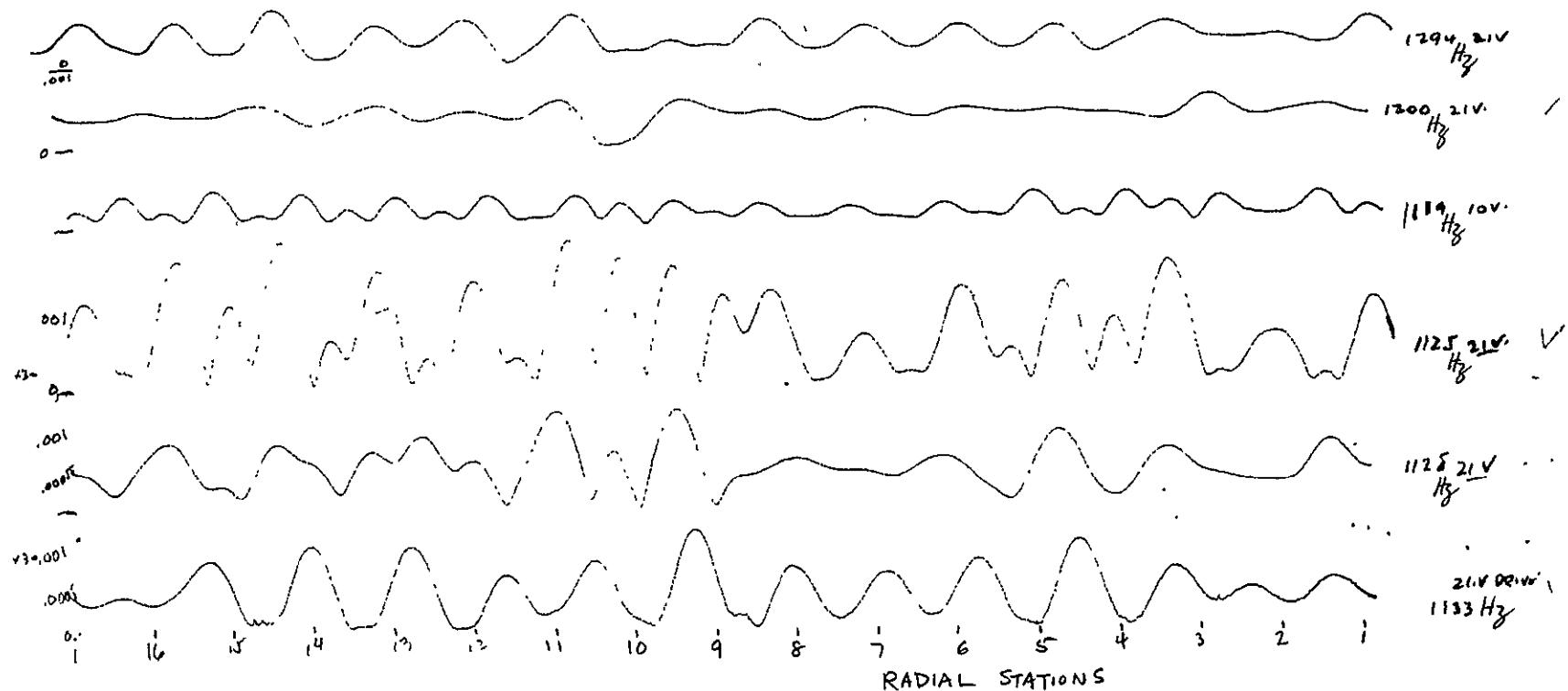
Figure XV-1. Mapping of N Modes (Sheet 18 of 26)

TEST RUN 8-3-V-P-"2"
          8-3-R-P-F
20V   3-26-69

ROTA⁻ONAL
TEST RUNS   1 2 3 4 5 6 7 8 9 10 11
LOCAT⁻ONS 'F 3"15 35 4⅜ F ¾ 1½ 2¼ 3½ 4¼'
              UP UP UP UP   DN DN DN DN DN
           0 1 + + + 0 - - - - -

VERT
706.7 Hz

ROTA⁻⁻on
706.7 Hz

ROTATION
706.7

VERTICAL-'2'-line

RADIAL STATION
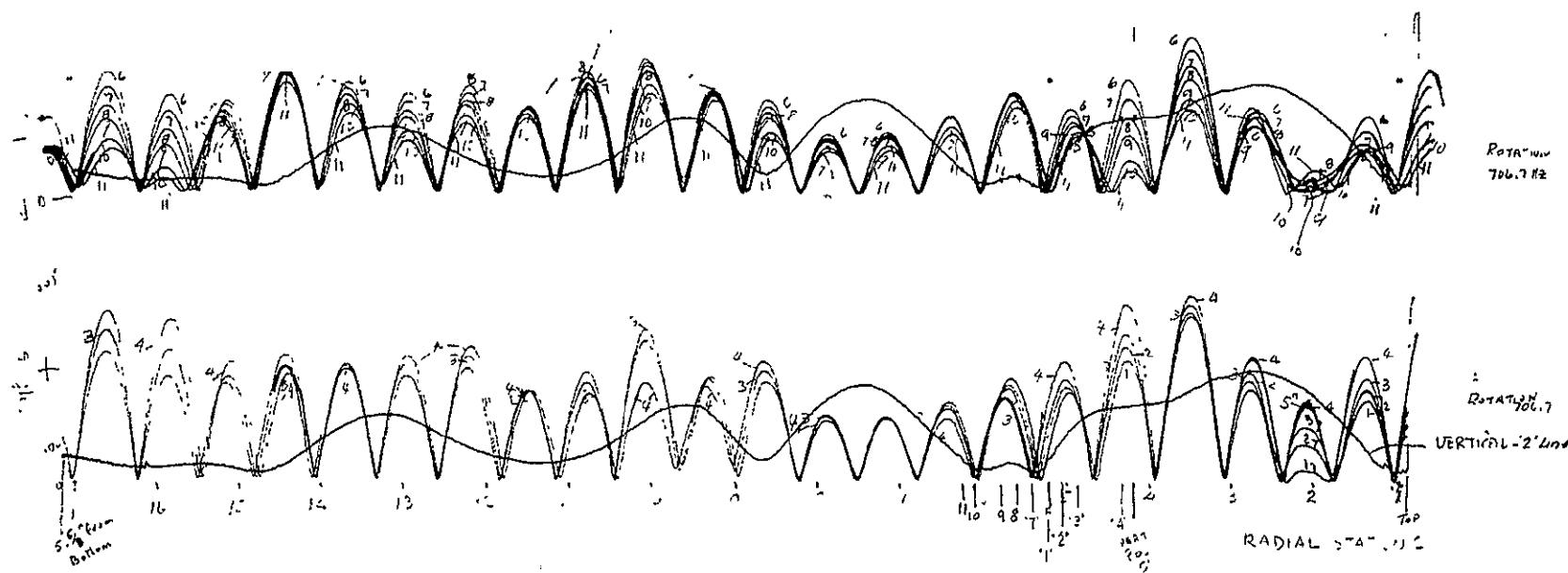
Figure XV-1.   Mapping of N Modes (Sheet 19 of 26)

Space Division
North American Rockwell
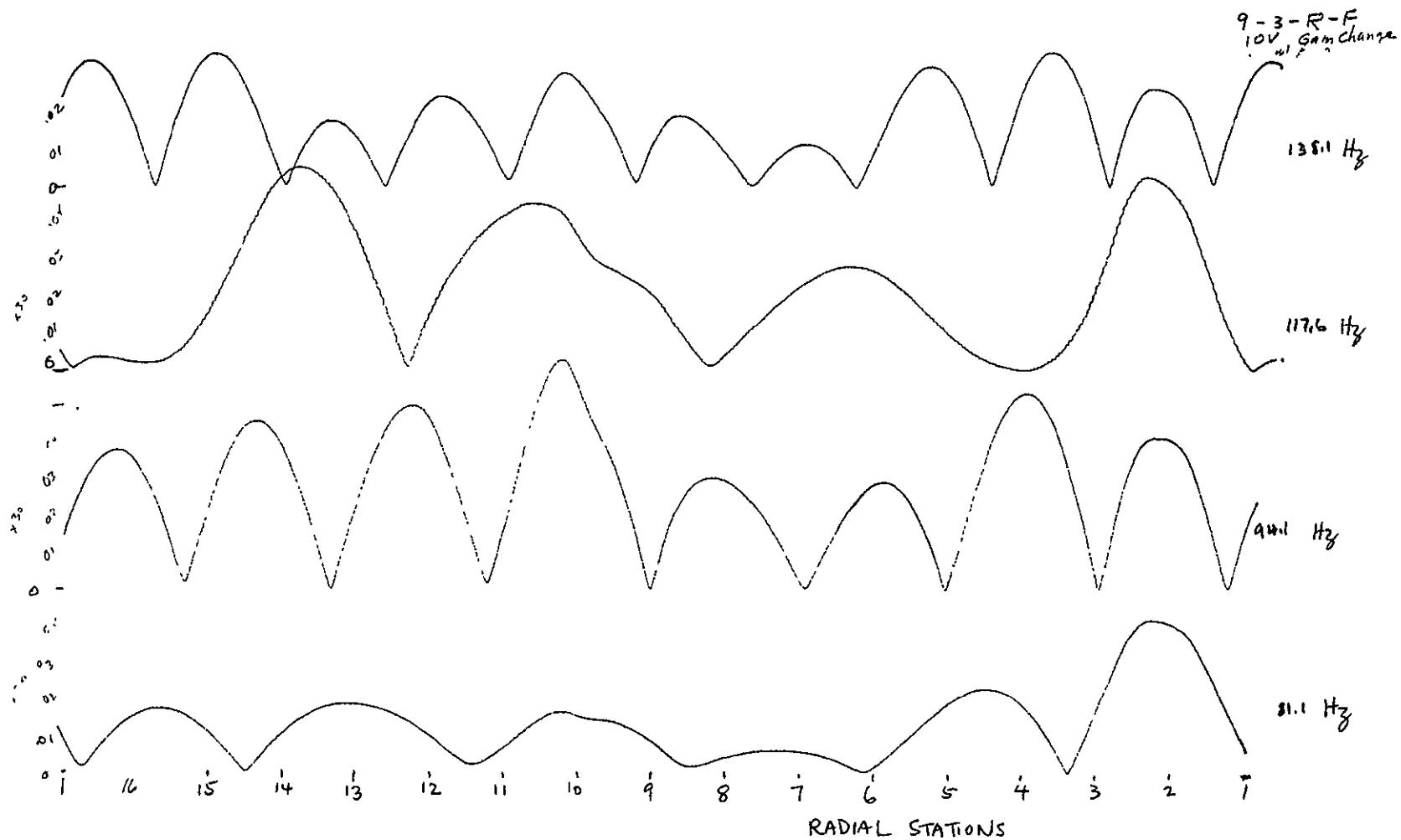
Figure XV-1. Mapping of N Modes (Sheet 20 of 26)

9 - 3 - R - F
10 V 3/5/9

.05
.04
.03
.02
.01
0

172.5 Hz

.01
0

244.0 Hz

175.7 Hz

.01
0

157.9 Hz

223.5 Hz

198.4 Hz

1   16   15   14   13   12   11   10   9   8   7   6   5   4   3   2   1

RADIAL STATIONS

Space Division
North American Rockwell
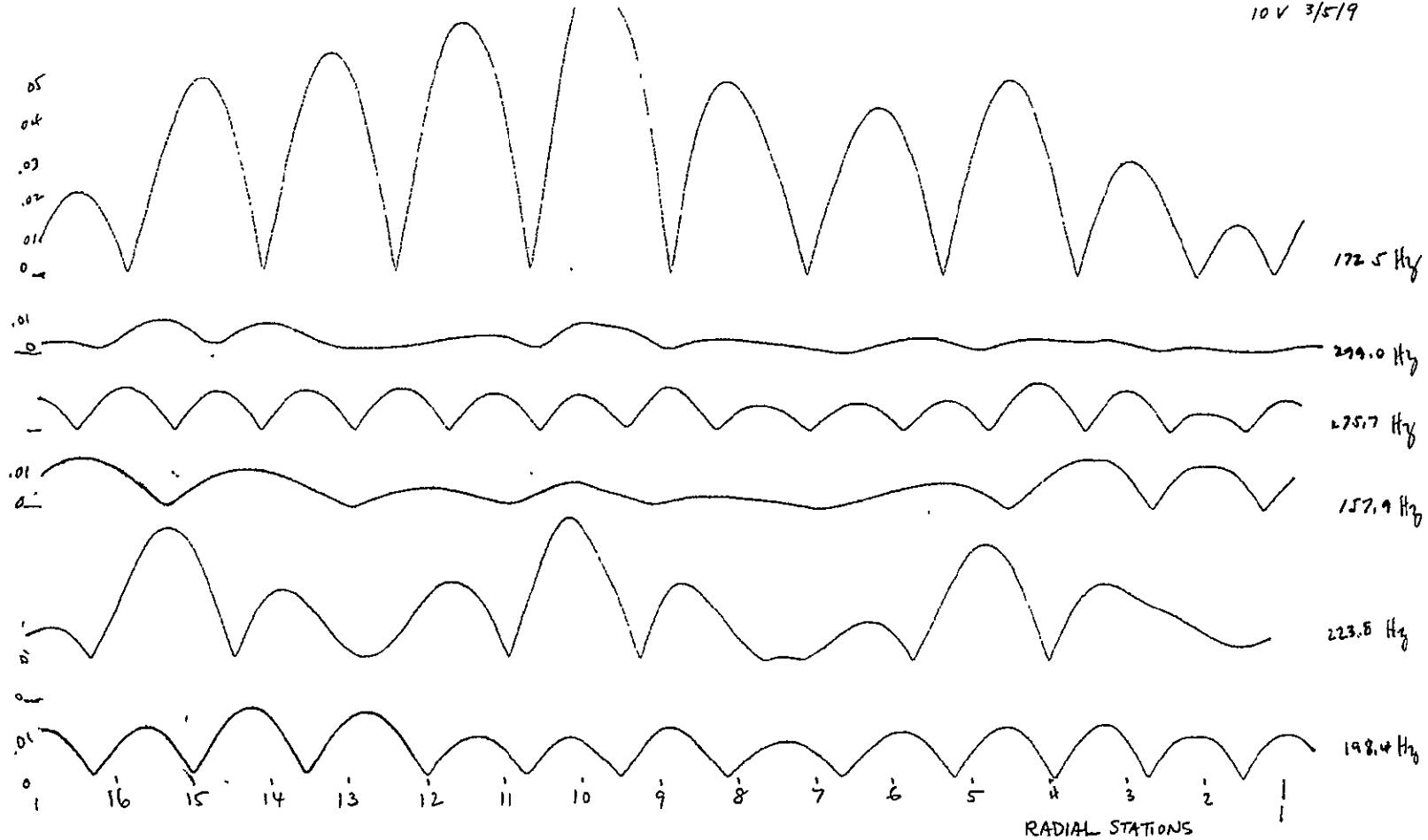
Figure XV-1.   Mapping of N Modes (Sheet 21 of 26)

Figure XV-1. Mapping of N Modes (Sheet 22 of 26)

Space Division
North American Rockwell

9-3-R-F
10V 3/6/9

1200 Hz ✓

1186 Hz (M.LV)

1125 Hz (2020) ✓

1028 Hz (10V) ✓

875.7 Hz ✓

815.8 Hz

822.0 Hz

RADIAL STATIONS
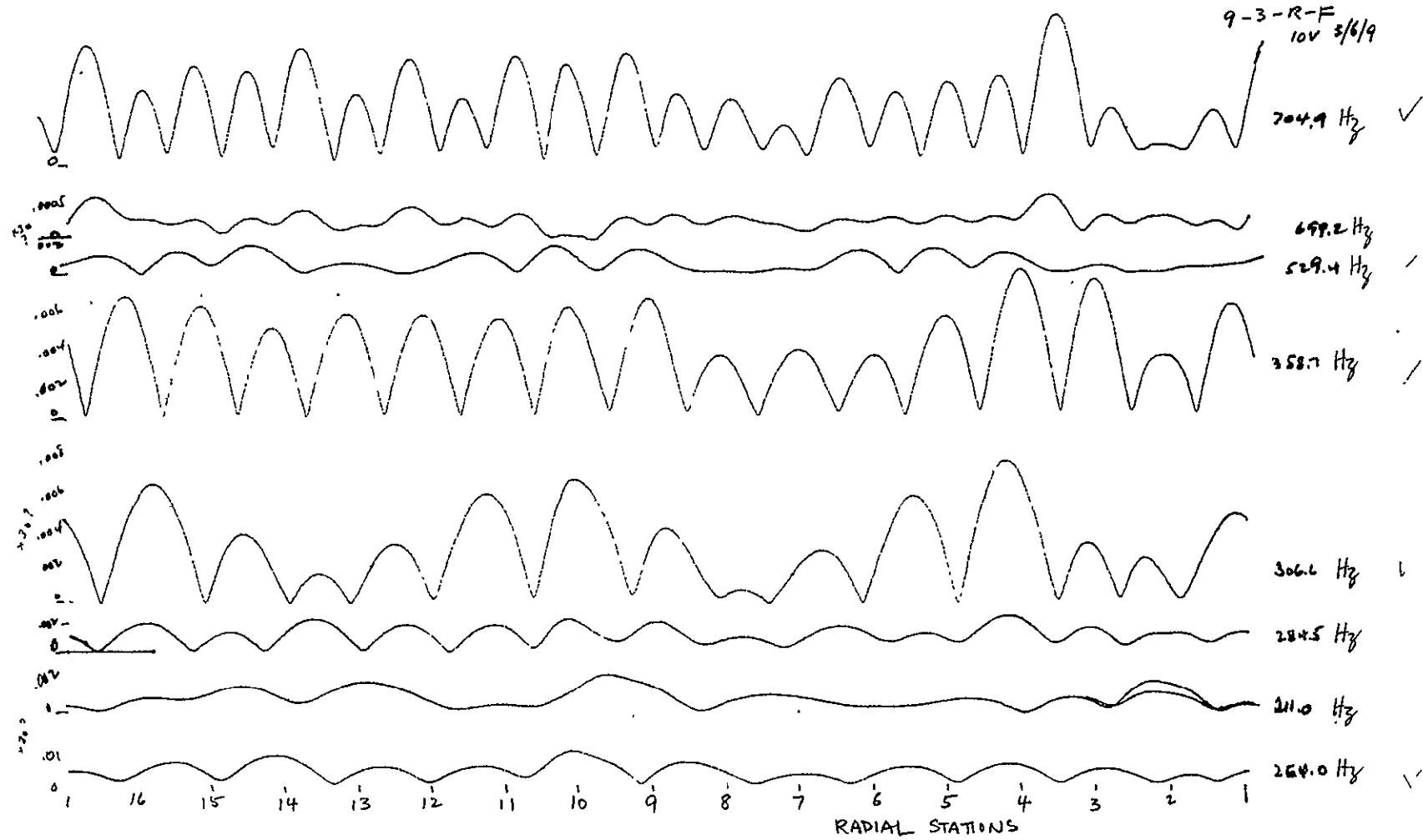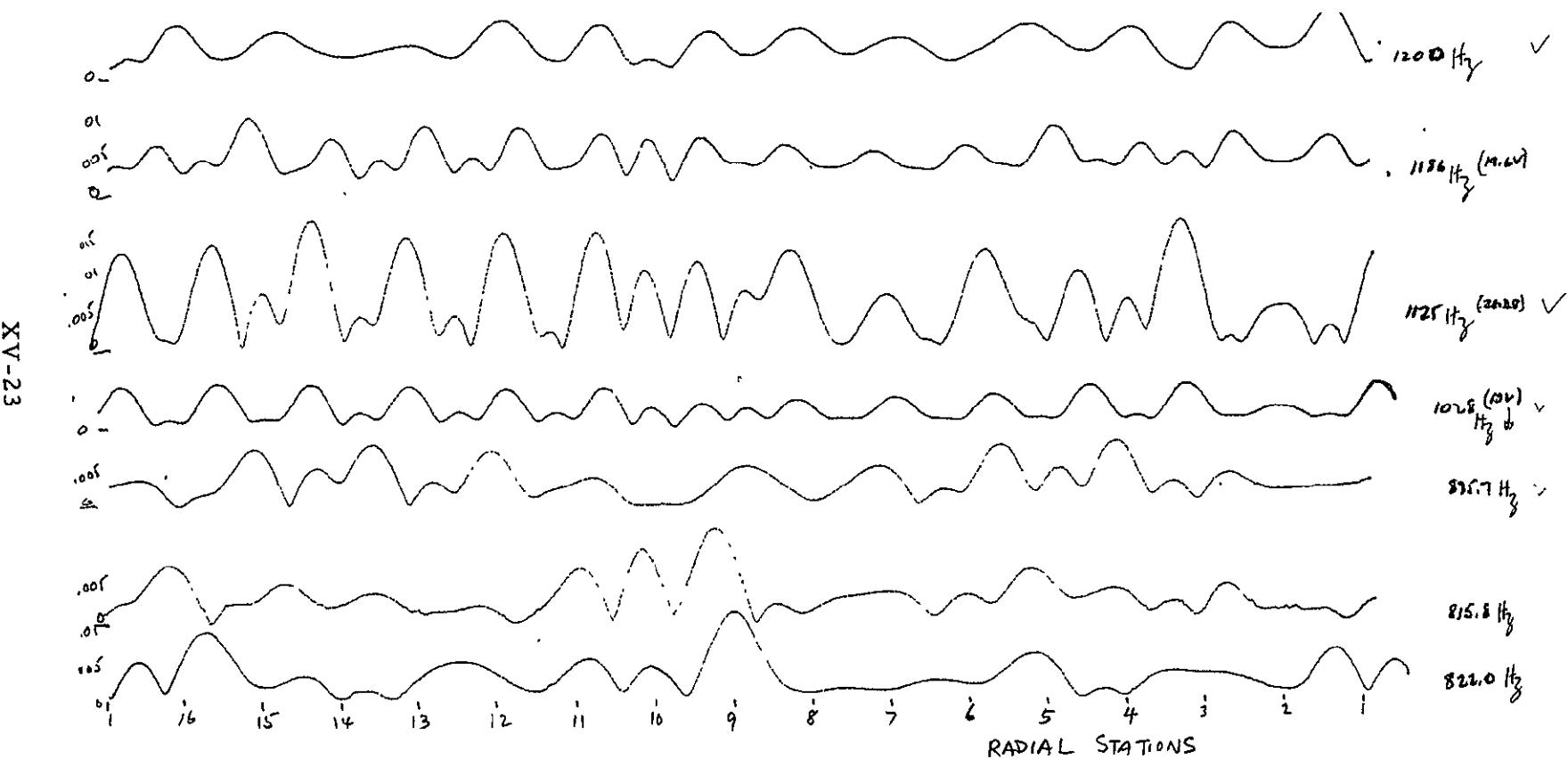
Figure XV-1. Mapping of N Modes (Sheet 23 of 26)

Space Division
North American Rockwell

10-3-R 10v 3/6/9

172.1 Hz

.152 6 Hz

134.5 Hz

113.4 Hz

92.5 Hz

76.3 Hz

RADIAL STATIONS

Space Division
North American Rockwell
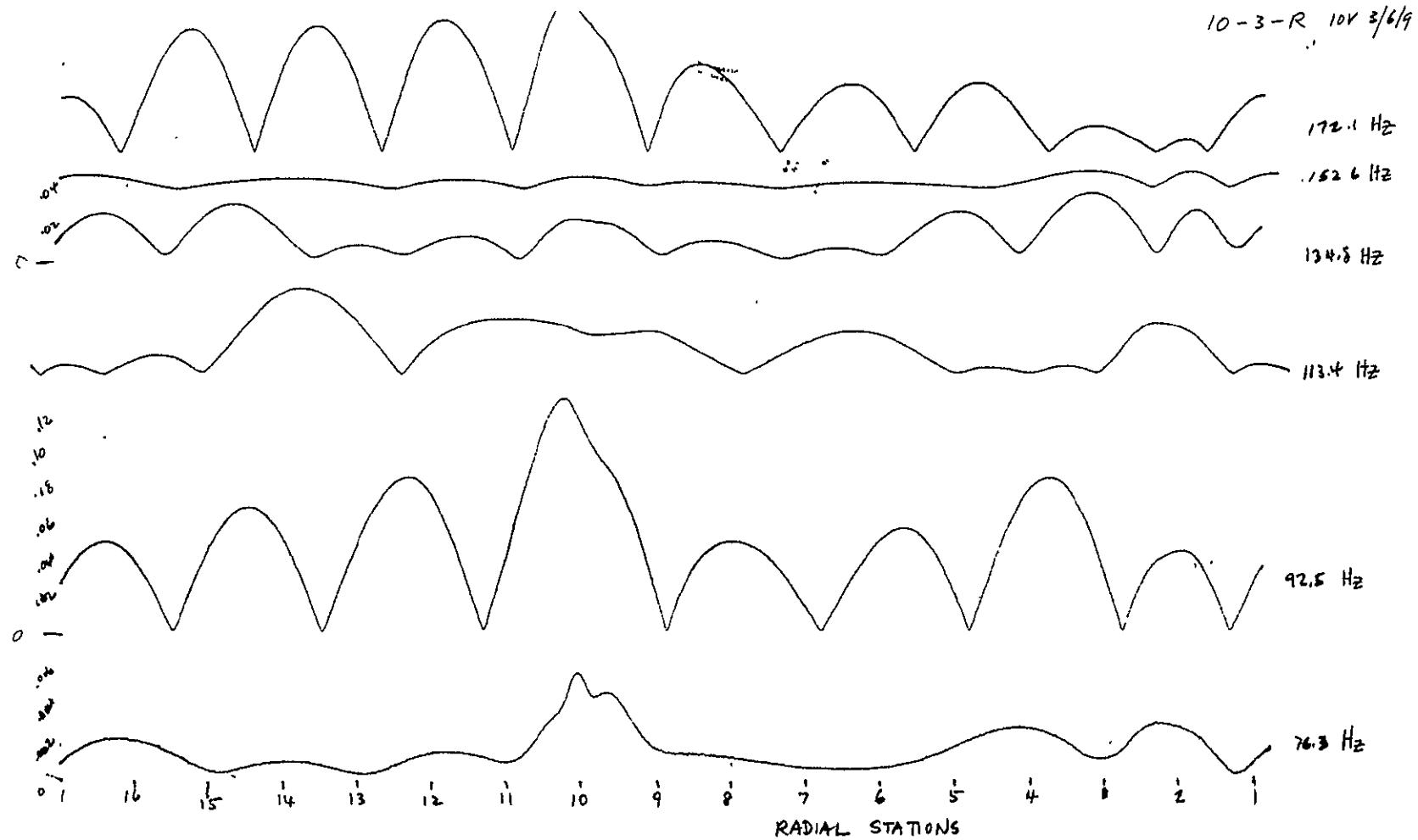
Figure XV-1.   Mapping of N Modes (Sheet 24 of 26)

Figure XV-1. Mapping of N Modes (Sheet 25 of 26)

XV-26

SD 69-766

821.2 Hz

814.6 Hz

RADIAL STATIONS
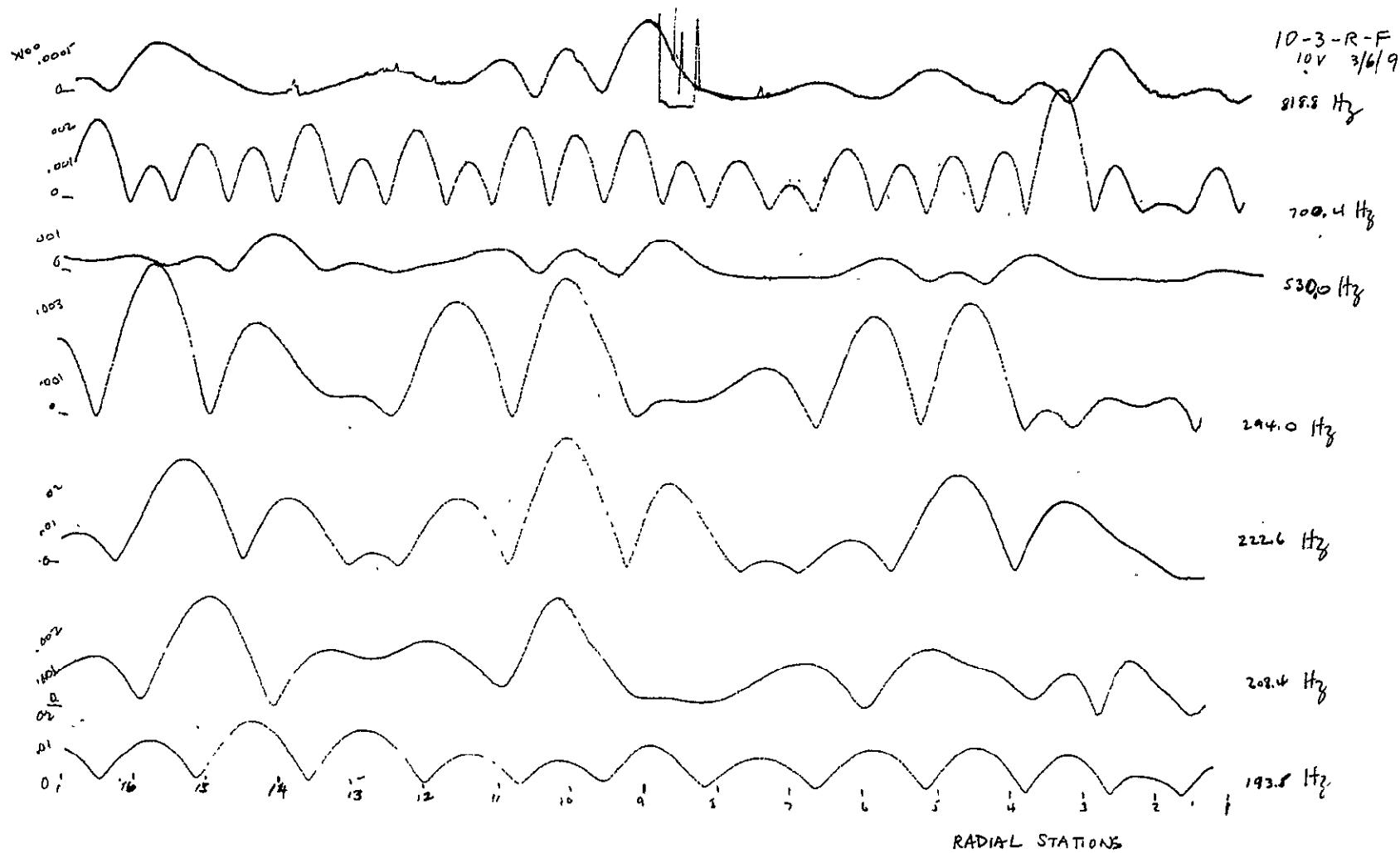
Space Division
North American Rockwell
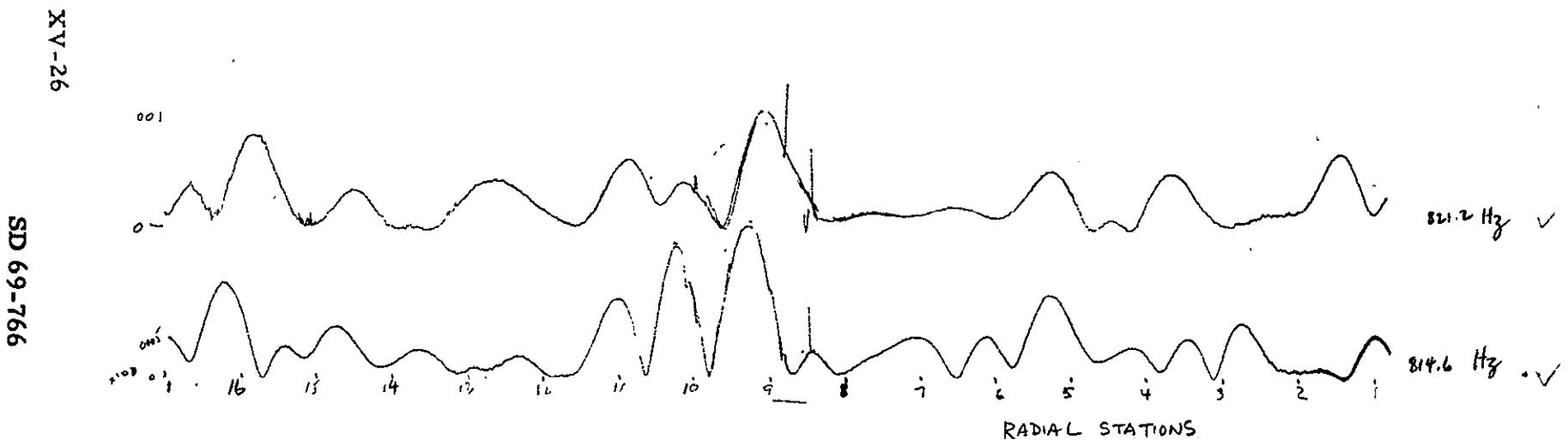
Figure XV-1.   Mapping of N Modes (Sheet 26 of 26)

XVI. M-MODE INVESTIGATIONS
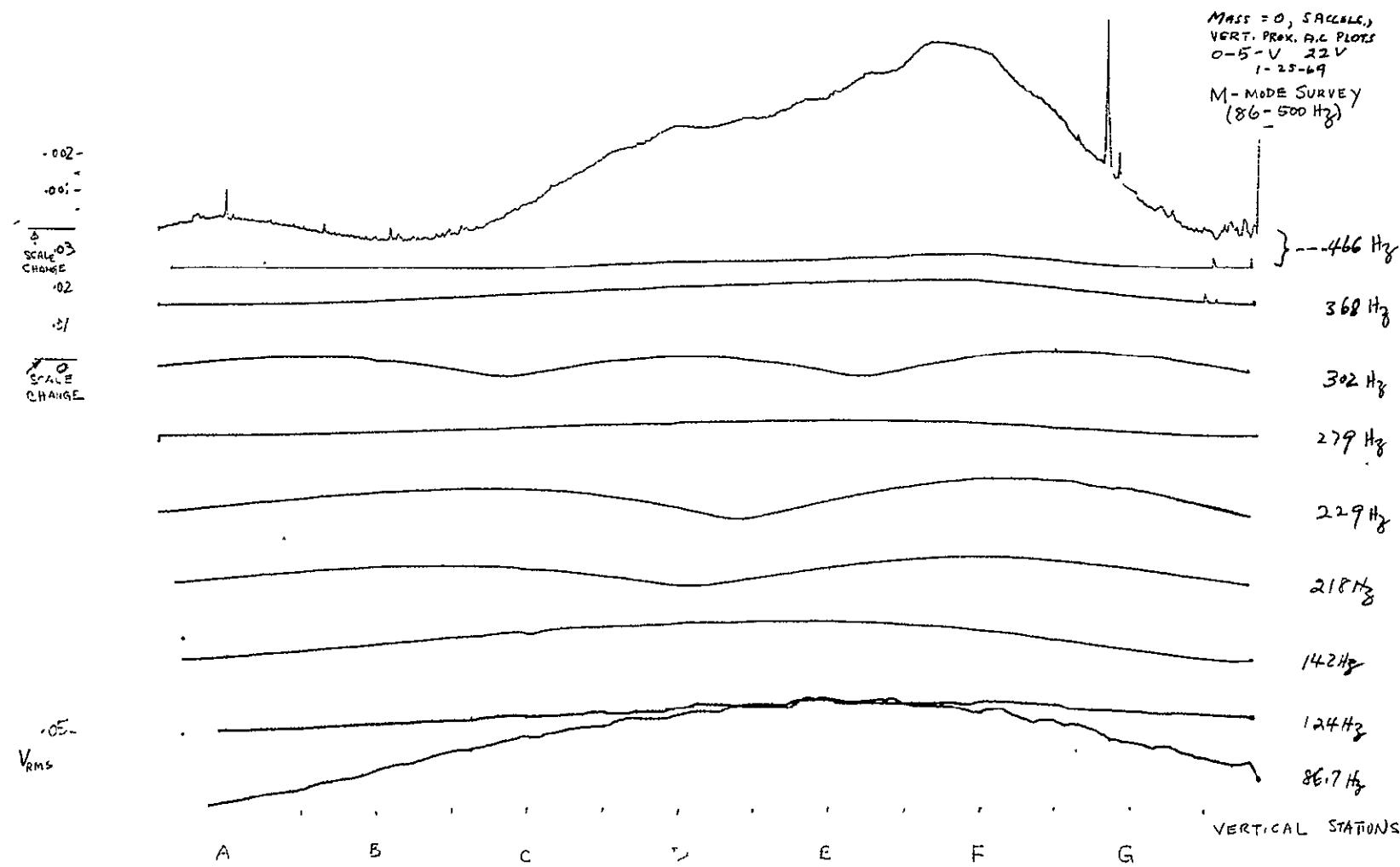
Figure XVI-1. M-Mode Investigations (Sheet 1 of 6)

Space Division
North American Rockwell

O-5-V-22V

M-MODE
SURVEY (499-801Hz)

801 Hz

702 Hz

645 Hz

579 Hz

538 Hz

499 Hz

V_{RMS}

.004

.003

.002

.001

0

A   B   C   D   E   F   G   H

AXIAL STATIONS
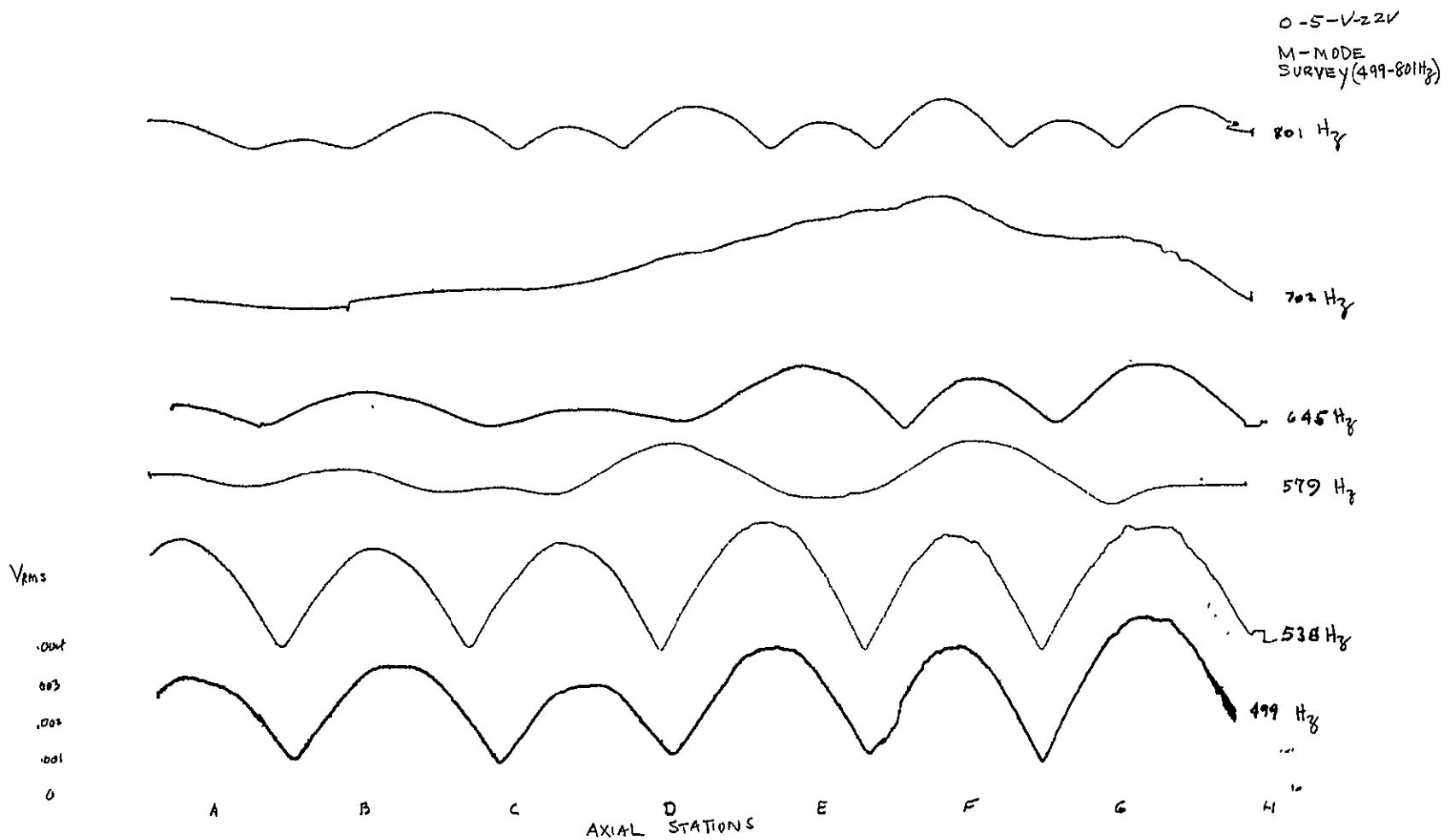
Figure XVI-1.   M-Mode Investigations (Sheet 2 of 6)

Space Division
North American Rockwell

Figure XVI-1. M-Mode Investigations (Sheet 3 of 6)

Space Division
North American Rockwell
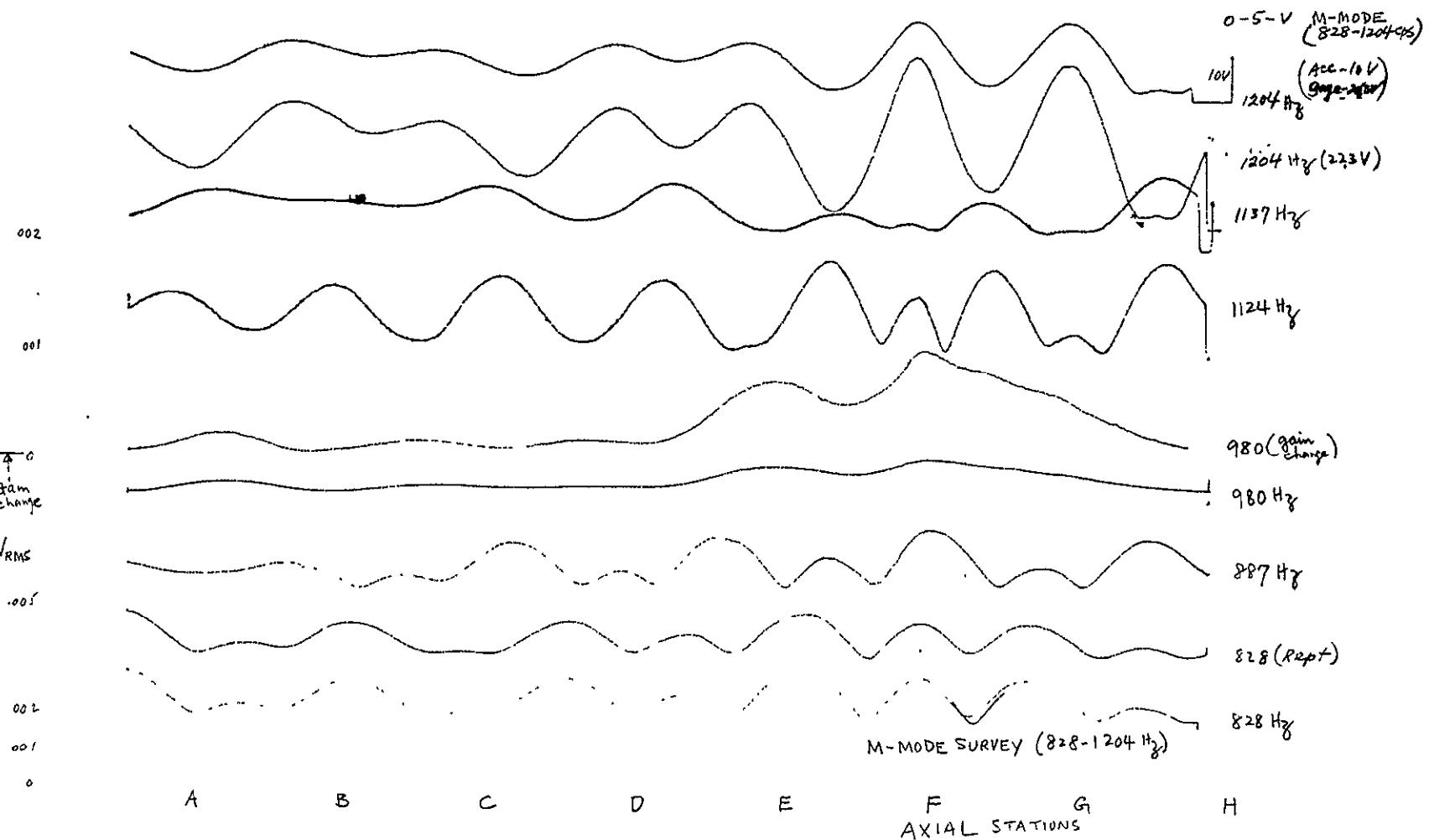
PROX SAGE #2 LINE
0-3-V-1312 Hz
3/4/9
NO MASS.
M-MODE SURVEY
1312 Hz.
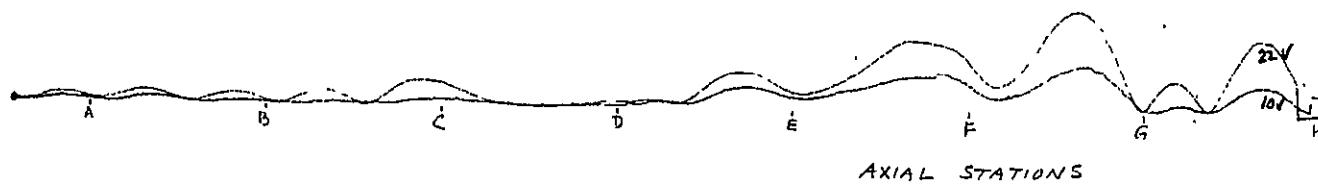
OUTPUT VOLTS

0.1

22V

10V

A   B   C   D   E   F   G   H

AXIAL STATIONS

Figure XVI-1.   M-Mode Investigations (Sheet 4 of 6)
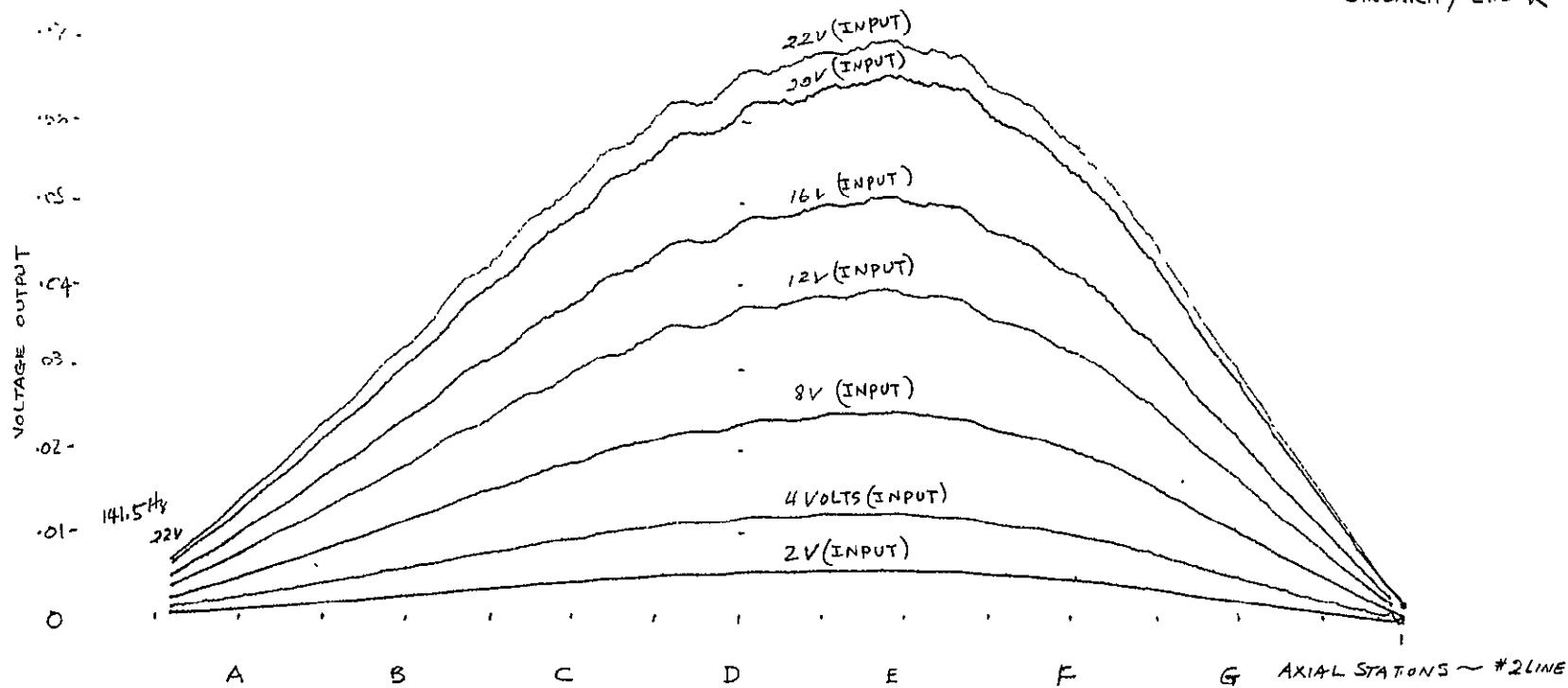
$0-5-V-(141.5 Hz)$

$2-26-9$

NO MASS VERTICAL SURVEY
M-MODE 5 ACCEL.
FREQ 141.5 Hz

M - MODE SURVEY
&
LINEARITY CHECK

VOLTAGE OUTPUT

.07

.06

.05

.04

.03

.02

.01

0

22V (INPUT)
20V (INPUT)
16V (INPUT)
12V (INPUT)
8V (INPUT)
4 VOLTS (INPUT)
2V (INPUT)

141.5 Hz
22V

A   B   C   D   E   F   G   AXIAL STATIONS ~ #2 LINE

Figure XVI-1.   M-Mode Investigations (Sheet 5 of 6)

Space Division
North American Rockwell

OUTPUT VOLTS

.02

.01

A   B   C   D   E   F   G   H

AXIAL STATIONS ~ "2" LINE

O-5-V-228 Hz
22V   2/27/9
NO MASS CASE
"M" MODE SURVEY
(228 Hz)
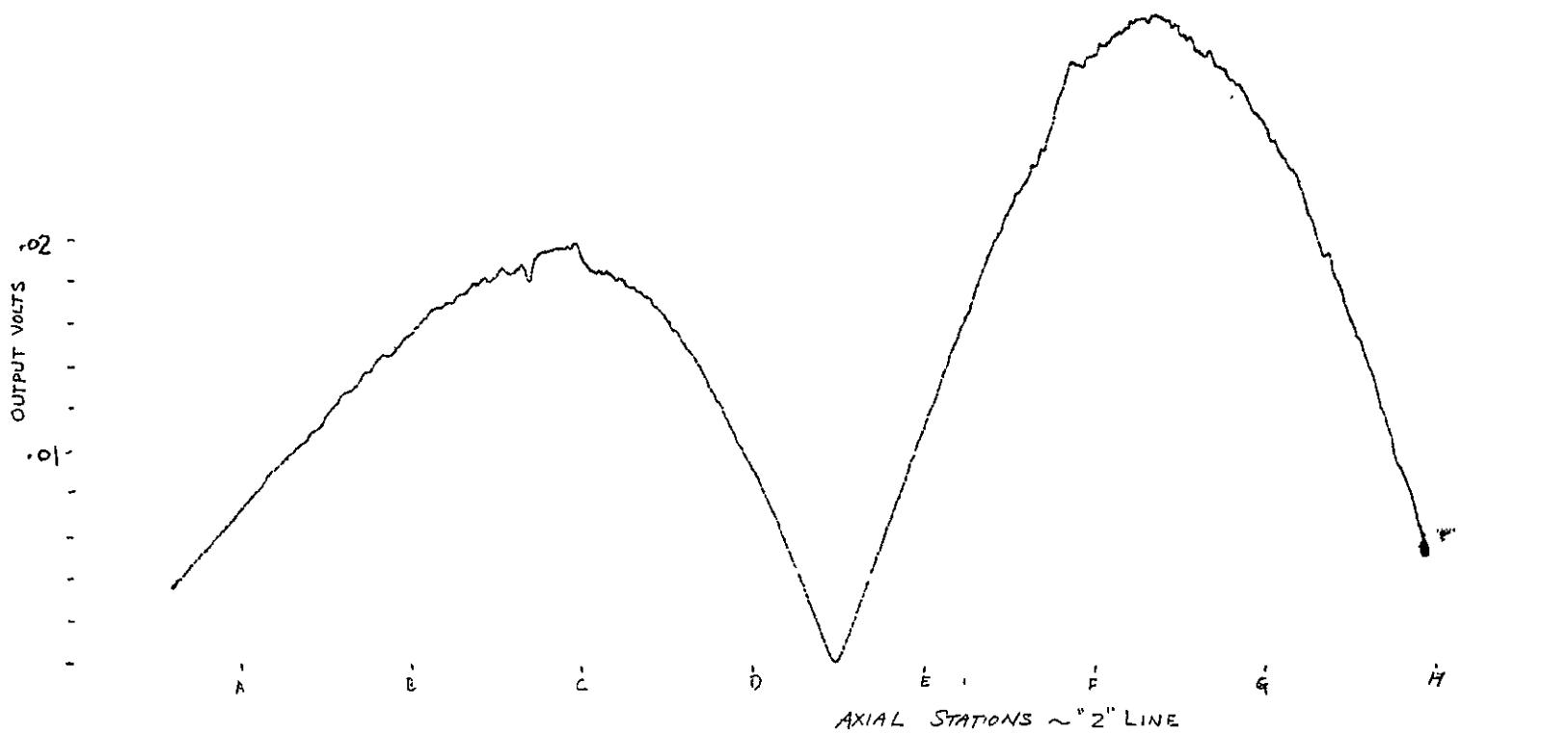
Figure XVI-1.   M-Mode Investigations (Sheet 6 of 6)

XVII. THEORETICAL MODE SHAPES AND FREQUENCIES FOR
MASS-LOADED SHELLS
(BY SERIES EXPANSION TECHNIQUE)
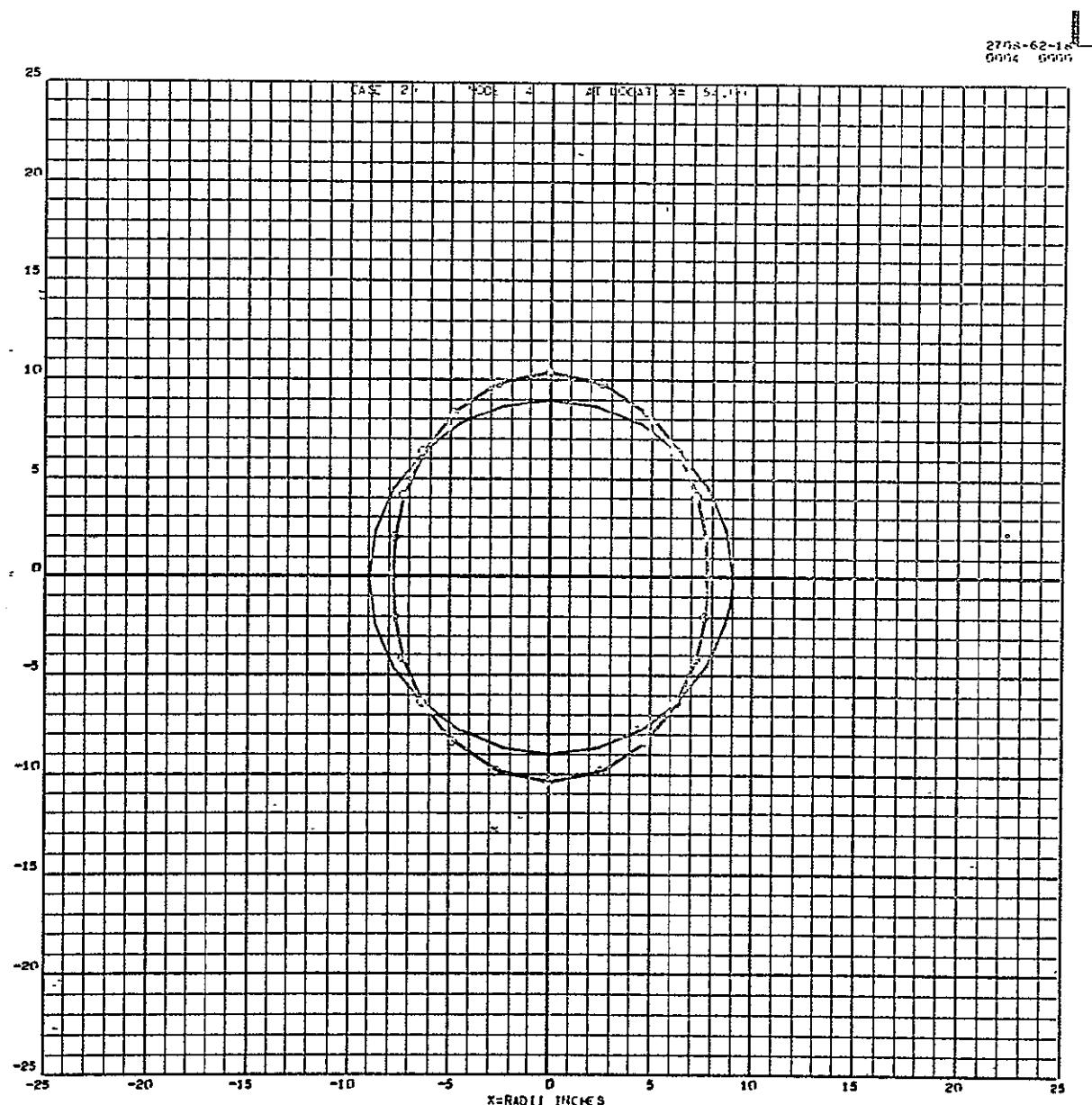
Figure XVII-1.   Theoretical Mode Shapes and Mass-Loaded Shells.
Case 20 - 52.32 Hz

XVII-1
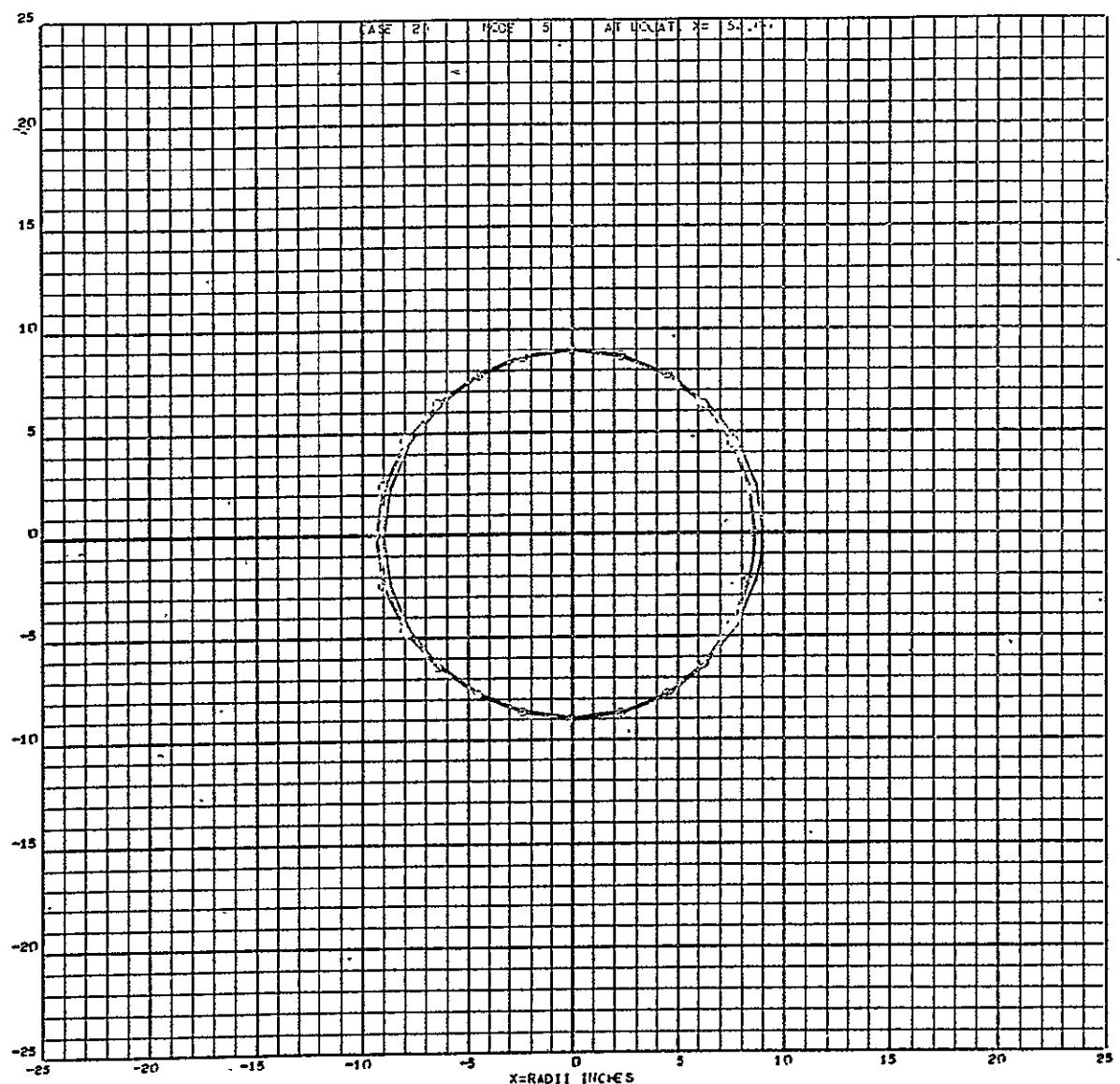
Figure XVII-2. Theoretical Mode Shapes and Mass-Loaded Shells.
Case 20 - 69.7 Hz

XVII-2
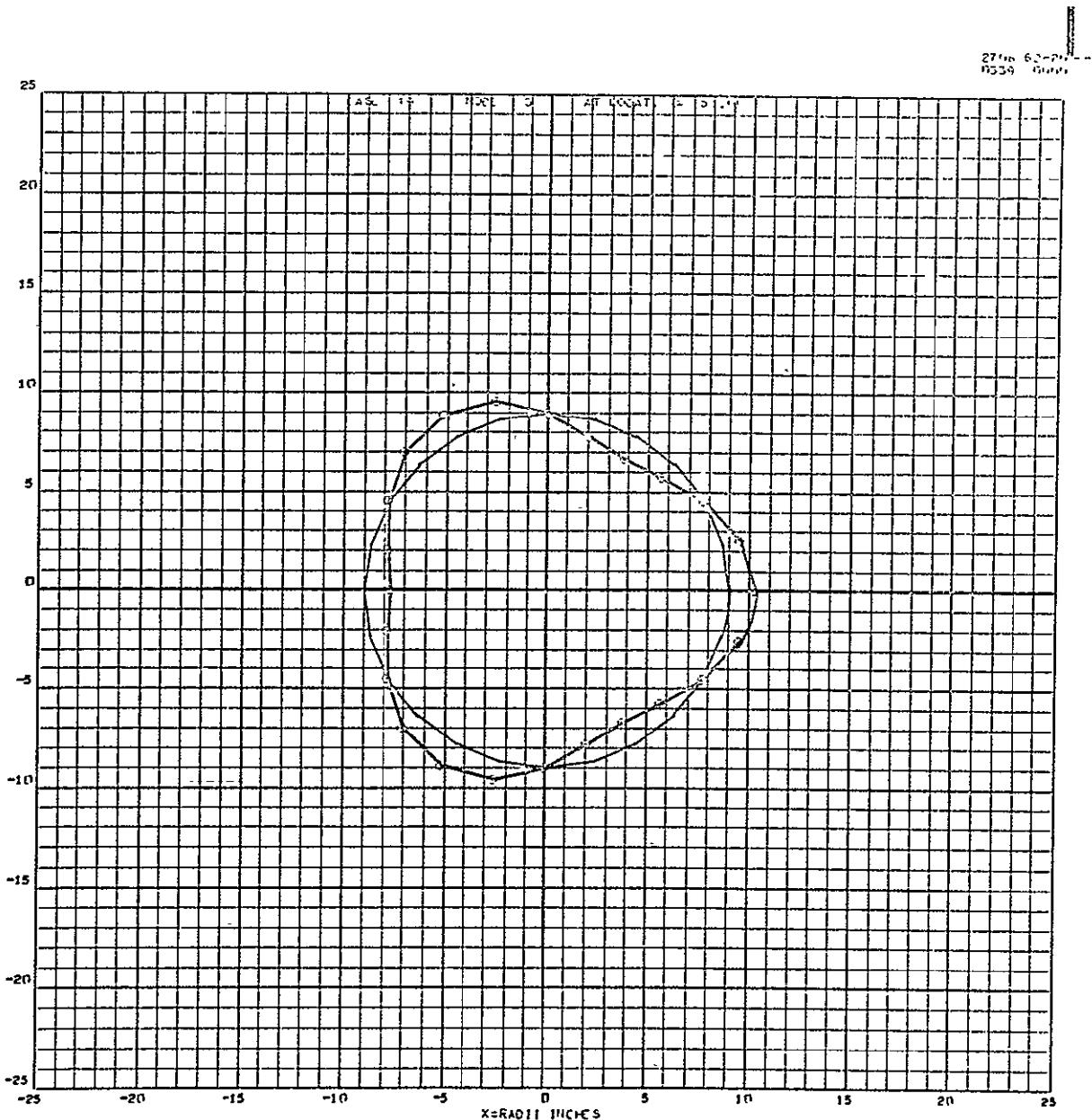
Figure XVII-3. Theoretical Mode Shapes and Mass-Loaded Shells.
Case 19 - 77.19 Hz

XVII-3
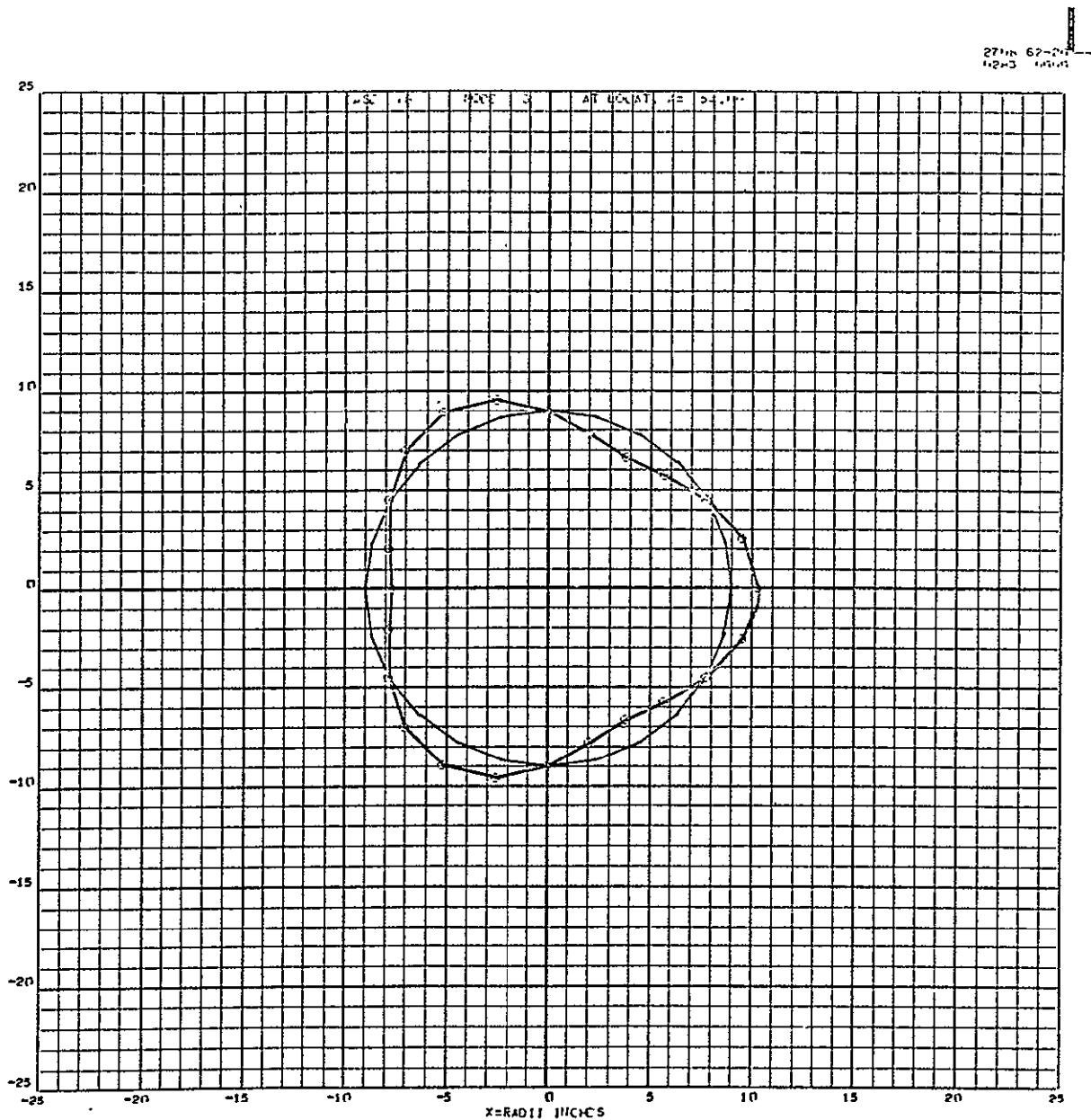
Figure XVII-4. Theoretical Mode Shapes and Mass-Loaded Shells.
Case 18 - 78.38 Hz

XVII-4
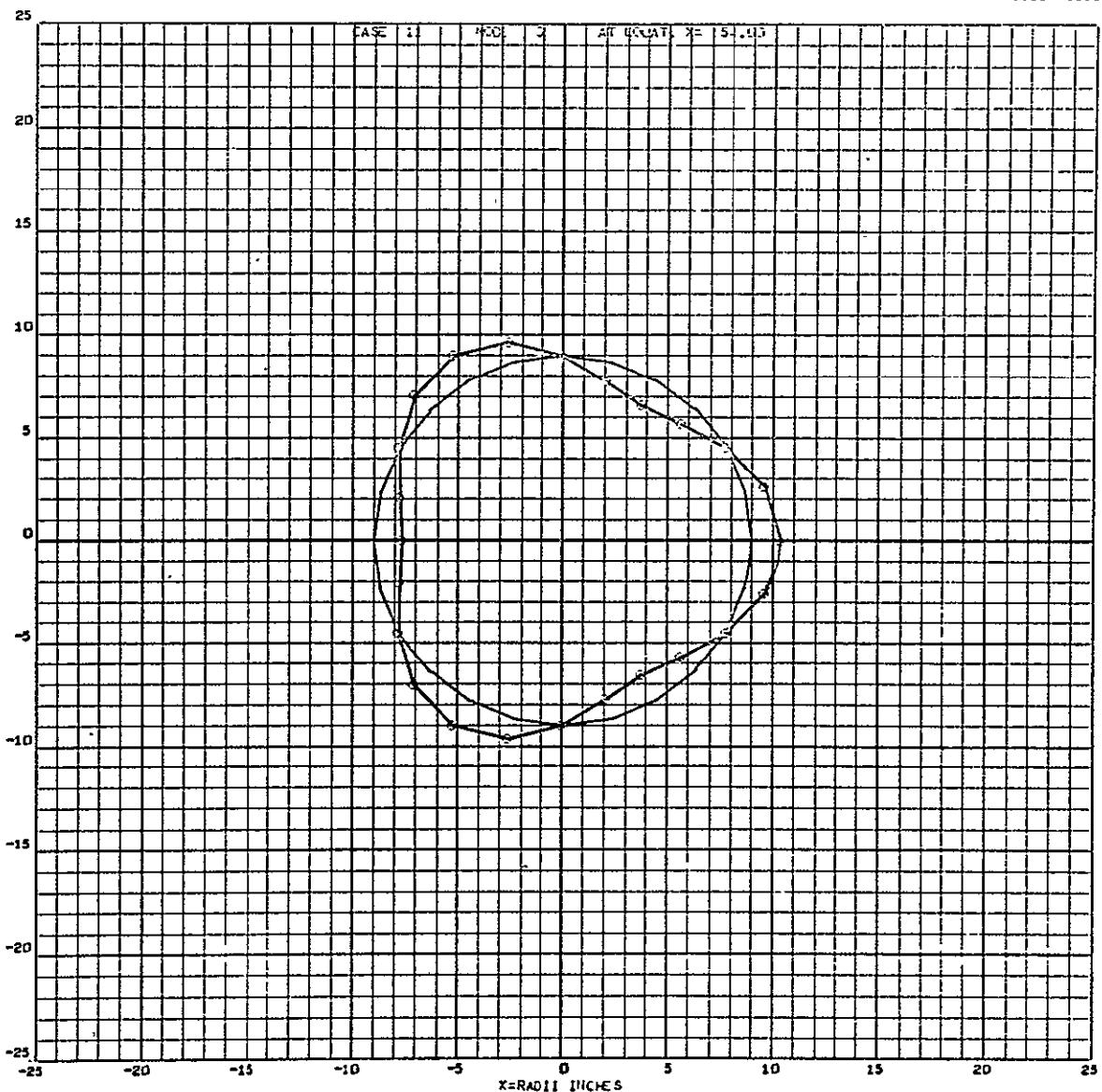
Figure XVII-5. Theoretical Mode Shapes and Mass-Loaded Shells.
Case 11 - 84.25 Hz

XVII-5
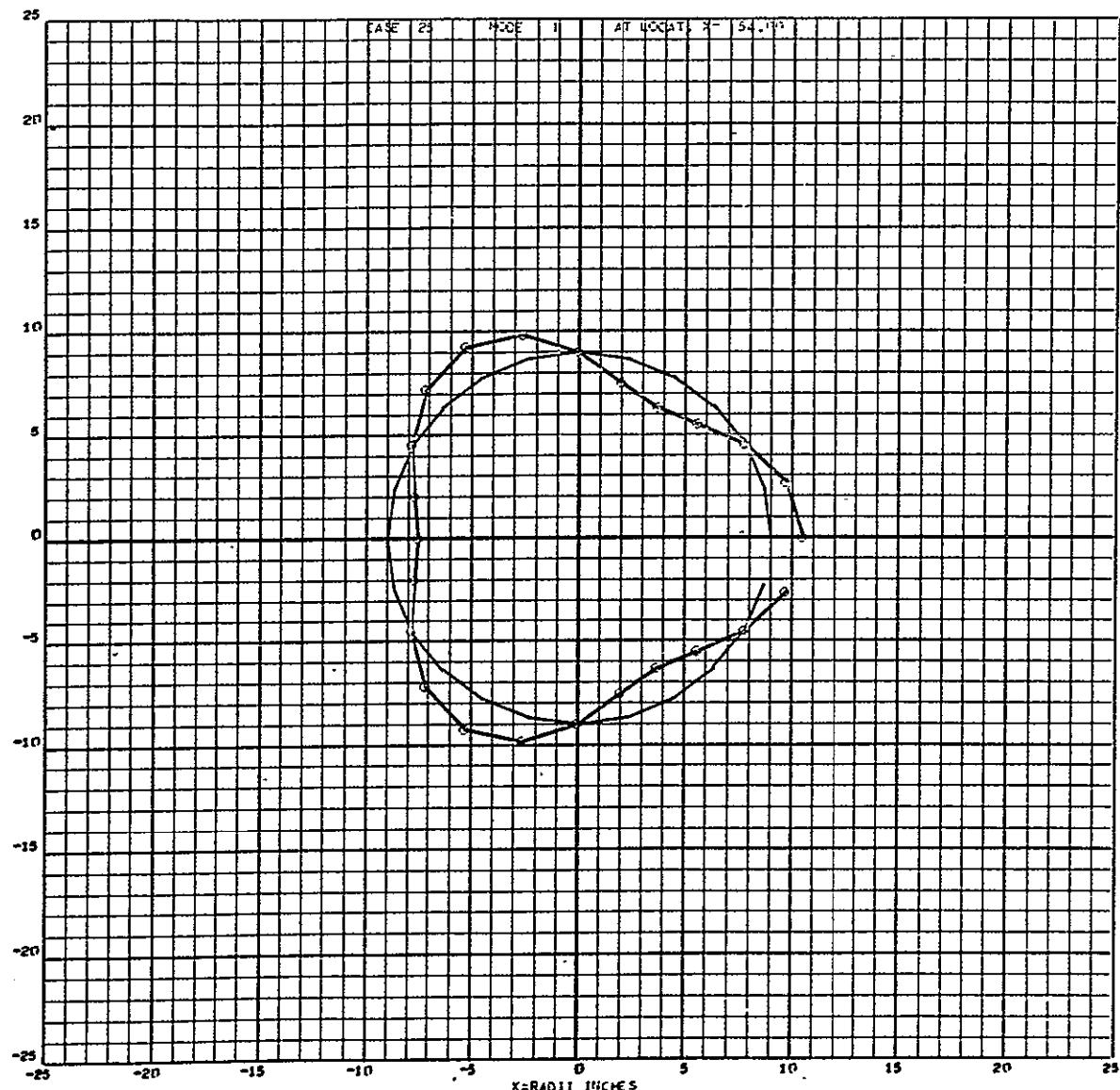
SD 69-766

Figure XVII-6. Theoretical Mode Shapes and Mass-Loaded Shells.
Case 25 - 86.89 Hz

SD 69-766
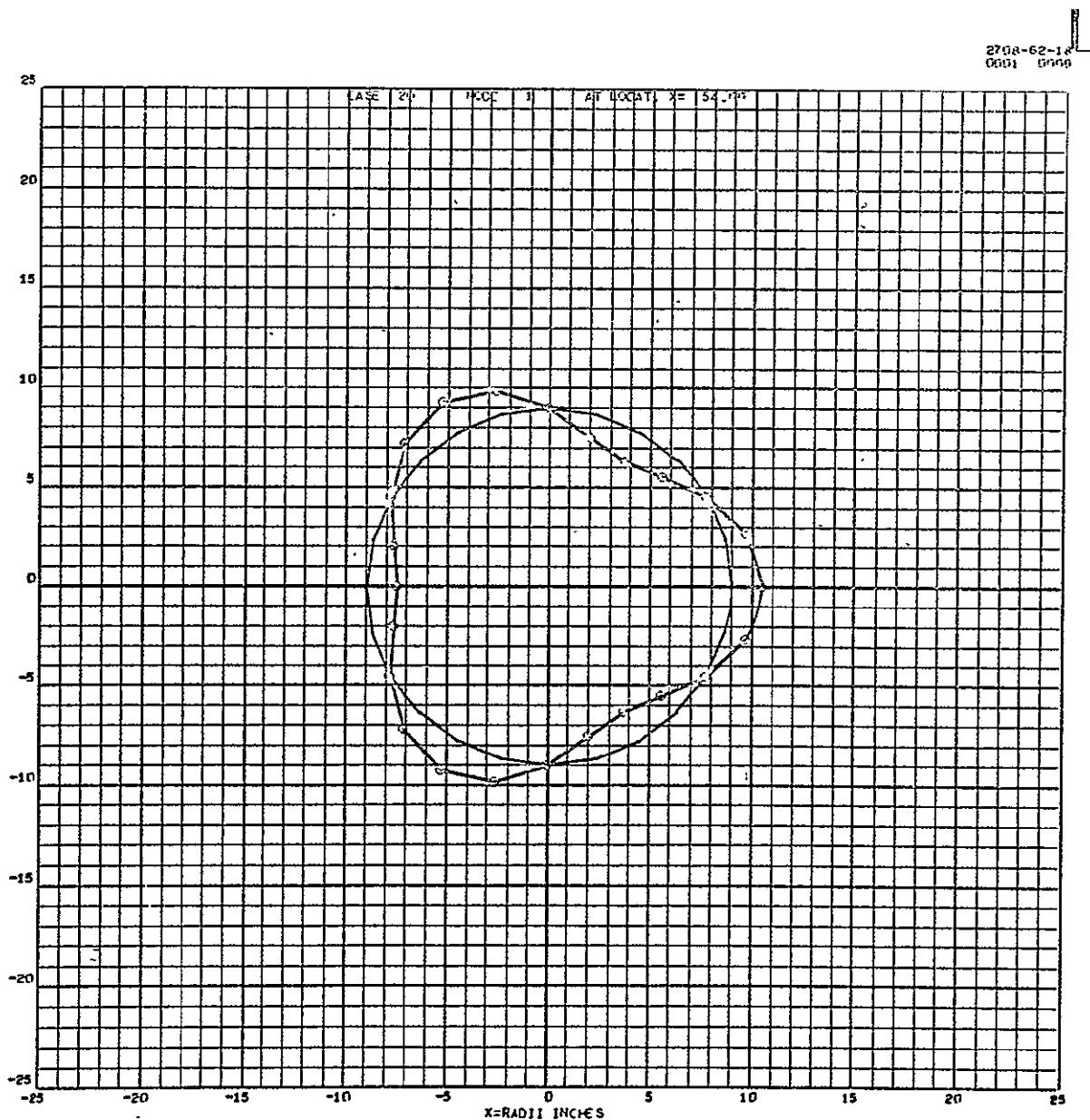
Figure XVII-7. Theoretical Mode Shapes and Mass-Loaded Shells.
Case 20 - 97 Hz
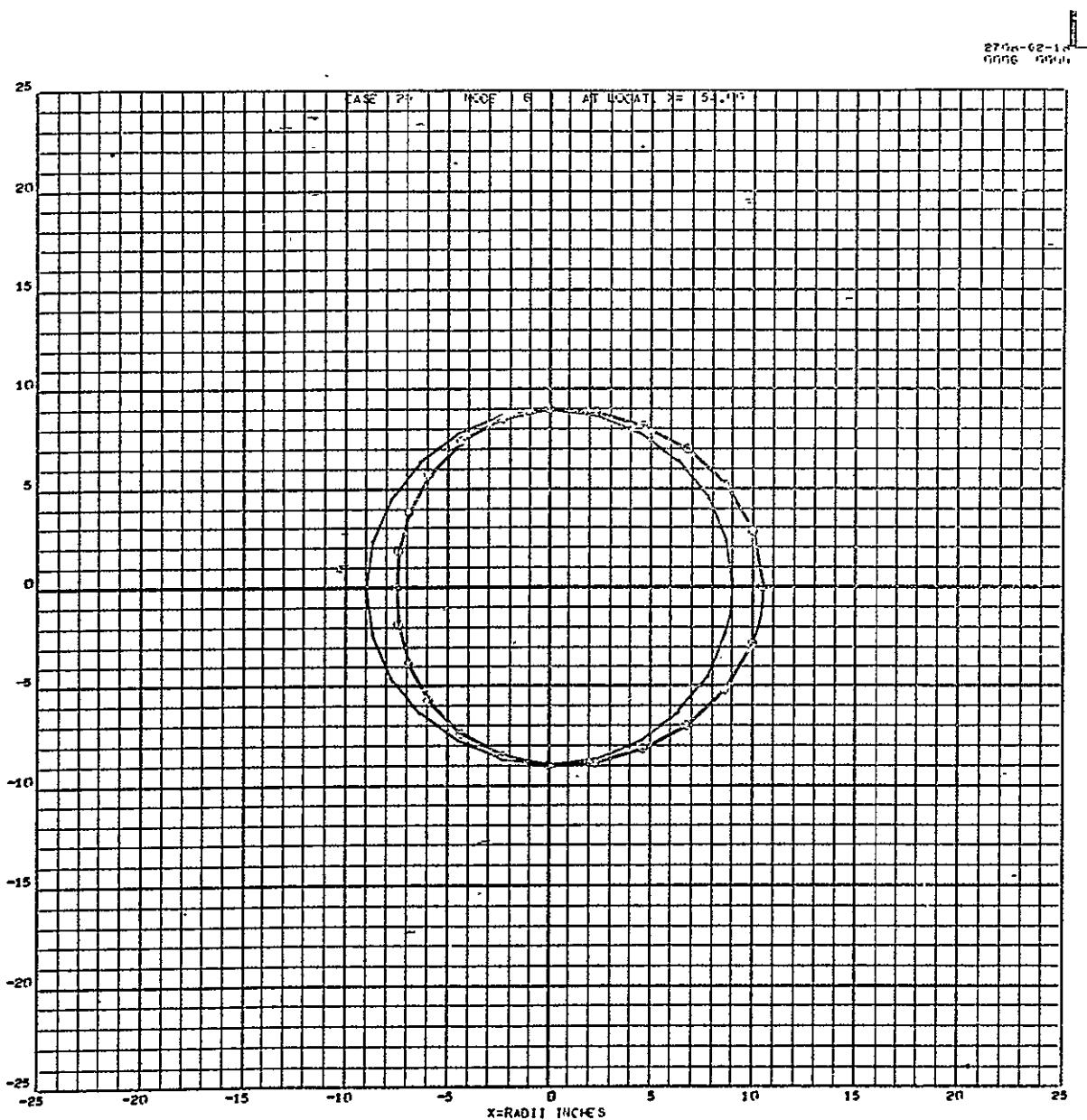
Figure XVII-8.   Theoretical Mode Shapes and Mass-Loaded Shells.
Case 20 - 106.61 Hz
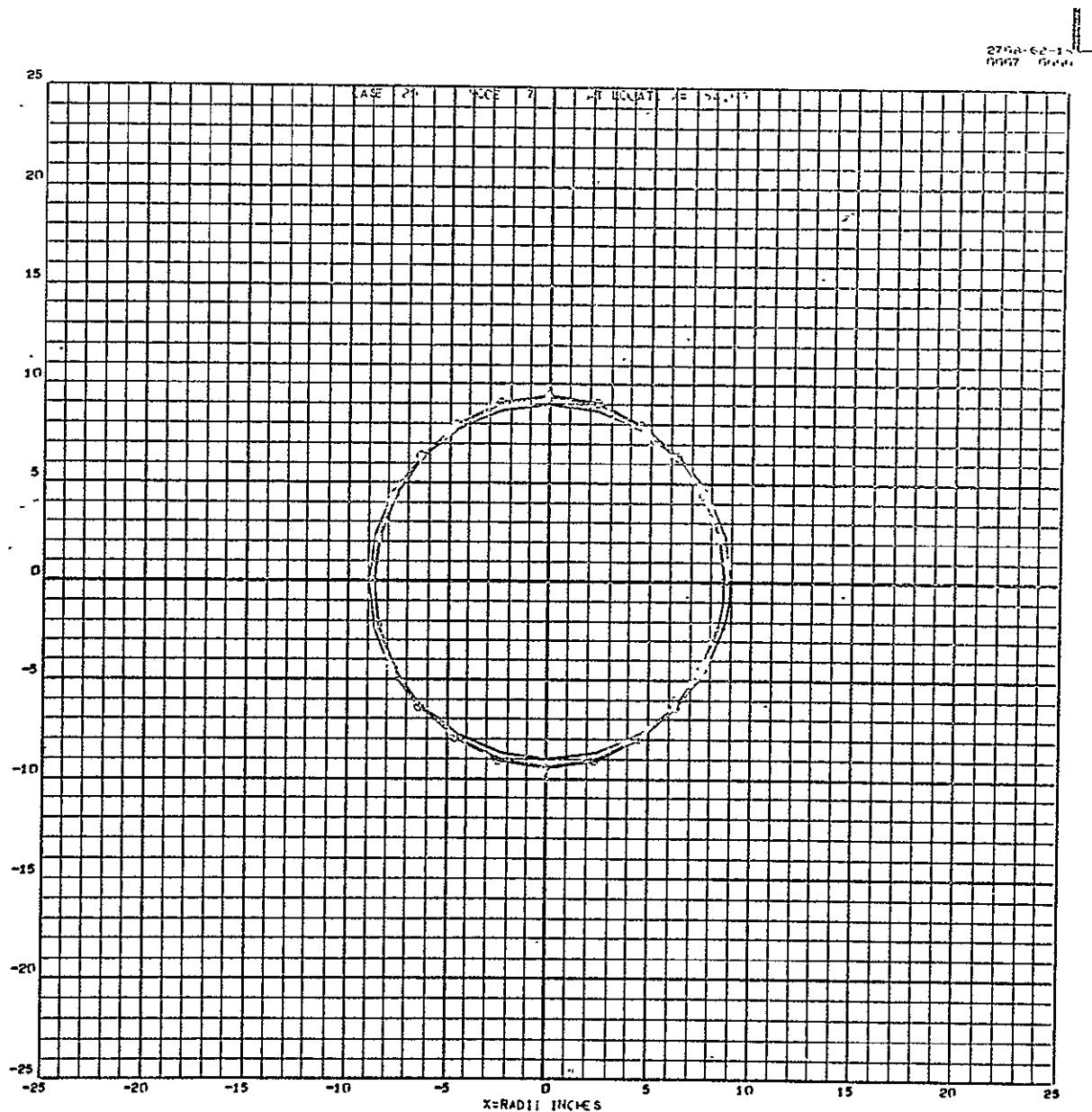
Figure XVII-9. Theoretical Mode Shapes and Mass-Loaded Shells.
Case 20 - 110. 85 Hz

XVII-9
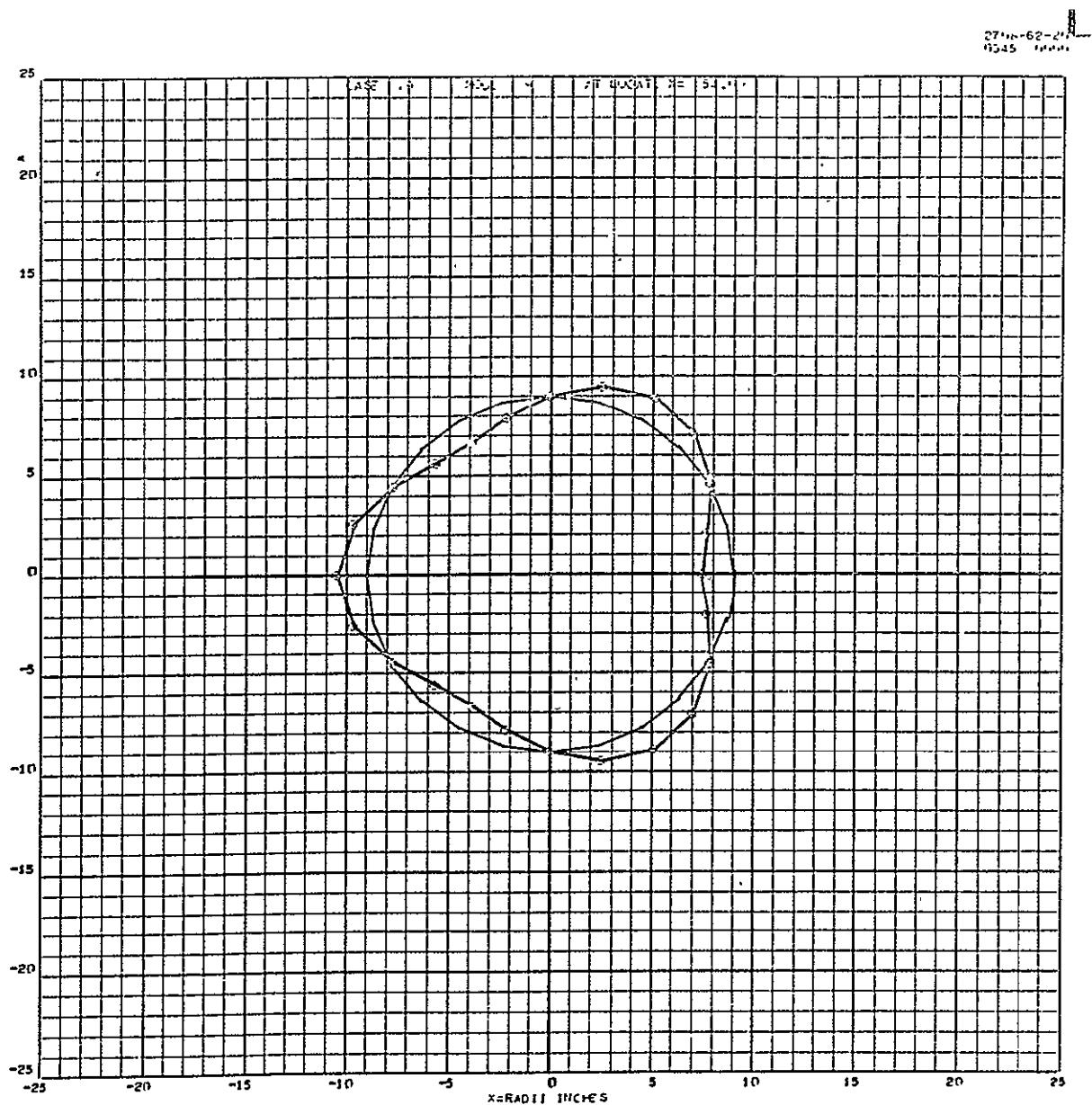
Figure XVII-10. Theoretical Mode Shapes and Mass-Loaded Shells.
Case 19 - 282.26 Hz
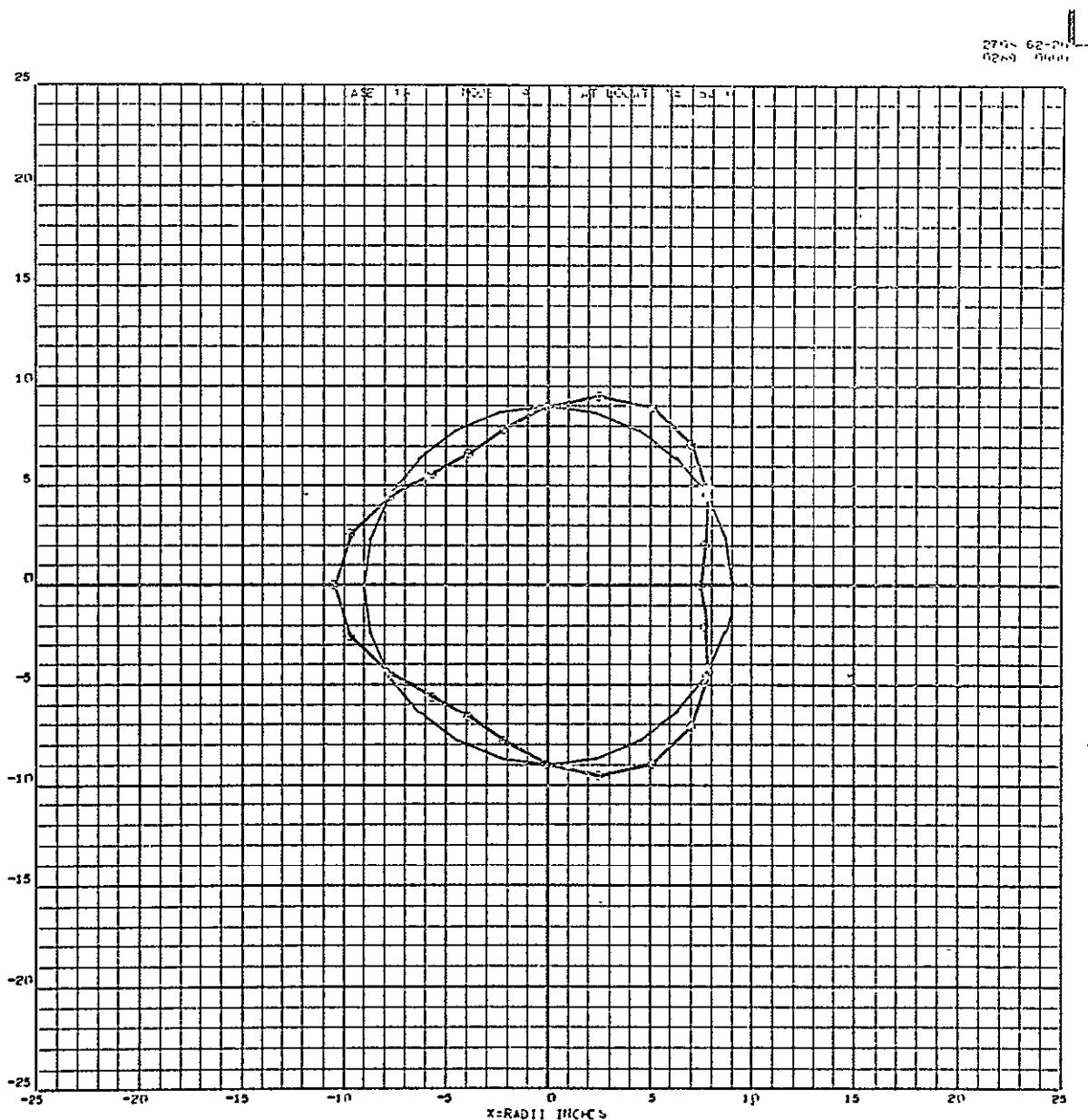
XVII-10

Figure XVII-11.   Theoretical Mode Shapes and Mass-Loaded Shells.
Case 18 - 283.86 Hz
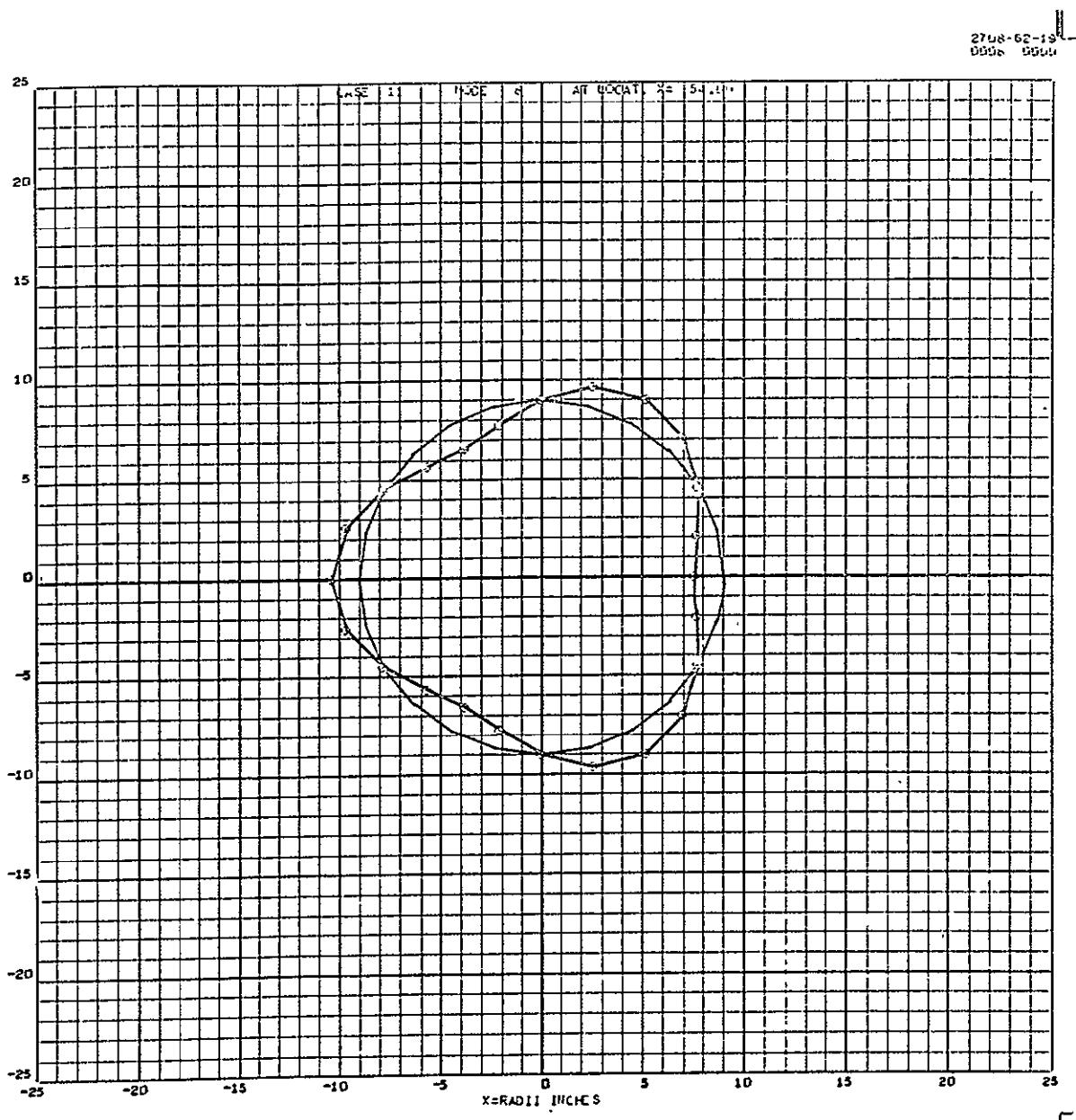
XVII-11

Figure XVII-12. Theoretical Mode Shapes and Mass-Loaded Shells.
Case 11 - 288.86 Hz
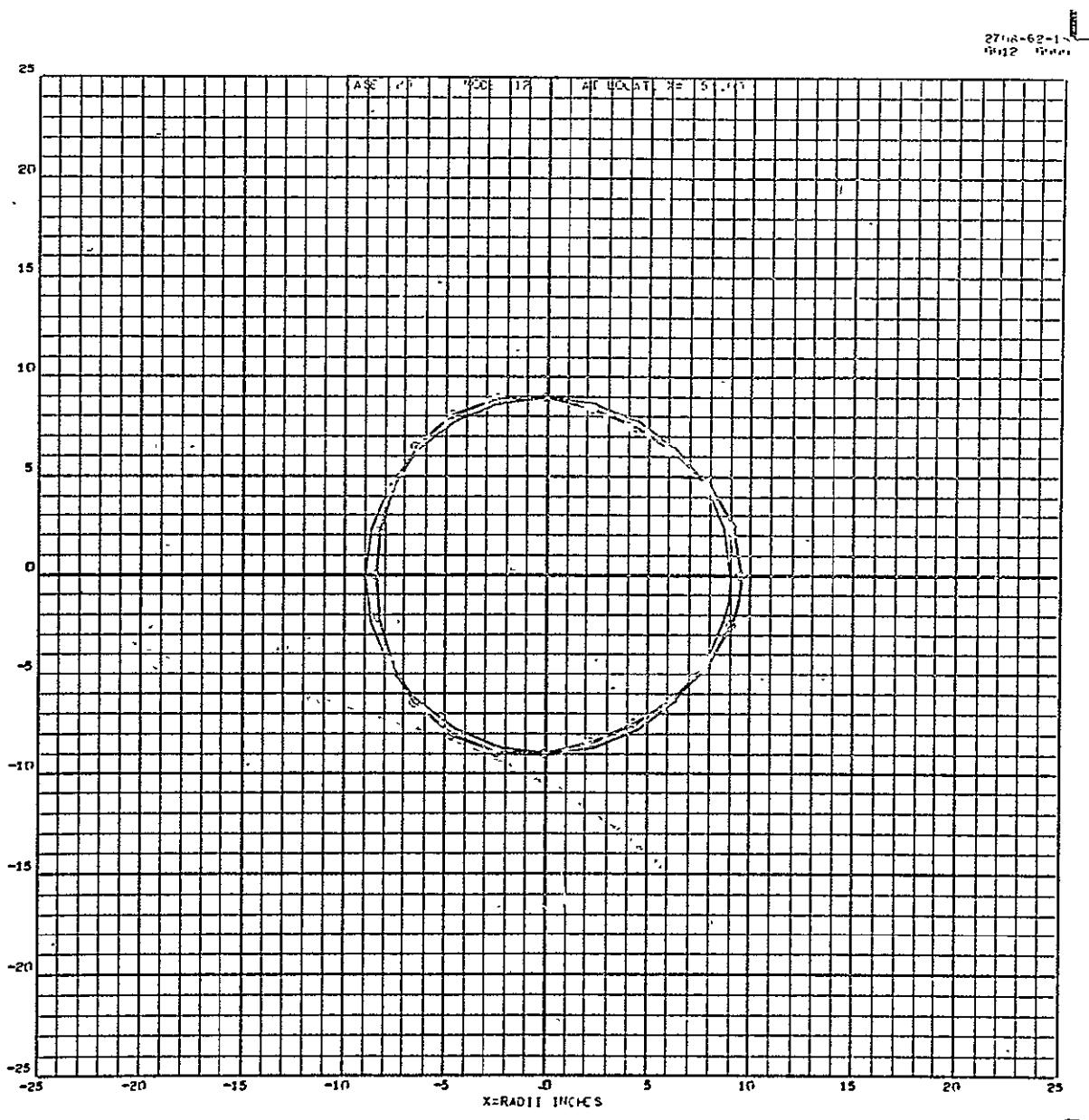
Figure XVII-13. Theoretical Mode Shapes and Mass-Loaded Shells.
Case 20 - 307.58 Hz
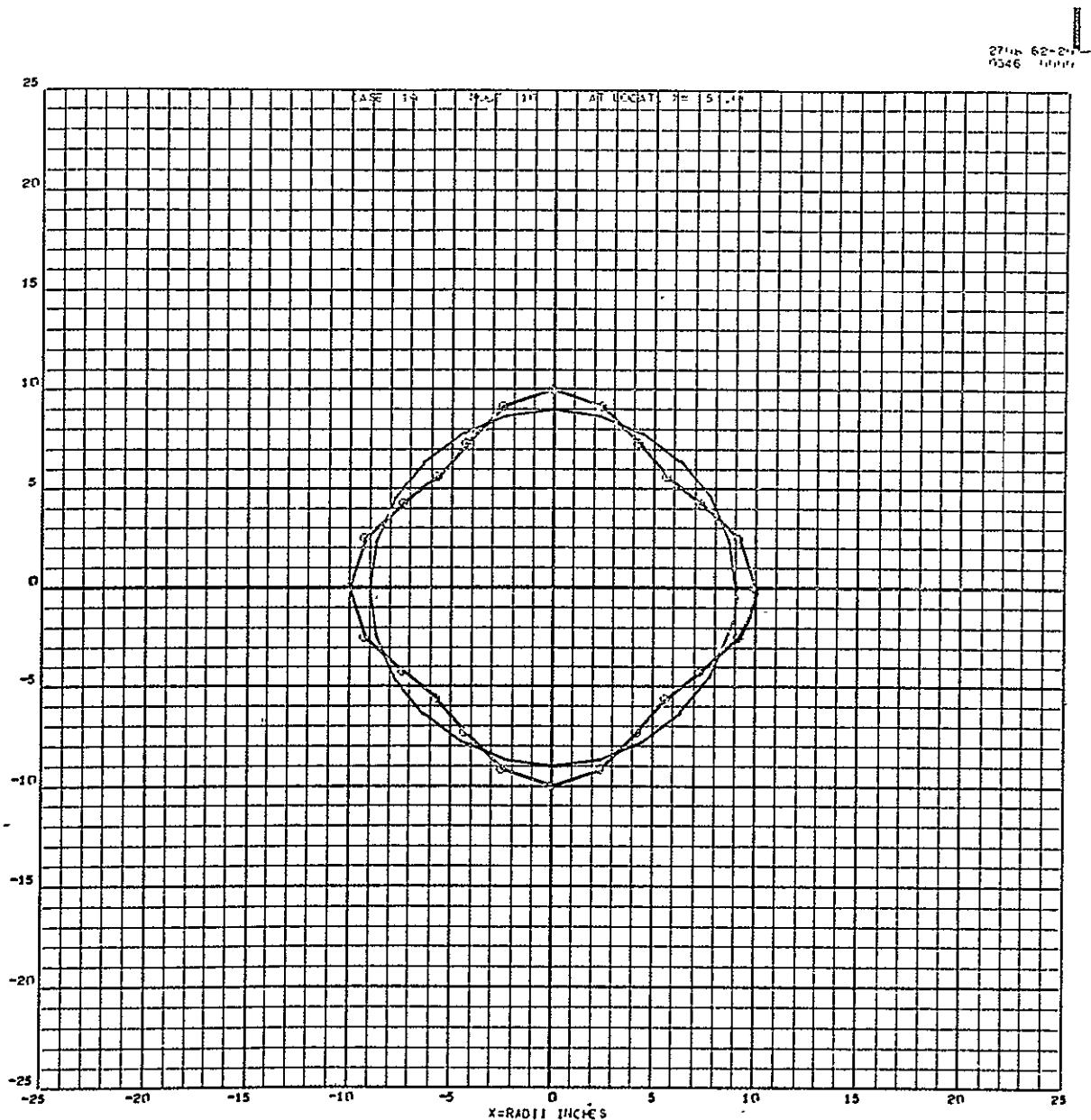
XVII-13

Figure XVII-14. Theoretical Mode Shapes and Mass-Loaded Shells.
Case 19 - 209. 02 Hz
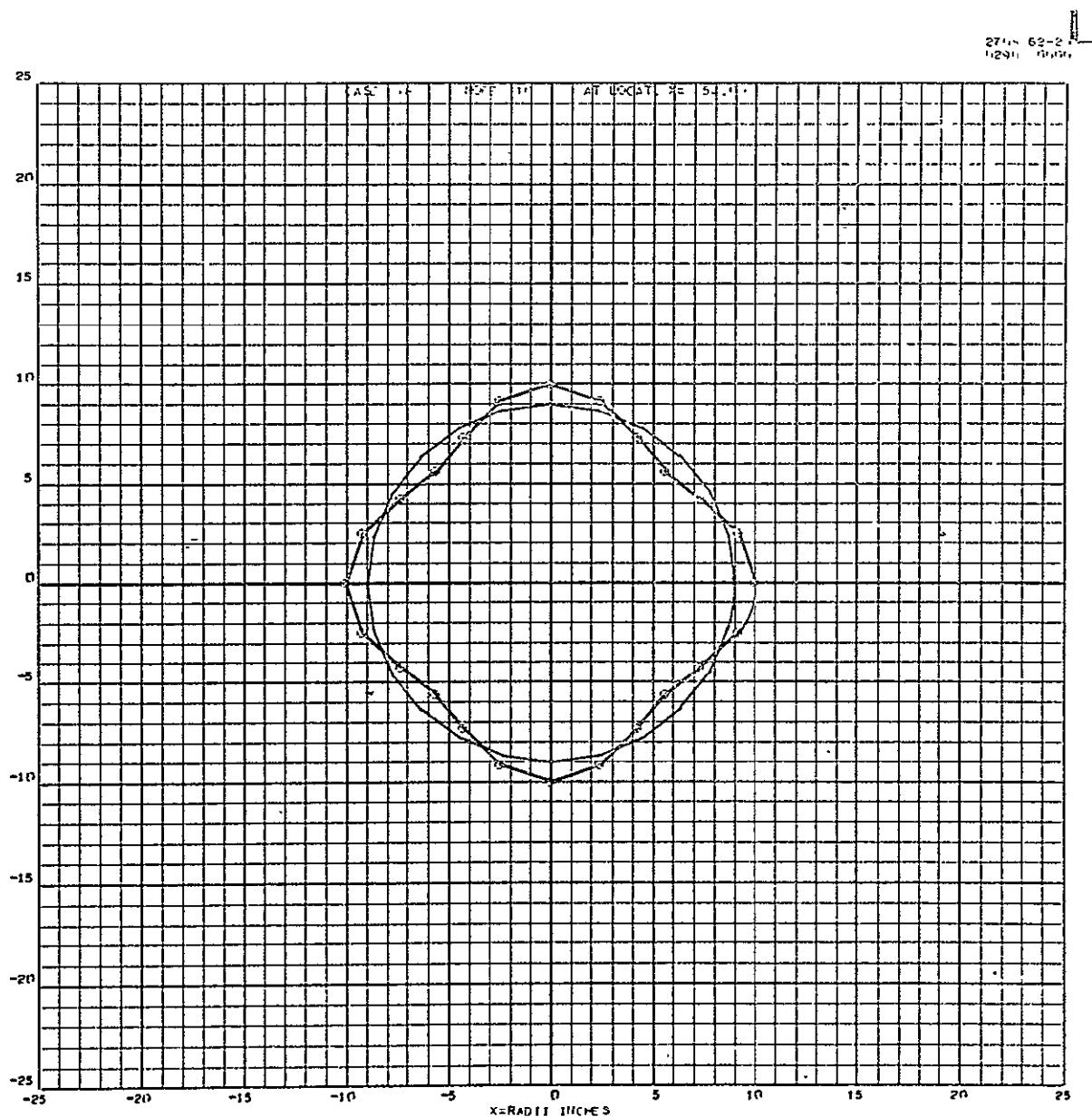
XVII-14

Figure XVII-15. Theoretical Mode Shapes and Mass-Loaded Shells.
Case 18 - 309. 17 Hz
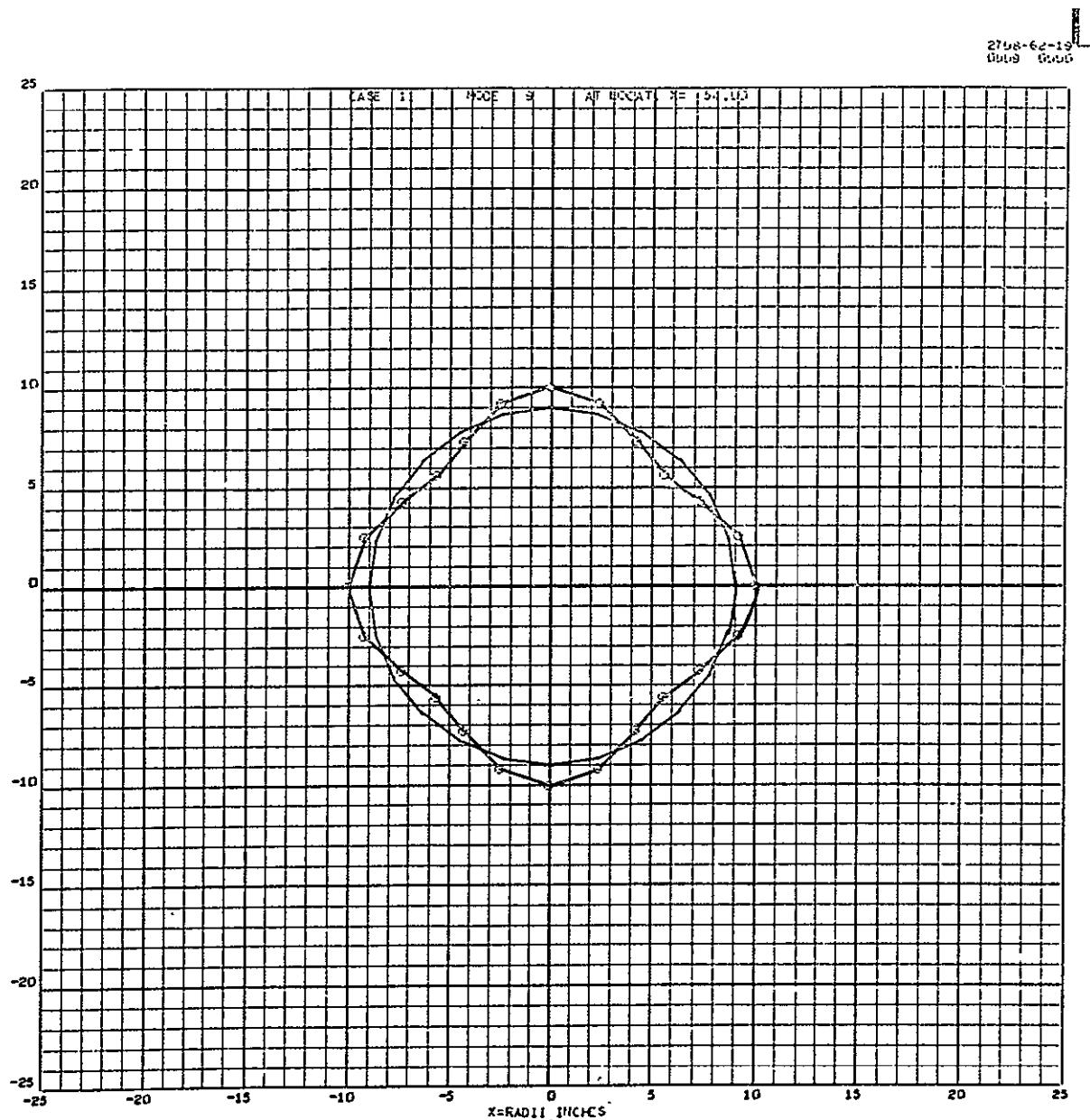
XVII-15

Figure XVII-16. Theoretical Mode Shapes and Mass-Loaded Shells.
Case 11 - 309.79 Hz
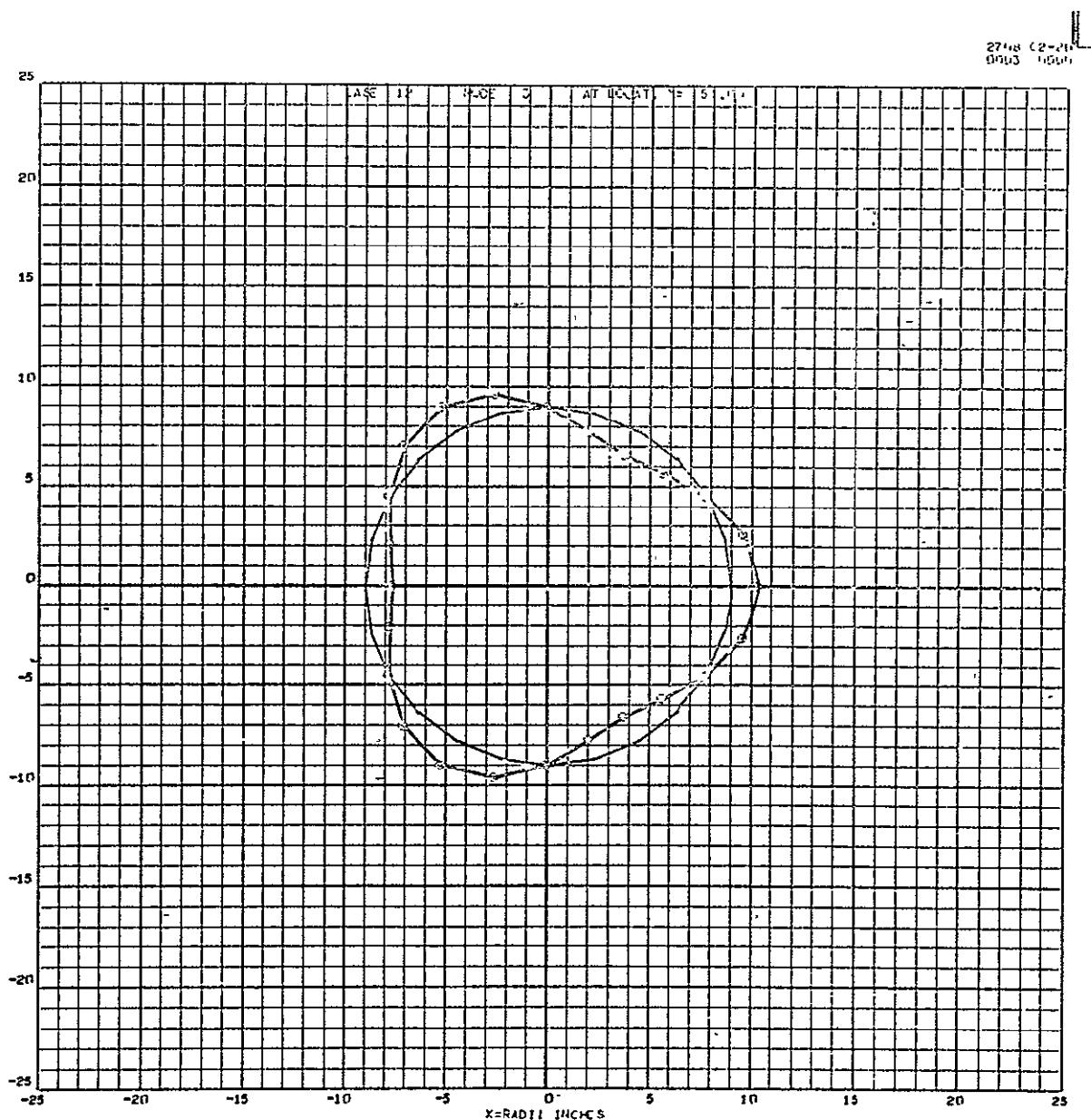
XVII-16

Figure XVII-17.   Theoretical Mode Shapes and Mass-Loaded Shells.
Case 12 - 84.09 Hz
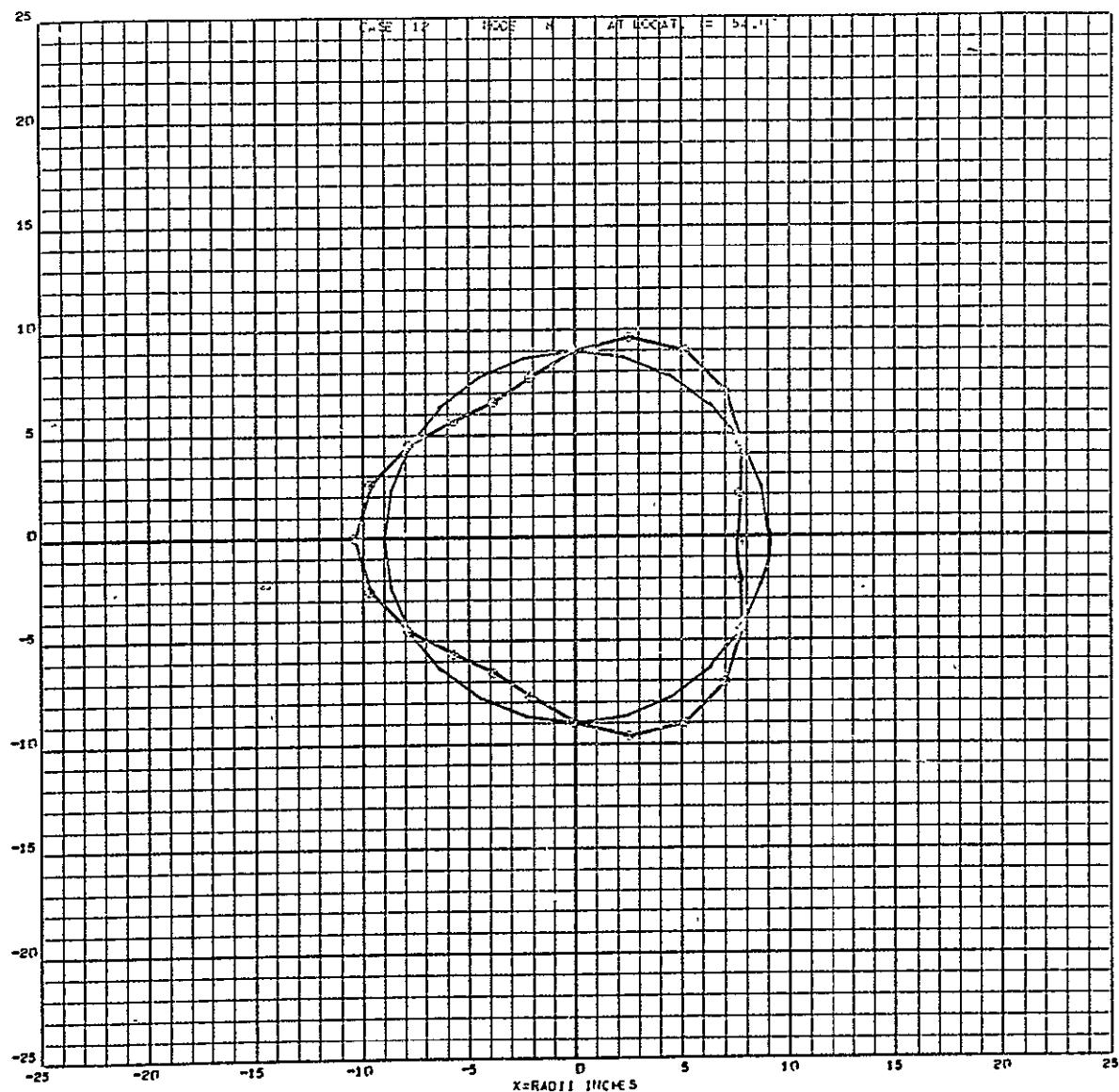
XVII-17

Figure XVII-18.   Theoretical Mode Shapes and Mass-Loaded Shells.
Case 12 - 288.69 Hz
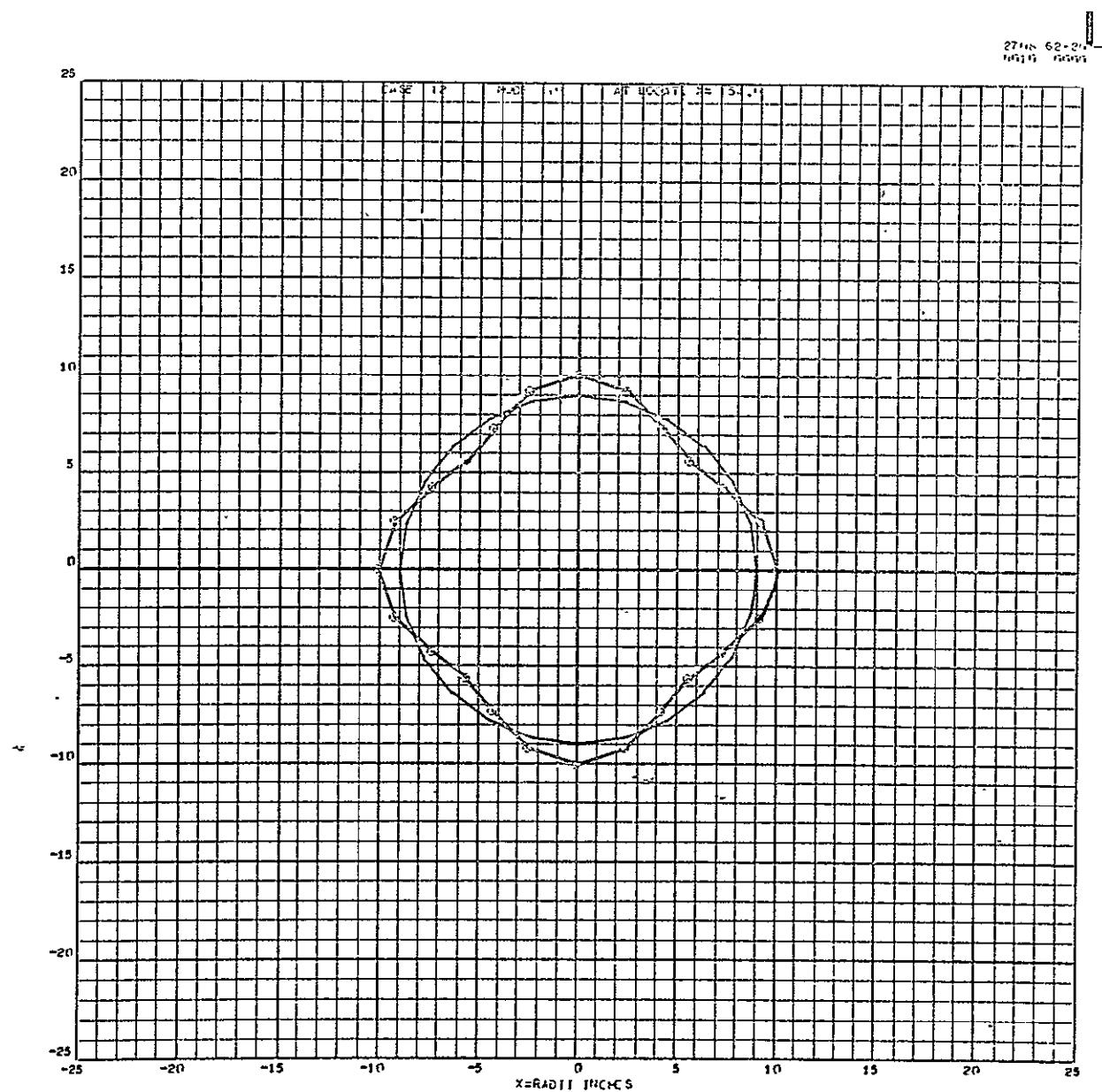
XVII-18

Figure XVII-19.   Theoretical Mode Shapes and Mass-Loaded Shells.
Case 12 - 309.77 Hz
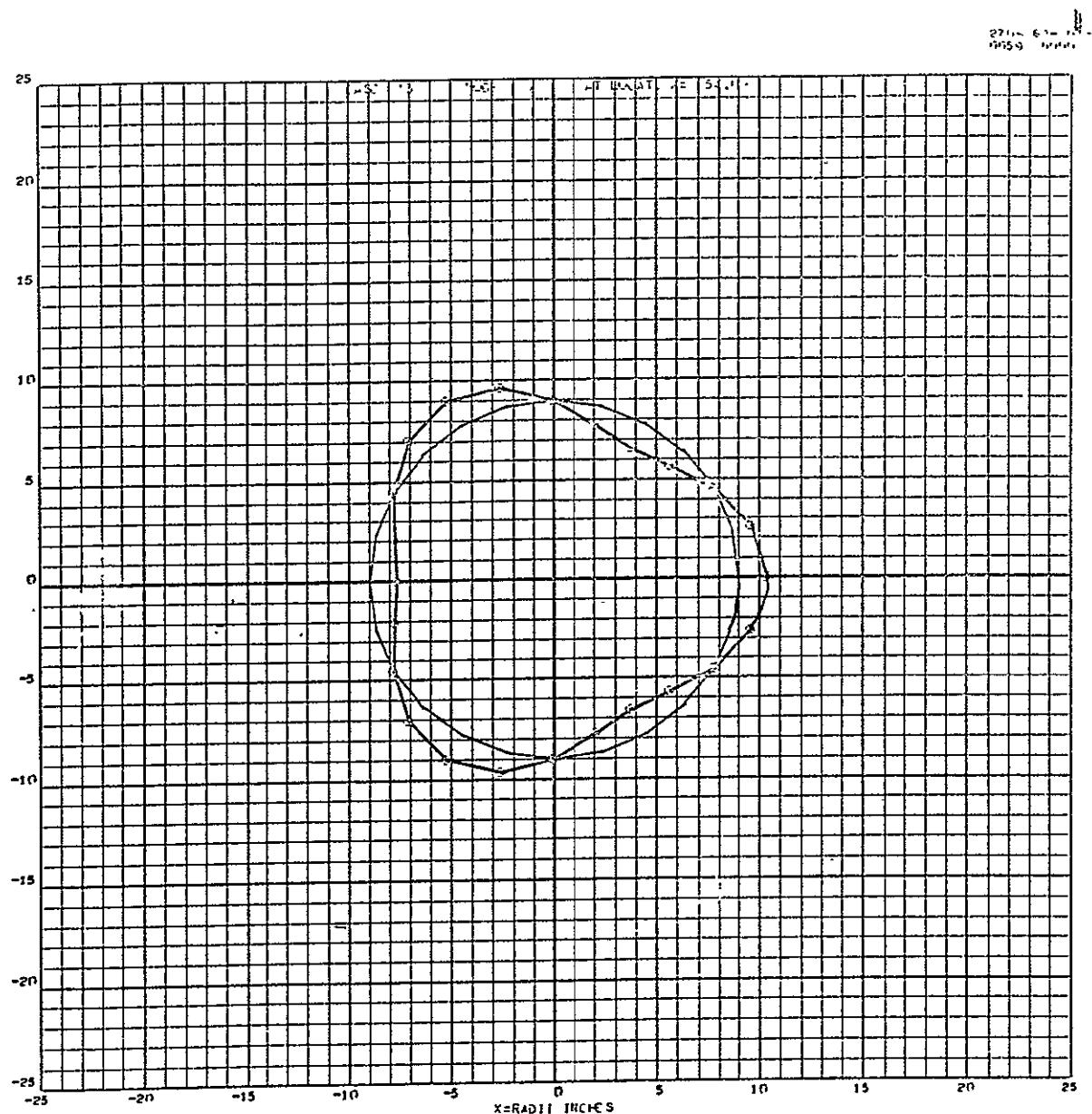
Figure XVII-20. Theoretical Mode Shapes and Mass-Loaded Shells.
Case 13 - 83.95 Hz
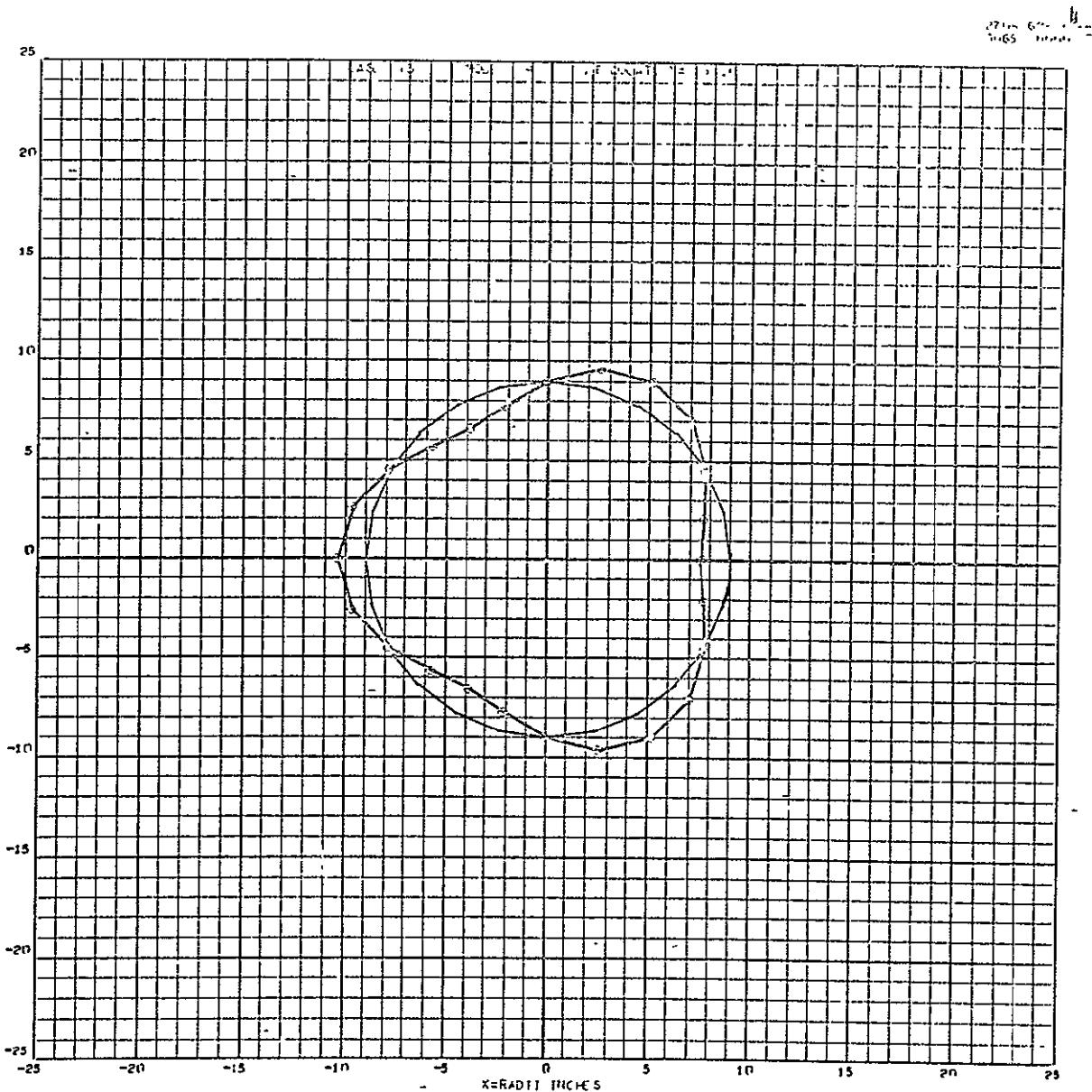
XVII-20

Figure XVII-21.   Theoretical Mode Shapes and Mass-Loaded Shells.
Case 13 - 288.44 Hz
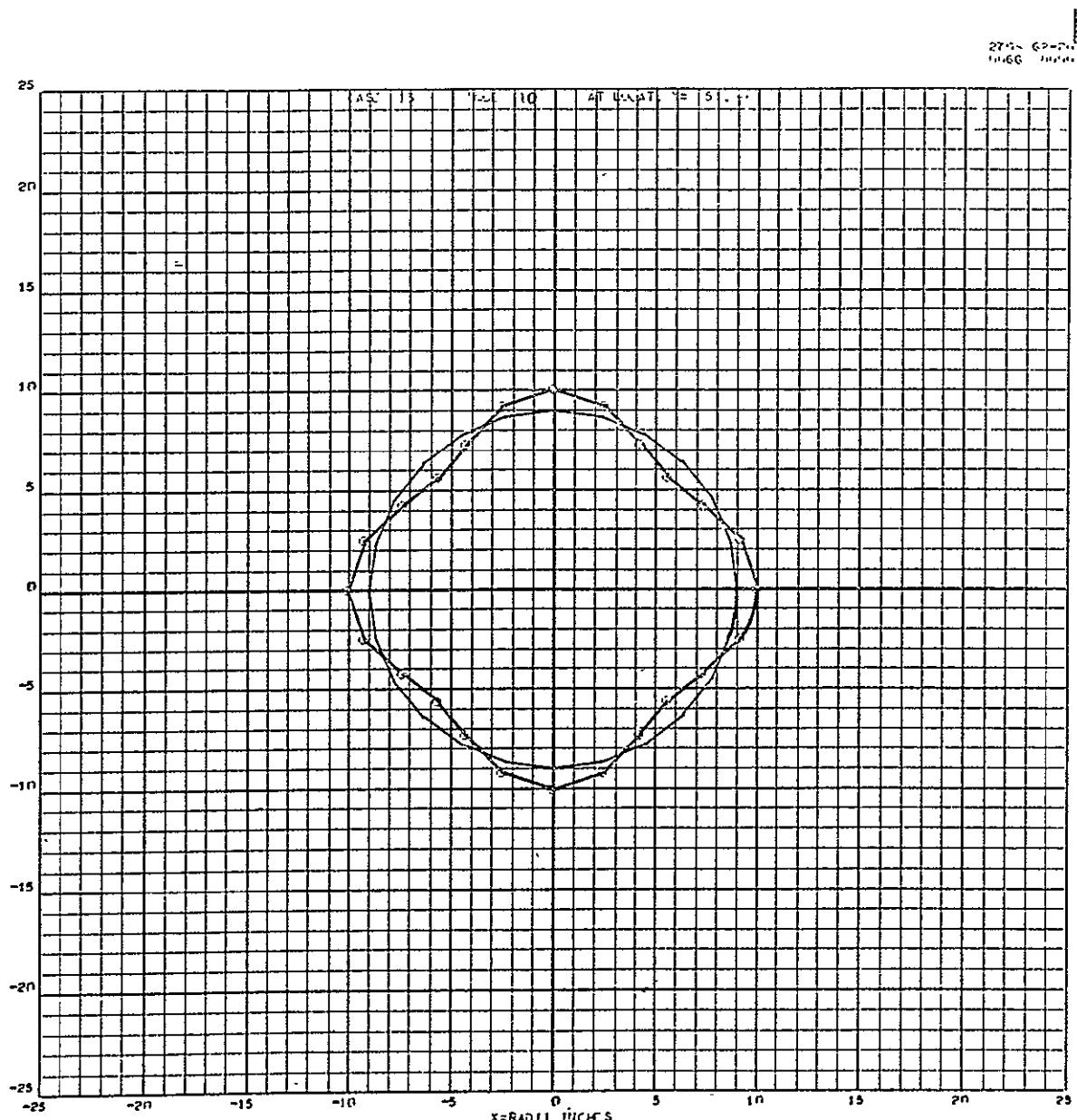
XVII-21

Figure XVII-22. Theoretical Mode Shapes and Mass-Loaded Shells.
Case 13 - 309.74 Hz
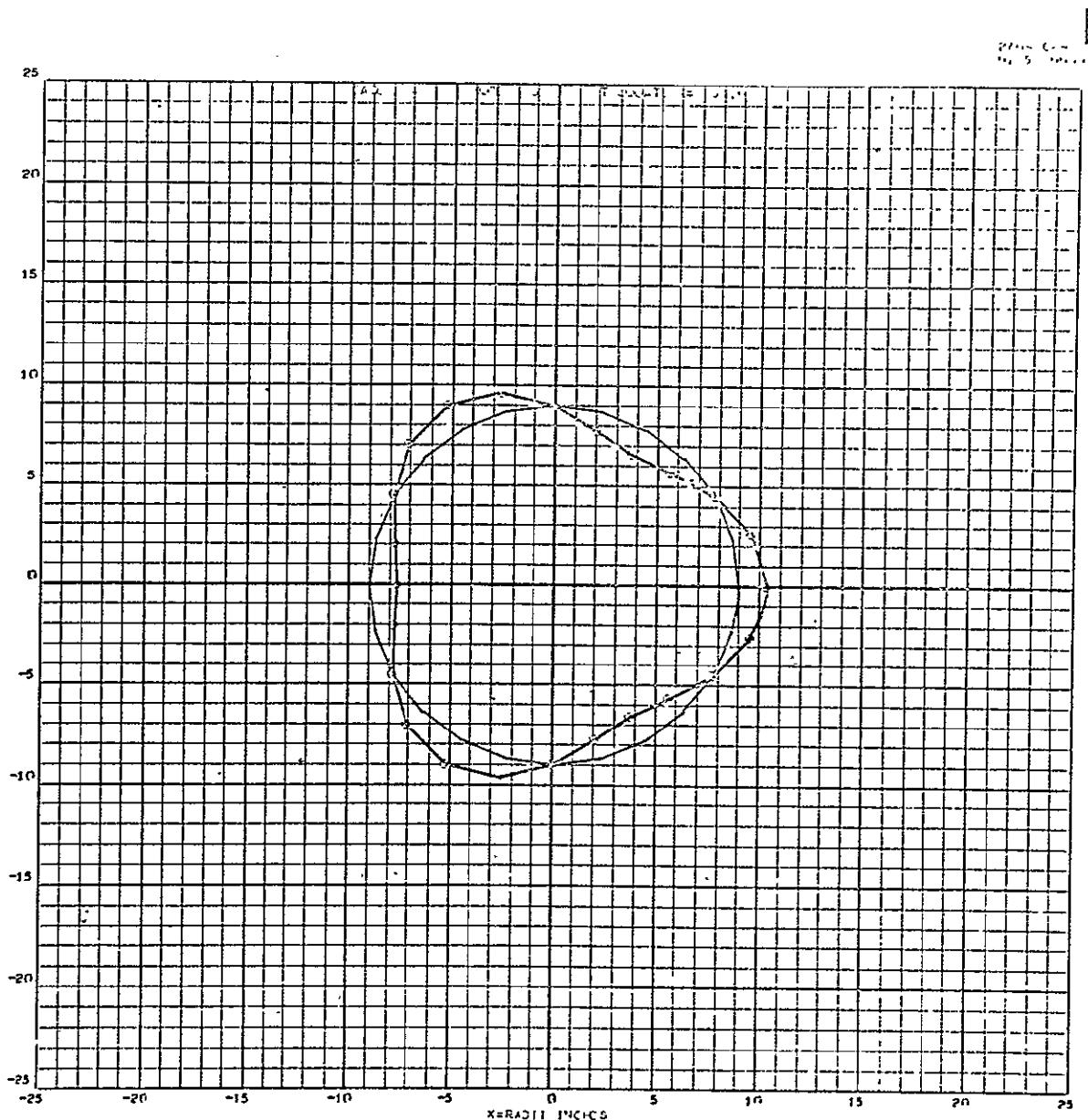
XVII-22

Figure XVII-23. Theoretical Mode Shapes and Mass-Loaded Shells.
Case 14 - 83.75 Hz
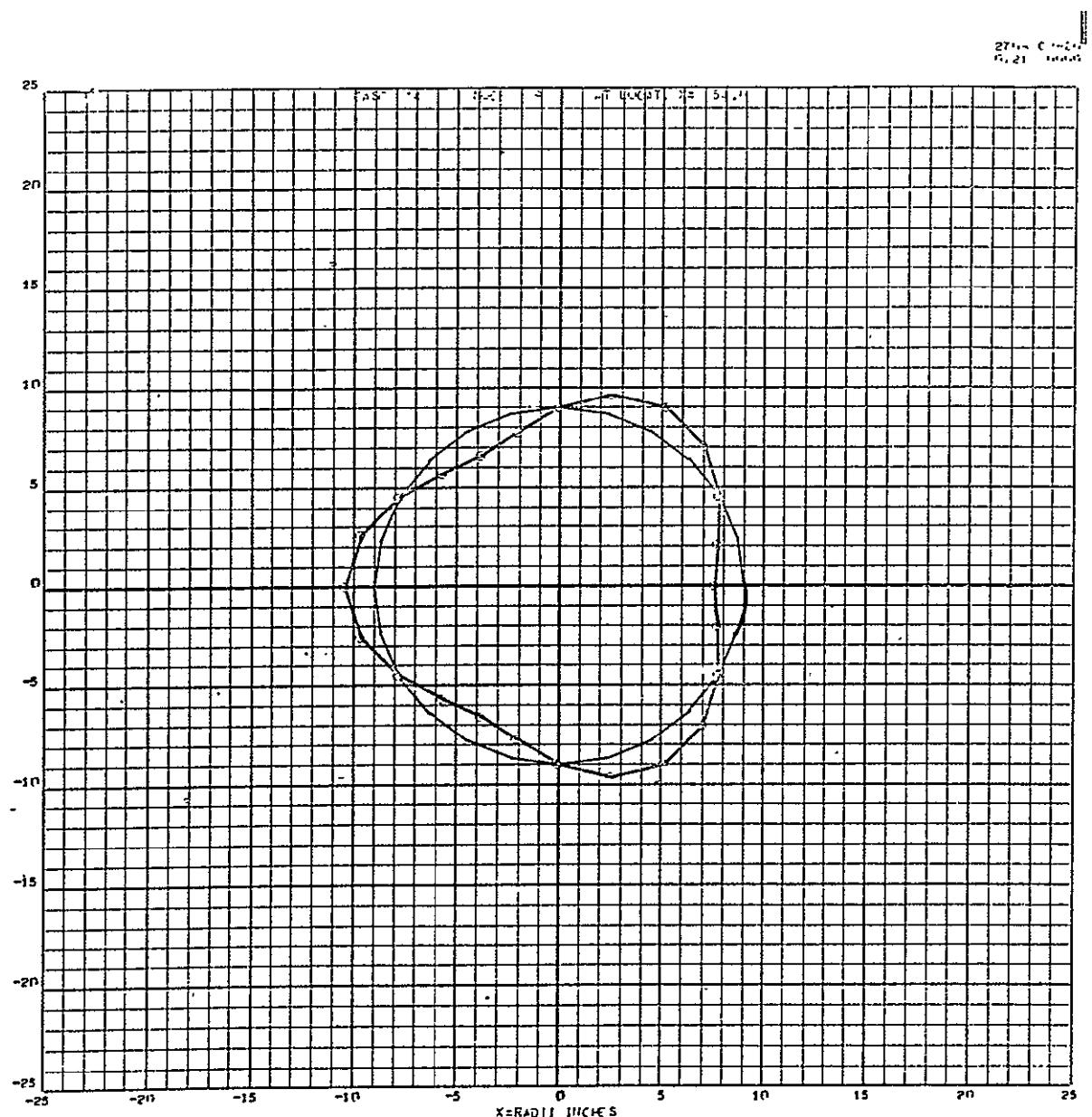
Figure XVII-24.   Theoretical Mode Shapes and Mass-Loaded Shells.
Case 14 - 288. 22 Hz
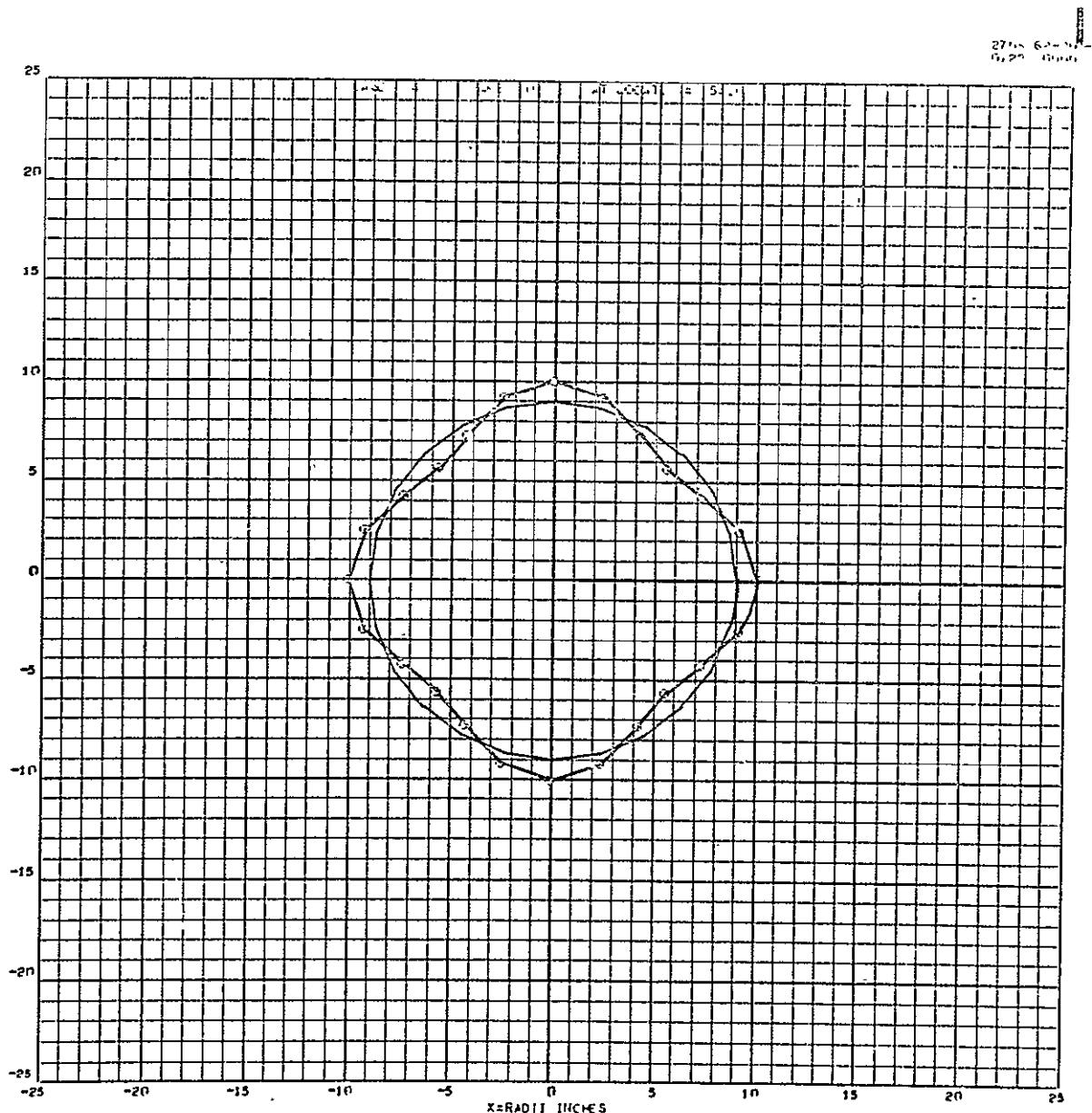
XVII-24

Figure XVII-25. Theoretical Mode Shapes and Mass-Loaded Shells.
Case 14 - 309.71 Hz
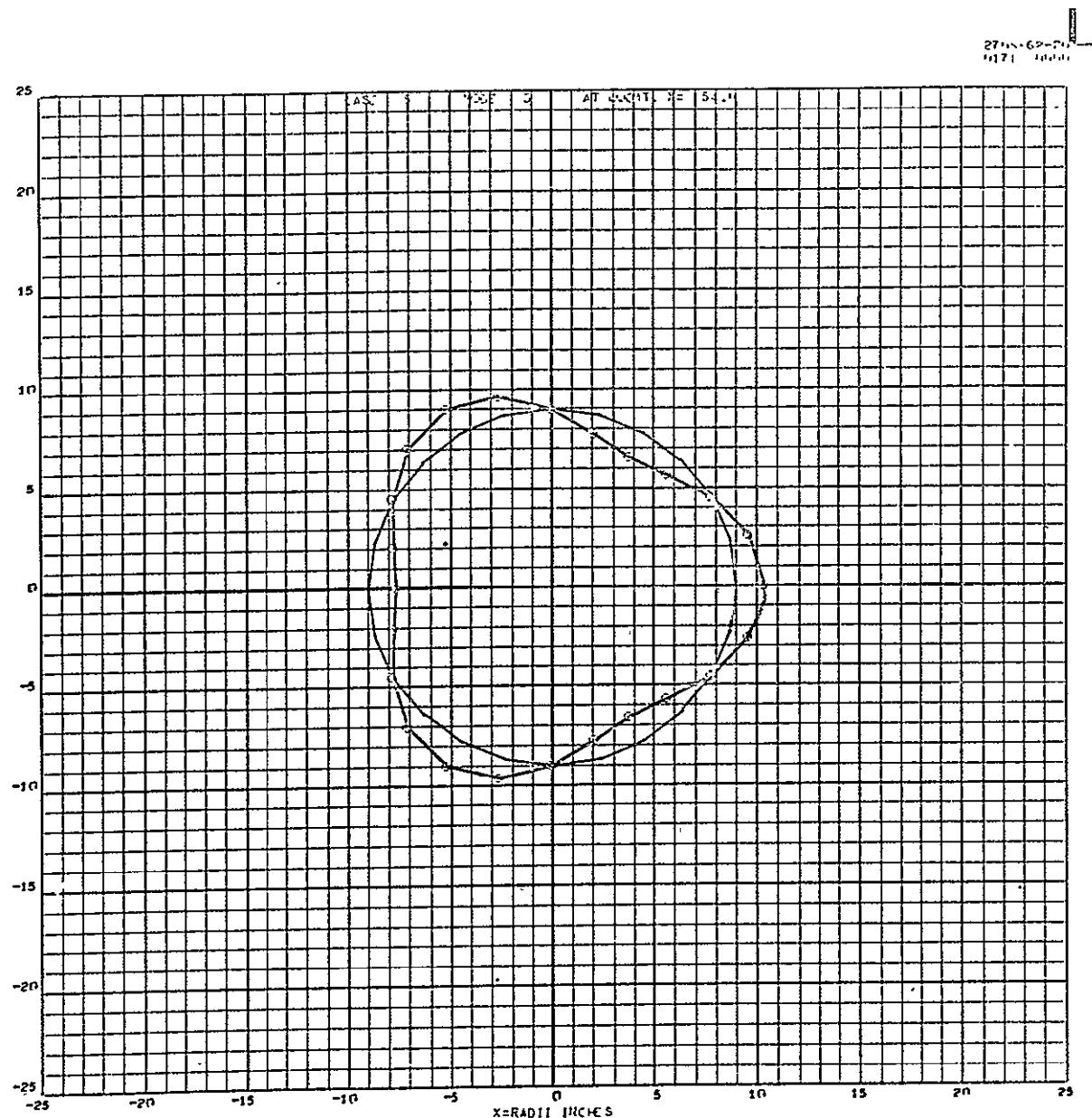
XVII-25

Figure XVII-26.   Theoretical Mode Shapes and Mass-Loaded Shells.
Case 15 - 83.57 Hz
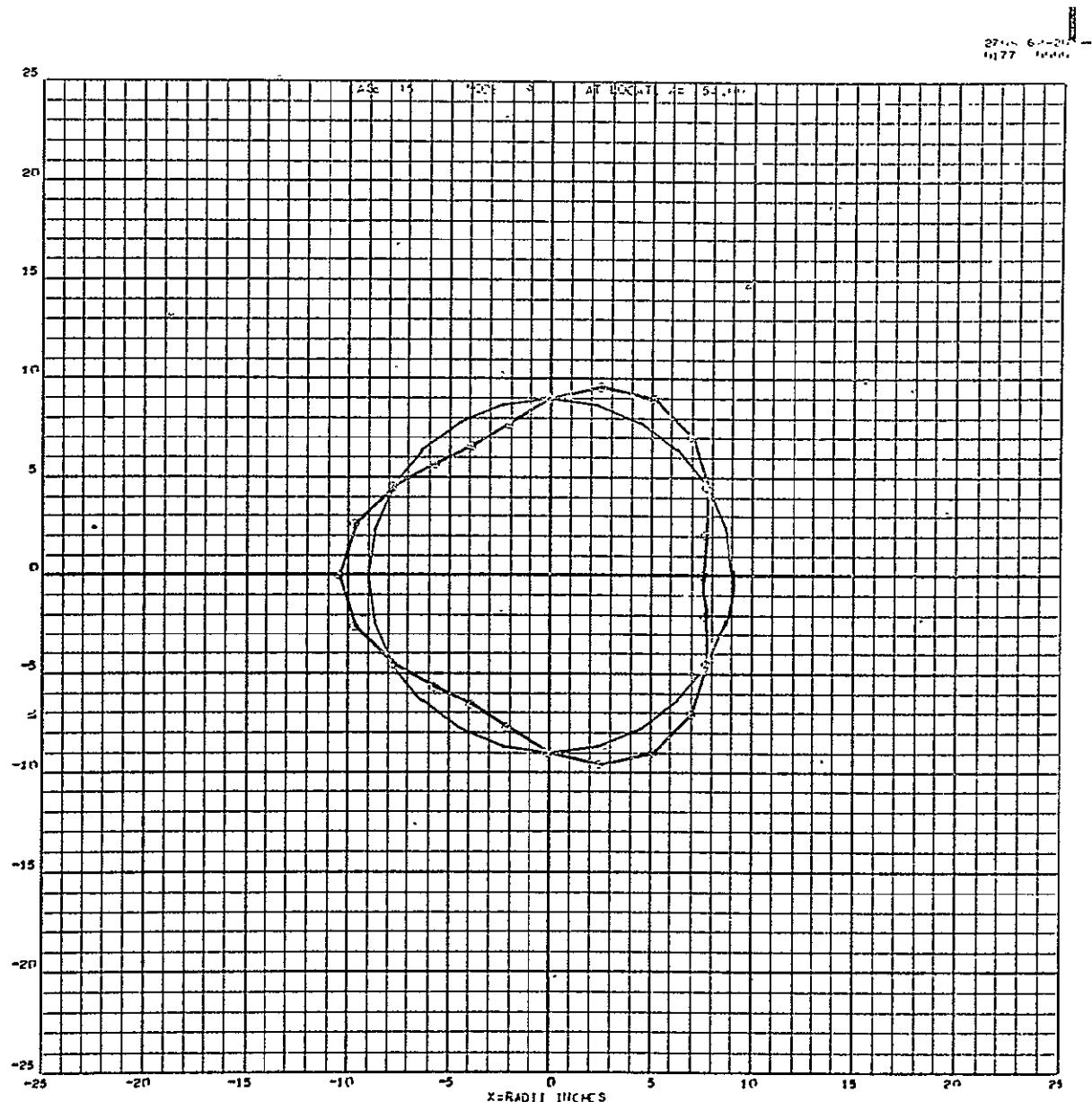
XVII-26

Figure XVII-27. Theoretical Mode Shapes and Mass-Loaded Shells.
Case 15 - 287.99 Hz
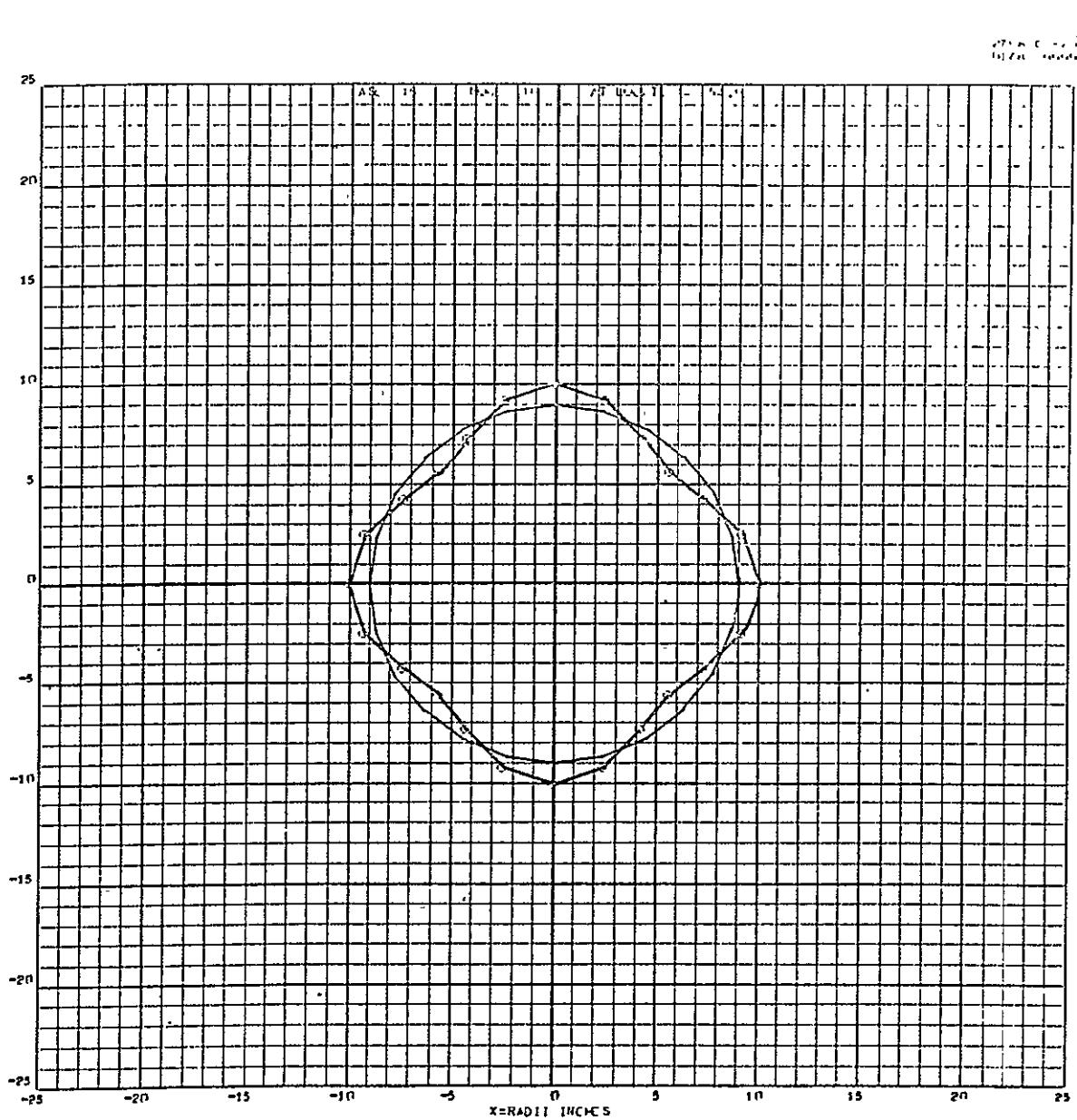
Figure XVII-28. Theoretical Mode Shapes and Mass-Loaded Shells.
Case 15 - 309.69 Hz
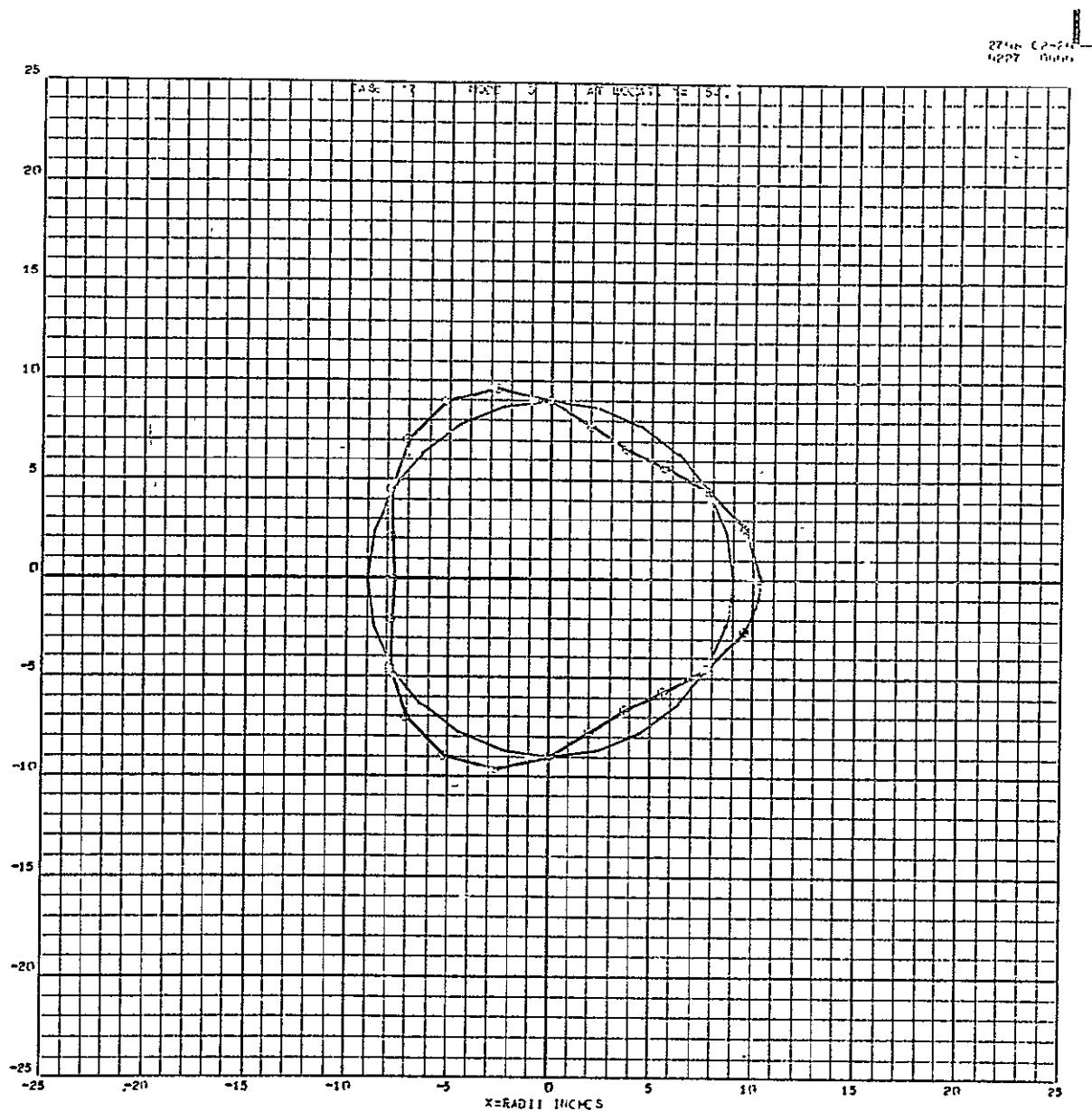
XVII-28

Figure XVII-29. Theoretical Mode Shapes and Mass-Loaded Shells.
Case 17 - 81.76 Hz
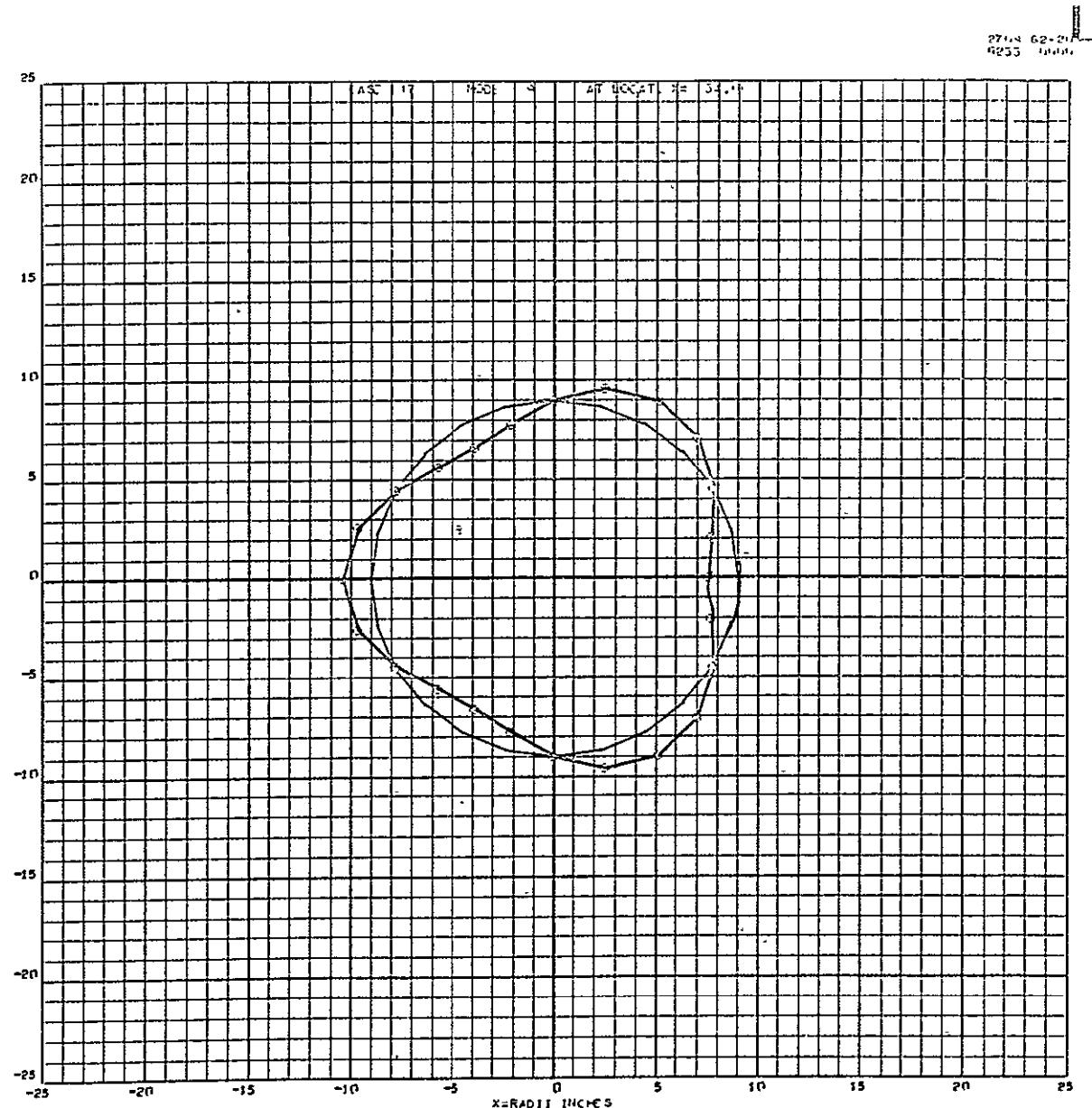
Figure XVII-30.   Theoretical Mode Shapes and Mass-Loaded Shells.
Case 17 - 286 Hz
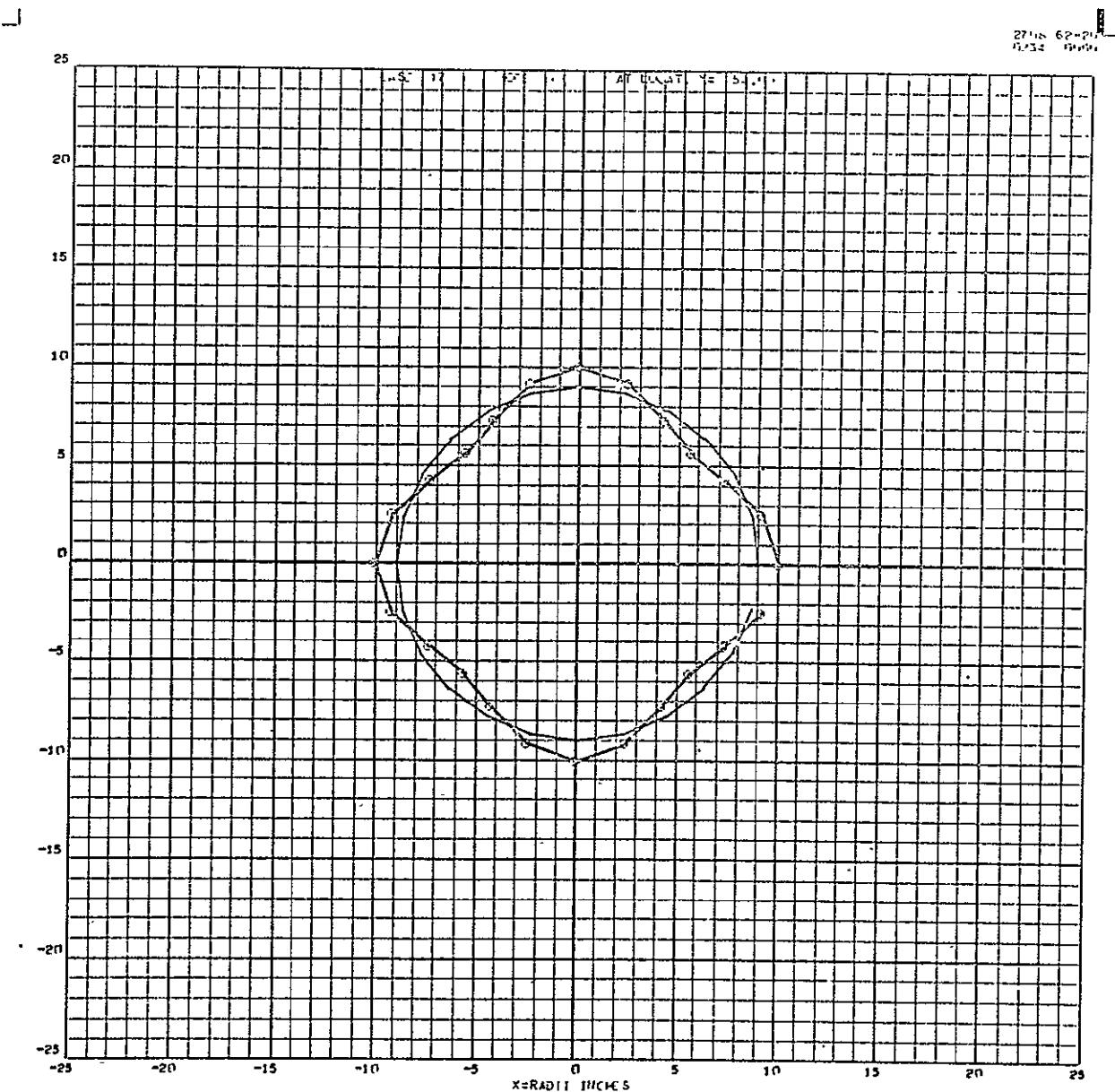
Figure XVII-31.   Theoretical Mode Shapes and Mass-Loaded Shells.
Case 17 - 309. 49 Hz

XVII-31